

AUG 11 1983

NAS 155:2269/pt.2

NASA Conference Publication 2269

Part 2

ORIGINAL

Large Space Antenna Systems Technology - 1982

*Proceedings of a conference held in
Hampton, Virginia
November 30 - December 3, 1982*



25th Anniversary
1958-1983

NASA

NASA Conference Publication 2269

Part 2

Large Space Antenna Systems Technology - 1982

Compiled by
E. Burton Lightner
Langley Research Center
Hampton, Virginia

Proceedings of a conference sponsored by
the NASA Office of Aeronautics and Space
Technology and NASA Langley Research Center
and held in Hampton, Virginia
November 30 - December 3, 1982

NASA
National Aeronautics
and Space Administration
Scientific and Technical
Information Branch

1983

PREFACE

This publication is a compilation of the unclassified papers presented at the NASA Conference on Large Space Antenna Systems Technology held at the Langley Research Center, Hampton, Virginia, November 30 - December 3, 1982. The conference was sponsored jointly by the NASA Office of Aeronautics and Space Technology (OAST) and the NASA Langley Research Center. The conference was organized into five sessions: Systems, Structures Technology, Control Technology, Electromagnetics, and Space Flight Test and Evaluation. All speakers and topics were selected by the session cochairmen and included representation from industry, universities, and government. The program was organized to provide a comprehensive review of space missions requiring large antenna systems and of the status of key technologies required to enable these missions.

In addition to the formal sessions, three forums were conducted on topics of current special interest. Forum topics were Systems Studies, Limitations of Ground Testing, and Structure and Control Interaction. Proceedings of the forums are not included in this publication.

The general cochairmen for the conference were Dell P. Williams, Director, Space Systems Division, NASA Office of Aeronautics and Space Technology, and Paul F. Holloway, Director for Space, Langley Research Center. The program chairman was Dr. Earle K. Huckins III, Head, Large Space Antenna Systems Technology Office, Langley Research Center. The conference committee wishes to express its appreciation to the session chairmen, authors, and conference administrative assistants for their outstanding contributions to the meeting.

This publication was expedited and enhanced through the efforts of the staff of the Research Information and Applications Division, Langley Research Center.

E. Larion Lightner
Langley Research Center

CONTENTS

PREFACE	iii
ATTENDEES	x

PART 1*

SYSTEMS

Communications

LARGE SPACEBORNE ANTENNA TECHNOLOGY: A SYSTEM PERSPECTIVE	1
F. Naderi	
LAND MOBILE SATELLITE SYSTEM REQUIREMENTS	17
John D. Kiesling	
SATELLITE SYSTEMS REQUIREMENTS FOR LAND MOBILE COMMUNICATIONS	29
M. Horstein	
AUDIO DIRECT BROADCAST SATELLITES	47
J. E. Miller	

Space Science

LARGE DEPLOYABLE REFLECTOR: AN INFRARED AND SUBMILLIMETER ORBITING OBSERVATORY	53
Paul N. Swanson and M. K. Kiya	
ANTENNA TECHNOLOGY FOR ORBITAL VERY LONG BASELINE INTERFEROMETRY (VLBI) . . .	61
E. C. Hamilton	

Military (Classified)

POTENTIAL APPLICATIONS OF LARGE SPACE SYSTEMS TECHNOLOGY TO THE INTEGRATED TACTICAL SURVEILLANCE SYSTEM (ITSS) S. A. Nichols	
PHASED ARRAY LENSES FOR SPACE-BASED RADAR (SBR) R. Schnieble	
STRUCTURAL AND RADIO FREQUENCY (RF) TEST RESULTS OF A PHASED ARRAY LENS WITH FOUR-BIT PHASE SHIFT MODULES J. Diglio	
SPACE-BASED RADAR (SBR) STRUCTURES AND DYNAMICS TECHNOLOGY ASSESSMENT F. Ayer, J. Turner, and T. Henderson	

*Part 1 is presented under a separate cover.

Earth Observations

PUSHBROOM RADIOMETRY AND ITS POTENTIAL USING LARGE SPACE ANTENNAS	81
Richard F. Harrington and Lloyd S. Keafer, Jr.	
EARTH OBSERVATION SYSTEM: SPACECRAFT DESIGN	105
J. J. Herbert and Will A. Schartel	
15-METER DEPLOYABLE APERTURE MICROWAVE RADIOMETER	131
J. V. Coyner, Jr.	

Systems Analysis

SYSTEMS DESIGN AND COMPARATIVE ANALYSIS OF LARGE ANTENNA CONCEPTS	157
L. Bernard Garrett and Melvin J. Ferebee, Jr.	
LARGE SPACE SYSTEMS AUXILIARY PROPULSION REQUIREMENTS	175
Joseph E. Maloy and William W. Smith	
A SUMMARY OF MISSION AND SYSTEM PERFORMANCE REQUIREMENTS FOR LARGE SPACE ANTENNAS	201
Lloyd S. Keafer, Jr., and W. R. Hook	

STRUCTURES TECHNOLOGY

Structures and Materials Technology

SPACECRAFT MATERIALS RESEARCH - A NASA PERSPECTIVE	213
Darrel R. Tenney	
SPACECRAFT MATERIAL APPLICATIONS - LONG-TERM STABILITY QUESTIONS	241
F. W. Crossman	
ADVANCES IN STRUCTURAL CONCEPTS	257
Martin M. Mikulas, Jr., and Harold G. Bush	
MANNED ASSEMBLY OF SPACE STRUCTURES	285
David Akin, Mary Bowden, and James Mar	
NASA/USAF RESEARCH IN STRUCTURAL DYNAMICS	301
L. D. Pinson and A. K. Amos	
PROGRESS IN THERMOSTRUCTURAL ANALYSIS OF SPACE STRUCTURES	345
Earl A. Thornton, Pramote Dechaumphai, Jack Mahaney, and Ajay K. Pandey	
STRUCTURES FOR LARGE PRECISION REFLECTORS	361
J. M. Hedgepeth and W. H. Greene	

Large Space Antenna Structural Systems

SURVEY OF DEPLOYABLE ANTENNA CONCEPTS	381
R. E. Freeland	

WRAP-RIB ANTENNA CONCEPT DEVELOPMENT OVERVIEW	423
A. A. Woods, Jr., and N. F. Garcia	
HOOP/COLUMN ANTENNA DEVELOPMENT PROGRAM	469
M. R. Sullivan	
STATUS OF DEPLOYABLE GEO-TRUSS DEVELOPMENT	513
J. A. Fager	
BOX TRUSS DEVELOPMENT AND APPLICATIONS	527
J. V. Coyner, Jr.	
INFLATED ANTENNAS	545
G. J. Friese, M. Thomas, and W. F. Hinson	
ELECTROSTATICALLY FIGURED MEMBRANE REFLECTORS: AN OVERVIEW	575
J. H. Lang	

PART 2

CONTROL TECHNOLOGY

CONTROL OF LARGE SPACE ANTENNAS	583
A. F. Tolivar and S. J. Wang	
ENABLING TECHNOLOGIES FOR LARGE PRECISION SPACE SYSTEMS	601
Robert R. Strunce, Jr., and James D. Turner	
REDUCED ORDER CONTROL DESIGN FOR LARGE SPACE STRUCTURES - A COMMUNICATION SATELLITE EXAMPLE	625
Richard Gran	
CURRENT STATUS OF SYSTEM IDENTIFICATION METHCDOLOGY	649
W. E. Larimore, R. K. Mehra, D. E. Gustafson, and J. Raillieul	
COMPUTER ANALYSIS AND GROUND TESTING OF LARGE SPACE SYSTEMS CONTROL STRATEGIES	665
J. N. Aubrun and J. A. Breakwell	
SHAPE DETERMINATION/IDENTIFICATION FOR LARGE SPACE ANTENNAS	687
G. Rodriguez, J. M. Cameron, and M. H. Milman	
PRACTICAL APPROACHES TO THE DESIGN OF CONTROL SYSTEMS FOR LARGE SPACE STRUCTURES	709
H. J. Buchanan	
RESULTS OF STUDIES AT LANGLEY RESEARCH CENTER ON THE CONTROL OF LARGE SPACE SYSTEMS	721
R. C. Montgomery and L. W. Taylor, Jr.	

ELECTROMAGNETICS

INTELSAT VI ANTENNA SYSTEM DESIGN AND DEVELOPMENT	743
M. F. Caulfield, R. A. Taormina, B. M. Flynn, S. O. Lane, T. M. Paige, and V. E. Cascia	
SCANNING BEAM ANTENNA CONCEPTUAL DESIGN FOR 20/30 GHz SATELLITE SYSTEMS . .	767
J. Smetana, R. Sorbello, and W. F. Crosswell	
MULTIMISSIION ADVANCED CONFIGURATION	797
A. Saitto and G. Berretta	
LARGE SPACE ANTENNA COMMUNICATIONS SYSTEMS - INTEGRATED LaRC/JPL TECHNOLOGY DEVELOPMENT ACTIVITIES. I. INTRODUCTION	809
Thomas G. Campbell	
LARGE SPACE ANTENNA COMMUNICATIONS SYSTEMS - INTEGRATED LaRC/JPL TECHNOLOGY DEVELOPMENT ACTIVITIES. II. LaRC ACTIVITIES	815
T. G. Campbell, M. C. Bailey, C. R. Cockrell, and F. B. Beck	
LARGE SPACE ANTENNA COMMUNICATIONS SYSTEMS - INTEGRATED LaRC/JPL TECHNOLOGY DEVELOPMENT ACTIVITIES. III. JPL ACTIVITIES	833
K. E. Woo, Y. Rahmat-Samii, and W. Imbriale	
THE EFFECTS OF MESH REFLECTING SURFACES UPON RADIOMETRIC MEASUREMENTS . . .	853
W. F. Crosswell	
DEVELOPMENT OF IMPROVED ANALYTICAL MODELS FOR MESH REFLECTOR SURFACES . . .	867
Jerry C. Brand and J. Frank Kauffman	
A SURVEY OF NEAR-FIELD TESTING METHODS FOR LARGE APERTURE ANTENNAS AND FUTURE TRENDS	877
Allen C. Newell	
NEAR-FIELD MEASUREMENT FACILITY PLANS AT LEWIS RESEARCH CENTER	899
R. G. Sharp	

SPACE FLIGHT TEST AND EVALUATION

THE NEED FOR SPACE FLIGHT EXPERIMENTS AND TESTING IN THE DEVELOPMENT OF LARGE SPACE ANTENNA SYSTEMS TECHNOLOGY	923
Earle K. Huckins III	
A ROBOT IN SPACE AS A LARGE SPACE STRUCTURES CONTROL EXPERIMENT	941
Richard Gran	
SPACE FLIGHT EXPERIENCE WITH THE SHUTTLE ORBITER CONTROL SYSTEM	949
Kenneth J. Cox, Kevin C. Daly, and Philip D. Hattis	
SPACE TECHNOLOGY EXPERIMENT PLATFORM (STEP). A SHUTTLE-BORNE SUPPORT FACILITY FOR STRUCTURES, STRUCTURAL DYNAMICS, AND CONTROL TECHNOLOGY FLIGHT EXPERIMENTS	969
Jack E. Harris and Larry D. Pinson	

SAFE ON-ORBIT EXPERIMENT FOR MEASUREMENT OF LARGE STRUCTURES DYNAMICS . . .	981
R. W. Schock	
SAFE II - LARGE SYSTEMS SPACE PLASMA EVALUATION EXPERIMENT	991
M. R. Carruth, Jr., L. E. Young, C. K. Purvis, and N. J. Stevens	
MAST SPACE RESEARCH FLIGHT EXPERIMENT	1007
John L. Allen and Brantley Hanks	
A LARGE ANTENNA SYSTEM FLIGHT EXPERIMENT	1021
Keto Soosaar	
SADE - A SPACE EXPERIMENT TO DEMONSTRATE STRUCTURAL ASSEMBLY	1029
James K. Harrison and David C. Cramblit	

ATTENDEES

NASA Headquarters Washington, DC

J. B. Dahlgren
J. D. DiBattista
Dr. D. A. Gilman
L. Holcomb
F. D. Kochendorfer
J. E. Miller
S. L. Venneri
D. P. Williams

NASA Langley Research Center Hampton, VA

Dr. D. P. Hearth
R. H. Petersen
P. F. Holloway
R. C. Goetz
H. T. Wright
Dr. M. F. Card
Dr. G. D. Walberg
I. Abbasy (GWU)
H. M. Adelman
E. L. Ahl, Jr.
F. O. Allamby
F. Allario
J. L. Allen, Jr.
M. J. Anderson
W. W. Anderson
E. S. Armstrong
G. C. Ashby, Jr.
Dr. M. C. Bailey
J. G. Batterson
M. E. Beatty III
F. B. Beck
W. K. Belvin
K. S. Bey
H. J. C. Blume
D. E. Bowles
L. Bowman
W. J. Boyer
O. H. Bradley
J. D. Buckley
H. G. Bush
D. H. Butler
T. G. Campbell
J. J. Catherines
H. K. Clark
Dr. C. R. Cockrell
M. Cooper (GWU)
R. H. Couch

NASA Langley Research Center Hampton, VA (Continued)

E. A. Crossley, Jr.
K. A. Crumbly
L. J. DeRyder, Jr.
L. A. Dillion-Townes
Dr. S. C. Dixon
J. A. Dodgen
J. T. Dorsey (GWU)
R. S. Dunning
J. R. Elliott
R. W. Faison
J. C. Fedors
M. J. Ferebee, Jr.
Dr. W. B. Fichter
W. Fitzgerald
A. Fontana
R. E. Fulton
Dr. L. B. Garrett
M. C. Gilreath
J. W. Goslee
W. L. Grantham
W. H. Greene
J. Hagaman
H. A. Hamer
B. R. Hanks
P. W. Hanson
Dr. R. F. Harrington
J. E. Harris
W. L. Heard, Jr.
C. L. Herstrom
W. F. Hinson
R. Hodges
S. E. Holloway III
W. R. Hook
Dr. G. C. Horner
L. G. Horta
Dr. J. M. Housner
Dr. E. K. Huckins III
J. W. Johnson
W. R. Jones
J. N. Juang
L. S. Keafer, Jr.
C. R. Keckler
B. M. Kendall
V. Klein (GWU)
P. Klich
F. Koprivier III
W. Lee
E. B. Lightner
S. A. T. Long

NASA Langley Research Center
Hampton, VA (Continued)

U. M. Lovelace
J. B. Lovell
M. H. Lucy
J. Mahaney (ODU)
J. A. Martin
H. G. McComb, Jr.
P. McGowan
M. McMillin
Dr. M. M. Mikulas, Jr.
R. Miserentino
Dr. R. C. Montgomery
J. C. Moorman
V. Mukhopadhyay (GWU)
J. R. Newsom
A. K. Noor (GWU)
G. C. Olsen
R. S. Pappa
Dr. L. D. Pinson
W. H. Reed III
M. D. Rhodes
D. K. Robertso
J. C. Robinson
R. A. Russeil
A. A. Schy
K. N. Shivakumar
Dr. J. J. Singh
F. M. Smith
J. Sobieski
L. D. Staton
J. S. Sutila
G. Sykes
J. B. Talbot
L. W. Taylor, Jr.
Dr. D. R. Tenney
Dr. E. A. Thornton (ODU)
J. D. Timmons
R. H. Tolson
Dr. S. S. Tompkins
L. F. Vosteen
W. W. Wagner, Jr.
J. E. Walz
J. C. Ward, Jr.
N. D. Watson
A. P. Wiehing
J. L. Williams
J. P. Williams
R. T. Wingate
R. L. Wright
J. W. Young

NASA Ames Research Center
Moffett Field, CA

M. K. Kiya
R. B. Pittman
B. L. Swenson

NASA Goddard Space Flight Center
Greenbelt, MD

H. Montgomery
W. T. Walton
J. P. Young

Jet Propulsion Laboratory
Pasadena, CA

K. C. Coon
W. A. Edmiston
R. E. Freeland
W. A. Imbriale
V. Jamejad
Dr. R. Levy
F. Naderi
Y. Rahmat-Samii
Dr. D. G. Rea
G. Rodriguez
Dr. P. N. Swanson
S. N. Swanson
S. Szirmay
A. F. Tolivar
K. E. Woo

NASA L. B. Johnson Space Center
Houston, TX

R. F. Baillie

NASA Lewis Research Center
Cleveland, OH

B. E. LeRoy
J. E. Maloy
R. Sharp

NASA Marshall Space Flight Center
Huntsville, AL

H. J. Buchanan
M. R. Carruth
E. C. Hamilton
R. W. Schock
W. E. Thompson

Advanced Technology Center
Huntsville, AL

B. Sallo

Aerojet Liquid Rocket Co.
Sacramento, CA

L. H. Luehr

Aerospace Corp.
Los Angeles, CA

E. Jacobs
G. Smit

AFOSR
Bolling Air Force Base, DC

A. K. Amos
R. Sierakowski

AFWAL
Wright Patterson Air Force Base, OH

H. C. Croop
G. R. Holderby
W. Johnston
J. Pearson
Lt. D. B. Ridgely
V. B. Venkayya

Astro Research Corp.
Carpinteria, CA

B. Cambell
Dr. J. M. Hedgepeth

Battelle Columbus Lab
Columbus, OH

S. A. Kingsley

The BDM Corp.
Albuquerque, NM

R. K. Hoppe
K. F. Probst

Bendix Field Engineering Corp.
Greenbelt, MD

M. J. Aucremanne
G. T. Foote

Boeing Aerospace Co.
Seattle, WA

T. H. Chase
R. M. Gates
C. T. Golden
W. W. Smith
E. E. Spear

Brunswick Corporation
Costa Mesa, CA

C. B. Kurz

C. S. Draper Laboratory
Cambridge, MA

F. N. R. Ayer
K. Daly
Dr. E. Fogel
S. D. Ginter
J. G. Lin
C. M. Satter
Dr. K. Soosaar
R. R. Strunce, Jr.
J. D. Turner

College of William and Mary
Williamsburg, VA

Dr. E. Kamaratos

Communications Research Center
Ontario, Canada

D. G. Zimcik

COMSAT Laboratories
Clarksburg, MD

P. M. Caughran
Y. S. Lee
H. Gerson
R. M. Sorbello
A. I. Zaghloul

Edighoffer
Hampton, VA

H. Edighoffer

Essex Corp.
Huntsville, AL

N. Shields, Jr.

European Space Agency
The Netherlands

A. Saitto
H. A. Superfine

Fairchild Space & Electronics Co.
Germantown, MD

L. DiBiasi
R. E. Kramer

Foldes Inc.
Wayne, PA

P. Foldes

Ford Aerospace & Communications Corp.
Palo Alto, CA

E. Nygren

General Dynamics Convair
San Diego, CA

N. L. Cohen
M. P. Dudeck
J. A. Fager
H. B. Henderson
S. Kulick
A. R. Robertson
J. R. Sesak
G. R. Stone
J. D. Weber

General Electric Company
Philadelphia, PA

D. J. Cuthbert
M. Garnek
J. D. Keising
E. J. Kuhar, Jr.
V. Navon
C. V. Stahle
R. B. Wiley

General Research Corporation
Santa Barbara, CA

R. F. Crawford
D. J. Mihora

Georgia Institute of Technology
Atlanta, GA

S. N. Atluri

Goodyear Aerospace Company
Washington, DC

R. W. Morris

Grumman Aerospace Corporation
Bethpage, NY

J. T. Diglio
R. Gran
R. R. Price
J. L. Schultz
W. E. Simpson
S. Wong

Harris Corporation
Melbourne, FL

B. B. Allen
H. J. Andrews
W. F. Croswell
J. W. Shipley
M. R. Sullivan

Honeywell, Incorporated
Minneapolis, MN

R. P. Singh

Howard University
Washington, DC

Dr. P. M. Baiman
R. Krishna
M. G. Mancharan
C. McKissack
A. S. S. R. Reddy

Hughes Aircraft Co.
Los Angeles, CA

V. E. Cascia
M. F. Caulfield
B. N. Flynn
S. G. Lane
T. M. Paige

Hydraulic Research TEXTRON
Irvine, CA

R. Quartararo

Itek Corp.
Lexington, MA

J. J. Cleary

Johns Hopkins University
Laurel, MD

T. B. Coughlin

Kentron International
Hampton, VA

C. L. Blackburn
E. P. Brien
R. E. Calleson

Kentron International
Hampton, VA (Continued)

R. A. Dacosta
J. K. Jensen
R. W. LeMessurier
J. E. Phelps
J. E. Price
R. E. Wallson

Lawrence Livermore National Lab
Livermore, CA

S. R. Arnold
H. S. Cabayan
W. E. Larimore
A. J. Spero

L'Garde, Inc.
Newport Beach, CA

G. J. Friese
M. Thomas

Lockheed Missiles and Space Company
Sunnyvale, CA

E. L. Becker
N. F. Garcia
R. R. Johnson
G. Turner
A. A. Woods, Jr.

Lockheed Palo Alto Research Laboratory
Palo Alto, CA

J. N. Aubrun

Martin Marietta Corporation
Denver, CO

J. V. Coyner, Jr.
Dr. R. C. Engels
T. C. Fenner
J. J. Herbert
W. H. Huang
M. W. Kuethe
F. K. Mattson
W. A. Schartel
F. R. Schwartzberg

Massachusetts Institute of Technology
Cambridge, MA

J. H. Lang
J. W. Mar

McDonnell Douglas Technical Services
Huntsville, AL

Dr. W. R. Mahaffey
T. P. Poole

MIT Lincoln Lab
Lexington, MA

S. E. Forman

MRJ Inc.
Fairfax, VA

W. L. Poesch
Dr. R. Shieh

National Bureau of Standards
Boulder, CO

A. C. Newell

Naval Electronics Systems Command
Arlington, VA

R. L. DuPuy
S. A. Nichols

Naval Research Laboratory
Washington, DC

K. T. Alfrend
R. E. Lindberg, Jr.
V. E. Noble

North Carolina State University
Raleigh, NC

J. C. Brand
C. Christodoulou
Dr. J. F. Kauffman

OCSE - Rome Air Development Center
Rome, NY

R. W. Carman
R. Schneible

Old Dominion University
Norfolk, VA

Dr. P. Dechaumpai
Dr. E. A. Thornton

ORI, Inc.
Silver Springs, MD

W. C. Hayes
L. R. Patterson
R. Whitman

RADC/EEC
Hanscom AFB, MA

D. J. Jacavaco

RCA Astro Electronics
Princeton, NJ

E. R. Ganssle
W. P. Manger
Dr. S. Parekh
H. H. Soule

Riverside Research Institute
Arlington, VA

A. L. DeVillers

Rockwell International
Downey, CA

H. S. Greenberg
D. Hays
J. Wokurka

SPAR Aerospace Limited
Ontario, Canada

F. Charron
R. T. Cooper
Dr. J. S.-C. Yuan

TRW
Redondo Beach, CA

W. Akle
Dr. J. S. Archer
J. T. Bennett
R. L. Hammel
M. Horstein
L. R. Mortaloni
R. H. Van Vooren

UCLA
Los Angeles, CA

L. A. Schmit

University of Kentucky
Lexington, KY

T. R. Tauchert

University of Virginia
Charlottesville, VA

J. K. Haviland
M. F. Mallette

U.S. Government
Washington, DC

R. Jeans
P. Schmid

Virginia Associated Research Campus (VARC)
of the College of William and Mary
Newport News, VA

A. Kyser

VPI&SU
Blacksburg, VA

R. T. Haftka
W. L. Hallauer, Jr.

Vought Corporation
Dallas, TX

R. . . Cox
J. J. Pacey

CONTROL OF LARGE SPACE ANTENNAS

A. F. Tolivar and S. J. Wang
Jet Propulsion Laboratory

Large Space Antenna Systems Technology - 1982
NASA Langley Research Center
November 30 - December 3, 1982

NASA LSS ANTENNA MISSIONS

The objectives of this paper are (1) to summarize the NASA large space antenna missions, (2) to examine the performance requirements, and (3) to define the resulting control technology requirements.

The NASA large space antenna missions can be categorized into three major classes: RF antennas, large segmented reflectors, and LSS flight experiments. The large RF antenna class includes near-term communications missions (e.g., LMSS), the radiometry missions, and the advanced communications missions. Their sizes range from 20 to 100 m and larger, and they include various reflector structural concepts such as mesh deployables, truss structures, and electrostatic membranes. The segmented reflector missions are primarily the IR and submillimeter astronomy missions that require multifacet solid-panel 10- to 30-m reflectors deployed on supporting structures. The flight experiments missions are specifically for evaluating LSS enabling technologies and establishing the required flight data base.

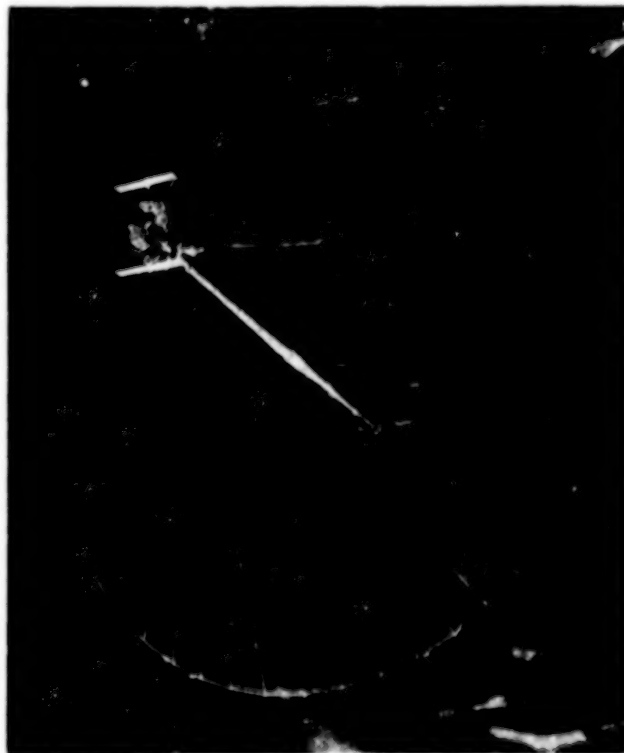
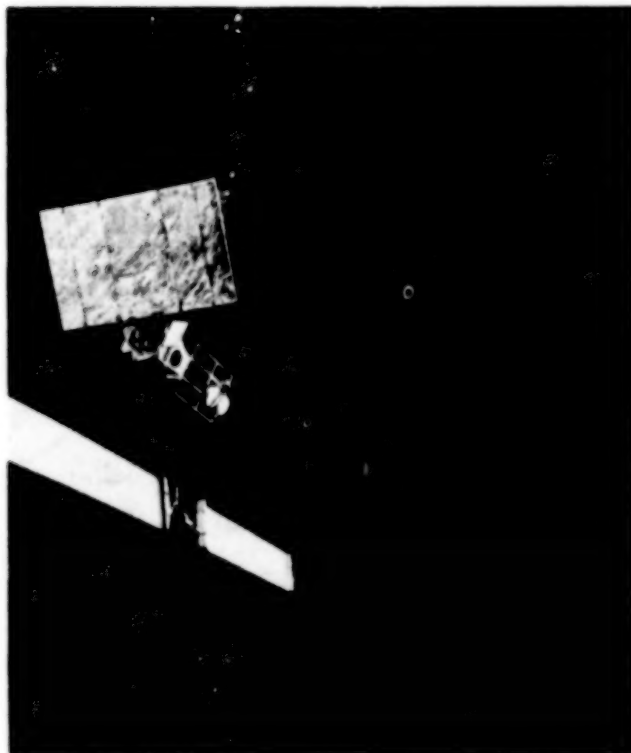
CLASS	OBJECTIVES
<ul style="list-style-type: none">• LARGE ANTENNAS 30-100 m<ul style="list-style-type: none">• MESH DEPLOYABLES• TRUSS• ELECTROSTATIC MEMBRANE, etc.	<ul style="list-style-type: none">• COMMUNICATIONS• RADIOMETRY/EARTH RESOURCES• RADIOASTRONOMY
<ul style="list-style-type: none">• SEGMENTED REFLECTORS 10-30 m<ul style="list-style-type: none">• LARGE DEPLOYABLE REFLECTOR	<ul style="list-style-type: none">• IR, SUBMILLIMETER ASTRONOMY
<ul style="list-style-type: none">• LSS FLIGHT EXPERIMENTS	<ul style="list-style-type: none">• VALIDATION LSS ENABLING TECHNOLOGIES• ESTABLISH REQUIRED FLIGHT DATA BASE

LMSS ANTENNA MISSION CONFIGURATIONS

The Land Mobile Satellite Service (LMSS) is a representative example within the large RF antenna mission class. The LMSS is one of the early large antenna applications which has been studied in considerable detail by a joint team of JPL/NASA and industry technologists. The LMSS is a multibeam communications mission utilizing a geosynchronous-orbit-based large antenna for providing telephone services to mobile users in the continental United States.

Two candidate LMSS configurations have been studied. One is a wrap-rib design consisting of a 55-m-diameter mesh reflector and a large 8- × 11-m RF feed. These are connected by two booms 34 and 80 m in length. The second configuration is a hoop-column design consisting of a 118-m-diameter mesh reflector, an 88-m mast, and four feed arrays of 4 × 4 m each. Each of the systems weighs about 10,000 lb and have moments of inertia of 10^6 to 10^7 kg-m².

The operating frequency for the LMSS mission is 0.87 GHz (UHF). The RF absolute pointing and jitter requirement is 0.02°, the required reflector surface accuracy is 6 mm, and the feed/dish lateral displacement is 30 mm. The LMSS pointing and control requirements can be met with new distributed control systems, which will be described. These systems require slight advancement of the state of the art.

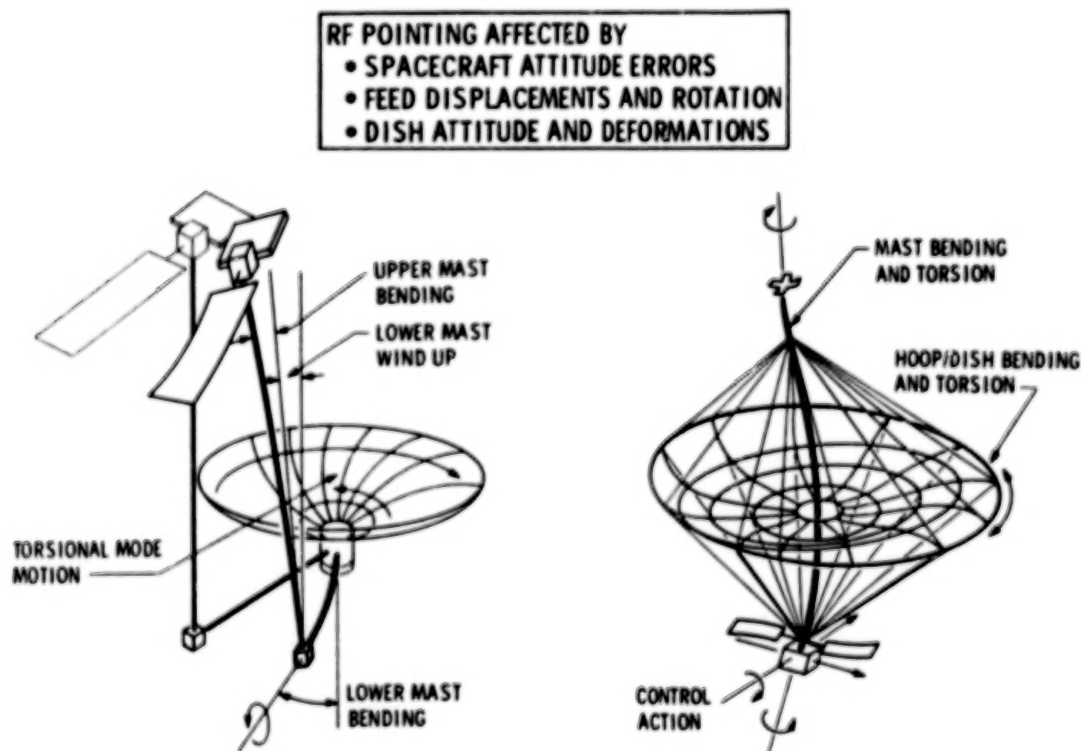


ANTENNA POINTING PROBLEM

The principal control system objective for a typical RF antenna is to point the RF beam(s) to the desired target(s) within prescribed pointing and jitter errors (typically, 0.020° to 0.002°) while maintaining overall system alignment and figure (typically within 5 to 0.5 mm) to insure the desired RF performance characteristics (main beam gain, low sidelobes, etc.). The actual RF pointing and jitter performance is dependent on the contribution of a large number of error sources, including geometrical errors due to quasi-static and dynamic disturbances, parameter errors, misalignments, and nonlinearities. By major contribution, these errors can be further classified as follows:

- (1) Spacecraft attitude errors due to overall static biases and dynamic motion of the antenna feed/bus about its nominal pointing direction
- (2) Relative feed/dish errors involving rotational and lateral motion about the optimal focal point location
- (3) Vibrational and quasi-static distortions of the dish about its nominal parabolic figure

Achieving the desired antenna pointing performance on a flexible structure of 50 to 100 m while maintaining the static and dynamic figure within an envelope of 0.5 to 5 mm represents a very substantial challenge to the technology. These problems are significantly compounded by the need to accommodate dynamic model uncertainties arising from the fact that the actual dynamic behavior of such structures will not be known accurately prior to launch. This behavior will only be established after the structure is deployed in orbit.



COMMUNICATION ANTENNA CONTROL TECHNOLOGY

Recent control system technology studies for the early communication missions have resulted in the identification of a hierarchy of control system options for large antennas and their evaluation by means of very detailed analysis and computer simulation. This hierarchy involves the following three levels of control technology:

- (1) Single lumped controller at the spacecraft bus with analytical modeling of the antenna flexibility in the estimator (this level represents current state of the art)
- (2) Distributed sensing: retain lumped actuation at bus but augment level 1 with an optical sensor which measures flexible dynamics of dish and boom directly rather than relying on estimation alone
- (3) Distributed sensing and control: augment level 2 with additional actuators at hub of dish to stabilize boom/dish vibrations

The results of these studies have led to the following major conclusions:

- (1) Distributed sensing and control provides a significant performance improvement of 1 order of magnitude over lumped control.
- (2) Model errors have great impact on control performance and stability margins. The system can be destabilized with even moderate parameter errors.
- (3) Preflight models for large space antennas are not accurate enough for closed-loop control. Therefore, in-orbit system identification is necessary. In addition, initial and periodical in-orbit identification of static characteristics, including figure alignment and calibration, is also required.

- SIGNIFICANT PERFORMANCE IMPROVEMENT WITH DISTRIBUTED SENSING AND CONTROL
- SYSTEM PARAMETER ERRORS RESULT IN PERFORMANCE DEGRADATION, EVEN INSTABILITY
- INFLIGHT SYSTEM ID OF CRITICAL STATIC AND DYNAMIC CHARACTERISTICS IS NECESSARY
 - OVERALL SYSTEM FIGURE ALIGNMENT AND CALIBRATION
 - IDENTIFICATION OF RELEVANT CLOSED LOOP DYNAMICS AND ON BOARD MODELS

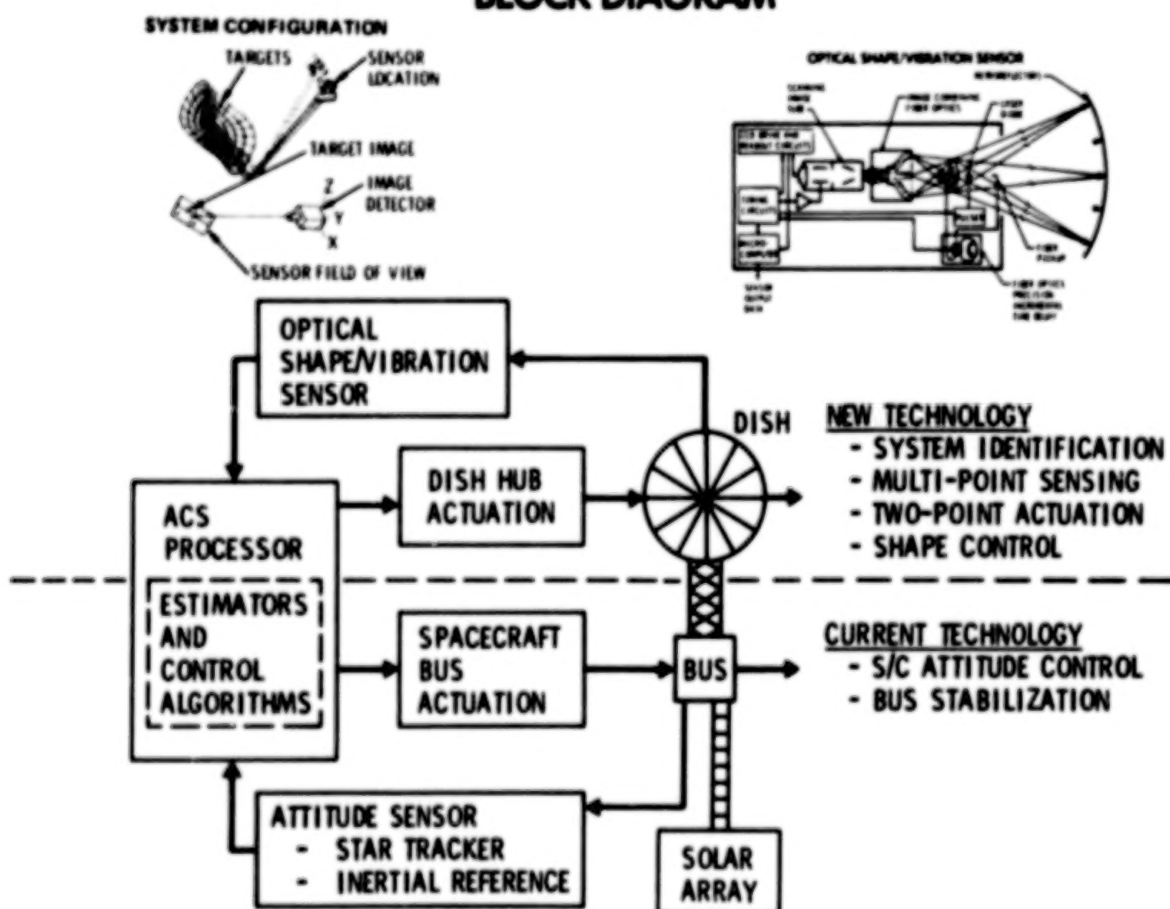
A TYPICAL CONTROL SUBSYSTEM FOR LARGE COMMUNICATION ANTENNAS

The figure illustrates the control system block diagram for a typical LMSS early communication antenna. The control system provides the required 0.02° pointing as follows:

- (1) Primary attitude control of bus/feed to 0.01° using reaction wheels and a high-bandwidth gyro-based control loop (nested within an attitude determination and gyro drift correction loop using star trackers)
- (2) Dish motion compensation and boom stabilization with respect to bus to 0.01° equivalent by means of
 - (a) Optical shape and vibration sensor at bus (top right)
 - (b) Six DOF (torque and force) control actuators at feed/bus and six DOF control actuators at dish
 - (c) Articulation actuators to reposition feed and dish to their correct static alignment

Note that in addition to being used as a control sensor, the optical shape and vibration sensor also provides the capability to carry out the initial in-orbit static alignment and the dynamic measurements required for system identification.

BLOCK DIAGRAM

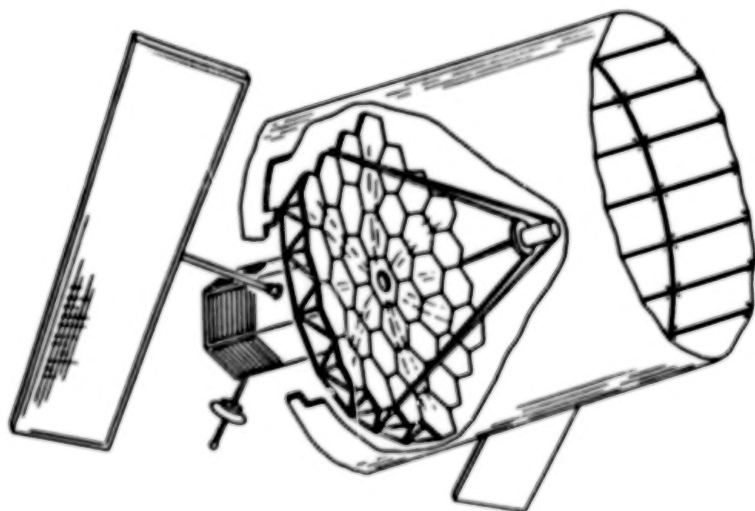


LARGE DEPLOYABLE REFLECTOR

The second major class of large antenna missions corresponds to applications where the wavelength is so short that solid reflectors are required. Typical of this class is the Large Deployable Reflector (LDR) which is an Earth-orbiting astronomical observatory operating from 50 to 1000 μm , a region of the spectrum where ground-based mapping of the sky is severely limited due to atmospheric opacity.

The LDR, illustrated below, carries a 20-m-diameter segmented primary reflector consisting of about 120 solid panel segments. The segments are deployed from their folded configuration into final reflector shape. To satisfy the observational requirements, the position and orientation of each segment must be sensed and controlled to extremely high precision. The major components are the segmented primary reflector, the secondary reflector, the backup structure, the spacecraft bus with its cryogenically cooled focal plane instruments, the solar arrays, and the thermal baffle.

The extremely short wavelengths of operation of this telescope call for stringent control requirement. Typically, active figure control will be required to maintain shape to within 0.5 μm , and advanced attitude control should provide overall system pointing to 0.05 arc sec and stability to 0.02 arc sec.

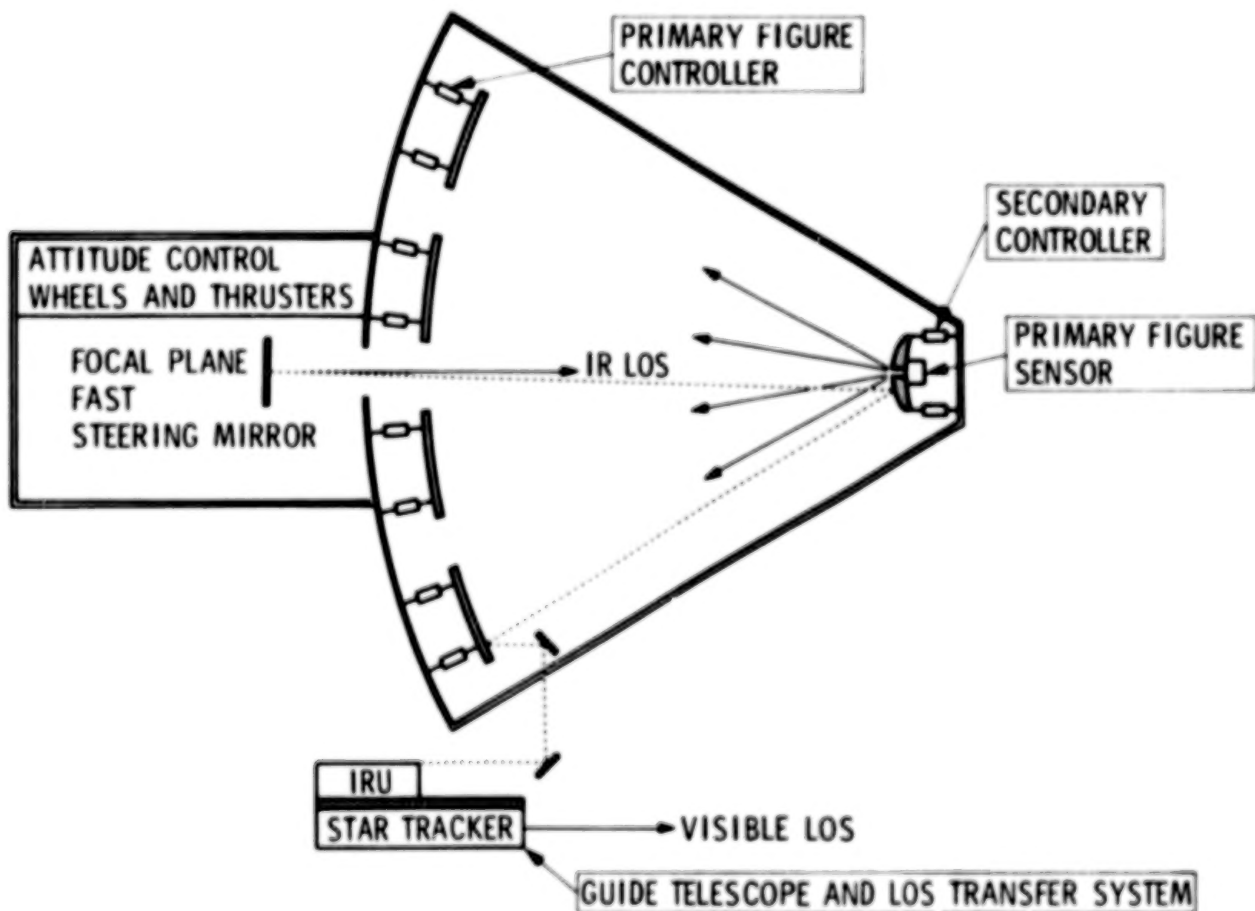


- 20 m SEGMENTED PRIMARY
- 120 SEGMENTS
- ACTIVE FIGURE CONTROL TO 0.5 μm
 - WITHIN PRIMARY
 - PRIMARY-TO-SECONDARY
- OVERALL SYSTEM POINTING TO
 - 0.05 arc sec - ABSOLUTE
 - 0.02 arc sec - STABILITY

LDR CONTROL APPROACH

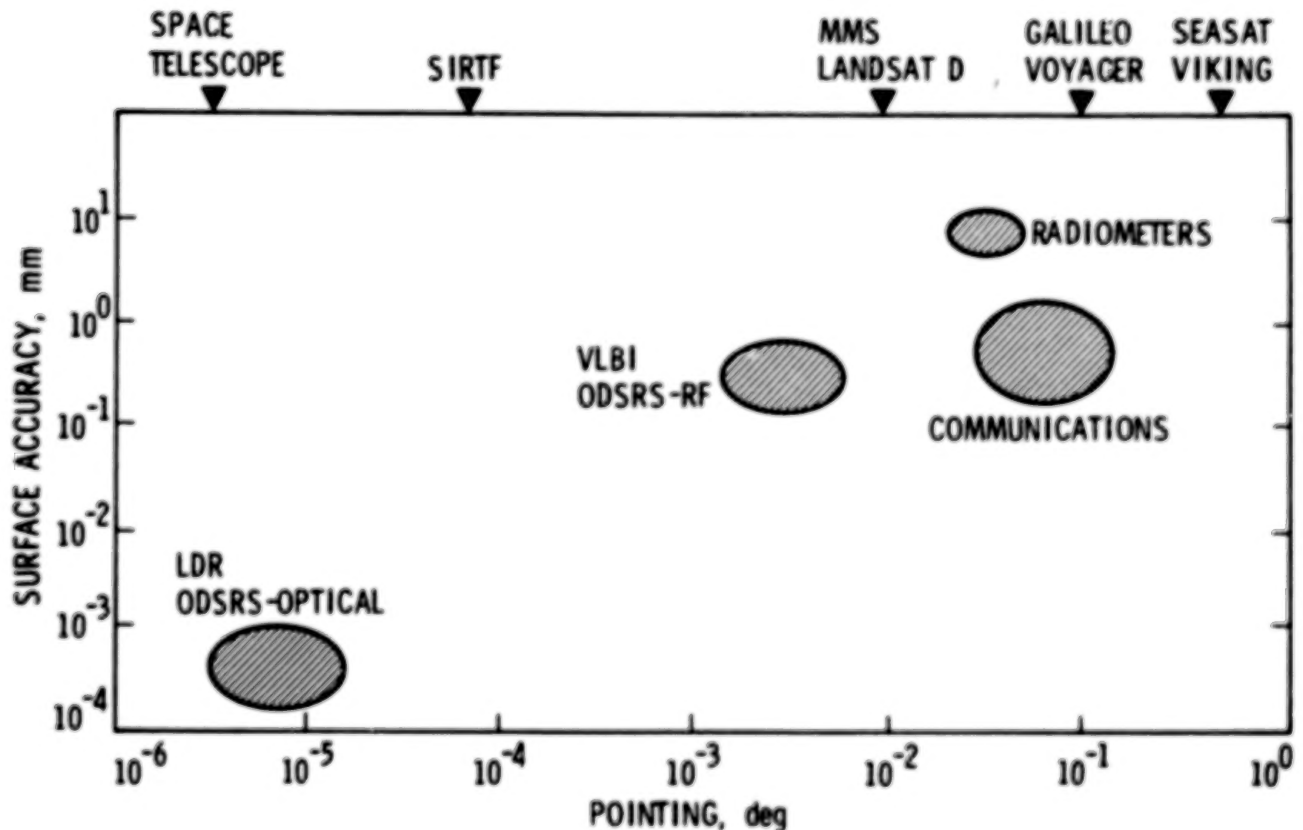
A potential control approach for LDR is shown below. This control approach calls for an attitude control system with wheels and thrusters to steer and stabilize the focal-plane assembly, with attitude sensing provided by the Guide Telescope and LOS (line of sight) transfer system. This ultra-precise IR LOS pointing of the focal plane is accomplished by transmitting a laser beam from the guide telescope to the focal plane via a set of mirrors, a selected segment reflector surface, and the secondary reflector. Fine pointing at the focal plane can be enhanced by means of a fast-steering mirror and detector electronics. The direction of the laser beam is determined by the guide telescope, which uses a star tracker, IRU (Inertial Rate Unit), and its own attitude controller to guide its orientation relative to the stars.

The shape of the primary reflectors is maintained by the Primary Figure Controller, which drives the segmented reflectors against the backup structure. The primary figure sensor unit is mounted in the vicinity of the secondary reflector, which is driven by a suitable drive mechanism actuating against its support structure.



SUMMARY OF ANTENNA CONTROL REQUIREMENTS

The figure illustrates the broad spectrum of pointing and figure control requirements spanned by large antennas. From the near-term communications antennas and radiometers to the VLBI and advanced communications antennas (such as the RF Orbiting Deep Space Relay Station), the surface and pointing requirements are at least 1 order of magnitude apart. From the advanced RF systems to the IR and optical systems (such as the laser Orbiting Deep Space Relay Station), the requirements are another 3 orders of magnitude tighter.



ANTENNA CONTROL TECHNOLOGY REQUIREMENTS

Broad control requirements call for equally wide-range technology support. The control technologies needed may be categorized into five groups:

- (1) Distributed control, sensing, and actuation
- (2) In-flight system and parameter identification
- (3) Adaptable and adaptive control
- (4) Figure determination and control
- (5) Long-life hardware components (sensors and actuators)

The application areas dictate the technology level of advancement. For near-term communications, such as LMSS, distributed sensing and control of 15 to 30 DOF will suffice. System ID and figure sensing and control are required for initial dynamic and static characterization, as are periodic system calibrations. For the advanced communications and radioastronomy antennas, however, higher order distributed control (30 to 60 DOF) with active vibration-damping capability is required. Long-life proof-mass dampers and figure sensors which are accurate to $1/20$ mm with 5 Hz bandwidth are also required.

IR and submillimeter astronomy antennas will require significant advances in control technology. Active damping and distributed control of a high-order (>500 DOF) is required. This will greatly impact on control design and computational capability and hardware. Real-time system dynamics parameter ID and estimation will be required. Real-time adaptive-gain adjustment is necessary to accommodate slewing and settling operations. Active figure control to provide $0.5\text{-}\mu\text{m}$ accuracy at 1 Hz rate will be required. High-resolution low-noise momentum wheels, lightweight proof-mass dampers, and figure actuators/sensors are required. Sensor accuracy will be to the $0.1\text{-}\mu\text{m}$ level, and LOS transfer system accuracy to 0.05 arc sec will be needed.

	NEAR TERM COMMUNICATIONS	ADVANCED COMMUNICATIONS AND RADIOASTRONOMY	IR, SUBMILLIMETER ASTRONOMY
DISTRIBUTED SENSING AND ACTUATION	15-30 DOF	30-60 DOF ACTIVE DAMPING	> 500 DOF ACTIVE DAMPING
SYSTEM IDENTIFICATION	INITIAL SYSTEM DYNAMICS, PERIODIC CALIBRATION	INITIAL SYSTEM DYNAMICS, PERIODIC CALIBRATION	REAL TIME SYSTEM DYNAMICS AND DISTURBANCES
ADAPTIVE CONTROL	GROUND-BASED REPROGRAMMING	GROUND-BASED REPROGRAMMING	REAL TIME GAIN ADJUSTMENTS
FIGURE DETERMINATION AND CONTROL	INITIAL ADJUSTMENT, PERIODIC CALIBRATION TO $1/2$ mm	INITIAL ADJUSTMENT, PERIODIC CALIBRATION TO $1/20$ mm	ACTIVE TO $1/2 \mu\text{m}$ AT 1 Hz
LONG-LIFE ACTUATORS AND SENSORS	FIGURE SENSORS TO $1/2$ mm AT 5 Hz	PROOF-MASS DAMPERS, FIGURE SENSORS TO $1/20$ mm AT 5 Hz	HIGH RESOLUTION, LOW NOISE WHEELS, PROOF-MASS DAMPERS, FIGURE ACTUATORS, FIGURE SENSORS TO $0.1 \mu\text{m}$, LOS TRANSFER SYSTEM TO 0.05 arc sec

NEED FOR FLIGHT EXPERIMENT

Every new technology requires extensive test and evaluation before it can be applied for space missions. Large flexible space structures have never been flown before. Uncertainties are so great that they can only be reduced by broad-based ground-test and flight experiments. Some specific fundamental needs are listed below.

- (1) Flight experience and a LSS data base must be established to reduce the uncertainties in control and structure dynamic interactions.
- (2) Structural damping at various modal frequencies, which cannot be predicted reliably, is a very important parameter that affects both open-loop and closed-loop behavior. Damping characteristics and closed-loop dynamics can be measured in a flight experiment.
- (3) Ground simulations and tests of LSS need validation. Flight experiments are necessary to establish quantitative levels of confidence and provide guidance for improvement.

Furthermore, there is no alternative to flight experiments. Flight conditions for LSS cannot be simulated on the ground. These include zero-g environment, full deployment of structures, and the required evaluation of structure and control interactions.

• LACK OF FLIGHT EXPERIENCE REQUIRES SPACE EXPERIMENT

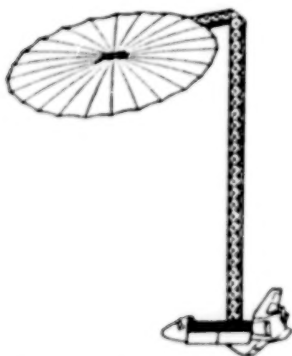
- UNCERTAINTY IN CONTROL/STRUCTURE INTERACTIONS REQUIRES FLIGHT EXPERIENCE/DATA BASE
- MEASURE CLOSED LOOP DAMPING AND DYNAMIC RESPONSE
- VERIFY AND ESTABLISH CRITERIA FOR GROUND TEST
- VALIDATE GROUND SIMULATIONS

• CANNOT GET THE BASIC DATA ANY OTHER WAY

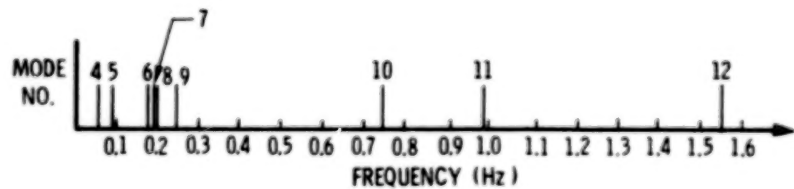
- CANNOT SIMULATE FLIGHT CONDITIONS ON GROUND
 - ZERO G
 - DEPLOYMENT
 - STRUCTURE/CONTROL INTERACTIONS

FLIGHT EXPERIMENT CONFIGURATION

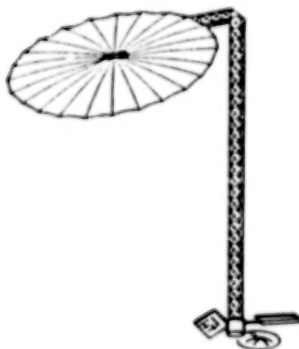
The figure illustrates a possible flight experiment configuration consisting of a 55-m offset wrap-rib antenna in which the feed can be gimballed or rigidly attached to the Shuttle. Although other configurations are possible (hub attached, etc.) the feed-rigid-attached mode has been selected for further study because of its simple interface with the Shuttle and the fact that it has the dynamic characteristics of the free-flier antenna as shown in the figure.



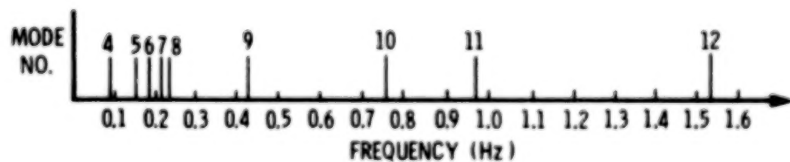
SHUTTLE-ATTACHED EXPERIMENT
CONFIGURATION



SHUTTLE-ATTACHED ANTENNA MODES



FREE-FLIER
CONFIGURATION



FREE-FLIER ANTENNA MODES

FLIGHT EXPERIMENT CONTROL GOALS

The control technology goal for an integrated control/structure interactions flight experiment is to evaluate fundamental technologies needed for the control of large space structure systems, including large antennas for communication and radiometry, space station missions, and also some of the basic needs for the more advanced IR and optics mission applications. The basic control technologies to be validated should include (1) distributed control and sensing, (2) system identification and parameter estimation, (3) adaptive control, (4) figure determination and shape control, (5) active vibration damping, (6) precision pointing, and (7) model error sensitivity and compensation.

TECHNOLOGY VALIDATED

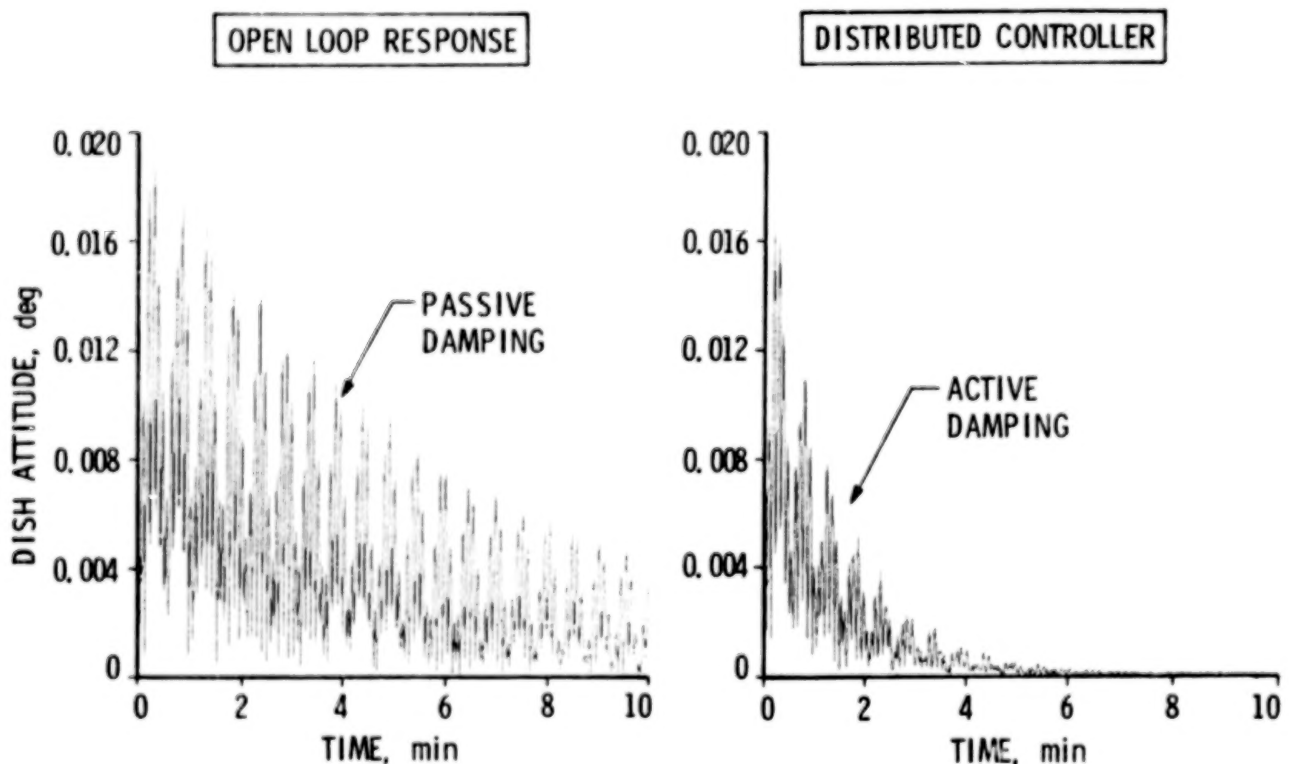
- DISTRIBUTED CONTROL / SENSING
- SYSTEM IDENTIFICATION
- ADAPTIVE CONTROL
- FIGURE CONTROL
- ACTIVE VIBRATION DAMPING
- PRECISION POINTING / STABILITY
- MODEL ERROR COMPENSATION

APPLICABLE MISSIONS

- COMMUNICATIONS
- RADIOMETRY
- IR / OPTICS
- SPACE STATION

DISTRIBUTED CONTROL EXPERIMENT SIMULATED SYSTEM RESPONSE TO
PROGRAMMED SHUTTLE VERNIER REACTION CONTROL SUBSYSTEM FIRING

The feasibility of carrying out the distributed control experiment has been investigated via computer simulations. Antenna-to-Shuttle dynamic interactions, system stability, Shuttle VRCS deadband and limit cycle properties, and VRCS firing transient have been simulated with a disturbance environment similar to that of a 400-km circular orbit. The plots below illustrate the simulated 10-minute time response of the system to preprogrammed VRCS thruster firings under the following two conditions: (1) open loop, with the control system turned off, and (2) the distributed control system enabled to provide vibration damping. Notice how the distributed control system damps out the pointing jitter about four times faster than the system free response under passive structural damping alone.



SHUTTLE-ATTACHED EXPERIMENT - PRELIMINARY CONCLUSIONS

Preliminary but positive conclusions have been obtained based on results of computer simulations.

- (1) The Shuttle-attached LSS antenna experiment is feasible.
 - (a) The static and dynamic disturbances must be handled with care, but they do not present problems.
 - (b) The Shuttle VRCS controller including the VRCS phase plane control laws and the vernier thrusters is compatible with the requirements.
 - (c) Control experiment can be defined to minimize the impact to Shuttle avionics system interface.
- (2) Performance of critical technology can be validated with the proposed experiments.
- (3) The configuration selected for this analysis does represent the free-flier large space antennas and first-order space stations.

• SHUTTLE ATTACHED EXPERIMENT IS FEASIBLE

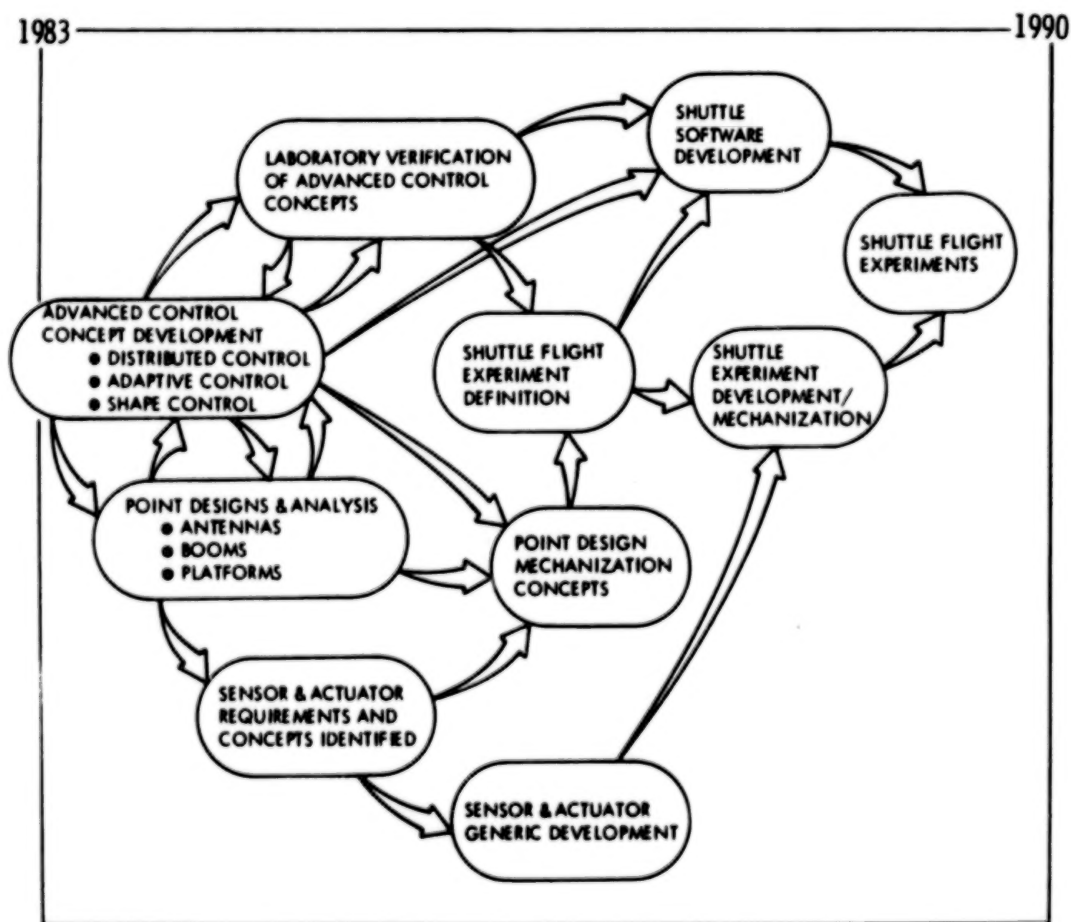
- STATIC AND DYNAMIC DISTURBANCES NOT A PROBLEM
- SHUTTLE CONTROLLER COMPATIBLE
- EXPERIMENTS DEFINED TO MINIMIZE SHUTTLE INTERFACE

• PERFORMANCE OF CRITICAL TECHNOLOGIES CAN BE VALIDATED

- EXPERIMENT CONFIGURATION REPRESENTS FREE FLIER AND FIRST ORDER SPACE STATION

TECHNOLOGY DEVELOPMENT APPROACH - LSS CONTROL TECHNOLOGY DEVELOPMENT

The chart below illustrates the approach for control technology development for large space systems. This process begins with the definition and development, analysis, and evaluation of advanced control concepts (figure control, distributed and adaptive control, system identification, etc.) for classes of antennas and platform/space station applications. This leads to point design mechanization concepts and to the definition of sensor and actuator requirements and the development of selected generic hardware concepts. Early evaluation of the technologies at the component level can effectively be achieved through ground demonstration of the individual technologies via scaled functional demonstrations. Actual evaluation of performance at the system level and calibration of tools and ground facilities must be accomplished via an actual space experiment such as the proposed Shuttle flight experiment.



SUMMARY OF KEY TECHNOLOGY NEEDS

The key technology needs for large space structure system controls may be summarized as follows:

- (1) Modeling and model reduction techniques require extensive research. Present day methodology is far from adequate. A unified and integrated structural and control modeling methodology must be developed.
- (2) The control and stabilization of large flexible structures represent a major challenge to the state of the art in control theory. Concepts and methodologies must be developed for distributed control, figure control, and active vibration damping.
- (3) Techniques must be developed to deal with the uncertainties associated with structural dynamics, disturbances, system nonlinearities, and control/structure interactions. Improvements in model development techniques can only solve part of the problem. In-flight system identification is needed even by the simple early users, such as LMSS, while adaptive-control approaches will become critical for those systems that involve high-speed slew operation and possible configuration changes.
- (4) Long-life and precision hardware components (such as sensors and actuators) are needed.
- (5) Ground and flight evaluation of the new technologies is a necessary part of the technology development process.

- MODELING AND MODEL REDUCTION TECHNIQUES
- CONTROL AND STABILIZATION OF FLEXIBLE STRUCTURES
 - DISTRIBUTED SENSING AND ACTUATION
 - FIGURE CONTROL
 - ACTIVE DAMPING
- UNCERTAINTY MANAGEMENT
 - SYSTEM IDENTIFICATION
 - ADAPTIVE APPROACHES
- HARDWARE AND SOFTWARE
- GROUND AND FLIGHT VALIDATION

ENABLING TECHNOLOGIES
FOR
LARGE PRECISION SPACE SYSTEMS

Robert R. Strunce, Jr., and James D. Turner
The Charles Stark Draper Laboratory, Inc.
Cambridge, Massachusetts

Large Space Antenna Systems Technology - 1982
NASA Langley Research Center
November 30 - December 3, 1982

During the Apollo era, the control designers became increasingly aware of the flight control system dynamic interaction with complex vehicle motion [1-4]. With the advent of large space structures [5-8] and increasing demands on precision pointing and control [9], active control of flexible space structures [10-14] will be necessary in order to satisfy stringent performance goals. This paper summarizes the surveys contained in references 15 and 16. These reports surveyed the current enabling technologies for large precision space systems in the following areas:

- 1) Multibody satellite dynamic modeling theory
- 2) Large space structure vibration control
- 3) Slewing maneuvers for flexible spacecraft
- 4) Sensor, actuator, and components
- 5) Array processor technology
- 6) Fault-tolerant considerations
- 7) Large space structure type experiments
- 8) Large space structure test facilities

The technology issues in these areas of structures, dynamics, and control were established by reviewing relevant space missions [17,18].

The major large space structure (LSS) technology issues (Figure 1) are:

- (1) Modeling Accuracy.--LSS modeling inaccuracies will limit achievable control system performance. The more stringent the mission performance requirements, the greater the LSS model fidelity required. These modeling errors are grouped into three categories:
 - (a) LSS Structural/Dynamic Models.--These errors may be introduced through initially assumed structural properties or by the truncation process implicit in the finite-element method. In space, LSS parameters may vary as a function of thermal gradients, configuration changes, or depletion of consumables.
 - (b) Environmental Models.--These models must be investigated and verified by appropriate experiments. Accurate knowledge of the external forces (e.g., Earth magnetic and gravitational fields, solar wind and radiation pressure, and drag) acting upon an LSS may be necessary to satisfy precision control requirements.
 - (c) Disturbance Models.--Internal/external disturbance phenomenon must be understood and sufficient models developed. The achievable control system performance will be a function of disturbance model fidelity.
- (2) System Identification.--LSS structural model verifications will be accomplished through system identification. Identification techniques must be developed to determine structural parameters, modal frequencies, damping ratios, and mode shapes. Such methods could be used to determine environmental and disturbance models. Consideration must be given to the type of sensors, onboard processing requirements, data reduction, and post-processing requirements.

- (3) Control Law Design Methodology.--The control law design approach will be a function of the structural/dynamic models, disturbance models, and mission performance requirements. The design methodology must address the following:
- (a) The model reduction process will reduce the high dimensional finite-element model to a tractable (lower order) design model.
 - (b) Reduced-order compensator design methods need to be developed which ensure overall closed-loop system stability. These methods must address the direct digital design problem.
 - (c) Implementation of these control laws will require analog/digital mechanizations, which must consider centralized versus decentralized processing, sensor/actuator configuration, fault-tolerant systems, redundancy management and reconfiguration.
- (4) Sensors and Actuators.--Techniques will be required to determine sensor/actuator placement as a function of the control objectives. The type of sensor/actuator which meets the necessary performance specifications must be determined. The dynamic characteristics of these devices will be essential for evaluation of controller closed-loop stability and robustness.
- (5) Avionics.--The high computational needs and sensor/actuator data rates will require development of advanced system architecture and integration in order to meet the 1990 type requirements. Fault detection, isolation, and reconfiguration must be an integral part of this development.

LSS CONTROL TECHNOLOGY ISSUES

Fundamental Problem: Design a finite dimensional compensator to control an infinite dimensional system

- Major Technical Issues:**
- (1) Modeling accuracy
 - Large space structures
 - Upper atmosphere
 - Disturbances
 - (2) System Identification
 - (3) Control Law Design Methodology
 - Model reduction techniques
 - Reduced order compensator design
 - Overall system closed-loop stability
 - Robustness of stability
 - Direct digital design and implementation
 - (4) Sensors and actuators
 - Specification
 - Type
 - Placement
 - Dynamics
 - (5) Avionics
 - System architecture and integration
 - Fault detection, isolation, and reconfiguration
 - Data acquisition

Figure 1

The large space structure technology issues with respect to spacecraft categories (space station, large antenna, space-based laser, IR surveillance) are detailed in Figure 2. Each spacecraft category is further subdivided into columns of technology, applied research, sensor/actuator development, avionics development, ground-based demonstration and space-based demonstration. The technology disciplines of control, identification, and modeling are subdivided into rows. The technologies which are required are shown as a solid black box while those which might be required are represented as a dotted box. A blank indicates either state-of-the-art technology or that the technology is not applicable. This figure emphasizes the broad need for sensor/actuator development and avionics development.

LARGE SPACE STRUCTURES TECHNOLOGY ISSUES

Spacecraft Categories →	Space Station	Large Antenna	Space-Based Laser	IR Surveillance
TECHNOLOGY ISSUES →	Technology Applied Research Sensor/Actuator Development Avionics Development Ground-Based Demonstration Space-Based Demonstration	Technology Applied Research Sensor/Actuator Development Avionics Development Ground-Based Demonstration Space-Based Demonstration	Technology Applied Research Sensor/Actuator Development Avionics Development Ground-Based Demonstration Space-Based Demonstration	Technology Applied Research Sensor/Actuator Development Avionics Development Ground-Based Demonstration Space-Based Demonstration
CONTROL				
Structural Vibration Suppression	REQUIRED	REQUIRED	REQUIRED	REQUIRED
Disturbance Isolation/Accommodation	REQUIRED	REQUIRED	REQUIRED	REQUIRED
Attitude Control	REQUIRED	REQUIRED	REQUIRED	REQUIRED
Station Keeping/Orbital Changes	REQUIRED	REQUIRED	REQUIRED	REQUIRED
Slew Maneuver	REQUIRED	REQUIRED	REQUIRED	REQUIRED
Static/Dynamic Figure Control	REQUIRED	REQUIRED	REQUIRED	REQUIRED
Fault Detection, Isolation, Reconfiguration	REQUIRED	REQUIRED	REQUIRED	REQUIRED
Deployment	REQUIRED	REQUIRED	REQUIRED	REQUIRED
Construction	REQUIRED	REQUIRED	REQUIRED	REQUIRED
Articulated Structures, Appendages	REQUIRED	REQUIRED	REQUIRED	REQUIRED
Robotics	REQUIRED	REQUIRED	REQUIRED	REQUIRED
Grappling	REQUIRED	REQUIRED	REQUIRED	REQUIRED
Docking	REQUIRED	REQUIRED	REQUIRED	REQUIRED
IDENTIFICATION				
Model Validation	REQUIRED	REQUIRED	REQUIRED	REQUIRED
Input/Output Characterization	REQUIRED	REQUIRED	REQUIRED	REQUIRED
Time Varying Characterization	REQUIRED	REQUIRED	REQUIRED	REQUIRED
Phenomenology Investigation	REQUIRED	REQUIRED	REQUIRED	REQUIRED
MODELING				
Deployment Dynamics	REQUIRED	REQUIRED	REQUIRED	REQUIRED
Environmental Models	REQUIRED	REQUIRED	REQUIRED	REQUIRED
Structural Characterization	REQUIRED	REQUIRED	REQUIRED	REQUIRED
Structural Damping	REQUIRED	REQUIRED	REQUIRED	REQUIRED
Arbitrary Motion of Multiple Flexible Bodies	REQUIRED	REQUIRED	REQUIRED	REQUIRED
Articulated Structures	REQUIRED	REQUIRED	REQUIRED	REQUIRED
Robotics	REQUIRED	REQUIRED	REQUIRED	REQUIRED
Grappling	REQUIRED	REQUIRED	REQUIRED	REQUIRED
Docking	REQUIRED	REQUIRED	REQUIRED	REQUIRED

REQUIRED ■

MIGHT BE REQUIRED ▤

Figure 2

The large space structures technology issues overview of Figure 3 uses the same format as the previous figure. Note that the solid black box represents technology required by all spacecraft categories while the dotted box represents those technologies required by some of the spacecraft. This figure demonstrates those areas of common technology issues: structural characterization, structural damping, fault detection, isolation and reconfiguration, sensor/actuator development, avionics development, and ground- and space-based demonstration.

LARGE SPACE STRUCTURES TECHNOLOGY ISSUES OVERVIEW

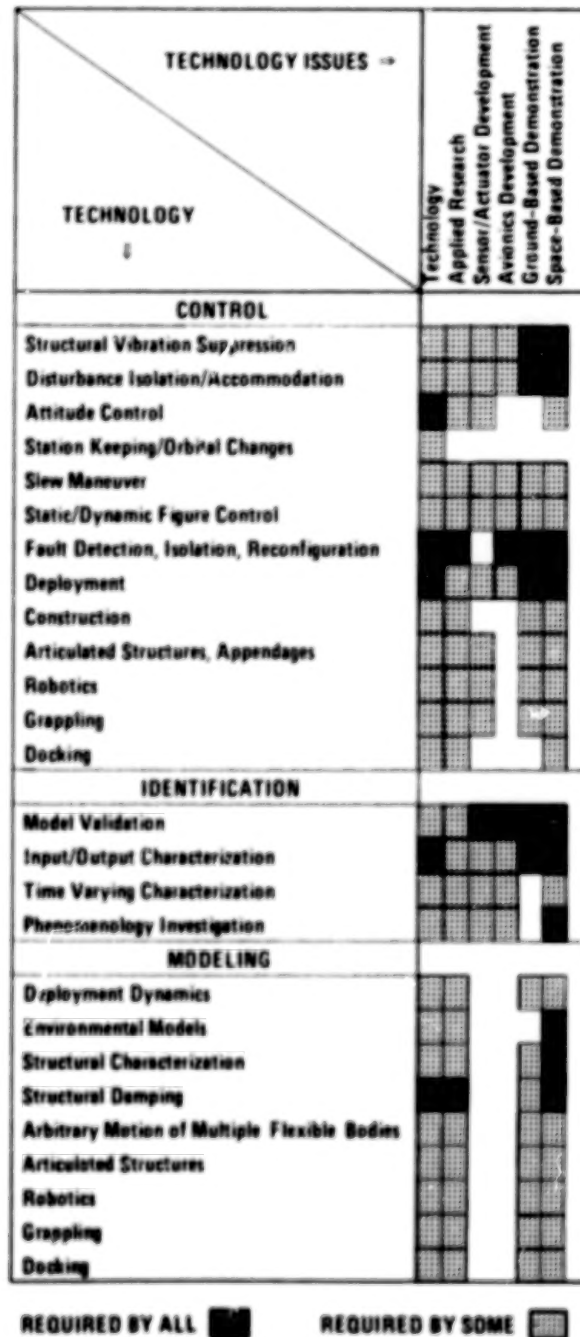


Figure 3

To date, multibody satellite dynamics modeling theory has not adequately addressed multibody systems in which all bodies are nonrigid or in which arbitrary bodies can be either rigid or nonrigid. The term "multibody dynamics modeling theory" here refers to the line of research that originated in the mid-1960s with the work of Hooker and Margulies and Roberson and Wittenberg [15,16]. As shown in Figure 4, it is clear why the Euler-Newton methods of early researchers have now been supplanted by the more general techniques of analytical dynamics. Moreover, researchers in the aerospace field have been particularly slow in eliminating the modeling geometry of topological tree structures. Furthermore, there has been little attention given to handling systems containing closed loops. Indeed, for LSS missions requiring a deployment phase, the techniques must be available for handling systems with closed loops. Moreover, as shown in Figure 5, careful attention must be given to the selection of coordinates used to model LSS, since the choice of coordinates can dramatically affect the complexity of the resulting equations of motion.

The reason that researchers have turned to analytical dynamic modeling methods can be traced to the ease with which the constraint forces and torques between contiguous bodies can be handled (see Figure 6). In particular, they have found that using an absolute coordinate approach, combined with a Lagrange multiplier approach or related methods, leads to significant efficiencies in both deriving and coding the equations of motion for LSS.

Nevertheless, it is necessary to do the following: (1) develop modeling techniques for reliability handling of systems where arbitrary bodies can be rigid or nonrigid, (2) develop procedures for handling interconnected structures of bodies containing closed paths, and (3) develop techniques whereby the constraints at joints can be very general.

COMPARISON OF EULER-NEWTON METHODS VERSUS ANALYTICAL DYNAMICS METHODS

Subject	Euler-Newton Methods	Analytical Dynamics Methods
Advantages	<ul style="list-style-type: none">● Physically motivated problem formulation● Handles rigid body topological tree structures (terminal body flexibility can be accounted for)	<ul style="list-style-type: none">● Easily determines the constraint forces and torques between contiguous bodies● Handles rigid/flexible body topological tree structures● Handles topological tree structures containing closed loops● Easily handles adding or deleting bodies from a model● Handles general joint constraints● Easily applied to multibody LSS (deployment)
Dis-advantages	<ul style="list-style-type: none">● Awkwardly handles the determination of the constraint forces and torques between contiguous bodies● Difficult to apply to LSS not connected in a topological tree structure● Difficult to apply to multibody LSS when arbitrary bodies can be nonrigid● Difficult to modify special purpose computer codes IF bodies are either added to or removed from the model	<ul style="list-style-type: none">● Abstract problem formulation● Techniques for handling holonomic constraints require some sophistication on the part of the analyst

Figure 4

COORDINATE MODELING TECHNIQUES FOR MULTIBODY DYNAMICS THEORY

Subject	The Absolute Coordinate Approach	The Relative Coordinate Approach
Description	<ul style="list-style-type: none"> Each body is modeled individually Each body possesses six rigid body DOF* and N generalized coordinates for modeling flexibility 	<ul style="list-style-type: none"> One body is selected as a reference body, then at each joint relative coordinates are assigned for each unconstrained DOF The total number of degrees of freedom for the model consists of: (1) six rigid body DOF for the reference body; (2) the relative DOF at the joints; and (3) the generalized coordinates for the flexible body effects of each body
Advantages	<ul style="list-style-type: none"> Great analytical simplicity Permits easy addition and deletion of bodies in a multibody computer simulation Naturally lends itself to multibody LSS simulations 	<ul style="list-style-type: none"> Minimum number of DOF required Eliminates the constraint forces and torques at the constrained DOF at the joints
Disadvantages	<ul style="list-style-type: none"> Maximizes the number of constraint equations to be dealt with 	<ul style="list-style-type: none"> Creates difficult bookkeeping problems Difficult to modify if the vehicle topology changes

*(DOF) degrees of freedom

Figure 5

SOLUTION TECHNIQUES FOR EVALUATING CONSTRAINT FORCES AND TORQUES

Observation: The ability to efficiently evaluate the constraint forces and torques arising in the equations of motion constitutes the principal reason analytical dynamics methods are superior to Euler-Newton methods for modeling LSS

Available Techniques:

Subject	Lagrange Multiplier Method	Jerkovsky's Transformation Operator Approach	Baumgarte's Method
Advantages	<ul style="list-style-type: none"> Simple algebraic solution Easily implemented 	<ul style="list-style-type: none"> Eliminates the constraint forces and torques altogether Computationally efficient 	<ul style="list-style-type: none"> Stabilizes differentiated constraint equations by requiring the constraint equation to satisfy a second-order differential equation with artificial stiffness and damping
Disadvantages	<ul style="list-style-type: none"> Requires artful techniques for maintaining integrated constraints (e.g., error impulse momentum corrections) 	<ul style="list-style-type: none"> The method is very abstract 	<ul style="list-style-type: none"> The artificial damping and stiffness matrices are selected in an ad hoc manner

Figure 6

Precision pointing and control trends [9] through the year 2000 will require pointing accuracies ranging from 10 arcsec down to 0.1 arcsec with corresponding stability requirements ranging from 1 arcsec down to 0.001 arcsec. These stringent requirements and the large space structure (LSS) characteristics (closely packed, lightly damped, low frequency modes) have motivated a plethora of research in active control of space structures (ACOSS) [11-14]. Figure 7 shows a hierarchy of vibration suppression methods. The level of vibration control complexity is a function of the LSS characteristics, performance requirements, and disturbance characteristics. Naturally, structural response minimization methods such as tuning, stiffening, and material damping should receive first consideration.

VIBRATION CONTROL HIERARCHY

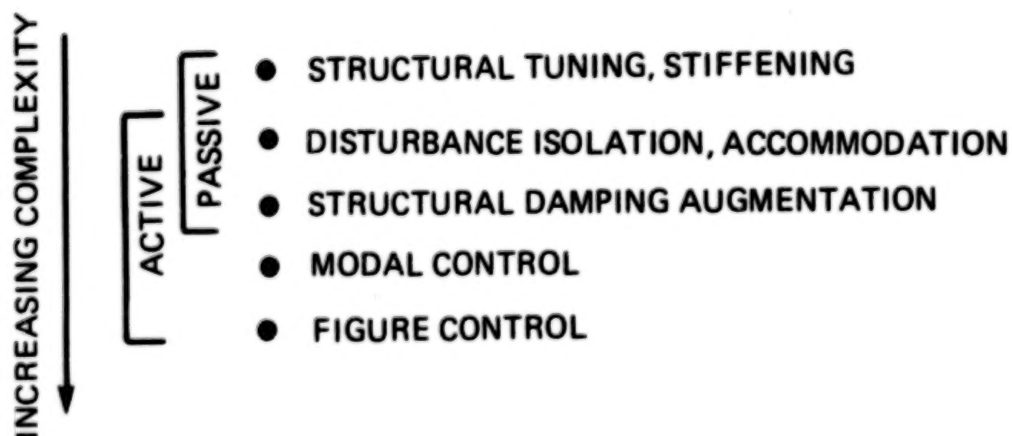


Figure 7

Reference 19 addressed the issue of passive and active suppression of vibration response in precision structures from a structural point of view. The results of this 1977 state-of-the-art assessment showed that the 1 to 3% achievable damping was insufficient for 1990 requirements. It is this study which motivated the current DARPA ACOSS program. The objectives of the ACOSS program are threefold:

- (1) Develop a unified technology base in structural dynamics and control for large precision space structures.
- (2) Demonstrate the applications of this technology through analysis and simulations.
- (3) Verify this technology through ground-based proof-of-concept experiments.

Figure 8 presents a summary of the ACOSS program.

ACOSS PROGRAM SUMMARY

Company	Control Theory	Control Design & Analysis	Experiments
Convair	Model Error Sensitivity Suppression (MESS)	MESS Disturbance Accommodation	Flyswatter Plate (IR&D)
Draper	Reduced-Order Modeling Reduced-Order Controller Output Feedback Sensor/Actuator Placement Optimal Slewing Maneuvers High Resolution System Identification	Structural Damping Augmentation (SDA) Modern Modal Control (MMC) SDA/MMC Actuator Synthesis Disturbance Rejection Sensor/Actuator Placement Optimal Slewing Maneuvers High Resolution System Identification	Beam (IR&D)
Honeywell	System Identification	Singular Values	
Hughes	Electronic Damping	Electronic Damping	Hollow Cylinder
Lockheed	Low Authority Control (LAC) High Authority Control (HAC) Modal Cost Analysis (MCA)	LAC, HAC LAC/HAC Frequency Shaping System Identification	Mini-Beam Maxi-Beam Vertical Pipe Circular Plate Wheel (frame) Toysat POC
TRW	Stability Ensuring Methodology System Identification Adaptive Control	Stability Ensuring Methodology System Identification	Plate (IR&D)

Figure 8

With the increasing size and inherent flexibility of many future satellites, there have come new and more difficult attitude control problems. In particular, the nature of the resulting attitude control problems can be divided into the two categories shown in Figure 9. It is important to understand and appreciate the fundamentally different control requirements which characterize the attitude stabilization and slewing control problem. In addition, as shown in Figure 10, one needs to understand the different techniques available for both defining and solving the two-point boundary-value problems which define optimal spacecraft slewing maneuvers.

The subject of spacecraft slewing maneuvers has received the attention of many authors (see Figure 11). The work to date encompasses many important subjects, including: (1) linear/nonlinear open-loop methods, (2) distributed control, (3) on-off thruster control, (4) feedback control, and (5) experimental results. Nevertheless, much additional theoretical and analytical work is required before reliable techniques will be commonly available for LSS applications.

COMPARISON OF THE ATTITUDE STABILIZATION PROBLEM VERSUS THE SLEWING PROBLEM

Attitude Stabilization Problem	Slewing Problem
<p><u>Plant Description</u></p> <ul style="list-style-type: none"> ● Small rigid body rotations and elastic deformations assumed (linear plant dynamics) <p><u>Control Law Formulation</u></p> <ul style="list-style-type: none"> ● Infinite time problem (steady-state control) ● Free end conditions ● Shape and/or figure control specifications ● Minimum control spillover effects 	<p><u>Plant Description</u></p> <ul style="list-style-type: none"> ● Large rigid body rotations and small elastic deformations assumed (linear/nonlinear plant dynamics) <p><u>Control Law Formulation</u></p> <ul style="list-style-type: none"> ● Finite fixed time (time-varying control) ● Fixed end conditions (e.g., $\theta(t_f)$, $\underline{\eta}(t_f)$, and $\dot{\underline{\eta}}(t_f)$ are specified) ● The elastic degrees of freedom are to be minimally excited during the maneuver ● A vibration suppression constraint is imposed at the end of the maneuver ● Free end conditions for $\theta(t_f)$ and $\dot{\theta}(t_f)$ for spin-up maneuvers, despin maneuvers, and slewing to engage moving targets

Figure 9

SOLUTION TECHNIQUES FOR OPTIMAL SLEWING MANEUVERS

$$\text{Minimum: } J = \int_{t_0}^{t_f} L(\underline{x}, \underline{u}, \dot{\underline{u}}, \dots, \underline{u}^{(k)}; t) dt$$

$$\text{Subject to: } \dot{\underline{x}} = f(\underline{x}, \underline{u}; t)$$

Given

$\underline{x}_0, \underline{x}_f$

Specified

$\underline{u}_0, \dot{\underline{u}}_0, \dots, \underline{u}_0^{(k-1)}$
 $\underline{u}_f, \dot{\underline{u}}_f, \dots, \underline{u}_f^{(k-1)}$

THE CALCULUS OF VARIATIONS APPROACH	THE OPTIMIZATION APPROACH
<p>Leads to:</p> <p>State $\dot{\underline{x}} = f(\underline{x}, \underline{u}; t)$</p> <p>Costate $\dot{\underline{\lambda}} = g(\underline{x}, \underline{\lambda}; t)$</p> <p>Control $\underline{u}(2k) = h(\underline{x}, \underline{\lambda}, \underline{u}, \dot{\underline{u}}, \dots, \underline{u}^{(2k-2)}; t)$</p> <p>→ Exponential matrix solution for the resulting two-point boundary-value problem</p> <p>8211A370-4</p>	<p>Assume:</p> $\underline{u}_i(t) = \sum_j^{2k-2} a_{ij} \phi_{ij}(t)$ <p>where</p> <p>$\phi_{ij}(t)$ denotes the j^{th} assumed time function for the i^{th} control</p> <p>a_{ij} denotes the unknown coefficient for the i^{th} control and j^{th} time function</p> <p>→ Iterative successive approximation strategy for the a_{ij} coefficients</p>

Figure 10

OVERVIEW OF RECENT WORK IN SLEWING MANEUVERS FOR FLEXIBLE SPACECRAFT [15,16]

Subject	Turner & Chen	Turner & Junkins	Breakwell	Forrenkopt	Swigert	Vander Velde & He	Longman & Alfriend	Markley	Lassen & Elliot
Rigid +1-Flexi-Mode Plant	✓	✓	✓	✓	✓	✓	✓	✓	✓
Rigid + Flexi-Modes Plant	✓	✓	✓			✓			
Distributed Control	✓					✓			
Parameter Variation Sensitivity			✓	✓				✓	
Open-Loop Control of Nonlinear Plants	✓	✓							
On-Off Thruster Control						✓		✓	
Control Smoothing Techniques	✓				✓				✓
Feedback Control	✓		✓			✓			
General End Condition Problems	✓								
Experimental Results			✓		✓				
Suboptimal Control				✓				✓	
Large-Angle Maneuvers	✓	✓				✓			
Small-Angle Maneuvers	✓	✓	✓	✓	✓	✓	✓	✓	✓

Figure 11

Figure 12 shows the block diagrams for an LQG controller and a HAC/LAC controller. Sizing the control law algorithms [15] for these two approaches assumed a 50 Hz control bandwidth, 250 Hz sampling frequency, 2 bytes/word accuracy, and a data flow rate of 500 bytes/sec per sensor or actuator. Figure 13 presents the floating point operations (FLOP) per control cycle as a function of the number of control states (2 states/mode) and the number of sensor/actuator pairs.

CONTROL LAW ALGORITHM SIZING

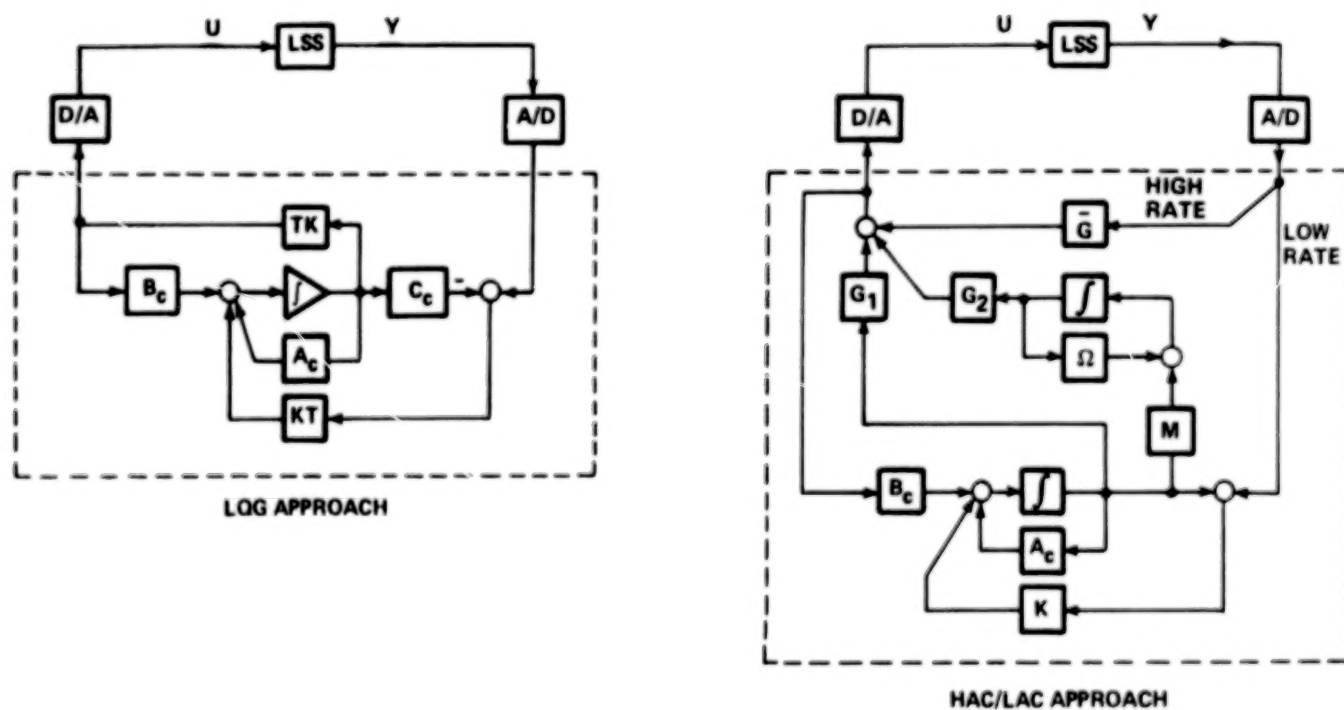


Figure 12

CONTROL LAW ALGORITHM SIZING (Cont)

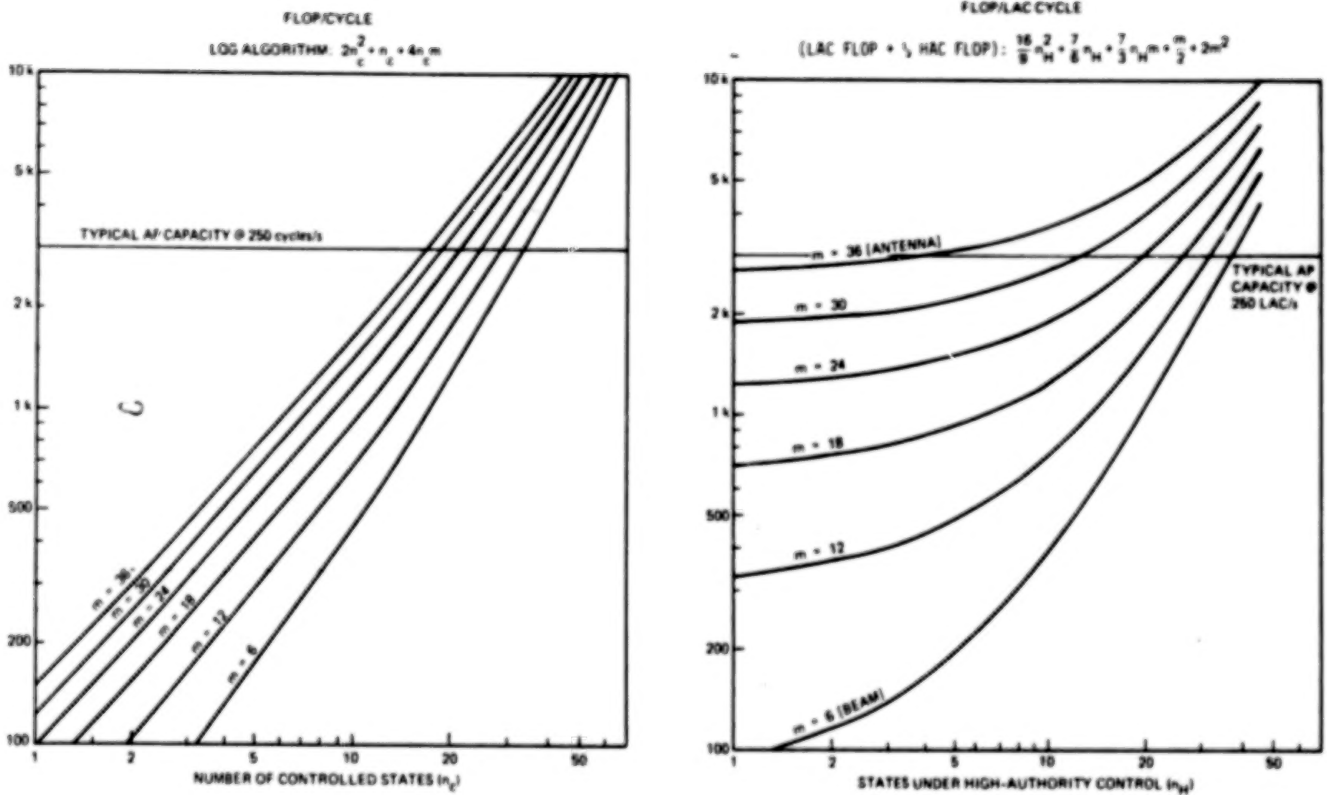


Figure 13

Regarding the array processors surveyed (Figure 14), the primary function of these devices is signal processing, which requires high throughput while performing filtering on data collected in real time. Because of their speed, the array processors would appear to be candidates for closed-loop control. Several array processors are ruled out for closed-loop control application because of their fixed-point arithmetic. The loss in speed incurred by the host/array processor transfer of sensor/actuator data prohibits those which have no direct I/O capability. Hence, FPS-100, FPS-164, AP-120B, AP-180R, AP-190L, Datawest 460, MAP 300, MAP 200, MAP 6400, Magnavox (Mil Spec of CSPI MAPs), and CIA MSP-300 are the major contenders. There are mixed reports concerning the success of array processors in real-time closed-loop control. Conflicting reports have indicated that a major rewrite of the operating system was necessary. Despite the negative tone, closed-loop control with an array processor capable of direct, programmed I/O poses no fundamental problem. It simply appears that no one has thought of this or has had the need to use them in such an application. In collecting data for this survey, array processor engineers were unfamiliar with closed-loop control applications but saw no difficulty in their implementation. The MCP-100 [20,21] is an untried prototype processor which was designed specifically to implement LQG controllers. Figure 14 presents an overview of the avionics data processing status.

AVIONICS DATA PROCESSING

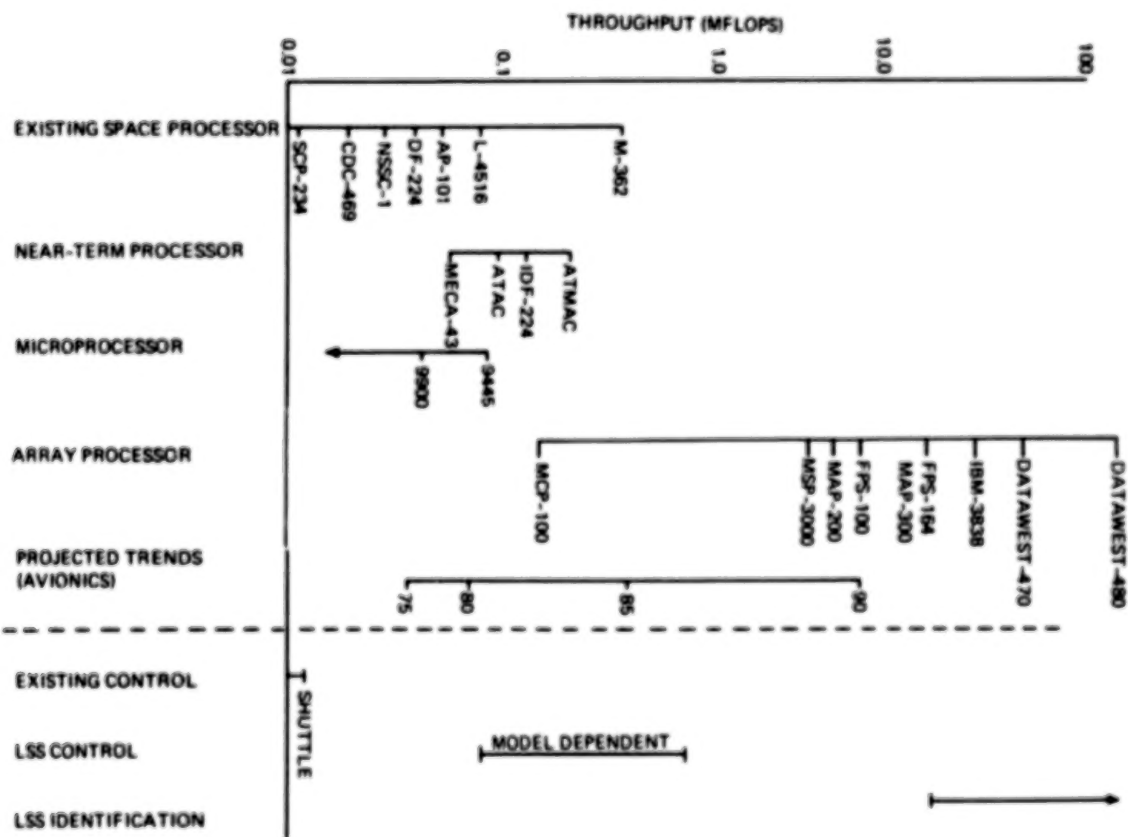


Figure 14

Sensor technology (see Figure 15) for sensing submicron vibration in large precision space systems is not available off the shelf. Optical measurement techniques provide the best potential because of their high bandwidth, accuracy and resolution. Piezoelectric sensors are another candidate. Lockheed, Hughes, TRW, and Itek are pursuing these technologies. The only inertial grade space accelerometer is the BELL XI which is expensive by comparison to optical devices. CSDL is investigating the potential of a Three-Axis Angular Rate Accelerometer (TAARA) and a Six-Axis Space Sensor (SASS). The high cost of inertial grade space gyros is the major disadvantage. Even though these gyros exhibit low noise and drift, their bandwidth is less than 50 Hz. Fundamentally, the sensor technology for submicron vibration sensing is available but exists only as a laboratory demonstration.

TABLE OF TYPICAL SENSORS

Type	Device	Bandwidth (Hz)	Range	Resolution	Power (W)	Weight (oz)	Size (in.)	Comments
Position	LVDT	0-500	± 1.0 mm	6 μ m	0.3	2.3	0.75 D \times 2.1	
	Capacitive probes	0-50k	0.1-1.52 mm	0.001 μ m	—	17.6	0.63 D \times 3.7	
	Interferometer microphase sensor	0-50 0-20k	± 0.01 m	0.00 μ m <0.00 μ m	0.0004	—	—	LMSC Φ 100 M LMSC
	SAMS	0-8	± 30 cm	± 0.2 mm	0.3	—	0.47 \times 0.59 \times 1.6	TRW Φ 45 M
	BIRD II	0-8	± 30 cm	± 0.3 mm	—	192	—	Bell Φ 32 M
Angle	RVDT	0-500	± 1 rad	0.01 rad	1.0	1.9	1.1 D \times 1.9	
	Optical encoder	0-75k	—	0.0008 rad	—	—	3.0 D \times 6.5	
Acceleration	Inertial accelerometer	0-100	100 g	0.1 μ g	1.5	1.7	0.9 D \times 1.4	Modified Bell XI
	Piezoelectric accelerometer	2-10k	± 84 g	800 μ g	—	1.4	0.75 D \times 1.5	
Force	Piezoelectric transducer	0-75	± 2.5 kN	10 mN	—	0.4	0.4 D \times 1.0	Force link
	Strain gauge	0-50k	± 40 μ m/m	5 μ m/m	0.025	0.04	0.25 \times 0.02 \times 0.002	
Rate	Inertial gyro	0-200	—	0.003 sec	—	29.2	2.5 D \times 3.6	CSDL IT66

Figure 15

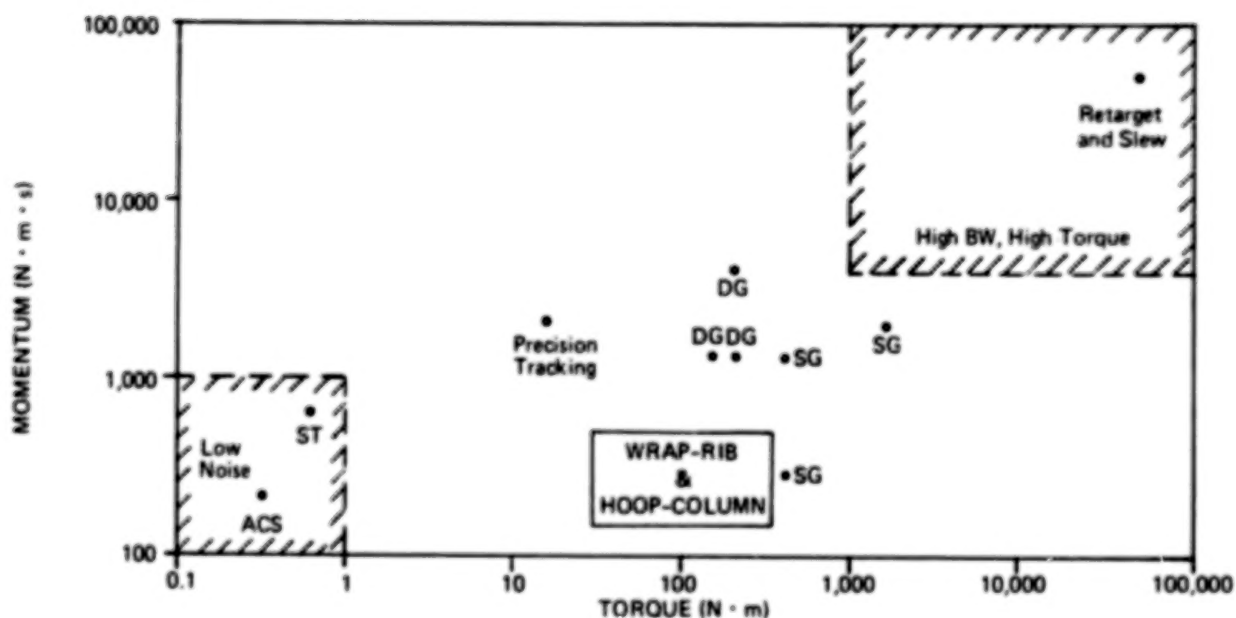
Actuator technology (see Figure 16) for submicron vibration control relevant to the large precision space systems problem is virtually nonexistent. Piezo-electric devices provide the best potential. With respect to slow maneuvering and attitude control, Control Moment Gyro/Reaction Wheel (CMG/RW) is not capable of either. For attitude control, the CMG/RW is required to have low noise/low bandwidth characteristics, while for maneuvering, it is required to have high torque/high bandwidth characteristics. Today's CMGs and RWs fall in between these diverse requirements as shown in Figure 17. Thruster technology has the potential for high torque; however, these devices lack a continuously variable thrust level.

TABLE OF TYPICAL ACTUATORS

Type	Device	Bandwidth (Hz)	Characteristics	Weight (lb)	Power (W)	Size (in.)
Torque	Reaction wheel	0-100	5 lb-in./7 ft-lb-s	12	15	12 D x 7.8
	Control momentum gyro	0-50	500 ft-lb/2300 ft-lb-s	418	50	49 sphere
Force	Pulsed plasma thrusters	—	0.0003 N/1000 s SPI	14.5	25	15 x 7 x 9
	Piezoelectric actuators	0-5k	1 Nm/15 μ m range	1	—	0.7 D x 2
	LMSC Proof Mass actuator PPM	2-200	10N	—	—	—

Figure 16

TORQUE/MOMENTUM CAPABILITIES AND REQUIREMENTS



 Technology Development Required

- NOTES: (1) ST = Space Telescope Reaction Wheel
 (2) ACS = Attitude Control System
 (3) DG = Double Gimbal Control Momentum Gyro
 (4) SG = Single Gimbal Control Momentum Gyro
 (5) WRAP-RIB (55 m Dish Diameter, 80 m Boom)
 (6) HOOP-COLUMN (118 m HOOP, 88 m MAST)

Figure 17

Very little work has been done in the area of fault detection, isolation, and reconfiguration for large space systems per se [22,23]. Therefore, a broad, well-planned technical effort is needed to successfully apply fault-tolerant technology to large space systems and gain the benefits of improved system performance and reliability which can result from it. Fortunately, a large amount of theoretical and applied work has been done in the fault-tolerant technology area, which forms a solid and broad basis for the development of a fault-tolerant large space system. This is especially true in the areas of computation, failure detection, isolation algorithm development, reliability analysis, digital system architecture, and the application of fault-tolerant technology to space, naval, and aircraft systems. Figure 18 shows that a system with 50 components ($N=50$) whose mean time between failure is 100,000 hours (12 years) can expect 4 component failures each year.

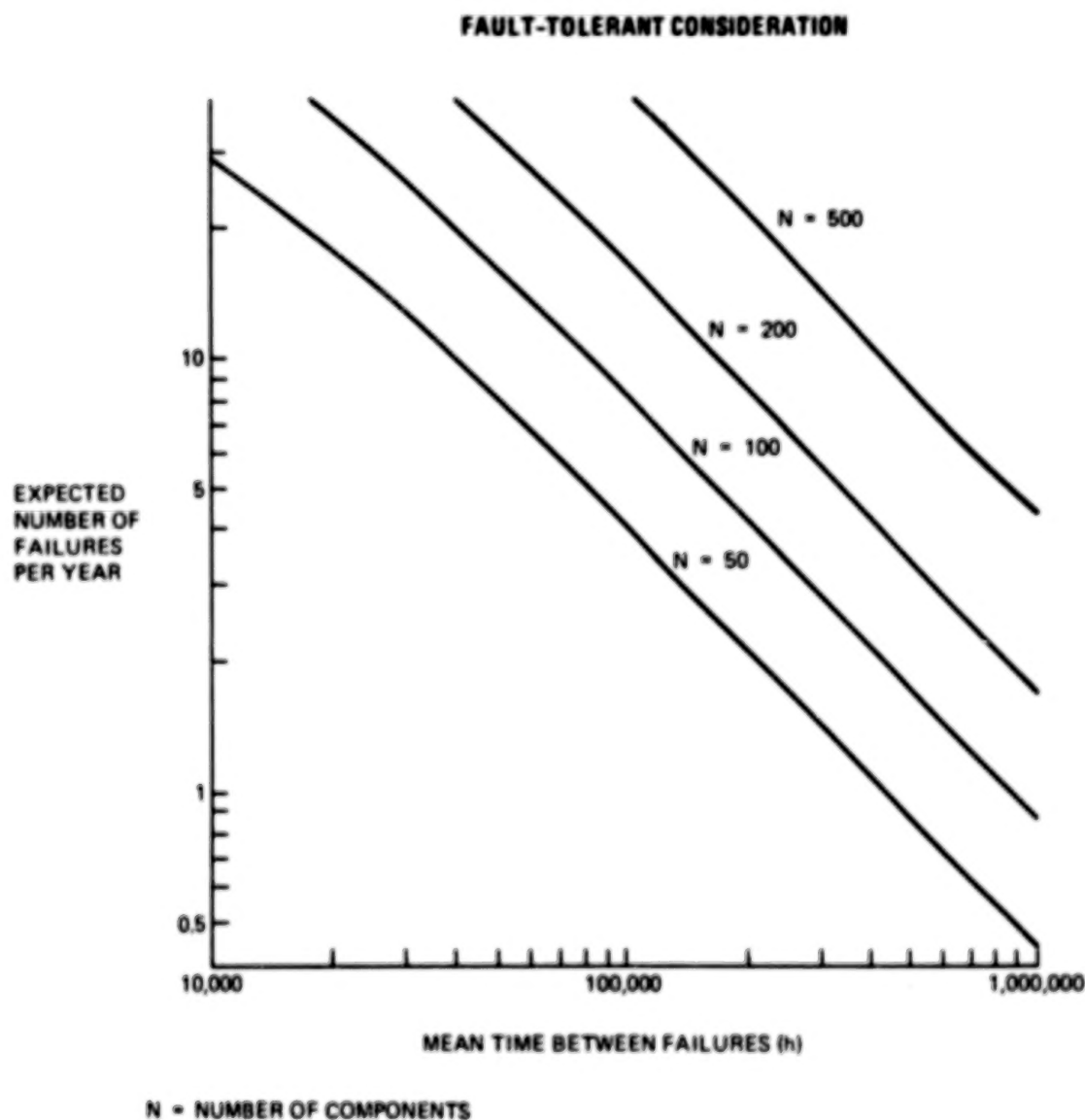


Figure 18

The relevant large space structure experiments (see Figure 19) to date considered either beams or plates, with one exception, Lockheed's proof-of-concept (POC). The advantage of these choices is the ability to analytically predict the dynamic behavior of the structure and thus compare the analysis to the experimental results. The obvious drawback of these experiments is the fact that almost no realistic large space structure has the characteristics of a beam or a plate, although it might contain a flexible beam (e.g., the boom connecting the feed and the reflector of an antenna). None of the experiments employed a truss structure--a likely large space structure configuration. The current level of performance in these experiments was for large deflections, even though deflections in the submicron range are anticipated for large precision space systems. The Draper RPL-EXP is the only experiment which incorporates thrusters.

RELEVANT LSS EXPERIMENTS

Company	Type	Description	Sensor	Actuator	Demonstration
Comair	Plate	Fixed-free 88" x 183" aluminum 4" x 5/16" welded beams	Rate gyros	Torque wheels	Model error sensitivity suppression
Draper	Beam	Fixed-free 1/4" x 1" x 60" aluminum	Piezoelectric accelerometers	Electrodynamic shaker	Observation/control spillover modern modal control
	RPL-EXP	4 beams (1/8" x 6" x 48" aluminum) cantilevered to hub on air bearing table	Angle encoder accelerometers	Cold gas thrusters	RCS controller Design methods for flexible spacecraft
Hughes	Cylindrical mast	Hollow fiberglass cylinder (8.23 cm x 4.3 cm dia. x 66 cm long)	Piezoelectric ceramic strain transducers	Piezoelectric ceramic strain transducers	Electronic damping
JPL	Beam	Pinned-free 150" x 6" x 1/32" stainless steel	Eddy current position sensor	Brushless dc torque motor	Modern modal control
LaRC	Beam	Suspended 12" x 6" x 3/16" aluminum	Noncontacting deflection sensor, load sensor	Electrodynamic shaker	
Lockheed	Beam	Fixed-free 40" magnesium	Optical rate sensor	Proof-mass	Low authority control
	I-Beam	Fixed-free 25' x 16" (400 lb) aluminum	Optical rate sensor	Single gimbal CMG	Low authority control
	Vertical Beam	Fixed-free 6' aluminum lead tip masses	Accelerometers, quad-detector photo diodes	Pivoted proof-mass	Low authority control System identification
	Circular plate	Suspended, 2 meter diameter, aluminum	Multi-channel micro-phase optics	Pivoted proof-mass	Low authority control Low/high authority control System identification
	Frame	Suspended 2 meter diameter aluminum tubes	Accelerometers, optics	Pivoted proof-mass	
	Toyot	Suspended rigid body 1.6 m cantilever beams aluminum	Accelerometers, LVDT velocity pickups	Electrostatic actuators	Open loop torque profile high authority control
	POC	4.5 meter boom with 3 meter reflector, aluminum on air bearing sphere	Accelerometers, rate gyrs, laser	CMG Proof mass	Classical and modern control of vibration and slew
TRW	Plate	Clamped 1.73 m x 1.22 m x 1.66 mm aluminum	Rate sensors, accelerometers	Bending moment actuator	Vibration suppression and damping augmentation

Figure 19

The major potential large space structures test facilities are the Air Force Rocket Propulsion Laboratory, Arnold Engineering Development Center, Boeing, Ford Aerospace, General Dynamics, Johnson Space Center, McDonnell Douglas, and the TRW Systems Group.

Ground-based environmental testing of large space structures sections or components may be required prior to actual space construction. The issues of zero-g and seismic disturbances cannot be ignored; however, experience has shown that prudent ground-based testing of spacecraft can reduce operational risk. Figure 20 presents a representative survey of large environmental space chambers which could be utilized in an appropriate large space structure ground-based test program.

LARGE SPACE STRUCTURE VACUUM CHAMBER SUMMARY

Organization	Equipment	Size (ft)	Pressure (torr)	Heat	Cooling	Solar	Comments
Air Force Rocket Propulsion Laboratory	SPEF	30 ft sphere	1×10^{-6}	Heated panel +400° F	Cryo panel -300° F	Solar heat simulator	
Arnold Engineering Development Center	Mark I	42 D x 82 L vertical	5×10^{-9}		Cryo	Yes	
	7V	7 D x 12 L horizontal	—		Cryo	No	Used for simulation of space mission for cold-optics and specialized infrared equipment
	10V	10 D x 20 L horizontal	—		Cryo	No	Used for low density aerodynamic studies and testing of small rocket engines
	12V	12 D x 35 L vertical	—		Cryo	Xenon arc	Heat flux system to simulate planet albedo and radiance
Boeing	Space Chamber	28 D x 40 L vertical					Structure mounted on 1×10^6 lb mass. Used to make optical level measurements
Ford Aerospace	Solar Simulation Chamber	10 D x 22 L	1×10^{-7}	NA	Yes	Off axis xenon arc	LN ₂ cold wall
General Dynamics		12 D x 30 L horizontal					
Johnson Space Center	SESL Chamber A	55 D x 90 L vertical	1×10^{-6}	Heat flux of 150 W/ft ²	90° K	Top and side	
	SESL Chamber B	25 D x 26 L vertical	1×10^{-6}	Heat flux of 150 W/ft ²	90° K	Yes	
McDonnell Douglas	38' spherical	30 x 30	—	NA	Cryo shrouds		Isolated seismic base vibration shaker
TRW System Group	Sphere	30 ft sphere		Shroud temp +275° F	Shroud temp -30° F	84 in diameter	-300° F cold wall
	Cylinder	22 D x 46 L vertical		Shroud temp +200° F	Shroud temp -80° F	10 feet square	-300° F cold wall

Figure 20

REFERENCES

1. Effects of Structural Flexibility on Spacecraft Control Systems, NASA SP-8016, Apr. 1969.
2. Noll, Richard B., John J. Deyst, Curtis H. Spenny, "A Survey of Structural Flexibility Effects on Spacecraft Control Systems," AIAA Paper No. 69-116, AIAA 7th Aerospace Sciences Meeting, New York, New York, January 20-22, 1969.
3. Farrenkopf, R.L., A Survey of Case Histories Involving Spacecraft Dynamic Interaction, TRW Report, TRW, Inc., Redondo Beach, CA, Mar. 30, 1968.
4. Likins, Peter W., H. Karl Bouvier, "Attitude Control of Nonrigid Spacecraft," Astronautics and Aeronautics, May 1971.
5. Disher, John H., "Next Steps in Space Transportation and Operations," Journal of Astronautics and Aeronautics, January 1978.
6. Hagler, Thomas, Herbert G. Patterson, and Allan C. Nathan, "Learning to Build Large Structures in Space," Journal of Astronautics and Aeronautics, December 1977.
7. Daros, Charles J., Robert F. Freitag, and Richard L. Kline, "Toward Large Space Systems," Journal of Astronautics and Aeronautics, May 1977.
8. Powell, Robert V., and Albert R. Hibbs "An Entree for Large Space Antennas," Journal of Astronautics and Aeronautics, December 1977.
9. Dahlgren, J.B. and S.M. Gunter, "Pointing and Control Technology Needs for Future Automated Space Systems," AIAA Convention on Large Space Platforms, Los Angeles, California, September 1978.
10. Mode, V.J., "Attitude Dynamics of Satellites with Flexible Appendages - A Brief Review," Journal of Spacecraft and Rockets, Vol. 11, No. 11, September 1974.
11. "Special Issue on Dynamics and Control of Large Space Structures," The Journal of the Astronautical Sciences, Volume XXVII, No. 2, April-June 1979.
12. Seltzer, Sherm M., "Active Control of Flexible Space Structures," AAS 80-026, American Astronautical Soc., Annual Rocky Mountain Guidance and Control Conference, February 17-21, 1980, Keystone, Colorado.
13. Likins, Peter, "The New Generation of Dynamic Interaction Problems," AAS 78-101, American Astronautical Soc., Annual Rocky Mountain Guidance and Control Conference, March 10-13, 1978, Keystone, Colorado.
14. Balas, Mark J., "Trends in Large Space Structure Control Theory: Fonddest Hopes, Wildest Dreams," IEEE Trans. Automat. Contr., Vol. AC-27, No. 3, June 1982.

15. Preliminary Flight Control Avionic Requirements for Orbiter-Attached Large Space Structures, CSDL-R-1531, The Charles Stark Draper Laboratory, Inc., Cambridge, MA, January 1982.
16. An Investigation of Enabling Technologies For Large Precision Space Systems, Vol. 1, 2, and 3, CSDL-R-1499, The Charles Stark Draper Laboratory, Inc., Cambridge, MA, November 1981.
17. Hord, R.M., Military Space Systems Technology Model, NASA CR-168720, 1982.
18. Large Space Systems Technology - 1981, Parts 1 and 2, NASA CP-2215, 1982.
19. Passive and Active Suppression of Vibration Response in Precision Structures: State of the Art Assessment, Vols. 1 and 2, CSDL-R-1138, Charles Stark Draper Laboratory, Inc., Cambridge, MA, 1973.
20. Travassos, Richard H., "The MCP-100: A Turnkey System for Implementing Multi-variable Flight Control Laws," Proceedings of the IEEE 1982 National Aerospace and Electronics Conference, 1982.
21. MCP-100 Operations Manual (draft), Integrated Systems Inc., Palo Alto, CA, Sept. 1982.
22. Deyst, J.J., J.V. Harrison, E. Gai, and K.C. Daly, "Fault Detection, Identification and Reconfiguration - An Emerging Discipline in the Development of Highly Reliable Space Systems," 1980 Annual Meeting of the American Astronautical Society, Boston, October 20-23, 1980.
23. Marshall, M., and G.D. Low, "Final Report of the Autonomous Spacecraft Maintenance Study Group," JPL Publication 80-88, Jet Propulsion Laboratory, Pasadena, CA, February 1981.

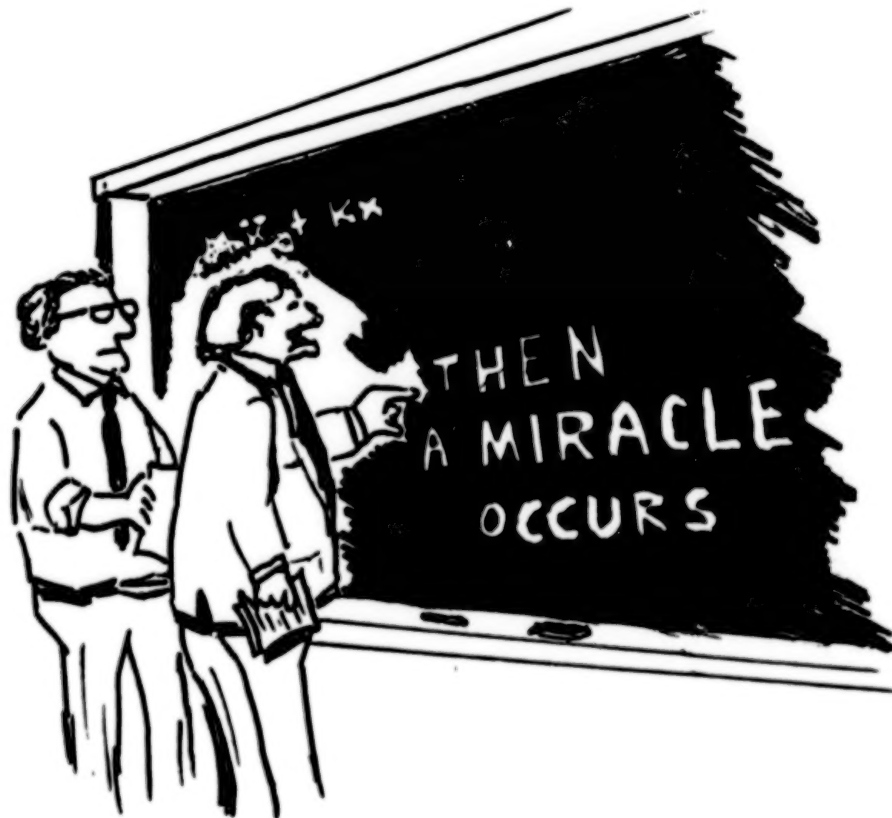
REDUCED ORDER CONTROL DESIGN FOR LARGE SPACE STRUCTURES -
A COMMUNICATION SATELLITE EXAMPLE

Richard Gran
Grumman Aerospace Corp.
Bethpage, New York

Large Space Antenna Systems Technology - 1982
NASA Langley Research Center
November 30 - December 3, 1982

This talk summarizes work that was performed under contract to the International Telecommunications Satellite Organization (INTELSAT). The problem posed was how does one design a controller for a large flexible communication satellite. The satellite that was developed for a "straw man" was configured as an offset fed paraboloid with a set of masts and booms that carry the antenna. The controllers were both a boom and mast actuator and a set of two degree of freedom actuators at the antenna to move it in order to satisfy both line of sight and defocus control.

One of the problems with the control of large space structures is that it has been given only limited attention because the control theorists have tended to sell control theory as a miracle medicine - like step two - but, while control theory can be very effective, the solutions that have been developed so far for the large space structures control problem are too unwieldy and difficult to implement.



"I think you should be more explicit here in step two."

Structural control problems are inherently infinite dimensional. They are infinite no matter how you look at them, and they don't lend themselves to simple reduction in order because you can't simply cut the loop and view the problem as finite. If you do, you could make errors. The only way is to iterate on the order reduction.

infinite

The procedures we developed for designing control systems are outlined in the 5 step iterative procedure described in this figure. The idea is to reduce the order based upon a preliminary control system bandwidth evaluation, then use this to design the control system. The bandwidth of the resulting controller is then known and you can return to step one to reevaluate the design model. Step 3 is therefore a point for iteration on the design and the way the loop is broken in the infinite dimensional problem.

STEP 1 – FINITE DIMENSION DESIGN MODEL

1. PICK CONTROL BANDWIDTH (ω_c) BASED ON CONTROL OBJECTIVE
2. BASED ON LEVEL OF DAMPING, DETERMINE MAXIMUM STRUCTURAL FREQUENCY TO BE RETAINED (ω_M)
3. USING MODE DESCRIPTIONS:
 - KEEP UNSTABLY INTERACTING MODES – EVEN THOUGH THEY HAVE LOW COSTS
 - DISCARD, IF NECESSARY, LOW FREQUENCY STABLE MODES WITH LOW MODE COSTS
 - DISCARD UNOBSERVABLE OR UNCONTROLLABLE MODES
NOTE: IF THESE MODES HAVE HIGH MODAL COST, THEN ADD SENSOR/ACTUATOR AT OTHER LOCATIONS
 - PLACE SENSORS/ACTUATORS USING STABLE INTERACTIONS AS CRITERIA, BUT REMEMBER THAT SOMETIMES NONCOLLOCATION IS NOT POSSIBLE

STEP 2 – DISTURBANCE MODELING

- INCLUDE IN MODEL ALL DISTURBANCES, BOTH STOCHASTIC AND DETERMINISTIC
IN GENERAL, MEASUREMENT OF DISTURBANCES IS ASSUMED TO BE IMPOSSIBLE

STEP 3 – DESIGN

- ITERATIVELY CHANGE DESIGN MODEL IF ω_c INCREASES

STEP 4 – ACTUATOR & SENSOR PROLIFERATION TO IMPROVE PERFORMANCE

- ITERATIVELY ADD SENSORS TO IMPROVE PERFORMANCE IF DESIGN DOES NOT MEET SPECS
- ITERATIVELY ADD ACTUATORS IN SAME MANNER AS SENSORS – AT EACH STEP REEVALUATE STABILITY OF MODES

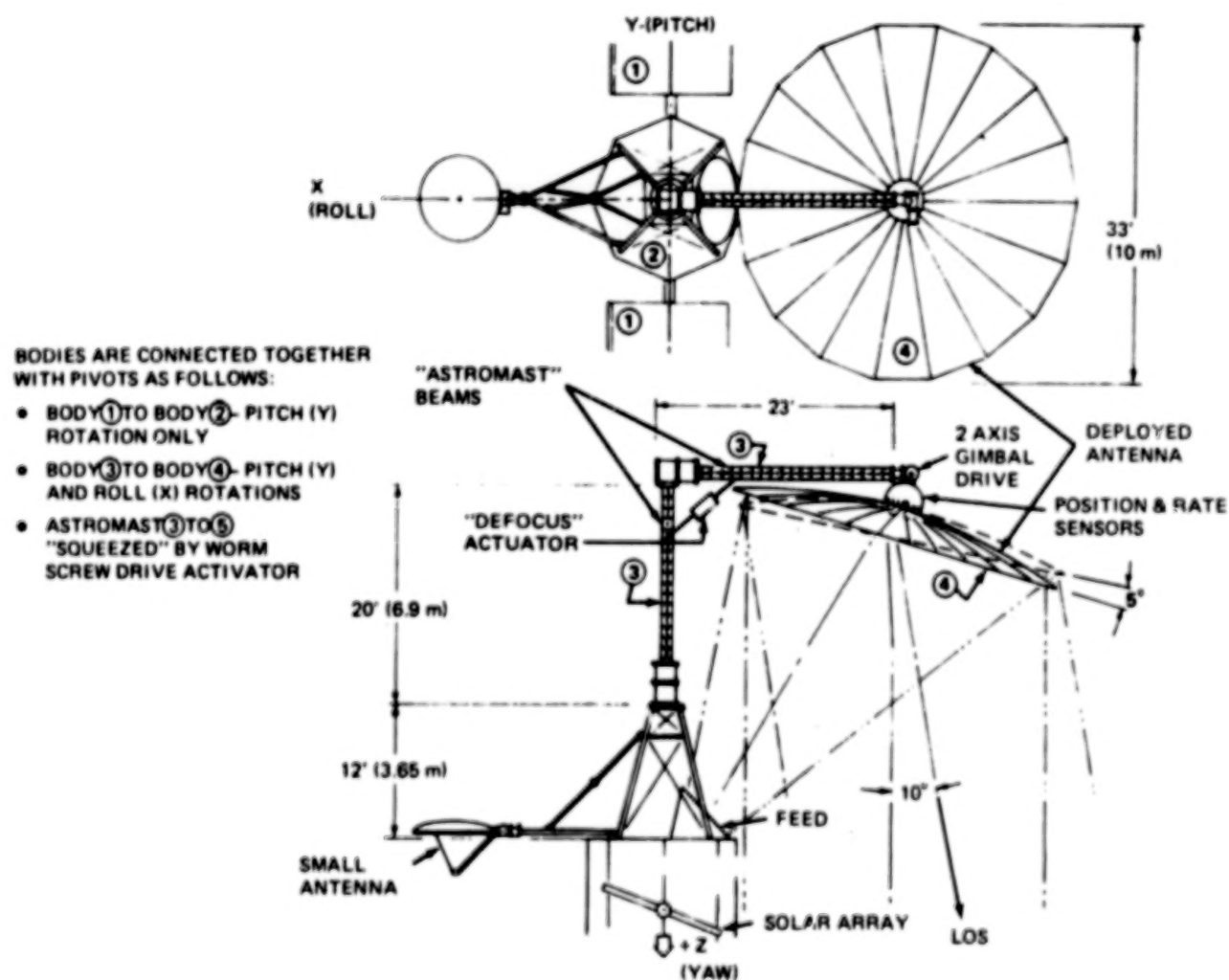
STEP 5 – ROBUSTNESS

- VERIFY DESIGN IS INSENSITIVE TO PARAMETER VARIATIONS

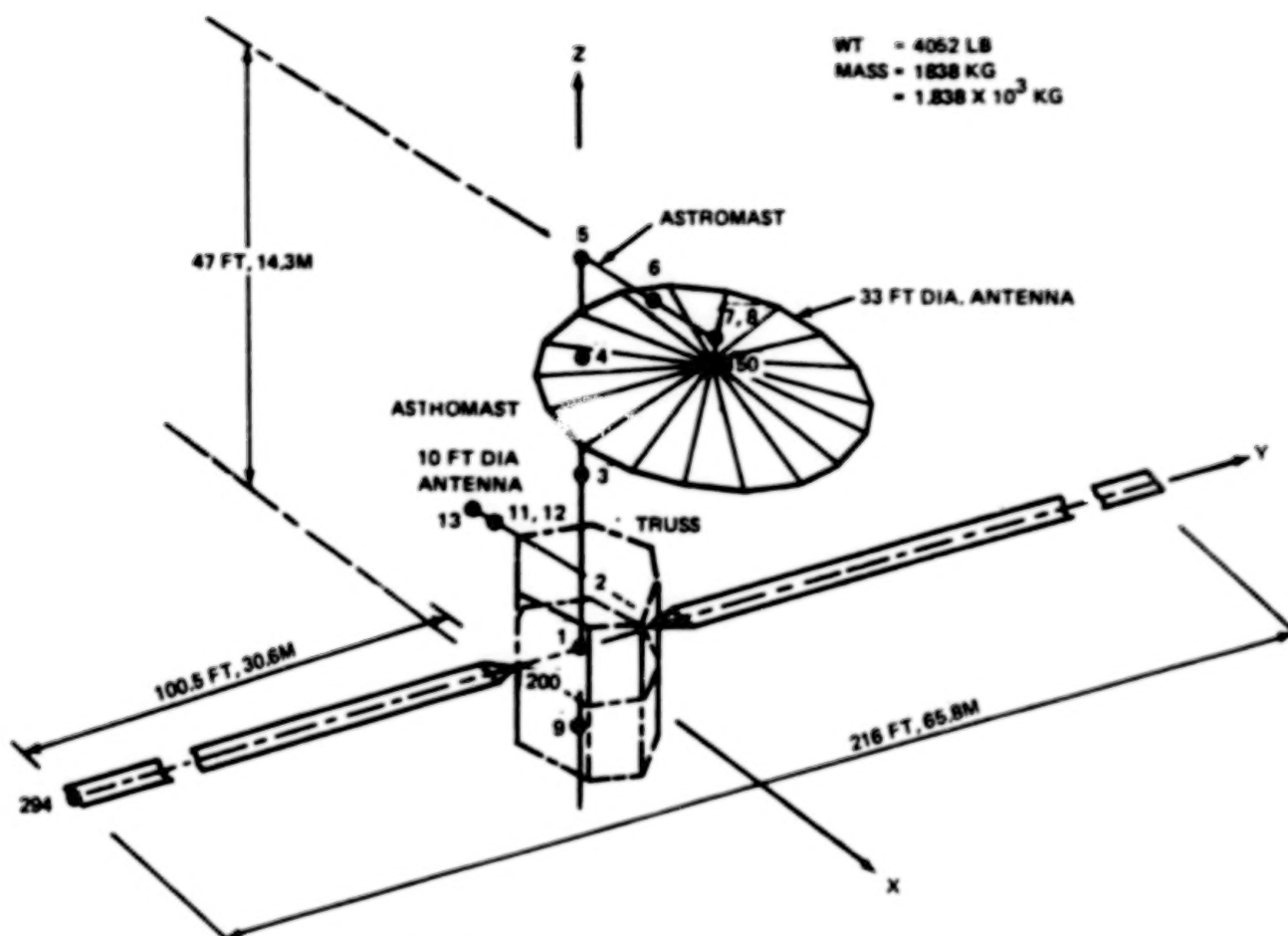
Large space structures control design.

The model spacecraft that was used to design the control systems for INTELSAT is shown in the following two figures. The structure is completely deployable using ASTROMASTs and a hoop antenna. The actuators are such that defocus and line of sight motion can be controlled (if desired) along with the rigid body (the central core where all of the electronics and the feed horn are located).

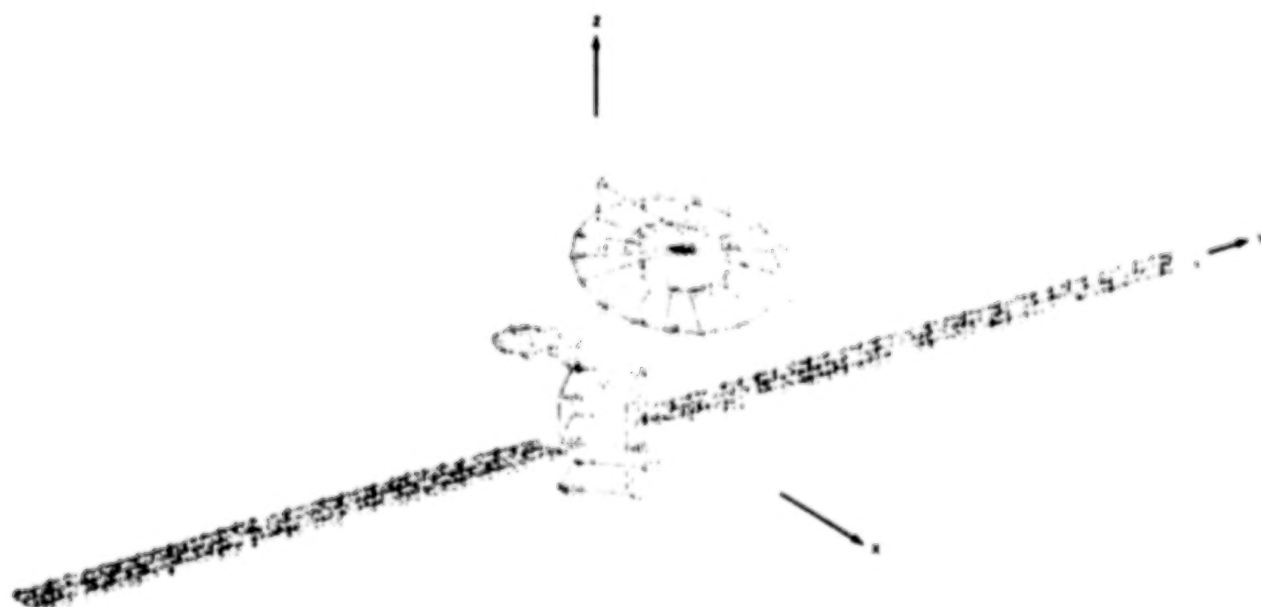
The finite element model is shown in the second figure. It offers enough detail so that the modes out to the antenna are accurately (consistently) defined.



Phase III configuration. (From ref. 1.)



(a) Schematic of finite element model.



(b) Finite element model.

Phase III spacecraft model. (From ref. 1.)

To reduce the model order to a finite model with accurate representation of the significant dynamics, one must know precisely how each mode affects the performance of the system. Thus the line of sight motion in pitch and roll is used along with the perturbation in the antenna-to-feed distance as the criteria for good control. The antenna feed perturbation, for example, is computed as shown.

$$L = \sqrt{(x_2 - x_{50})^2 + (y_2 - y_{50})^2 + (z_2 - z_{50})^2}$$

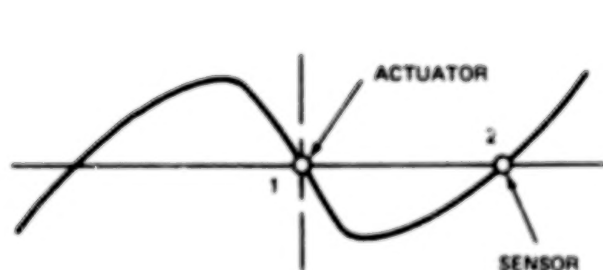
$$\partial L = \left(\frac{\partial L}{\partial x_2} \right)_0 \partial x_2 + \left(\frac{\partial L}{\partial y_2} \right) \partial y_2 + \left(\frac{\partial L}{\partial z_2} \right) \partial z_2 + \left(\frac{\partial L}{\partial x_{50}} \right) \partial x_{50} + \left(\frac{\partial L}{\partial y_{50}} \right) \partial y_{50} + \left(\frac{\partial L}{\partial z_{50}} \right) \partial z_{50}$$

$$= \alpha_x (\partial x_2 - \partial x_{50}) + \alpha_y (\partial y_2 - \partial y_{50}) + \alpha_z (\partial z_2 - \partial z_{50})$$

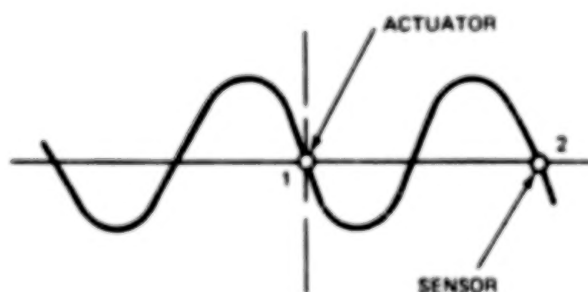
Line of sight motion.

The modes that have a significant effect on the performance measure (line of sight motion and defocus) are the only ones that are usually retained. This can lead to disastrous consequences when actuators and sensors are not at the same location. This is illustrated by the two mode shapes in this figure. The one on the left is unstably interacting and the one on the right is stably interacting. The argument is simple and straightforward. The mode on the left will be driven unstable because if the sensor detects a clockwise rotation it would normally send a signal to the actuator to cause a counterclockwise torque. In this case, that torque would further twist this mode, causing it to increase in amplitude. For the mode on the right, just the opposite is true. The interaction is stable.

The only way a control system can control a mode such as the one on the left is to introduce an 180° phase shift at that mode frequency and nowhere else.



Unstably interacting.

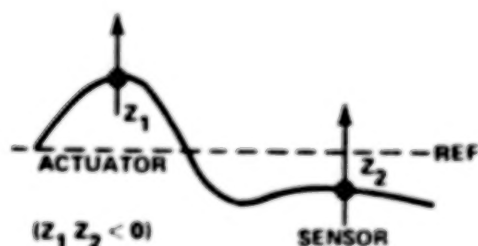


Stably interacting.

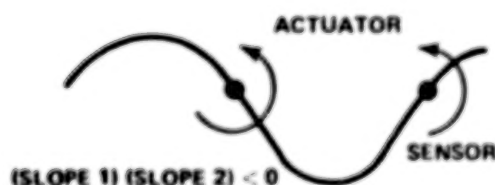
Mode shapes for stable and unstable interactions. (From ref. 1.)

For a control design, unstable modes show up as pole-zero dipoles where the pole is before the zero. In severe cases, the zero moves to infinity and reappears as non-minimum phase zeros (zeros in the right half plane).

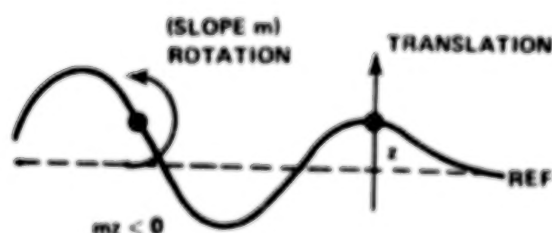
The lesson is that unstably interacting modes must always be retained in the model unless they are so high in frequency that they don't interact with the control loop. To do otherwise could lead to an unstable control system.



Unstably interacting mode for translational actuator/sensor pair.

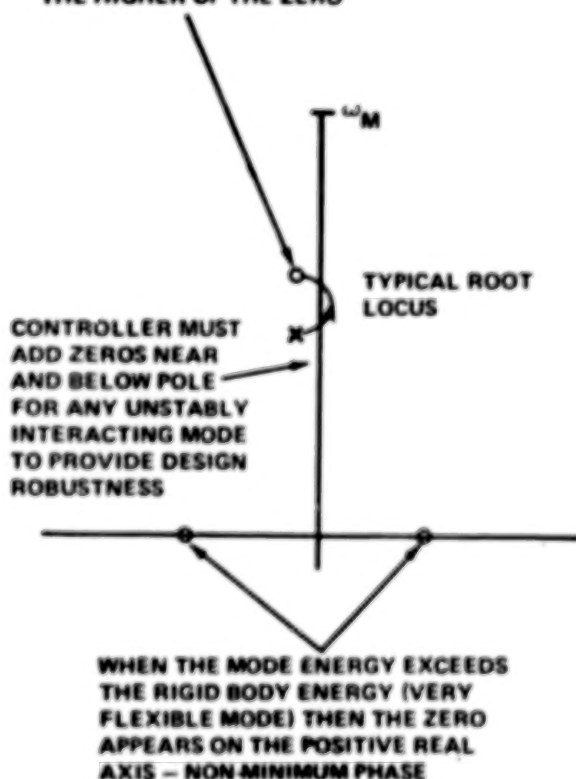


Unstably interacting mode for rotational actuator/sensor pair.



Unstably interacting mode for mixed sensing/actuation.

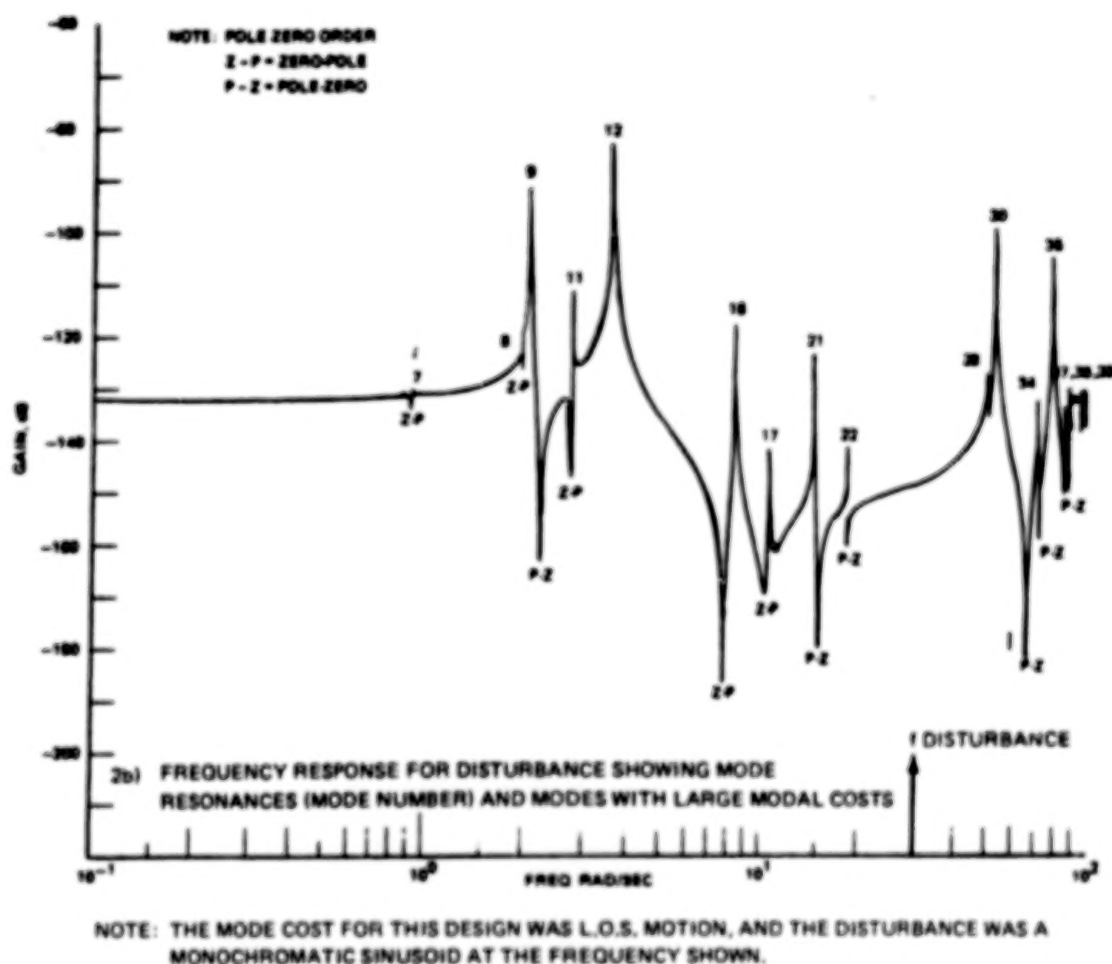
THE "MORE FLEXIBLE" THE MODE THE HIGHER UP THE ZERO



Pole-zero configuration for unstably interacting modes.

Example: shapes for unstable interactions. (From ref. 1.)

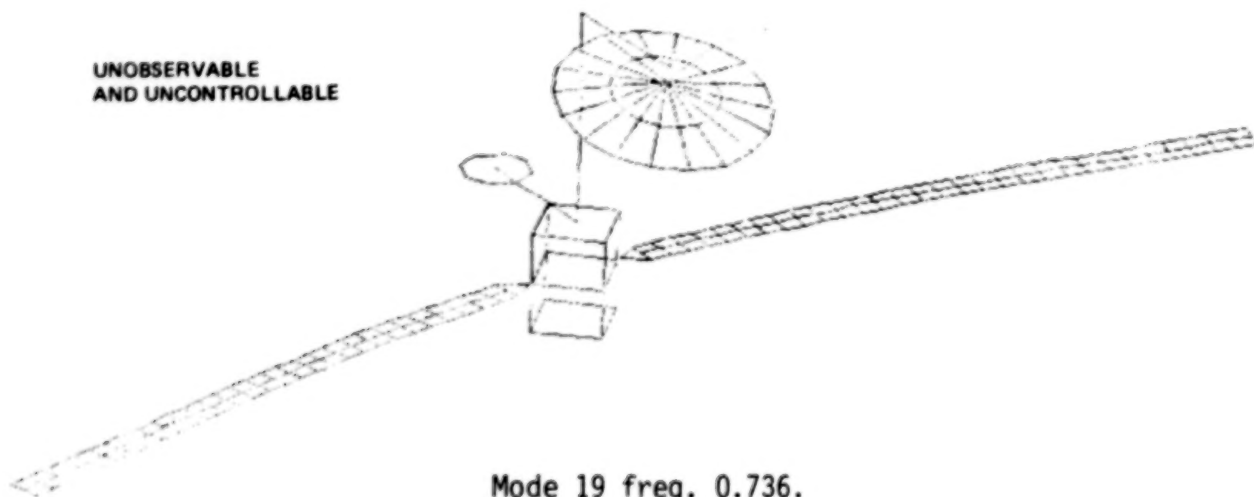
One way of evaluating the cost of each mode is to put the disturbances into the structural model and draw a power spectral density function (or Bode plot) of the performance criteria. This plot not only shows the modes that contribute to the cost, but also those modes that are unstably interacting (those whose zeros "Z" come before the poles "P" are stable and vice versa).



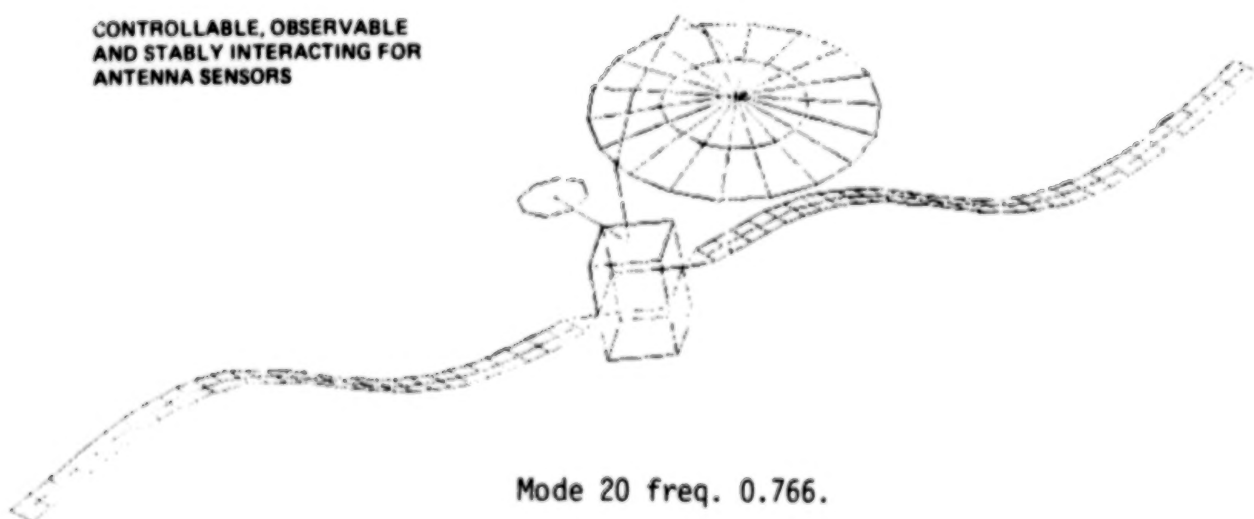
Mode costs for a structure. (From ref. 1.)

The following three mode shapes are all useful for evaluation of the modes to retain. Once again they can be used by themselves to determine which modes to retain. They are interpreted using the mode shapes that are drawn along with the locations of the actuators and sensors. Stably interacting and unstably interacting modes can be picked out rapidly with a little practice.

**UNOBSERVABLE
AND UNCONTROLLABLE**

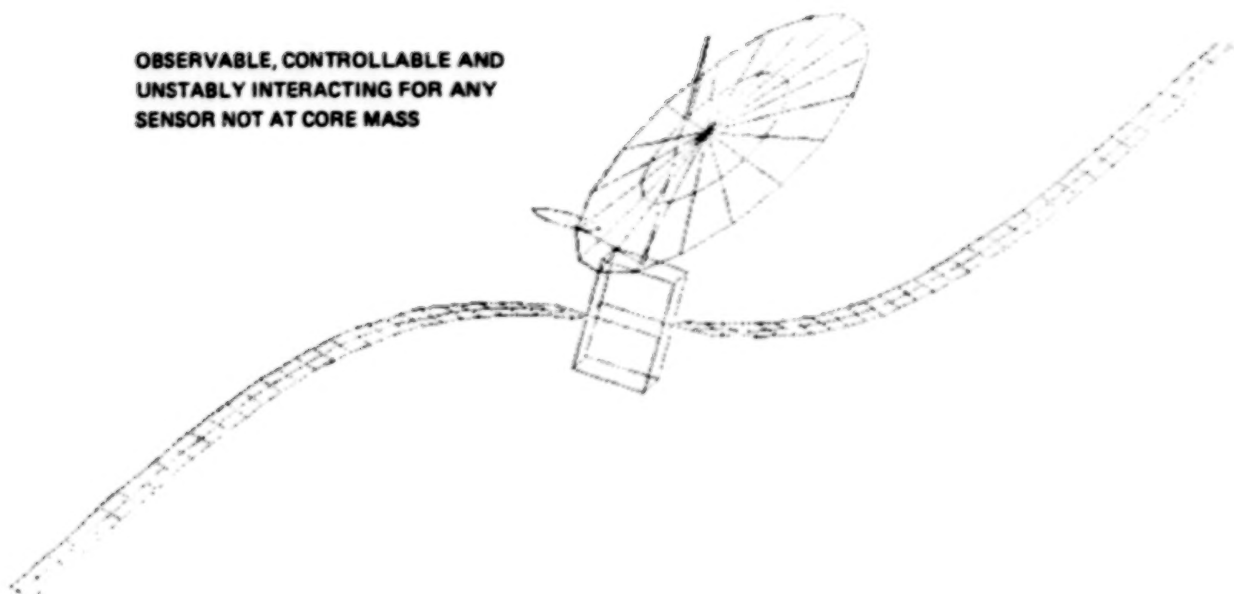


**CONTROLLABLE, OBSERVABLE
AND STABLY INTERACTING FOR
ANTENNA SENSORS**



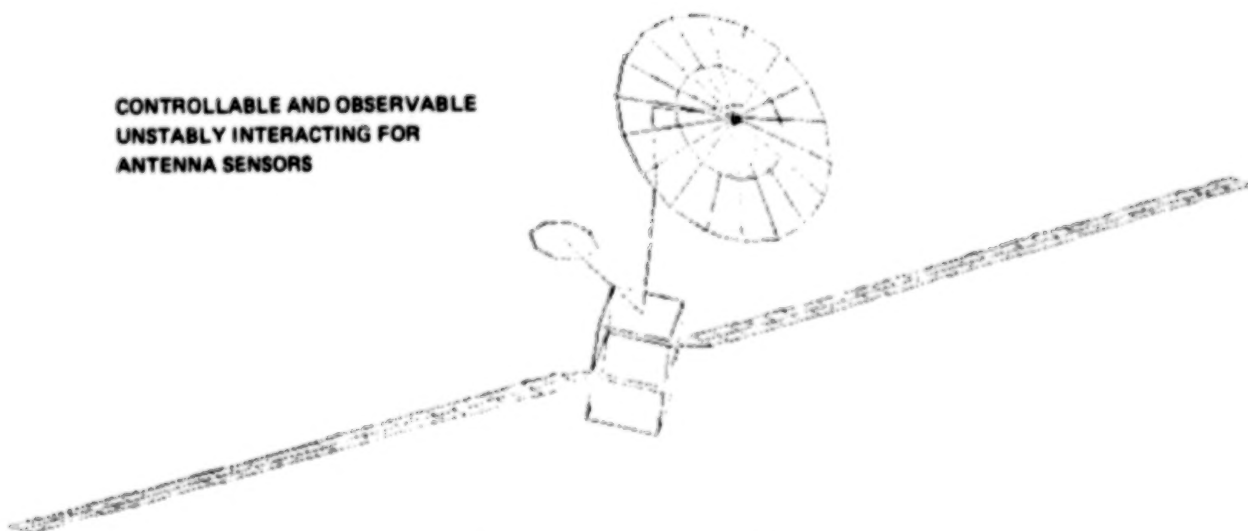
Configuration 2 deployable antenna and solar array. (From ref. 1.)

OBSERVABLE, CONTROLLABLE AND
UNSTABLY INTERACTING FOR ANY
SENSOR NOT AT CORE MASS



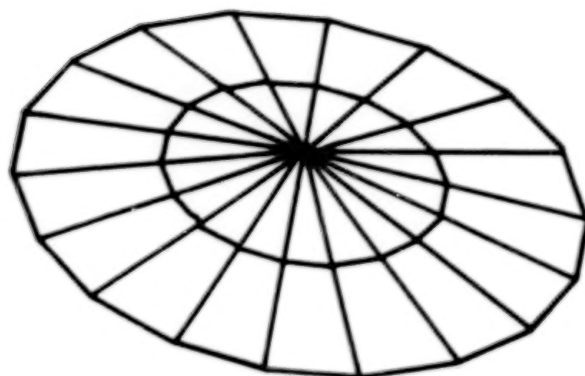
Mode 13 freq. 0.179.

CONTROLLABLE AND OBSERVABLE
UNSTABLY INTERACTING FOR
ANTENNA SENSORS

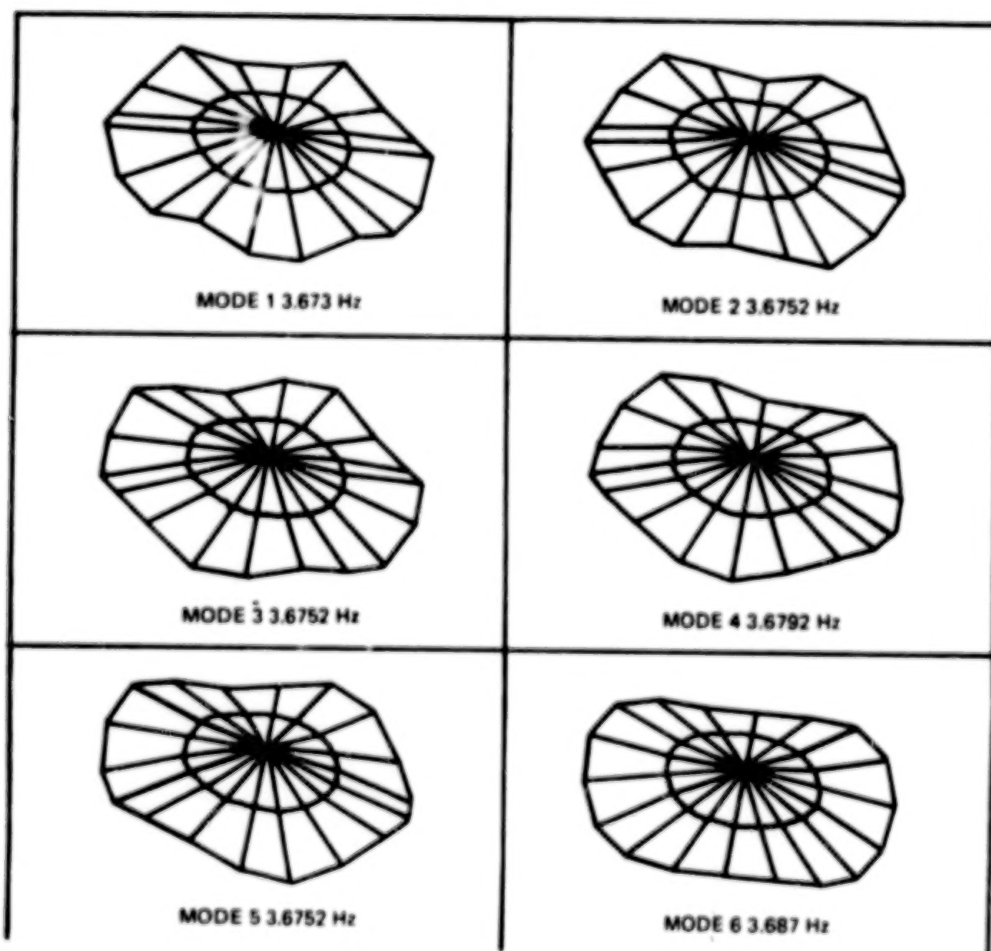


Mode 14 freq. 0.220.

Configuration 2 deployable antenna and solar array (concluded).

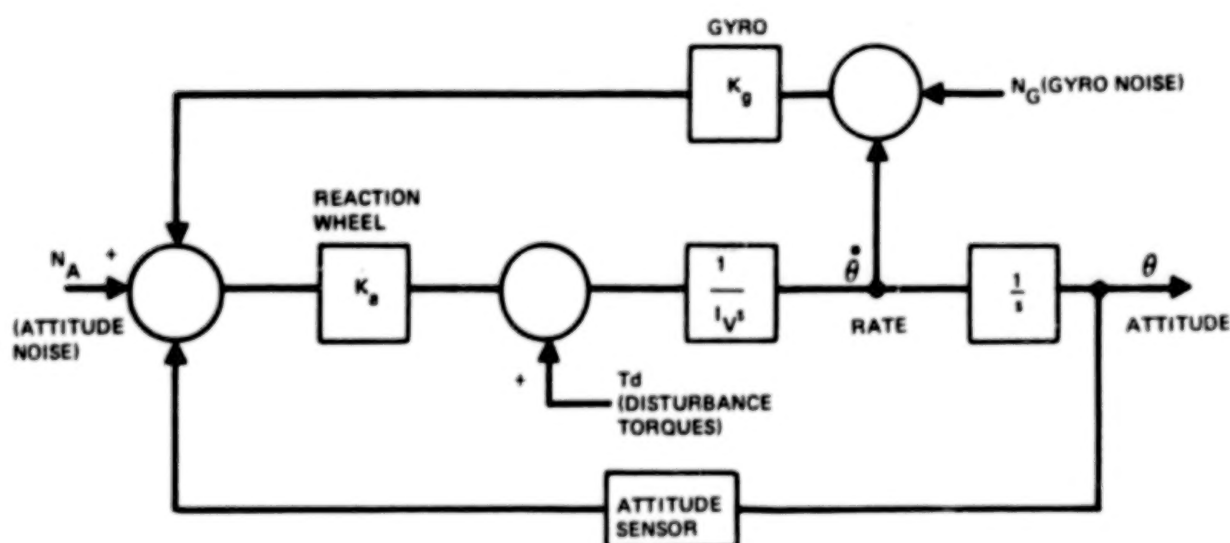


UNDEFORMED SHAPE



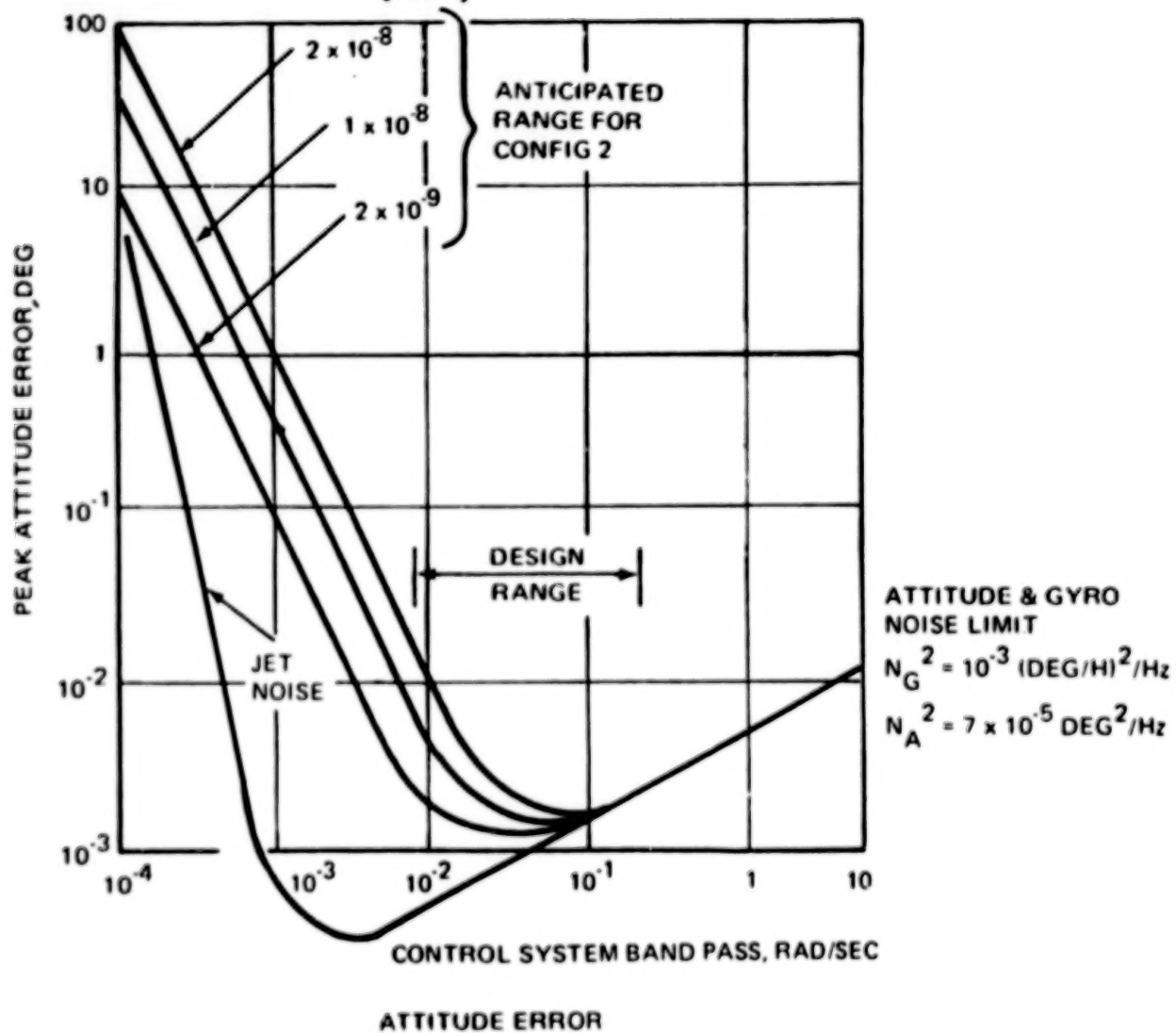
Configuration 2 antenna modes.

To determine the preliminary control bandwidth, a simplified analysis such as that shown in these two figures is used. The noises (disturbances) are modeled as white noises exciting linear systems, and the simplest block diagram that can be conceived of as achieving the design objective (here a rigid body controller) is used. The bandwidth of the control loop is then varied to see what the effect of the disturbances on the performance is. There is always a minimum noise response that determines the bandwidth. This bandwidth is then used to truncate the model to a maximum frequency that is, say, 10 times higher than the bandwidth. (There is a criterion that we have developed that is based on the damping levels expected in the structure. See ref. 2.)



Simplified block diagram of attitude control system. (From ref. 1.)

SOLAR DISTURBANCE TORQUE $\left(\frac{1}{\text{SEC}^2} \right)$
INERTIA



Performance tradeoff analysis. (From ref. 1.)

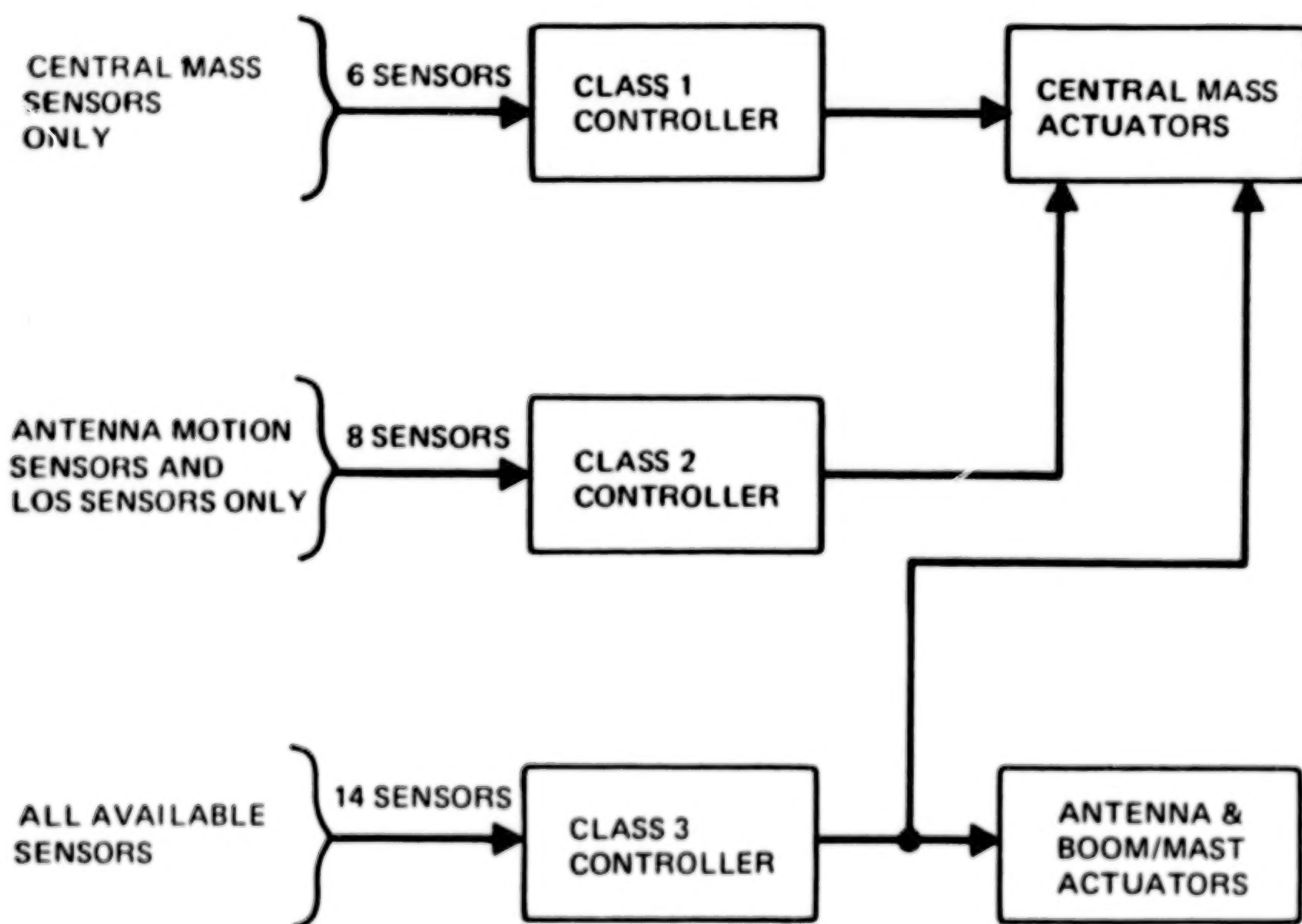
This chart delineates the first 31 modes and whether or not they were retained or discarded and why.

OBSERVABILITY AND CONTROLLABILITY OF STRUCTURAL MODES

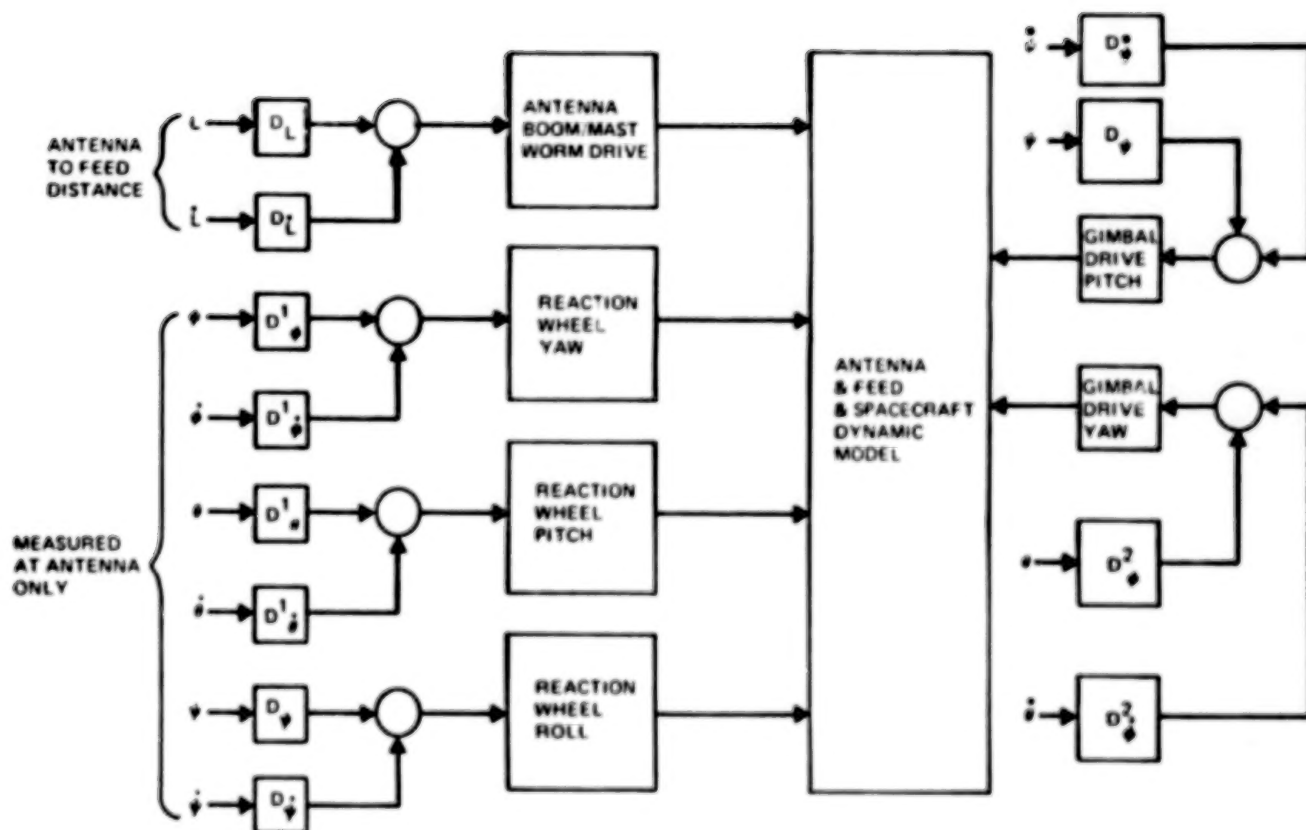
Mode No.	Observability		Stable or Unstable Interactive at		Retain R or Discard D		
	No	Yes	Solar Array	Antenna	Class 1	Class 2	Class 3
7	✓				D	D	D
8	At Core	At Antenna			D	R	R
9	At Core	At Antenna			D	R	R
10	At Core	At Antenna			D	R	R
11	✓				D	D	D
12	✓				D	D	D
13		✓	U	U	R	R	R
14		✓	2	S	R	R	R
15	✓				D	D	D
16		✓	S	U	R	R	R
17	✓				D	D	D
18	✓				D	D	D
19	✓				D	D	D
20		✓	S	U	R	R	R
21	✓				D	D	D
22		✓	U	U	R	R	R
23		✓	3	U	R	R	R
24	✓				D	D	D
25	✓				D	D	D
26		✓	U	S	R	R	R
27	✓				D	D	D
28		✓	S	S	R	R	R
29	✓				D	D	D
30	✓				D	D	D
31		✓	S	U	R	R	R
NOTES: 1 For attitude sensor located in center body, nodes 400 through 410 2 Will not excite solar array 3 Neutral because control torque is uniformly distributed on solar array about Y axis							

Observability and controllability of structural modes. (From ref. 1.)

Three classes of controllers were investigated during the contract. They are shown in the figure. The class 3 design is shown in more detail in the next figure. The gains denoted by D in this figure were the only ones that were optimized. The combined structural dynamics, actuator dynamics, and sensor dynamics led to a system of order 44 (24 for the retained modes, 6 for the actuators, 12 for the sensors and 2 to model the sinusoidal disturbance due to the solar array motion). Thus the full state solution would have required 528 gains (44 times 12) to achieve almost the same performance as was achieved here with only 12 gains. Incidentally, this calculation ignores the number of gains one would use to implement the Kalman filter.

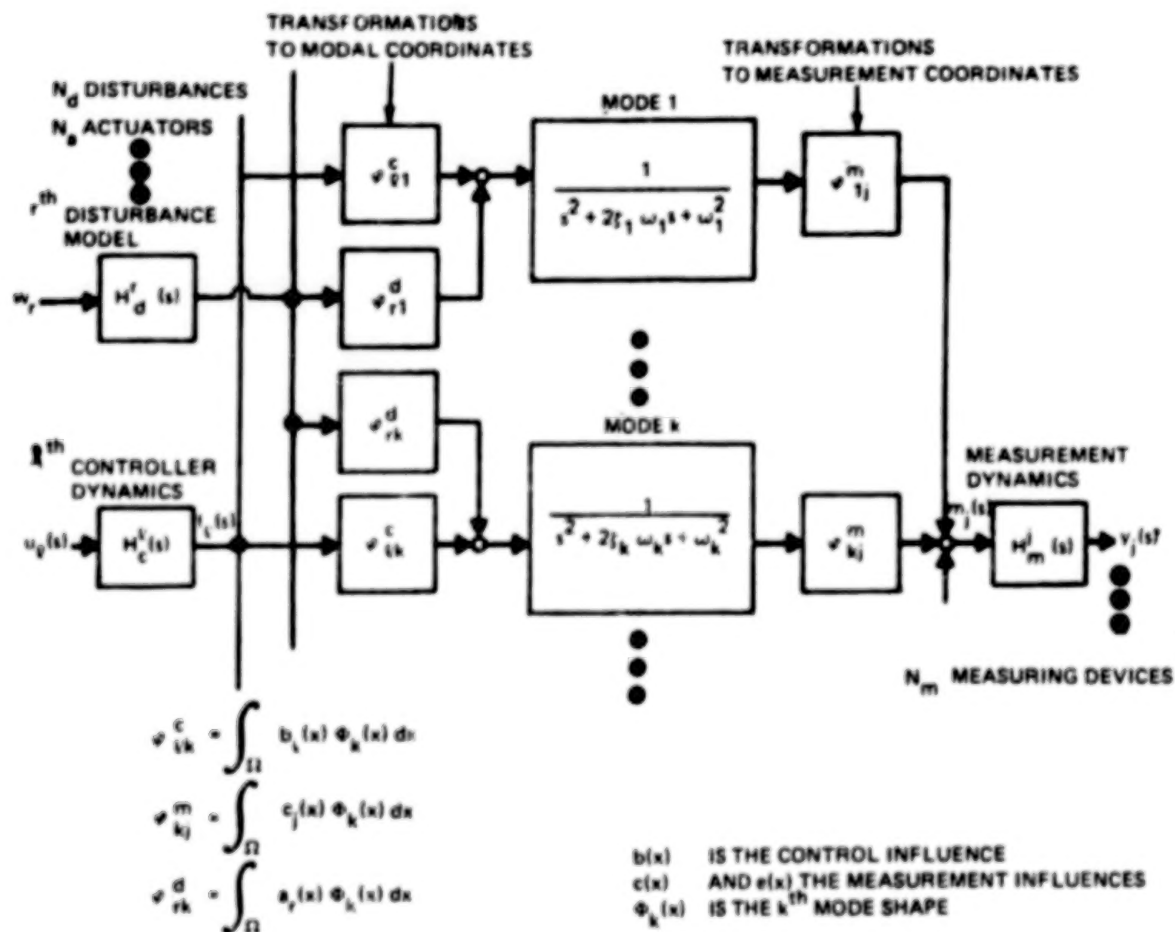


Structure of Class 1, 2, and 3 controllers. (From ref. 1.)

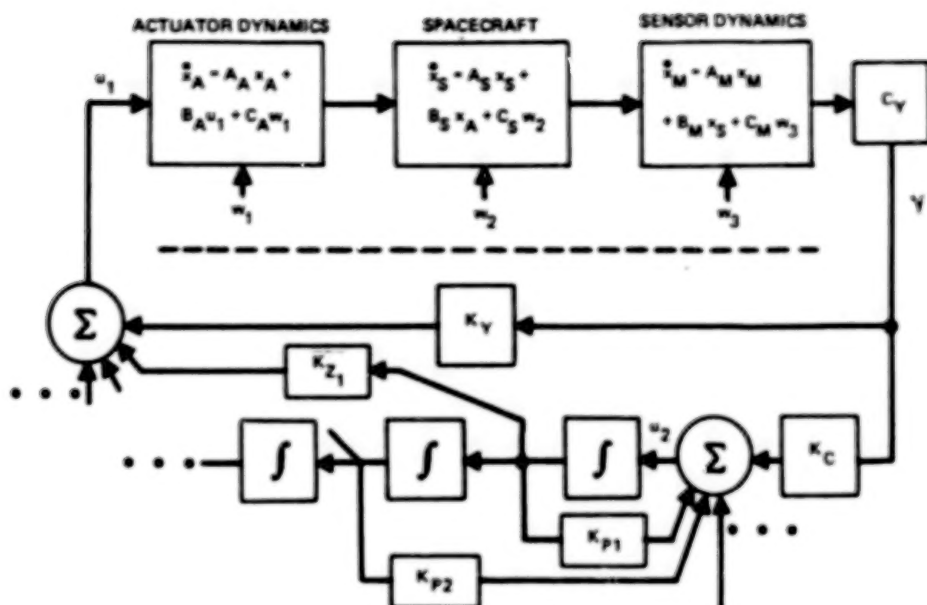


Class 3 design. (From ref. 1.)

The next four figures illustrate the design procedure. An iterative algorithm is used to determine the gains which minimized the cost. For this problem the cost was the expected value of the line of sight errors and the defocus error. The reduced state algorithm allows sensor and actuator dynamics to be included, and allows the noises to be accounted for in a very direct and straightforward way. The compensation (if any) for such problems as unstably interacting modes (these require notch filters to introduce the 180° phase shift) is simply designed along with the control system.



Structural dynamics control problem. (From ref. 1.)



NOTE: THE CONTROL GAINS SHOWN ARE SELECTED TO PROVIDE THE LOWEST COST J FOR THE CONFIGURATION SHOWN. ONLY THE GAINS SHOWN ARE DERIVED BY THE ALGORITHM GIVING BOTH THE FEEDBACK CONTROL AND THE COMPENSATOR.

Reduced state feedback control design. (From ref. 1.)

$$J = \int_0^\infty (y^T Q_y y + u^T R u) dt = x_0^T P x_0$$

$$\dot{x} = \begin{bmatrix} A_S & B_S & 0 & B_{D1} & 0 \\ 0 & A_A & 0 & B_{D2} & 0 \\ C_S & 0 & A_M & B_{D3} & 0 \\ 0 & 0 & 0 & A_D & 0 \\ 0 & 0 & 0 & 0 & A_C \end{bmatrix} x + \begin{bmatrix} 0 & 0 \\ I_A & 0 \\ 0 & 0 \\ 0 & 0 \\ 0 & I_C \end{bmatrix} u + \begin{bmatrix} 0 \\ 0 \\ 0 \\ C_D \\ 0 \end{bmatrix} w$$

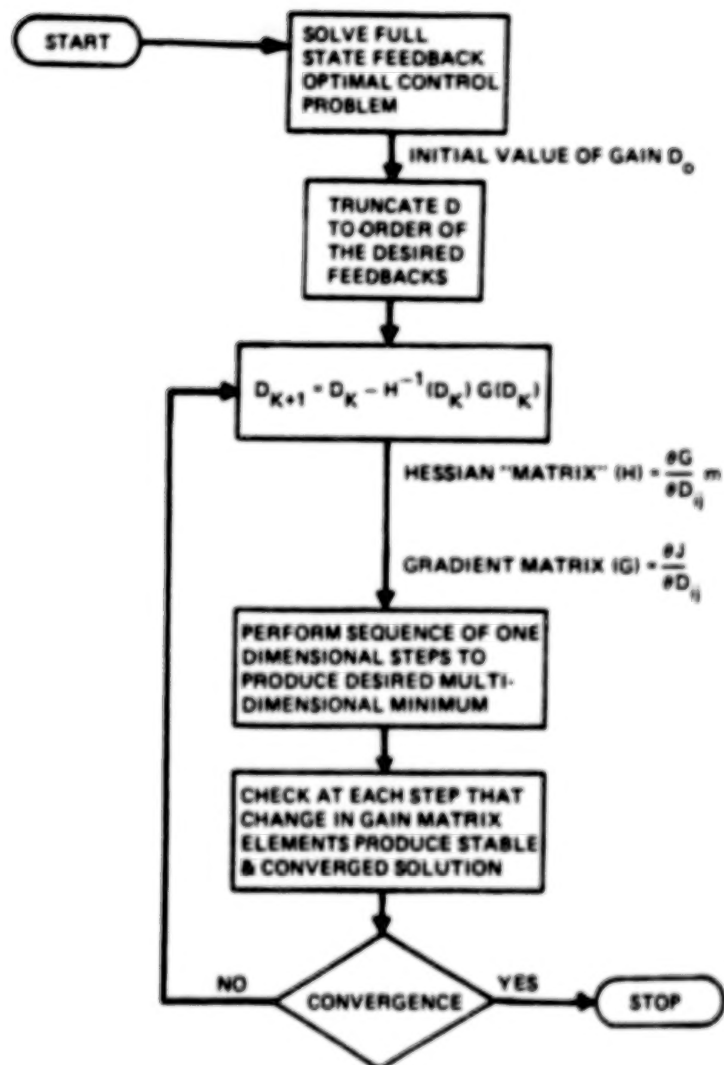
where

S = system
A = actuator
M = measurement
D = disturbance
C = compensator

System input: $u_S = K_1 y_M + K_2 x_C$ — determine compensator zeros
Compensator input: $u_C = K_3 y_M + K_4 x_C$ — determines compensator poles
 $y_M = C_M x_M$ is the measurement

$$K_1, K_2, K_3, K_4 \text{ minimize } x_0^T P x_0$$

Reduced state (output) feedback. (From ref. 1.)



Constrained optimal control. (From ref. 1.)

As was alluded to before, the reduced state design performance was 35×10^{-3} degrees compared to 6×10^{-3} degrees for the full state design (with no filter). Thus if the filter errors were included, the performances of the two designs were comparable. The robustness of the designs as determined from loop gain and phase margins was also comparable to that of the full state designs.

ACTUATORS		SENSORS AT ANTENNA							
		ROLL (X)		PITCH (Y)		YAW (Z)		ANTENNA TO FEED DISTANCE	
		POS	RATE	POS	RATE	POS	RATE	POS	RATE
RIGID BODY ROTATION ACTUATORS	REACTION WHEELS X Y Z	3E6	-2E7	6E6	-2E7	-1E5	-2E5		
ANTENNA ACTUATORS	2DOF GIMBAL MAST/BEAM WORM SCREW X Y	3E4	5E4	7E5	4E6			6E2	4E6
FULL STATE LOS RMS ERROR						6×10^{-3} DEG.			
REDUCED STATE LOS RMS ERROR						35×10^{-3} DEG.			

Gains for the reduced state design. (From ref. 1.)

REFERENCES

1. Gran, Richard; and Proise, Michael: Flexible Spacecraft Attitude Control. Research and Development Center Report No. RE-652, Grumman Aerospace Corp., Sept. 1982.
2. Gran, Richard: Control of Flexible Structures, A Systematic Overview of the Problem. Presented at NASA/JPL Conference on Applications of Distributed Control Techniques to Large Space Structures (Pasadena, CA), June 1982.

CURRENT STATUS OF
SYSTEM IDENTIFICATION METHODOLOGY

W. E. Larimore, R. K. Mehra, D. E. Gustafson, and J. Baillieul
Scientific Systems, Inc.
Cambridge, MA

Large Space Antenna Systems Technology - 1982
NASA Langley Research Center
November 30 - December 3, 1982

THE LARGE SPACE STRUCTURES PROBLEM

The proposed use of large space structures (LSS) poses some very challenging problems in the identification and control of high order dynamical systems. In addition some of these systems have requirements for very accurate pointing and shape control. These systems are infinite dimensional distributed parameter systems that are very lightly damped. It is not feasible to determine the LSS dynamics by earthbound testing so that the identification and control must take place largely in orbit in an adaptive manner after construction. To some degree, there may be requirements to identify the system dynamics and structural characteristics while under closed-loop control in orbit. This may severely restrict the type and amplitude of input signals which are allowable for enhancing identification of the system.

THE LARGE SPACE STRUCTURE PROBLEM

- STRINGENT REQUIREMENTS FOR SHAPE, ORIENTATION POINTING AND VIBRATION REDUCTION
- VERY LIGHTLY DAMPED—MANY SHARP RESONANCES
- DISTRIBUTED PARAMETER SYSTEM—INFINITE STATE ORDER
- LIMITED EARTHBOUND TESTING—MANY CHARACTERISTICS MUST BE DETERMINED IN ORBIT
- LIMITED PERTURBATION ALLOWED FOR SYSTEM IDENTIFICATION

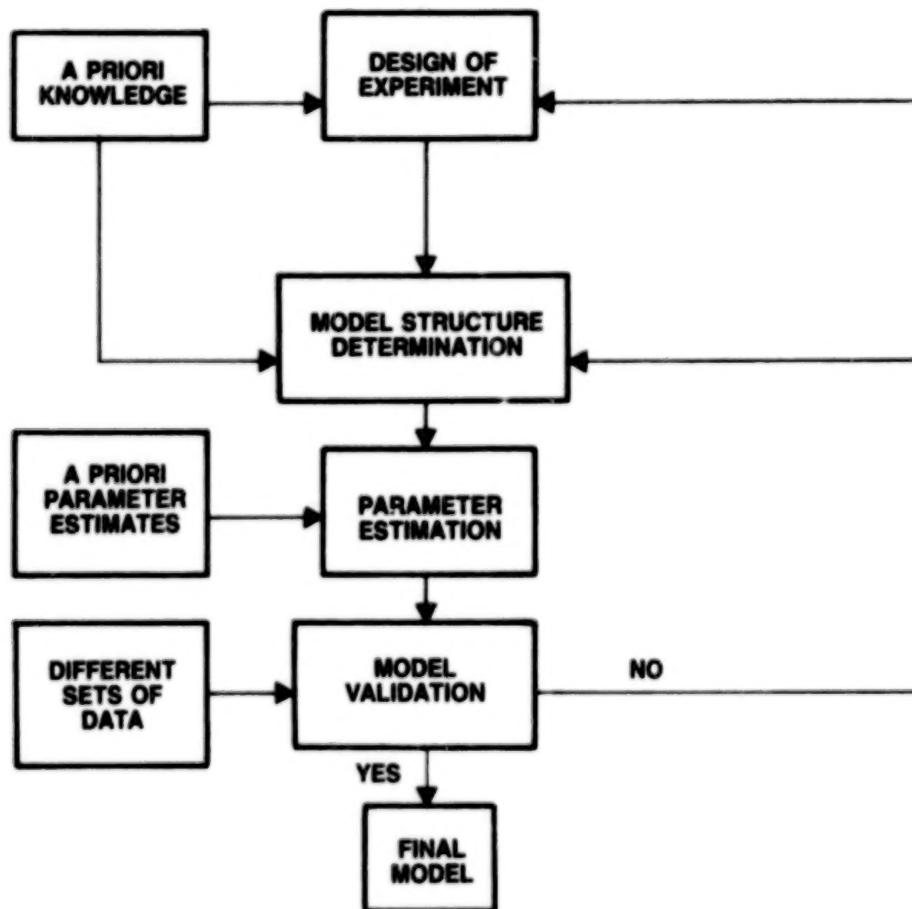
OBJECTIVE OF SYSTEM IDENTIFICATION

The objective of system identification varies considerably for the different schemes. In physical model identification, particular parameters of the structure describing mass, stiffness, and damping are considered the important quantities to determine. In empirical model identification, an input-output system description is obtained relating the control and other inputs to measured sensor outputs. Such an approach does not explicitly estimate structural parameters, but may offer advantages in obtaining a reduced-order model which accurately describes the important structural behavior. In control model identification or adaptive control, a plant (LSS) is to be identified while under closed-loop control. This may be the more important problem in some LSS systems. Identification while under control could also involve the use of either physical or empirical models as well as full- or reduced-order methods.

- DESCRIBING PHYSICAL CHARACTERISTICS AND PARAMETERS
 - STRUCTURAL PARAMETERS OF: STIFFNESS, DAMPING, MASS DISTRIBUTION
- EMPIRICAL DYNAMICS MODELING
 - TRANSFER FUNCTION, STATE SPACE, SPECTRAL ANALYSIS, REDUCED ORDER
- CONTROL MODEL IDENTIFICATION AND ADAPTIVE CONTROL

STEPS IN SYSTEM IDENTIFICATION

The complete system identification process consists of an iterative use of the four steps: 1) experimental design, 2) model structure determination, 3) parameter estimation, and 4) model validation. The purpose of experimental design is to select inputs and outputs, sensors, actuators and other variables in such a way that the remaining three steps of identification can be performed successfully. During model structure determination, a mathematical functional form for the model is selected with unknown parameters from a set of such functional forms. In estimation of these parameters in step 3), the use of a priori information about the parameters may be involved. In model validation, the validity of the model in describing various different sets of data is considered. The result of model validation is either a final validated model or a return to one of the other steps in the system identification process.



MODEL FORMULATION

In the problem formulation step, the LSS is generally described by a system of partial differential equations (PDE) in space x and time t together with an appropriate set of boundary conditions, where $u(x,t)$ is a vector of instantaneous displacements of the structure from equilibrium including both translational and rotational displacements, $F(x,t)$ are the applied forces and torques, Au is the restoring force, Du_t is the damping term, and $m(x)$ is the mass density. Observations $y(t)$ are considered to be linear combinations of translation and rotation displacements and their rates.

While there has been some work on identification of systems of PDE's (Goodson and Polis (1974)), the methods for identification of systems of ordinary differential equations (ODE) are more developed and better understood. Among the methods of spatial discretization of PDE, the finite element method is one of the more popular and produces a system of ODE's. Defining the state $x^T = (u^T, u_t^T)$ and inverting the mass matrix, this system can be written in the standard state-space form.

- DISTRIBUTED PARAMETER SYSTEM

$$m(x)u_{tt}(s,t) + Du_t(s,t) + Au(s,t) = F(s,t)$$

$$y(t) = Cu(s,t) + Eu_t(s,t)$$

- SPATIAL DISCRETIZATION AND REARRANGEMENT GIVES
STATE SPACE FORM

$$\dot{x}_r(t) = Ax(t) + Bf(t) + w(t)$$

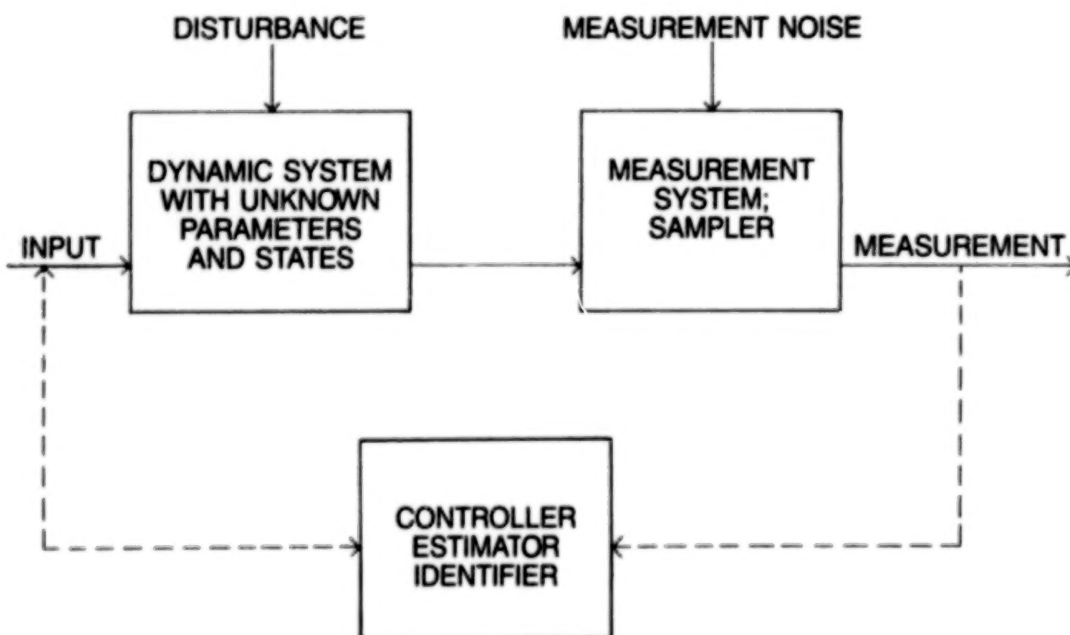
$$y(t) = Cx(t) + v(t)$$

- APPROXIMATION ERRORS—FINITE ORDER, LUMPED SYSTEM

EXPERIMENTAL DESIGN

The system considered for experimental design consists of a dynamic system (plant) with unknown parameters and states excited by an observed input and unobserved disturbance. The sampler and measurement system involves measurement noise. From knowledge of the input and output measurements, the estimator determines a state estimate, the identifier estimates unknown parameters, and the controller determines a signal, using the measurements, to feed back to the input.

The basic experimental design problem addresses the questions 1) what measurements to make, 2) when to make them, and 3) what input to use in the experiment. Experimental design thus involves selection of initial conditions, input signals, sensors, their location, sampling rates, and other aspects of LSS test design to enhance the identifiability of unknown parameters. Systematic procedures exist for solving these problems (Mehra (1974, 1976, 1981)). For LSS identification, the use of inputs in addition to control inputs may be required to assure identifiability of the unknown parameters. Such additional inputs to excite various structural modes sufficiently for identification may lead to motions unacceptable in terms of control requirements. It may be necessary to select inputs in such a way that modes over a limited frequency band are excited.



DESIGN PROBLEMS:

1. WHAT TO MEASURE
2. WHEN TO MAKE MEASUREMENTS
3. WHAT INPUT TO USE (DUAL CONTROL)

MODEL ORDER AND STRUCTURE DETERMINATION

Suppose a parametric model form is chosen which could involve a physical structural model or a mathematical form such as an autoregressive or polynomial form. A particular model structure corresponds to specifying which parameters are considered fixed and known and which are unknown (to be estimated). The alternative model structures are fitted to the observed data; i.e., the unknown parameters are estimated. A variety of methods are available for comparing a set of alternative model structures. Some of these are (a) information criteria (Larimore (1982, 1983a), Akaike (1974a), Rissanen (1976)); (b) rank tests (Tse and Weinert (1975), Van Den Boom and Van Den Enden (1974), Wellstead (1978)); (c) goodness of fit tests (Parzen (1974)); and (d) generalized likelihood ratio tests (Larimore (1977)). These methods can be used to supplement physically based methods of model structure determination.

- CHOOSE PARAMETRIC MODEL FORM
 - E.G., POLYNOMIALS, PHYSICAL STRUCTURE, AUTOREGRESSIVE
- CHOOSE PARTICULAR ALTERNATIVE MODEL STRUCTURES AND ORDERS TO BE COMPARED — I.E., WHICH PARAMETERS ARE SPECIFIED OR UNKNOWN
- FIT THESE PARTICULAR MODELS (ESTIMATE PARAMETERS)
- COMPARE ALTERNATIVE MODEL FITS
 - GOODNESS OF FIT (CHI-SQUARED, ETC.)
 - GENERALIZED LIKELIHOOD RATIO TESTS
 - INFORMATION OR ENTROPY MEASURES (AKAIKE'S AIC)

(1974(a))

PARAMETER ESTIMATION METHODS

The field of parameter estimation is very vast in scope, but has been summarized quite well in several survey papers, volumes and books (e.g. Eykhoff (1974), Kailath (1974), Mehra and Lainiotis (1976), Young (1979)). A very broad classification of parameter estimation methods may be done as follows: (1) equation error methods (including linear least squares, instrumental variable, etc), (2) output error methods (including nonlinear least squares, quasi-linearization, extended Kalman filter, etc.), and (3) prediction error methods (including maximum likelihood, Bayesian and maximum entropy).

The above ordering represents increasing complexity, generality and accuracy (or estimation efficiency). Output error and prediction error methods require nonlinear searches and therefore need good starting values. Equation error methods, though less accurate, can provide good starting estimates if they are used properly. Another major advantage of equation error methods is that they can be made recursive with respect to both model order and sample size. The order-recursive property is useful for on-line identification and adaptive control. Equation error methods have another interesting property for multiinput-multioutput systems: parameter estimation can be done one equation at a time. In aircraft parameter identification (Mehra and Tyler (1973)), a combination of the equation error method to obtain starting values and the maximum likelihood method to refine the parameter estimates was found to have the best performance in terms of convergence and accuracy.

- LEAST SQUARES, EQUATION ERROR, OR REGRESSION
- INSTRUMENTAL VARIABLES
- OUTPUT ERROR
- EXTENDED KALMAN FILTER (PARAMETERS AS STATES)
- MAXIMUM LIKELIHOOD

PARAMETER ESTIMATION DIFFICULTIES

The parameters of a model are identifiable if a change in any of the parameters results in a change in the distribution of the measurement random variables. The selected parameter set should be identifiable and related easily to physically meaningful coefficients. In the case of poor identifiability, some parameters or functions of the parameters have very little effect upon the expected observations and may need to be constrained to some fixed nominal value in order to estimate the other parameters. In many realistic parameter estimation problems, there is a very nonlinear dependence of the output observations on the parameters. To find the optimum set of parameters requires a sophisticated and robust optimization procedure such as the quadratic hill-climbing (also called Levenberg-Marquardt) method. The presence of both measurement noise and input process noise considerably complicates the methods and effort required for good parameter identification, and usually necessitates the use of a Kalman filter or equivalent approach to compute a white innovation sequence for which a likelihood function is easily evaluated. On-line procedures are especially attractive in adaptive control schemes, but some of these such as the extended Kalman filter with some states as parameter estimates may diverge in some situations. An algorithm with guaranteed convergence properties is much to be preferred.

- **POOR IDENTIFIABILITY—LARGE CHANGES IN PARAMETERS HAVE VERY SMALL EFFECT ON EXPECTED OBSERVATIONS**
 - NEED TO FIX SOME OF PARAMETERS
- **NONLINEAR DEPENDENCE OF OUTPUT ON PARAMETERS**
 - USE ROBUST QUADRATIC HILL-CLIMBING OPTIMIZATION
- **SENSOR AND INPUT (PROCESS) NOISE**
 - REQUIRES KALMAN FILTER OR SIMILAR APPROACH
- **DIVERGENCE OF SOME ON-LINE PROCEDURES**

MODEL VALIDATION

The objective of model validation is to determine if the identified model predicts the observed response, not only for the data used for identification but also for other available data sets. There are a number of procedures for evaluating the validity of an identified model on a given data set. Residual analysis involves the analysis of residuals or innovations to determine if they are indeed white noise or have significant correlation properties indicating the presence of unmodeled structure in the process. The adequacy of a model can be evaluated by comparing it with the response predicted by more general or higher order models. Such a comparison can be made on a sound theoretical basis using the AIC procedure (Akaike (1974a)) which has a likelihood interpretation (Larimore (1982, 1983a)). Data splitting and cross-validation methods involve using part of one set of data in fitting the model and the rest of that data set in evaluating the adequacy of the prediction. And of course the model may also be required to satisfy certain reasonability requirements for particular problems such as stability, stationarity, positive definiteness, causality, etc.

- DOES THE IDENTIFIED MODEL PREDICT THE OBSERVED RESPONSE
- RESIDUAL ANALYSIS (CORRELATION & WHITENESS TESTS)
- COMPARE RESPONSES PREDICTED BY VARIOUS MODELS
- COMPARE LIKELIHOOD OF VARIOUS MODELS (AIC)
- DATA SPLITTING AND CROSS-VALIDATION METHODS
- REASONABILITY TESTS

REDUCED ORDER MODELING AND IDENTIFICATION

The Akaike stochastic realization (Akaike (1974b), (1976)) method identifies a multioutput system in a canonical form using the method of canonical correlations and variates. It has been used successfully by Mehra (1978) for multiple time series modeling and forecasting. The method has been extended to include measured inputs in the presence of noise (Larimore (1983b)). One obtains in this fashion a transfer function model. The parameters are asymptotically efficient and order determination is done automatically using an approximate AIC procedure. The use of a singular value decomposition is a major computational advantage of this method over other methods so that no iterative nonlinear optimization problem needs to be solved. All order state space models up to a given order are determined simultaneously from one singular value decomposition. Furthermore, since a state vector model is identified, it can be related to a physical model and used to provide an alternative set of estimates for the physical parameters.

- THE CANONICAL VARIATE METHOD (AKAIKE (1974b, 1976))
- DECOMPOSE CORRELATION STRUCTURE OF RECENT PAST AND NEAR FUTURE
- OPTIMAL CHOICE OF REDUCED ORDER STATE SPACE STRUCTURE
- COMPUTATION VIA SINGULAR VALUE DECOMPOSITION
— NUMERICALLY ACCURATE, STABLE, EFFICIENT
- DETERMINES OPTIMAL MODELS FOR ALL ORDERS AT ONCE
- APPROXIMATE AIC FOR CHOOSING OPTIMAL ORDER

CLOSED-LOOP IDENTIFICATION

Identification of a plant while under closed-loop control has some special problems that were not fully appreciated until recently (Caines and Chan (1976), Ljung et al. (1974), Phadke and Wu (1974)). Much of the difficulty stems from the correlation between past outputs and future inputs of the plant. Many identification procedures explicitly or implicitly assume that there is independence between past outputs and future inputs. The application of these procedures has been shown to lead to biased and inefficient parameter estimates and in some cases loss of parameter identifiability. More sophisticated procedures allow for correlation between past outputs and future inputs such as the maximum likelihood and canonical variate analysis procedures. Some methods do not explicitly constrain the identified plant model to be causal which can lead to unreasonable results. If a closed-loop identification procedure is used on-line while the system is under control, additional gain margin or other precautions may be required to insure control system stability.

- CORRELATION BETWEEN PAST OUTPUTS AND FUTURE INPUTS
- MOST SYSTEM IDENTIFICATION PROCEDURES DO NOT ALLOW FOR THIS AND GIVE BIASED ESTIMATES
- CANONICAL VARIATE ANALYSIS WILL ALLOW FOR SUCH CORRELATION
- IT IS IMPORTANT TO MAINTAIN STABLE CONTROL WHILE IDENTIFYING THE PARAMETERS

ISSUES IN LSS SYSTEM IDENTIFICATION

The LSS control and identification problem has a number of crucial, practical difficulties which are not present in most other systems. The system is fundamentally a distributed system, and finite order state-space models are only an approximation. A very high state order may be required to model all of the aspects of interest from the structural, input-output, and control system points of view. In terms of a primary control objective, empirical reduced-order modeling which includes the states of dominant influence on control is a promising approach to the problem. Recent advances in reduced-order modeling with flexible weighting criteria involve the use of numerically stable and efficient computational methods. Other issues which must be addressed include maintaining control system stability while adapting parameters in on-line adaptive control schemes. In some situations, such as calibration after initial deployment, additional input signals for model identification may be required, and these may have to be designed to excite specific models of the system so that the number of parameters during a single identification experiment can be kept small.

- PHYSICAL STATE SPACE MODELS ARE ONLY APPROXIMATE
- HIGH SYSTEM STATE ORDER
- LARGE NUMBER OF PARAMETERS
- REDUCED-ORDER MODELING PROBABLY NECESSARY
- PRIMARY OBJECTIVE OF IDENTIFICATION IS CONTROL
- EMPIRICAL REDUCED ORDER IDENTIFICATION ATTRACTIVE
- MUST MAINTAIN CONTROL SYSTEM STABILITY WHILE ADAPTING PARAMETERS
- INPUT SIGNALS FOR MODEL IDENTIFICATION MAY BE SEVERELY RESTRAINED

REFERENCES

- Akaike, H. (1974a) A New Look at Statistical Model Identification. *IEEE Trans. Auto. Control*, vol. AC-19, pp. 716-723.
- Akaike, H. (1974b) Stochastic Theory of Minimal Realizations. *IEEE Trans. Auto. Control*, vol. AC-19, pp. 667-674.
- Akaike, H. (1976) Canonical Correlation Analysis of Time Series and the Use of an Information Criterion. *System Identification: Advances and Case Studies*, R. K. Mehra and D. G. Lainiotis, eds., New York: Academic Press.
- Caines, P. E., and Chan, C. W. (1976) Estimation, Identification and Feedback. *System Identification: Advances and Case Studies*, R. K. Mehra and D. G. Lainiotis, eds., New York: Academic Press.
- Eykhoff, P. (1974) *System Identification*. New York: John Wiley & Sons.
- Goodson, R. E., and Polis, M. P., eds. (1974) *Identification of Parameters in Distributed Systems*. New York: ASME Publ.
- Kailath, T., ed. (1974) *IEEE Trans. Automatic Control - Special Issue on Identification*. New York: IEEE.
- Larimore, W. E. (1977) Nontested Tests on Model Structure. *Proc. Joint Automatic Control Conf. (San Francisco, CA)*, New York: IEEE, pp. 686-690.
- Larimore, W. E. (1982) A Survey of Some Recent Developments in System Parameter Identification. *Proc. 6th IFAC Symposium on Identification and System Parameter Estimation*, vol. 1, A. Bekey, ed., Oxford: Pergamon Press, pp. 979-984.
- Larimore, W. E. (1983a) Predictive Inference, Sufficiency, Entropy, and an Asymptotic Likelihood Principle. *Biometrika*, in press.
- Larimore, W. E. (1983b) System Identification, Reduced-Order Filtering and Modeling Via Canonical Variate Analysis. *Proc. 1983 American Control Conference*, H. S. Rao and T. Dorato, eds., New York: IEEE.
- Ljung, L., Gustavsson, I., and Soderstrom, T. (1974) Identification of Linear Multivariable Systems Operating Under Linear Feedback Control. *IEEE Trans. Auto. Control*, vol. AC-19, pp. 836-840.
- Mehra, R. K. (1974) Optimal Input Signals for Parameter Estimation in Dynamic Systems: Survey and New Results. *IEEE Trans. Auto. Control*, vol. AC-19, pp. 753-768.
- Mehra, R. K. (1976) Synthesis of Optimal Inputs for Multi-Input Multi-Output (MIMO) Systems With Process Noise. *System Identification, Advances and Case Studies*, R. K. Mehra and D. G. Lainiotis, eds., New York: Academic Press.
- Mehra, R. K. (1978) A Survey of Time-Series Modeling and Forecasting Methodology. *Modeling, Identification and Control in Environmental Systems*, E. Vansteenkiste, ed., North Holland Publ. Co.

- Mehra, R. K. (1981) Choice of Input Signals. Trends and Progress in System Identification, P. Eykhoff, ed., IFAC, Oxford: Pergamon Press.
- Mehra, R. K., and Lainiotis, D. G., eds. (1976) System Identification: Advances and Case Studies. New York: Academic Press.
- Mehra, R. K., and Tyler, J. S. (1973) Case Studies in Aircraft Parameter Identification. Proc. 3rd IFAC Conf. on Identification and System Parameter Estimation, P. Eykhoff, ed., Oxford: Pergamon Press, pp. 117-144.
- Parzen, E. (1974) Some Recent Advances in Time Series Modeling. IEEE Trans. Auto. Control., vol. AC-19, pp. 723-730.
- Phadke, M. S., and Wu, S. M. (1974) Identification of Multiinput-Multioutput Transfer Function and Noise Model of a Blast Furnace From Closed-Loop Data. IEEE Trans. Auto. Control, vol. AC-19, no. 6, pp. 944-951.
- Rissanen, J. (1976) Minimax Entropy Estimation of Models for Vector Processes. System Identification: Advances and Case Studies, R. K. Mehra and D. G. Lainiotis, eds., New York: Academic Press.
- Tse, E., and Weinert, H. L. (1975) Structure Determination and Parameter Identification for Multivariable Stochastic Linear Systems. IEEE Trans. Auto. Control, vol. AC-20, pp. 603-613.
- Van Den Boom, A. J. W., and Van Den Enden, A. W. M. (1974) The Determination of the Orders of Process and Noise Dynamics. Automatica, vol. 10, pp. 245-256.
- Wellstead, P. E. (1978) An Instrumental Product Moment Test for Model Order Estimation. Automatica, vol. 14, pp. 89-91.
- Young, P. C. (1979) Parameter Estimation for Continuous Time Models - A Survey. Proc. of 5th IFAC Symposium on Identification and System Parameter Estimation, R. Isenmann, ed., Oxford: Pergamon Press, pp. 17-41.

COMPUTER ANALYSIS AND GROUND TESTING
OF
LARGE SPACE SYSTEMS CONTROL STRATEGIES

J. N. Aubrun and J. A. Breakwell
Lockheed-California
Palo Alto, California

Large Space Antenna Systems Technology - 1982
NASA Langley Research Center
November 30 - December 3, 1982

INTRODUCTION

This presentation is a summary of the investigations undertaken at Lockheed Missiles & Space Co. for the past few years in the area of large space structure (LSS) control. Both analytical and experimental results are presented. Control strategies were developed and their validity was tested on somewhat realistic models of large spacecraft, principally on the computer model developed by Charles Stark Draper Laboratory, the so-called CSDL #2 model. The research was also directed toward experimental validations. These are very unique and constitute an essential step in the LSS control technological developments.

Participating in this research were Integrated Systems, Inc., for analytical developments and Synergistic Technology, Inc., for hardware and control software implementations.

TECHNOLOGY DEVELOPMENTS OVERVIEW

Two distinct problems were addressed in this research. The first concerns the active injection of damping in the structure, the so-called "modal damping" approach. The Low Authority Control (LAC) technique, which is based on collocated actuators and sensors with low gain rate feedback loops, was used for broadband but moderate damping. The High Authority Control (HAC), which is based on linear quadratic Gaussian (LQG) techniques with a generally non-collocated system of actuators and sensors, was used to obtain large amounts of damping in specific vibration modes.

The second problem concerns the rejection of on-board disturbances with given power spectrum density (PSD). Optimal control is the technique used to achieve high performance in this case; the control laws are minimizing a performance metric and usually affect the mode shapes more than the poles themselves.

DAMPING AUGMENTATION

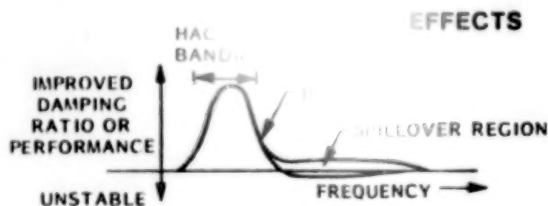
	PERFORMANCE	LIMITATIONS
BROADBAND	15% OF CRITICAL	SENSOR/ACTUATOR TYPES, LOCATIONS
SPECIFIC MODES	50% OF CRITICAL	MODEL (IDENTIFICATION) SENSITIVITY

DISTURBANCE REJECTION ON PERFORMANCE METRIC

	PERFORMANCE	LIMITATIONS
NARROWBAND	3 TO 4 ORDERS OF MAGNITUDE	SYSTEM ID OF MODEL AT DISTURBANCE FREQUENCY
BROADBAND	2 ORDERS OF MAGNITUDE	SENSOR NOISE, PERFORMANCE MEASUREMENT

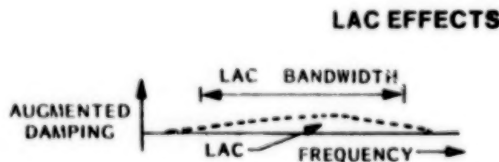
HIGH- AND LOW-AUTHORITY CONTROL INTEGRATION

The simultaneous use of HAC and LAC in the control design is explained by this chart. The necessarily finite bandwidth of the HAC controller provokes the phenomenon called "spillover"; i.e., a destabilization of the vibration modes situated in the roll-off region. This is generally not exactly predictable because modal frequencies and shapes are poorly known in this region. This instability can, however, be compensated for by the use of a superimposed LAC system, which is very insensitive to model errors and can provide the necessary broadband damping. So, in this integrated system, HAC is used to achieve performance, LAC to achieve stability.



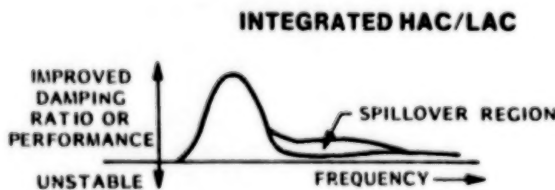
HIGH AUTHORITY

- LARGE DAMPING RATIO CHANGES
- EIGENVECTOR CHANGES
- LQG SYNTHESIS WITH FREQUENCY SHAPING
- ENHANCED CONVENTIONAL LQG ROBUSTNESS



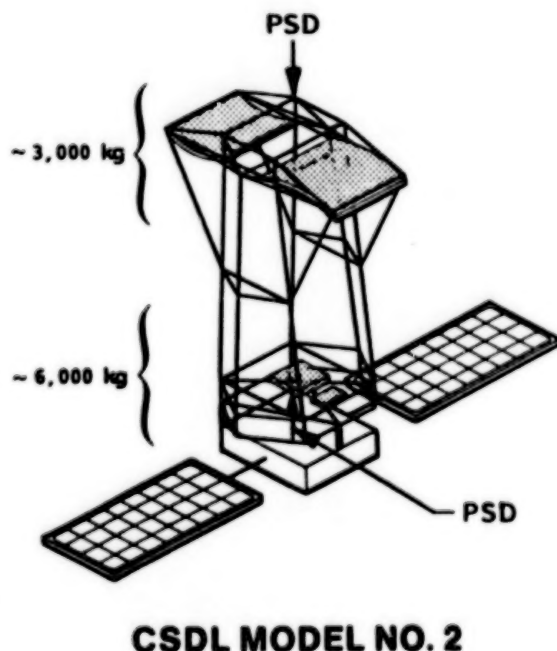
LOW AUTHORITY

- BROADBAND DAMPING AUGMENTATION
- ROBUST AGAINST MODELING ERROR
- SIMPLIFIED SYNTHESIS (LEAST SQUARES, JACOBI'S PERTURBATION)



ANALYTICAL STUDIES TEST MODEL (CSDL #2)

The main model for analytical studies and computer simulations has been the CSDL #2 finite element model of an optical space system. This structure contains three mirrors and a focal plane and is excited by two disturbances, one on top and one on the bottom, as shown in the picture. The problem was to reduce the line-of-sight (LOS) error using active control. To evaluate the robustness of the controller, two perturbed models were created by Draper Laboratory (P2 and P4), where stiffness and mass of some elements had been modified. A typical example of the resulting spectrum for the original (solid line) and the perturbed models (dotted lines) is shown in the picture.



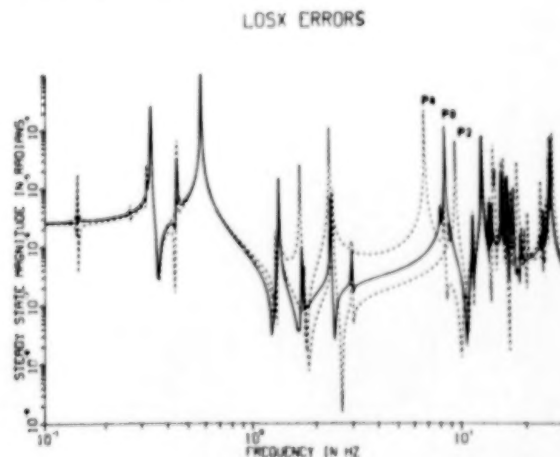
CHARACTERISTICS

- HEIGHT - 28 m, WEIGHT 9,300 kg
- 306 DOF
- 137 STIFFNESS ELEMENTS
- 51 NODES
- 84 NONZERO MASS ELEMENTS

CONTROL IMPLEMENTATION

- 3 RIGID-BODY MODES
- 41 FLEXIBLE MODES

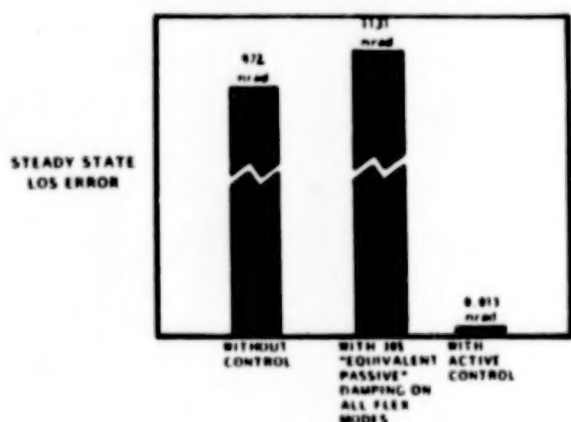
DYNAMICS



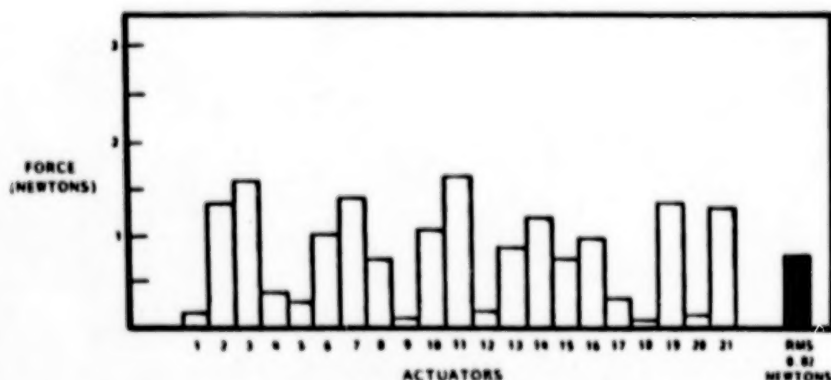
SINE DISTURBANCE REJECTION - CSDL #2

The case of sinusoidal disturbances was looked at first. The top bar chart shows a comparison between the open-loop LOS error on the left and the closed-loop LOS error on the right. Several orders of magnitude reduction was shown to be achievable (at least on the computer). This result was obtained by combining LQG techniques with a frequency shaping method, which increases the penalty function at the disturbance frequency. The middle value resulted from the blind application of 30% of critical damping in all modes. It shows that in this case, damping was not the solution, and tended to facilitate the transmission of energy between the disturbance sources and the line of sight.

The bottom chart shows the control effort of the 21 actuators that were used in this example. Very little control effort was needed. Again this is because this control system acts more by modifying the eigenvectors of the system than by trying to freeze the whole structure.



LOS PERFORMANCE



CONTROL EFFORT

INPUT DISTURBANCE

- TOP - 10 N AT 10 Hz
- BOTTOM - 20 N AT 5 Hz

CONTROL IMPLEMENTATION

- FREQUENCY SHAPED HAC
- LAC STABILITY AUGMENTATION
- 12-MODE CONTROL DESIGN MODEL
- 44-MODE EVALUATION MODEL
- SENSOR NOISE NOT INCLUDED

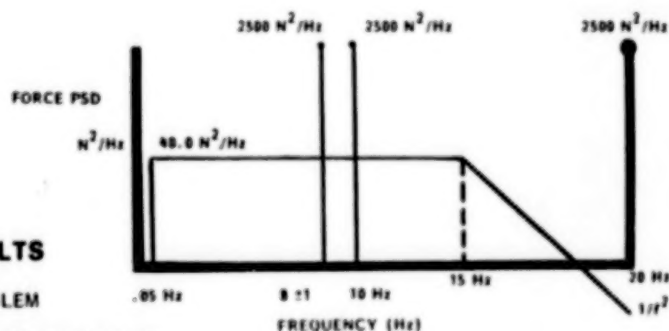
PERFORMANCE

- 10^5 REDUCTION IN LOS ERROR
- ROBUST OVER P_0, P_2, P_4

DISTURBANCE REJECTION PSD

A more complete problem was addressed by using a PSD model (defined by Riverside Research) containing continuous wide-band as well as discrete distributions. In this case, the sinusoidal excitations were still very easily eliminated. The 20-Hz disturbance was in the unmodelled frequency range and system identification would have been required to properly design the controller. Once this assumption is made (i.e. the system's transfer function at 20 Hz is known) this disturbance can be eliminated along with the others using the same frequency shaping techniques.

The wide-band PSD was the most difficult to reduce. However, two orders of magnitude reduction was achieved, as shown in the figure.



• WIDEBAND DISTURBANCE RESULTS

- DOMINATES THE CONTROL PROBLEM
- ACHIEVES 2 ORDER-OF-MAGNITUDE REDUCTION
- REQUIRES RSS CONTROL EFFORT COMMENSURATE WITH DISTURBANCE
- ACHIEVES HIGHER PERFORMANCE THROUGH ONLINE SYSTEM ID
- RIGID-BODY MODE STABILITY IS SENSITIVE TO LOW-FREQUENCY MODELING ERROR

• SINUSOIDAL DISTURBANCE RESULTS

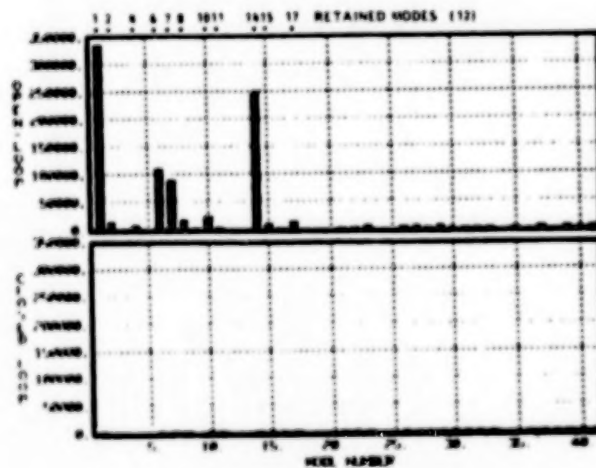
- IN-BAND DISTURBANCE EFFECTS ELIMINATED
- REJECTION IS ENSURED IF CLOSED-LOOP SYSTEM IS STABLE
- RELATIVELY LOW RSS CONTROL EFFORT
- OUT-OF-BAND DISTURBANCES REQUIRE SYSTEM ID AT DISTURBANCE FREQUENCIES

LSS CONTROL - ANALYTICAL RESULTS

The HAC/LAC control laws, designed on a reduced 12-mode model, were tested with success on the full 41 mode evaluation model and the two perturbation models. The nominal performance results are depicted in this chart. The bottom bar graph shows the contribution to the total cost of each separate mode in open and closed-loop cases. In the closed-loop case, the cost of the modes being controlled becomes on the same order as the cost of the unmodelled modes, which is, of course, the limiting, nonreducible factor.

	OPEN-LOOP	HAC/LAC	REDUCTION FACTOR
RMS LOS x (nrad)	114110	3273.0	34.87
RMS LOS y (nrad)	425390	4636.2	91.75
TOTAL RSS LOS (nrad)	441430	5675.1	77.61
RSS CONTROL EFFORT (N)	0	63.46	

PERFORMANCE RESULTS



COMPONENT COST

EXPERIMENTAL DEVELOPMENTS OVERVIEW

This chart summarizes the main achievement of the experimental program. This is basically the laboratory validation of the control technology on test structures exhibiting the most critical properties expected from LSS (mainly low damping, close frequencies, and a requirement for distributed systems of actuators and sensors). The significant result is that it is indeed feasible to design and implement on 3-D structures optimal controllers with predictable and reasonable performance.

**OBTAINED FIRST STABLE CLOSED-LOOP CONTROL
OF FULL 3-D EXPERIMENTIAL STRUCTURE**

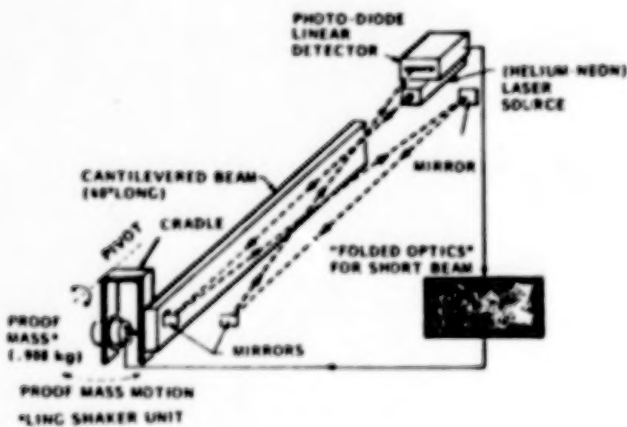
**USED REAL SPACE INSTRUMENTATION
FOR SENSING AND ACTUATION**

**DESIGNED CONTROL SYSTEM USING SYSTEMATIC,
MODERN CONTROL APPROACH**

**DEMONSTRATED CONTROL OF MULTIINPUT
MULTIOUTPUT SYSTEM WITH
NEARLY REPEATED MODAL FREQUENCIES**

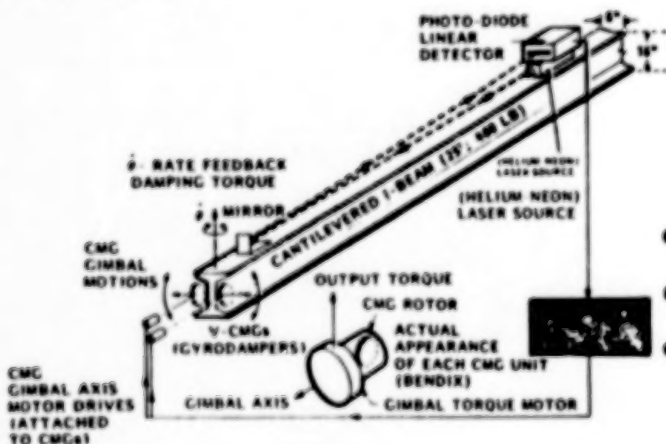
EARLY EXPERIMENTAL DEMONSTRATIONS

Historically, the experimental program started in 1978 with some simple demonstrations of control concepts. Proof mass actuators and control moment gyros were used in separate experiments to show the real possibilities of actively damping beam vibrations. Collocated rate feedback mechanizations were used very successfully in these early tests, with simple but efficient optical sensing using laser beams, mirrors and linear detectors. The vibration was damped either by a reaction force (proof mass actuators) or a gyroscopic torque (CMGs) opposing the rate of change of the corresponding variable (i.e. tip displacement and tip rotation respectively).



MINIBEAM LAC DEMONSTRATION

- 40-in. BEAM, LASER OPTICS
- PROTOTYPE PROOF MASS TESTED
- LAC CONCEPT - 2-MODE DEMONSTRATION
- 50 PERCENT DAMPING PRODUCED - MODE 1
- 20 PERCENT DAMPING PRODUCED - MODE 2



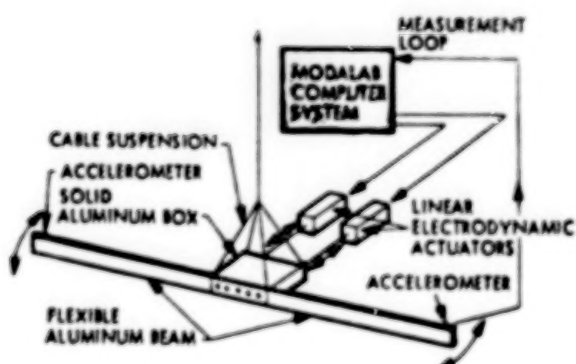
MAXIBEAM LAC DEMONSTRATION

- 400-lb 25-ft BEAM, 1-Hz LASER OPTICS
- CMG BEAM END ROTATION CONTROL
- > 20 PERCENT DAMPING - MODES 1 AND 7

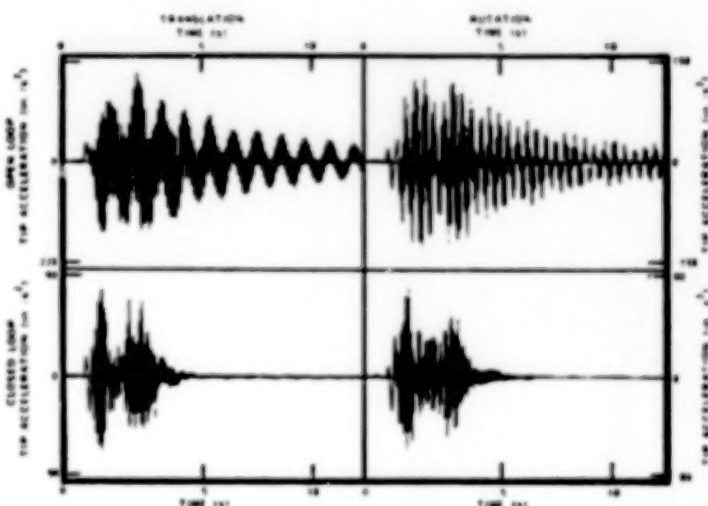
TOYSAT EXPERIMENT SETUP

First of the digital control experiments, the "Toysat" setup consists of a 12-ft flexible beam fastened to the side of a 1.3-ft square block of aluminum. To accentuate bending, a 2-lb. weight is attached to each end of the beam. The beam is suspended from the ceiling in such a way as to allow free motion in the horizontal plane.

Control of the motion of the specimen is provided by two linear actuators. When the actuators act together, translational motion results, and when equal but opposite commands are given, pure rotational motion results. Sensing is provided by accelerometers mounted at the ends of the flexible beam and by linear position sensors mounted in tandem with the linear actuators.



EXPERIMENT



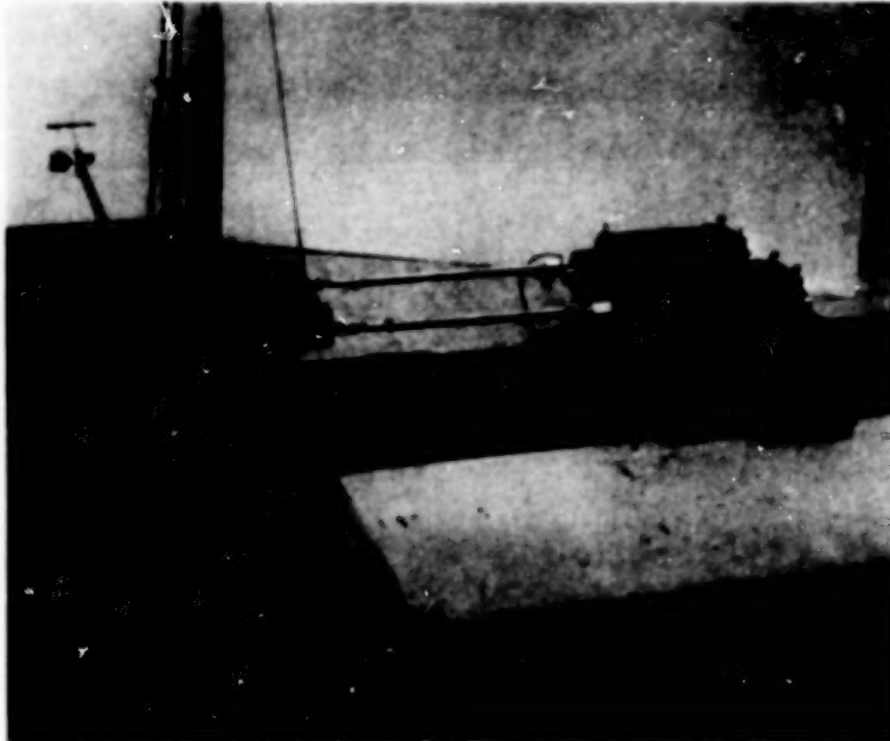
RESULTS

HAC DEMONSTRATED — FOR TRANSLATION AND ROTATION, RIGID-BODY AND 2 FLEXIBLE MODES

- NONCOLLOCATED ACTUATORS AND SENSORS
- DIGITAL MECHANIZATION WITH CSPI MAP-200 ARRAY PROCESSOR
- ELECTROSESIS ACTUATORS TIED TO LABORATORY FRAME

TOYSAT SLEWING EXPERIMENT

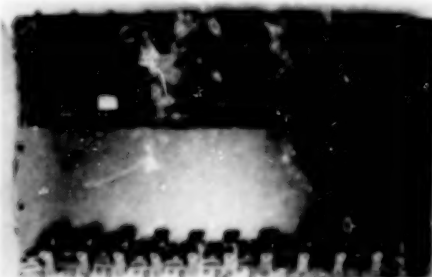
The Toysat was originally designed as an experiment to test optimal slewing techniques. These were closed-loop slewing strategies which left an arbitrary number of bending modes quiescent at the end of the slewing maneuver. Upon the successful conclusion of these experiments, the Toysat was used to demonstrate a twelve-state HAC controller, with which two rigid-body and four bending modes were subdued using the central actuators.



NEW CONTROL HARDWARE

In order to meet the special requirements arising from this new field of LSS control, special hardware needed to be developed. Precise sensing of very small vibration amplitudes (submicron) such as are needed for optical systems, with the capability for simultaneous multichannel and wide bandwidth, was achieved with the development of the "microphase" sensor. This sensor measures the phase changes between outgoing and incoming laser beams (reflected by corner cube mirrors on the structure). Inertially reacted actuators for space application, capable of applying vibratory forces to the structure with precision and bandwidth, were developed in the form of the pivoted proof mass (PPM) actuator. An internal velocity servo-loop makes this actuator very linear in frequency and amplitude.

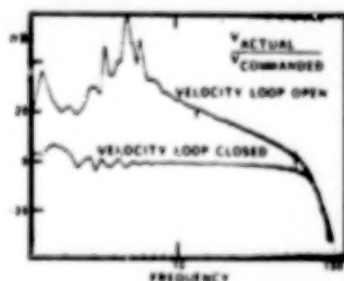
MICROPHASE MULTICHANNEL SENSING



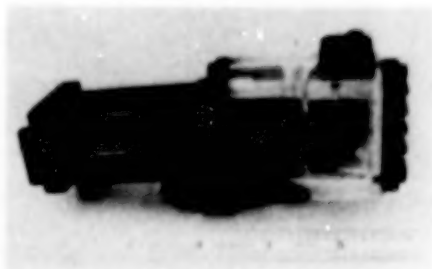
MICROPHASE OPTICS PACKAGE

- 10-CHANNEL "STARRING" SYSTEM
- 0.08 μm RESOLUTION
- 20 kHz BANDWIDTH
- DIGITAL 12-BIT OUTPUT
- BRAGG CELL MODULATION TECHNIQUE

PIVOTED PROOF-MASS ACTUATOR



RESPONSE



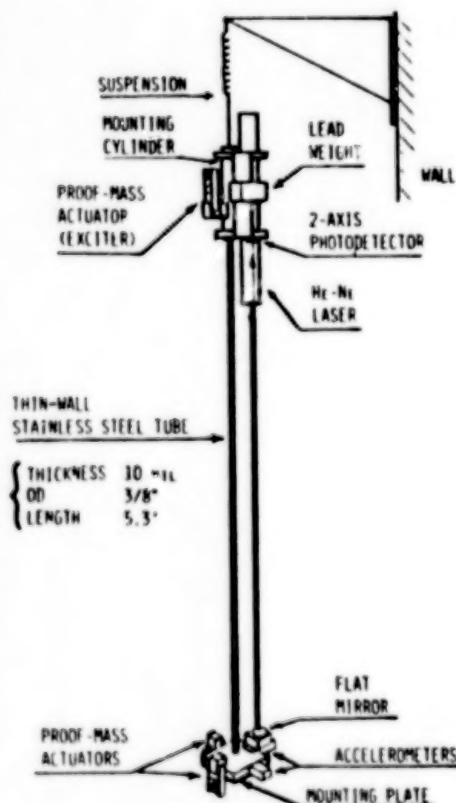
PPM ACTUATOR

- VELOCITY-CONTROLLED PROOF-MASS
- ELECTRODYNAMIC MOTOR
- RUGGED, FLEXURE SUSPENSION
- INERTIALLY REACTED
- SIMPLE TO MODEL
- SCALING LAWS DEVELOPED
- IMPLEMENTABLE FOR FLIGHT

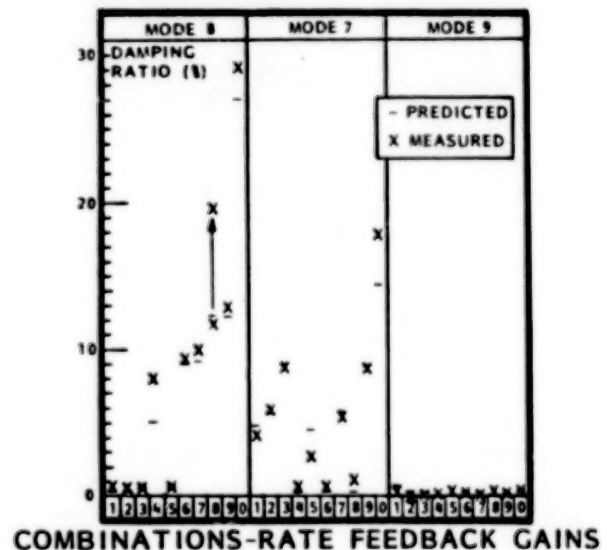
- EXPERIMENTAL RESULTS -

SLIM BEAM TEST

This experiment was directly aimed at verifying the LAC theory and was the first to use the PPM actuators. This vertically suspended slim beam was controlled in two axes by two PPMs situated at its free end. Sensing was purely optical, measuring the angular difference between the two ends. Thus the controller was not purely collocated nor consistent, and consequently it violated the unconditional stability characteristic of LAC systems. Nevertheless, a careful finite element model was constructed, and measured results were in excellent agreement with the predicted values, including the stability limits due to the noncollocation/nonconsistency effects.



SLIM BEAM TEST

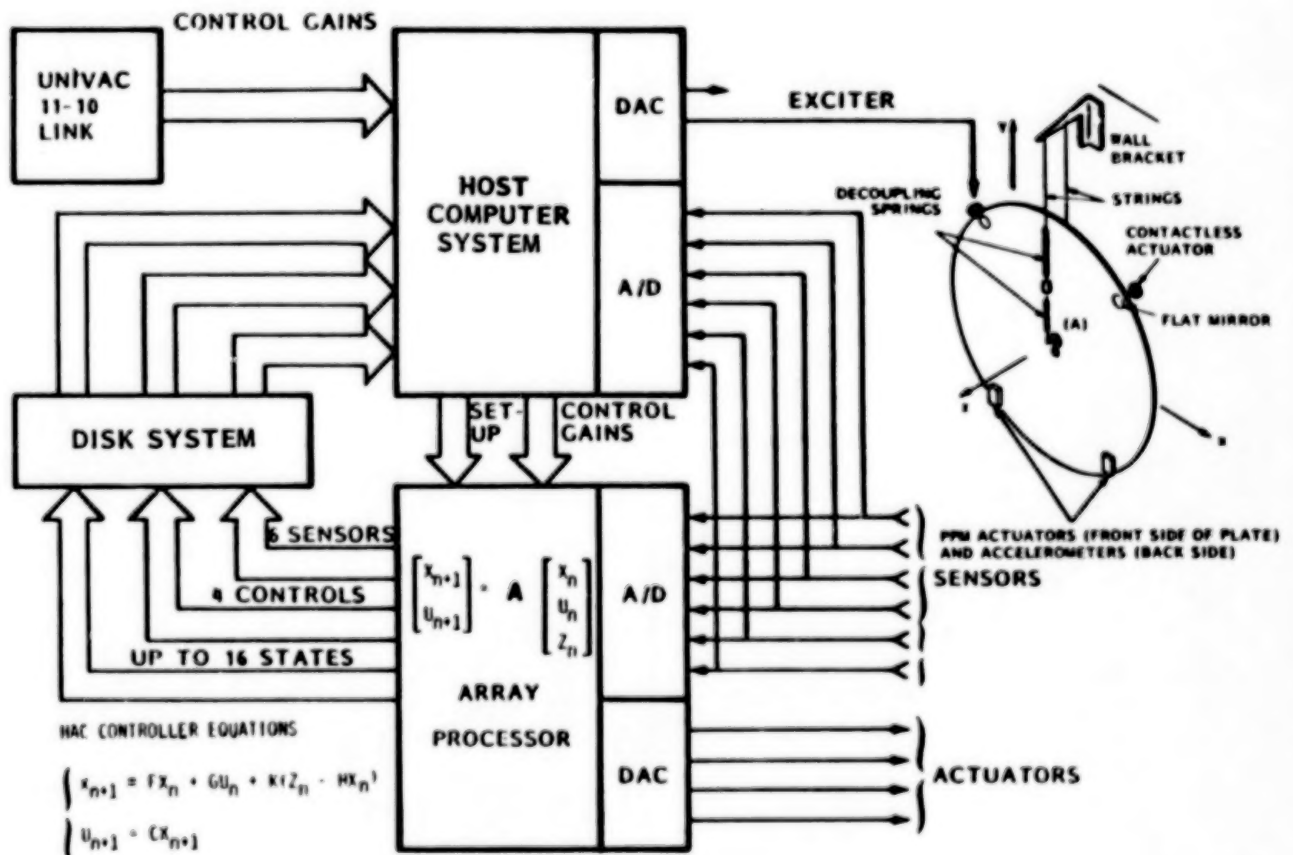


RESULTS

- VERIFICATION OF LAC THEORY
- 2-D CROSS-COUPLED EFFECTS CHARACTERIZED
- NONCOLLOCATION/NONCONSISTENCY IMPLEMENTATION DEMONSTRATED

PLATE EXPERIMENT OVERALL CONFIGURATION

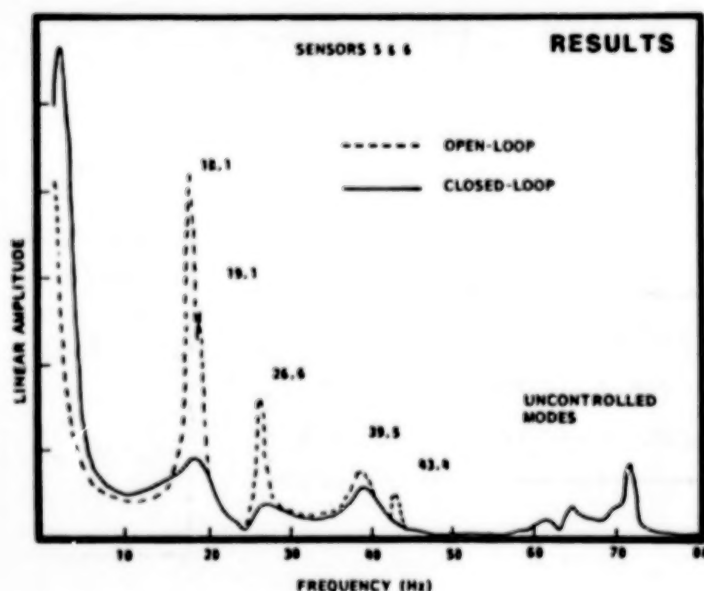
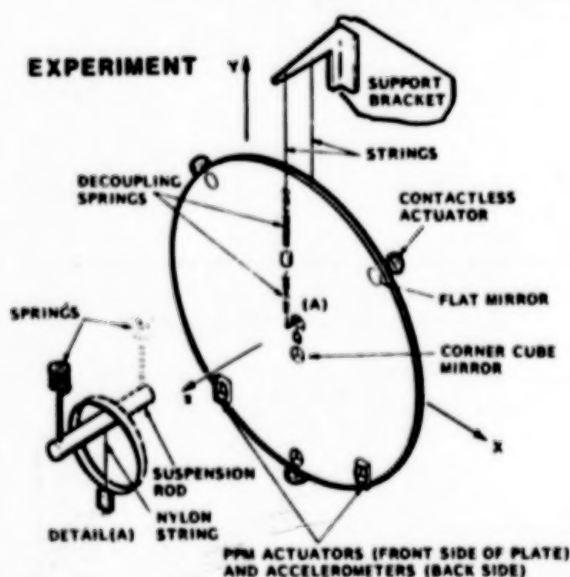
The next step of the experimental program was to start controlling more complex structures presenting as much similarity to LSS as possible, and implementing high order digital control systems. The chart below describes the general experimental set-up used for the circular plate experiment. The digital controller is implemented in an array processor (AP). The host computer is used principally to acquire and process data for open- and closed-loop characterizations. Its secondary function is to load the gain matrices in the AP and start or stop the control algorithm. Control gains are generated before the experiment by large scale control synthesis programs such as OPTSYS, residing in the UNIVAC 11-10 computer.



CIRCULAR PLATE EXPERIMENT - MIRROR-TYPE STRUCTURE

The circular plate experiment uses a circular aluminum plate as a test structure. This plate is about 3 mm thick and 1.2 m in diameter. It is suspended by its center with a system of springs and strings to approximate unconstrained conditions, and basically simulates a large reflector in space. Flat and corner-cube mirrors are used for optical sensing of local rotations or displacements. Contactless electro-magnetic actuators (for attitude/vibration control) and PPM actuators (for vibration control only) are mounted on this plate. A 16th order Kalman filter was implemented on the array processor using 6 optical sensors. Four actuators were used by the controller (3 contactless, 1 PPM). Three rigid-body modes were controlled (2 rotations, 1 translation) along with the first five bending modes ranging from 18 to 43 Hz. The open- and closed-loop transfer functions obtained experimentally show the controller effect of the system and are in good agreement with theoretical predictions.

CIRCULAR PLATE EXPERIMENT - MIRROR-TYPE STRUCTURE

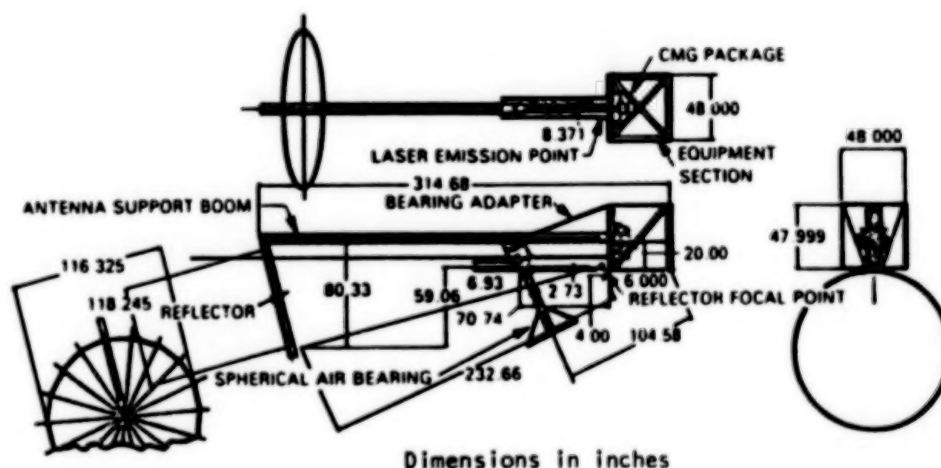


RIGID BODY AND MODAL CONTROL DEMONSTRATION

- 3 RIGID BODY MODES (2 ROTATIONS, 1 TRANSLATION)
- 5 BENDING MODES (FROM 18 TO 43 Hz)
- LAC STABILIZATION OF UNMODELLED MODES

PROOF OF CONCEPT EXPERIMENT BLUEPRINT OF TEST SPECIMEN

The proof of concept (POC) test specimen was conceived as a scaled down model of an RF offset feed antenna. Actuators and sensors were chosen to duplicate as closely as possible those which will be used on the real article.

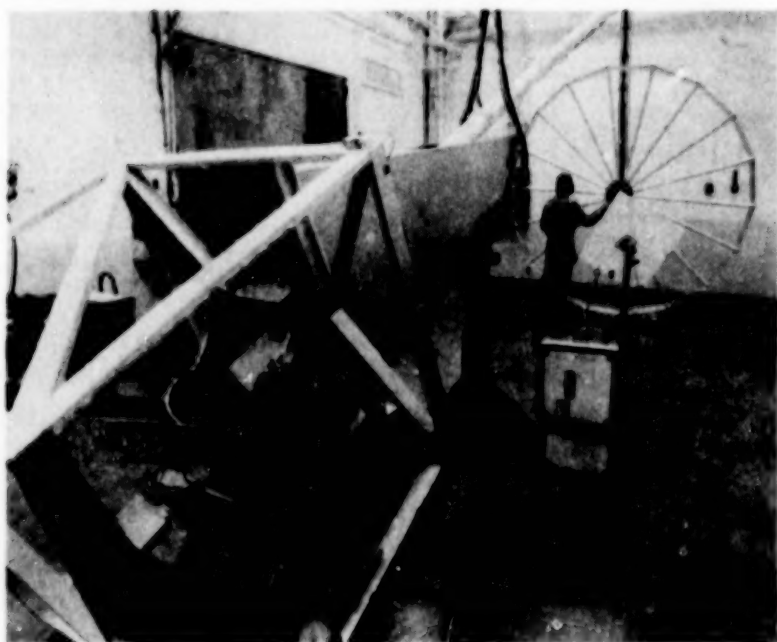
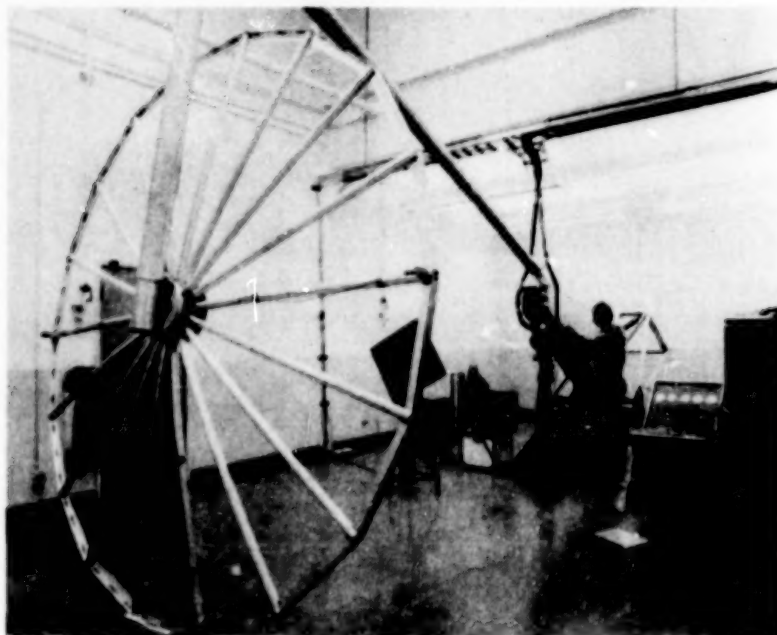


WEIGHT OF SPECIMEN: _____ 600 lb
OVERALL LENGTH: _____ 25 ft
DISH DIAMETER: _____ 10 ft

ACTUATORS: _____ 3 - CMG CLUSTER, PIVOTED
PROOF-MASS ACTUATORS
SENSORS: _____ LASER ATTITUDE SENSORS
RATE GYROS
ACCELEROMETERS
SUSPENSION: _____ AIR BEARING
COMPUTATION: _____ PDP 1145 WITH CSPI ARRAY
PROCESSOR, VAMP SOFTWARE

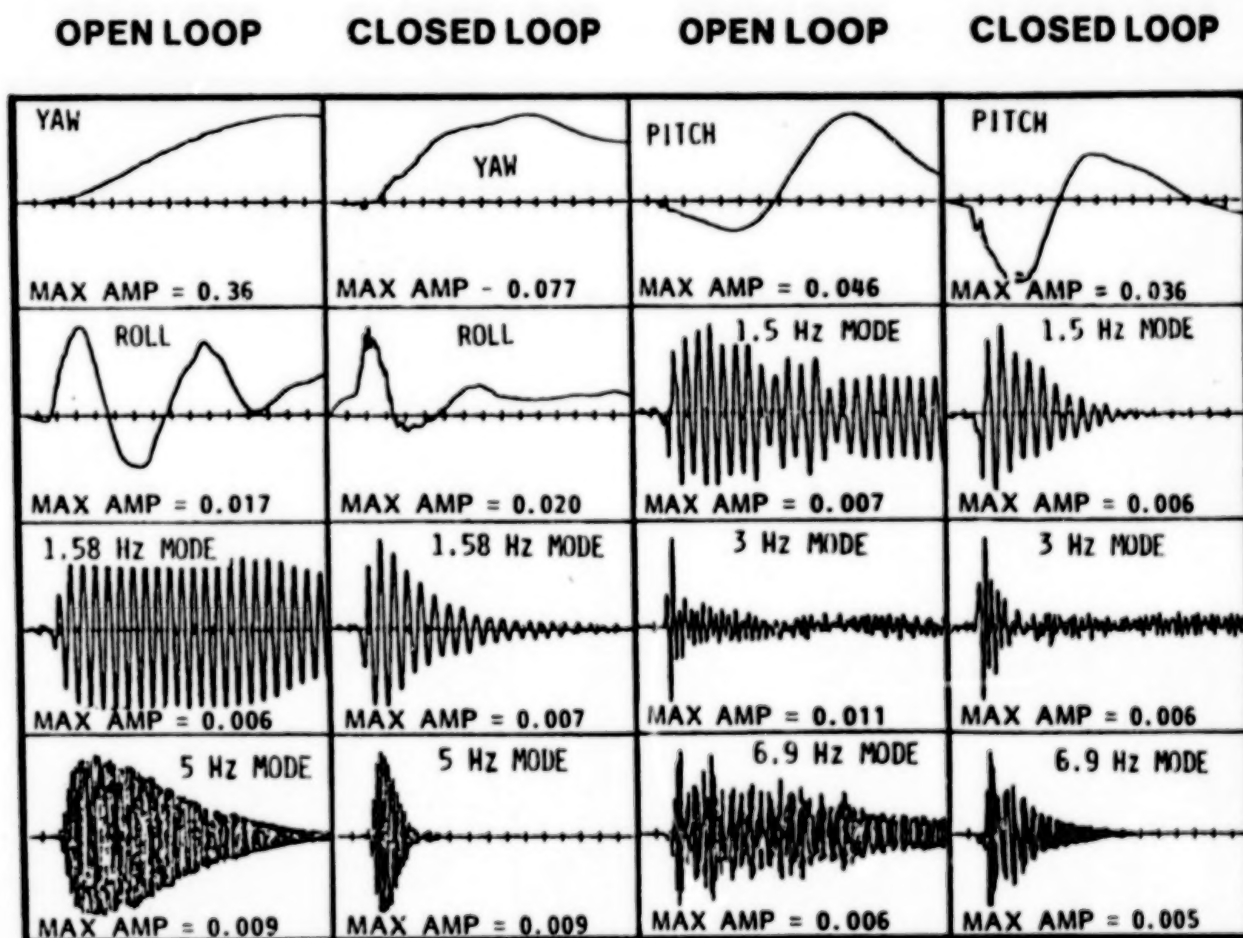
POC EXPERIMENT SETUP

These 2 pictures shows the POC mounted on the air bearing. The structure was instrumented with 78 accelerometers in a first phase, for system characterization purposes. The digital processing setup was similar to that of the plate experiment. For control purposes, 10 accelerometers and three rate gyros were used. The control actuators were three single-gimbal CMGs mounted in the back body (two of them are seen on the triangular-shaped support).



POC EXPERIMENTAL RESULTS

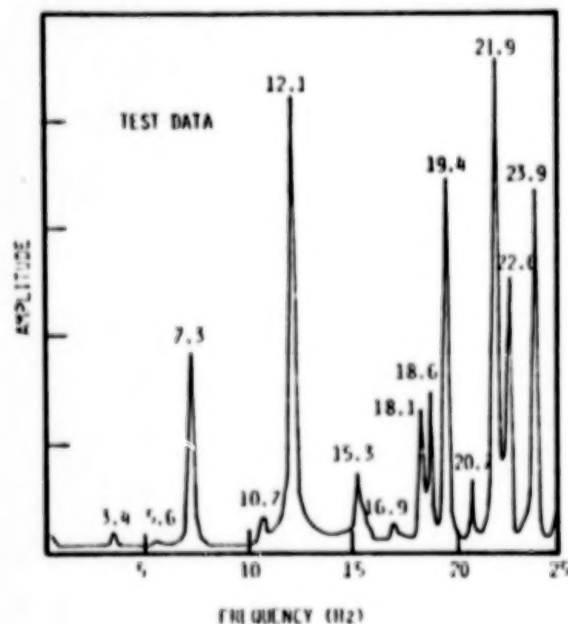
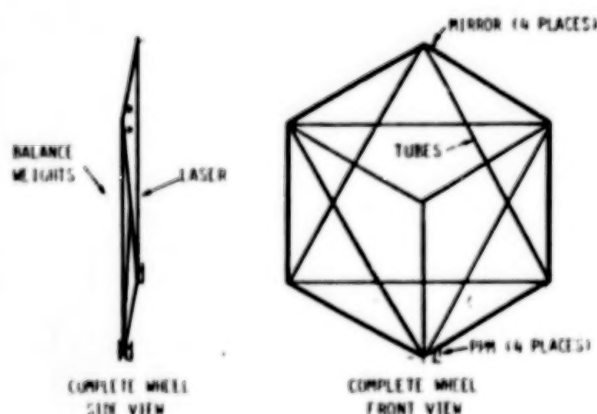
This real-time output of the Kalman filter estimates of the bending states for both uncontrolled and controlled tests demonstrates dramatically how the sixteen-state ACOSS controller succeeds in controlling bending of the POC specimen. The tests are conducted by applying an external excitation for the first four seconds of the test, and then allowing the structure to ring for the next twelve seconds. The closed-loop models not only exhibit much faster settling times, they also have significantly reduced peak amplitudes.



TIME IS 16 s, DISTURBANCE APPLIED DURING FIRST 4 s

TRUSS EXPERIMENTAL RESULTS

The truss "wheel" structure, designed in 1979, is the most complex of the present test structures in terms of its modal behavior. Although its geometry is relatively simple, a high modal density is found. The theoretical model shows numerous occurrences of double and triple roots, which, even though slightly separated in the actual structure, are difficult to identify. The agreement between finite element models and test results is only fair at this time, as can be seen in the figure. The development of a control system for this structure represents a real challenge, because modelling and system identification are already difficult. However, this is probably still much easier than it would be for any real LSS.



FREQUENCY SPECTRA (Hz)	
TEST DATA	COMPUTED DATA
3.397	3.525
3.403	3.527
7.264	7.328
10.594	10.53
10.828	10.89
12.117	11.58
15.230	13.66
15.521	14.31
15.755	14.38
16.899	14.71
18.107	15.25
18.570	15.46
19.352	15.62
20.628	16.17
	16.59
	19.95
	19.98
	20.03
	21.94
	23.86
	24.73
	29.08

CONCLUSIONS

The important lesson to be learned from this research is that modern control theory is a very powerful tool to solve LSS control problems, but it had to be seriously tested against real cases and amended accordingly. The significance of the experiments has been that, with the proper adjunct of more classical approaches, such as LAC and frequency shaping, LQG mechanizations can be made to work in real applications and with significant performance. However, the tight relationship between this performance and the model accuracy indicates the almost sure necessity for system identification and further adaptive control schemes in future real space applications.

- **GENERIC CONTROL STRATEGY HAS BEEN**
 - DEVELOPED FOR LSS
 - APPLIED IN LARGE SCALE COMPUTER SIMULATIONS
 - TESTED IN REALISTIC HARDWARE EXPERIMENTS
- **ACTIVE CONTROL**
 - CAN BE IMPLEMENTED
 - PROVIDES SIGNIFICANT PERFORMANCE IMPROVEMENT
- **PERFORMANCE COULD BE FURTHER IMPROVED BY BETTER KNOWLEDGE OF SYSTEM PARAMETERS**

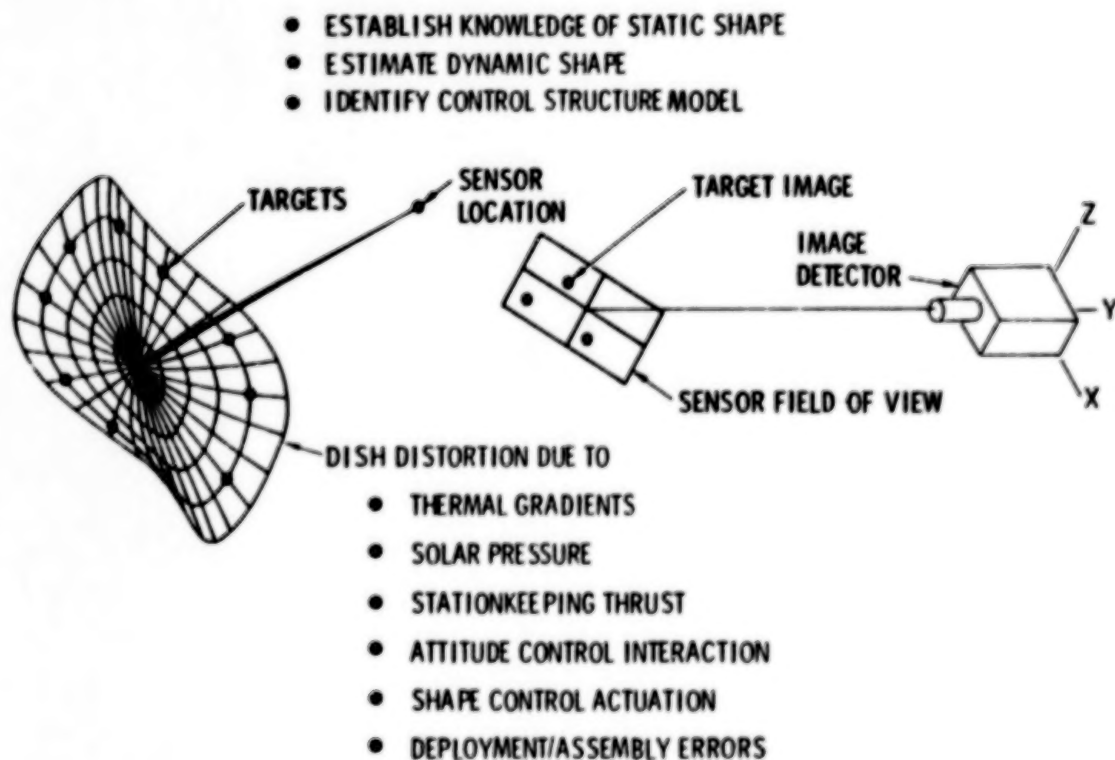
SHAPE DETERMINATION/IDENTIFICATION
FOR LARGE SPACE ANTENNAS

G. Rodriguez, J. M. Cameron, and M. H. Milman
Jet Propulsion Laboratory
California Institute of Technology
Pasadena, California

Large Space Antenna Systems Technology - 1982
NASA Langley Research Center
November 30 - December 3, 1982

IDENTIFICATION PROBLEM

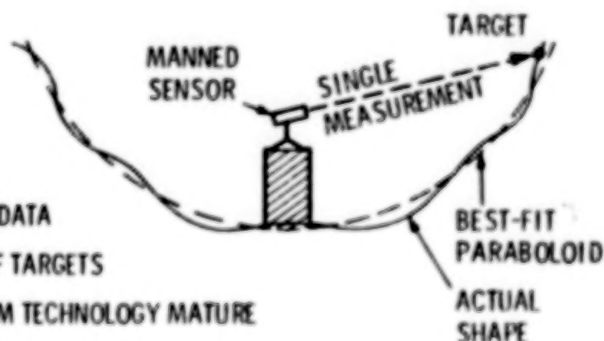
The shape determination problem is to reconstruct an antenna surface given discrete (noisy) measurements. Typically, a large flexible antenna will be perturbed from a nominal desired shape by both control actuation and environmental disturbances. To meet future antenna performance requirements will require a description of the dynamical interaction between these disturbances and the static deformation and vibration of the structure. Some antenna systems may also require active shape control to satisfy requirements. Performing these additional functions will in turn impose new constraints on the shape determination process, particularly in the areas of speed, autonomy, and sensor data rates.



SHAPE DETERMINATION CURRENT TECHNOLOGY FEATURES

Current methods for antenna calibration entail a painstaking survey of the entire surface of the structure. This is usually accomplished by a technician armed with a theodolite. Once the survey is complete, a least-squares fit of the data to the parameters of a paraboloid is performed. The entire process takes on the order of days. This approach is clearly inadequate for systems requiring autonomous operation and real-time estimation.

- SEQUENTIAL SURVEY SENSING
- MAN-IN-THE-LOOP OPERATIONS
- LEAST-SQUARES PARABOLOID FIT TO DATA
- ACCURACY DEPENDENT ON NUMBER OF TARGETS
- SENSING AND ESTIMATION ALGORITHM TECHNOLOGY MATURE
- SURFACE RECONSTRUCTION TAKES DAYS
- INFORMATION ABOUT ACTUAL SHAPE NOT READILY AVAILABLE
- NOT SUFFICIENTLY ACCURATE AT SHORT WAVELENGTHS



TYPICAL APPLICATION

- LARGE GROUND ANTENNAS
64-m DSN
- GROUND CALIBRATION
OF FLIGHT ANTENNAS

SHADES: AN INTEGRATED HARDWARE/SOFTWARE SYSTEM FOR SHAPE DETERMINATION AND IDENTIFICATION

The previous "brute force" methodology neglects to exploit the inherent structural dynamics of the system. Incorporating a dynamical description into the estimator design overcomes the aforementioned shortcomings. Specifically, better estimates of surface deformation can be realized with fewer sensor placements. The aspects of reduced data requirements and accurate autonomous sensing are the key features of the Shape Determination System (SHADES) described below. In addition to the shape estimator design, SHADES will contain multipurpose subroutines performing such functions as system identification, tracking of feed movement, and RF pointing. SHADES is an integrated system and is made up of two fundamental technologies: multipoint spatially distributed sensing, provided by SHAPES (Spatial High-Accuracy Position Encoding Sensor), and estimation and identification methodology for processing the sensor data in order to establish knowledge of the vehicle's static and dynamic shape. In addition, SHADES will contain the system identification algorithms required for estimating poorly known parameters (modal frequencies, damping, etc.) in the dynamical models. While the figure illustrates an application of SHADES to a large antenna, the basic sensing, estimation, and identification capabilities of the integrated system are more generally applicable to a wider range (platforms and space stations) of large structure configurations.

SHADES

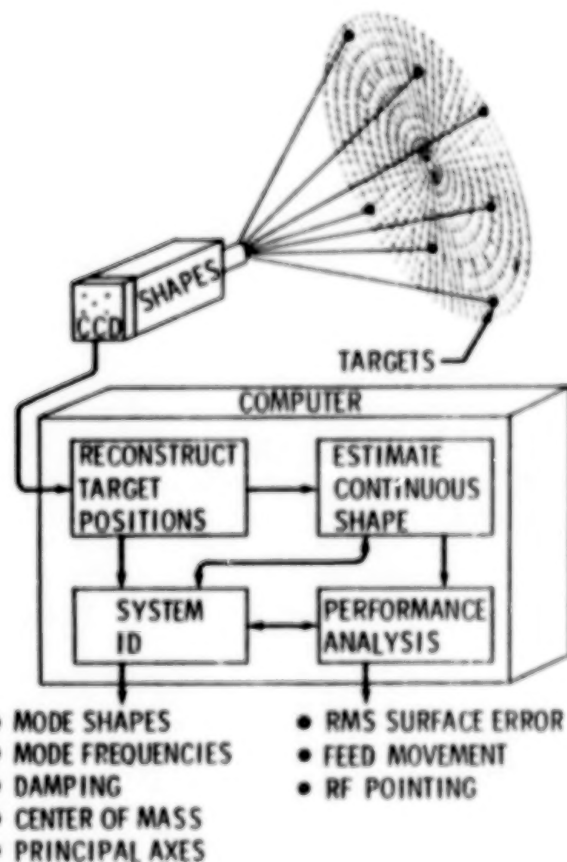
- AN INTEGRATED HARDWARE/
SOFTWARE SYSTEM FOR
SHAPE DETERMINATION
AND SYSTEM IDENTIFICATION
OF LARGE FLEXIBLE STRUCTURES

FEATURES

- SELF-CONTAINED PORTABLE
MODULE (SUITCASE)
- MULTIPOINT OPTICAL SENSING
VIA SPATIAL HIGH-ACCURACY
POSITION ENCODING SENSOR
(SHAPES)
- RECURSIVE MAX LIKELIHOOD
ESTIMATION ALGORITHMS FOR
ON-BOARD IMPLEMENTATION
- INTEGRATED SHAPE ESTIMATION /
IDENTIFICATION

APPLICATIONS

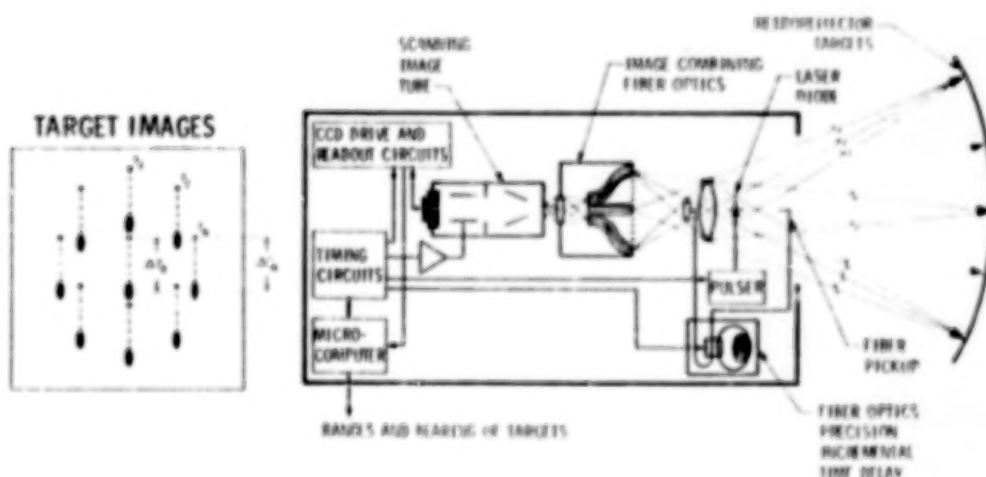
- LSS FLIGHT EXPERIMENT
- GROUND/SPACE ANTENNAS



THREE DIMENSIONAL MULTIPPOINT SENSOR

The SHAPES concept is designed to meet the need for a shape determination and system identification sensor that can measure the three-dimensional coordinates of many points on a large space structure simultaneously. It utilizes recent developments in short-pulse laser diodes, fiber optics, integrated optics, streak tubes, and CCD technology. It operates by measuring the range to and angular position of targets on the structure from a single location. Range is measured by the time of flight of very short light pulses. The precision of this measurement is improved by the use of a discrete-delay reference path consisting of fiber-optics links switched by integrated-optics switches. The time delay is determined by a streak tube with a CCD readout. The angular position is determined by the direct imaging of the targets on a second CCD.

The projected performance for SHAPES is 10 readings per second from up to 50 targets per optics head with range uncertainties of 0.15 mm and angular position uncertainties of 10^{-4} of the field of view. More targets can be accommodated in parallel with the addition of a second optics head.



NEW TECHNOLOGY

- PICO-SECOND LASER PULSES
- PICO-SECOND STREAK TUBE
- INTEGRATED OPTICS SWITCH
- FIBER OPTICS FOR CALIBRATION REFERENCE

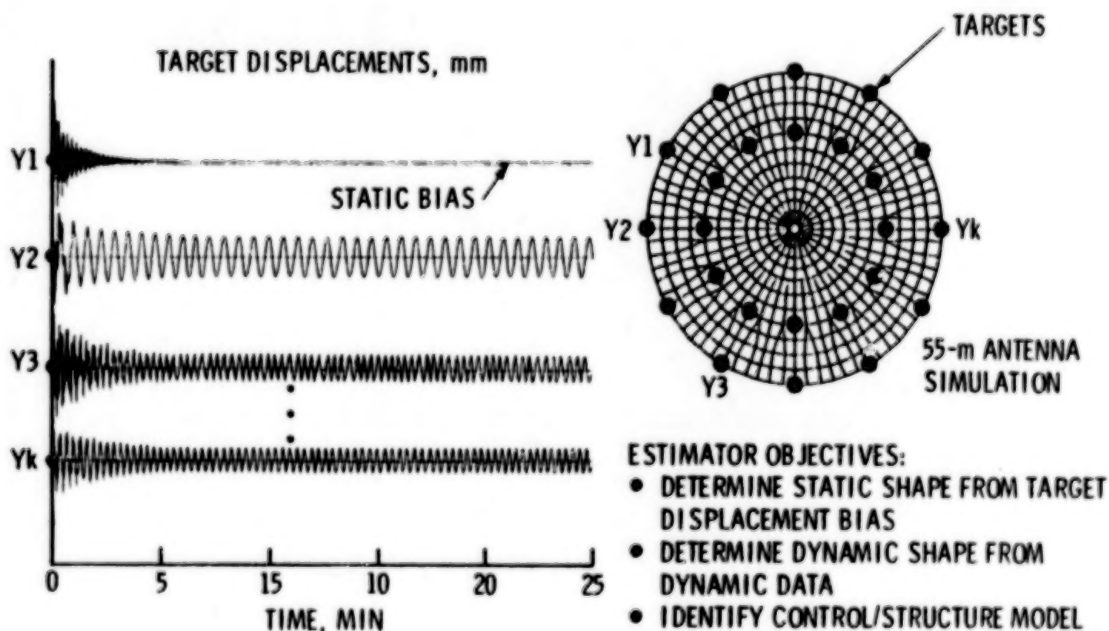
PERFORMANCE

- $1:10^4 - 10^5$ ANGLES ACCURACY
- 0.1 mm RANGE
- 50 TARGETS FOR OPTICS HEAD
- 10 TARGET SETS/SEC UPDATES

MULTIPOINT SENSOR DATA - 55-m ANTENNA SIMULATIONS

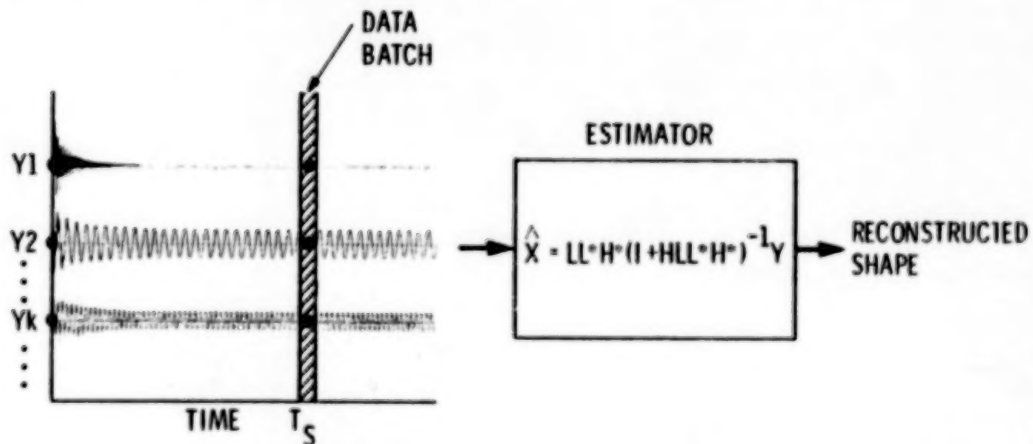
Shown below are simulated target motions as interpreted by a sensor. They depict structural vibrations superimposed on a static deflection. In an actual system, the static deflection could be produced by "slow" environmental disturbances such as thermal gradients, while the vibration could be a result of an attitude control actuation. As antenna performance is degraded by either of these disturbances, the need arises for estimation processes to determine both the static deflection and dynamic response of the antenna.

The estimator objectives are to process the target displacement data provided by the sensor in order to obtain estimates of the vehicle static deflection and dynamic shape and to establish knowledge of the control/structure model parameters. This data processing can be performed in either a batch mode or a recursive scheme as described in the following few figures.



BATCH PROCESSING

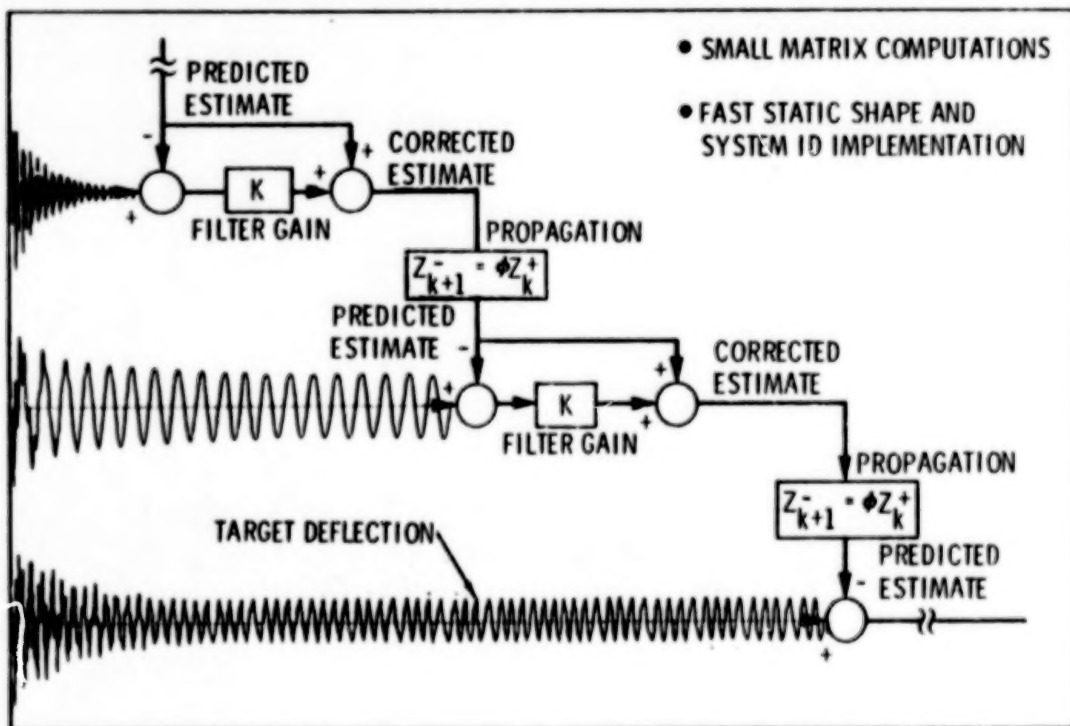
By definition, batch processing requires the collection of all measurement data prior to estimation. This has a negative computational impact in that matrix computations on the order of the number of sensor targets result. With a single optical head, the SHAPES sensor can accommodate about 50 targets at 10 Hz. This number can be increased by using multiple optical heads or by decreasing the data rate. (Also, angular accuracy can be enhanced by restricting the field of view.) Thus, to fully utilize the sensor's capabilities necessitates alternate processing schemes.



- COLLECTION OF ENTIRE DATA SET PRIOR TO ESTIMATION
- LARGE MATRIX COMPUTATIONS
- SUITABLE FOR STATIC SHAPE ESTIMATION (SMOOTHING)
- ONBOARD IMPLEMENTATION FOR SMALL DATA SETS ONLY

SCANNING ALGORITHMS - RECURSIVE PROCESSING

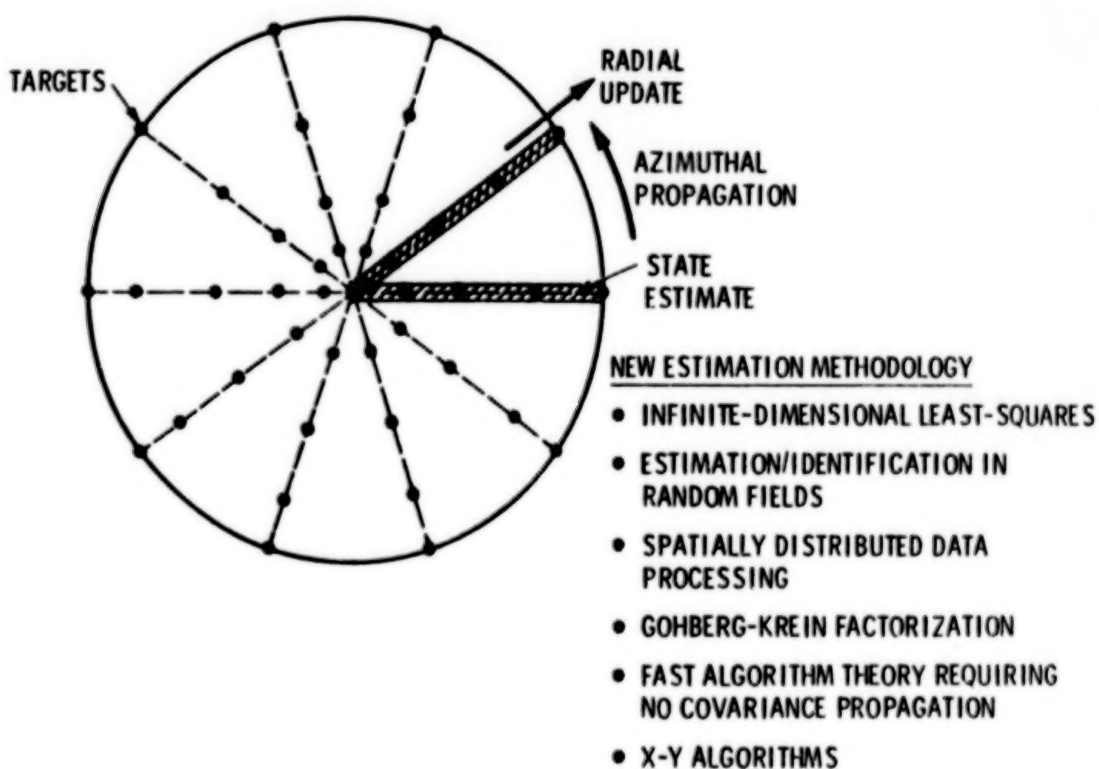
An alternative to batch processing is recursive processing, which involves an update of the state estimate with each new observation set. After initialization of the estimator, the state is updated by processing the measurement residual. The state update in the continuous-discrete Kalman filter can, in many cases, be reduced to scalar operations. A possible recursive scheme is presented below. Here, the state is updated with each individual measurement; this results in simplified computations and overall reduction in estimator complexity. The practical implementation of infinite-dimensional estimators of this type requires new theoretical tools and techniques as indicated in the following figure.



SCANNING ALGORITHMS - AZIMUTHAL SWEEPS

Some current research areas in estimation methodology are described below. For example, new applications of the Gohberg-Krein factorization combined with the theory of random fields and random processes with values in an infinite-dimensional space are expected to yield scanning type algorithms. An azimuthal sweep scheme involving state update in the radial direction and state propagation in the azimuthal direction is currently under investigation.

Another development that is anticipated to facilitate the realization of infinite-dimensional filters is the "x-y" type algorithms for fast estimation, which circumvent the need for covariance propagation and thereby result in very efficient on-board implementations that take full advantage of the emerging parallel processing computer technology.



BATCH VERSUS SCANNING - HIGHEST OBSERVABLE MODAL FREQUENCY

For quasistatic estimation, large quantities of data can be processed simultaneously in a batch mode. But for real-time applications, this amount of data processing will have to be reduced considerably. The scanning solutions have a potential to provide this reduction. A rough estimate of frequencies that can be tracked versus the number of sensor targets to be processed in both batch and scanning modes is shown below. It can be seen from the chart that the highest observable frequency increases as more of the data is processed in a scanning mode, thereby leading to estimator designs that can respond more quickly to a changing shape. Conversely, the estimator response becomes slower and less able to track high-frequency structural vibrations as more data is processed in a batch mode. An efficient combination of both scanning and batch data processing (implemented by means of parallel computations) will be under investigation for the SHADES application.

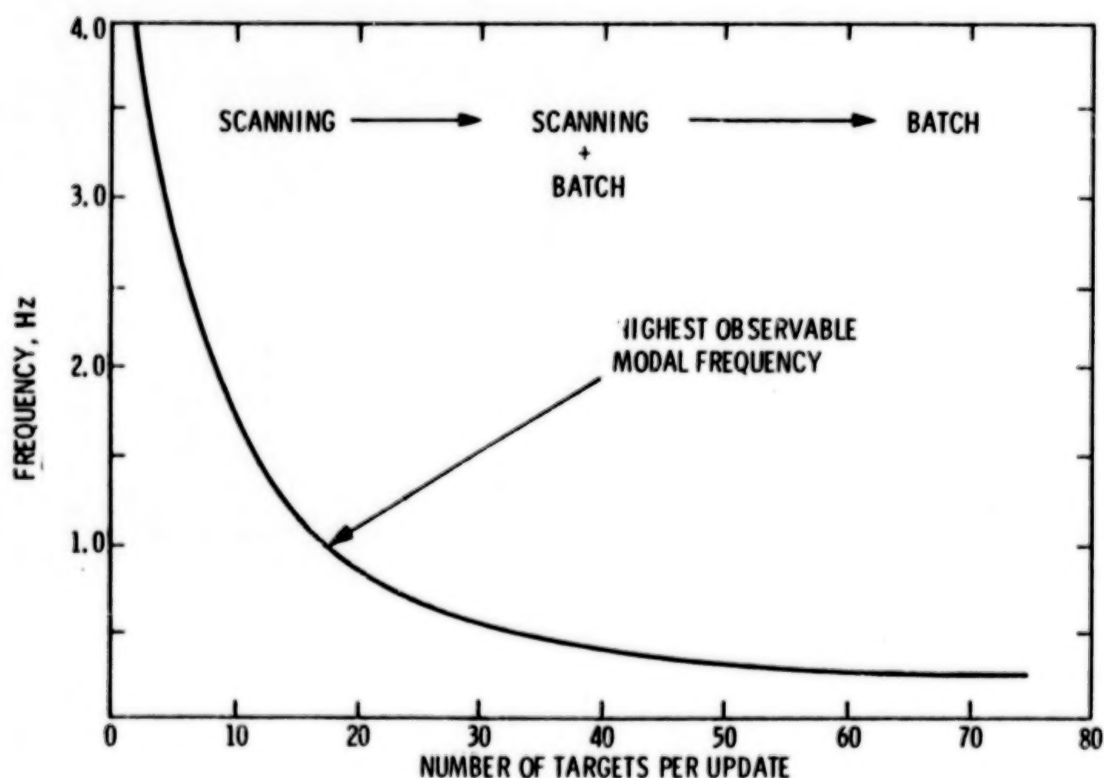
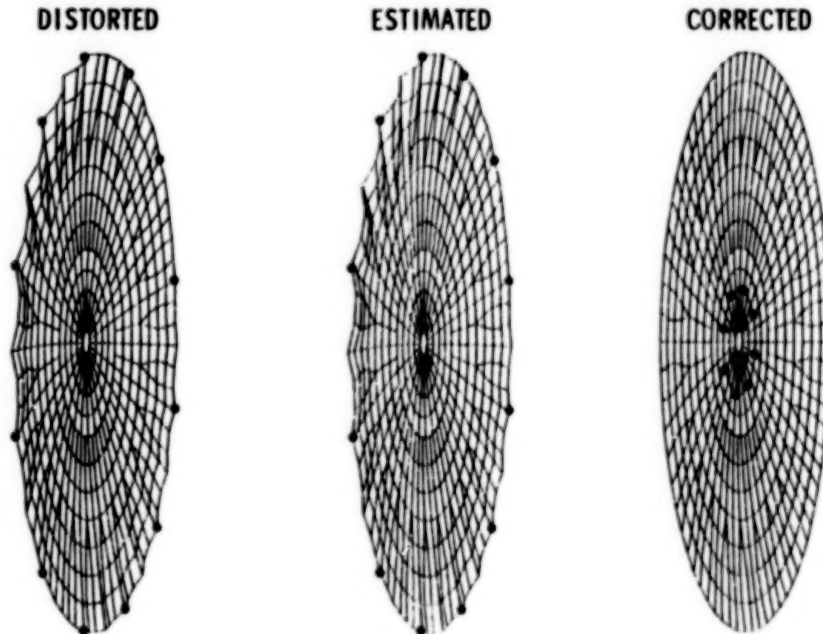


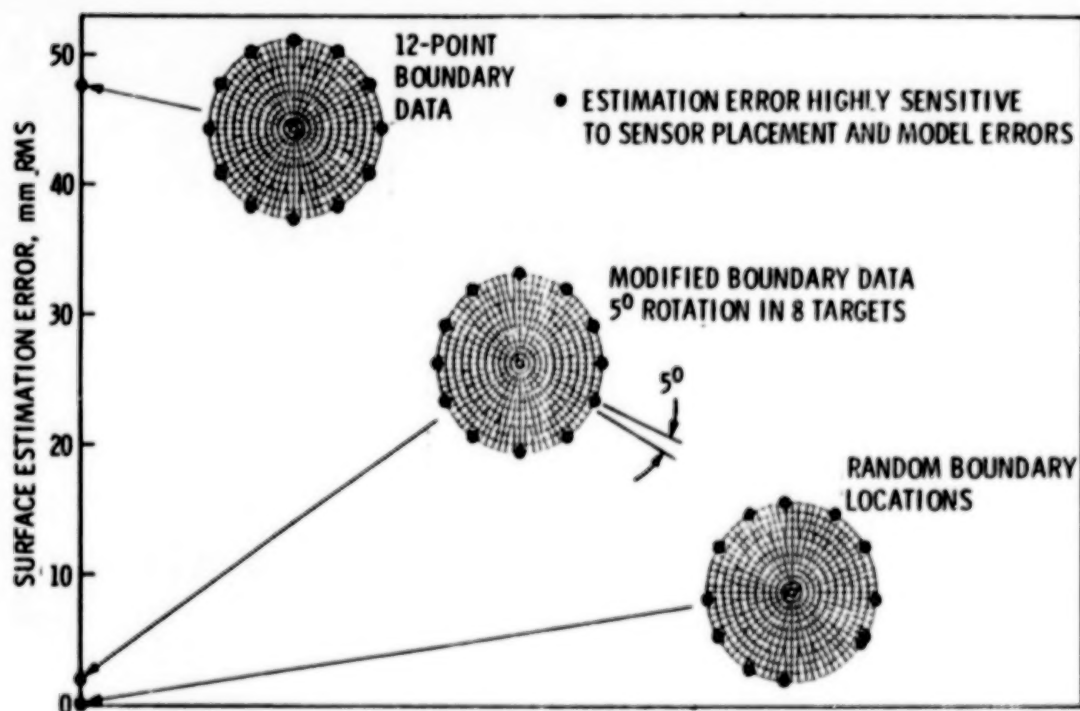
FIGURE ESTIMATION AND CONTROL PERFORMANCE ILLUSTRATION

The focus of recent JPL work in the shape estimation area has been on sensor placement sensitivity studies based on a 55-m wrap-rib antenna model. These results are presented in the next few figures. The simulations involved reconstructing the antenna surface from a set of discrete measurements as shown in the figure. In each simulation a deformation of a nominal antenna shape was produced by a linear combination of the first 18 modes provided by a finite element model of the antenna. The estimator performance in a batch mode was then investigated for several sensor placement configurations. A parallel investigation of the sensitivity of figure control performance to actuator placement (as opposed to sensor placement) was also conducted. Most of the results for the sensor placement study presented here have a parallel, analogous (dual) interpretation in terms of actuator placement.



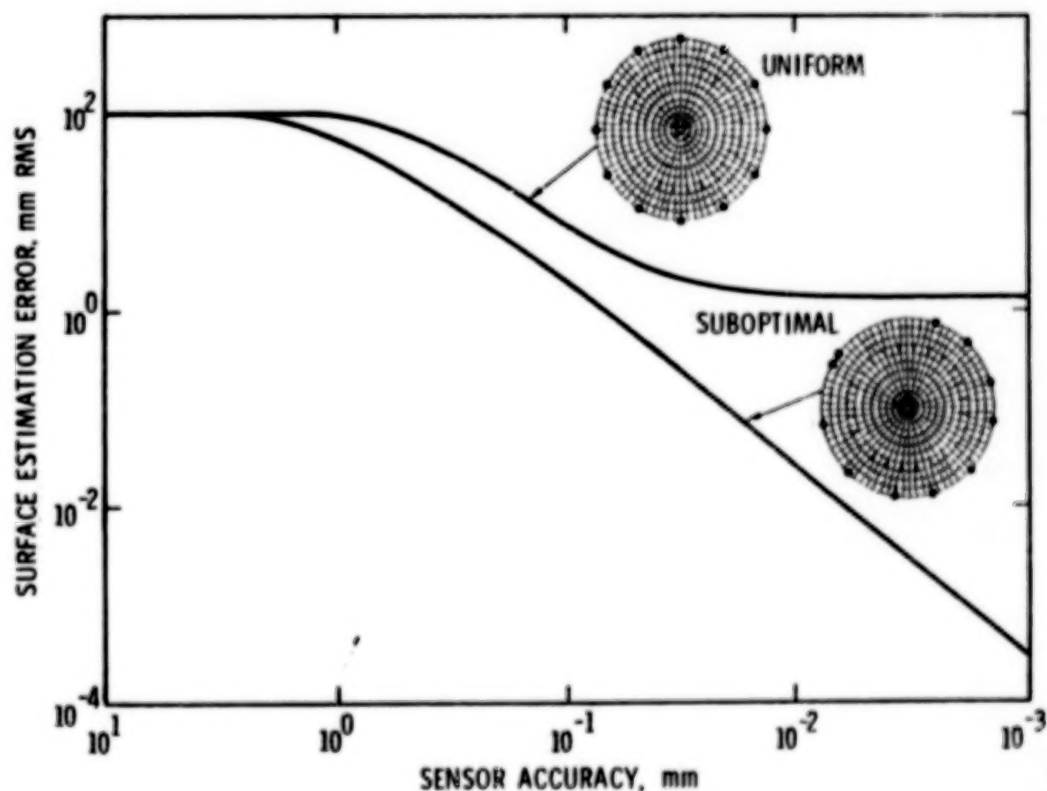
ESTIMATION ERROR SENSITIVITY TO SENSOR PLACEMENT

This figure illustrates the sensitivity in estimation error due to small repositionings of the sensors. This sensitivity has two important ramifications. First, it suggests an equal sensitivity to perturbations of the mode shapes. This underscores the need for good modeling of modes. The second consequence is the implication that methods for determining "optimal" sensor placement must carefully address the issue of constraints on the set of admissible placement because a small repositioning of the sensors could have a significant effect on the estimation performance.



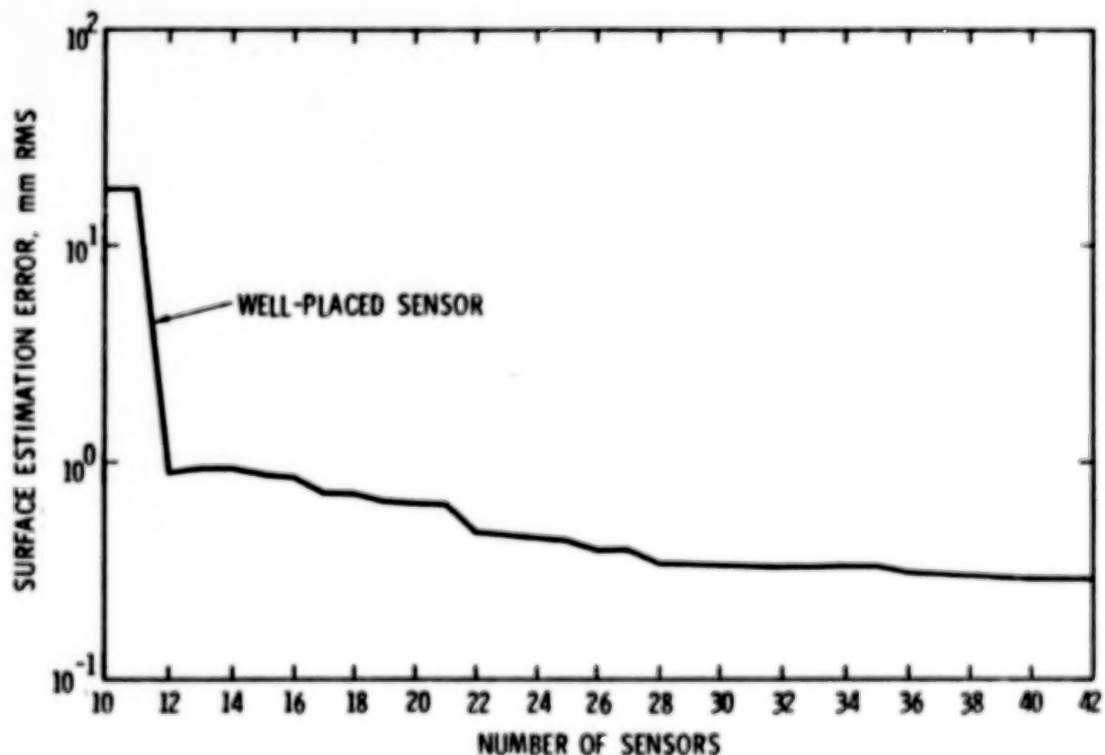
SENSITIVITY TO SENSOR ACCURACY

Intuitively, it is clear that estimator performance improves with sensor accuracy. However, the role of sensor placement in the amount of improvement to be gained is important here also. Note the contrast between performance improvement versus sensor accuracy for the two different sensor configurations below. The configuration using a uniform placement of sensors improves very little once the sensor error drops below 10^{-2} mm, while a "suboptimal" placement continues to improve. The suboptimal placement was motivated by a desire to maximize, in a general and somewhat empirical sense, the signal-to-noise ratio for each sensor position. This was accomplished by positioning sensors at points of maximal deflection for each of the active modes. Although the problem of optimizing sensor placement involves more than the consideration of reducing the effect of sensor noise, this suboptimal approach is suggestive of general guidelines or directions for choosing sensor placement.



SENSITIVITY TO SENSOR NUMBER

Here, the effect of arbitrarily adding new sensors to a given configuration is illustrated. More than an order of magnitude improvement was realized from going from an initial set of 10 sensor targets to a set of 42 targets. Note also the drastic improvement in performance obtained by the addition of a "well-placed" 12th sensor target. This result suggests that the indiscriminate addition of targets does not necessarily lead to significant improvements in performance. Much better improvements can be expected if the sensor target placement strategies are based on a detailed understanding of the estimation and modeling problems. The parallel (and integrated) development of the sensor technology and of the estimation/identification methodology will ensure that such an understanding exists as SHADES evolves and will result in better overall system performance.



SENSOR PLACEMENT SENSITIVITY -
FY'82 RESULTS SUMMARY

A recapitulation of the major FY'82 findings is given below. The most significant aspect of the analysis is the rather broad spectrum of expected performance that can be realized from varying the number of either sensor targets or positions. So, although it is premature to make definitive conclusions concerning the ability to meet shape determination requirements for a specific mission (e.g. a 55-m antenna), the preliminary analysis does indicate that there is a lot of potential in the area of improving performance by means of selective sensor placement.

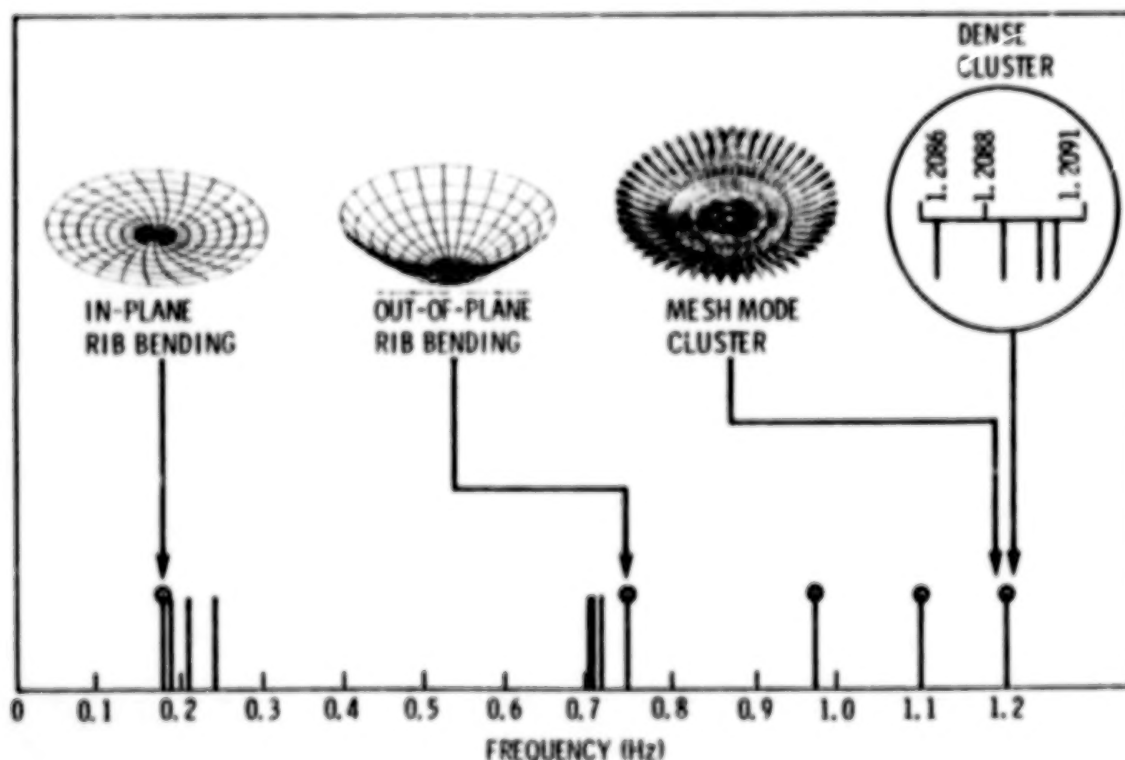
- ESTIMATOR PERFORMANCE VERY SENSITIVE TO SENSOR PLACEMENT
- PERFORMANCE DEPENDENT UPON SENSOR PLACEMENT AND ACCURACY
- EXHAUSTIVE SEARCH TECHNIQUES FOR OPTIMAL PLACEMENT DIFFICULT TO IMPLEMENT
- SUBOPTIMAL TECHNIQUES UNDER DEVELOPMENT
- SENSITIVITIES TO PLACEMENT AND TO MODEL ERRORS ARE EQUIVALENT

55-m WRAP-RIB MODAL FREQUENCIES
ILLUSTRATION OF SYSTEM ID PROBLEM

Presented below is an illustration of some of the modes of a 55-m wrap-rib antenna dish. The figure shows: (1) an in-plane bending mode at a frequency of about 0.2 Hz in which the dynamics are governed primarily by the rib mass and bending stiffness; (2) an out-of-plane bending mode at a frequency of about 0.7 Hz; and (3) a mesh mode cluster in which the overall dynamics are still dominated by the rib mass and stiffness while the mesh stiffness causes a cluster of an infinite number of modes with almost identical frequency.

While the model is very detailed and has been generated by one of the most advanced finite element programs available, it is nonetheless inherently limited in terms of its accuracy because of the unavoidable presence of a large number of model errors. For instance, inaccurate knowledge of the rib stiffness will result in incorrect values for the rib bending modal frequencies and mode shapes. Similarly, the linear approximation used for the mesh elastic behavior leads to errors in the characterization of combined rib/mesh dynamics. For the static shape estimation problem, the inaccuracies in the mesh model could also result in incorrect mesh shape estimates.

Because recent control/structure interaction studies have shown that such errors (which are typical of many large space systems) could seriously degrade overall system performance, it is widely recognized that a process of in-flight identification will be required in order to improve preflight dynamical models. SHADES addresses this need by providing for a system identification capability that is an integral part of the combined sensor/algorithm system. It should be stressed at this point that the system ID capability incorporated into SHADES is applicable to a wide range of structural configurations and is not limited to the large antenna illustrations in this paper. The methodology to achieve the identification process is discussed in the following figures.



MAXIMUM LIKELIHOOD IDENTIFICATION APPROACH SUMMARY

A maximum likelihood approach has been selected for the purpose of identifying system parameters. This method is based on sound statistical principles and has the potential for extracting the maximum amount of information from the data. It is also a method that has been quite successfully advanced in the area of aircraft parameter identification.

The main ideas underlying the maximum likelihood approach are illustrated in the figure. The method assumes a system model that contains a vector θ of unknown parameters. The objective of the identification process is to estimate this vector from measurements of the system behavior as well as from the system model itself. In this particular application, the maximum likelihood approach seeks to find an optimal (maximum-likelihood) parameter estimate that minimizes what is referred to as the negative log-likelihood functional. The minimization is conducted by means of a numerical search based on the Newton-Raphson method that, from an initial estimate, generates a sequence of estimates θ^n based on computations of the gradient g and the approximate Hessian matrix M , as illustrated in the figure.

SYSTEM MODEL

$$\dot{x} = A(\theta)x + B(\theta)w$$

$$y_k = H(\theta)x(t_k) + n_k$$

- θ = UNKNOWN PARAMETERS
- x = STATE
- y_k = OBSERVATIONS
- w, n_k = MODEL ERRORS

NEGATIVE LOG LIKELIHOOD (INNOVATIONS REPRESENTATION)

$$\text{MINIMIZE}_{\theta} J(\theta) = \frac{1}{2} \sum_{k=1}^N [\text{Tr} \log D_k(\theta) + e_k^T(\theta) D_k^{-1}(\theta) e_k(\theta)]$$

- $e_k = y_k - H(\theta)Z(t_k^-) = \text{INNOVATIONS PROCESS}$
- $D_k = E[e_k e_k^T] = \text{PREDICTION ERROR COVARIANCE}$
- $Z(t_k^-) = \text{PREDICTED STATE ESTIMATE}$

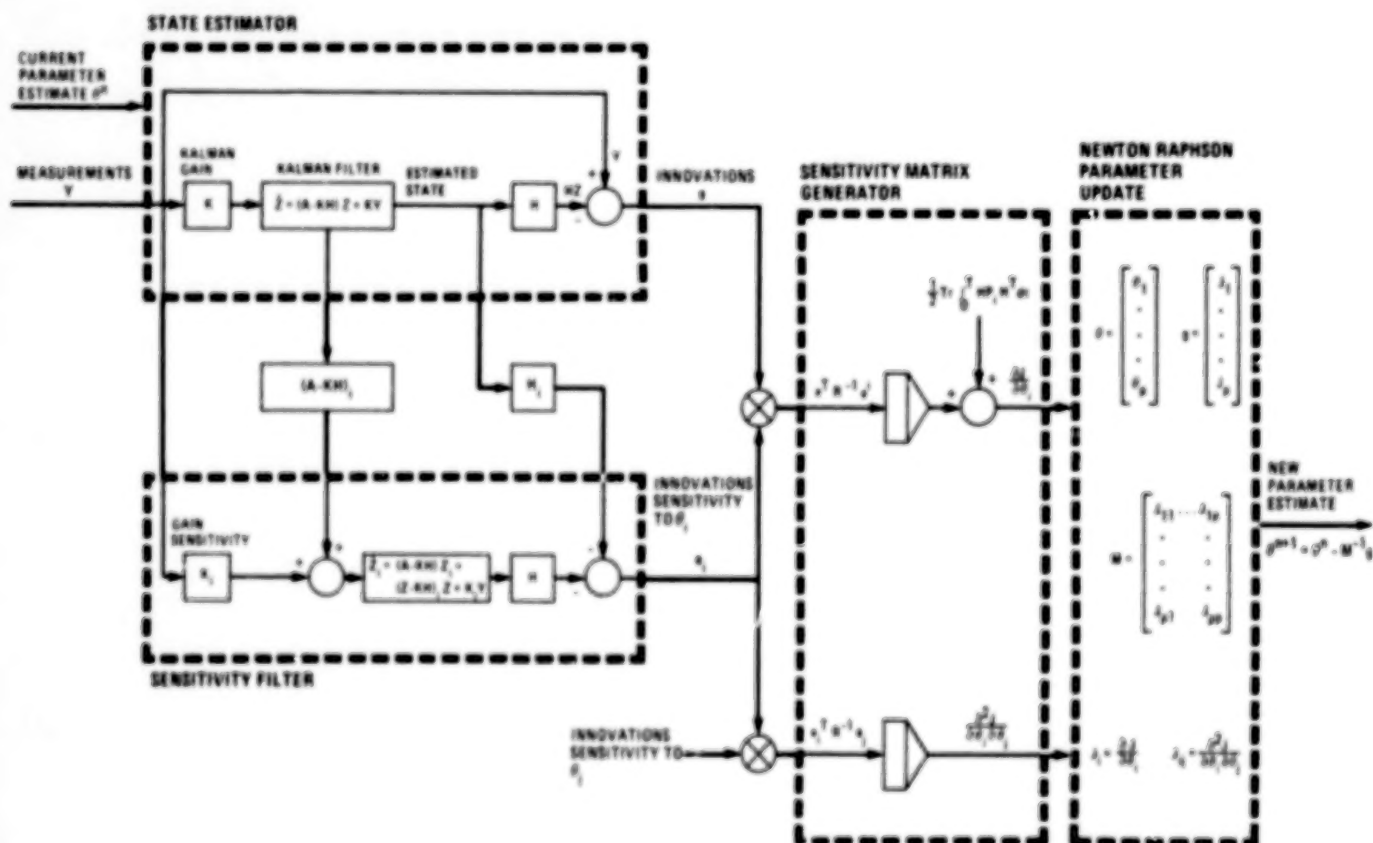
NEWTON-RAPHSON NUMERICAL SEARCH

$$\theta^{n+1} = \theta^n - M^{-1} g$$

- θ^n = CURRENT PARAMETER ESTIMATE
- θ^{n+1} = NEW PARAMETER ESTIMATE
- g = GRADIENT
- M = APPROXIMATE HESSIAN

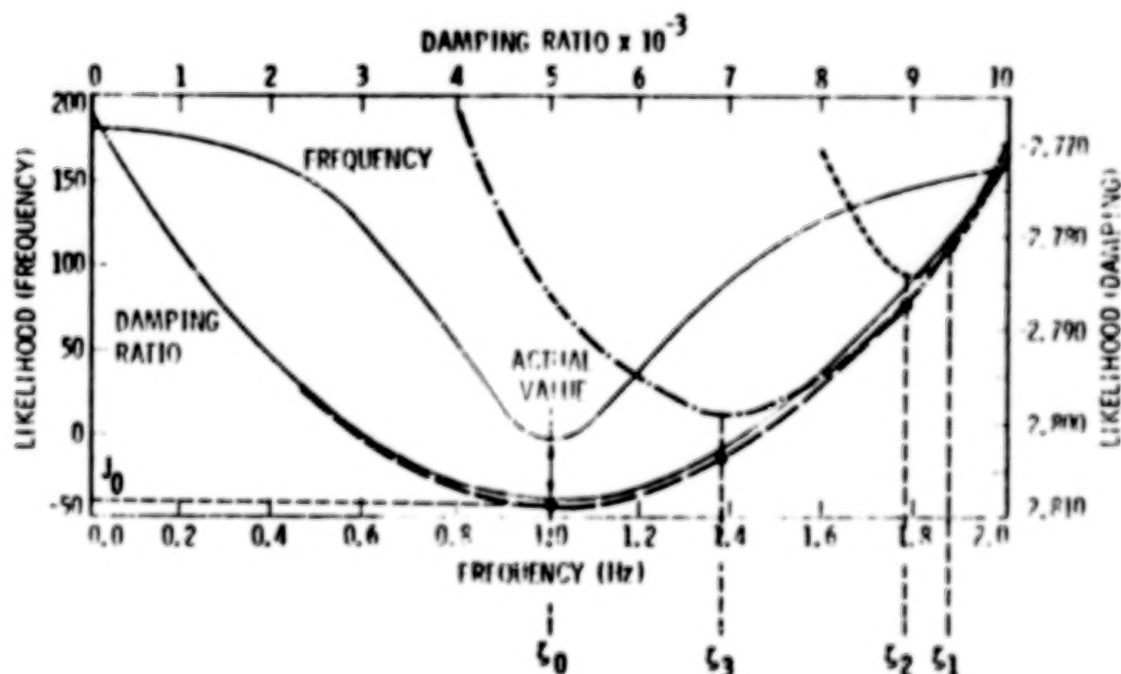
MAXIMUM LIKELIHOOD IDENTIFICATION FUNCTIONAL BLOCK DIAGRAM

The computations involved in the maximum likelihood approach are summarized in the block diagram. The approach assumes that an initial value for the parameter estimates is available to start the process. This initial estimate is used to design a Kalman filter and a corresponding sensitivity filter that generates the sensitivity of the innovations process with respect to the poorly known parameters (see STATE ESTIMATOR and SENSITIVITY FILTER blocks). The innovations and their related innovations sensitivities are then used in a SENSITIVITY MATRIX GENERATOR to form: (1) the gradient of the likelihood functional with respect to the parameters being identified; and (2) an approximation to the Hessian matrix which reflects the curvature of the functional corresponding to the current value of the parameter estimates. Based on the gradient and the approximate Hessian matrix computation, a new parameter estimate is established as shown in the NEWTON-RAPHSON PARAMETER UPDATE block of the diagram. Once the new parameter estimate is determined, the new estimate becomes the current one, and the overall process (including filtering and sensitivity matrix generation) is repeated as many times as necessary until convergence to the optimal parameter estimate is achieved.



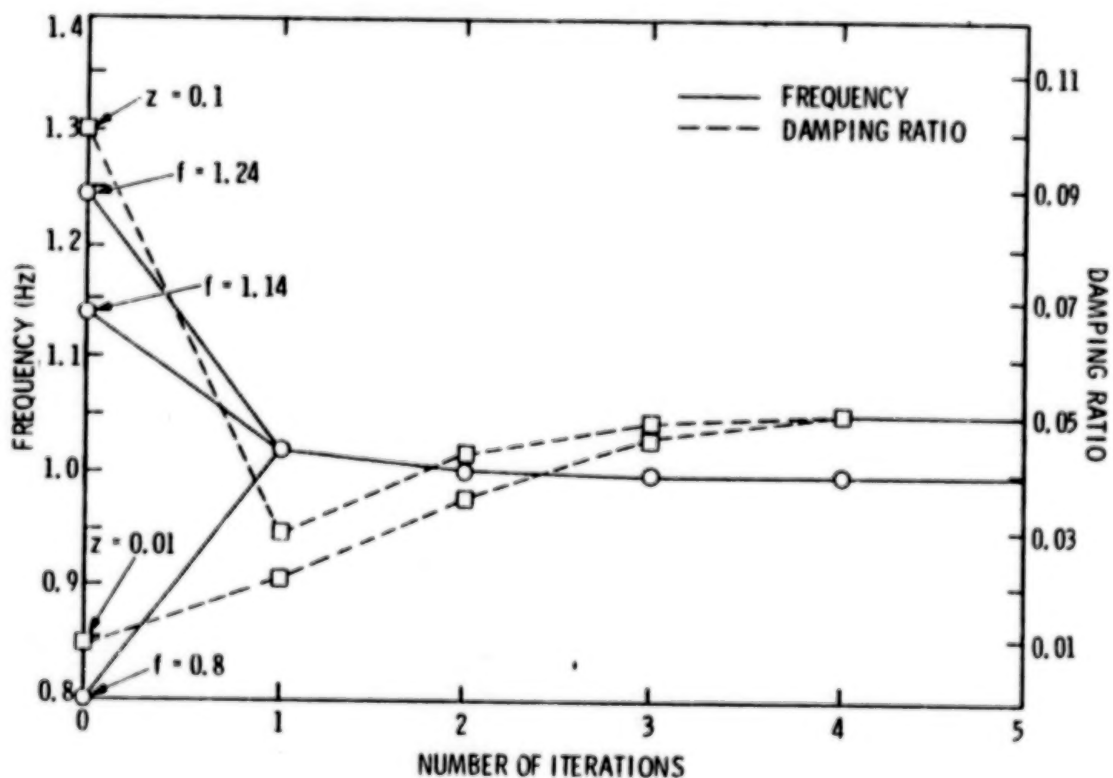
TYPICAL LIKELIHOOD FUNCTIONALS - NEWTON-RAPHSON ITERATION

The plots below show typical negative log likelihood functionals for frequency and damping resulting from an initial displacement in a one-mode model. Both identification problems are tractable to numerical search methods for optimization in the displayed neighborhoods since the true values are also the only minima in the regions. The figure also illustrates the sequence generated by the Newton-Raphson method for the case of damping ratio identification. Starting from an initial damping ratio estimate denoted by ξ_1 , the numerical search generates a sequence ξ_1, ξ_2, \dots which ultimately converges to the actual value. The frequency identification problem cannot be solved for this case by the Newton-Raphson method alone due to the occurrence of the inflection points near the minimum. Thus, a hybrid approach using a gradient method to get "close", followed by Newton-Raphson iteration to improve convergence, is more applicable to this particular example.



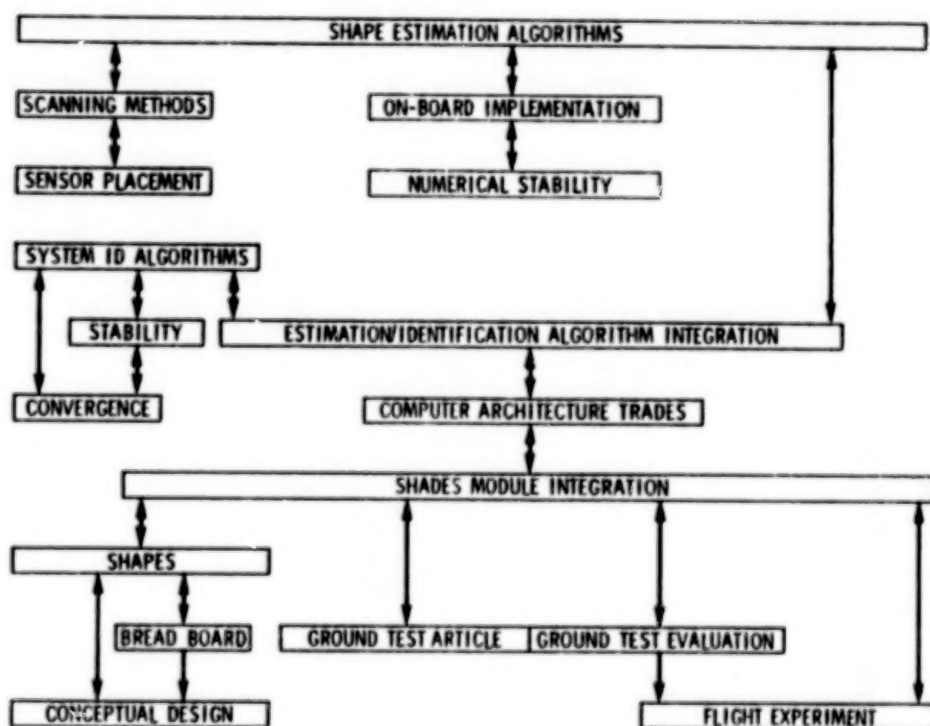
FREQUENCY AND DAMPING IDENTIFICATION ITERATED CONVERGENCE

Preliminary algorithm convergence results for damping and frequency identification illustrate the numerical search minimization of the likelihood functional described in the previous figures. This figure shows plots of estimated frequency and damping versus the number of iterations for the case of a structure described by a single vibrational mode. In the frequency identification problem, the Newton-Raphson method converged for a range of nominal values from 0.37 Hz to 2.6 Hz where the true value was 1 Hz. This contrasts with the (proportionally) wider range of convergence of the method in the damping identification problem. The convergence properties are, however, very highly dependent on the type of excitation that is used to generate the data used for identification. Improved convergence can be obtained by designing inputs that in some sense maximize the information that the data contains about the parameters being identified. Therefore, although in this particular case a wider range of convergence was obtained for the damping problem, other cases have shown that (with an appropriate excitation) the frequency identification search can also be made to converge for a wider range of the initial parameter estimates.



SHADES DEVELOPMENT APPROACH

A flowchart describing the approach being used in the development of the Shape Determination System (SHADES) is shown below. Preliminary algorithms for static figure determination and system identification have been developed. Detailed design work has been completed for the SHAPES sensor, and hardware is currently being prepared for experimental tests. Work is now beginning on suboptimal sensor placement methods and on fast algorithm theory in the figure determination area. In the system identification area, the initial algorithms are being expanded and modified to accommodate multimodal and distributed system models as well as fast scanning and processing of sensor data. Once the algorithms for shape determination and system identification have matured, software requirements will be generated for the integration of the system. This will then be followed by the implementation and evaluation phases in ground tests and possible flight experiments.



PRACTICAL APPROACHES TO THE DESIGN OF CONTROL SYSTEMS
FOR LARGE SPACE STRUCTURES

H. J. Buchanan
Marshall Space Flight Center
Huntsville, Alabama

Large Space Antenna Systems Technology - 1982
NASA Langley Research Center
November 30 - December 3, 1982

INTRODUCTION

This paper will deal with some of the practical problems that face the control system designer over the next decade. These are generally deficiencies in tools or knowledge, sometimes both.

The first step is, of course, an assessment of the problem at hand. While some aspects of future large systems have been given much discussion, other problems of practical significance have been largely ignored.

FUTURE SPACE SYSTEMS

Large spacecraft now being contemplated for development before the end of this century will differ vastly from the smaller vehicles of the 60's and 70's. Although these differences will impact the design of all subsystems, the effect will be felt in particular by the control system designer.

Perhaps the most publicized difference is the enormous size of some of these vehicles. Much has also been made of system flexibility as exemplified by low and closely spaced modal frequencies. System complexity has not yet received so much attention, but previous spacecraft tended to be configured to fit launch vehicles, leading to relatively compact, simple structures. Most of the proposed large systems consist of deployable modules of Shuttle transportable size attached to one another (see figure 1). This can lead to configurations which are topologically quite complex.

Another area of difference has to do with the evolving nature of these systems. Earlier satellites were built to fit a well specified mission. Many of these future systems have the nature of a general facility to be used over a period of many years by a wide range of users. The requirements imposed on all subsystems and particularly the attitude control system can be expected to change with time. Even the vehicle itself can be expected to expand and contract as new missions and requirements are imposed.

At Marshall Space Flight Center we are making an effort to anticipate these problems and develop tools and procedures to fit the tasks shown in figure 2. This paper will discuss three such developments and describe how they relate to one another as well as to the anticipated problems.

• • • • •

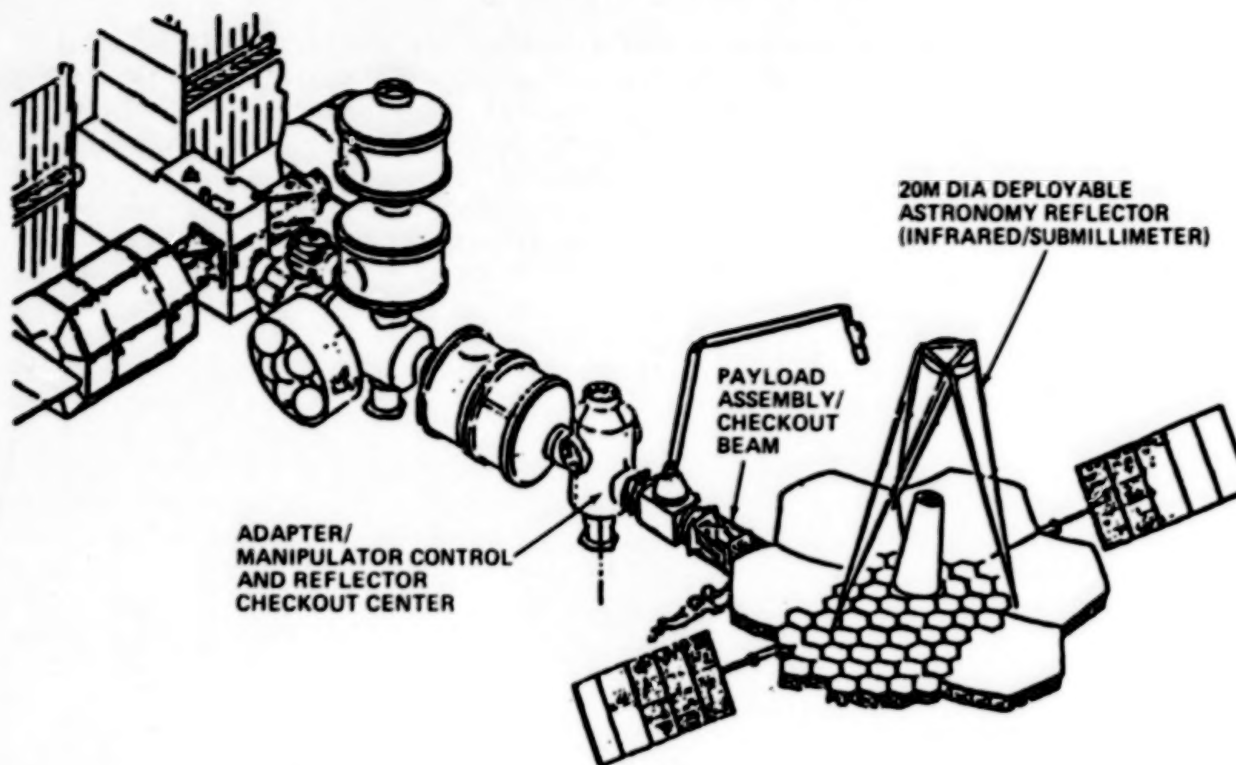


Figure 1

SIZE - LINEAR DIMENSIONS AND AREAS ARE LARGE.

FLEXIBILITY - MODAL FREQUENCIES ARE LOW AND CLOSELY SPACED.

TOPOLOGY - SYSTEM IS COMPLEX WITH MANY CONNECTIONS.

EVOLUTIONARY - SYSTEM CHANGES IN SIZE, SHAPE, AND PURPOSE.

Figure 2

AUGMENTED FLEXIBLE BODY ANALYSIS

The evolving nature and complex geometry of many currently proposed space structures poses an obstacle to both the structural dynamic analyst and the control system designer. As the structure grows, economical modeling procedures which provide for the adding of major elements without remodeling the entire system will be in demand by the control community. In a related factor, growth implies that the system topology may change significantly. For example, figure 3 shows three classic configurations we may expect to encounter. The first is a chain of bodies. The second shows a chain with many appendages, branching like a tree. The final example is a ring with branches extending from it. A unified modeling technique needs to be developed which is capable of treating all of these cases.

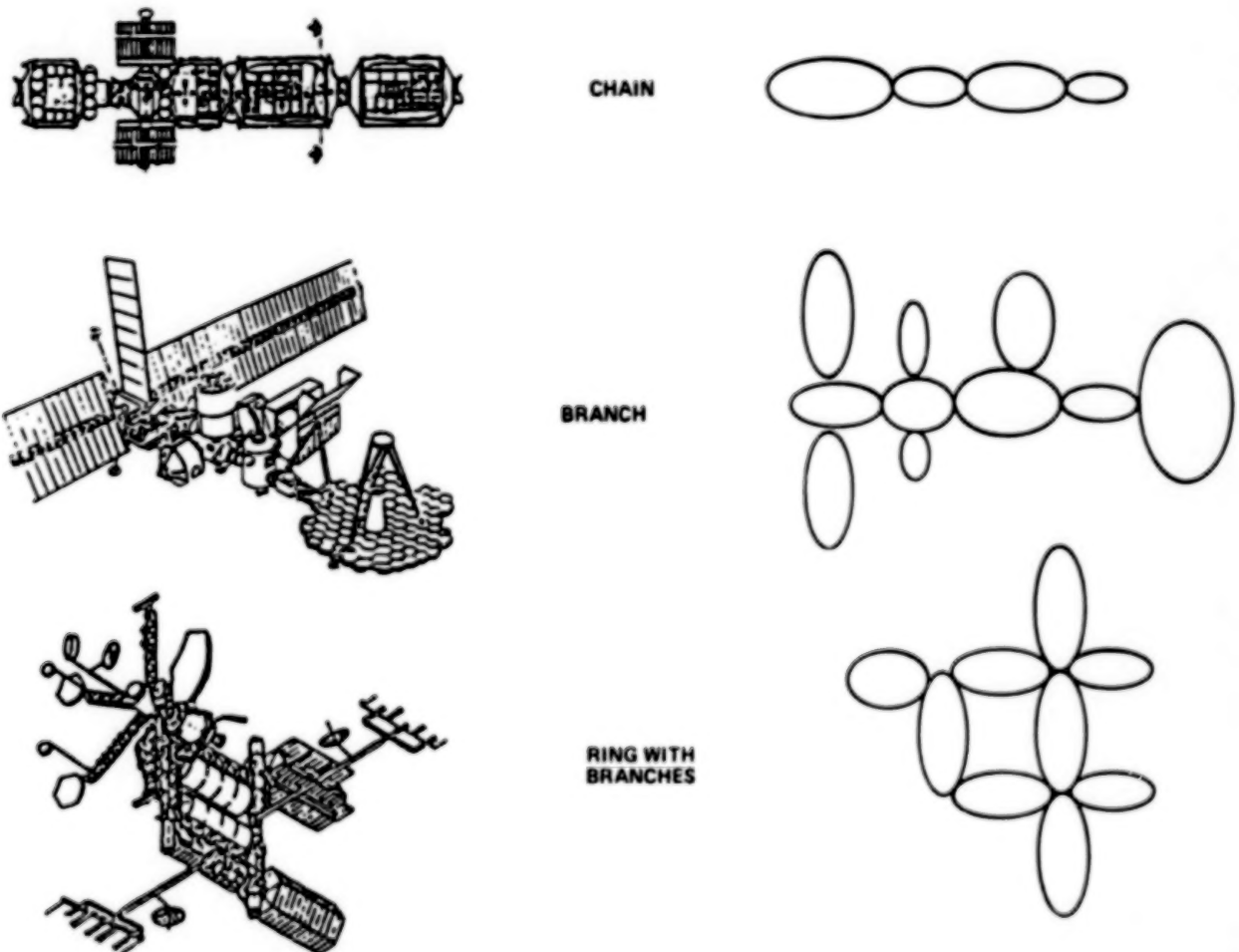


Figure 3

AUGMENTED FLEXIBLE BODY ANALYSIS

Honeywell is developing for NASA an Augmented Flexible Body Analysis package (reference 1) which will encompass all of these topologies and allow large angular motion between any segments of the topology. A special Direct Matrix Abstraction Program (DMAP) of the latest version of NASTRAN was effected to generate the flexible body data base. Currently a version of this program is available for conducting time response simulations of a chain topology and work is well along on the extension to cover rings and branches. The program is based on a unique formulation of the multi-body differential equations by Likins and Singh (reference 2) which offers an advanced capability for analyzing complex flexible structures. The program treats the total structure as an interconnected set of individual bodies, each with its own modal characteristics and boundary conditions. Thus models of specific modules can be developed and then combined in a variety of configurations. Active control elements can be included if desired. The time response capability will be most useful in verifying the performance of controllers developed using simplified models. A planned option will generate the linearized coefficients of the equations of motion for use in off-line design tools.

Four relatively simple steps (figure 4) are required to use the system. 1) System configuration and initial conditions must be defined. If a controller is being used it must be specified. 2) A modal data file for each flexible body must be created (this can be done by an off-line program such as NASTRAN). 3) Run an interactive program which creates the job control and data files necessary to execute the simulation. 4) Run the simulation and create plot and output files as desired.

We are working with the initial version of this program and expect it to have great utility.

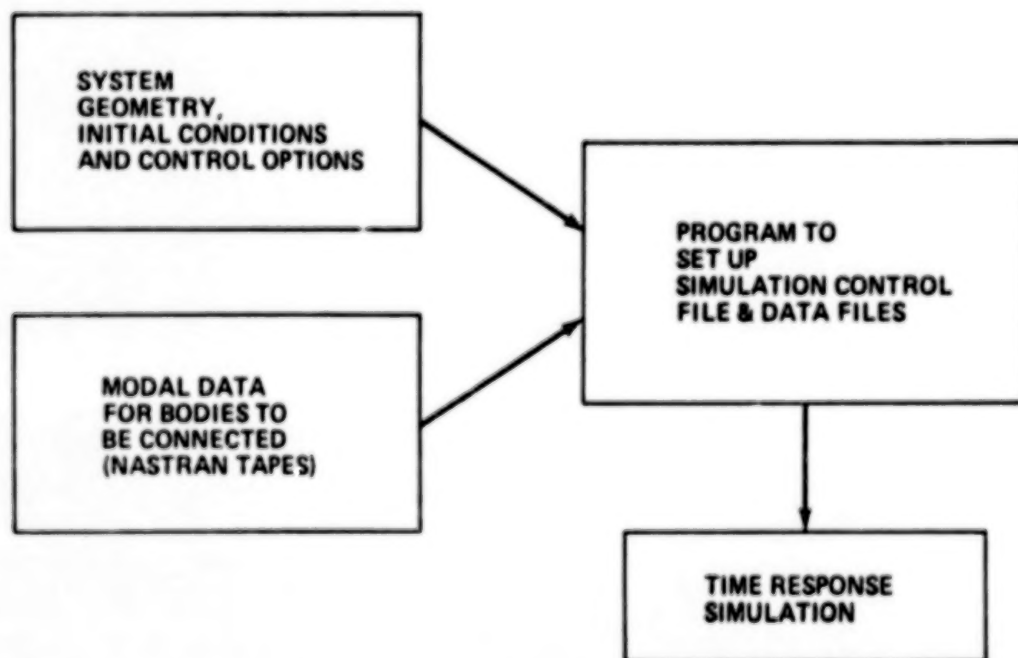


Figure 4

MODULAR CONTROL

For large evolving spacecraft the control system requirements will grow rapidly as the vehicle matures. A means for adding to the system efficiently with minimum impact to the existing plant has been identified as a priority technological issue. A modular control concept is one approach to this goal. Such a modular configuration is pictured in figure 5. Here individual station modules would be provided with their own control subsystem consisting of actuators, sensors, control computers, etc. At a higher level a supervisory controller coordinates the module subsystems to insure that attitude control of the entire body is maintained and to eliminate the potential for undesirable interaction at the module interfaces. With a successful solution, addition of a module would only require re-instruction of the supervisory controller and provisions for connecting the module subsystem to it.

Bendix, under NASA contract, has been actively pursuing one approach to this problem. To date the concept has been implemented in a simulation for a somewhat restricted case (reference 3). Future efforts will concentrate on reducing these restrictions and rendering the concept more practical. A solution to this problem can create new flexibility in system design, leading to lower front-end cost and probably lower life cycle cost.

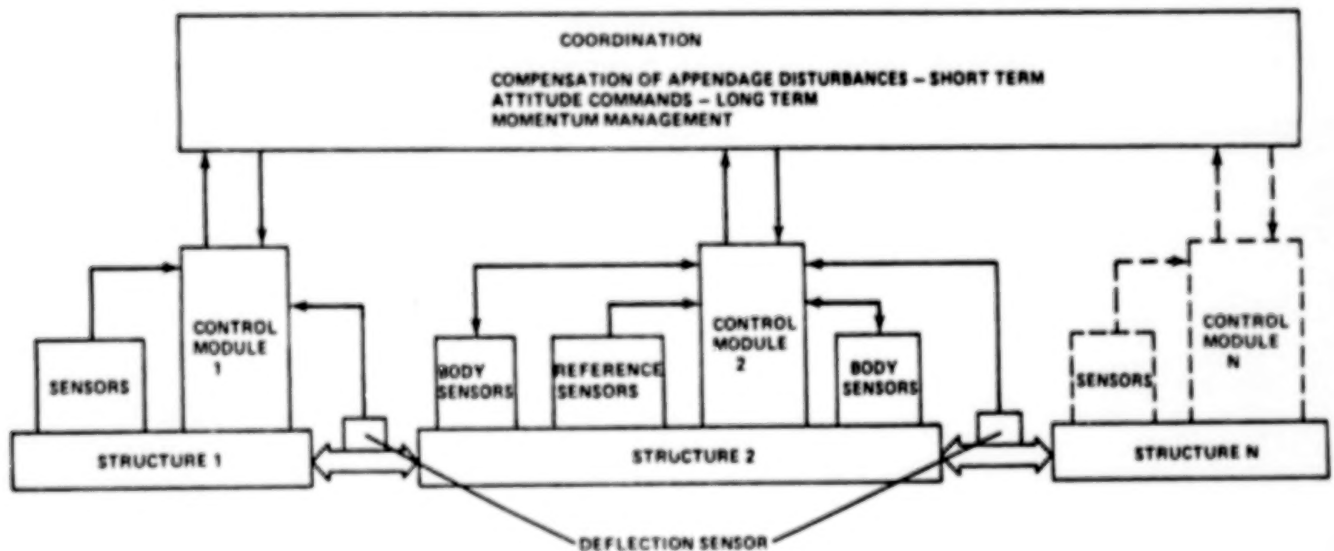


Figure 5

DESIGN-TEST-REVISE CYCLE

In the recent past the design process (figure 6) has consisted of: 1) characterizing the structure analytically; 2) designing the controller; 3) dynamic testing of the structure to improve the characterization; 4) revising the controller design based on this knowledge, and finally 5) evaluating the actual performance, which contributes to the experience base for future work. The changes to this sequence are primarily that steps 3 & 4 must now be postponed until the flight phase. Ground vibration test of large structures is difficult to accomplish and the information obtained may still be inadequate. This means that one should probably plan for on-orbit vibration testing if accurate structural dynamic data is critical to system performance. An approach to this problem would see the spacecraft launched with a 'caretaker' control system design based on the best available dynamic data set. The control system would emphasize 'robustness' over performance. Once on orbit a dynamic test would be performed and the actual dynamics used to optimize control system parameters to meet performance goals. If the configuration or requirements change significantly, the test-design update can be repeated. Eventually this operation will be done on line in real time (i.e., an adaptive control scheme), but in the near future only a well-structured, streamlined procedure will probably be required. This 'shake-down period' will not be a great sacrifice for a system with an operational lifetime spanning tens of years.

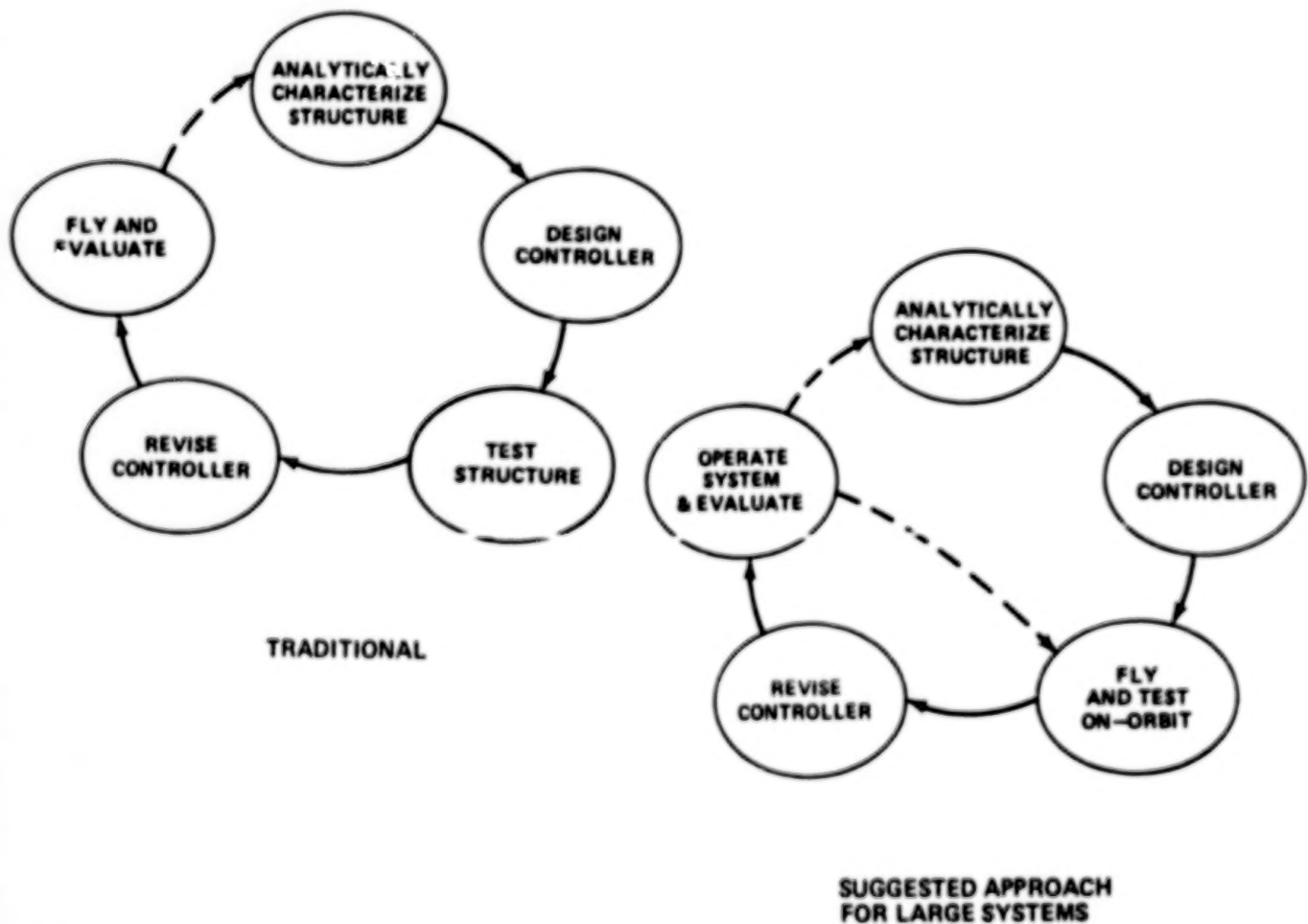


Figure 6

CONTROL TECHNIQUE VERIFICATION

NASA is developing an on-orbit test capability in conjunction with the Solar Array Flight Test Experiment (SAFE). Since another paper deals specifically with SAFE (reference 4), it will not be discussed further here. The second goal lies more in the domain of the control system designer and is being pursued in laboratory demonstrations under way in several places around the country. These generally emphasize slightly different aspects of the problem and compliment one another. The MSFC control demonstration deals with the problem of stabilizing and pointing flexible bodies mounted to a base structure. The test set-up is pictured in figure 7. The test article is a 33 ft x 7 in. Voyager Magnetometer boom and the control system is built around a two-axis gimbal system developed for the Advanced Gimbal System (AGS) program. Sensors mounted on the gimbal plate and also at the far end of the boom are connected to a microprocessor containing the control logic. The structure is vertical with both the upper suspension and the base supported on air bearings. Tests will investigate robust controller designs with structural frequencies within the control bandwidth. At present, system elements have been delivered and interface equipment built up. Following integration, which is now in progress, a dynamic test of the system will be performed, followed by the beginning of control system experiments later in this fiscal year. This cycle of dynamic characterization and controller investigation is designed to give more insight into the design of the 'caretaker controller' and the process of revising the system once the dynamics are known.

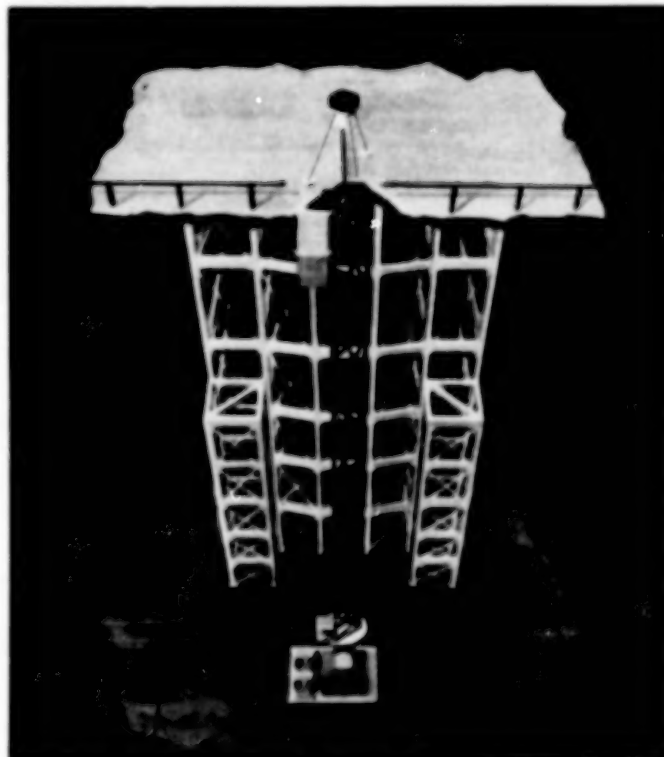


Figure 7

SUMMARY

In 1981 an effort was made to anticipate some of the practical problems the control engineer would have to deal with in the next few years. With that in mind we have shaped our research program to address solutions to some of these problems. As indicated, progress is being made and we expect to produce some useful methodology and design tools in addition to contributing to the general body of knowledge in the area of control systems.

REFERENCES

1. User's Manual for Augmented Flexible Body Dynamic Analysis Program. No. 18262, Honeywell Avionics Division, July 1982.
2. Singh, R. P.: Dynamics of a Chain of Flexible Bodies. Ph.D. Thesis, Univ. of Alabama, Huntsville, 1980.
3. Chichester, F. D.: Modular Design Attitude Control System. NASA CR-161998, 1982.
4. Schock, R. W.: SAFE On-Orbit Experiment for Measurement of Large Structures Dynamics. Large Space Antenna Systems Technology - 1982, Part 2, NASA CP-2269, 1983, pp. 981-990.

RESULTS OF STUDIES AT LANGLEY RESEARCH CENTER
ON THE CONTROL OF LARGE SPACE SYSTEMS

R. C. Montgomery and L. W. Taylor, Jr.
NASA Langley Research Center
Hampton, Virginia

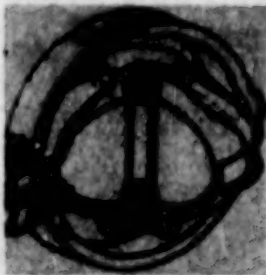
Large Space Antenna Systems Technology - 1982
NASA Langley Research Center
November 30 - December 2, 1982

Control Moment Gyro (CMG) research efforts are aimed at establishing the technology deemed essential to permit the precise, robust, long-term, and reliable control of large space systems. As such, research will be concentrated on the laboratory evaluation of a double-gimbal CMG having a momentum capacity of 4500 ft-lb-sec and a torque output capability of 200 ft-lb through the utilization of two direct-drive, brushless DC torquers per gimbal. Results obtained from the characterization testing program will be used to generate a high-fidelity mathematical model of the CMG for use in system simulations and trade-off studies.

CONTROL MOMENT GYRO (CMG)

TECHNOLOGY AREAS

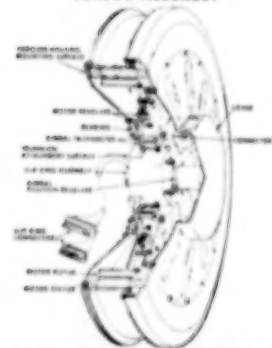
IMPROVED H/M RATIO
ROTOR STIFFNESS
SPIN BEARING
LUBRICATION



MOMENTUM - 4500 FT-LB-SEC
TORQUE - 200 FT-LB
WEIGHT - 630 LBS

TECHNOLOGY AREAS

DIRECT-DRIVE BDC MOTORS
GEAR TRAIN BACKLASH
LOW TORQUE CAPABILITY
LONG LIFE
DIRECT DRIVE TORQUER/
SENSOR ASSEMBLY



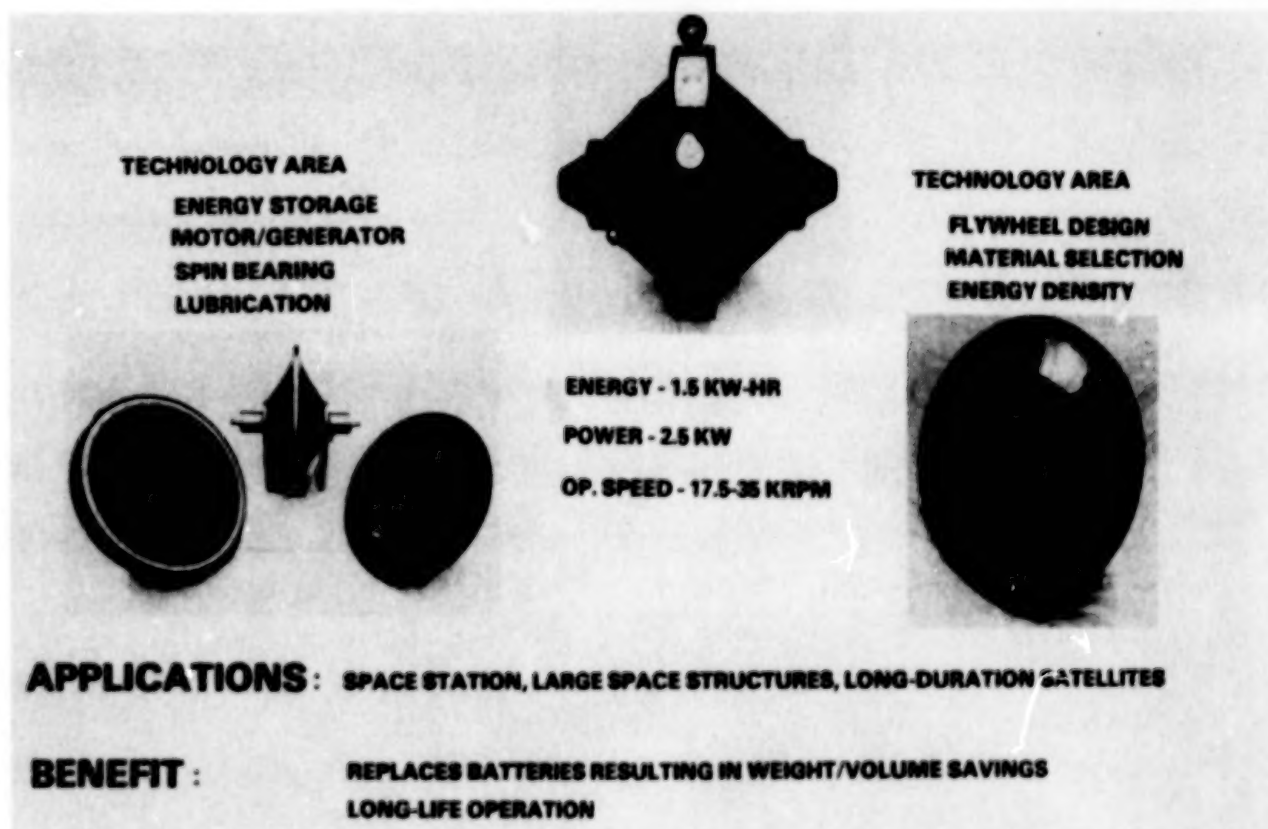
APPLICATIONS : MANNED SPACE STATION, LARGE SPACE STRUCTURES, LONG DURATION SATELLITES

BENEFIT :

LARGER MOMENTUM PERMITS FEWER DESATURATION MANEUVERS
LARGER MOMENTUM MEANS FEWER UNITS, THUS LOWER WEIGHT/VOLUME
FEWER UNITS RESULTS IN REDUCED SOFTWARE COMPLEXITY

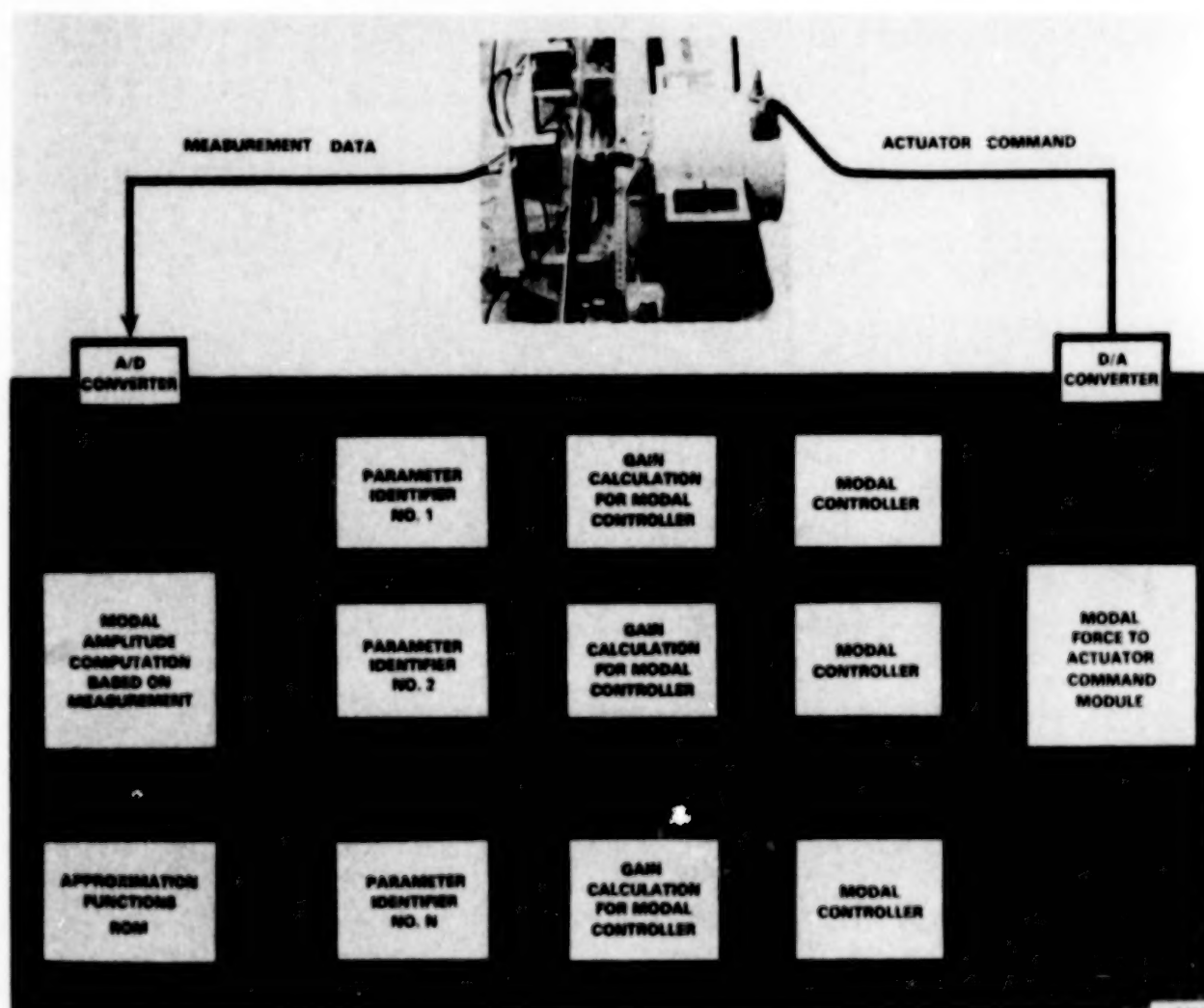
The effectiveness of momentum storage devices for providing control of a space vehicle's attitude has been demonstrated in flight. However, in most cases, the full potential of these devices was not utilized. One approach to realizing the full capability of a gimballed momentum device is to combine the control functions associated with such a unit with those attendant with energy storage and power generation. The unit shown in the figure is the rotating assembly of a double-gimbal IPACS (Integrated Power/Attitude Control System) unit. This device is capable of storing 1.5 kW-hr of energy and of delivering 2.5 kW of power at 52 V DC. In addition, it is designed to provide 20 ft-lb of torque required for control of an unmanned spacecraft. The research on this device will concentrate on establishing the generic technology associated with such a concept to permit future applications. These efforts will consist of characterization testing, math modeling, and utilization of such models in system trade-off analyses.

INTEGRATED POWER/ATTITUDE CONTROL SYSTEM (IPACS)

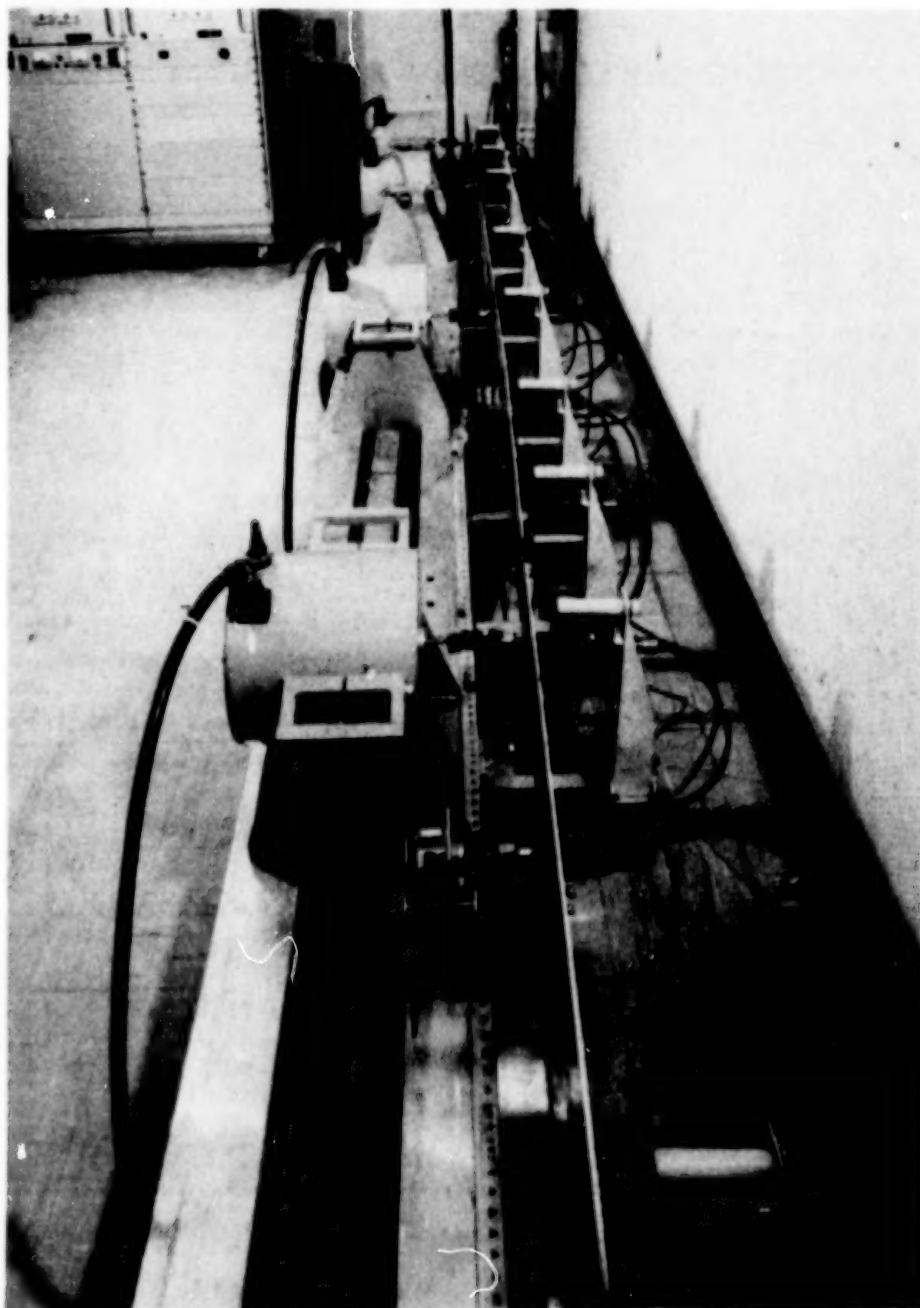


Research is in progress on modal adaptive control wherein measurement data are converted to modal amplitudes using a modal decomposition based on approximate mode shapes. The problems of on-line testing to obtain mode-shape approximations and the number of parallel channels required are treated further on in this presentation. After modal amplitudes are obtained, an ARMA parameter identification is made to identify modal frequency, damping, and control effectiveness for each mode. These parameters are used in a modal control design algorithm to calculate modal control feedback gains. Both proportional and on-off modal controllers have been examined in our research facility.

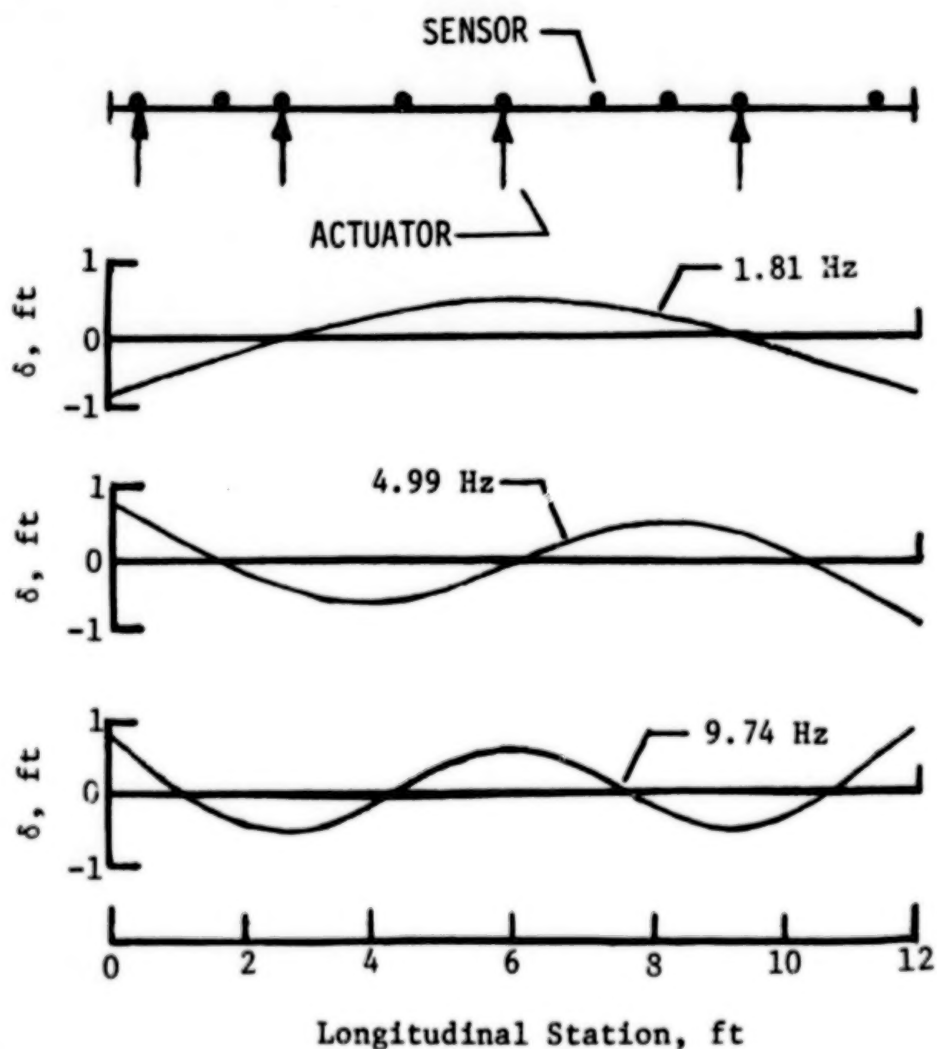
DISTRIBUTED ADAPTIVE CONTROL



The facility used for all experimental results presented herein is shown below. The photograph shows the end view of a beam, which is the structural test article. Four actuators are attached to the beam and can move it in the horizontal plane. Noncontacting displacement sensors measure the deflection of the beam at nine stations along the longitudinal axis of the beam. Compensation networks are used to reduce the effect of friction and viscous damping at the actuator attachments. Thus, the beam should behave essentially as a free beam in space with respect to transverse motions in the horizontal plane.



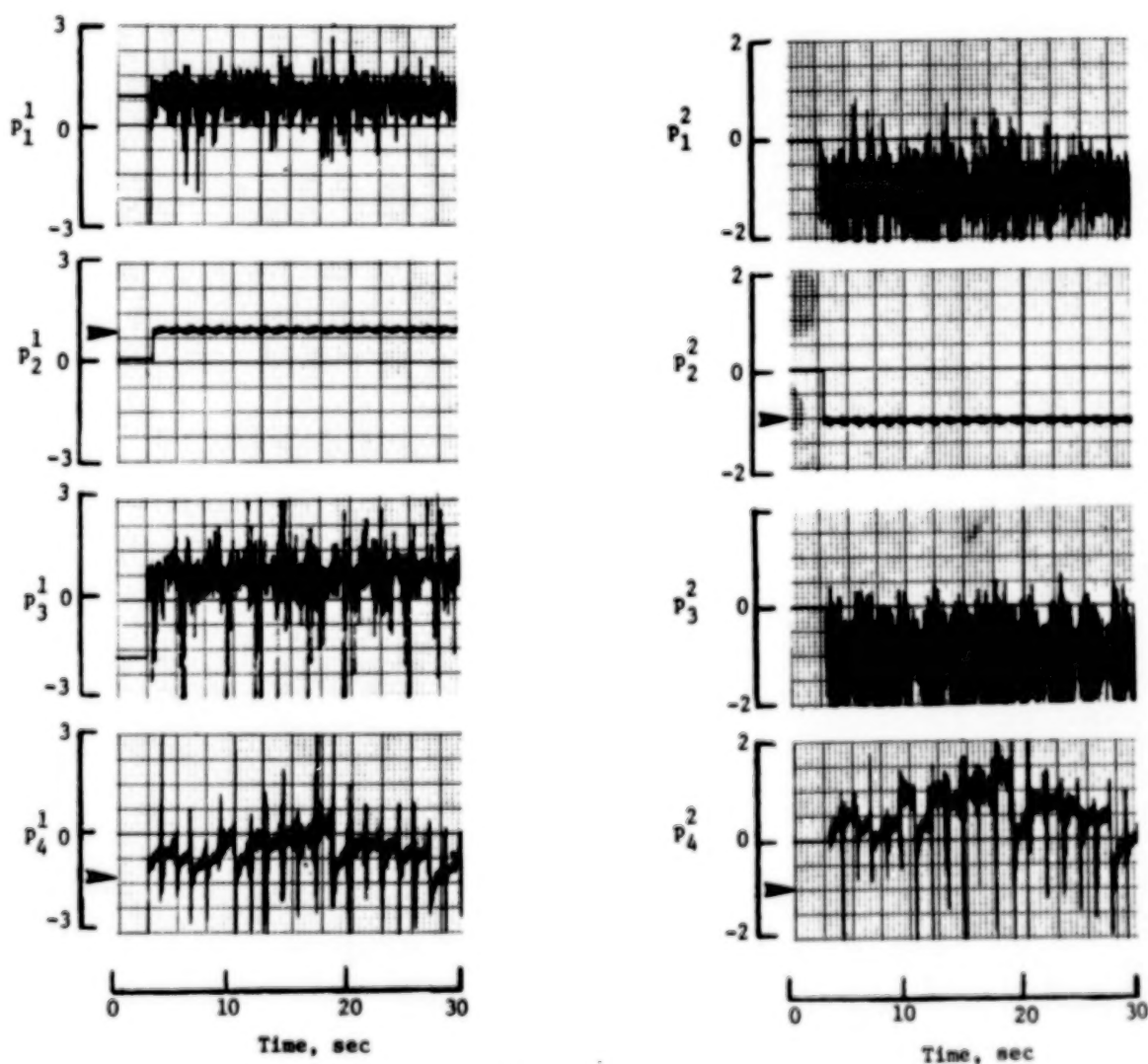
The studies reported herein were carried out using the free-free beam experimental setup at NASA Langley. The system consists of nine deflection-measuring sensors and four electromagnetic actuators. The mounting locations are indicated in the figure below. For the study, the first three flexible mode shapes and frequencies obtained using SPAR are also illustrated.



The parameter identification of the frequency and damping terms in an ARMA model of the dynamics of the beam is shown here. In this case only the second flexible mode was excited in an infrared vibration. Note that the characteristics of that mode are well identified (second set of graphs from the top), in agreement with a SPAR model, whereas the others are not. This indicates the need for testing the validity of the parameter estimates before modifying the control system design model.

OUTPUT OF PARAMETER IDENTIFIERS

MODE 2 EXCITED



► SPAR DERIVED VALUES

The main advantages of using lattice filters in large space systems control are described below.

- PROPOSED METHOD:

USE OF RECURSIVE, LEAST-SQUARE, LATTICE FILTERS FOR THE
IDENTIFICATION OF LSS DYNAMICS

- LATTICE FILTER:

RECURSIVE BOTH IN ORDER AND TIME

WIDELY USED IN ADAPTIVE SIGNAL PROCESSING (SPEECH, COMMUNICATION)

EASY IMPLEMENTATION - IN CHIP FORM

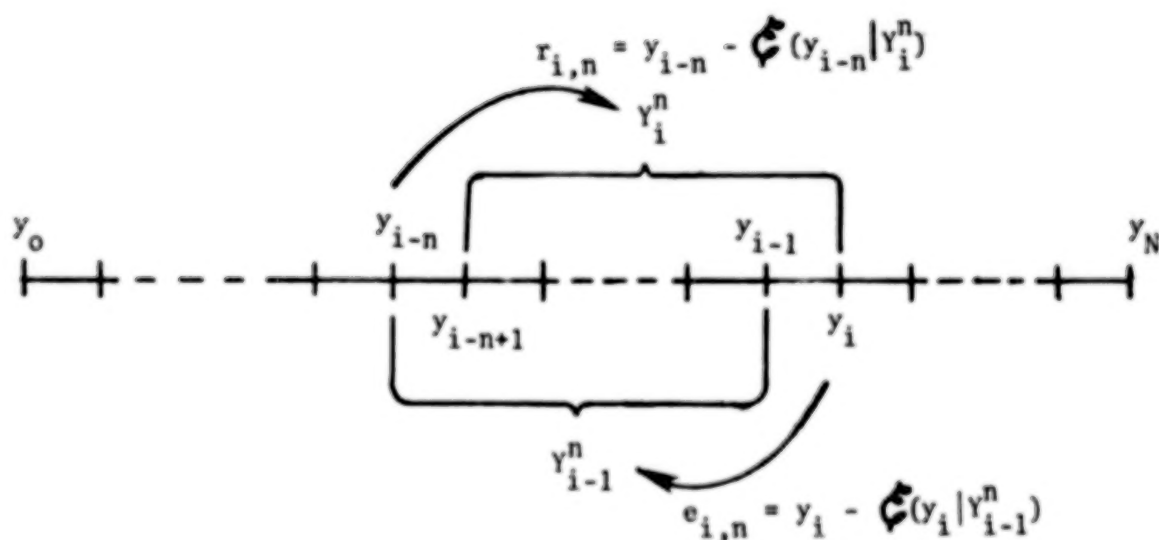
EXCELLENT NUMERICAL BEHAVIOR

- THE METHOD:

DETERMINES SYSTEM ORDER ON-LINE AND ALSO THE MODE SHAPES
FROM OUTPUT MEASUREMENTS

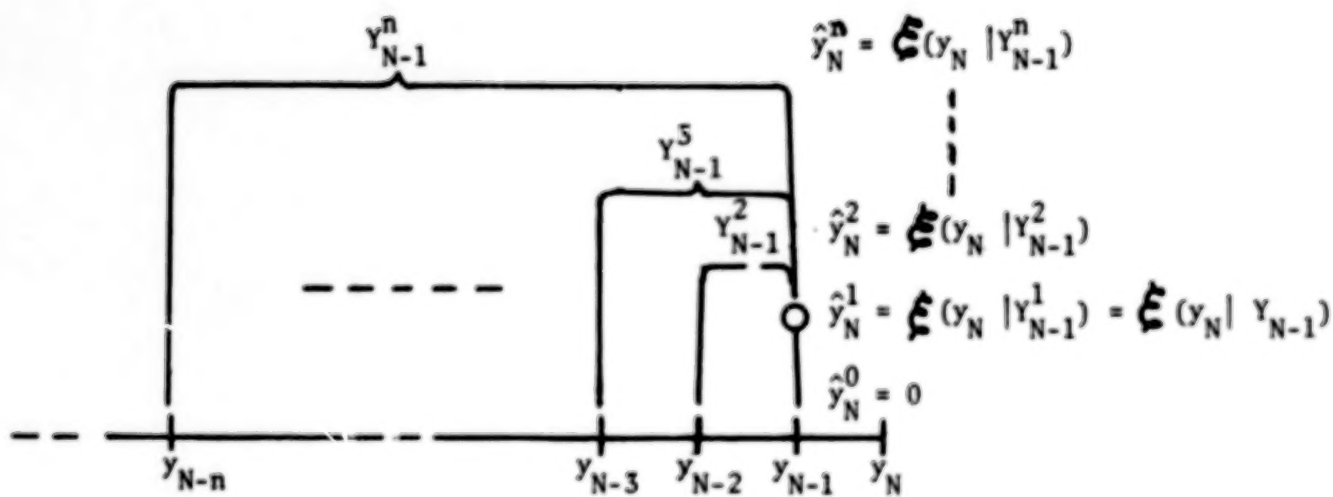
The lattice filter essentially uses two kinds of residual sequences, namely the forward residual $e_{i,n}$ and the backward residual $r_{i,n}$. In the symbol $e_{i,n}$, i stands for time instant and n stands for order. Thus it is seen that $e_{i,n}$ is recursive in both time and order. The symbol \mathcal{E} stands for orthogonal projection operator, with $\mathcal{E}(y_i/y_{i-1}^n)$ meaning the orthogonal projection of y_i on the space spanned by the last n measurements.

FORWARD AND BACKWARD RESIDUALS



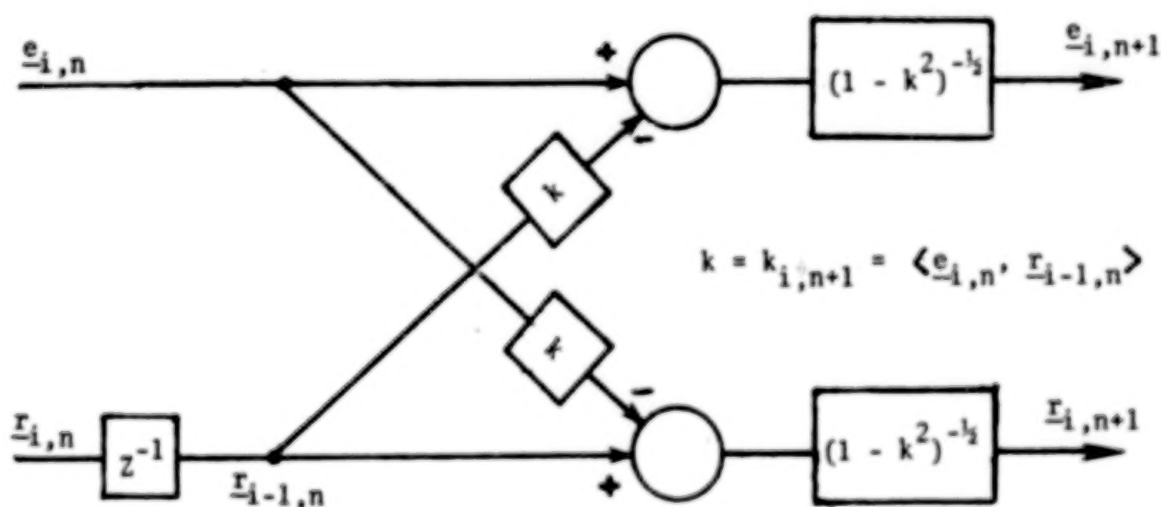
The most useful property of lattice filters is that, at any instant, all estimators of order from 0,1,2...n are available. This is clearly brought out in the figure below, and this property can be used for on-line change in estimator order, depending upon the system characteristics.

NESTING OF ESTIMATION



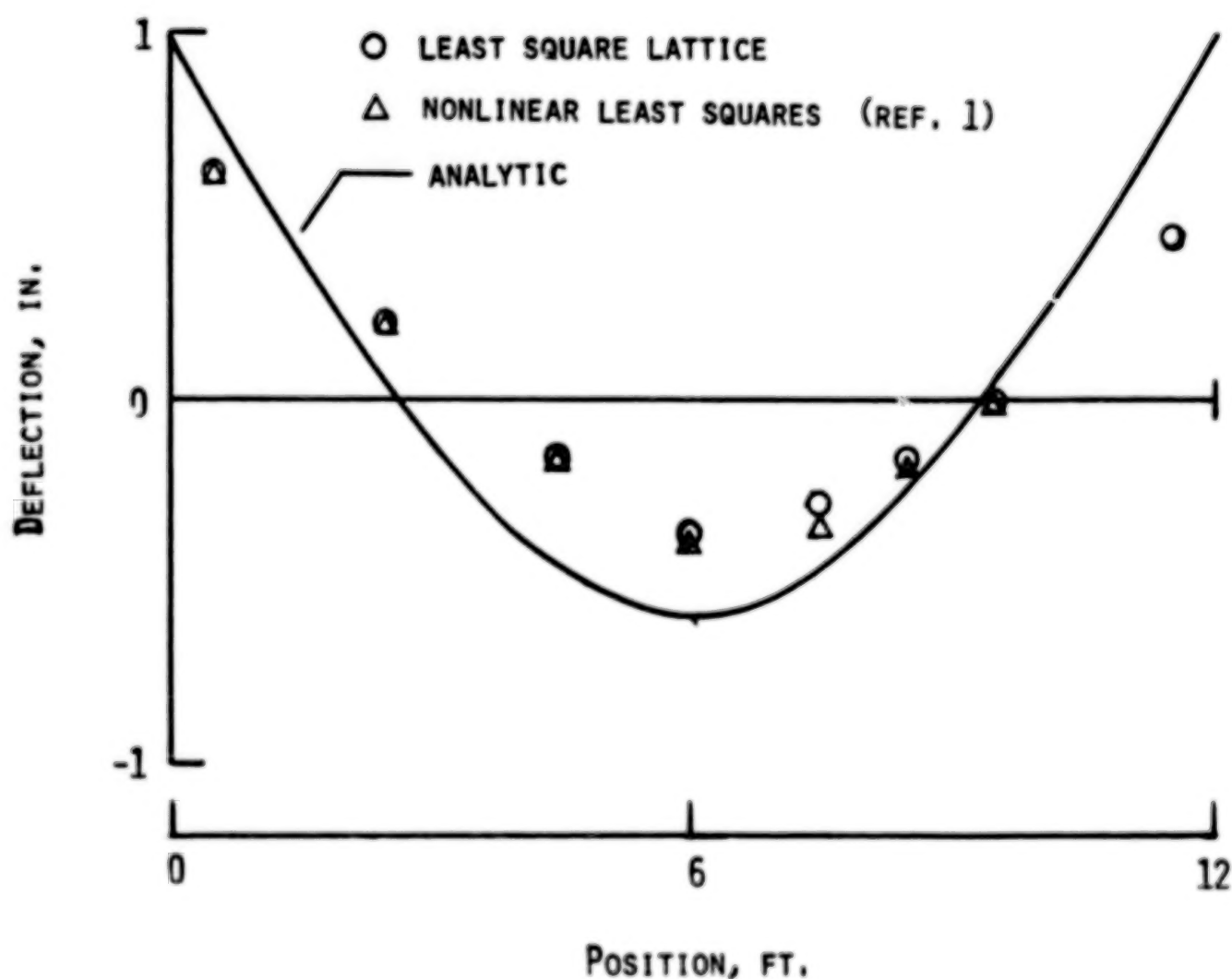
A typical block diagram for the lattice section is given below. It can be seen that the forward and backward residuals are interrelated by the reflection coefficient $k_{i,n}$. Also, this involves a delayed backward residual $r_{i,n}$, indicated by z^{-1} . The "lattice" filter derives its name because of this kind of lattice section, which is commonly described in the network synthesis area.

LATTICE SECTION



Here, two algorithms operating on different sets of measurement data are compared. Both obtain essentially the same primary mode shape from the experimental apparatus. For reference, the mode shape predicted from SPAR is also plotted. The disparity is believed to be caused by the spring and mass characteristics of the actuators, which were not included in the SPAR model.

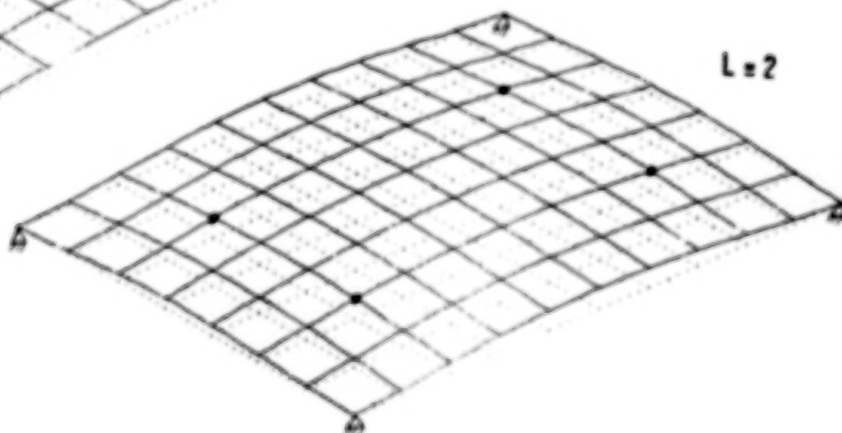
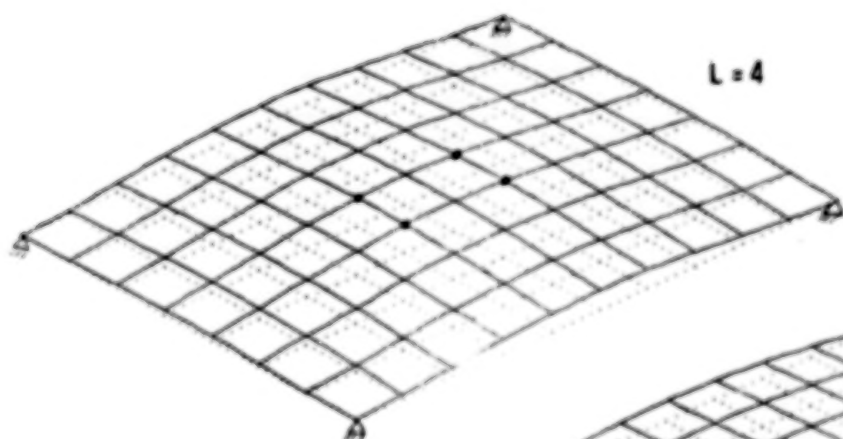
COMPARISON OF ESTIMATED MODE SHAPES



A minimization criterion has been developed to determine optimal sensor and actuator placement. It has been used successfully to determine optimal actuator placement for static shape control of the beam and the grid (plate) shown in the figure. It is assumed that the actuator loads are to be readjusted following any failures, but that the locations cannot be changed. The overall criterion is the shape control of the grid; that is, the integral square error between the actual shape of the grid and a desired one should be minimized.

PERFORMANCE OPTIMIZATION OVER MISSION LIFE CONSIDERING RELIABILITY

Application to Grid Structure

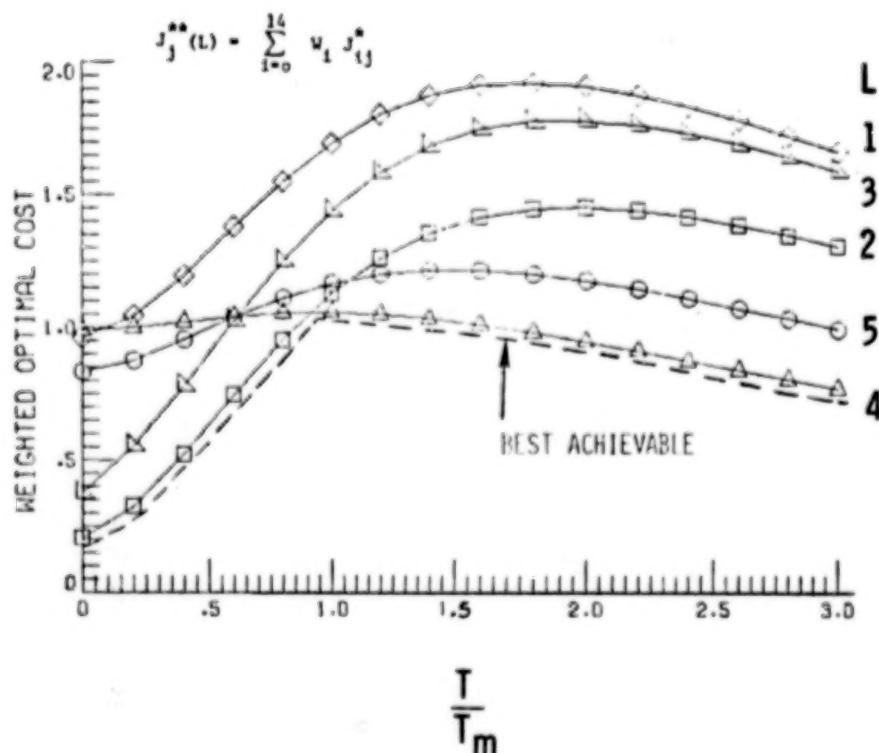


$$J^*(L) = \min_u \int_0^1 (\delta - \delta_d)^2 ds$$

When reliability of the actuators is considered, the criterion is modified to the expected value of the integral error; that is, the sum of the integral square error for each possible failure state considered, multiplied by the probability that the state will occur. The criterion is shown plotted as a function of the ratio between the mean time to failure of the actuators (T_M) and design mission life (T). The optimal location of the actuators indicates configuration 2 for short design mission life and configuration 4 for long design life. This result is expected, since for short life the actuators probably will not fail, and the designer will opt for the higher performance achievable by distributing the actuators, without considering the performance degradation that will result if one or more components fail. On the other hand, if the design mission life is long, the designer should select configuration 4 because the actuator locations are such that, by increasing the load, one actuator can nearly substitute for any failed one.

SELECTION OF BEST CONFIGURATION

Relation to Design Mission Life and Component MTBF



The table shows the effects of parameter errors on the closed-loop stability of the beam using a modal control law. The table shows the range of parameter errors that can be tolerated and still yield stability in the noncollocated modal control design. It appears that the system will be stable for parameter identification errors in the range of the algorithm tested. A linear modal distributed control system has been developed and tested using the beam facility. The tests demonstrated the ability to use noncollocated feedback of sensors to actuators through a modal control scheme. Noncollocated design is of fundamental importance in analytic redundancy management to handle the sensor-actuator control loop reconfiguration in the event of failure of control system components.

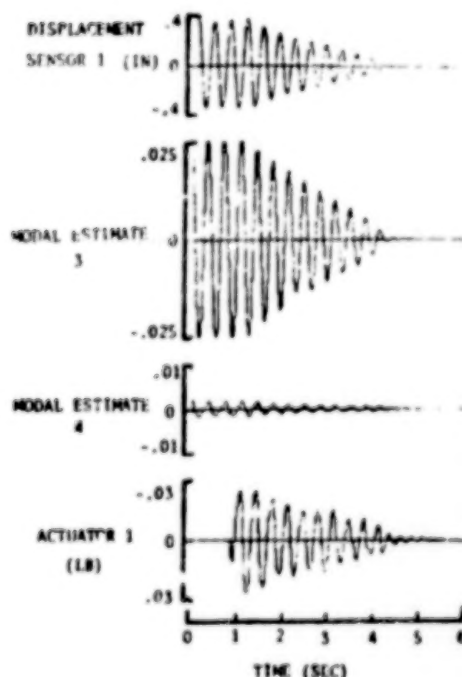
CONTROLLER DESIGN STUDIES

PARAMETER ERROR SENSITIVITY

CASE	MODE 3	MODE 4	MODE 5	MODE 6
I 4 CONT. 4 ACT.	-4 to +6%	-10 to >30%	Not controlled	Not Controlled
II 5 CONT. 4 ACT.	-6 to +14%	Initially unstable	-14 to >30%	Not Controlled
III 6 CONT. 5 ACT.	-8 to +8%	-12 to >30%	-16 to >30 %	-2 to +2%

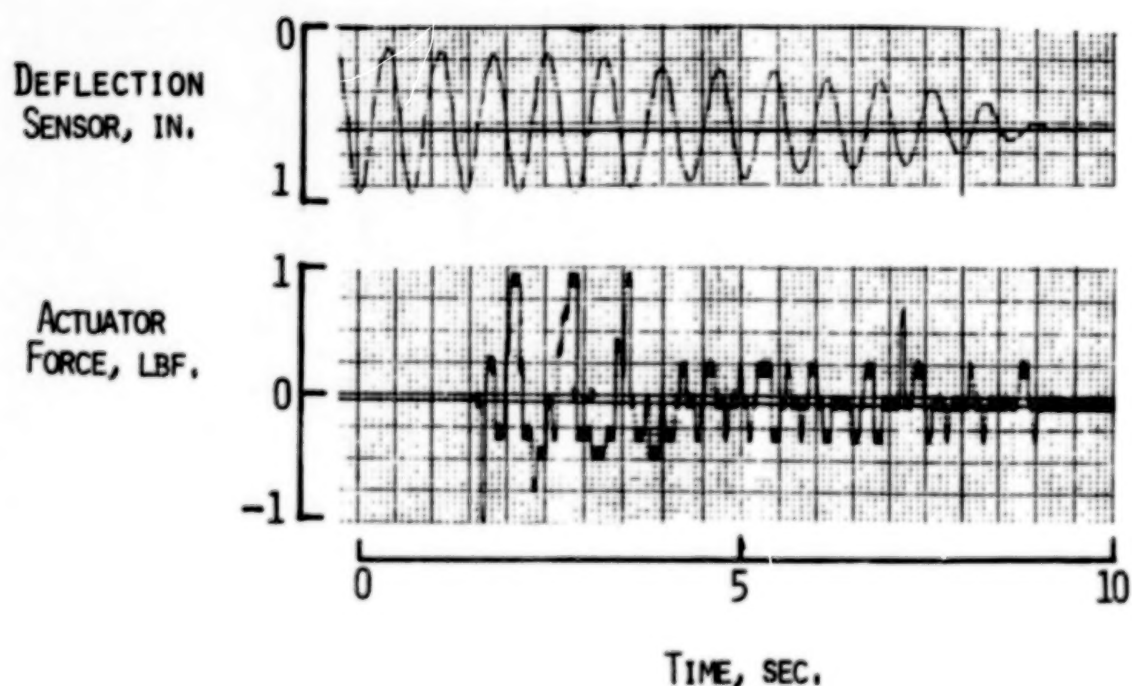
EXPERIMENTAL RESULTS

FIRST FLEXIBLE MODE EXCITED

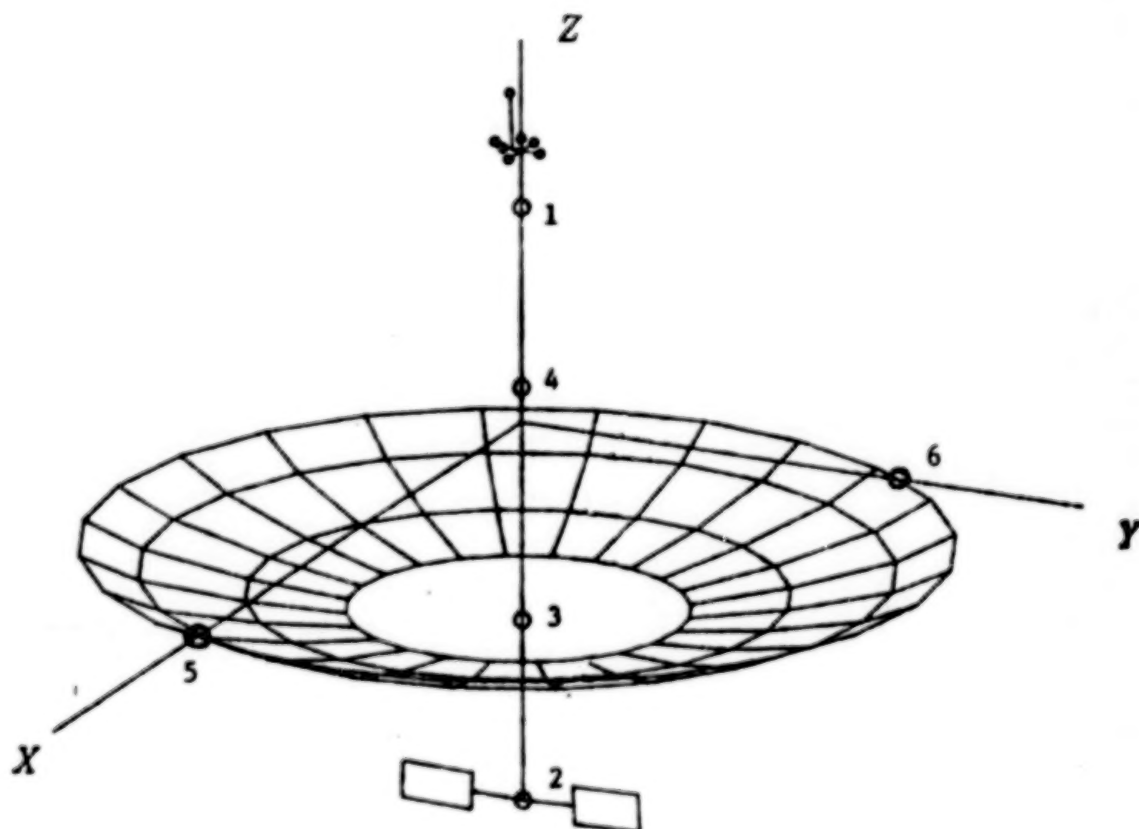


An on-off modal control law has also been implemented on the experimental facility. The top graph shows the displacement of the beam as recorded by the sensor located at $x = 2.5$ ft from the end. The bottom graph shows the force exerted on the beam by the actuator at the same location. The quantization in the actuator space is evident. It is clear that the control system suppressed the vibratory motion of the beam in a very short period of time.

ON - OFF MODAL CONTROL



A control-design analysis is under development for a large space-based antenna system. A NASTRAN model of a 122-m-diameter hoop-column antenna is being used as the basis for the design. The schematic sketch shows possible locations for the two types of controllers employed in the simulated studies. Control moment gyros and/or reaction control jets can be located at positions 1 to 4 along the mast, and reaction control jets can be located at positions around the hoop.



ANTENNA CHARACTERISTICS

Diameter = 400 ft.

$$W = 10020 \text{ lb}$$

$$I_x = 1.360 \times 10^8 \text{ lb-ft}^2$$

$$I_y = 1.365 \times 10^8 \text{ lb-ft}^2$$

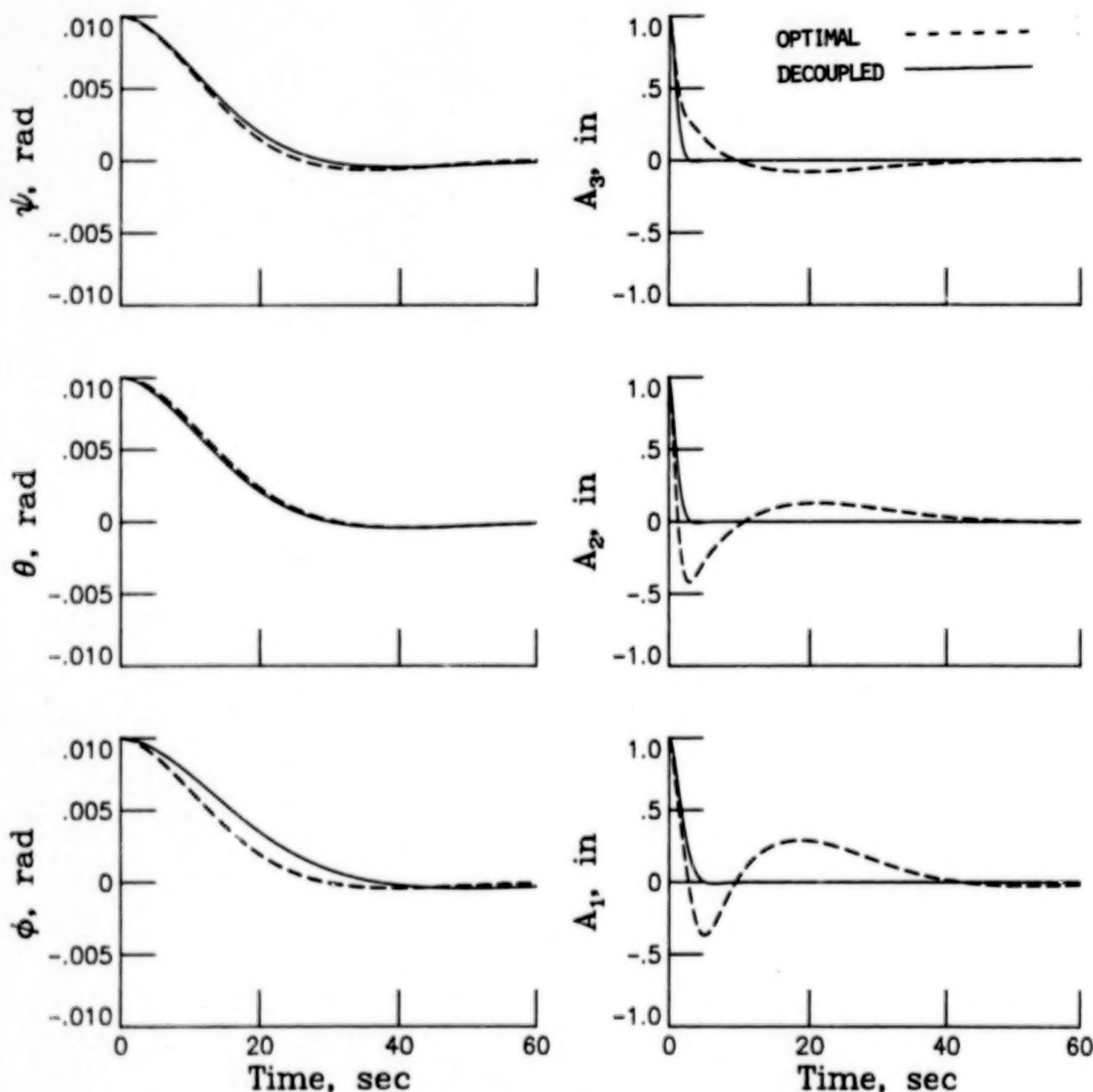
$$I_z = 1.041 \times 10^8 \text{ lb-ft}^2$$

$$I_{xz} = 0.58 \times 10^6 \text{ lb-ft}^2$$

MODE	ω_n , rad/sec	Period, sec
1	.7466	8.42
2	1.346	4.67
3	1.7025	3.69
4	3.1813	1.98
5	4.5294	1.39
6	5.5905	1.12

Various control techniques are being investigated to establish the most reliable and efficient design procedures for the hoop-column antenna. The figure illustrates typical results for two of the design methods investigated. The linear quadratic regulator (LQR) optimal control technique is being used as the basis for comparison of the various techniques. The plots show that the LQR and decoupled control methods produce comparable results for nulling disturbances in the three rigid-body modes and in the first three structural (vibration) modes. Of the two methods, the LQR method is the more complicated because of the iterative process required to achieve desired performance. The decoupled method provides a simple closed-form solution and produces the exact closed-loop dynamics specified for the system.

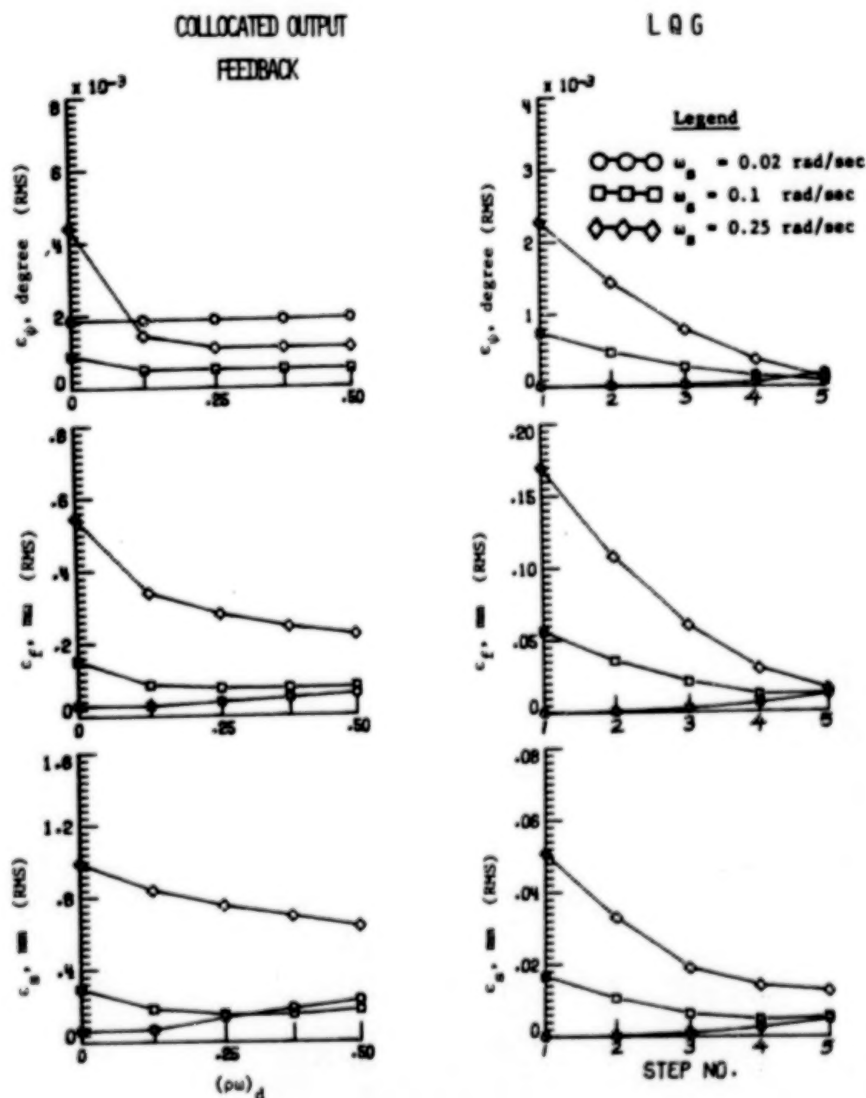
COMPARISON OF OPTIMAL AND DECOUPLED RESPONSES



Control systems were designed for the hoop/column antenna using collocated output feedback and LQG techniques. This figure shows a comparison of performances obtained using the two methods. The controllers were designed for three different closed-loop, rigid-body bandwidths (ϵ_s), and for various values of the (closed-loop) time constant corresponding to the structural modes. (The horizontal axis for the collocated controller figures indicates the desired negative shift in the closed-loop eigenvalues corresponding to the structural modes, which is used as a design parameter. The horizontal axis for the LQG controller indicates successive increase at each step in the "Q" matrix, which indirectly achieves the same effect.)

The expected values of pointing errors, feed-motion errors, and surface errors were computed in the presence of sensor and actuator noise. Although both controllers satisfy the requirements, the LQR controller is found to perform significantly better, especially when a smaller number of sensors and actuators was used.

CONTROLLER PERFORMANCE ANALYSIS



System identification with dynamic models represented by partial differential equations is currently being investigated at Brown University and Langley Research Center. The general approach is to select a distributed model for the system to be identified and apply a Galerkin procedure with spline basis functions to project the problem onto a finite dimensional subspace within which the identification is performed. Theory and software are being developed for a two-dimensional stretched membrane in a form descriptive of the mesh surface of the hoop-column antenna. Given a set of measured displacements $u_m(r, \theta)$ and applied forces $f(r, \theta)$, the solution u is expressed as a finite (bilinear) combination of splined $\alpha_i(r)$ and $\rho_j(\theta)$ with coordinates ω_{ij} . The tension is similarly expressed with coordinates γ (expressed in vector form). The Galerkin procedure defines ω_{ij} as an implicit function of γ , and γ is chosen to minimize a least-squares function of the fit error. Theory has been derived which guarantees that as the order of the u approximation increases, the spline approximation converges to the solution of the distributed model with a stable underlying system identification procedure defining γ .

SYSTEMS IDENTIFICATION APPROACH

- RESEARCH GRANT (BROWN UNIVERSITY)
- GALERKIN PROJECTION USING SPLINE BASIS FUNCTIONS
- STATIC TWO-DIMENSIONAL STRETCHED MEMBRANE EQUATION

$$-\frac{1}{r} \frac{\partial}{\partial r} \left(r E \frac{\partial u}{\partial r} \right) - \frac{\partial}{\partial \theta} \left(\frac{E}{r^2} \frac{\partial u}{\partial \theta} \right) = f$$

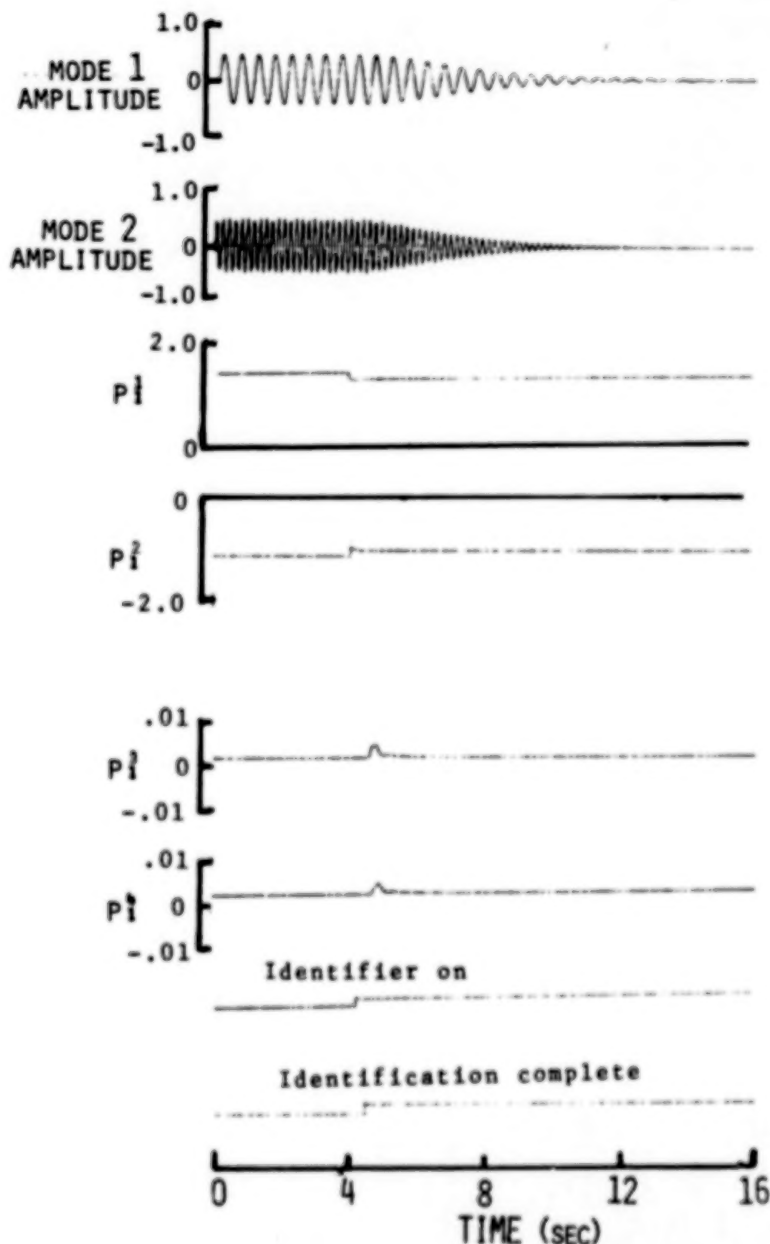
IDENTIFY $E(r, \theta, v)$

$$u(r, \theta, v) = \sum_{i=1}^M \sum_{j=1}^N \alpha_i(r) \omega_{ij}(v) \beta_j(\theta)$$

$$\min_v \sum_n \| u(r_n, \theta_n, v) - u_m(r_n, \theta_n) \|^2$$

A complete closed-loop parameter adaptive control system has been simulated. The system uses an output error formulation to identify parameters for a second-order ARMA model for each excited mode. Linear control gains are then calculated for each mode, and the modal control forces are converted to actuator forces. The first two time histories in the figure below show modal amplitudes for the first two modes. The output of the parameter identifier is shown in the next four time histories. These show rapid convergence to correct parameters. The control is initiated shortly after completion of the identification, and results are as desired.

SIMULATION OF PARAMETER ADAPTIVE CONTROL



REFERENCE

1. Thau, F. E., Eliazov, T., and Montgomery, R. C.: Least-Squares Sequential Parameter and State Estimation for Large Space Structures. Proc. of the 1982 American Control Conference, Vol. 1, IEEE, 1982, pp. 16-21.

INTELSAT VI ANTENNA SYSTEM DESIGN AND DEVELOPMENT

M. F. Caulfield, F. A. Taormina, B. M. Flynn,
S. O. Lane, T. M. Paige, and V. E. Cascia
Hughes Aircraft Company, Space and Communications Group
El Segundo, California

Large Space Antenna Systems Technology - 1982
NASA Langley Research Center
November 30 - December 3, 1982

INTELSAT VI OVERVIEW

As communications between countries continue to grow, so does the need for increasingly complex satellite systems. To meet that need, the International Telecommunications Satellite Organization (INTELSAT) signed a contract with Hughes Aircraft Company for the most sophisticated commercial communications satellite program ever undertaken. This contract is the largest of its kind in history.

INTELSAT, an organization of 106 shareholding countries, supplies to more than 150 countries the capacity to send and receive telephone calls, telegraphs, and television programming. The system presently carries more than 60 percent of the world's overseas traffic and almost all international television via a fleet of satellites operating in synchronous orbit 22,300 miles above Earth.

A team of top international electronics and aerospace firms will join in designing and building the next generation Intelsat VI. These firms are British Aerospace in England, Spar Aerospace Ltd. and COMDEV in Canada, Thompson-CSF in France, Selenia in Italy, Nippon Electric in Japan, and MBB and AEG-Telefunken in Germany.

The Intelsat VI spacecraft will carry 33,000 circuits, the equivalent of 33,000 two-way telephone calls, as well as four television channels. This increased capacity doubles the service of the current Intelsat spacecraft. The satellite's growth capability can expand international service to 100,000 circuits. Each satellite will have 50 transponders operating over the C- and K-band portions of the frequency spectrum. The transponders will be interconnectable using either static switch matrices or a network which provides satellite-switched time division multiple access (SS/TDMA) capability, a major new technology sponsored by INTELSAT. This interconnection provides channel-to-channel connection flexibility.

In order to achieve the communications capacity just described, extensive frequency spectrum reuse is required through the use of spatial and polarization isolation among the various antenna beam coverages. As will be described in this presentation, the performance requirements placed on the Intelsat VI antenna system will make it the largest and most complex commercial antenna system built to date. (See Figs. 1 and 2.)

INTELSAT VI OVERVIEW

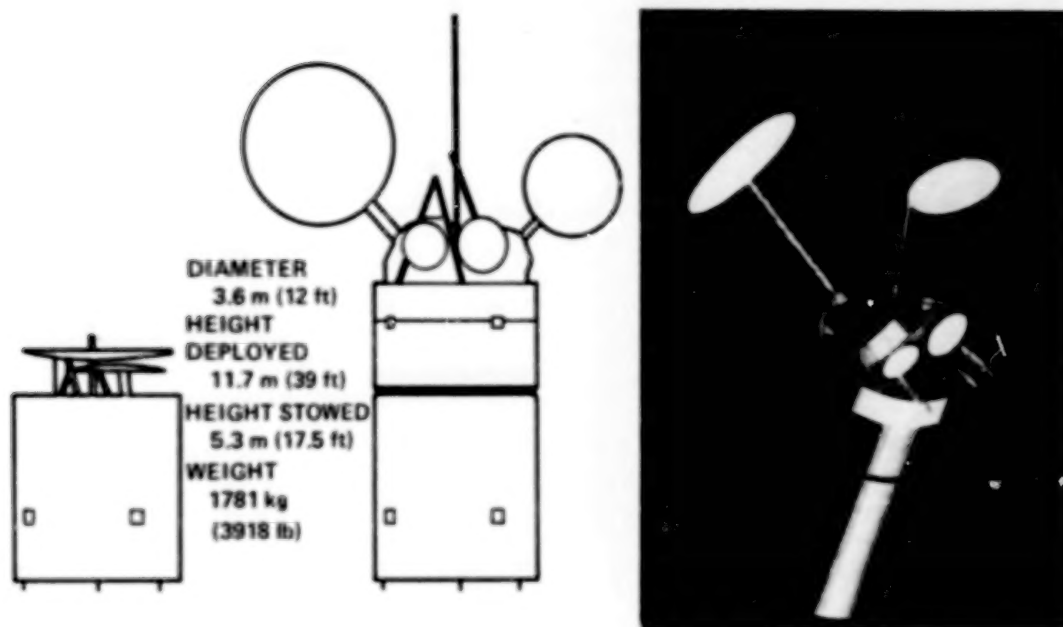


Figure 1

INTELSAT VI ACTUAL SIZE RENDERING

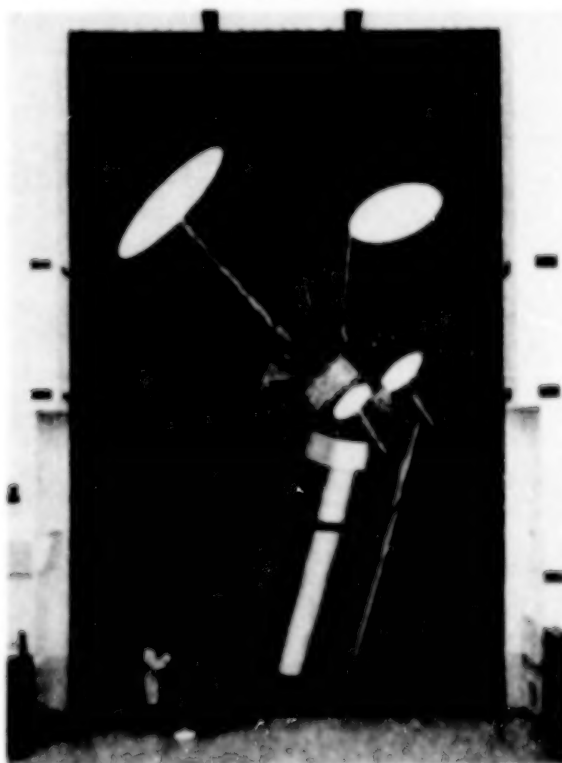


Figure 2

INTELSAT VI SPACECRAFT OVERVIEW

Intelsat VI will be a combination of two satellite designs currently in production at Hughes: 1) the HS 376 extended power spacecraft which in just five years has become the world's standard for providing domestic communications service, and 2) the HS 381 widebody satellite designed to exploit the potential of the Space Shuttle orbiter as a launch vehicle.

The Intelsat VI spacecraft is a spin-stabilized configuration. Its basic bus is derived from the dual spin technology developed at Hughes in the early 1970's and used for Intelsat IV, Intelsat IVA, and Comstar. This technology is used today on 29 of the 37 revenue-bearing satellites in orbit, and has demonstrated over 200 satellite years of successful service.

Intelsat VI is basically a larger and more powerful version of the HS 376 domestic satellite. It incorporates the dual solar panel concept which allows the HS 376 to generate twice the power of earlier spinners. During launch, the outer panel is placed over the inner array and main body of the satellite like a telescope. Once in orbit, the outer array is deployed downward, to expose the upper panel. The deployable solar panel gives the spinning configuration great potential for growth.

Other features of the HS 376 design are also incorporated in Intelsat VI. The communications payload is placed on a stationary cylindrical shelf and heat is rejected radially, similar to the HS 376 design. This arrangement also was chosen to facilitate communication capacity growth for Intelsat VI. The system dynamics and attitude stabilization are similar to the HS 376, as are the spacecraft structural concepts. (See Fig. 3.)

A number of important design features have been taken from the HS 381 widebody satellite program. The "Frisbee" ejection concept provides a simple, reliable technique for releasing the spacecraft from the Space Shuttle. A spring and latch mechanism gives an upward motion to the spacecraft. As the spacecraft leaves the orbiter bay, this ejection provides a slow spin for gyroscopic stability. The perigee boost into transfer orbit is then provided by a simple solid rocket motor controlled by an onboard timer. Other features of these widebody satellites found in Intelsat VI include a liquid bipropellant propulsion subsystem, nickel-hydrogen batteries, and microprocessor control of the command, telemetry, and despun functions.

The Intelsat VI spacecraft is nearly 39 feet (11.8 meters) tall in orbit. It is dominated by the large hemi/zone C-band antenna system. The transmit reflector alone measures over 10 feet (3.2 meters) in diameter. The antennas are mounted on the large shelf which also holds the communications equipment. This shelf and the antennas are despun and point constantly to Earth. The antennas will maintain a pointing accuracy within 0.1 degree at all times. For satellite stabilization, the lower portion of the satellite spins at 30 rpm. The spinning section holds most of the supporting subsystems, including the solar panels, batteries, and propulsion tanks.

The Intelsat VI spacecraft can be launched on either an Ariane 4 or the Space Shuttle with equal efficiency. Its launch configuration is 17.5 feet (5.3 meters) tall and its dry weight is 3918 pounds (1777 kg). Diameter of the satellite is nearly 12 feet (3.6 meters).

INTELSAT VI SPACECRAFT OVERVIEW

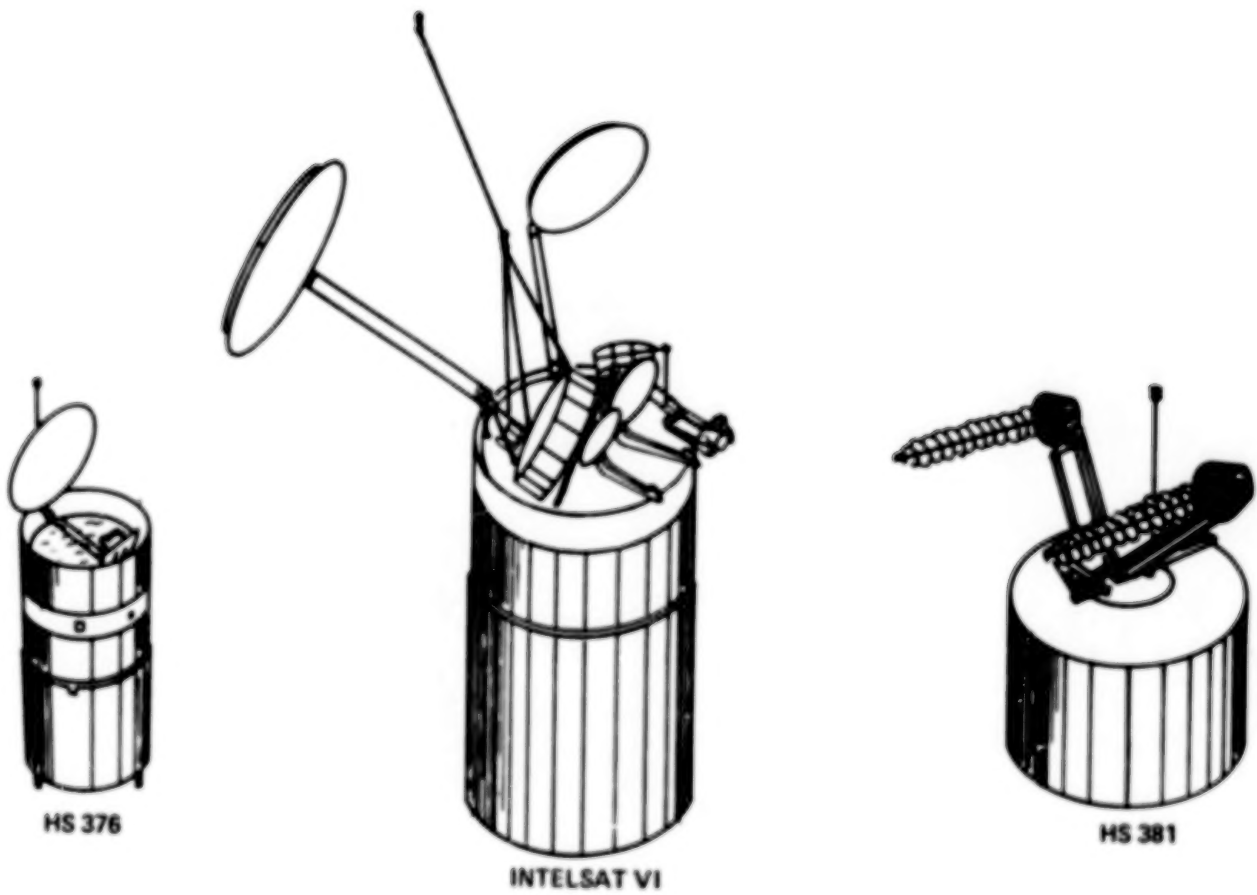


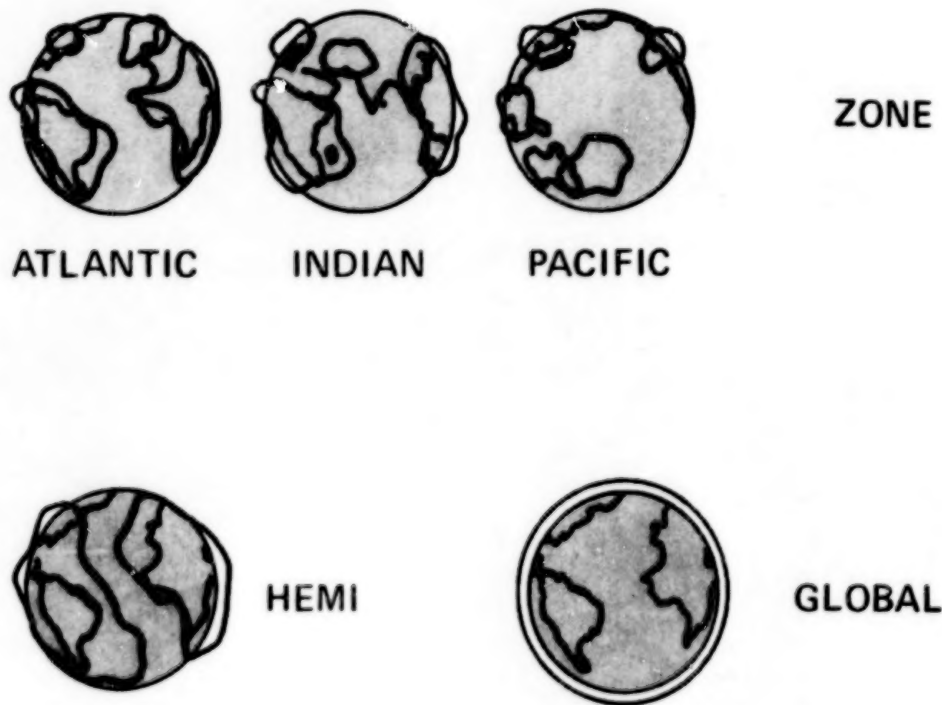
Figure 3

REQUIRED COMMUNICATION COVERAGES

The required communications antenna coverages for Intelsat VI are summarized in Figure 4. At C-band (6 GHz satellite receive, 4 GHz satellite transmit) 3 different types of coverages are required. The 3 coverages are: 1) four spatially isolated zone beams which must be reconfigured for each of the 3 ocean service regions, 2) spatially isolated east and west hemispheric coverage, and 3) global coverage. The closest angular beam-to-beam separation between the spatially isolated beams is 2.08 degrees for the zone beams and 2.80 degrees for the hemispheric.

At K-band (14 GHz satellite receive, 11 GHz satellite transmit) a $3.04^\circ \times 1.64^\circ$ elliptical spot beam and 1.54° diameter circular spot beam are required. The two spot beams must be steerable over the Earth's disc and are isolated from each other by both spatial and polarization isolation.

6/4 GHz COVERAGES



14/11 GHz COVERAGES



Figure 4

ANTENNA COVERAGE C/I REQUIREMENTS

The number, types and carrier-to-interferer (C/I) isolation levels required among the various antenna coverages are illustrated in Figure 5. A six-fold frequency reuse occurs between the 6/4 GHz hemi and zone coverages. For a particular ocean region, the four zone beams which are of the same sense of circular polarization are spatially isolated from each other resulting in four reuses. The two hemi beams are spatially isolated from each other but are oppositely polarized from the zone beams. Hence the polarization isolation between the hemi and zone beams results in two additional frequency reuses yielding the total of 6 reuses. The spatial and polarization levels required between the hemi and zones is either 27 or 30 dB depending upon beam-to-beam separation and/or overlap.

The 6/4 GHz global coverage beams operate in a different part of the 6/4 GHz frequency band from the hemi/zone coverages. In the global channels two-fold reuse is obtained by polarization isolation. The required polarization isolation requirement is specified in terms of meeting a voltage axial ratio of 1.09 volts for the two circularly polarized global coverage beams.

The 14/11 GHz steerable spot beams are linearly polarized. The polarization of the east spot beam is orthogonal to that of the west spot in both the 14 and 11 GHz coverages. Since the two beams are spatially separated, two frequency reuses are obtained by both spatial and polarization isolation. The C/I isolation values required vary between 25 to 33 dB depending upon the beam-to-beam separation of the two spots.

6/4 GHz HEMI ZONE



6 REUSES
C/I: 27 OR 30 dB

6/4 GHz GLOBAL



2 REUSES
C/I: VOLTAGE AXIAL
RATIO OF < 1.09

14/11 GHz SPOTS



2 REUSES
C/I: 25 TO 33 dB
DEPENDING ON
SEPARATION

Figure 5

14/11 GHz SPOT BEAM IMPLEMENTATION

The 14/11 GHz receive/transmit east and west steerable spot beam antennas consist of two separate offset reflectors, each fed by a single dual-polarized/dual-frequency feed horn. Except for the method chosen for beam steering, the antennas are identical in design to those used on the Intelsat V spacecraft (Fig. 6).

The west spot beam antenna has an offset parabolic reflector with a projected aperture diameter of 1.12 meters, a focal length of 1.12 meters, and an offset height of 0.06 meter. The east spot beam antenna has an offset reflector which is quasi-parabolic in that its surface is shaped to achieve optimum performance for the elliptical coverage beam. It has a projected aperture diameter of 1.0 meter, a focal length of 1.0 meter, and an offset height of 0.04 meter.

The reflector and feed horn of each antenna are rigidly connected together via a graphite support structure. The entire antenna including the support structure is then connected to an antenna positioning mechanism which is used for both beam steering and deployment from the stowed position. This method of steering the beam by moving the reflector and feed horn together has the advantage of incurring no scan loss as the spot beams are moved through their required steering ranges. The two spot beam antennas are mounted directly onto the despun shelf in front of the receive and transmit hemi/zone feed networks.

The spot beam reflectors will be designed and manufactured by British Aerospace. The feed horn and support structure design and manufacture and the overall antenna testing will be performed by Selenia.

- **SPECS IDENTICAL TO INTELSAT V**

- USE EXISTING INTELSAT V REFLECTOR AND FEED HORN DESIGN**

- **INTELSAT V DESIGN**

- WEST SPOT – CIRCULAR PARABOLIC REFLECTOR**

- EAST SPOT – CIRCULAR QUASI-PARABOLIC REFLECTOR**

- CORRUGATED DUAL FREQUENCY FEED HORN**

- NEW SUPPORT STRUCTURE TO TIE REFLECTOR AND FEED TOGETHER**

- **SUBCONTRACT SUPPORT**

- BAE – REFLECTOR**

- SELENIA – SUPPORT STRUCTURE**

- FEED HORN**

- OVERALL INTEGRATION AND TESTING**

Figure 6

HEMI/ZONE MAJOR DESIGN CONSIDERATIONS

The Intelsat VI hemi/zone antennas must provide high performance hemispheric and zone coverage beams which allow frequency reuse via both spatial and polarization isolation and exhibit a high degree of structural and thermal stability. The important design considerations are summarized in Figure 7.

The basic antenna design parameters are determined by the above noted requirements as well as by the need to minimize antenna weight. Antenna geometry, including the reflector diameter, focal length, and offset, is determined by the need for spatial isolation between the zone beams. Choice of a 3.2 meter aperture diameter for transmit is based on the worst case spacing between zones 1 and 3 in the Indian Ocean region (IOR) and has been shown by analysis and experiment to provide adequate margin over the requirements. However, since the technique used to achieve low sidelobes is not sufficiently broadband to accommodate both the receive and transmit frequencies, separate receive and transmit hemi/zone antennas are required. Given this arrangement, a proper choice of the number and dimensions of the feeds and optimization of the amplitude and phase excitations provide the appropriate beam shaping. A high degree of crosspolarization isolation is obtained by the use of multimode Potter feed horns. The hemispheric and zone coverages are orthogonally and circularly polarized for both transmit and receive. Both hemispheric and zone coverages are achieved with one antenna by employing dual polarized feed horns.

Reconfigurability of the zone beams for the three ocean regions is obtained by providing an independently optimized squareax (square coaxial) feed distribution network for each region with switching provided by a group of newly developed squareax switches driven by a common mechanism. An additional squareax layer provides the hemispheric coverages.

The stringent spatial and crosspolarization isolation requirements for the hemi/zone antennas require the appropriate placement of all antennas on the antenna farm. Computer studies were performed to determine the correct placement of the transmit and receive hemi/zone antennas, and the scattering interactions have been reduced to a negligible level.

The design consideration of obtaining a compact, lightweight, and thermally stable feed network is provided by utilizing the Hughes developed TEM squareax line technology. The feed network will be constructed of aluminum to ensure that the amplitude and phase excitations will remain within the necessary bounds to maintain high performance shaped main beams and spatial carrier-to-interference (C/I) ratio performance.

To ensure that the communications antenna subsystem maintains pointing alignment while on station, a structurally and thermally stable antenna structure is provided by using graphite for construction of the reflectors and the antenna support structure. Further reduction of thermal gradients on the antenna structure is achieved by placing thermal blankets around the feed networks, support structure, and feed horns.

A two-axis antenna positioning mechanism is provided on both the transmit and receive reflectors. The mechanisms are used to remove initial prelaunch/launch deployment beam pointing errors, and in a backup mode they are used to continually remove dynamic and thermally induced spacecraft pointing error through a beacon tracker system.

HEMI/ZONE MAJOR DESIGN CONSIDERATIONS

<u>DESIGN CONSIDERATIONS</u>	<u>APPROACH</u>
<ul style="list-style-type: none">● PROVIDE HIGH PERFORMANCE SHAPED BEAMS	SELECT APPROPRIATE FEED HORN DIMENSION AND SPACING USE COMPUTER OPTIMIZATION OF AMPLITUDE AND PHASE EXCITATIONS
<ul style="list-style-type: none">● PROVIDE SPATIAL ISOLATION BETWEEN BEAMS	SELECT OPTIMUM SIZE FOR REFLECTORS TO PROVIDE ADEQUATE C/I WHILE MINIMIZING WEIGHT
<ul style="list-style-type: none">● PROVIDE CROSSPOLARIZATION ISOLATION	USE MULTIMODE, DUAL POLARIZED FEED HORNS
<ul style="list-style-type: none">● PROVIDE THREE OCEAN RECONFIGURABILITY FOR ZONES	USE INDEPENDENT FEED DISTRIBUTION NETWORK FOR EACH REGION, SELECTED BY SQUAREX SWITCHES
<ul style="list-style-type: none">● MINIMIZE SCATTERING INTERACTIONS BETWEEN ANTENNAS	PROVIDE ANGULAR OFFSET BETWEEN TRANSMIT AND RECEIVE REFLECTORS PLACE SPOT ANTENNAS IN FRONT OF HEMI/ZONE FEEDS
<ul style="list-style-type: none">● MINIMIZE NUMBER OF REFLECTORS	USE CONTINGUOUS MULTIPLEXING TO ALLOW SINGLE MODE DESIGN COMBINE HEMI/ZONE COVERAGE ANTENNAS USING DUAL POLARIZED FEEDS
<ul style="list-style-type: none">● PROVIDE LIGHTWEIGHT DESIGN WITH THERMAL STABILITY	USE GRAPHITE REFLECTORS AND SUPPORT STRUCTURE USE ALUMINUM FOR FEED DISTRIBUTION NETWORKS USE THERMAL BLANKETS OVER FEED NETWORKS AND SUPPORT STRUCTURE
<ul style="list-style-type: none">● ALLOW CORRECTION OF POINTING ERRORS	USE TWO-AXIS ANTENNA POSITIONING MECHANISM FOR REFLECTORS AND CLOSED LOOP BEACON TRACKING

Figure 7

HEMI/ZONE AND GLOBAL BEAM IMPLEMENTATIONS

The Intelsat VI communications system requirements are fulfilled through the use of 11 different antennas: 4 GHz transmit hemi/zone, 6 GHz receive hemi/zone, 14/11 GHz receive/transmit steerable east spot beam, 14/11 GHz receive/transmit steerable west spot beam, 4 GHz transmit global, 6 GHz receive global, 11 GHz global beacon, 6 GHz command bicone, 4 GHz telemetry bicone, and two 4 GHz telemetry on-station horns. The arrangement of all of these antennas on the spacecraft in both their stowed and deployed configurations is illustrated in the next figure. This compact stowed arrangement minimizes the Shuttle bay length required and therefore minimizes the launch costs.

Both the receive and transmit hemi/zone antennas consist of offset parabolic reflectors, each fed by an array of 146 dual polarized feed horns (Fig. 8). The transmit reflector antenna has a projected aperture diameter of 3.2 meters, a focal length of 4.19 meters, and an offset height (distance from the bottom of the reflector to the focal axis) of 1.68 meters. The symmetry axis of the transmit antenna is rotated 45° from the spacecraft spin axis. The receive antenna is a scaled version of the transmit antenna. It has a projected aperture diameter of 2.0 meters, a focal length of 2.62 meters, and an offset height of 1.05 meters. The symmetry axis of the receive antenna is rotated 45° also from the spacecraft spin axis but in the direction away from the transmit antenna.

Two dielectrically loaded dual mode horns, based on a proven design used on the Intelsat IV-A spacecraft, are used for the 6/4 GHz global coverages. Each antenna is fed by a polarizer and orthomode-tee combination. All of the global antennas as well as the telemetry horns will be mounted on a common steerable support structure which in turn is mounted directly to the despun shelf. This design provides $\pm 2.0^{\circ}$ azimuth steering to repoint the global antennas when azimuth bias is used for the hemi/zone antennas.

HEMI/ZONE COVERAGES

- USE OFFSET PARABOLIC REFLECTOR WITH 146 FEEDS
- COMBINE HEMI/ZONE FUNCTIONS USING DUAL POLARIZED FEEDS
 - TRANSMIT HEMI/ZONE ANTENNA
 - RECEIVE HEMI/ZONE ANTENNA
- SEPARATE FEED NETWORK FOR EACH ZONE AND HEMI COVERAGES

GLOBAL

- USE DIELECTRICALLY LOADED DUAL MODE HORN

Figure 8

ANTENNA FARM CONFIGURATION

Figure 9 illustrates the entire Intelsat VI antenna farm layout in both the deployed and stowed configuration. As can be seen from this figure, the two hemi/zone antennas dominate the spacecraft configuration.

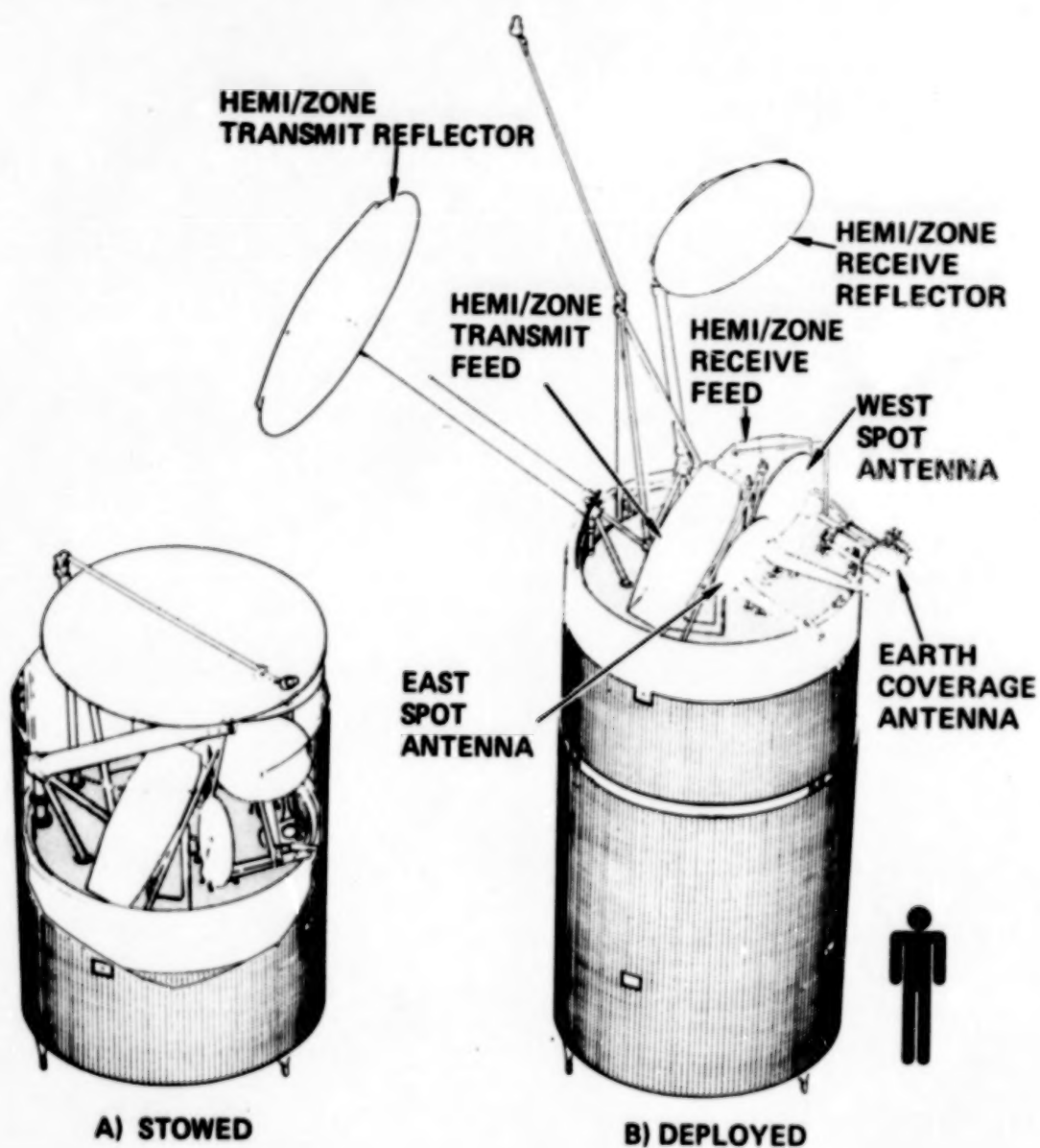


Figure 9

ANTENNA FARM DIMENSIONS

Relevant dimensions of the deployed antenna farm are illustrated in Figure 10.

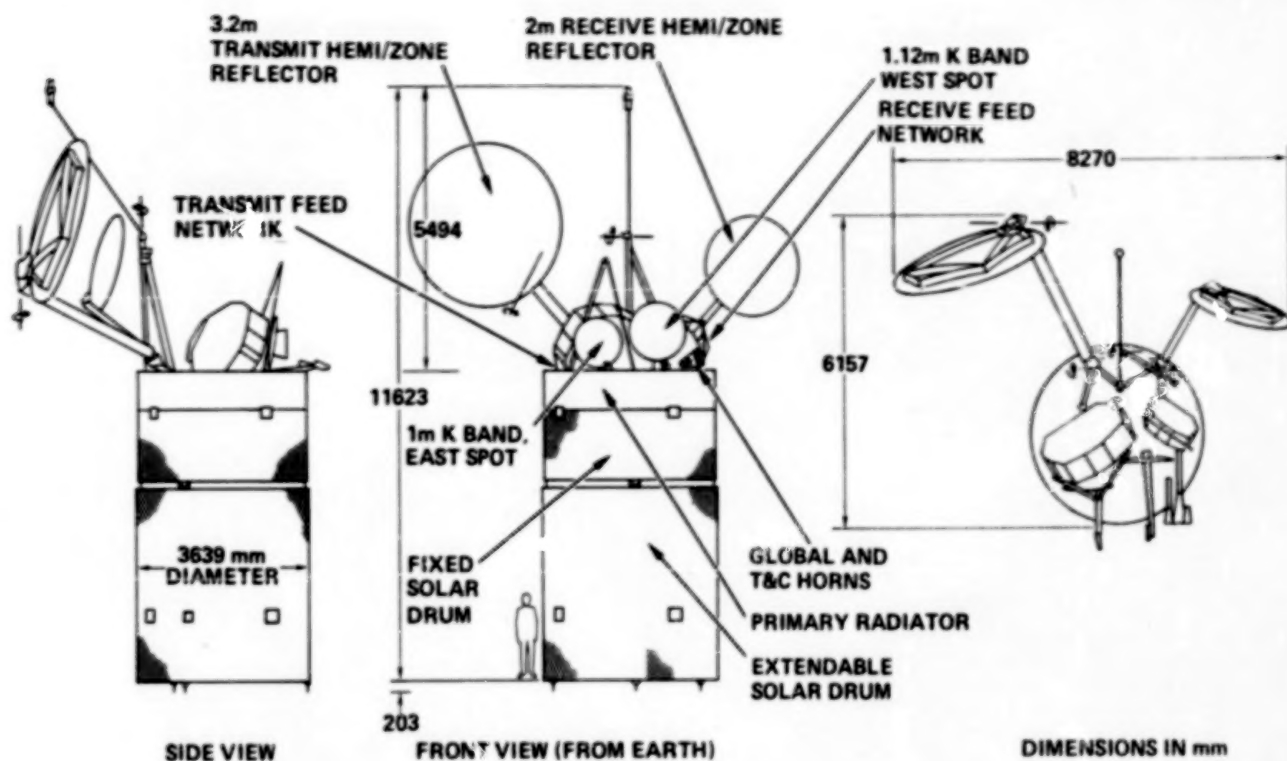


Figure 10

TRANSMIT FEED ARRAY CONFIGURATION

The feed array configurations used for the hemi and the Atlantic, Indian, and Pacific Ocean zones are illustrated in Figure 11. The horns designated as shared horns are used in more than two zone beams simultaneously. Ninety-two switches are required to reconfigure to the transmit zone coverages.

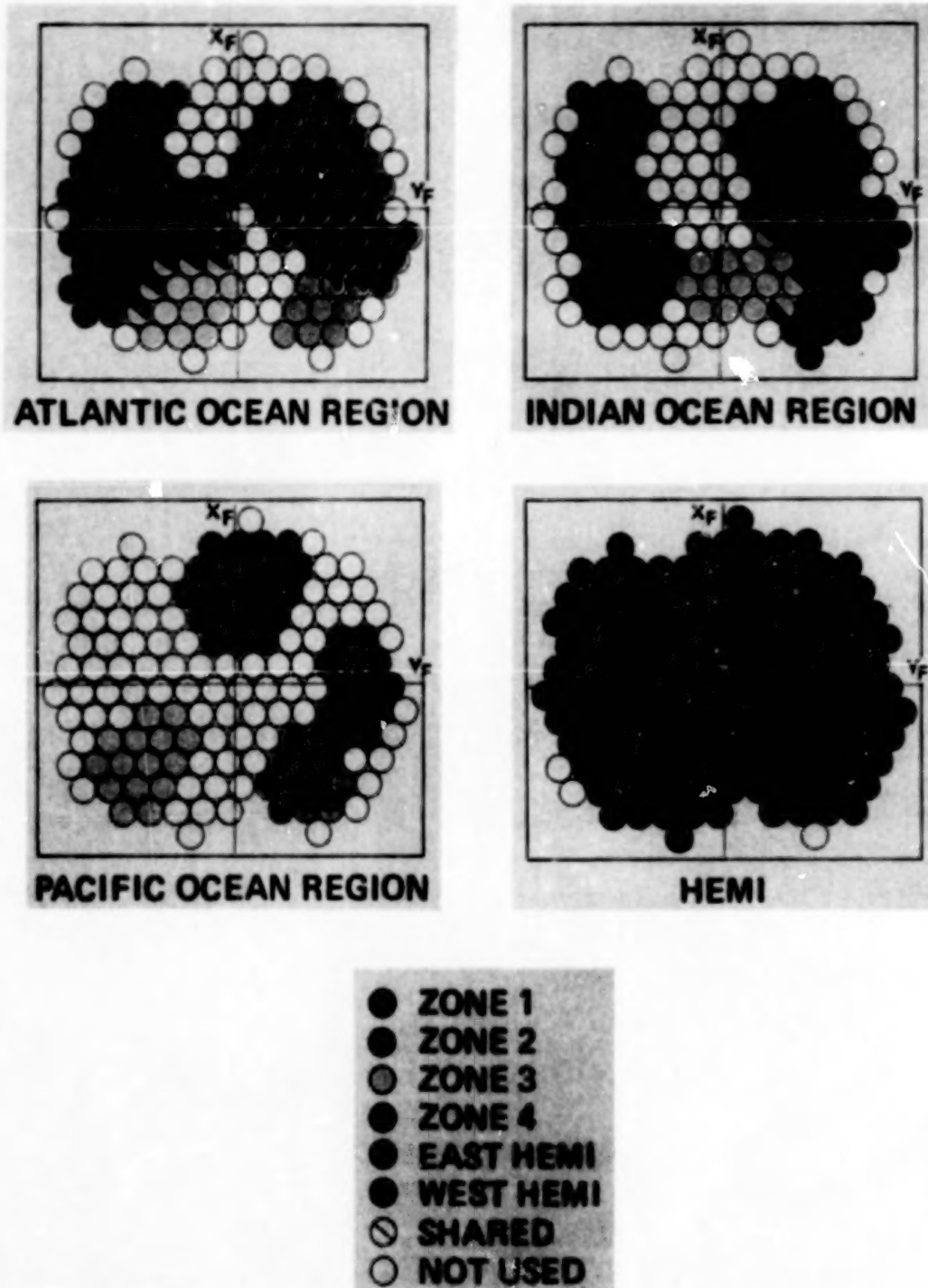


Figure 11

HEMI/ZONE FEED NETWORK IMPLEMENTATION

The hemi/zone antennas provide oppositely polarized hemispheric and zone beams by simultaneously exciting both polarizations in the feed horn array. The feed horn array is fed by four separate feed networks. One feed network is for the hemispheric beams and is used in all three ocean regions. The remaining three networks are used to form the Atlantic, Indian and Pacific zone beams. All four feed networks utilize Hughes developed TEM line squareax technology. An additional squareax layer containing electromechanical switches is used to select the appropriate squareax zone beam feed network for a particular ocean region. The four squareax networks and the switching layer are stacked to obtain a highly compact feed network assembly, as shown in Figure 12. The hemispheric beam feed network and the zone network selected by the switch layer are connected to the four probe polarizers, which generate the two oppositely polarized circular polarizations.

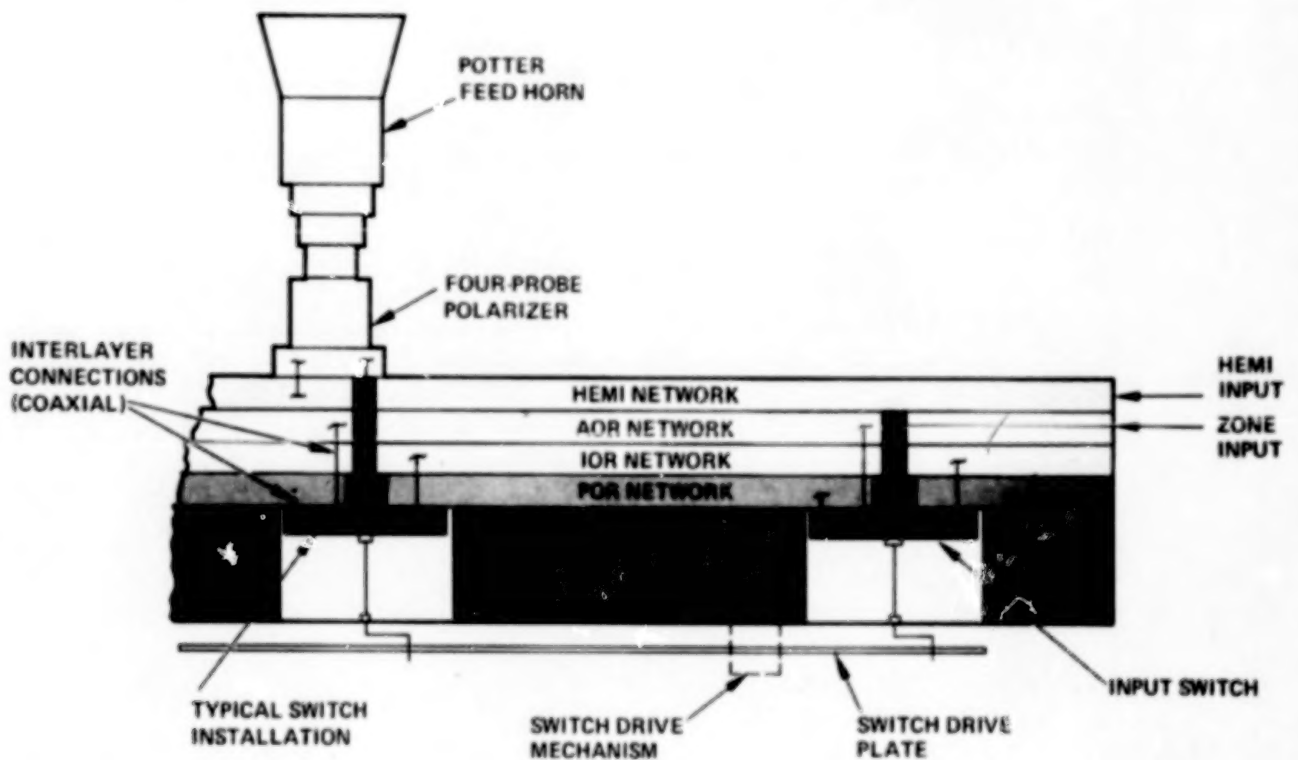


Figure 12

HEMI/ZONE ANTENNA FEED HORN DESIGN

The feed horn design utilized for the Intelsat VI hemi/zone beam antennas is a dual mode circular horn or Potter horn [1] which uses the fundamental TE_{11} mode and a TM_{11} higher order mode. With the proper amplitude and phase combination between the two modes at the horn aperture, equalized E and H plane far field patterns are obtained. Consequently, this horn design is capable of providing better polarization purity (i.e., lower axial ratio) when circularly polarized. The dual mode circular horn design inherently requires the use of a large aperture to support both modes. When a multihorn feed cluster is formed to provide a shaped beam, the larger horn aperture contributes to less mutual coupling between the horns, a fact that has been experimentally observed at Hughes and elsewhere. [2] Less mutual coupling means less degradation in axial ratio in the far fields and better agreement between the theoretically predicted and the measured far field antenna patterns.

Figure 13 illustrates the relative overall dimensions of transmit and receive dual mode feed horns. The excitation of the TM_{11} mode is provided by the final step discontinuity. The length of the horn from the step discontinuity to the horn aperture is adjusted to provide the correct phase relationship between the two modes. Electrical breadboard testing has shown that the correct TM_{11} amplitude excitation and phasing between the TE_{11} and TM_{11} modes can be achieved over the required 11.5 percent transmit and 7.5 percent receive bandwidths.

The feed horns will consist of a one piece, thin-wall aluminum construction. The entire horn will be machined to a nominal wall thickness of 0.51 mm (0.020 in) except in the flange area. It is felt that this approach has resulted in a desirable combination of enhanced production, repeatable quality and minimum weight that is superior to that offered by other fabrication techniques.

- DUAL MODE "POTTER" HORN
- GOOD CROSSPOLARIZATION PERFORMANCE
- LESS MUTUAL COUPLING IN ARRAY ENVIRONMENT

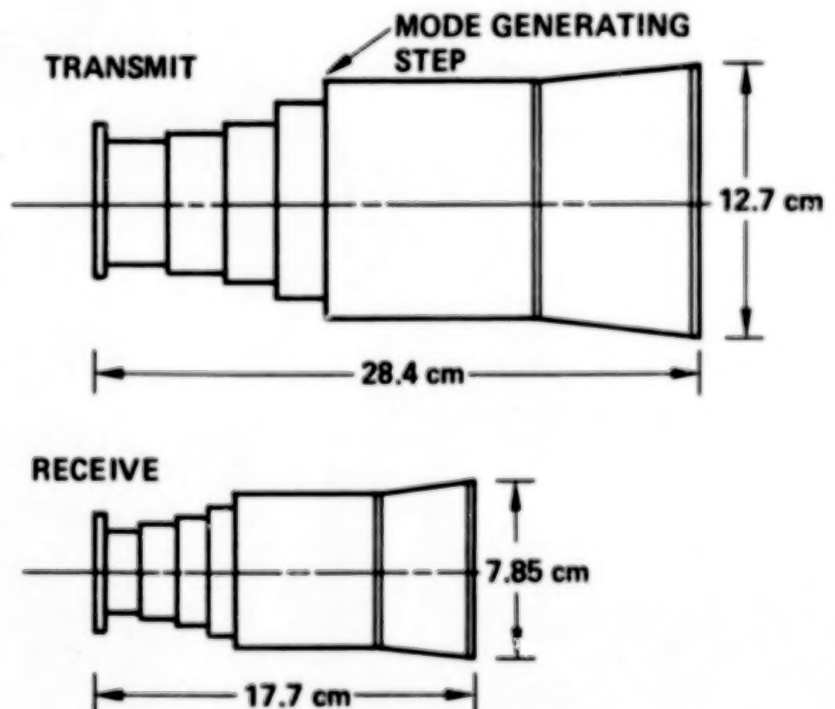


Figure 13

FOUR-PROBE POLARIZER

A circular polarization generating circuit has been designed which permits each feed horn to simultaneously excite both senses of circular polarization with high polarization purity. This design incorporates a four-probe circular waveguide launcher whose opposite ports are driven by three-port 3 dB tees which in turn are fed by a 3 dB quadrature hybrid. An electrical circuit diagram and side view of the four-probe launching circuit are shown in Figure 14.

To generate each sense of circular polarization the four probes must be excited equally in amplitude and with the correct phase progression. This is accomplished by a squareax network which has two inputs and four outputs as shown schematically. The two inputs of the network are connected to the hemispheric and zone TEM squareax networks and the four outputs are attached to the four orthogonal launching probes. The 3 dB hybrid and 3 dB tees generate the four equal amplitude excitations from the two input ports. The correct phase progression of the four probes is obtained by the 90° phase shift of the quadrature hybrid and by proper design of the squareax electrical line lengths to the four probes. Opposite phase progressions are obtained among the probes depending upon which of the two input ports is accessed. Thus circular polarizations of opposite sense are generated for the hemispheric and zone coverage beams.

The four-probe polarizers will be fabricated in aluminum using 4-axis machining. In 4-axis machining, an additional rotational axis is used along with the standard three translational axes in order to perform a circumferential machining operation.

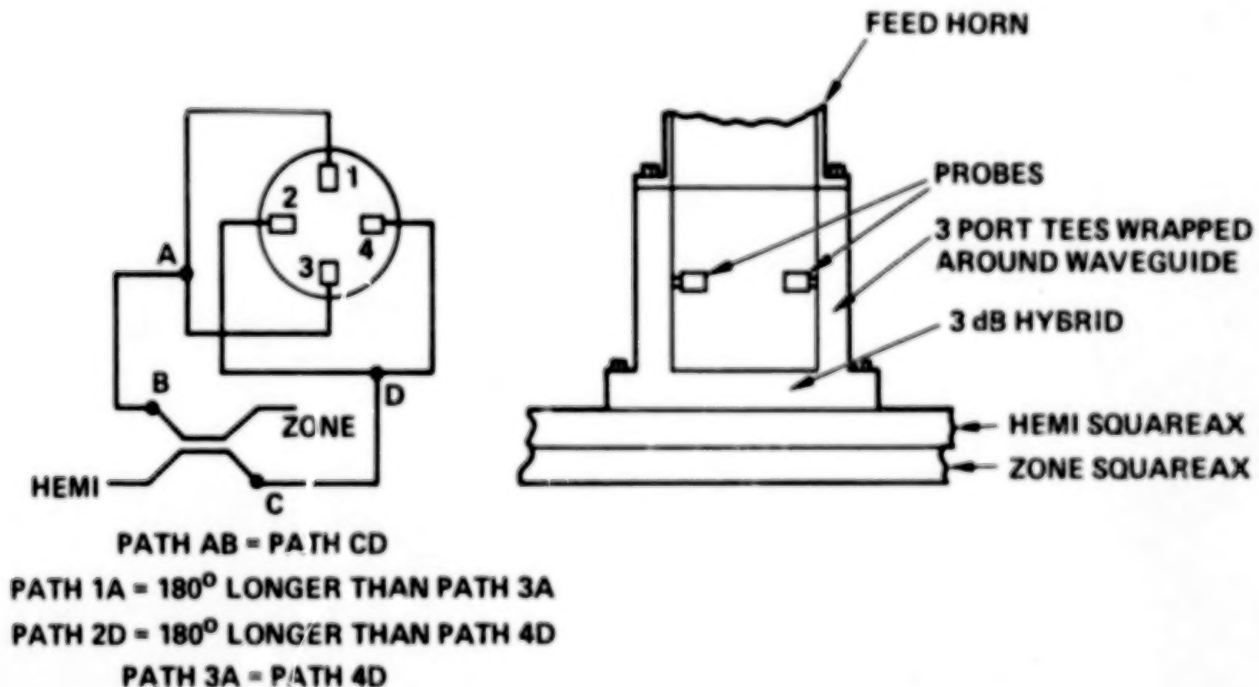


Figure 14

NETWORK IMPLEMENTATION

The feed networks for the transmit and receive hemispheric and zone antennas use the TEM square coaxial (squareax) transmission line technology which was developed by Hughes for Intelsat IV-A and is used extensively on current ongoing Hughes C-band programs. This transmission line combines the layout design features of conventional etched circuit stripline with the performance features of waveguide microwave networks. The squareax transmission line provides a low loss, broadband power division network with switching capabilities in a physically compact, lightweight package.

The TEM squareax transmission line is a shielded coaxial line consisting of a square outer conductor and a square center conductor and is supported by Teflon standoffs appropriately spaced throughout the circuit. The transmission line has a characteristic impedance of 50 ohms. The squareax networks utilize hybrid directional couplers for power division, transitions to conventional waveguide for power entry and exit, internal termination loads, and electromechanically operated switches for switching the feed horns to the appropriate zone feed network. A typical squareax layout is shown in Figure 15.

Extensive use of CAD/CAM (Computer Aided Design/Computer Aided Manufacturing) facilities has been made in the electrical and mechanical design layouts of the squareax networks. Upon satisfactory completion of the design, the CAD/CAM system generates an output file which is directly compatible with certain numerically controlled milling machines. Transferring the network data to the machines in this manner saves considerable programming time and reduces errors.

The squareax networks will be fabricated out of aluminum as are the feed horns and four probe polarizers.

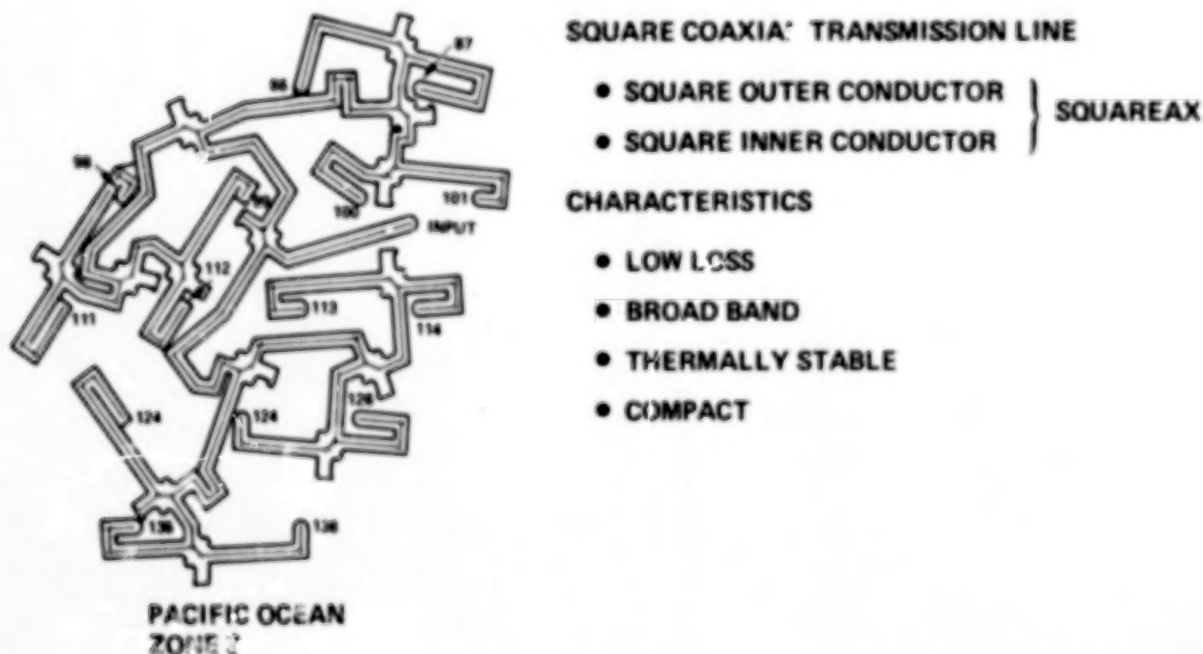


Figure 15

SQUAREAX SWITCH

As illustrated in Figure 16, the squareax switch is a single pole, triple throw device. Three stationary squareax lines are angularly spaced 120° apart to form the input lines. A rotating squareax center conductor at the center of the device selects the appropriate input line. Capacitive coupling allows power to be coupled between the input and output lines. High isolation between ports and low input VSWR are maintained over the required frequency bands.

Movement of the squareax switch center conductor is achieved by a crank shaft which is connected to it and protrudes out of the bottom of the squareax network. All the switch crank shafts are connected to a common orbiting plate. A single redundant mechanism moves the orbiting plate in a circular motion thus turning all the crank shafts in unison.

The individual zone beam switches are designed as independent preassembled and pretested modules. This module approach ensures meeting the high rate of switch production required by the overall spacecraft test and delivery program.

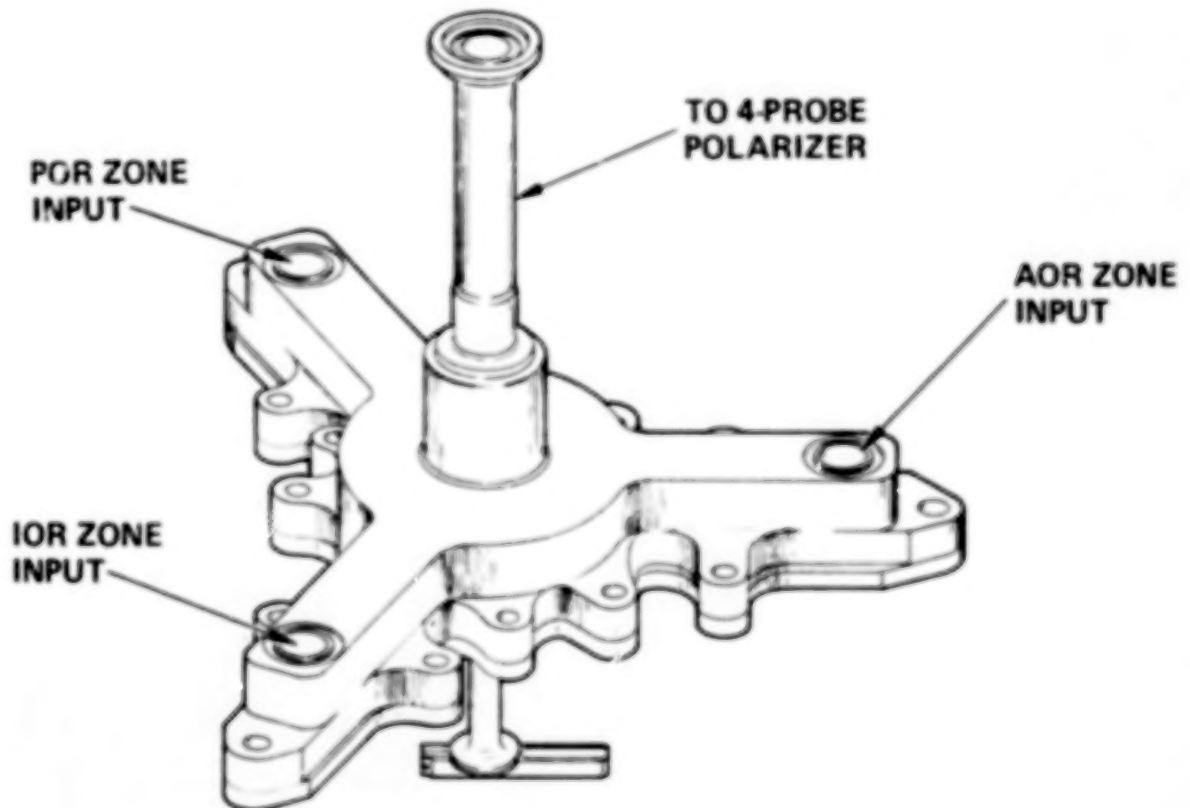


Figure 16

STOWED ANTENNA CONFIGURATION

The Intelsat VI stowed configuration is shown in Figure 17. Note that the stowed spot antennas and global horn clusters have been omitted for clarity.

The large hemi/zone reflectors stow horizontally, back-to-back with the transmit reflecting surface facing away from the spacecraft. Three point support for each of the reflectors is provided by the primary boom structures and by a shared monopod, bipod, and tripod. The monopod supports both reflectors directly. An interconnecting bracket atop the monopod provides an axial and shear tie between reflectors. The bipod supports both receive reflector and transmit boom near the top of the boom structure. The third support for the transmit reflector is provided by the tripod structure which supports the omni antenna mast. The third support for this receive reflector is provided by its own boom assembly. The omni telemetry and command stow directly over the transmit reflector/boom interface. The spot beam antennas and global cluster (not shown) slew inward and stow within the envelope of the extendable solar drum.

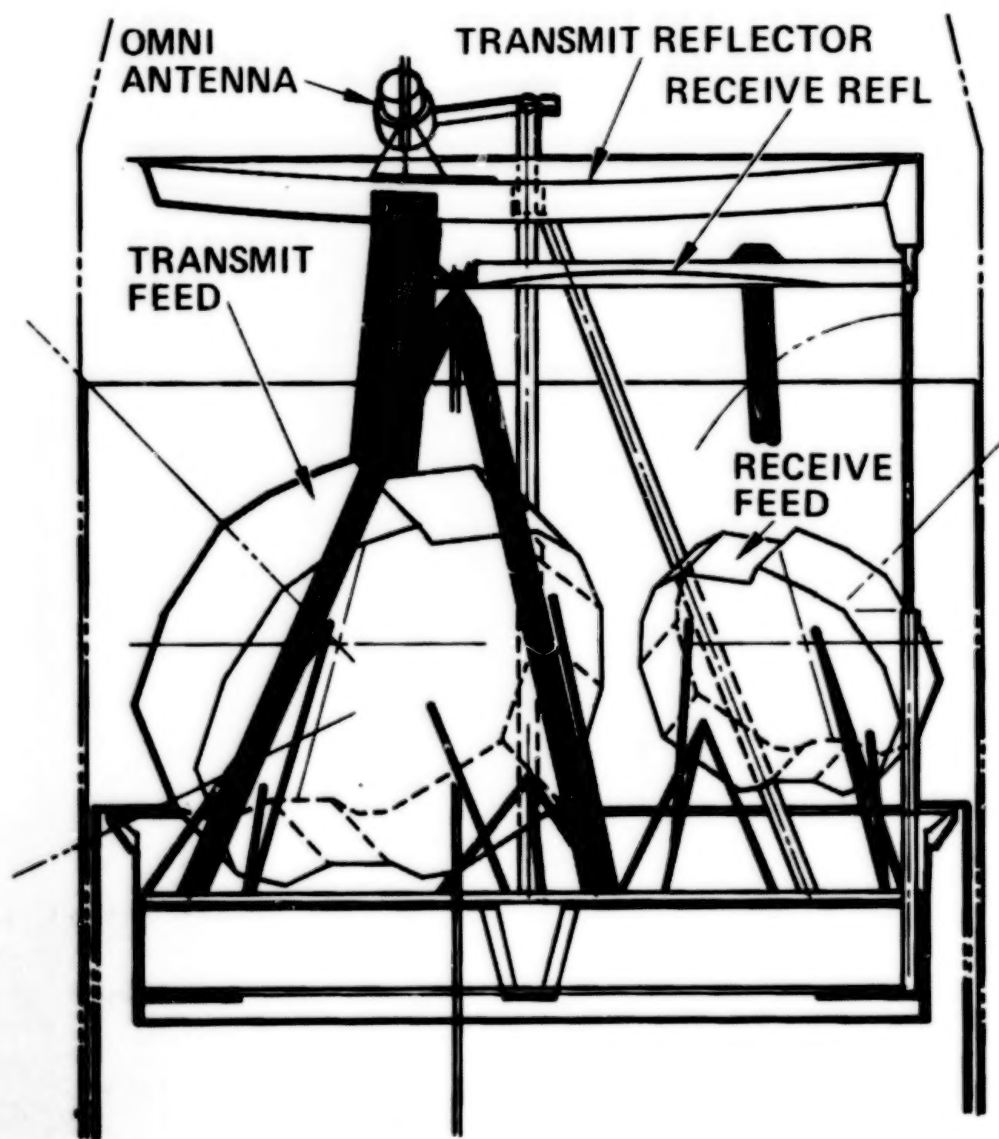


Figure 17

DEPLOYED CONFIGURATION

The deployed spacecraft configuration is illustrated in Figure 18. The antenna supports consist primarily of tubular ultra high modulus graphite structures which tie the various antenna components directly to hard points on the payload equipment shelf. The deployed hemi/zone reflectors are supported off their back edges by booms. Tripod structures tie the lower ends of the booms to the equipment shelf. Hinge mechanisms in the booms (2 transmit, 1 receive) enable compact stowage within the launch vehicle envelope. Beam pointing can be adjusted by positioner mechanisms located at the reflector/boom interfaces.

The hemi/zone feed networks are supported by tubular structure, the transmit network at five locations, the receive network at four. The 14/11 GHz spot antennas and global horn cluster are supported on individual tripod structures. Both east and west spot antennas are steerable to provide full Earth coverage.

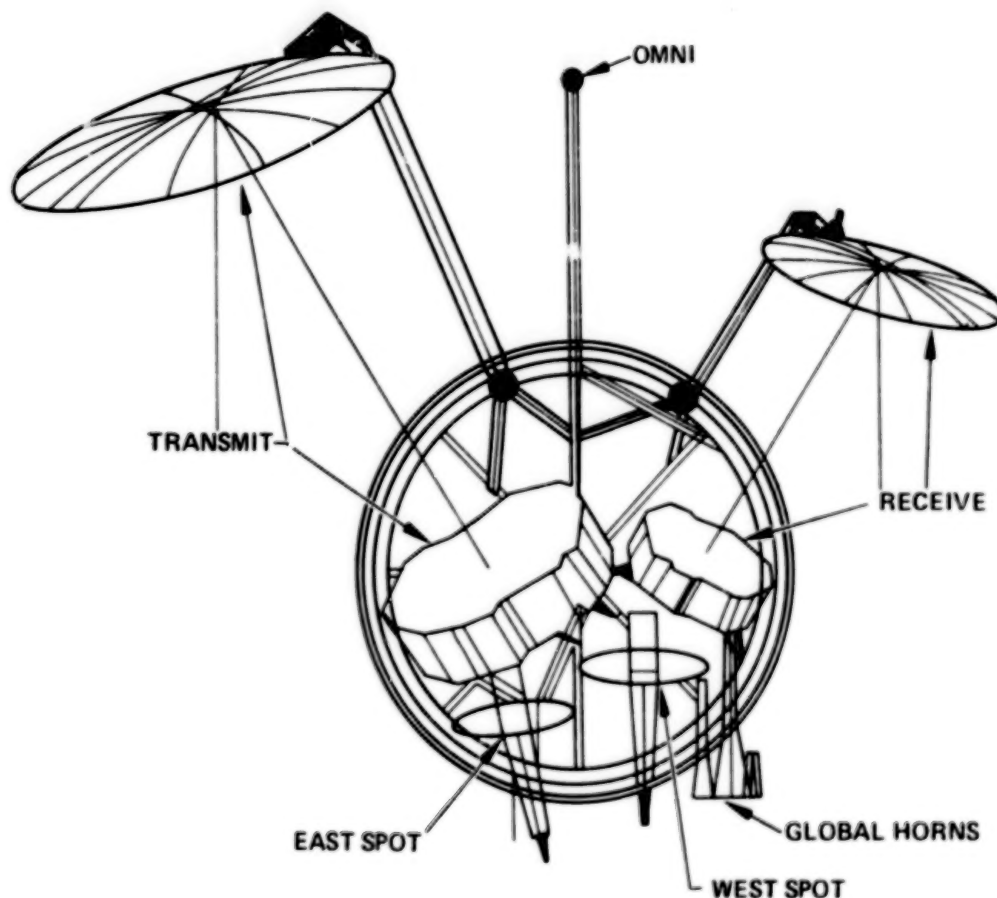


Figure 18

ANTENNA DEPLOYMENT SEQUENCE

Deployment of the Intelsat VI antenna is illustrated in Figure 19. After separation from the launch vehicle, the telemetry and command antenna (omni) is erected to a position above the spacecraft (A). The spacecraft remains in this configuration until reaching its final orbit location. The outer solar drum is then extended, and the communications payload is despun (B). Next, the omni completes its deployment by rotating to a position above and behind the spacecraft (C). Deployment of the C-band reflectors is accomplished in three motions (D, E and F). The transmit reflector is first rotated to a position overhanging the forward side of the spacecraft. The receive reflector and boom assembly then rotates to its operational position above and behind the spacecraft. In a similar motion, the transmit reflector and boom assembly rotates to its operational position. Finally, the global horn cluster and two K-band spot antennas slew eastward to complete the system deployment (G).

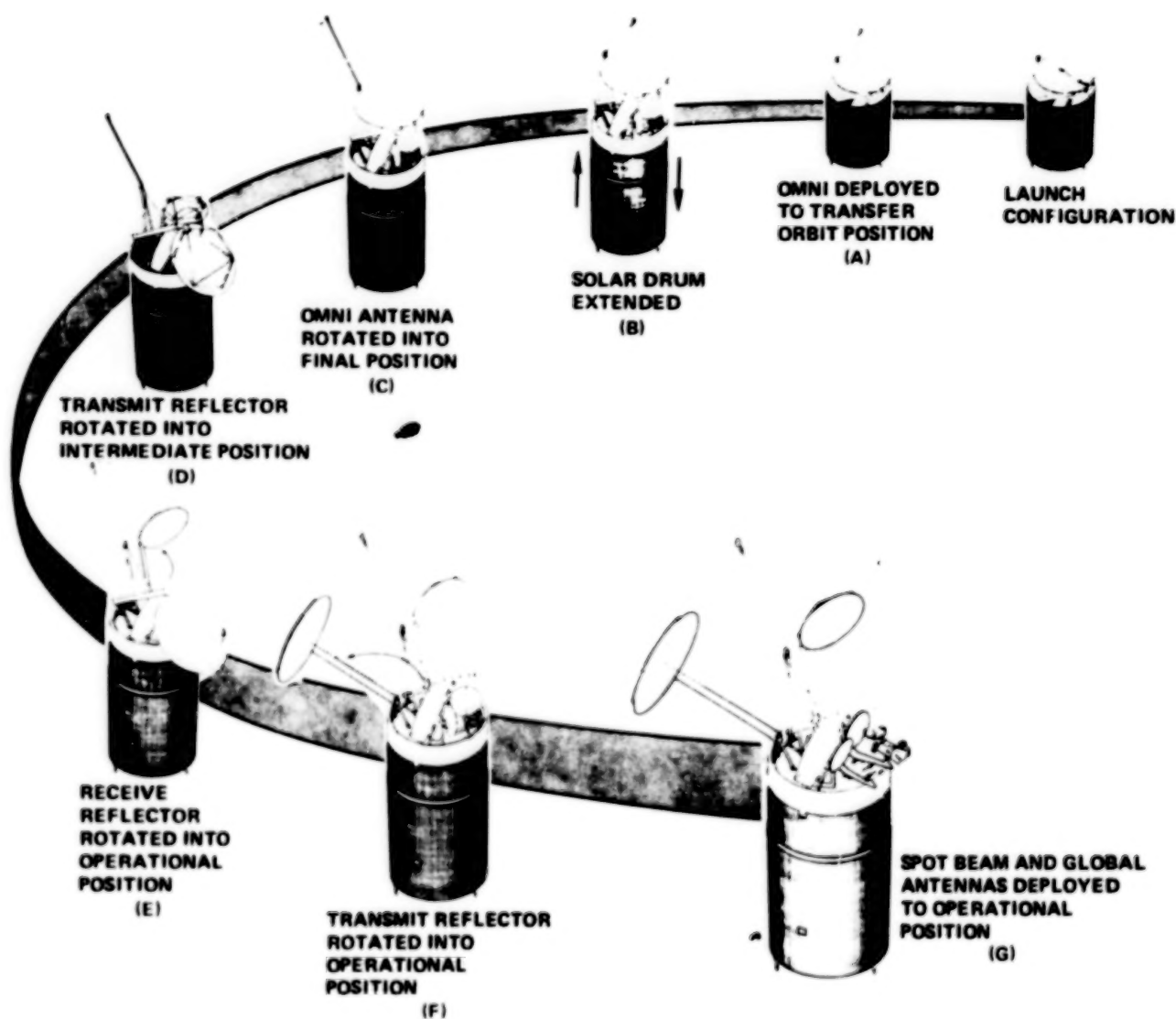


Figure 19

REFERENCES

1. Potter, P.D.: A New Horn Antenna with Suppressed Sidelobes and Equal Beamwidths. Microwave Journal, June 1963.
2. Neyret, F.: Experimental Study of Cross Polarization of Feed Horn Clusters. COMSAT Technical Review, Vol. 8, No. 2, Fall 1978, pp. 405-420.

SCANNING BEAM ANTENNA CONCEPTUAL DESIGN
FOR 20/30 GHz SATELLITE SYSTEMS

J. Smetana
NASA Lewis Research Center
Cleveland, Ohio

R. Sorbello
COMSAT Laboratories
Clarksburg, Maryland

W. F. Crosswell
Harris Corporation
Melbourne, Florida

Large Space Antenna Systems Technology - 1982
NASA Langley Research Center
November 30 - December 3, 1982

APPLICATION OF MMIC MODULES IN MULTIPLE SCANNING SPOT BEAM ANTENNAS

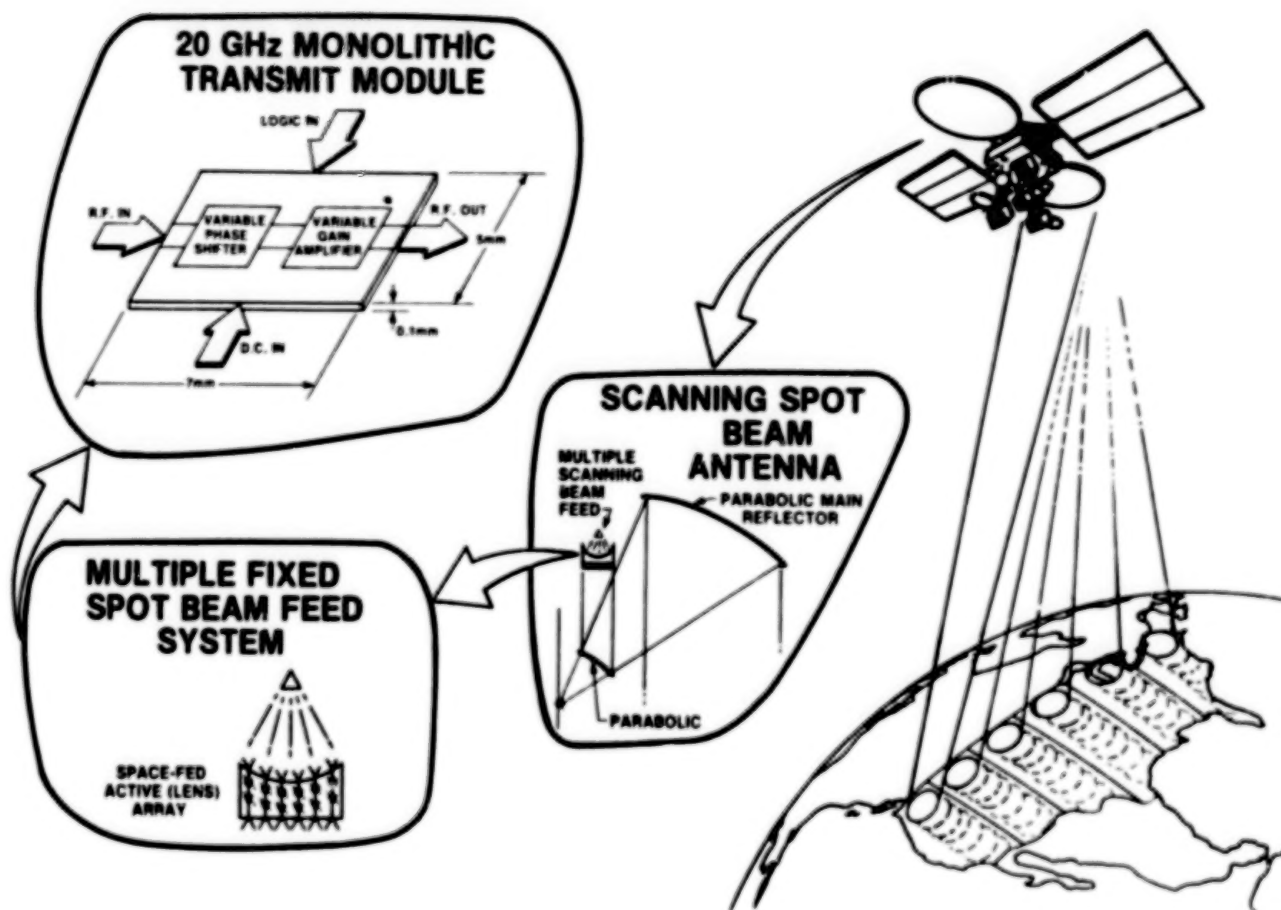
Two-phased array-fed dual-reflector antenna configuration studies are currently under way in contractual efforts by COMSAT Laboratories and the Harris Corporation. The studies are the first part of a program to develop 20-GHz multiple scanning spot beam and multiple fixed spot beam array-fed antenna systems having monolithic microwave integrated circuit (MMIC) modules in each radiating element of the feed array. This work is done in support of NASA's Advanced Configuration Satellite Base R&T Program.

One of the promising scanning spot beam antenna configurations will have a 12-ft (nominal) diameter parabolic main reflector, a confocal parabolic subreflector, and a feed system having three space-fed active (lens) arrays. Each array, which may have 177 to 2000 elements, illuminates the reflector system and develops a very narrow scanning spot beam (0.3°). The subreflector is positioned in the near field of the array. The narrow spot beams will permit a large volume of TDM and FDM traffic between thousands of ground terminals in each of six sectors in the United States. These terminals will be located on the premises of large commercial firms and their subsidiaries.

Two GaAs 20-MHz modules in each of the elements of each array provide variable phase shift and variable power amplification functions for each of two orthogonally polarized beams. The variable phase shift functions have five-bit resolution, and they are used for dynamic phase weighting and are programmed to incrementally reposition the beam to completely cover all parts of a sector. The variable power amplification function, which has five levels of gain, is used for dynamic amplitude weighting to reduce sidelobe level. The combination of low sidelobes and orthogonal polarization will provide excellent isolation between adjacent sectors (30 dBi).

The configuration described herein is one of four antenna system configurations developed in each contract using a variety of MMIC module arrangements and optical systems. A parametric analysis is expected to produce a data base for the selection of design points for a variety of applications. Soon to be accomplished is the design concept of the active (lens) array, which will take into consideration such factors as, for example, coupling effects, the space-fed power divider network design, input bias and control layout, investigation of thermal distribution, and analysis of module failure (graceful degradation).

MULTIPLE SCANNING SPOT BEAM ANTENNA



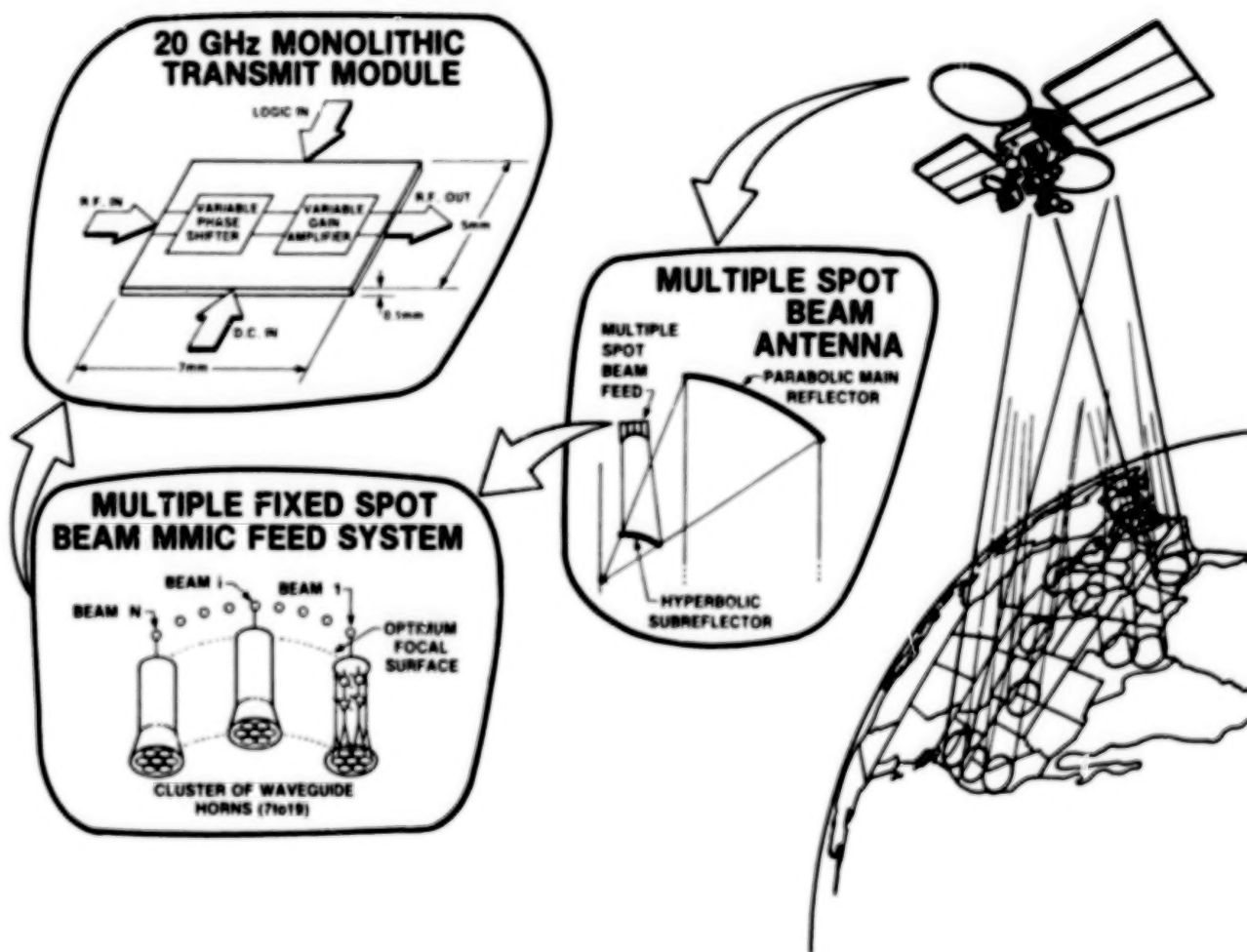
APPLICATION OF MMIC MODULES IN MULTIPLE FIXED SPOT BEAM ANTENNAS

One of the promising multiple spot beam antenna configurations will have a 12-ft (nominal) diameter parabolic main reflector, a hyperbolic subreflector, and a feed system having 10 to 18 clusters on a curved focal surface. Each cluster, which may have 7 to 19 elements, illuminates the reflector system and develops a very narrow fixed spot beam (0.3°). Its position on the curved surface determines the pointing angle. The narrow spot beams will permit large volume traffic between single ground terminals located at a carrier's facility in each of 10 to 18 major communications centers in the United States, with minimum RF power requirements.

GaAs 20-GHz MMIC modules in the elements of each cluster provide variable phase shift and amplification functions. The phase and amplitude of each element are weighted to provide low sidelobes. The combination of low sidelobes and orthogonal polarization will provide excellent spatial isolation (30 dBi). Control of the phase and amplitude weighting in space can be used for additional isolation improvement after launch.

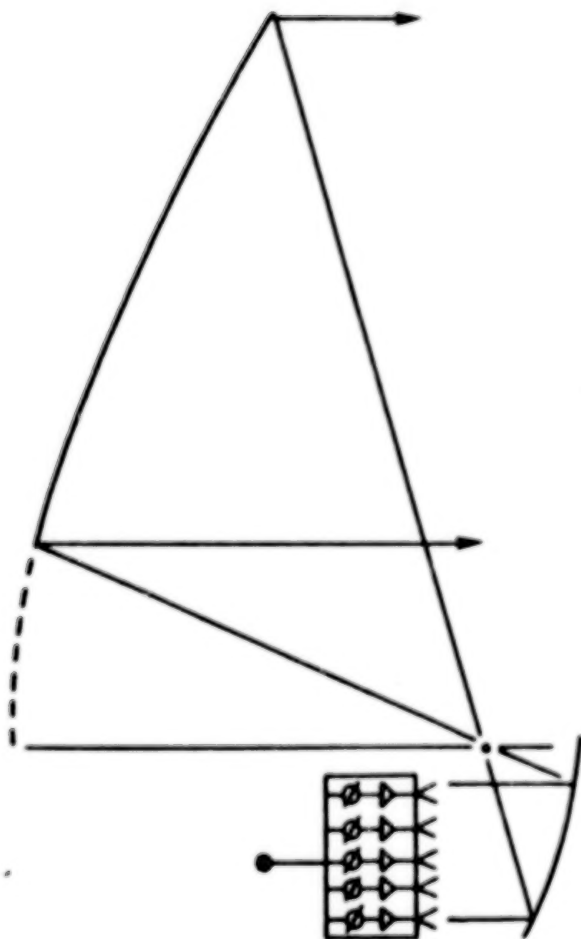
The configuration described herein is one of four antenna system configurations developed in each contract using a variety of MMIC module arrangements and optical systems. A parametric analysis is expected to produce a data base for the selection of design points for a variety of applications. Soon to be accomplished is the design concept of the clusters, which will take into consideration such factors as, for example, coupling effects, beam forming network design, input bias and control, investigation of thermal distribution, and analysis of module failure (graceful degradation). Follow-on work is planned for a contractual effort to design and fabricate an experimental antenna system and for in-house testing and evaluation of the system to the proof-of-feasibility level.

MULTIPLE FIXED SPOT BEAM ANTENNA

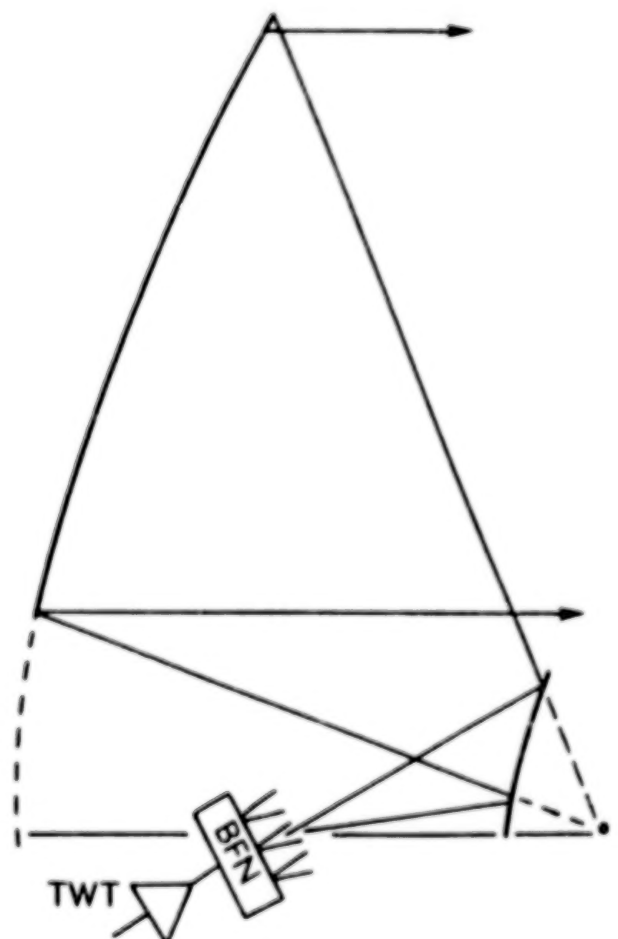


PHASED ARRAY FED
CONFIGURATION STUDY -
COMSAT LABORATORIES

MULTIPLE BEAM REFLECTOR ANTENNA

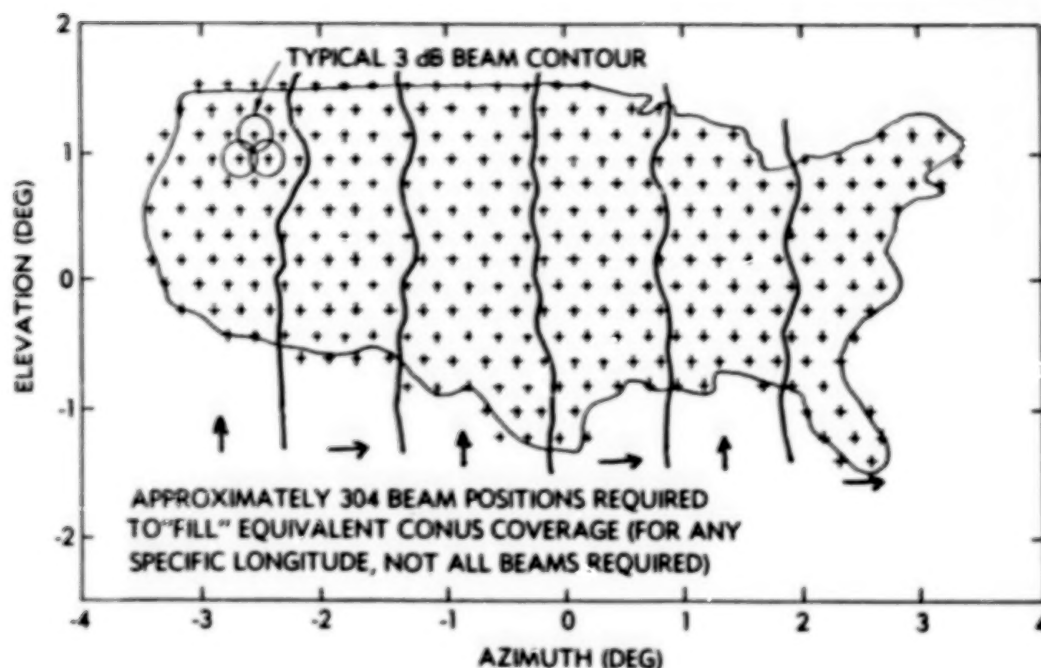


PHASED ARRAY FED
DUAL REFLECTOR SYSTEM



FOCAL REGION FED
DUAL REFLECTOR SYSTEM

SCANNING BEAM COVERAGE REQUIREMENT



ANTENNA SYSTEM REQUIREMENTS

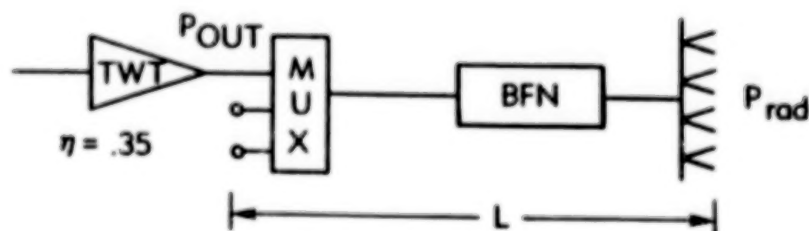
	REQUIREMENT	BASELINE
FIELD OF VIEW	$\pm 3.5^{\circ}\text{E-W}$, $\pm 1.5^{\circ}\text{N-S}$	SAME
MAIN APERTURE ~	9-14 FT	12.5 FT
FREQUENCY RANGE	17.7-20.2 GHz	SAME
BANDWIDTH	500 MHz	SAME
COMPONENT BW (3 dB)	0.4° - 0.25°	0.27°
TOTAL NO. OF BEAMS (6 AT ANY ONE TIME)	180-450	304
ON-AXIS PEAK GAIN ($\eta = 0.6$)	52.5-56.5 dBi	55.5 dBi
MINIMUM GAIN FOV (2.5-dB SCAN LOSS)	50-54 dBi	53 dBi

SYSTEM POWER CONSIDERATIONS

ANTENNA GAIN (WORST CASE)	53 dBi (BASELINE)
REQUIRED E.I.R.P.	67-75 dBW
RADIATED POWER/BEAM	25-158 W/BEAM
TOTAL RADIATED POWER	125-950 W

OBJECTIVE: GIVEN THESE REQUIREMENTS, COMPARED CONVENTIONAL
VS DISTRIBUTED AMPLIFIER APPROACH.

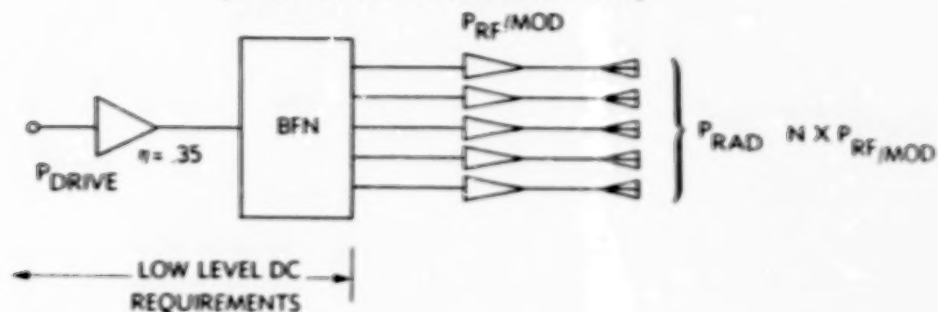
CONVENTIONAL (FOCAL REGION FED) APPROACH



E.I.R.P.	GAIN	P_{rad}/BEAM	L^*	η	P_{out}/BEAM	PDC/BEAM	TOTAL % EFF.
67 dBW	53 dBi	25 W	4 dB	.35	63 W	180 W	13.9%
71	53	80	4	.35	200 W	270 W	13.9%
75	53	158	4	.35	400 W	1140 W	13.9%

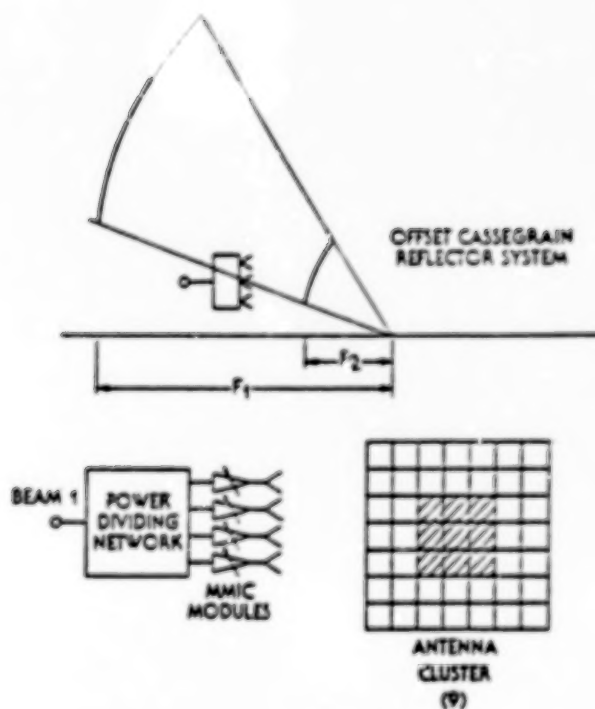
*L includes all output network, BFN, and antenna losses. Total % eff. depends on η and L.

DISTRIBUTED AMPLIFIER (PHASED ARRAY FED) APPROACH (SINGLE-BEAM PHASED ARRAY)



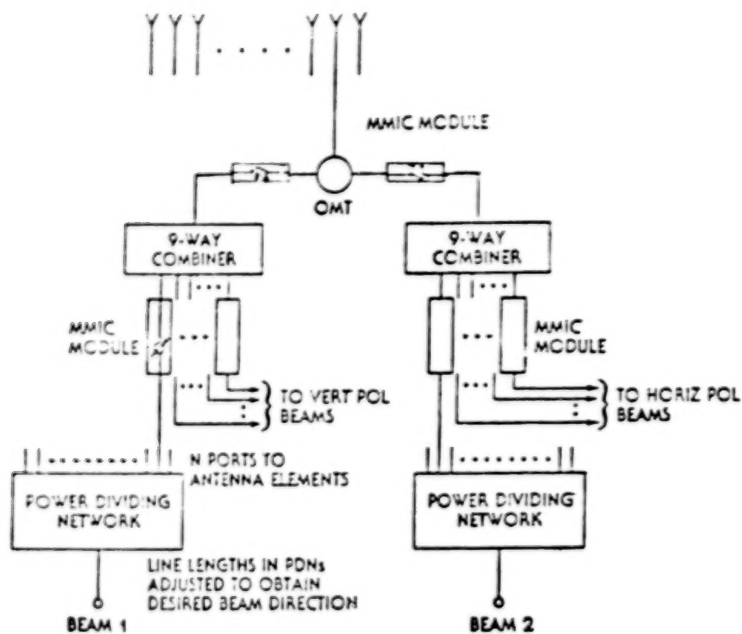
(dBW) E.I.R.P.	(dB) GAIN	(watts) P _{RAD} /BEAM	(watts) P _{RF} /MOD	(%) MOD. EFF.	#ELEM	(watts) P _{DC} /MOD	(watts) P _{DC} /BEAM*	TOTAL # EFF.
67	53	25	.5	15	50	3.3	170	14.5
71	53	80	.5	15	160	3.3	500	14.5
75	53	150	.5	15	316	3.3	1075	14.5

*Includes RF Drive to BFN (Driver Efficiency + 35%).



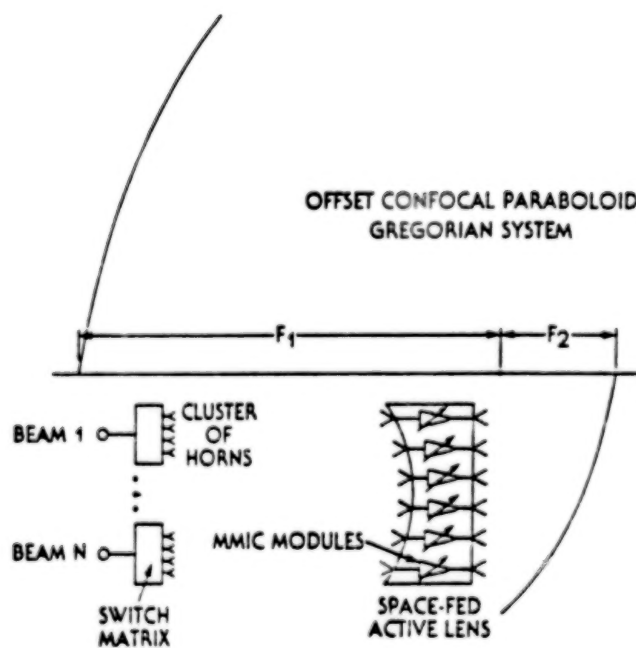
CONFIGURATION E

- MULTIPLE BEAMS (18)
- 52-62 dBW/BEAM (E.I.R.P.)
- VARIABLE GAIN (.5 W MAX OUTPUT, 5 LEVELS) MMIC
- ONE FEED CLUSTER FOR EACH BEAM

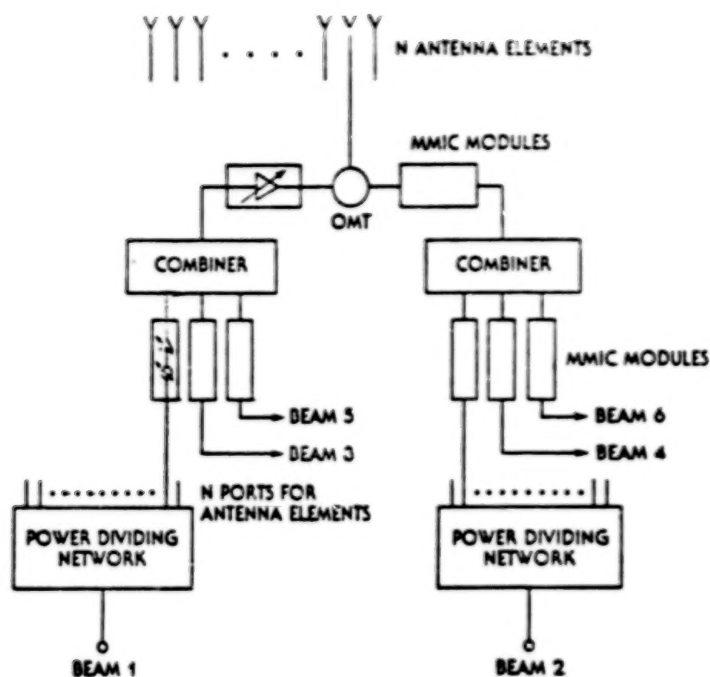


CONFIGURATION D1

- MULTIPLE BEAMS (18)
- 52-62 dBW/BEAM (E.I.R.P.)
- CONSTANT GAIN (.2 W MAX OUTPUT) AND 3-BIT PHASE-SHIFTER (FOR TRIMMING) MMIC

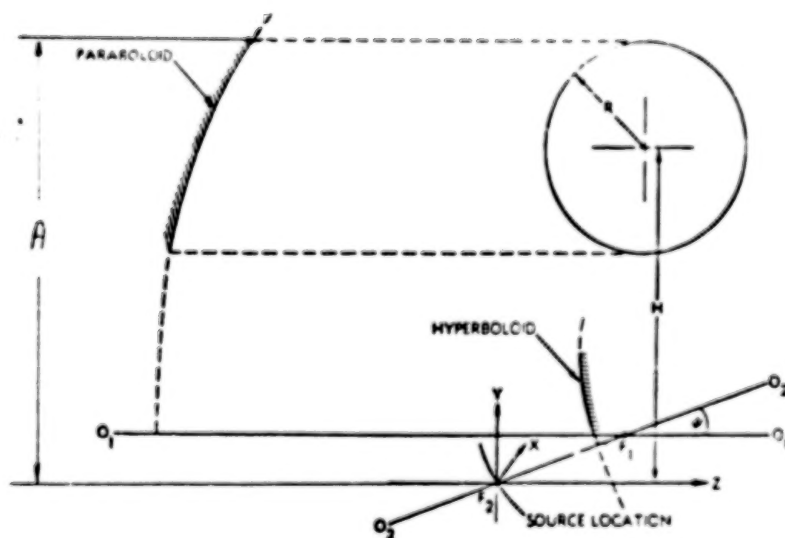


CONFIGURATION F



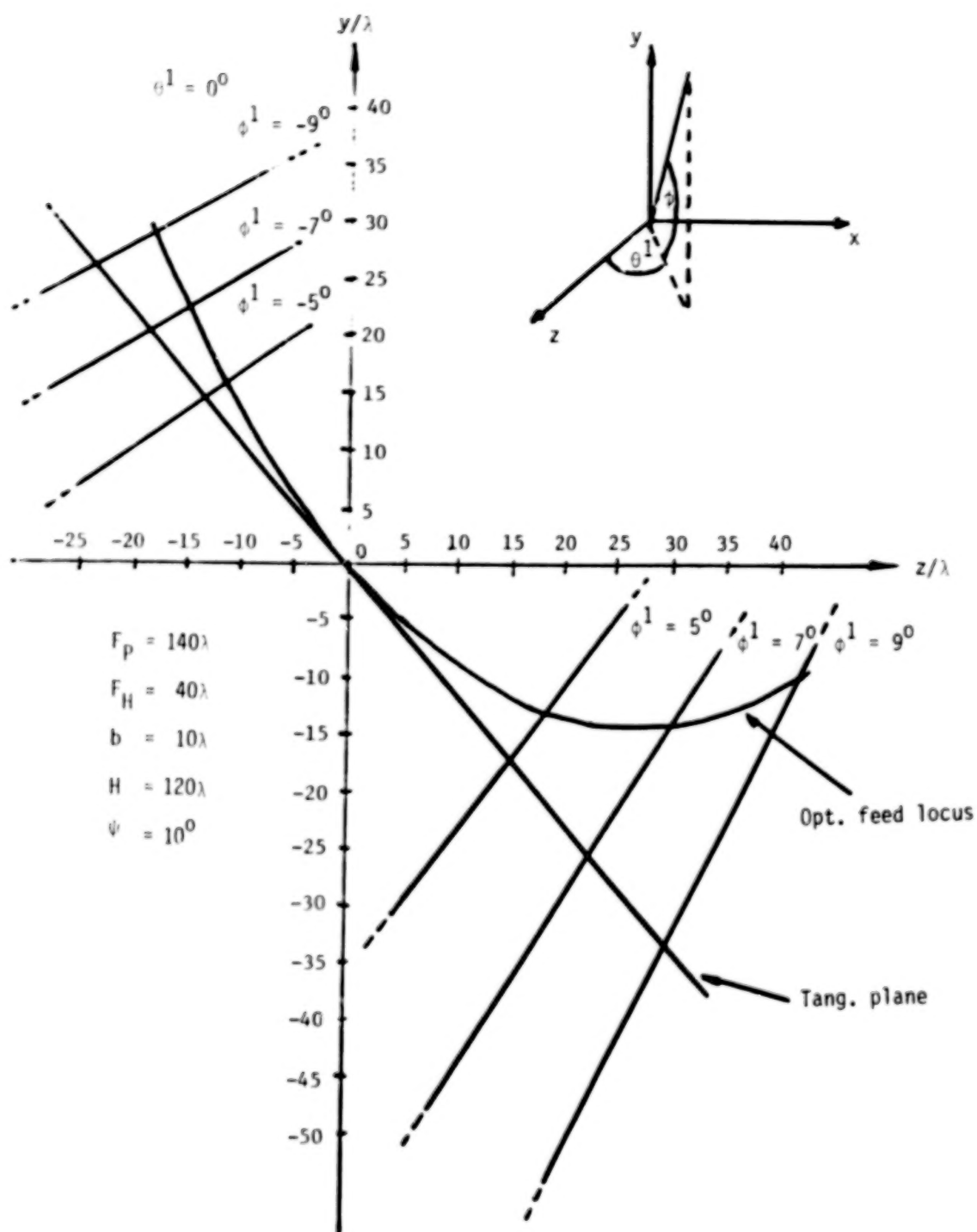
CONFIGURATION C

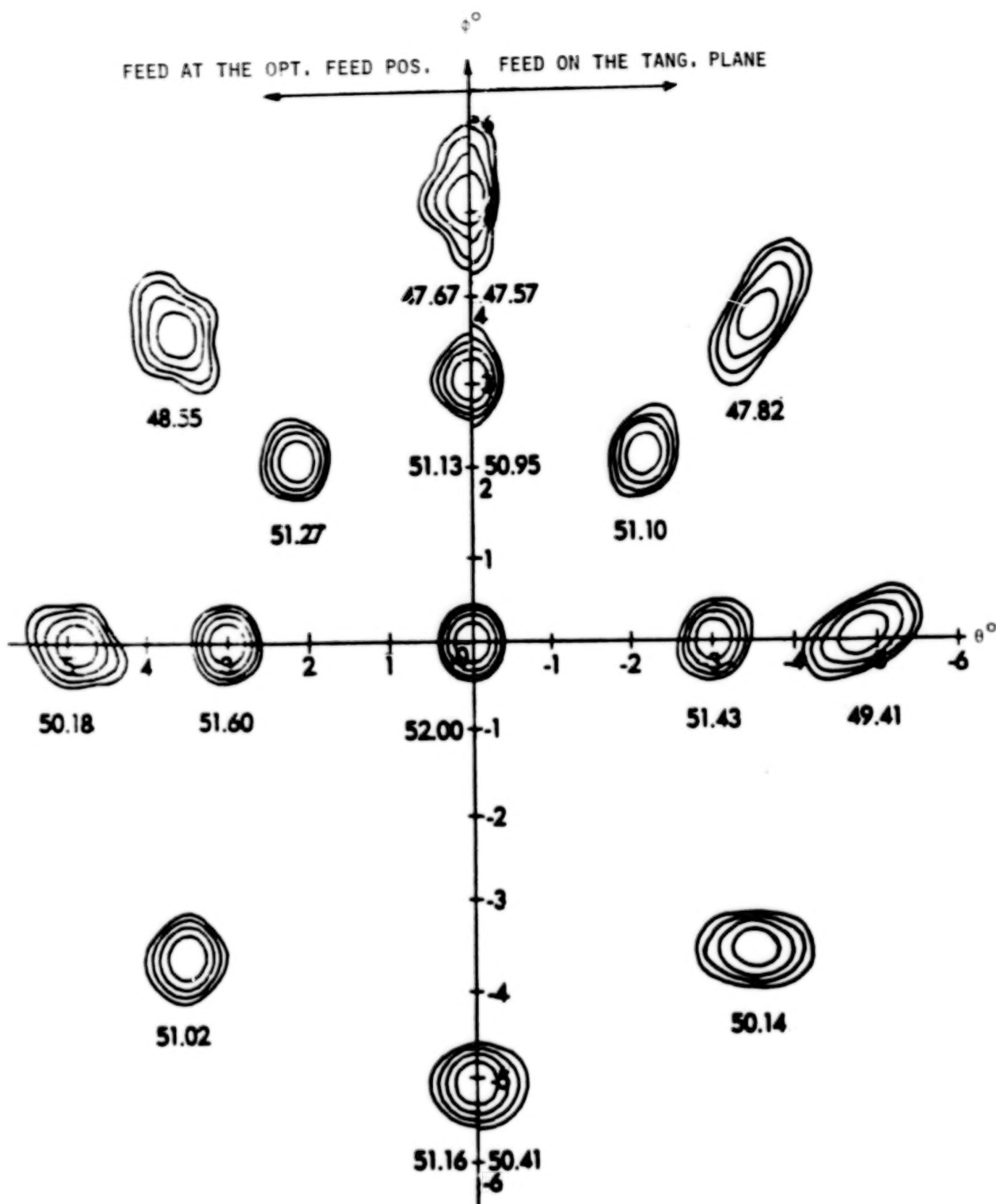
- SIX SCANNING BEAMS
- 67-75 dBW/BEAM (E.I.R.P.)
- VARIABLE GAIN/VARIABLE PHASE MMIC (.5 W MAX OUTPUT, 3 LEVELS/3 BIT)
- AND VARIABLE GAIN MMIC (.5 W MAX OUTPUT, 3 LEVELS)



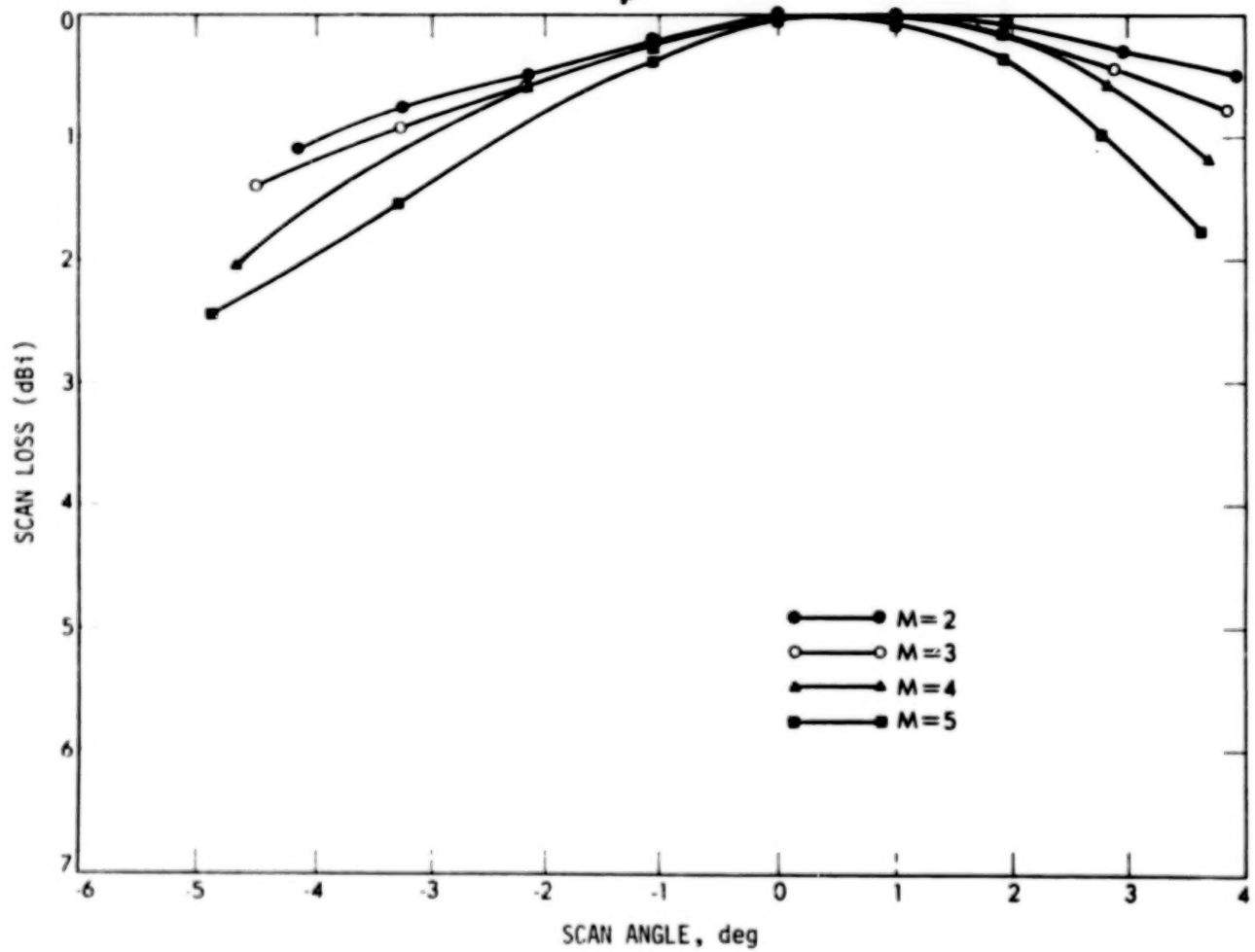
$$F_p = 140\lambda; F_H = 40\lambda; b = 10\lambda; R = 60\lambda; H = 120\lambda; \psi = 10^\circ$$

$$f = 12 \text{ GHz}; \lambda = 2.5 \text{ cm}; \phi = 2R = 300 \text{ cm}; A = H + R = 180\lambda = 450 \text{ cm}$$

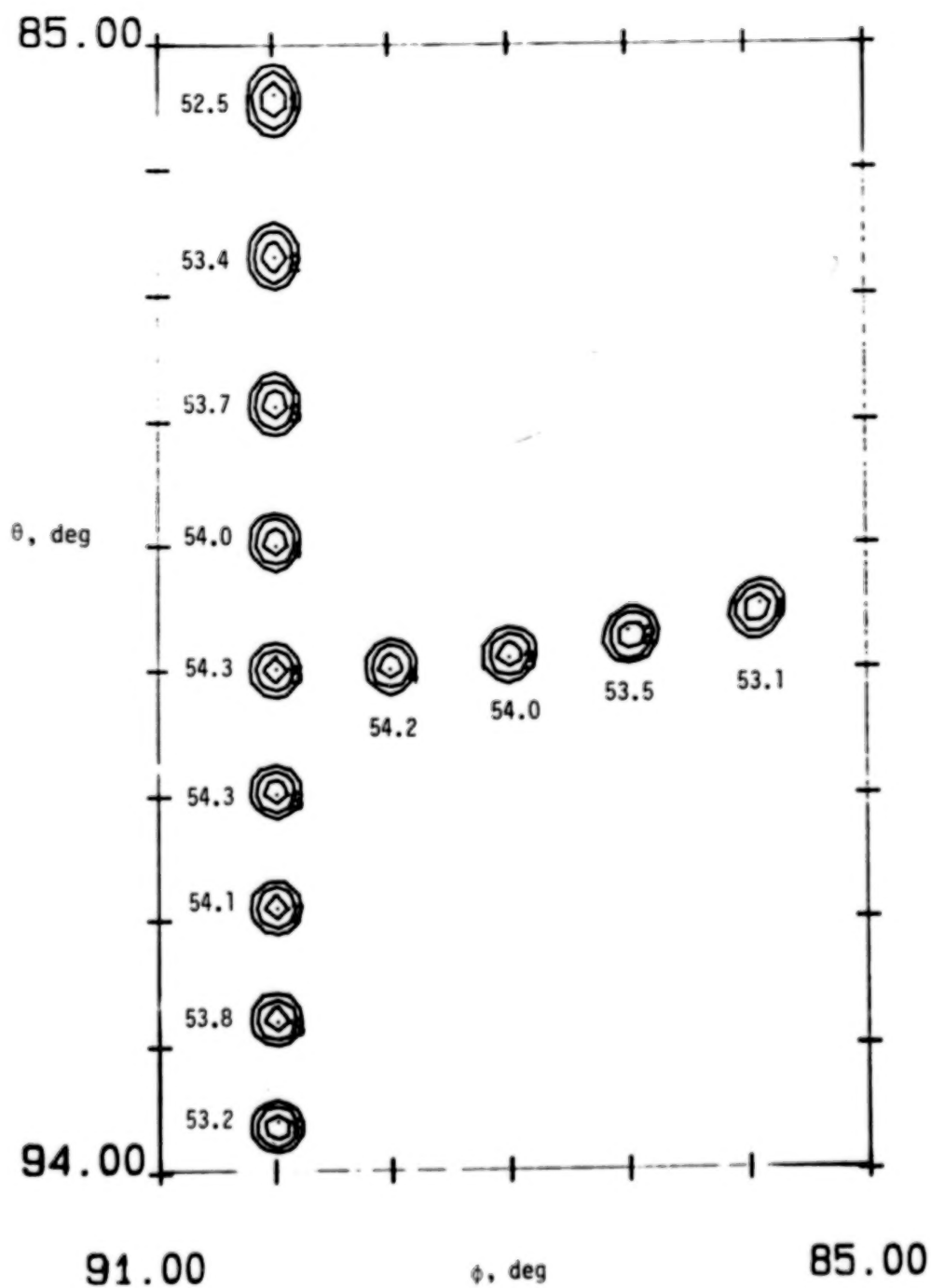


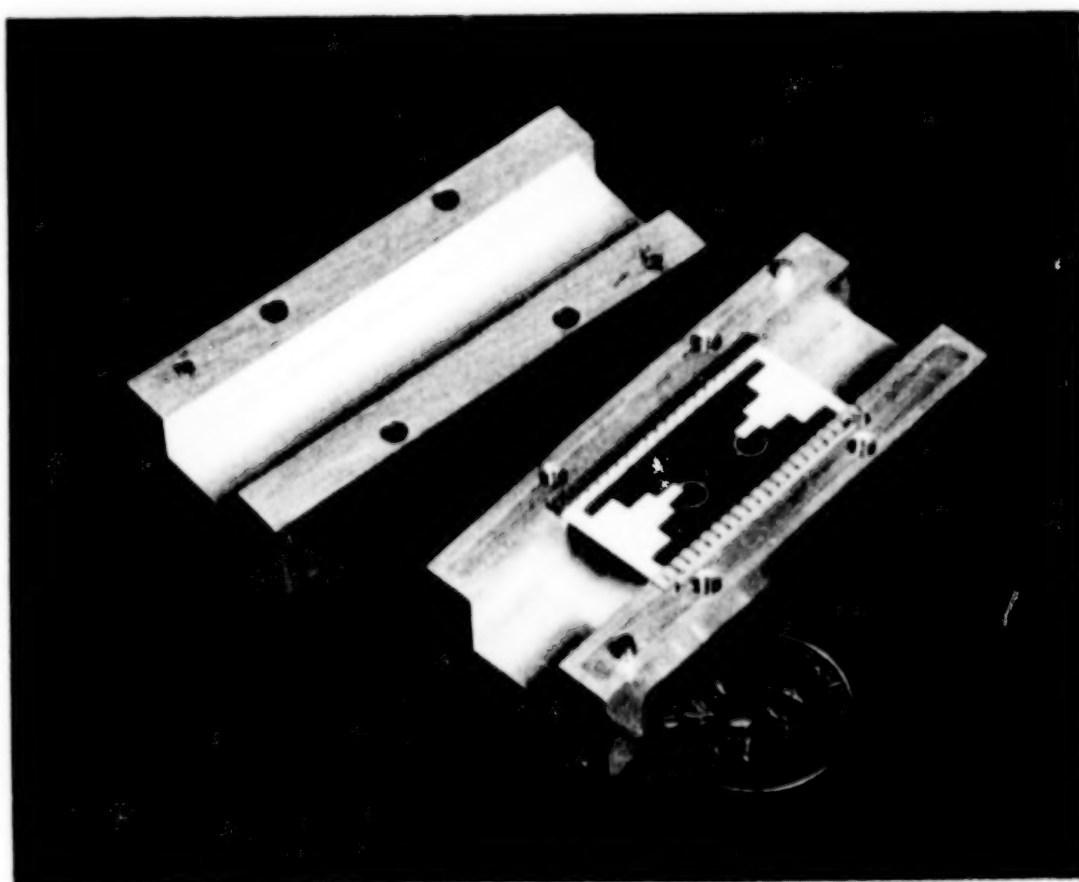
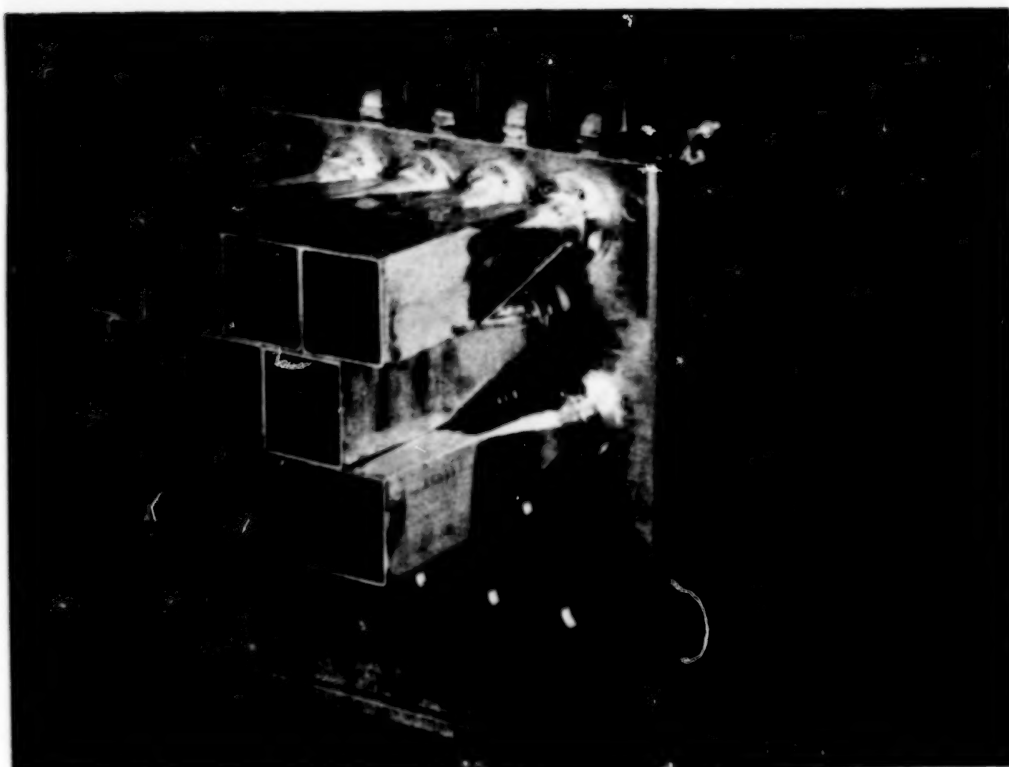


Scan Loss VS Scan Angle
 $F/D_p = 0.5$

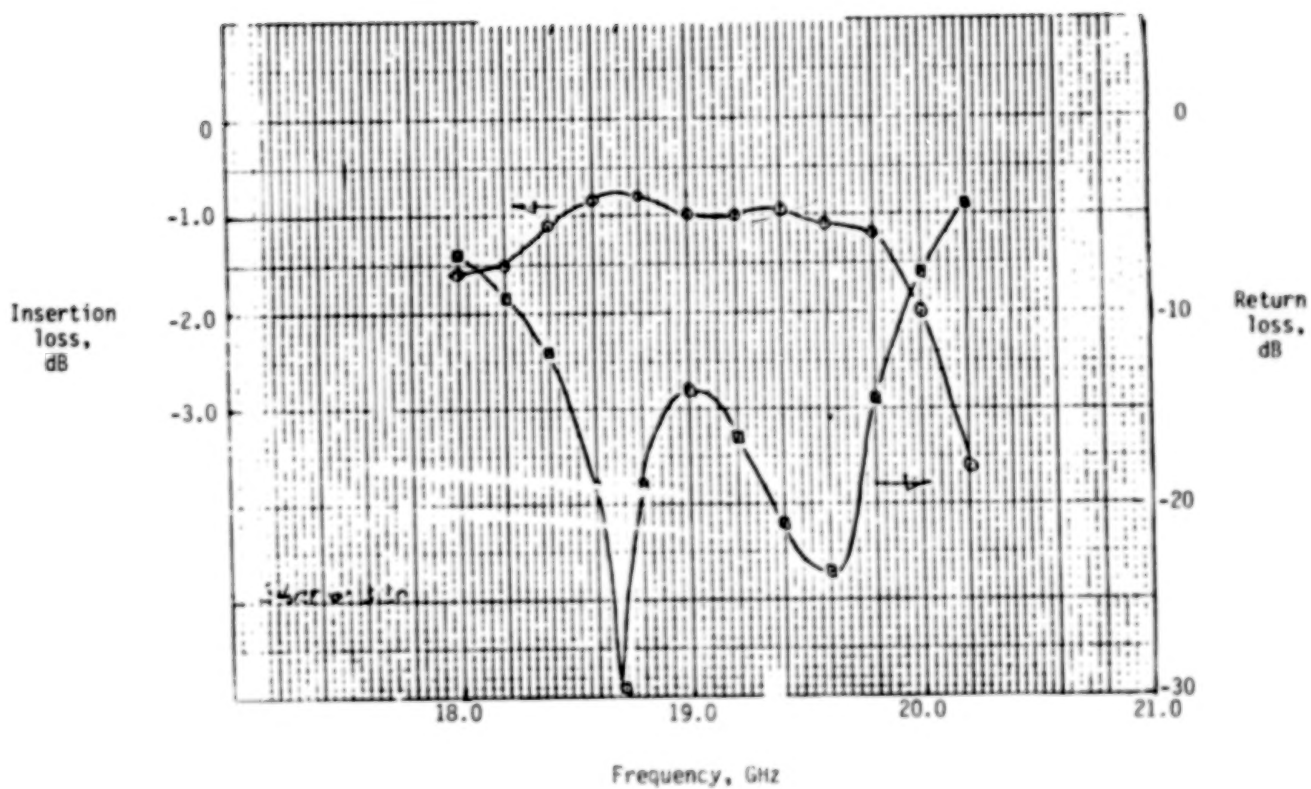


SCAN PERFORMANCE OF CONFOCAL PARABOLOID - $F/D = 0.5$; $M = 4$





RETURN LOSS AND INSERTION LOSS OF WAVEGUIDE/MMIC TRANSITION



PHASED ARRAY FED CONFIGURATION STUDY - HARRIS CORPORATION

CONTRACT REQUIREMENTS

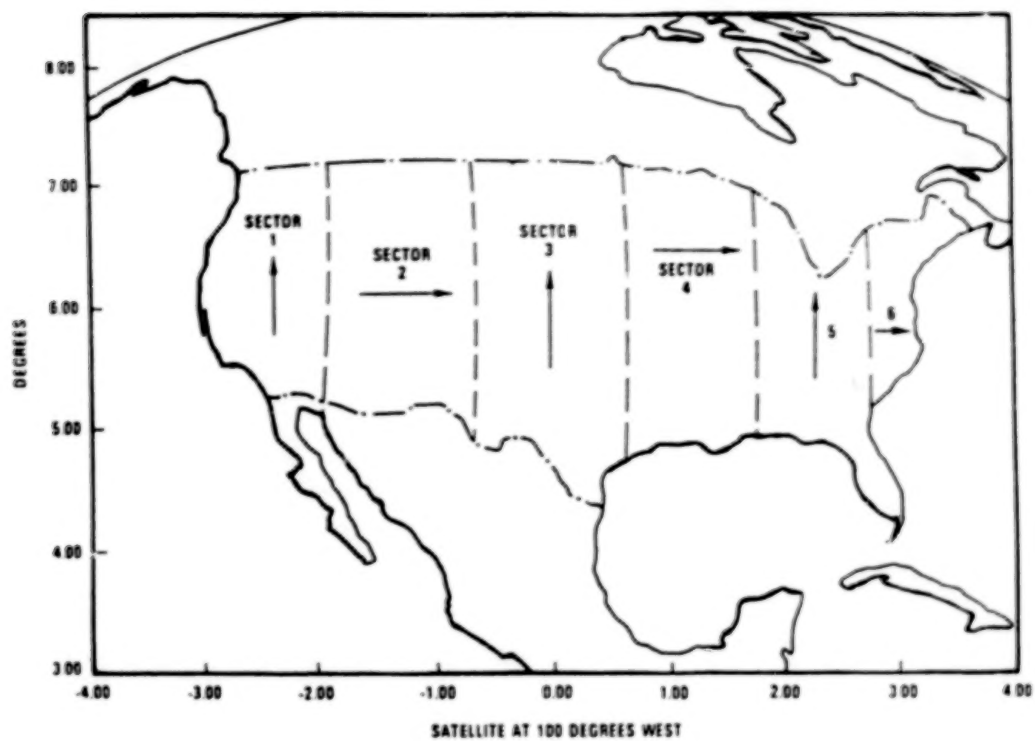
• DESIGN GOALS FOR MULTIBEAM AND SCANNING BEAM ANTENNA

BEAM CONFIGURATION		MULTIBEAM	SCANNING BEAM
ANTENNA SIZE		SHUTTLE COMPATIBLE	SHUTTLE COMPATIBLE
OPERATION FREQUENCY	-DOWNLINK	17.7-20.2	17.7-20.2
RANGE (GHz)	-UPLINK	27.5-30.0	27.5-30.0
NUMBER OF BEAMS	-OPERATIONAL	10-18	6 TRANS
MINIMUM GAIN (dB)	-20 GHz	53	53
	-30 GHz	56	53
BANDWIDTH (MHz)	-20 GHz	500	500
	-30 GHz	500	500
POLARIZATION		LINEAR	LINEAR
C/I PERFORMANCE (dB) ⁽¹⁾		30	30
POINTING ACCURACY	-E & H PLANE	0.02	0.02
(DEGREES)	POLARIZATION	0.4 ⁽²⁾	0.4
POWER/BREAM (EIRP) dBW		52-62	67-75

(1) CARRIER TO INTERFERENCE RATIO FOR EACH BEAM RELATIAVE TO ALL OTHER BEAMS

(2) DEGREES ROTATION FROM REFERENCE (I.E., TRUE SATELLITE VERTICAL OR HORIZONTAL)

A PROPOSED SCANNING BEAM CPS
ANTENNA COVERAGE SCENARIO



MULTIBEAM COVERAGE MAP

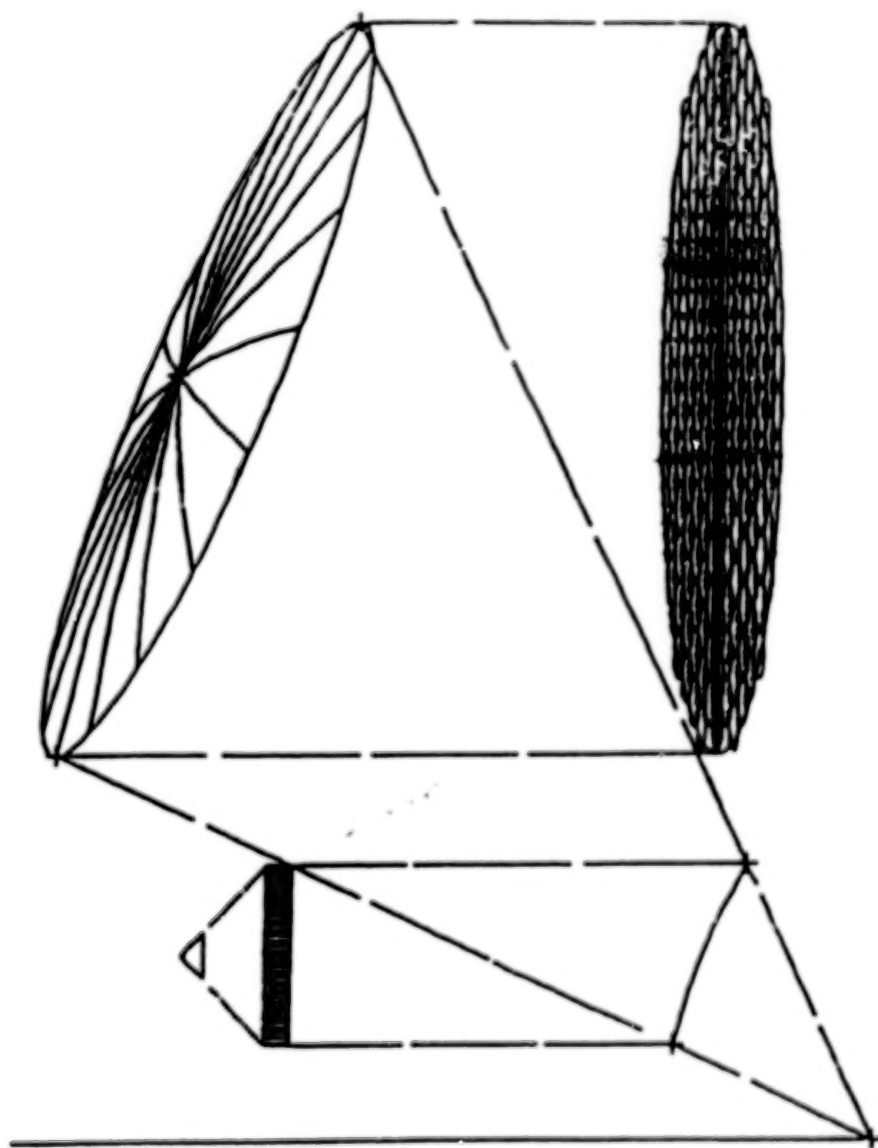


MMIC MODULE CONCEPT

- LARGE NUMBER OF LOW POWER MODULES - ONE FOR EACH ELEMENT OF THE ARRAY
 - HIGHER RELIABILITY - ELIMINATES SINGLE POINT FAILURES
 - HEAT GENERATION IS DISTRIBUTED OVER LARGER VOLUME
 - STATE-OF-THE-ART MMIC EFFICIENCIES ARE BEGINNING TO APPROACH TWT EFFICIENCY
- FAST SWITCHING OF PHASE SHIFTER AND POWER AMPLIFIER STATES (10-100 NANoseconds)
 - FAST BEAM SWITCHING FOR TDMA SYSTEMS
 - POTENTIAL FOR MULTIPLE BEAMS
 - DYNAMIC BEAM CONTROL
 - ELIMINATION OF HIGH SWITCHING CURRENTS

SCANNING BEAM ANTENNA SYSTEMS

OFFSET NEAR-FIELD CASSEGRAIN GEOMETRY SHOWING APERTURE ARRAY



SPACE VS CORPORATE FEED

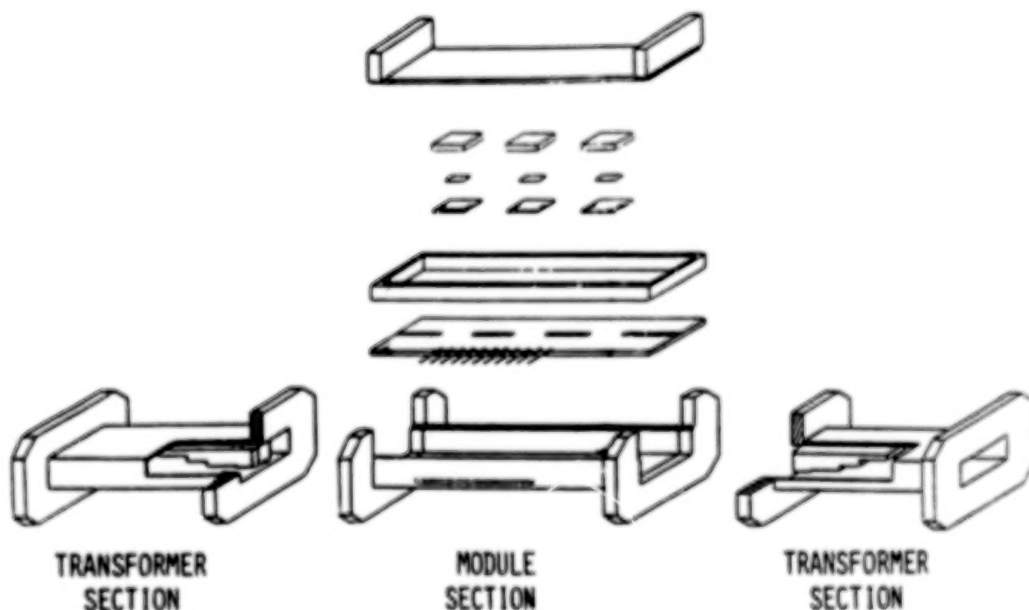
FEED TYPE	MODULE TYPE	RF INPUT POWER PER ELEMENT	NUMBER OF ELEMENTS	TOTAL RF INPUT POWER*	DC INPUT POWER REQUIRED	TOTAL RF OUTPUT POWER	EIRP**	ARRAY EFFICIENCY
CORPORATE	VPS-VPA	10 mW	177	3.7 W	254.9 W	32.75 W	68.15 dBW	11.397%
SPACE	VPS-VPA	10 mW	177	4.5 W	254.9 W	32.75 W	68.15 dBW	11.083%
CORPORATE	VPS-CGA-VPA	0.125 mW	177	46.2 mW	260.7 W	32.75 W	68.15 dBW	12.545%
SPACE	VPS-CGA-VPA	0.125 mW	177	56.0 mW	260.7 W	32.75 W	68.15 dBW	12.541%

* INCLUDES FEED LOSSES

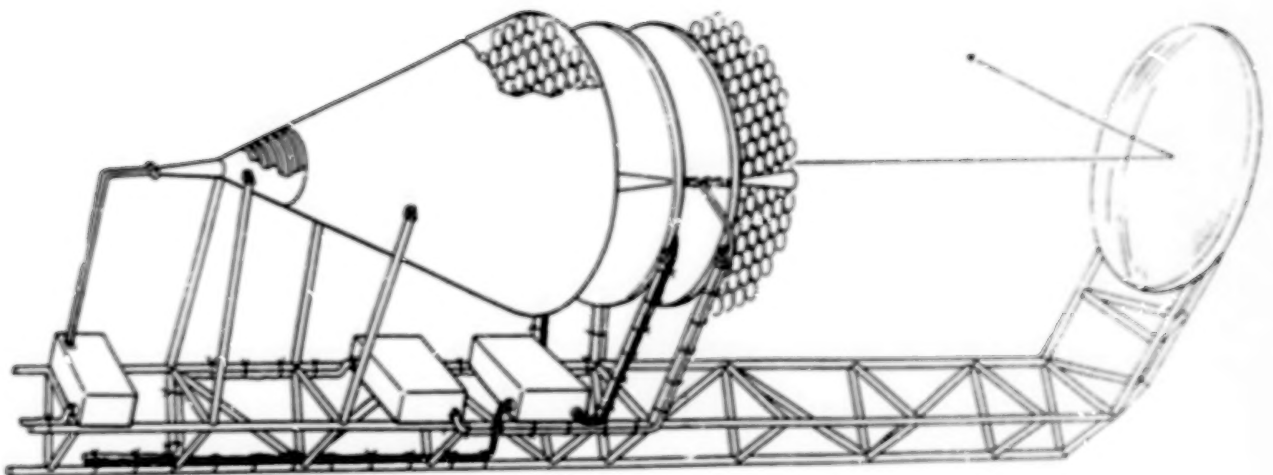
** INCLUDING 53 dB REFLECTOR GAIN

$$\text{ARRAY EFFICIENCY} = \frac{\text{RF OUTPUT} - \text{RF INPUT}}{\text{DC INPUT}}$$

MONOLITHIC MODULE TRANSITION AND MOUNTING CONFIGURATION



SCANNING BEAM SPACE FED PHASED ARRAY



SUMMARY AND CONCLUSIONS

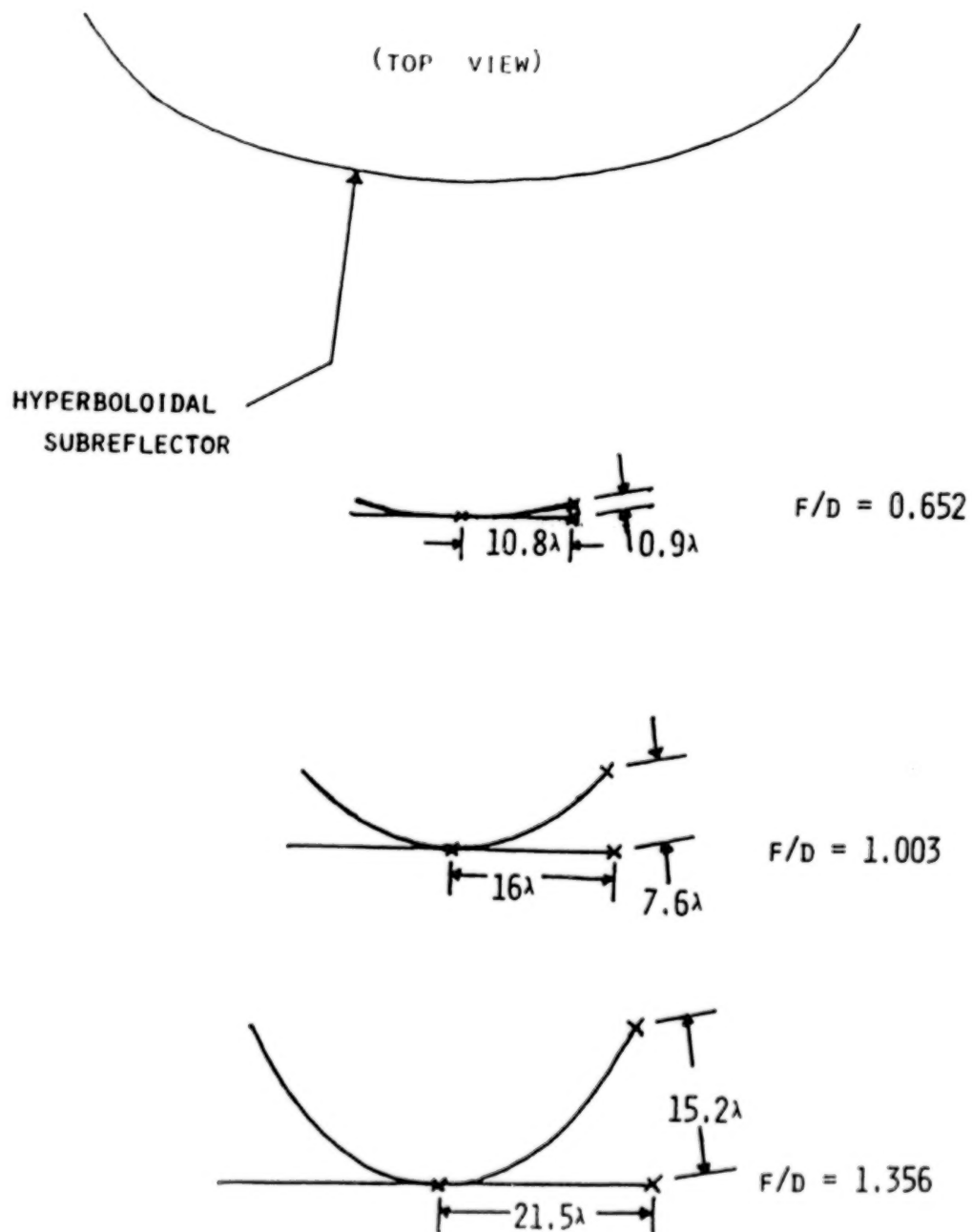
SCANNING BEAM ANTENNA CONCEPTUAL DESIGN

SUMMARY

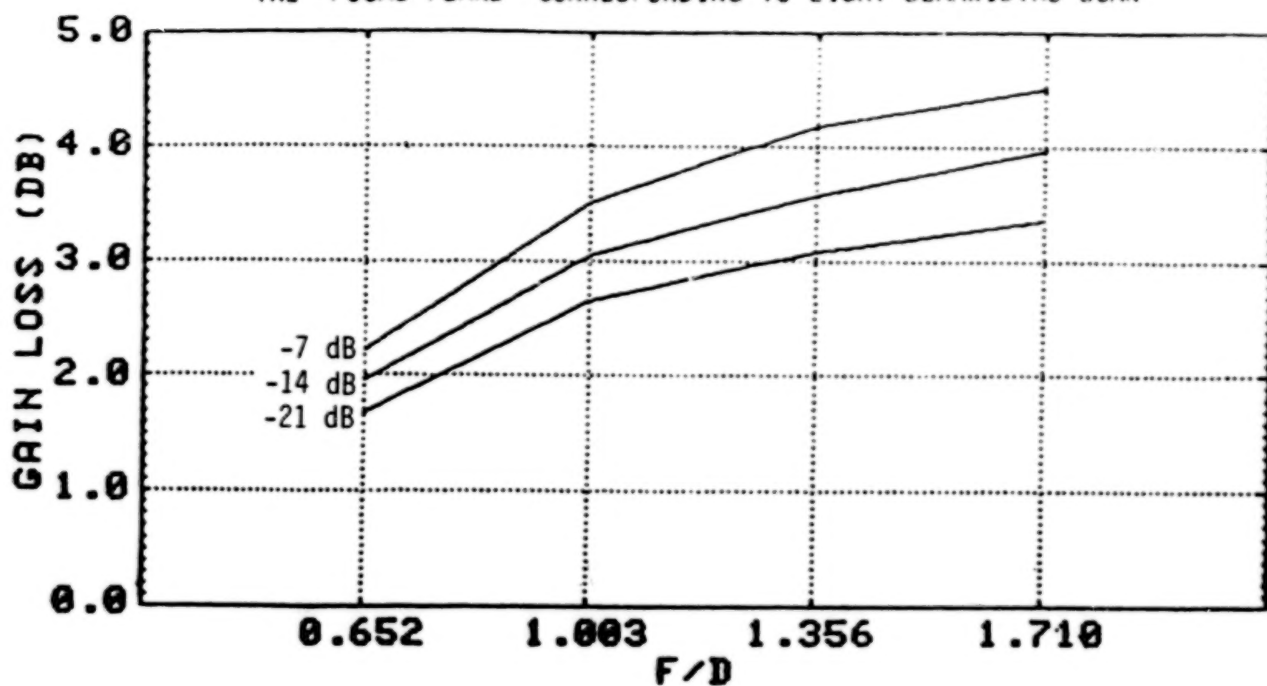
- NEAR-FIELD OPTICS NECESSARY TO OBTAIN EIRP
- SPACE FED LENS OFFERS IMPORTANT ADVANTAGES OVER CORPORATE FED BFN
- PRELIMINARY THERMAL/PACKAGING ANALYSIS INDICATES THAT UP TO TWO SCANNING SECTORS CAN BE ACCOMMODATED IN ONE ARRAY LENS
- SHAPED TRI-FOCAL OPTICS IMPORTANT FOR 6 SECTOR SCANNING BEAM COVERAGE
- MMIC MODULES SPECIFIED HAVE SUFFICIENT QUANTIZATION OF PHASE; FINER QUANTIZATION OF AMPLITUDE IS HIGHLY DESIRABLE

MULTIPLE BEAM ANTENNA SYSTEMS

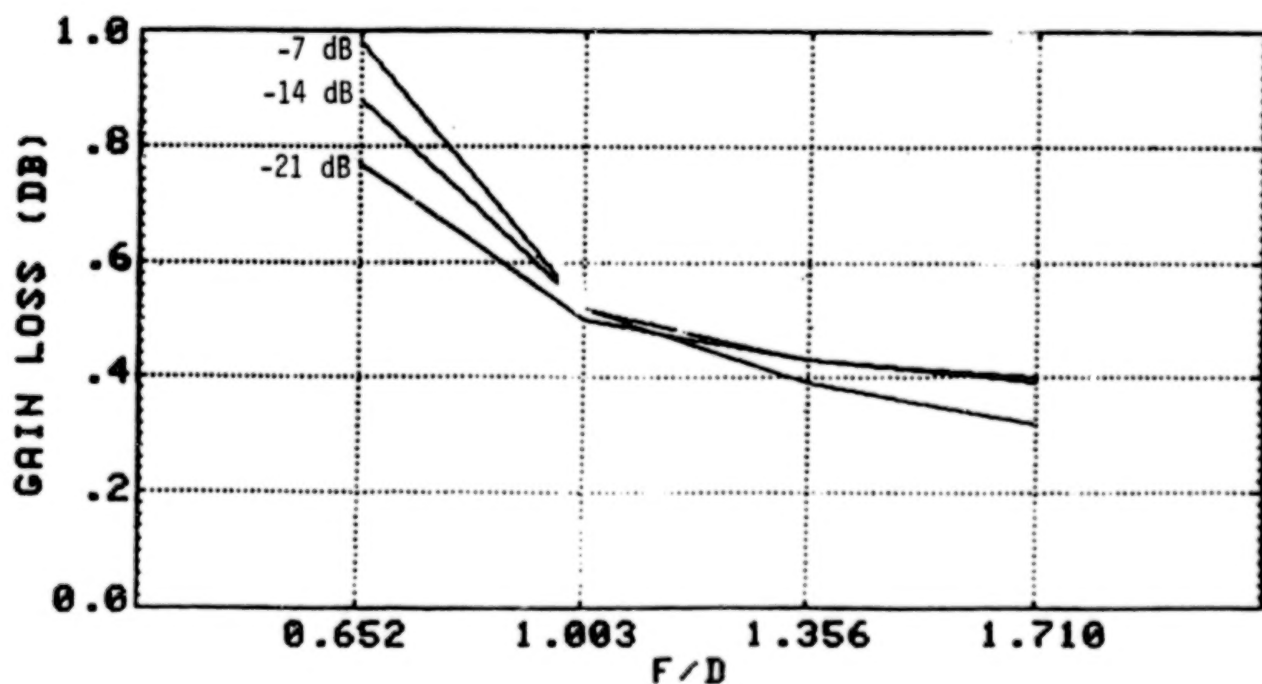
FEED PLANE VS OPTIMUM FOCAL SURFACE



GAIN LOSS VS F/D RATIO IN AN OFFSET CASSEGRAIN ANTENNA - FEED OFFSET ALONG THE "FOCAL PLANE" CORRESPONDING TO EIGHT BEAMWIDTHS SCAN



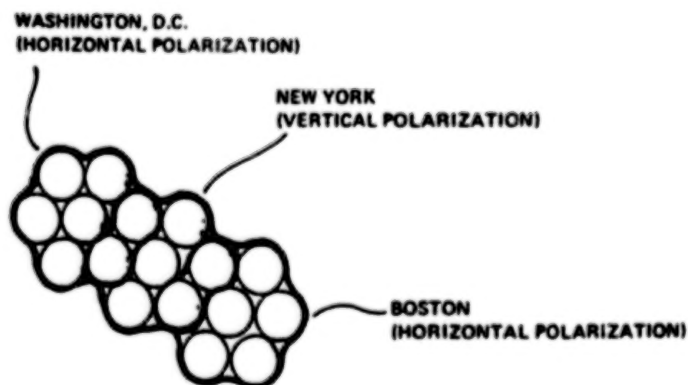
GAIN LOSS VS F/D RATIO IN AN OFFSET CASSEGRAIN ANTENNA - FEED OFFSET ALONG THE OPTIMUM "FOCAL SURFACE" CORRESPONDING TO EIGHT BEAMWIDTHS SCAN

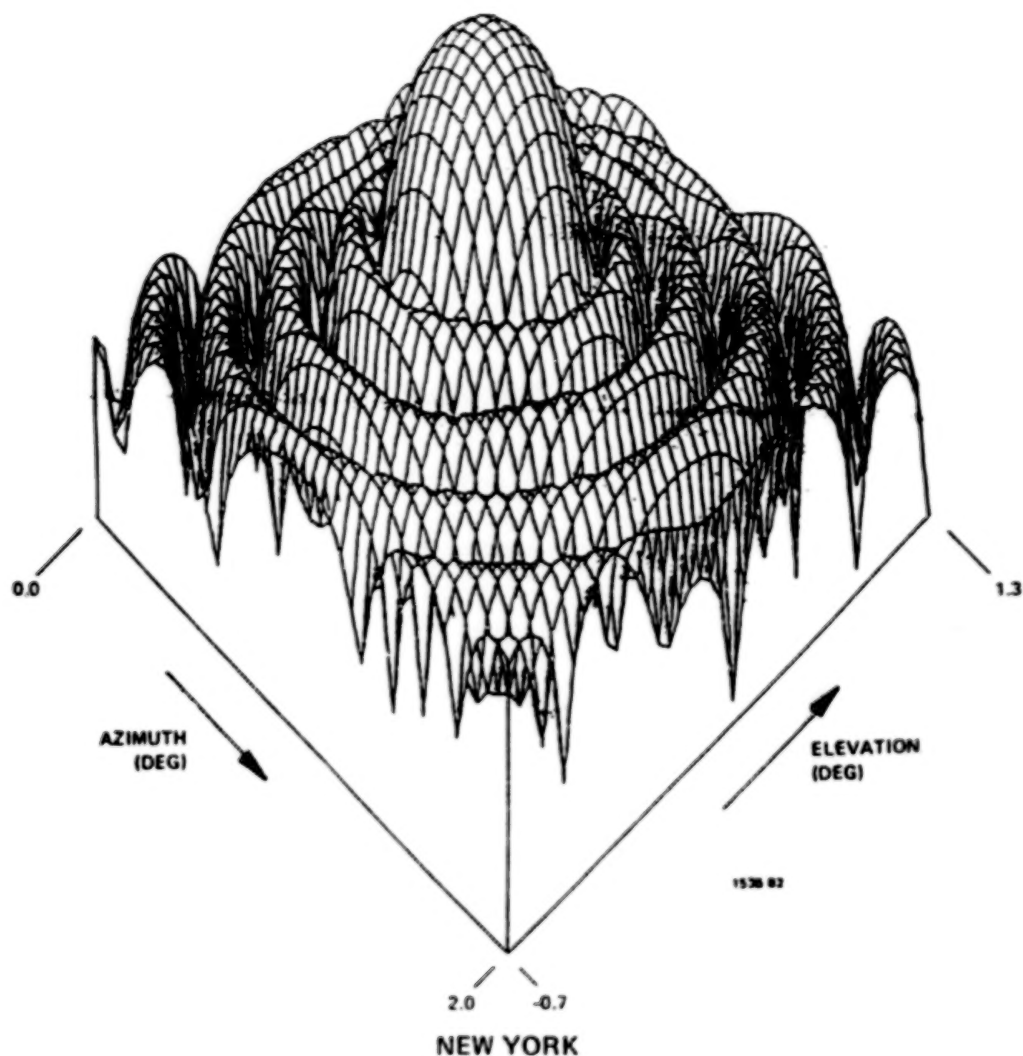


TYPICAL CLUSTER DESIGN

- WASHINGTON - NEW YORK - BOSTON
- WORST CASE C/I PERFORMANCE
- EACH CITY BEAM GENERATED BY 7-ELEMENT FEED CLUSTER
- OVERLAPPING FEEDS REQUIRED
- ELEMENT WEIGHTS DETERMINED BY CONJUGATE MATCHING TECHNIQUE

FEED CLUSTER LAYOUT





STUDY OBJECTIVES

- DEVELOP SPACEBORNE MULTIBEAM AND SCANNING BEAM PHASED ARRAY FEED DESIGN APPROACHES
- PARAMETRIC STUDY OF DUAL OFFSET REFLECTOR SYSTEMS CONFIGURED FOR MULTIPLE FIXED/SCANNING BEAMS
- INTEGRATION OF SOLID STATE AMPLIFIERS AND PHASE SHIFTERS INTO THE ARRAY DESIGN

CITY BEAM PERFORMANCE

<u>CITY</u>	<u>(AZ, EL) LOCATION</u>	<u>C/I RATIO</u>	<u>PEAK GAIN</u>	<u>CROSS-POL</u>	<u>EIRP</u>
WASHINGTON	(0.65°, 0.1°)	33.9 dB	54.8 dB	-42.1 dB	54.0 dBW
NEW YORK	(0.95°, 0.25°)	44.3 dB	54.8 dB	-41.7 dB	54.0 dBW
BOSTON	(1.2°, 0.45°)	31.7 dB	54.9 dB	-37.9 dB	53.9 dBW

DYNAMIC BEAM CONTROL

- C/I PERFORMANCE AT BOSTON IS 31.7 dB
- DOMINANT INTERFERENCE IS WASHINGTON SIDELobe LEVELS
- RE-OPTIMIZE WASHINGTON BEAM AT NEW LOCATIONS
RESULTING IN SMALL AMOUNTS OF SCAN WITHOUT
SIGNIFICANT DEGRADATION IN BEAM PERFORMANCE
- NEW WEIGHTS ARE ACHIEVED USING A COMBINATION OF
POWER DIVIDERS AND MMIC MODULES
- NOW LIMITED BY DISCRETE LEVELS OF GAIN AVAILABLE
WITH THE VPA MODULE

COMPUTED WASHINGTON BEAM PERFORMANCE FOR THREE SETS OF ELEMENT EXCITATIONS

<u>WEIGHT</u>	<u>LOCATION (AZ, EL)</u>	<u>C/I RATIO AT BOSTON</u>	<u>GAIN AT WASHINGTON</u>	<u>CROSS-POL</u>	<u>EIRP</u>
ORIGINAL	(0.65, 0.1)	31.7 dB	54.8 dB	-42.1 dB	53.9 dBW
A	(0.65, 0.0)	33.9 dB	53.2 dB	-42.0 dB	54.8 dBW
B	(0.7, 0.0)	34.8 dB	53.0 dB	-42.0 dB	55.5 dBW

SUMMARY AND CONCLUSIONS

MULTIPLE FIXED BEAM ANTENNA CONCEPTUAL DESIGN

SUMMARY

- USING TWO REFLECTOR ANTENNAS, OFFSET CASSEGRAIN OPTICS IS SUFFICIENT; TO USE ONE REFLECTOR WILL REQUIRE HIGHLY CONTOURED ARRAY STRUCTURE OR SHAPED SUBREFLECTOR
- LIMITED DYNAMIC BEAM CONTROL IS FEASIBLE USING CONVENTIONAL BFN AND SEPARATE MMIC MODULES (IMPROVED C/I RATIO)
- IMPROVED DYNAMIC BEAM CONTROL IS POSSIBLE WITH FINER AMPLITUDE QUANTIZATION
- BEAM-TO-BEAM ISOLATION IS ACHIEVABLE WITH POLARIZATION DIVERSITY AND SPATIAL SEPARATION ALONE

MULTIMISSION ADVANCED CONFIGURATION

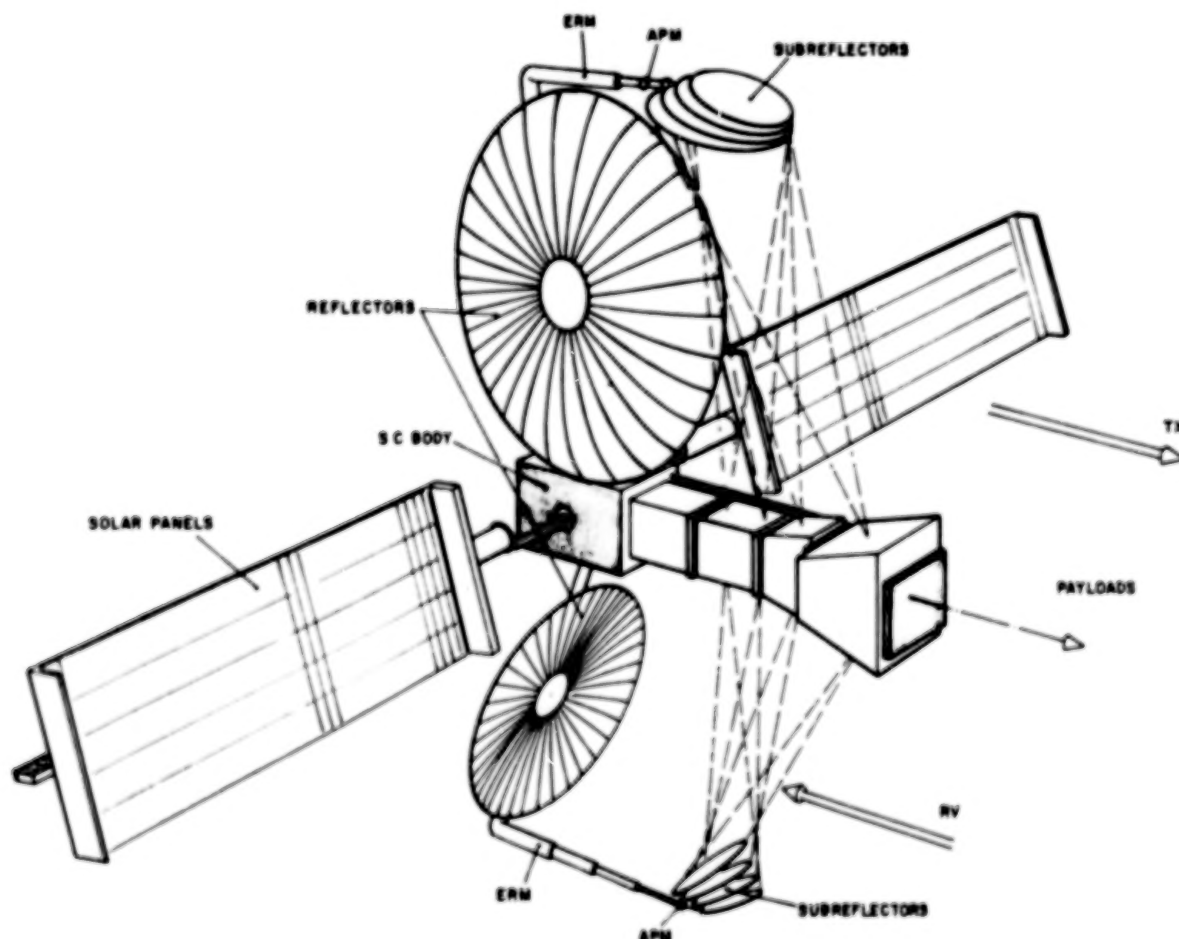
A. Saitto and G. Berretta
European Space Agency
Noorwijk, Holland

Large Space Antenna Systems-Technology - 1982
NASA Langley Research Center
November 30 - December 3, 1982

The proposed multimission configuration aims to reduce the number of reflectors present on the spacecraft and their related supporting structure (masts, booms) and at the same time divide the feed system from the reflector system for possible maintenance and/or payload substitution. This implies:

- o An antenna systems that is split into two parts:
 - (1) the reflector with the platform
 - (2) the feed subsystem with the payload
- o Reuse of the same reflector at different frequencies (to achieve this, the reflector system will use additional components, i.e., frequency-sensitive subreflectors (FSS))
- o In case of in-orbit refurbishment or maintenance, the reflector system may remain in orbit with the platform
- o The presence of the FSS allows separation of the focal position sufficiently for the multiple-contoured beam applications required by future missions

There are two of these reflectors (one for TX function, one for RV deployed) on the east and west sides of the spacecraft, and the solar panels are on the north and south sides. The payloads are aligned along the yaw axis. Apart from the size, this configuration looks like a conventional spacecraft.



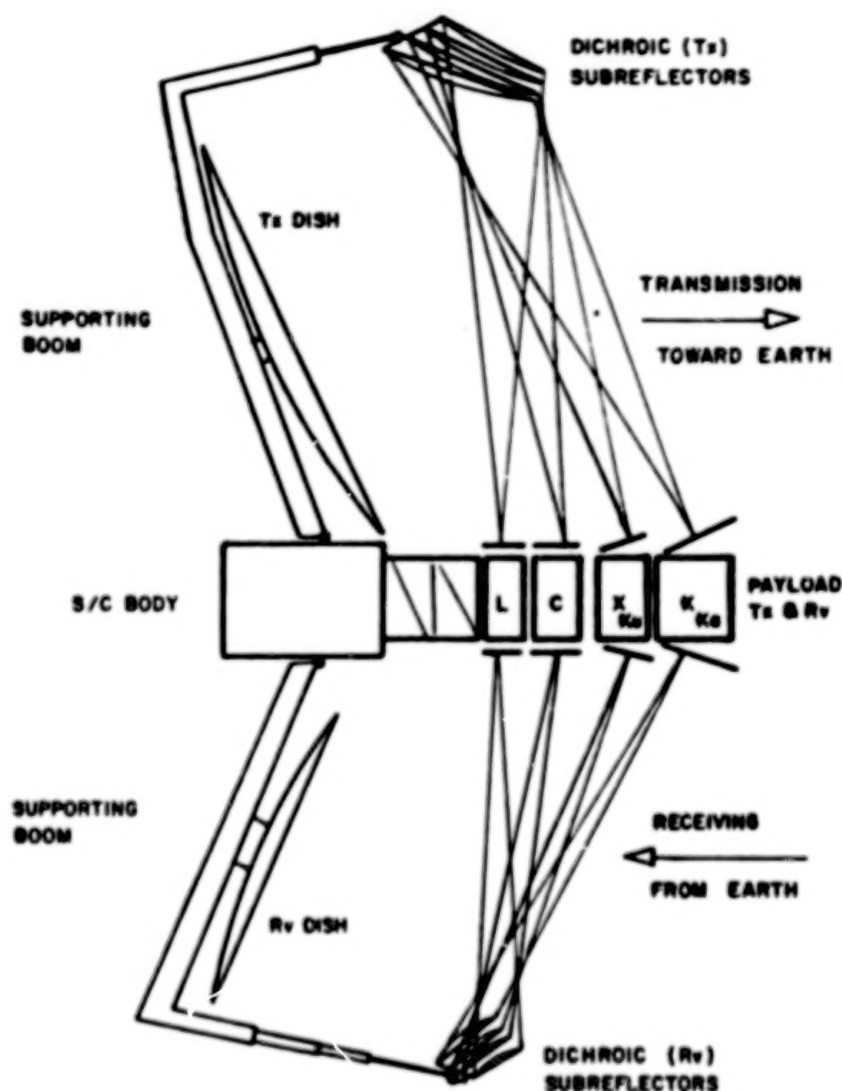
MULTIMISSION SPACE SEGMENT
ARTISTIC VIEW

The mission advantages are listed below. Additionally, the reuse of the same reflector gives a better reliability and a simpler orbit control system.

- REDUCING THE TOTAL MASS IN ORBIT
- MAXIMISING THE PAYLOAD DENSITY
- REDUCING SERVICING FLIGHTS TO THE MINIMUM NUMBER
- REDUCTION OF BOOM NUMBER
- MINIMUM LOSS CONFIGURATION (WAVEGUIDE RUN OPTIMISED)

MISSION ADVANTAGES

The two reflectors have four subreflectors with frequency-sensitive elements on each of them, except for the last one (for one band), which is solid. Each subreflector is reflecting at its own frequency and is transparent to the other three. The subreflectors cause a split of the relative feed position. In this way a feed system for each frequency can be designed with the maximum freedom in the allowed space. The space shown here is compatible within European coverage (5°). The figure shows a side view of the spacecraft with four different payloads (one TX and one RV).



MULTIMISSION SPACE SEGMENT
SCHEMATIC CONFIGURATION

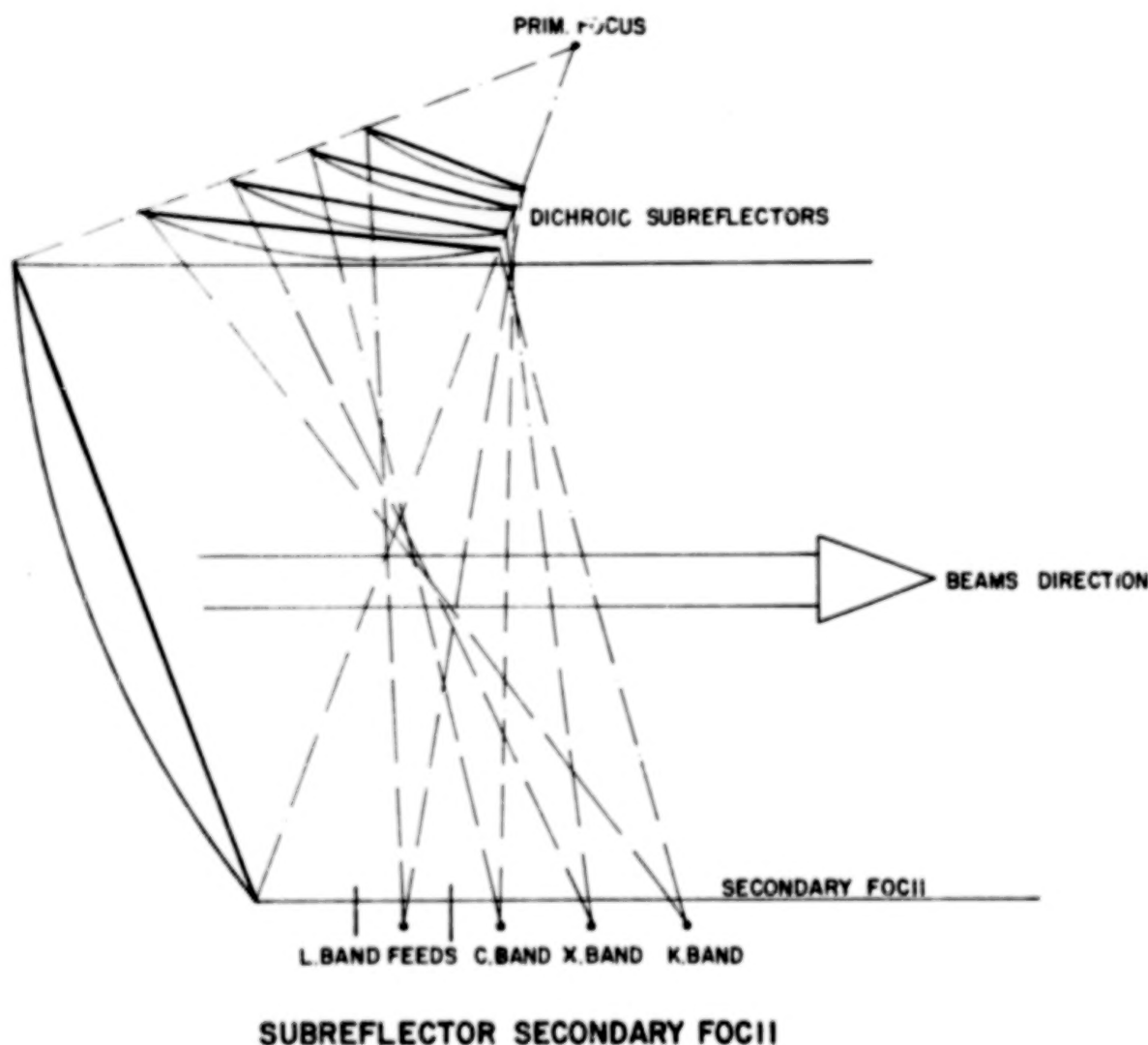
The characteristics of the antenna systems are summarized in the figure.

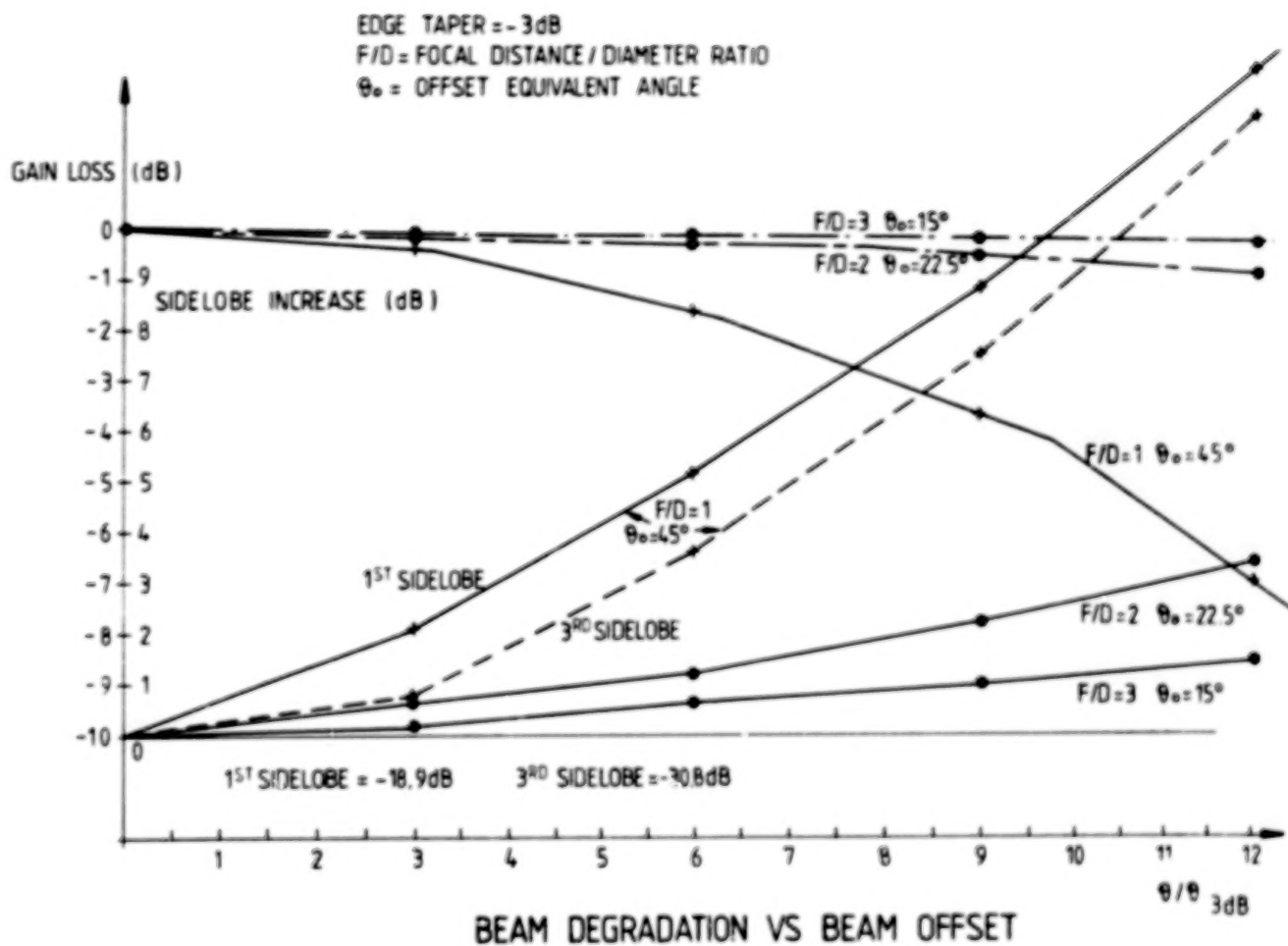
- VERY LARGE UNFURLABLE (OR INFLATABLE) REFLECTOR
- A NUMBER OF RIGID DICHROIC SUBREFLECTORS IN AN OPTIMUM CONFIGURATION FOR MULTIPLE / CONTOURED BEAM USE
- DIFFERENT PAYLOADS POSITIONED IN THEIR OWN FOCAL REGION
- ANTENNA POINTING MECHANISM FOR EACH SUBREFLECTOR POSSIBLE
- ARIANE COMPATIBILITY OF THE REFLECTOR SUBSYSTEM

ANTENNA SYSTEM CHARACTERISTICS

The figure shows a blowup of the reflector system with the different subreflectors. This configuration is a stable-reflector folded configuration for each frequency band, and has two advantages, a large equivalent F/D and small equivalent offset angles. These imply small beam distortions. (See figure on following page.) The small equivalent offset angle is obtained by folding the configuration in such a way that the feed principal ray (i.e., the normal to the feed aperture) is as close as possible to the trace of the focal plane on the plane of symmetry. (The best case is when it is parallel. Separate control of the beam directions is possible by moving each subreflector separately.)

The frequency-selective surfaces have a bandwidth larger than 20% depending on the incident angle on the surface. The corresponding loss may go from 0.2 dB (first subreflector) to 0.4 dB (last subreflector). The area between two consecutive foci may be shared between two different frequencies.



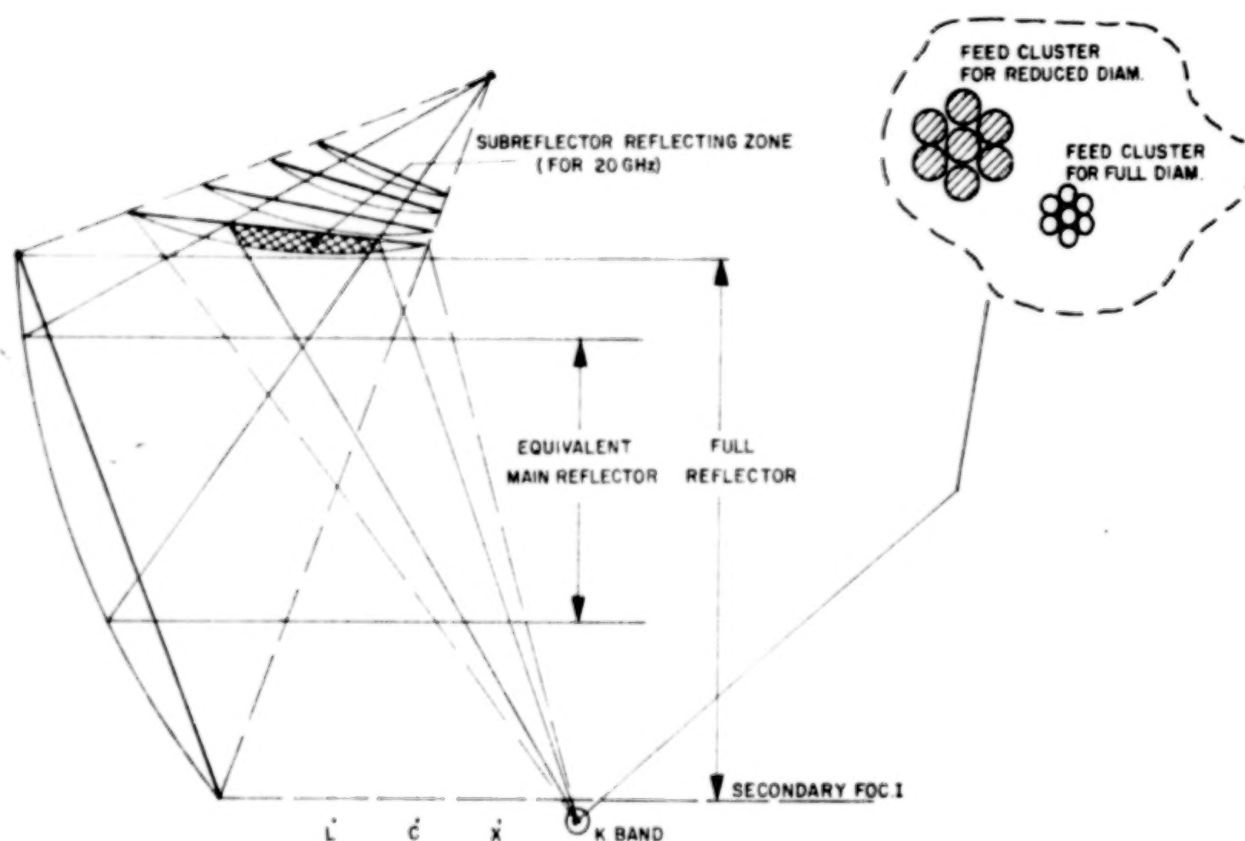


It is likely that different frequencies will require different reflector diameters. A possible way to get this result is to use only a part of the sub-reflector (i.e., make it frequency sensitive). In this way it is possible to select only a part of the main reflector. Because the subreflector part of the reflector system cannot be changed in orbit from payload to payload, the reflector reduction shall not be at the lower limit and some optimization of the 3 dB beamwidth shall be performed at the feed level.

Advantages of such an approach are:

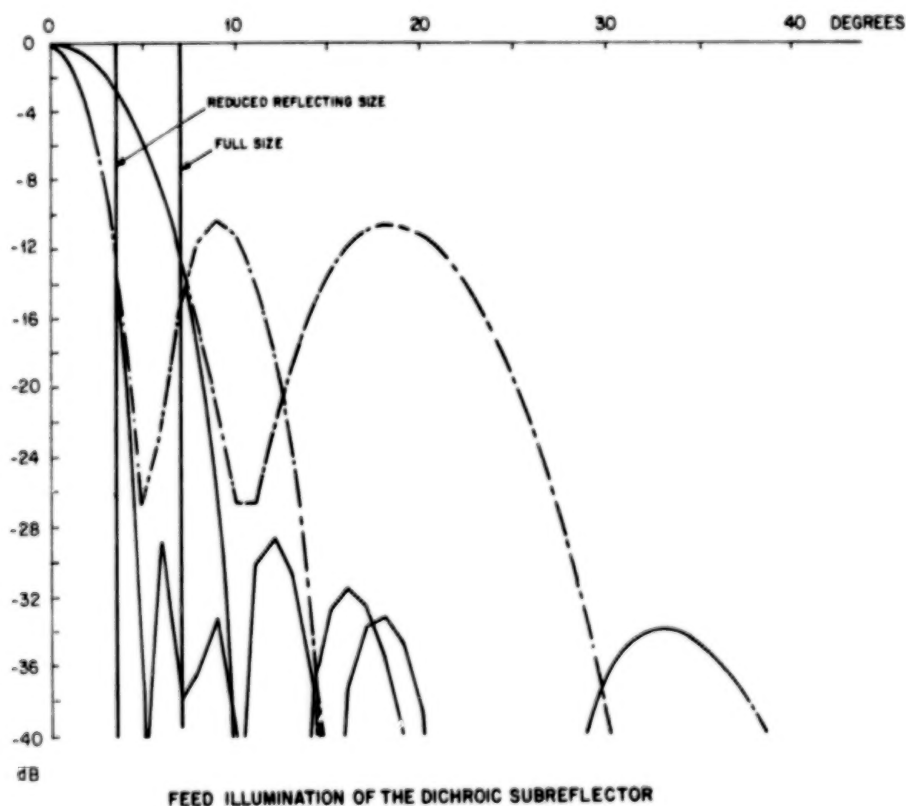
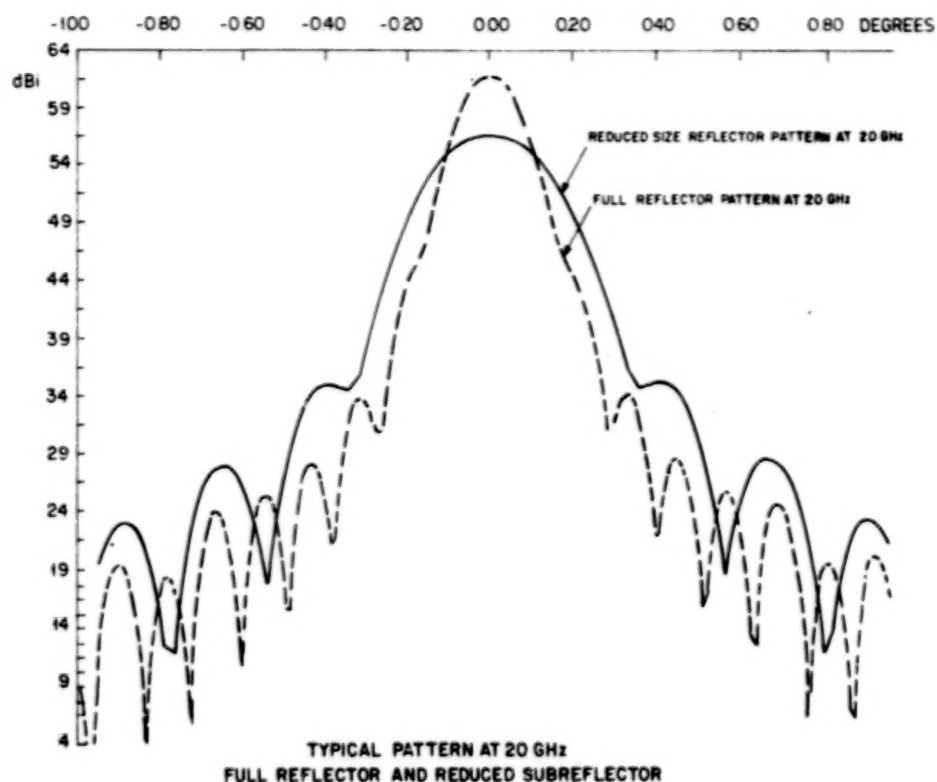
- o F/D increase (better performances)
- o Use of the control part of the reflector (less distortions)

A clear disadvantage is the increase (inversely proportional) of the feed dimensions.

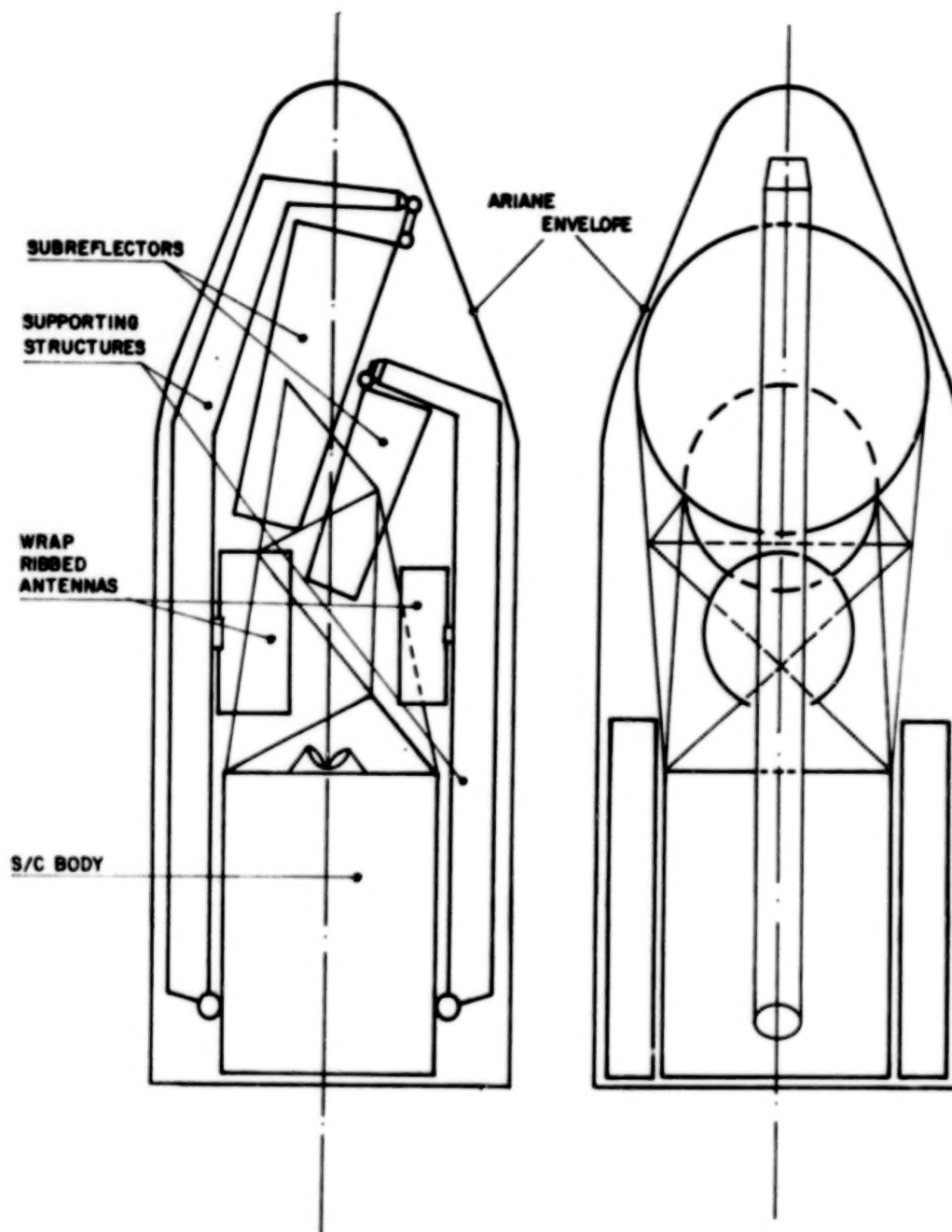


MAIN REFLECTOR OPTIMISATION FOR EACH FREQUENCY BAND (SHOWN 20 GHz) THROUGH AN INDEPENDENT REDUCTION OF THE REFLECTOR AREA OF EACH SUBREFLECTOR

The next two figures show the secondary and primary patterns of the full-size and reduced-size reflector.



The proposed configuration is compatible with the Ariane 4 fairing, as shown in the figure.



REFLECTORS & SUBREFLECTORS FOLDED
TO FIT THE ARIANE IV ENVELOPE

For the antenna subsystem (except for the spacecraft definition) there are three main points of investigation:

- o Reflector design for a large frequency range (surface roughness, tolerances, etc.)
- o Multidichroic subreflector performance (mutual effects, spurious resonances, etc.)
- o Mechanism subsystem (independent pointing mechanism for the subreflectors, reflector pointing and deployment, supporting mast, etc.)

LARGE SPACE ANTENNA COMMUNICATIONS SYSTEMS -
INTEGRATED LaRC/JPL TECHNOLOGY DEVELOPMENT ACTIVITIES
I. INTRODUCTION

Thomas G. Campbell
NASA Langley Research Center
Hampton, Virginia

Large Space Antenna Systems Technology - 1982
NASA Langley Research Center
November 30 - December 3, 1982

INTRODUCTION

The Jet Propulsion Laboratory and the Langley Research Center have been developing technology related to large space antennas (LSA) during the past several years. The hardware development activities were initiated during the Large Space System Technology (LSST) Program in 1978 and are now being continued by OAST through concept verification stages. During these concept development activities the structural aspects of the reflector configuration have been emphasized, but, due to funding constraints, feed system technology could not be addressed. Now, through the Communication System (R/T) Program of OAST, the problems associated with the feed systems that could be used with the LSA reflectors are now being investigated. Since the elements of the reflector program are directed by JPL and LaRC, an integrated feed development program has been initiated. This program will be synergistic with the reflector development and the electromagnetic research activities under way at JPL and LaRC.

OBJECTIVES FOR THE INTEGRATED TECHNOLOGY DEVELOPMENT PLAN

The need for a communication system research program became apparent during the recent studies for the Land Mobile Satellite System (LMSS). This study indicated the need for additional research in (1) electromagnetic analysis methods, (2) design and development of multiple beam feed systems, and (3) the measurement methods for LSA reflectors. The objectives of the integrated technology development program are listed below.

RECENT COMMUNICATIONS SYSTEMS **STUDIES FOR LMSS HAVE DEMONSTRATED** **THE FOLLOWING NEEDS:**

- VERIFIED E/M ANALYSIS METHODS FOR LARGE MESH
DEPLOYABLE REFLECTORS

- TECHNOLOGY DEVELOPMENT OF MULTIPLE BEAM FEED SYSTEMS
SUITABLE FOR L S A APPLICATIONS

- EVALUATE MEASUREMENT TECHNIQUES FOR LARGE
DEPLOYABLE REFLECTORS

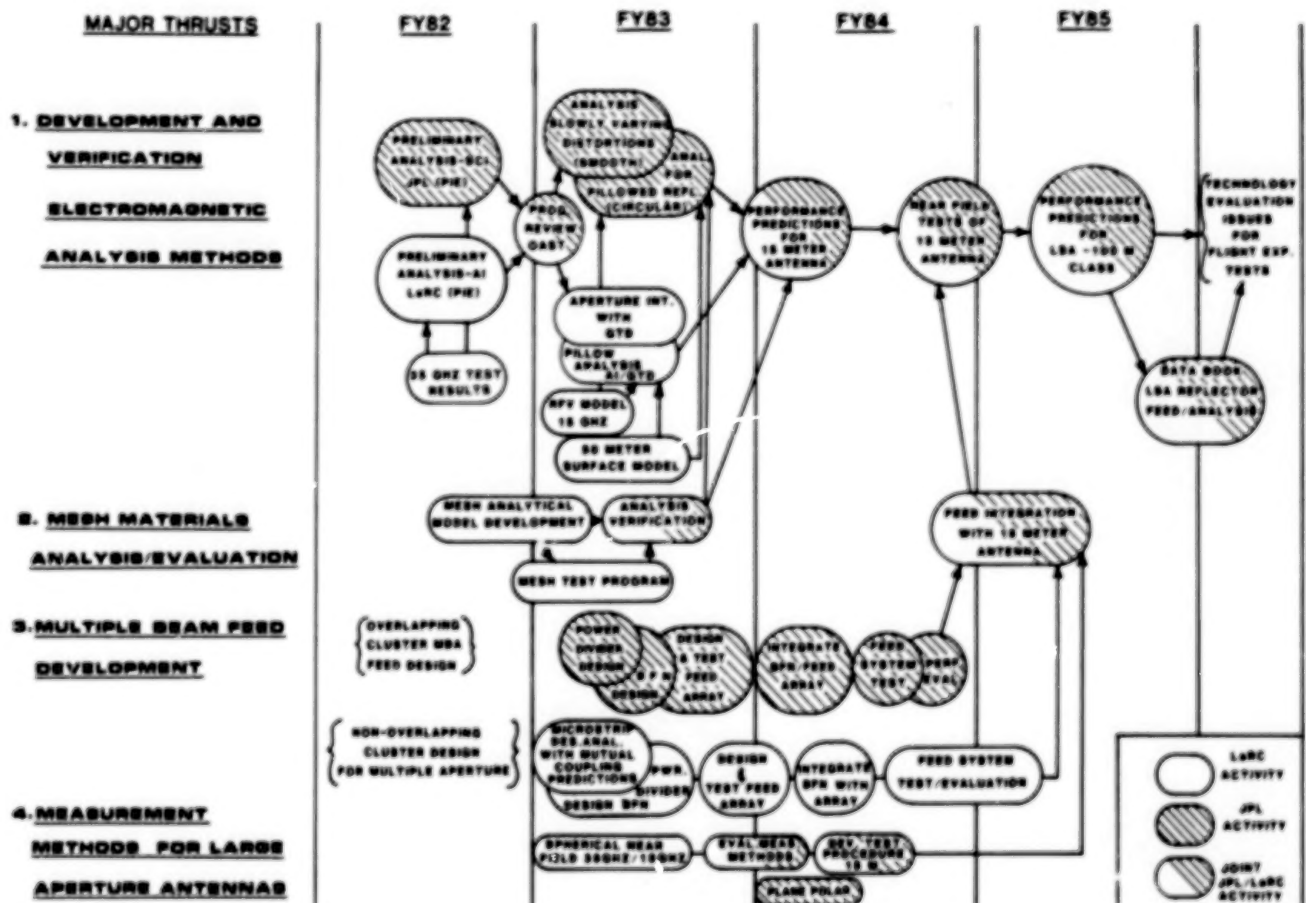
SPACECRAFT CONFIGURATIONS FOR THE LAND MOBILE SATELLITE SYSTEM (LMSS)

The recent LMSS studies at JPL and LaRC have identified two spacecraft configurations for the multiple beam missions. The JPL approach is to use a single 55-meter offset reflector and a feed system composed of overlapping feed cluster elements for the transmit and receive RF functions. The LaRC configuration is a larger symmetrical space frame structure that contains four 55-meter offset sub-apertures. The overall diameter is 122 meters. This approach is proposed in an effort to ease the packaging constraint imposed on the feed system by using additional apertures. The beams would then be interleaved from the respective apertures in providing the CONUS coverage required. Therefore, each LMSS configuration has different structural and radio frequency technological problems that will be addressed through the integrated program.



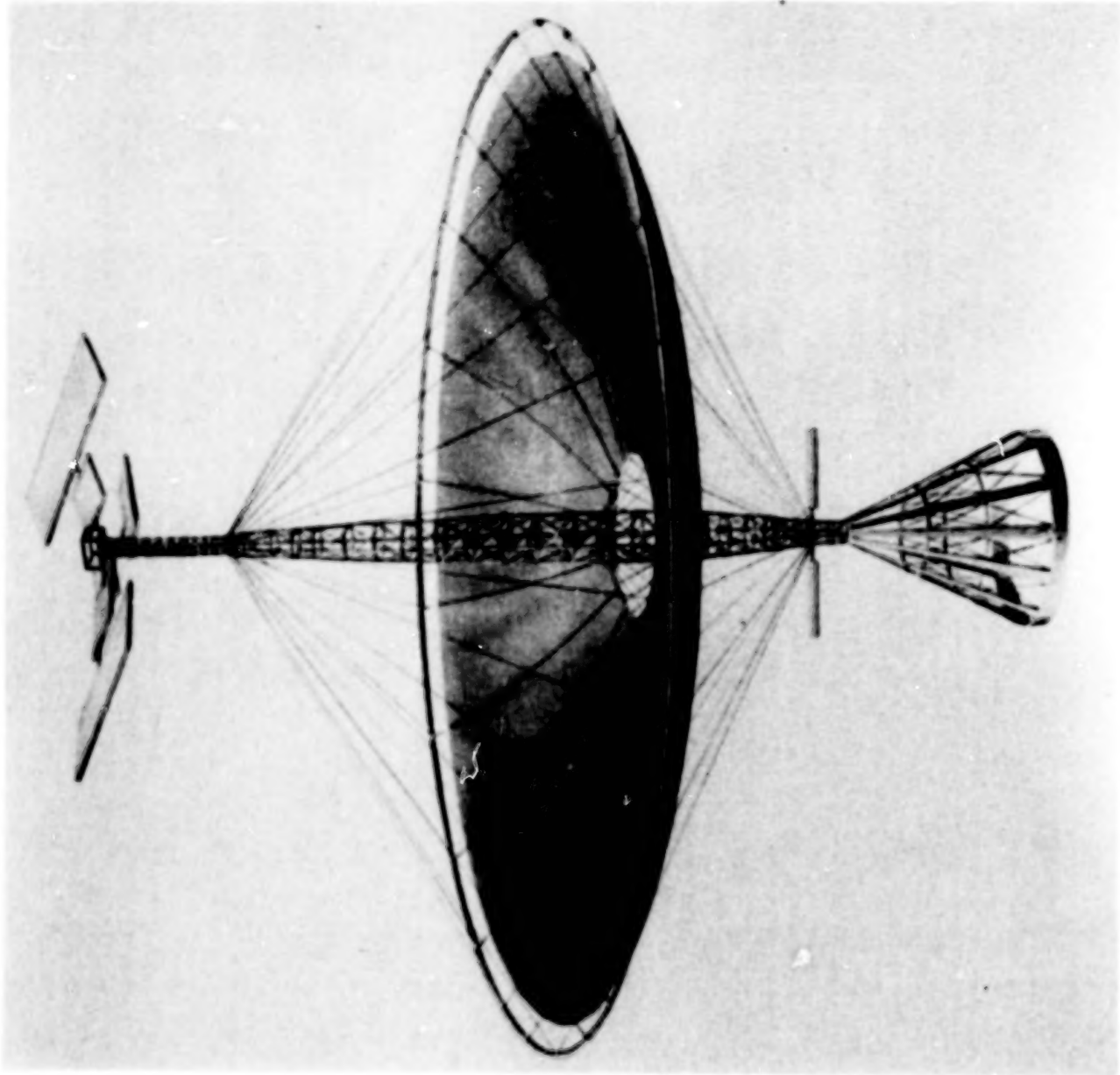
COMMUNICATIONS SYSTEMS TECHNOLOGY DEVELOPMENT PLAN

The technology development plan for the integrated communications systems program at JPL and LaRC is shown below. The major thrusts of the program are listed on the left-hand column of the plan and the major milestones for each thrust are scheduled as shown. The separate JPL and LaRC tasks are integrated through the development and testing of the 15-meter hoop/column deployable antenna model. This reflector model is being developed by the Harris Corporation under contract to Langley. The 15-meter model will provide a test bed for evaluating the LMSS feed system configuration that will be developed by JPL and Langley. In addition, the 15-meter model will serve as a verification model for the reflector analysis codes that are being modified and improved to include the characteristics of mesh reflector surfaces. The 15-meter antenna system will be tested in a planar near-field facility.



15-METER MODEL

An artist's rendering of the 15-meter antenna model is shown below. The 15-meter model will be deployed and the multiple beam feed panels will be attached to the center column as shown. The RF tests shall be designed by scaling the 15-meter reflector to the frequency and aperture size required for the LMSS communications mission. The single and multiple aperture approaches shall be tested and evaluated during this program.



LARGE SPACE ANTENNA COMMUNICATIONS SYSTEMS -
INTEGRATED LaRC/JPL TECHNOLOGY DEVELOPMENT ACTIVITIES
II. LaRC ACTIVITIES

f. G. Campbell, M. C. Bailey, C. R. Cockrell,
and F. B. Beck
NASA Langley Research Center
Hampton, Virginia

Large Space Antenna Systems Technology - 1982
NASA Langley Research Center
November 30 - December 2, 1982

ELECTROMAGNETIC ANALYSIS ACTIVITIES AT THE LANGLEY RESEARCH CENTER

The objective of the electromagnetic analysis activities at the Langley Research Center is to develop efficient and accurate analytical methods for predicting both far- and near-field radiation characteristics of large off-set multiple-beam multiple-aperture mesh reflector antennas.

REFLECTOR ANALYTICAL TECHNIQUES

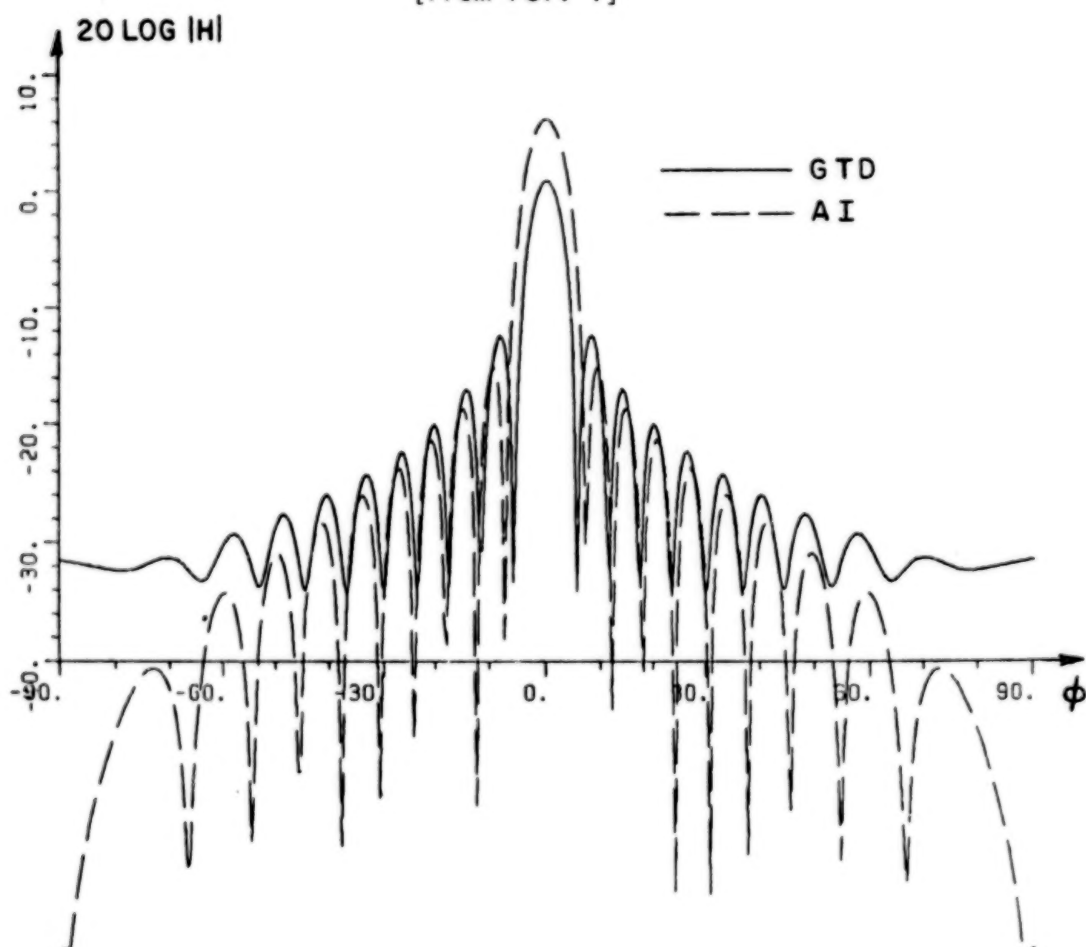
The Langley Research Center is emphasizing the utilization of aperture integration (AI) augmented with Geometrical Theory of Diffraction (GTD) in analyzing the large reflector antenna system. Typically, aperture integration is used to compute the main beam and near sidelobes and GTD will be used to compute the wide-angle sidelobes and backlobes. GTD can also be used to compute the near field radiation characteristics for certain near field aperture conditions. Reflector rim shapes, such as the segmented hoop of the 15-meter model, can be analyzed by GTD. The Langley analytical tasks shall be supported by the Electro Science Laboratory at the Ohio State University. Preliminary results are presented in reference 1.

- Aperture Integration - Aperture Field Method (AI) is used to compute the main beam and near sidelobes.
- Aperture Integration and Geometrical Theory of Diffraction - GTD coupled with AI will provide capability to compute wide-angle sidelobes and backlobes, as well as main beam.
- Aperture Integration Extended and GTD - Improved accuracy in computing the radiation pattern is expected if the aperture is extended to include vertex diffraction. AIE-GTD will be required when AI and GTD solutions have no common region of validity.

CALCULATED FAR FIELD PATTERN USING APERTURE INTEGRATION
AND GEOMETRICAL THEORY OF DIFFRACTION

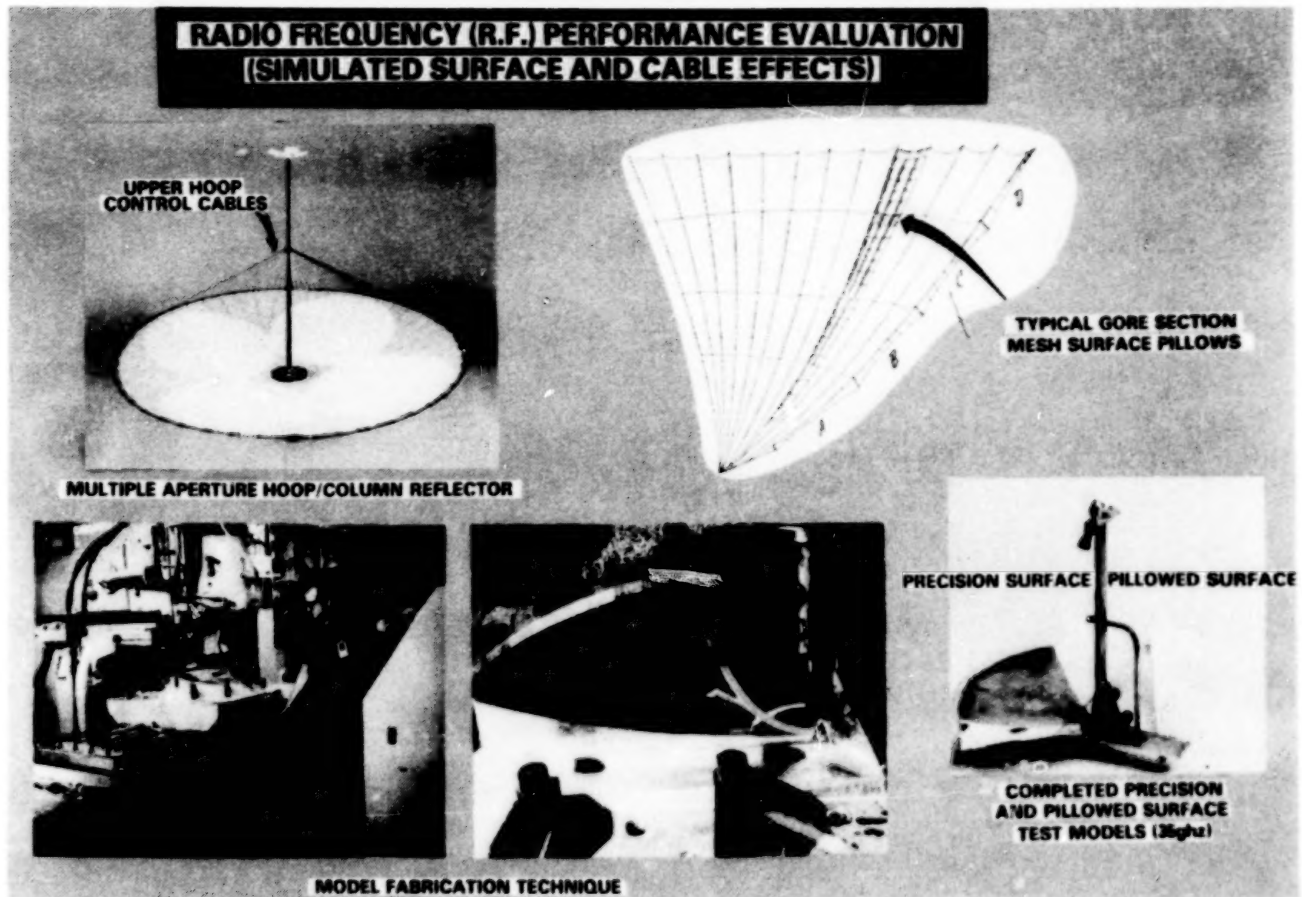
An example for the field radiation pattern calculations for tapered illumination and non-offset reflector using AI and GTD is shown below. The differences, especially in the sidelobes, can be noted. These particular results were obtained from Ohio State University (ref. 1) and they exemplify the need for AIE and GTD in order to obtain the complete 360-degree coverage about the antenna. The analysis methods developed will be evaluated using sub-scale engineering models for RF verification.

[From ref. 1]



35 GHz RF VERIFICATION MODEL ($D_{\lambda} = 35$)

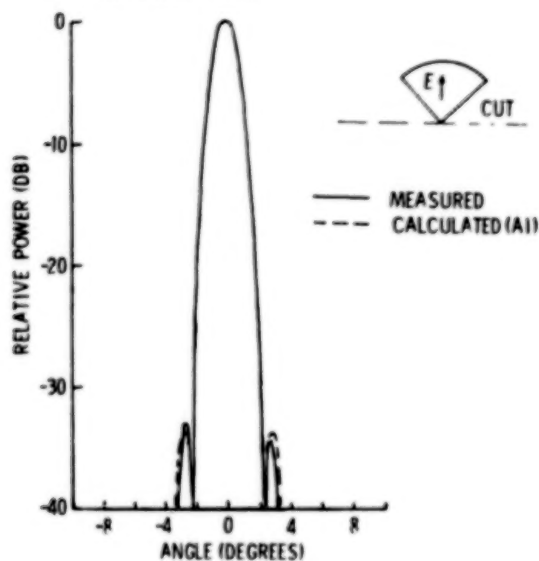
The first RF verification model operates at 35 GHz and preliminary test results are discussed in reference 2. The configuration of the offset fed reflector geometry and the machining process are shown below.



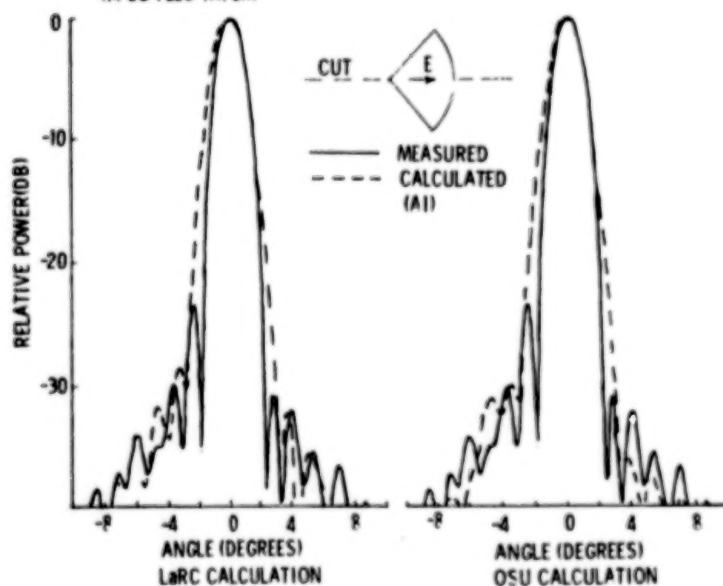
ANALYTICAL AND EXPERIMENTAL RESULTS USING THE 35-GHz TEST MODEL

Preliminary analytical results are compared with the measured results for the 35-GHz antenna model (precision surface - no pillows) in the figures below. The principal plane patterns are shown. It can be seen that good agreement was obtained for the H-plane (symmetric plane) pattern cut, but poor agreement was observed for the E-plane. These results are being investigated and further tests and analysis are under way. These results emphasize the need for experimental testing coupled with each reflector analysis activity.

MEASURED AND CALCULATED PATTERNS FOR 35 GHZ MODEL
(14 DB FEED TAPER)



MEASURED AND CALCULATED E-PLANE PATTERNS FOR 35 GHZ MODEL
(14 DB FEED TAPER)



RF VERIFICATION MODEL ($D_\lambda = 150$)

A larger RF verification model has been fabricated and is shown below. This model consists of 2.6-m-radius reflectors with the capability of testing two adjacent reflectors simultaneously. This RF verification model operates at 15 GHz and is the largest aperture that could be tested on the far field range available for testing. In fact, a (D^2/λ) range condition existed using this aperture that required defocusing the feed in order to achieve the far field pattern.

FABRICATION OF PRECISION RF VERIFICATION MODEL



A MOLD WITH 0.05 mm
(0.002 IN.) RMS ACCURACY
IS USED TO BUILD
FIBERGLASS
FACE SKINS

FACE SKINS ARE
ASSEMBLED TO
RIGID BACKUP
STRUCTURE



ASSEMBLED
ANTENNA TEST
MODEL

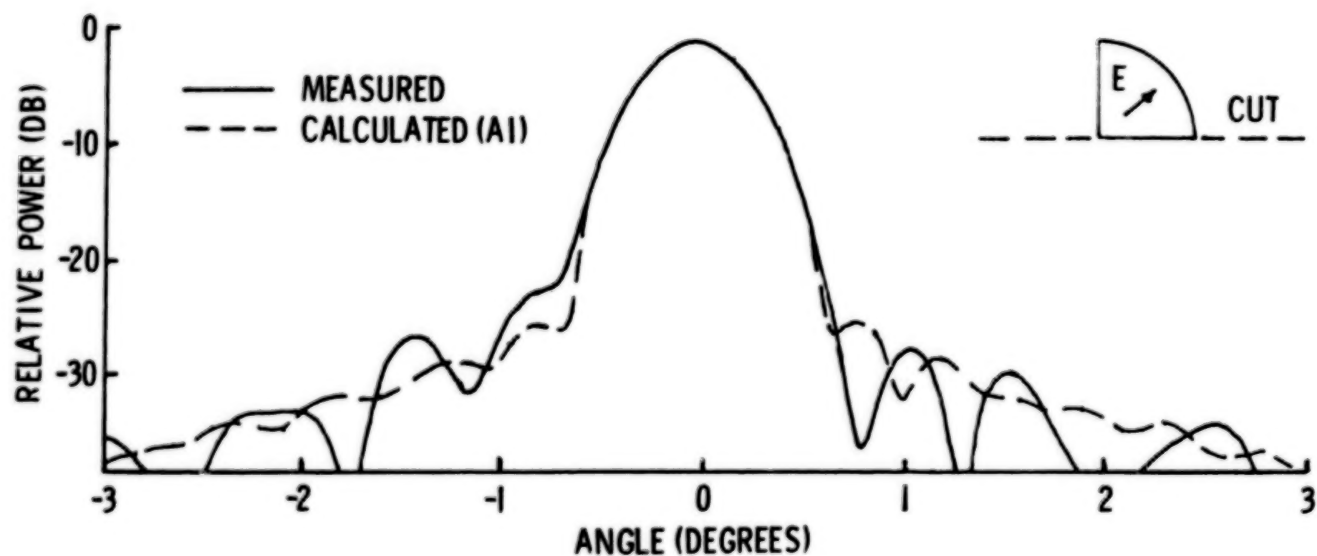


ADJUSTMENT SCREWS
BETWEEN FACE SKINS AND
BACKUP STRUCTURE PROVIDE
A REFLECTOR ACCURACY OF
0.2 mm (0.008 IN.) RMS

ANALYTICAL AND EXPERIMENTAL RESULTS - 150λ MODEL

The measured and calculated radiation patterns for the RF verification model (15 GHz) are shown below. AI was used to compute the pattern and further improvements in analysis and experimental modeling are expected.

MEASURED AND CALCULATED PATTERNS FOR RADIO FREQUENCY VERIFICATION MODEL (14 DB FEED TAPER)



MULTIPLE BEAM FEED DESIGN

Microstrip antenna design techniques will be used in developing the proof-of-concept LMSS feed configuration scaled to the 15-meter (6.09-meter sub-aperture) test model. Extensive research in microstrip antenna techniques have been conducted at Langley, and these analysis methods will be used for the LMSS feed design using multiple apertures. The analytical capability for predicting the radiated field, impedance, and mutual impedance characteristics of microstrip elements has been developed.

MICROSTRIP ANTENNA ANALYSIS

(vector potential)	$\vec{A} = \iint \vec{J} \cdot \vec{G}$
(radiated field)	$\vec{E}_r = k^2 \vec{A} + \nabla(\nabla \cdot \vec{A})$
(impedance)	$Z = \iint \vec{E}_r \cdot \vec{J}$
(mutual impedance)	$Z_{12} = \iint \vec{E}_1 \cdot \vec{J}_2$

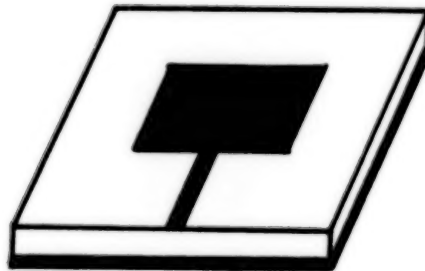
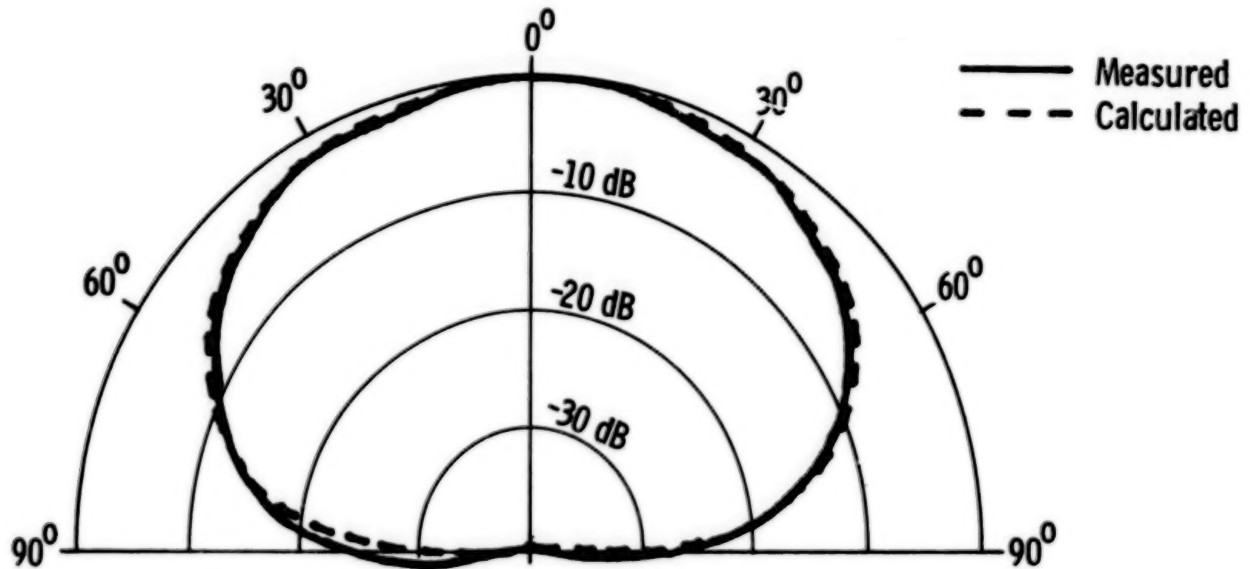


Analysis of Electromagnetics Problem

1. Derive \vec{G} by solving boundary value problem with impulse current.
2. Express \vec{J} in series with appropriate expansion functions.
3. Solve for coefficients of \vec{J} by matrix methods.

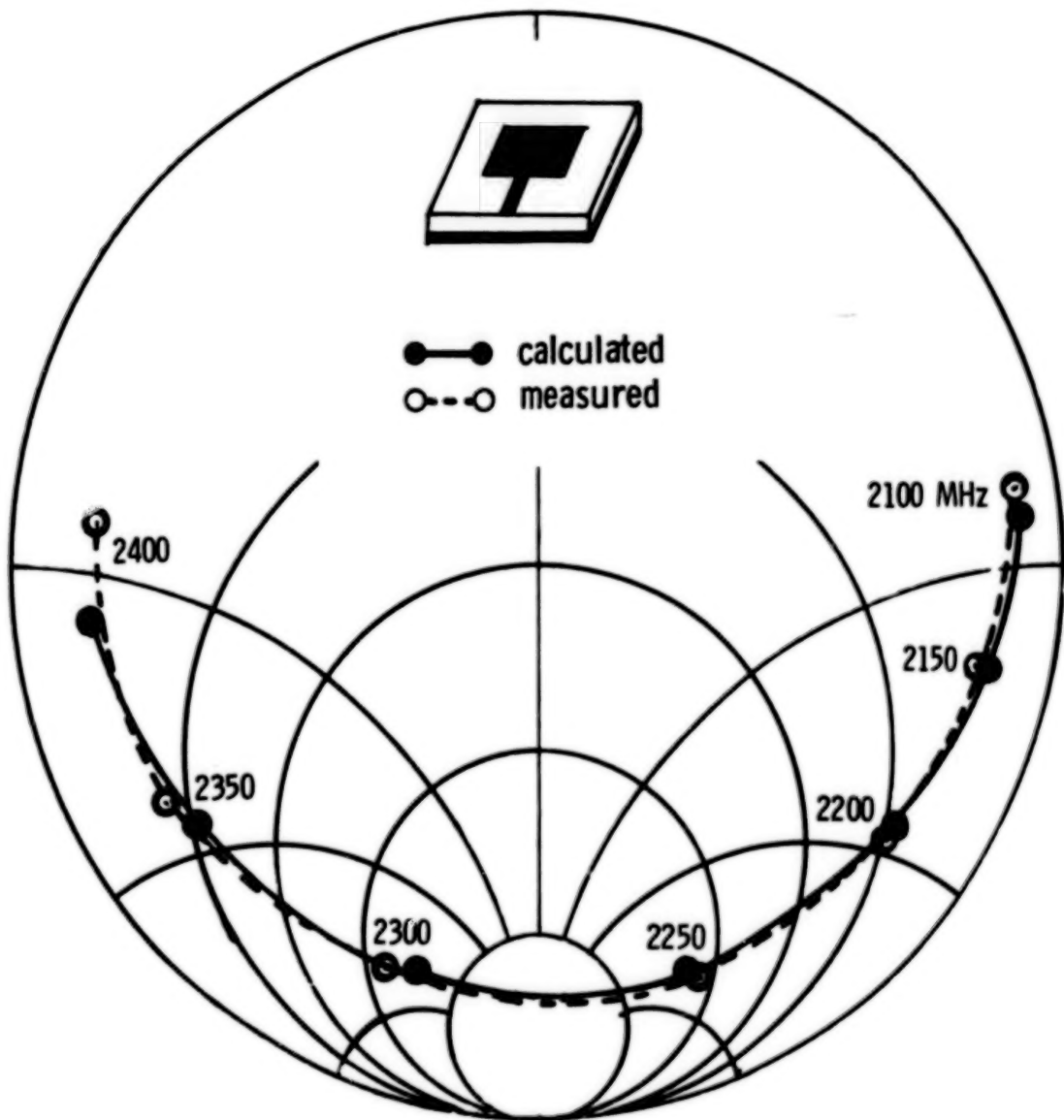
RADIATION PATTERN OF MICROSTRIP ANTENNA

An example of the accuracy of the microstrip analysis methods for predicting the radiation patterns is shown below. A rectangular microstrip, line fed antenna was used.



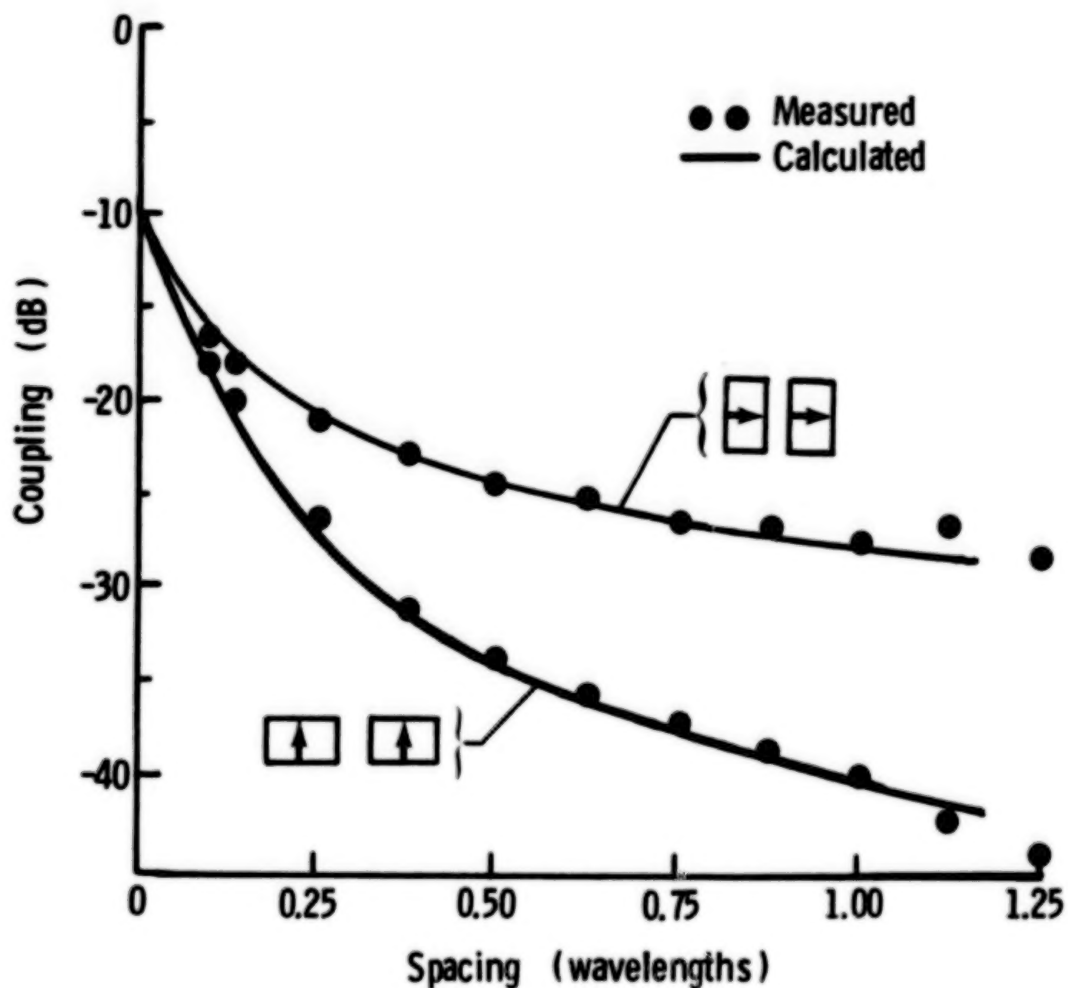
IMPEDANCE OF MICROSTRIP ANTENNA

An example of the accuracy of the microstrip analysis methods for predicting the impedance is shown below. A rectangular element configuration was used. Good agreement has been obtained for the matched impedance (50 ohms) as well.



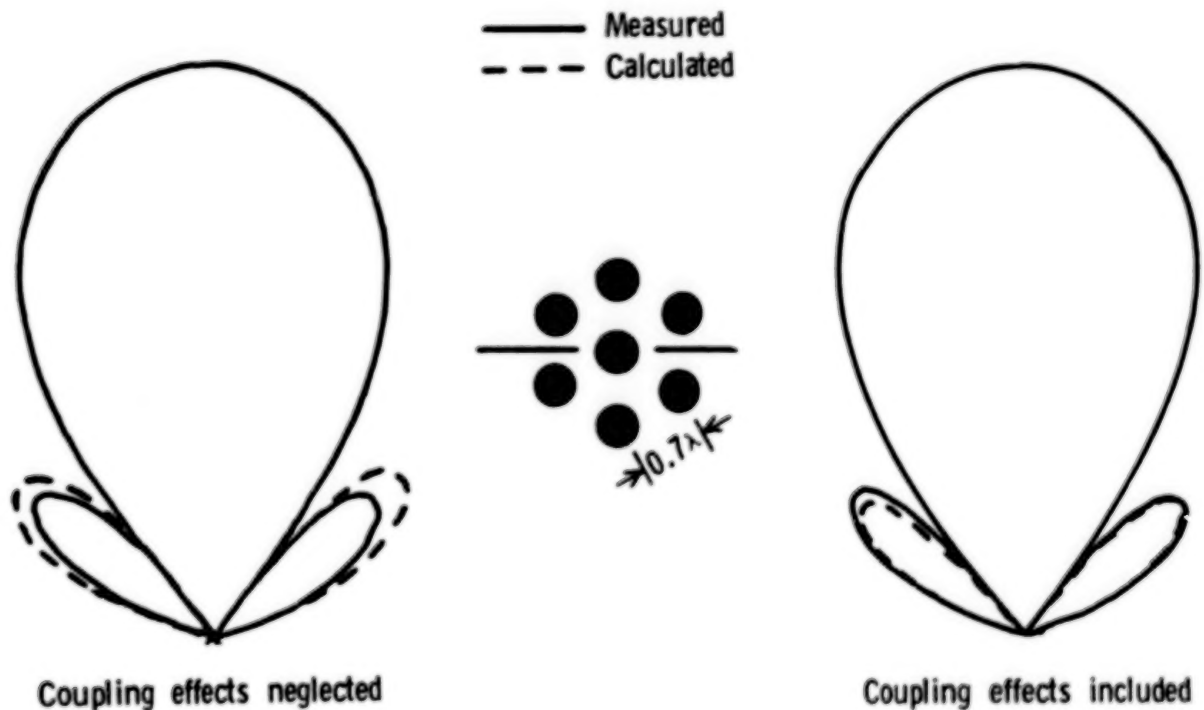
INTER-ELEMENT COUPLING OF MICROSTRIP ANTENNAS

Analysis methods for calculating the inter-element coupling of rectangular elements have been developed for the E- and H-planes. The analysis is being developed for circular microstrip elements. The coupling effect must be included in any microstrip cluster feed concept.



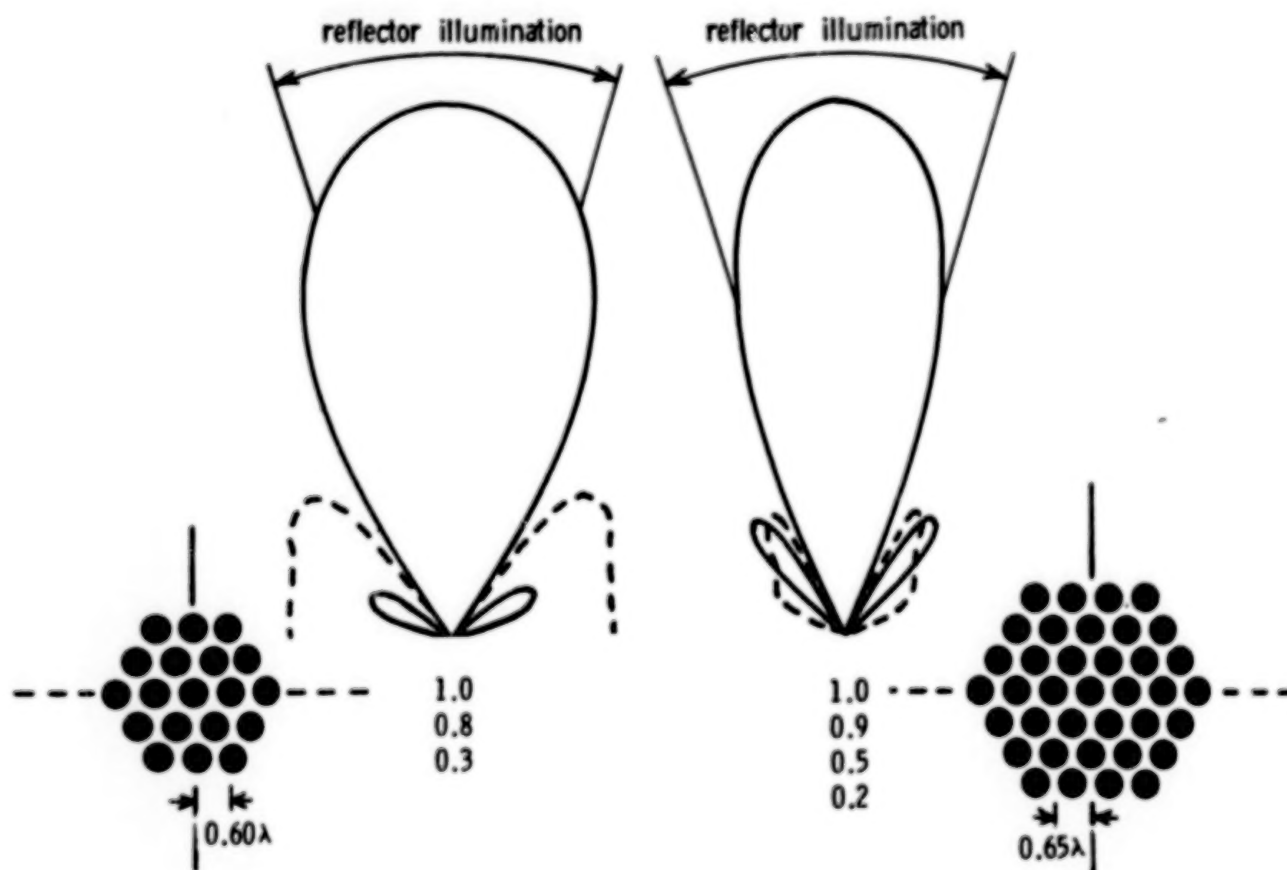
MEASURED AND CALCULATED RADIATION PATTERNS FOR A 7-ELEMENT MICROSTRIP FEED CLUSTER

A 7-element microstrip feed cluster has been considered in producing a single spot beam for the LMSS. Therefore, an engineering model of such a 7-element feed (3-GHz scale frequency) has been analyzed. Circular microstrip elements were used and the measured and calculated patterns are shown below. The effects of mutual coupling were considered as the radiation patterns were calculated with coupling effects neglected and then included as indicated below. The primary effect for the case considered was on the sidelobe level. In fact, mutual coupling for this example lowered the side levels by about 2 dB.



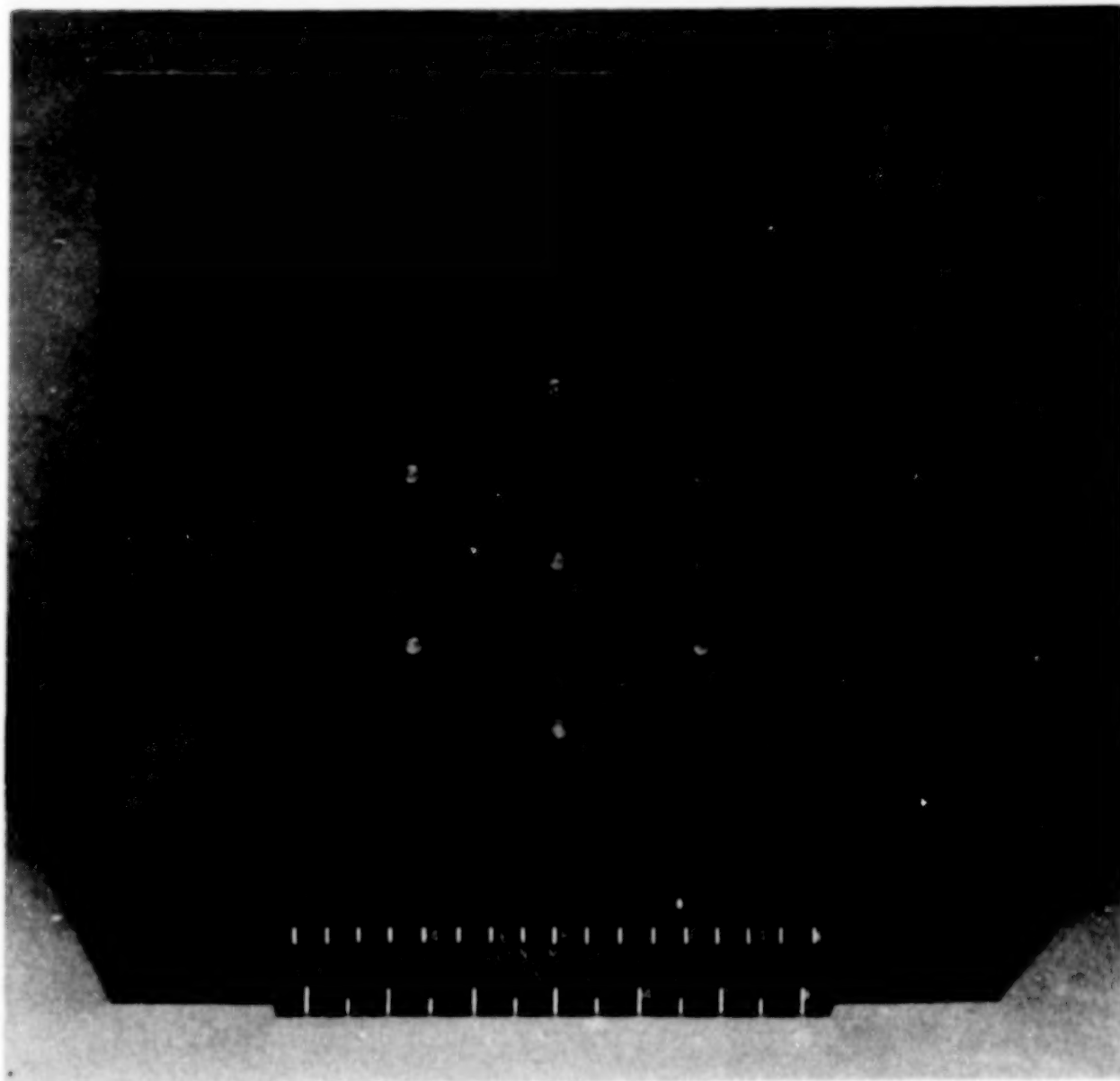
FEED CLUSTER DESIGNS WITH AMPLITUDE TAPERING

In the use of offset reflectors for communication and/or radiometric applications, different reflector illumination functions will probably be required. In the RF verification tests that have been under way with the 35-GHz and 15-GHz test models, two feed illuminations were used: 6 dB and 14 dB edge tapers. Therefore, microstrip feed clusters that would provide the 6 dB and 14 dB reflector edge illuminations were modeled at 3 GHz. A hexagonal element pattern was selected that would facilitate packaging a multiple beam configuration. The numbers of elements required for the 6 dB and 14 dB illuminations are 19 and 37, respectively. The amplitude distribution for each hexagonal ring of elements is indicated below for each cluster configuration.



PHOTOGRAPH OF 7-ELEMENT CONFIGURATION

A photograph of the 7-element microstrip cluster design is shown below. A Teflon fiberglass laminate ($\epsilon_r = 2.4$) was used. Circular microstrip elements were fed by coaxial probes and then combined using coaxial transmission lines and power dividers. A single probe feed was used on each element as linear polarization was produced.



TECHNOLOGY DELIVERABLES

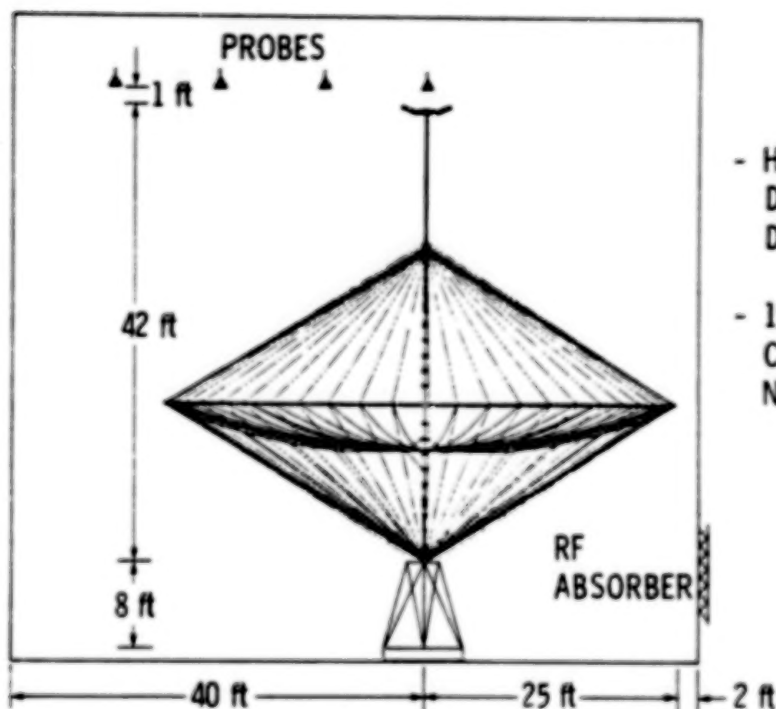
The technology deliverables expected from this Integrated Technology Development Program (JPL/LaRC) are listed below. The results should prove to be significant in assessing the readiness of deployable antenna technology for future multiple beam missions.

- **VERIFIED INTEGRATED FEED/REFLECTOR ANALYSIS
METHODS FOR MULTIPLE BEAM ANTENNAS**
 - **EVALUATED THROUGH SUB-SCALE MODELING AND
15 M ANTENNA R F TESTS**
- **MICROSTRIP MULTIPLE BEAM FEED SYSTEM DESIGN /
DEVELOPMENT (OVER-LAPPING CLUSTER AND
NON-OVERLAPPING CLUSTERS)**
- **NEW MESH ANALYTICAL MODELS**
- **VERIFIED MEASUREMENT METHODS FOR LARGE APERTURE,
MULTIPLE BEAM ANTENNAS**

NEAR FIELD TESTS USING THE 15-METER ANTENNA MODEL

A significant milestone in this Integrated Technology Development Program (JPL/LaRC) will be the RF testing of the 15-meter model in a near field facility. The Near Field Testing Laboratory (NFTL) at Martin-Marietta-Denver has been investigated and adjudged suitable for such tests. The NFTL is discussed in reference 3. The test configuration with the 15-meter model in the NFTL is shown below (ref. 4). It is anticipated that after the RF tests verifying mesh reflector surface characteristics have been completed, then the JPL and LaRC feed engineering models will be tested. These results should prove to be significant as the performance capabilities of mesh deployable antenna systems will be evaluated.

[From ref. 4]



- HARRIS CORP IS CURRENTLY DEVELOPING HOOP/COLUMN DEPLOYABLE ANTENNA FOR LaRC
- 15-m MODEL OF 100-m CONCEPT CAN BE ACCOMMODATED BY NFTL FOR TESTING UP TO 18 GHz

REFERENCES

1. Paknys, J. Robert: A Generalized Method for Determining Radiation Patterns of Aperture Antennas and Its Application to Reflector Antennas. Technical Report 710964-11, Electro Science Laboratory, Ohio State University, Sept. 1982.
2. Campbell, T. G.; and Young, W. R.: Preliminary Experimental Test Results Using 35 GHz Offset Fed Reflector Simulating Surface Pillows and Aperture Cables. Large Space Systems Technology - 1981, Part 1, NASA CP-2215, 1982, pp. 557-582.
3. Lang, G. J.: Near-Field Testing of LaRC Multiple-Beam Antenna. Large Space Systems Technology - 1981, Part 2, NASA CP-2215, 1982, pp. 657-680.
4. Near-Field Testing of LaRC Multiple-Beam Antenna. Report No. P81-62041-1, Martin Marietta Corp., Dec. 1981.

LARGE SPACE ANTENNA COMMUNICATIONS SYSTEMS -
INTEGRATED LaRC/JPL TECHNOLOGY DEVELOPMENT ACTIVITIES
III. JPL ACTIVITIES

K. E. Woo, Y. Rahmat-Samii, and W. Imbriale
Jet Propulsion Laboratory
Pasadena, California

Large Space Antenna Systems Technology - 1982
NASA Langley Research Center
November 30 - December 3, 1982

BEST AVAILABLE COPY

OVERVIEW

This paper describes the portion of JPL antenna R/D work that is performed co-operatively with Langley Research Center in support of the demonstration and evaluation of the 15-m unfurlable antenna. Figure 1 presents the activities that will be performed during FY 83 and FY 84.

- DEVELOP OVERLAPPING CLUSTER-OF-ELEMENTS MULTIPLE-BEAM FEED FOR LaRC 15-M UNFURLABLE ANTENNA
- MODIFY AND/OR VERIFY EXISTING JPL SCATTERING PROGRAMS NECESSARY FOR EVALUATING RF PERFORMANCE OF THE 15-M ANTENNA, INCLUDING:
 - PIE-SHAPED REFLECTORS
 - SURFACE DISTORTIONS DUE TO THERMAL EFFECTS
 - SURFACE DISTORTIONS DUE TO PILLOWING EFFECTS
 - MESH REFLECTORS
- EVALUATE SUITABILITY OF USING EXISTING JPL PLANE-POLAR NEAR-FIELD MEASUREMENT CAPABILITY FOR DESIGN VERIFICATION AND ACCEPTANCE TESTING OF LARGE OFFSET ANTENNAS

Figure 1

BEST AVAILABLE COPY

OVERLAPPING FEED CONCEPT

The basic way to generate multiple beams is to place the feed for each beam at the focal plane of a reflector system as shown in Figure 2(a). For adjacent beams to have a high cross-over level, their feeds must be close together. For beams to have low sidelobes, the aperture of each feed must be large so as to illuminate the reflector with high edge taper. When both low sidelobe and high cross-over are needed, as in the case of LMSS, it is necessary for the feed apertures to overlap. Such overlapping is physically impossible if single feeds are used, as shown in Figure 2(b). The overlapping can be achieved, however, if the aperture of each feed is made up of a number of subapertures or elements, as shown in Figure 2(c). In this case, each aperture is composed of a cluster of 7 elements with 4 common elements serving both feed apertures to produce both beams. For LMSS applications, the use of 7-element clusters provides sufficient flexibility to meet sidelobe and cross-over requirements.

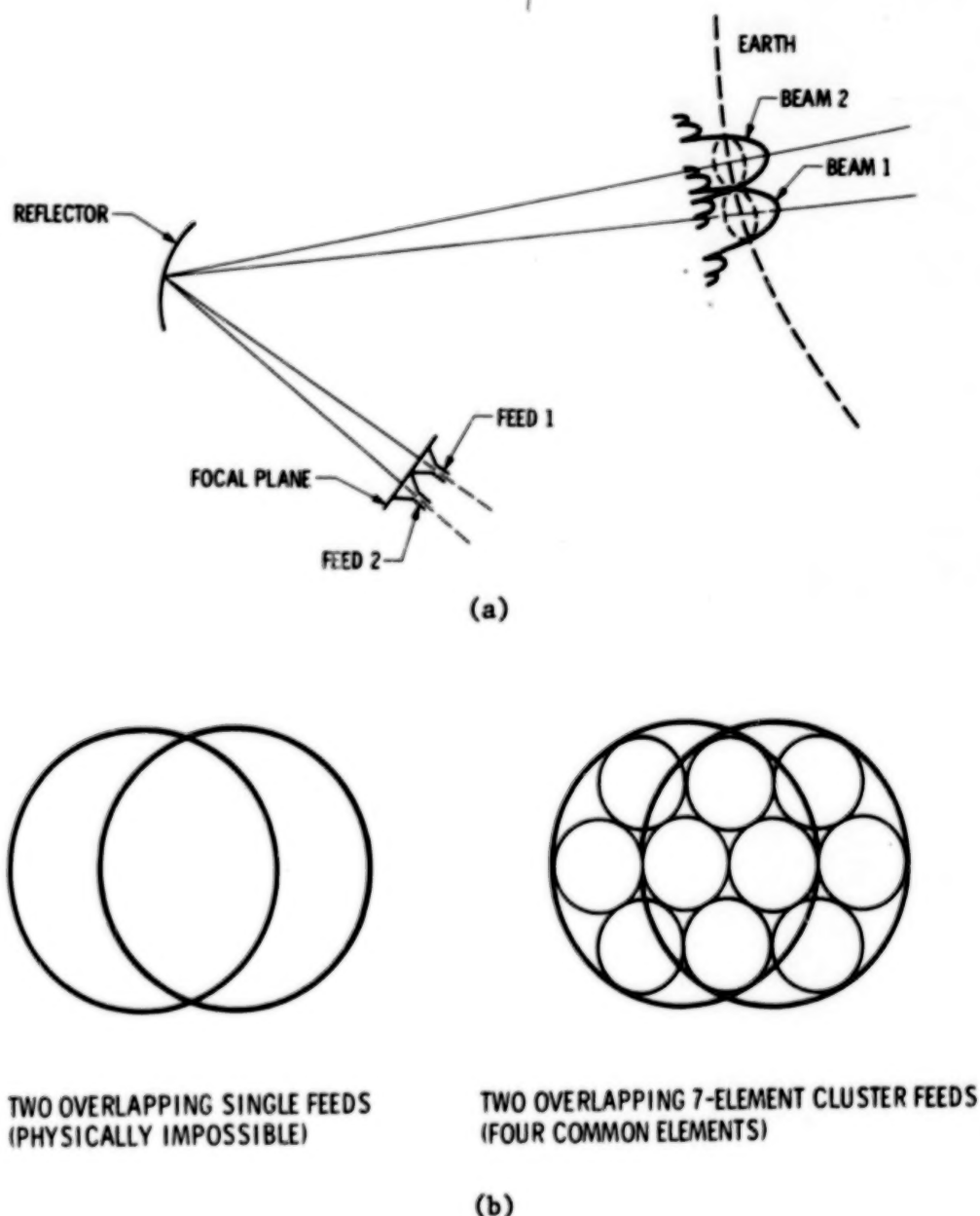


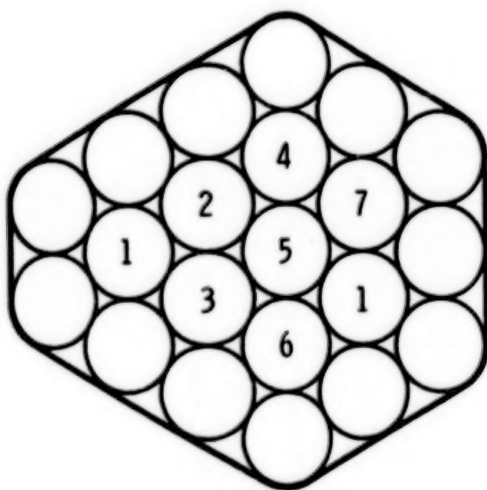
Figure 2

OVERLAPPING CLUSTER FEED DESIGN FOR 15-m ANTENNA

For the 15-m antenna, a circularly polarized overlapping cluster feed is to be developed to illuminate one quadrant of the antenna. Two alternatives are under consideration. One design is to produce 8 beams by using 21 elements, simulating a section of the feed for the 7-frequency reuse case of LMSS, as shown in Figure 3(a). The numerals 1 to 7 denote the center elements of seven 7-element clusters for producing seven far-field beams (from the reflector) at seven different frequencies. The cluster with center element 1 on the right is to produce an eighth beam operating at the same frequency as the beam produced by the cluster with center element 1 on the left. The presence of two beams of same frequency enables the study of inter-beam isolation characteristics of the design and the verification of existing computer programs for isolation calculations. The other design, as shown in Figure 3(b), is to produce 5 beams by using 16 elements, simulating a section of the feed for the 4-frequency reuse case of LMSS. Dual polarization is needed in this design in order to satisfy the LMSS isolation requirement.

For relative ease of deployment for future applications, microstrip square patch radiators will be utilized in that they are flat and thin. Each element is to consist of four such radiators, as shown in Figure 3(c).

The frequency of operation of this feed has not yet been selected. It will be determined jointly with LaRC in order to be compatible with their feed design for the multiple antenna aperture concept.

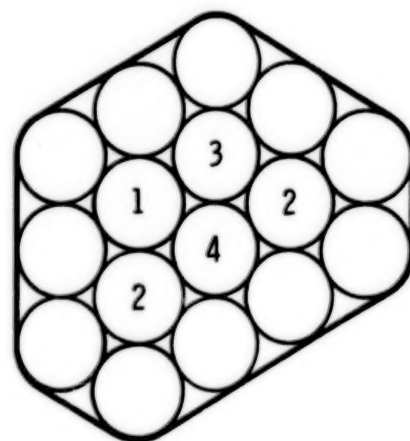


21 ELEMENTS

8 BEAMS

SIMULATING 7-FREQUENCY
REUSE CASE OF LMSS

(a)



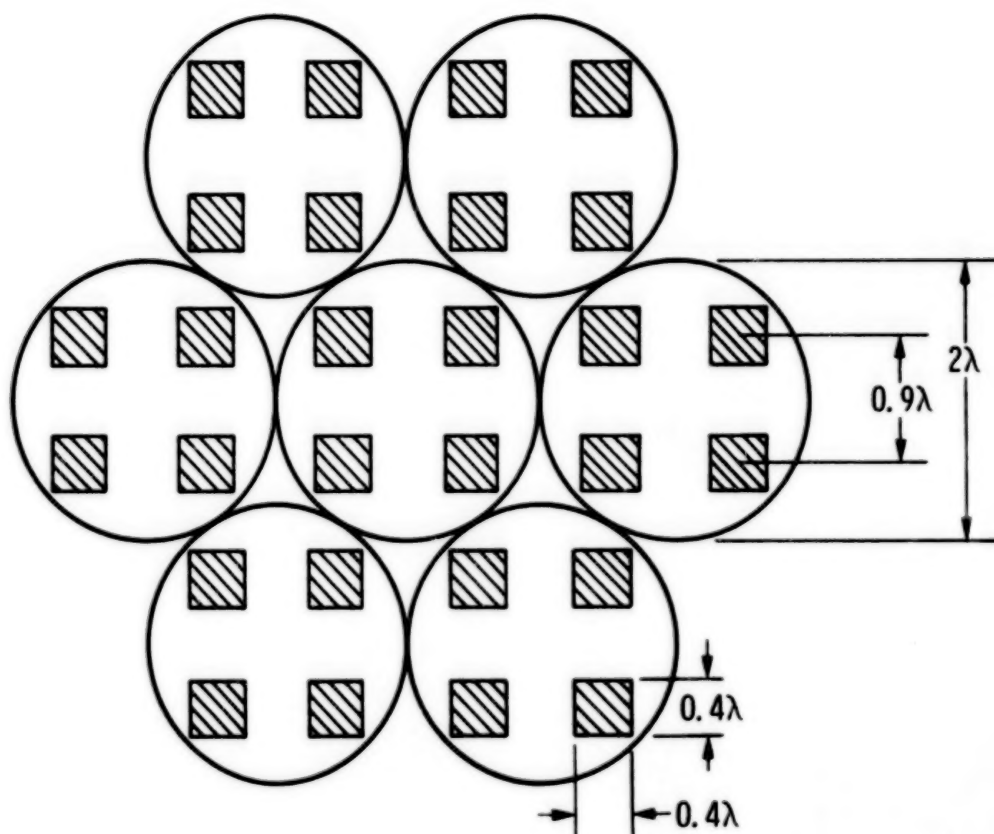
16 ELEMENTS

5 BEAMS

SIMULATING 4-FREQUENCY
REUSE CASE OF LMSS

(b)

Figure 3



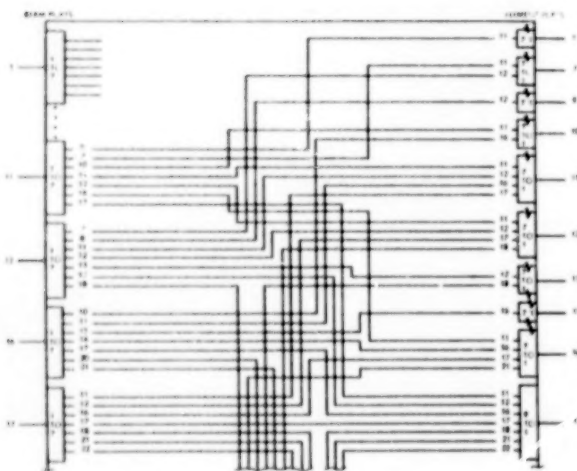
A CLUSTER OF 7 ELEMENTS PRODUCES ONE BEAM
 EACH ELEMENT IS COMPOSED OF 4 MICROSTRIP SQUARE PATCHES

(c)

Figure 3 (Concluded)

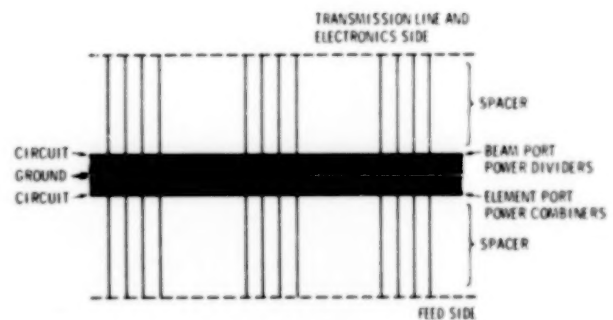
BEAM FORMING NETWORK (BFN)

To form individual beams, a beam forming network is required to divide the power feeding each beam port of the feed and route it to the cluster of 7 elements associated with that port. Due to the overlapping requirement, the element connected to each element port of the feed receives and combines power from as many as 7 beam ports for many of the elements. A schematic of this network for LMSS applications is shown in Figure 4(a). A design concept to implement this scheme using present day technology has been devised. Two microstrip panels are stacked ground to ground, as shown in Figure 4(b). Curved power dividing circuits are etched on the beam port side, and similarly curved power combining circuits are etched on the element side, as shown in Figure 4(c). The use of the stacked panels permits direct connections through the panels between appropriate terminals of the power dividing circuits and the power combining circuits, avoiding the otherwise severe routing problems of transmission lines. The use of curved circuits allows the combining of uplink and downlink BFN's on the same set of panels, thereby reducing the overall weight by half. The BFN for the 15-m antenna will be developed based on this concept unless the frequency of operation to be selected does not permit the use of this design.



SCHEMATIC FOR OVERLAPPING
7-ELEMENT CLUSTERS

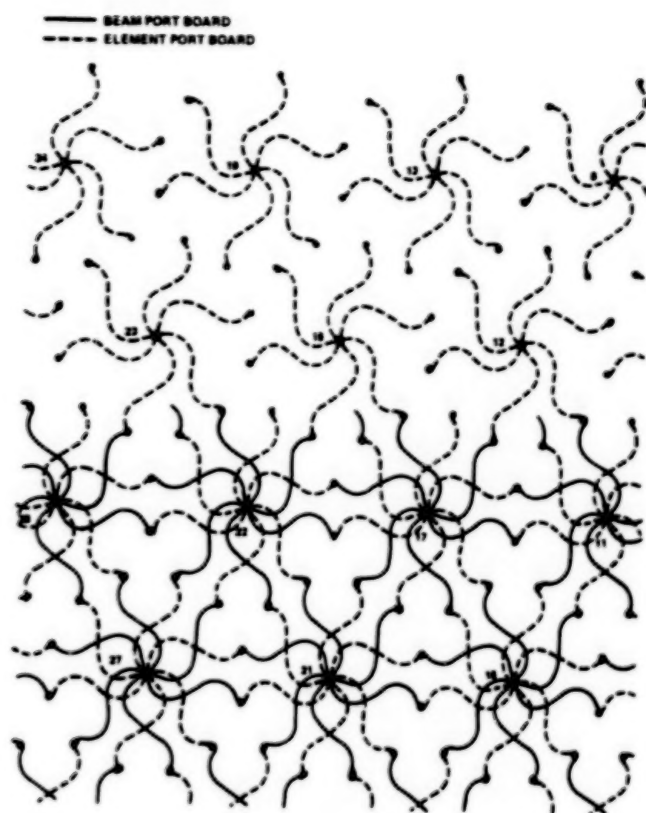
(a)



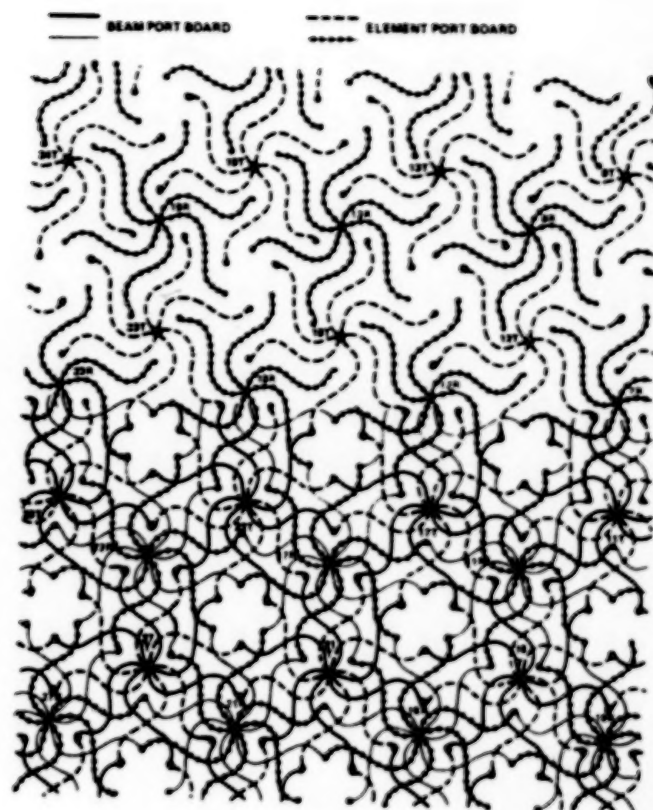
MICROSTRIP PANEL CONSTRUCTION

(b)

Figure 4



DOWNLINK



UPLINK AND DOWNLINK COMBINED

MICROSTRIP CIRCUIT CONFIGURATION

(c)

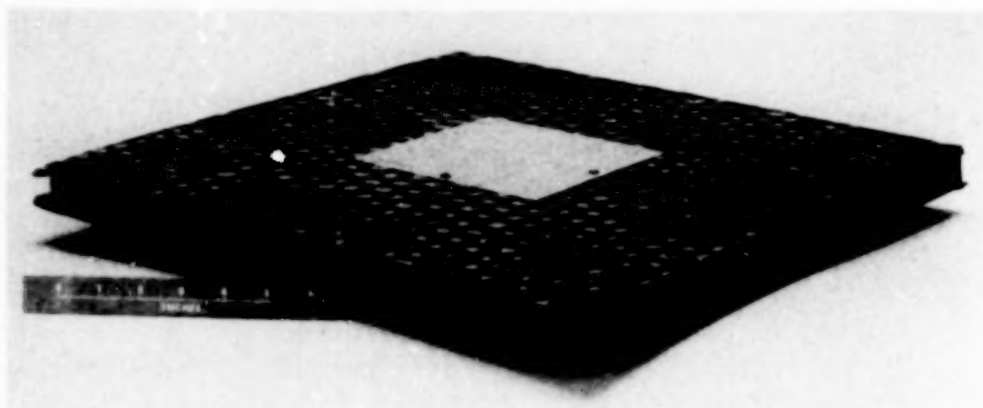
Figure 4 (Concluded)

MICROSTRIP PATCH AND BFN DEVELOPMENTAL ACTIVITIES

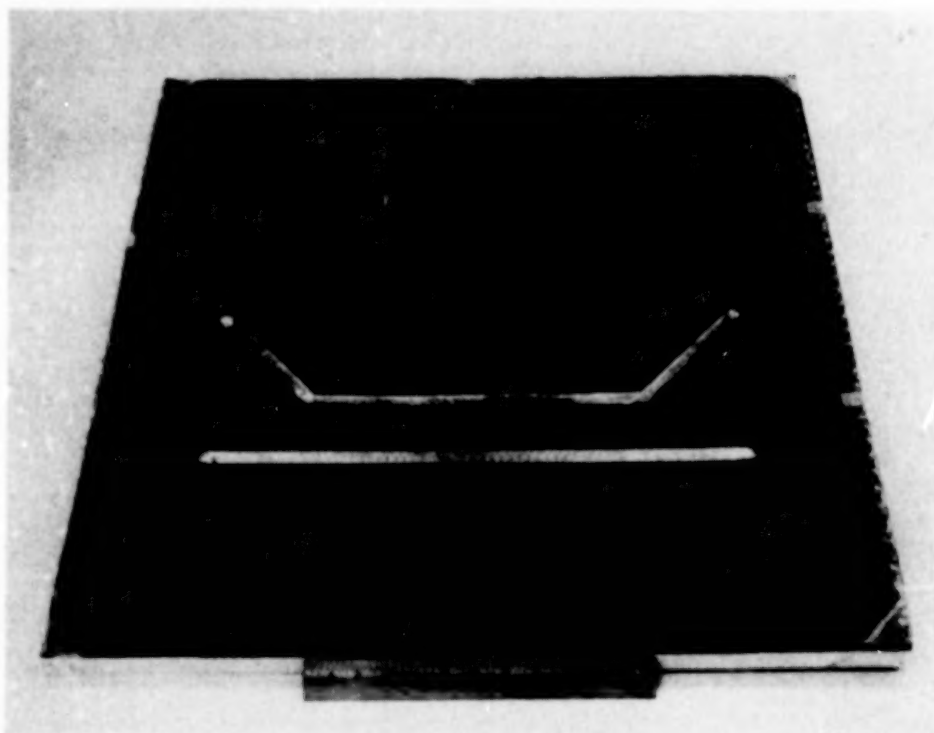
A circularly polarized microstrip square patch radiator has been developed at UHF, as shown in Figure 5(a). The radiator consists of a square metallic patch above a ground plane with honeycomb substrate in between. The radiator provides not only the proper radiation characteristics but also the relatively broad bandwidth (7%) required by LMSS.

A study for determining the loss and coupling characteristics of the proposed LMSS beam forming network has been performed. By using two UHF microstrip transmission lines, as shown in Figure 5(b), and by varying their separation, it is concluded that:

- (1) There are no significant losses in the circuits of the BFN
- (2) There is no significant coupling between adjacent circuits of the BFN



(a)



(b)

Figure 5

CONCEPTUAL VIEW OF FEED ARRAY FOR 15-m ANTENNA

Figure 6 shows the conceptual view of the LMSS integrated planar feed array. The feed array for the 15-m antenna will have a similar design except that no electronics and thermal capabilities will be provided.

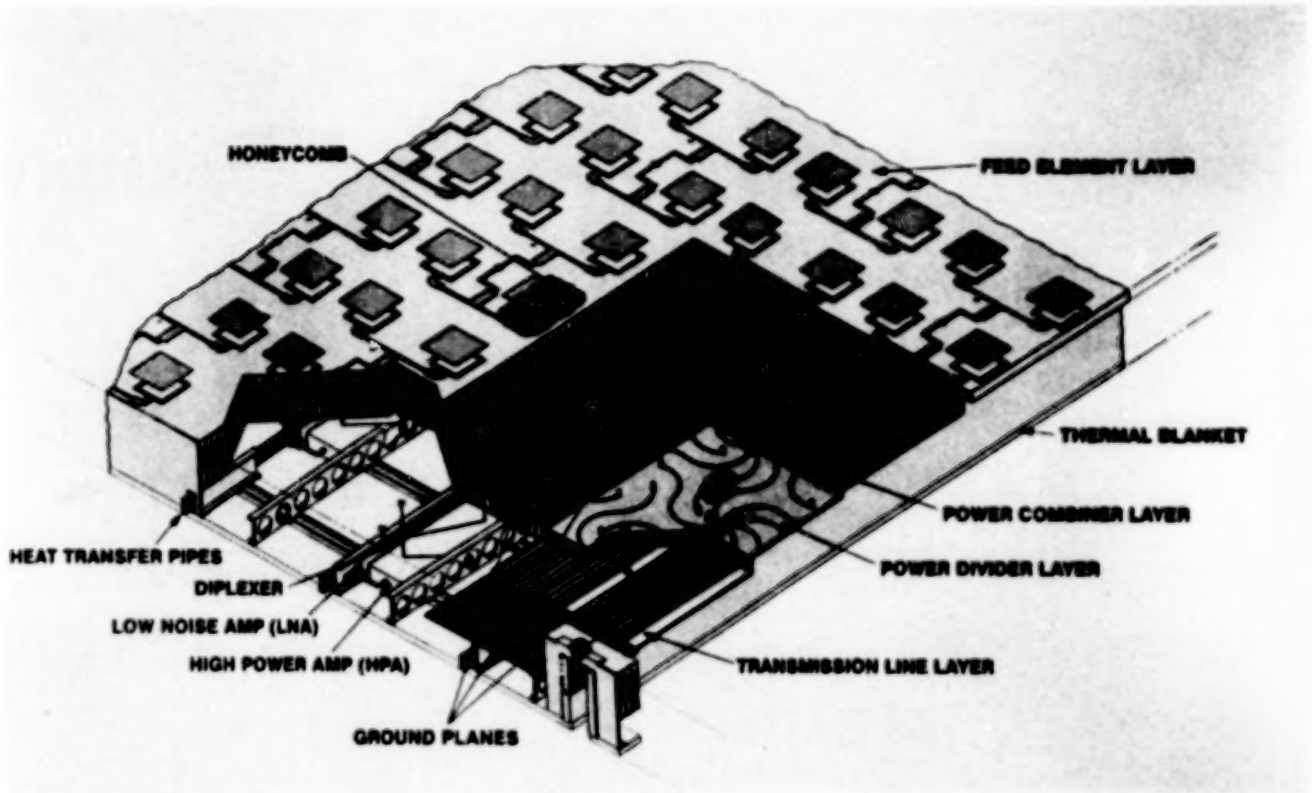


Figure 6

DIFFRACTION ANALYSIS OF REFLECTORS

Demands for accurate and efficient analysis of reflectors have resulted in the development of advanced computational techniques in vector diffraction methods. These advanced techniques are particularly useful in parametric studies of multiple and contour beam satellite antennas which require many computations. Figure 7 describes several of these techniques and identifies their interrelationships as far as the construction of the far-field pattern is concerned. At JPL, computer programs based on Physical Optics (PO) and the Geometrical Theory of Diffraction (GTD) have been developed for analyzing both single and dual offset reflectors (refs. 1 to 3). Recent methods, such as the application of sampling theorems, are also being investigated for increasing the efficiencies of the numerical computations involved.

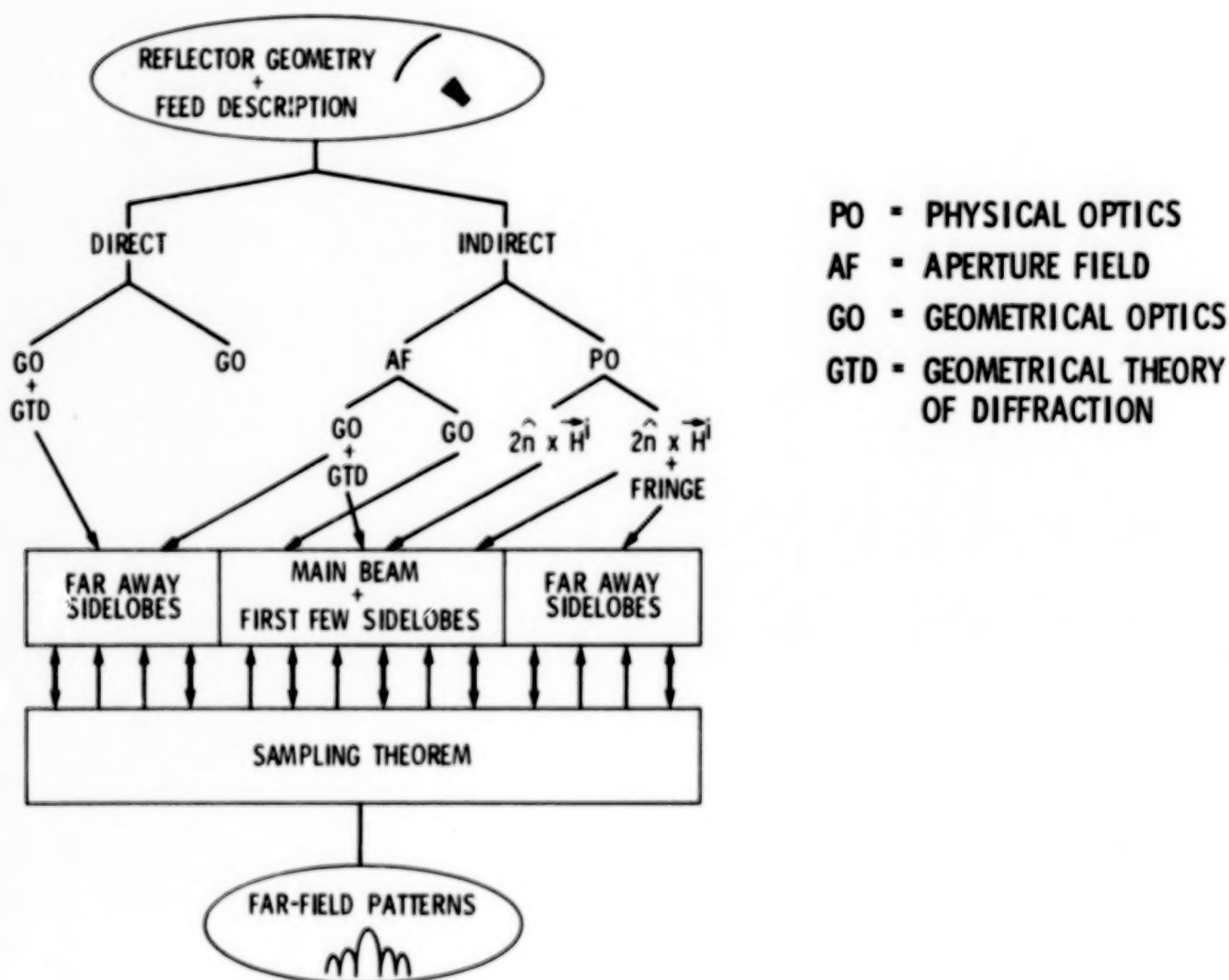


Figure 7

PHYSICAL OPTICS USING JACOBI-BESSEL EXPANSION

The Physical Optics (PO) diffraction analysis method has been proven to be a very accurate and powerful technique for analyzing and predicting the radiation characteristics of reflectors. Since a two-dimensional integration on a curved surface must be performed for any specified observation point, the standard integration algorithms can become very time-consuming when a repeated evaluation is needed. A method based on the Jacobi-Bessel expansion has been developed and tested which allows for a very efficient computation of the radiation pattern for many observation points (refs. 1 and 3). This method has many advantages, particularly for multiple-beam reflector systems. The key feature of the method is that a set of coefficients, independent of the observation points, can be assigned to any reflector/feed configuration and then the radiation pattern can be computed, using only these coefficients. A block diagram of the steps involved in this procedure is shown in Figure 8.

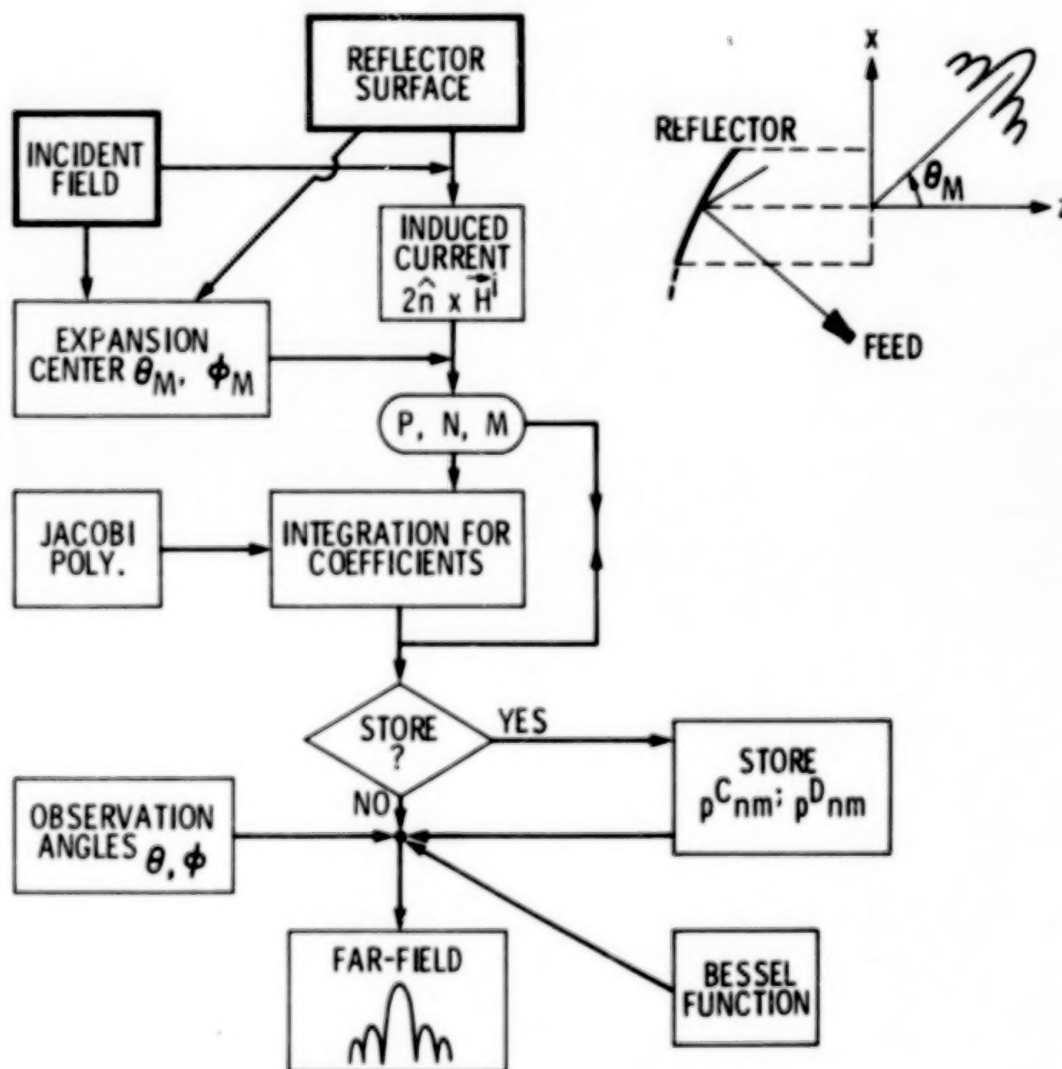


Figure 8

SCAN PERFORMANCE OF AN OFFSET REFLECTOR WITH CIRCULAR APERTURE

The performance of a multiple-beam reflector antenna cannot be properly assessed without detailed information concerning the radiation pattern of each beam. This includes the gain loss, sidelobe degradations, cross-polarization patterns, boresight beam location, etc. In particular, detailed knowledge of these parameters is vital for predicting the carrier/interference (C/I) ratio among the beams, which is a paramount factor in the assignment of frequency reuse plans (ref. 4). For example, Figure 9 shows how the radiation pattern of an offset parabolic reflector with circular projected aperture of diameter = 100λ and $F/D_p = 0.4$ ($F/D = 0.96$) can become degraded as the feed is positioned at different locations on the focal plane. In this figure, θ_p is an angle which is measured from the central reflected ray for each position of the feed. For this reflector/feed configuration, the beamwidths $\approx 0.7^\circ$. Notice that, for numbers of beamwidths scanned larger than four, the pattern is substantially degraded. For this reason, whenever a large number of beamwidths scanned is required, offset parabolic reflectors with large F/D_p (>0.7) ratios must be employed. The results shown in Figure 9 have been obtained using the Jacobi-Bessel algorithm.

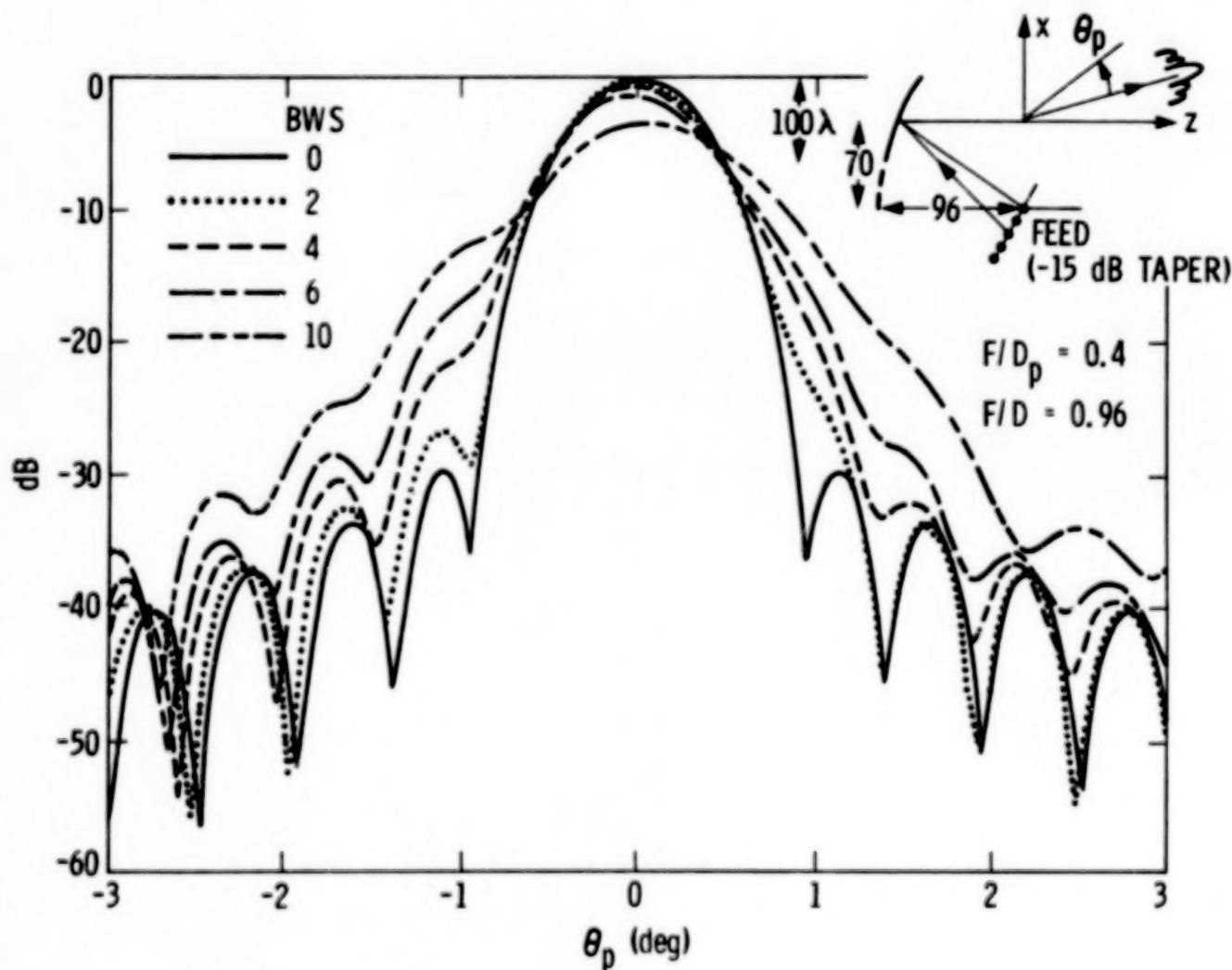


Figure 9

PIE-SHAPED REFLECTOR

When the hoop-column antenna configuration is used to generate multiple beams, the reflector's projected aperture takes a "pie" shape. Nevertheless, the objective is to achieve a radiation pattern which resembles a circularly projected aperture reflector. This may be achieved by using mesh reflectors with variable reflectivities such that only the portions of the pie which are confined to the circular aperture contribute to most of the radiation. Although this is conceptually feasible, it may be very costly. The alternative would be to use a uniform mesh structure and illuminate the pie shape with feeds having high aperture edge tapers, which is also necessary to produce low sidelobe levels. To assess the usefulness of this approach, an experimental setup has been constructed at LaRC. This setup consists of a metallic reflector with a pie-shaped projected aperture, which is illuminated by a feed having approximately -13 to -15 dB edge tapers, as shown in Figure 10. The dimensions of the reflector, operating at a frequency of $f = 35$ GHz, are also shown in the figure.

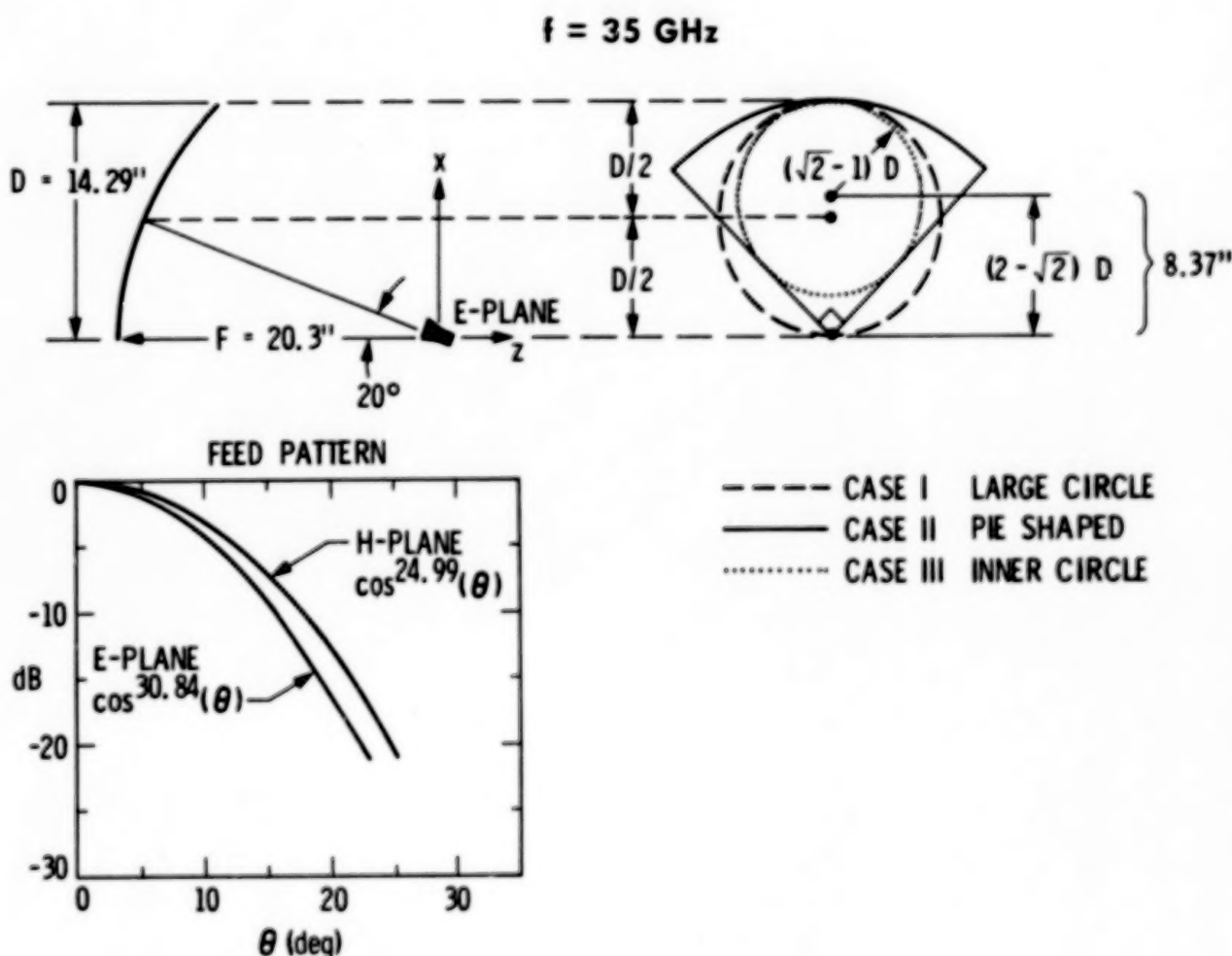


Figure 10

REFLECTOR PATTERNS

A numerical simulation of the LaRC pie-shaped reflector/feed configuration has been initiated using the Jacobi-Bessel diffraction analysis. Although this method is most efficient for circular-type apertures, nevertheless, satisfactory results have also been obtained for the pie-shaped configuration. For the sake of simplicity, the feed patterns are modeled as shown in Figure 10. Three cases have been considered: two circular and one pie-shaped aperture, as shown in Figure 10. The E- and H-plane patterns of these configurations are shown in Figure 11 in different columns. The reader can easily compare the patterns and conclude that the pie-shaped reflector has patterns similar to circular reflectors in the main beam region. Perhaps the comparison between the pie and the inner-circle cases would have been more representative if the feed direction had been tilted toward the center of the inner-circle case. Further studies are currently being pursued to compare these results with the measured data and to arrive at a detailed parametric evaluation of pie-shaped reflectors.

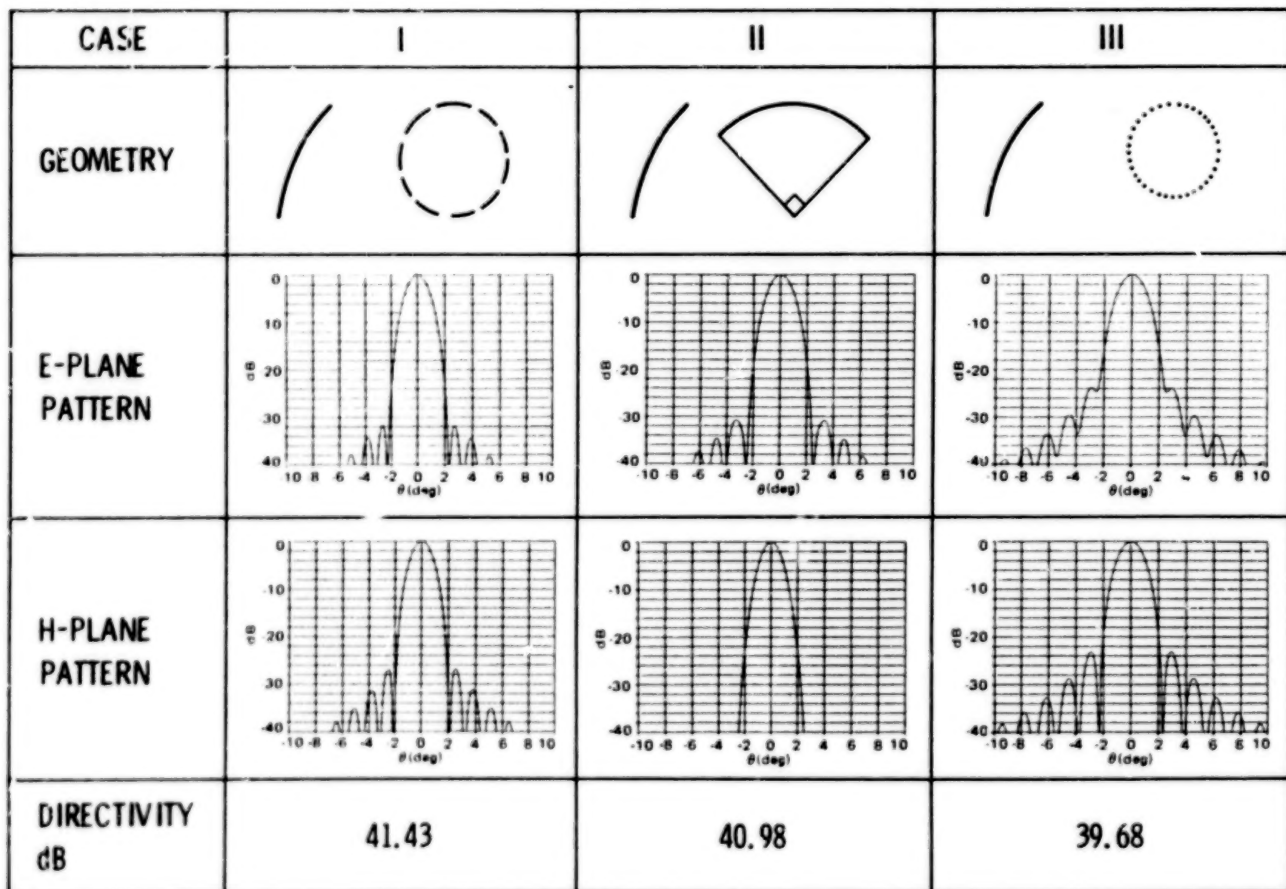


Figure 11

OFFSET REFLECTOR WITH SLOWLY VARYING DISTORTION

Both systematic distortions and random irregularities of reflector antenna surfaces can cause antenna radiation patterns to be markedly different from those of perfectly smooth reflector surfaces. How different the patterns are depends on many factors, such as the distribution, magnitude and shape of the irregularities, reflector illumination taper, the F/D ratio, etc. Commonly, the systematic errors result from thermal and dynamic effects. Thermal effects are relatively slowly varying (quasi-static) and are due to the different angles of the Sun's illumination on the reflector caused by diurnal motions of the satellite. Dynamic effects can cause rapid variations in the surface and are usually more difficult to analyze. A computer program has been developed at JPL for the analysis of slowly varying distortions. The results of this computer program are now being tested against measured data. The configuration of the reflector is shown in Figure 12(a). This is a very accurately machined reflector and its profile deviates from a best-fit parabolic reflector as shown in the figure. (This reflector was originally constructed for maximum gain dual offset reflector application.) The measurement setup will use a corrugated horn as the feed and many far-field pattern cuts will be measured for different locations of the feed. Preliminary numerical results for both the best-fit parabola and the distorted surface are shown in Figure 12(b). It is observed that the patterns become substantially degraded for the distorted reflector of Figure 12(a) at a frequency of 31.4 GHz.

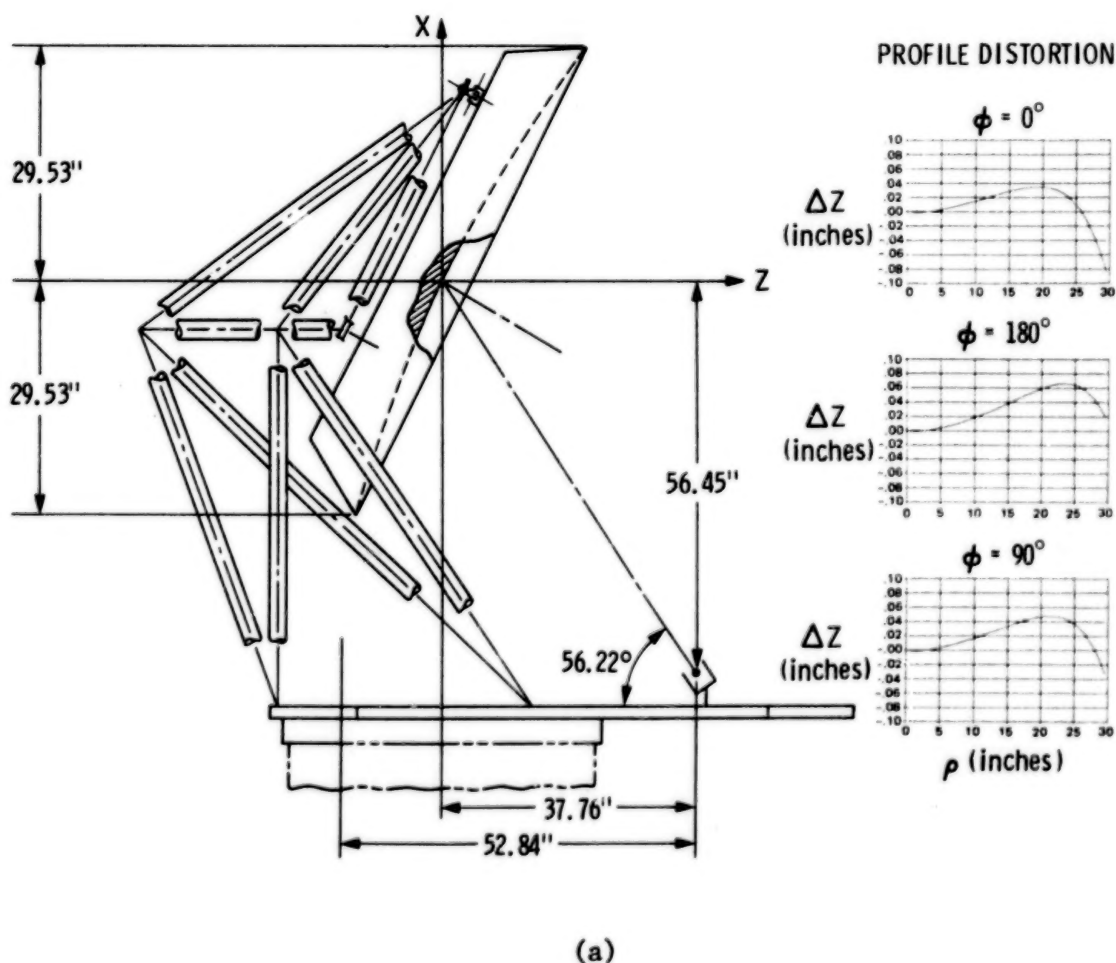
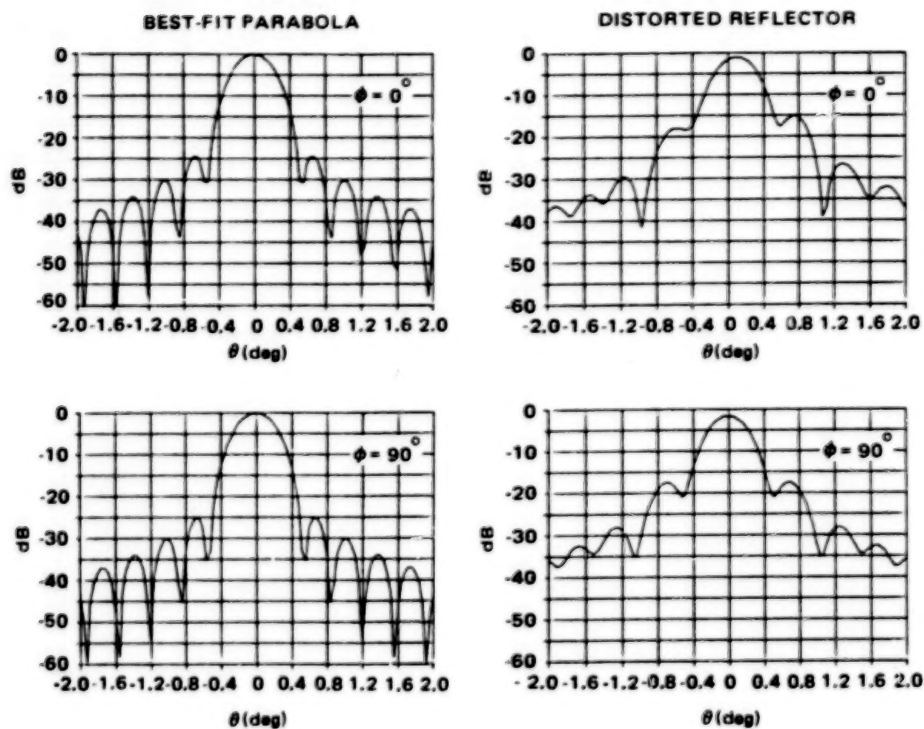


Figure 12

PATTERNS OF UNDISTORTED AND DISTORTED REFLECTORS

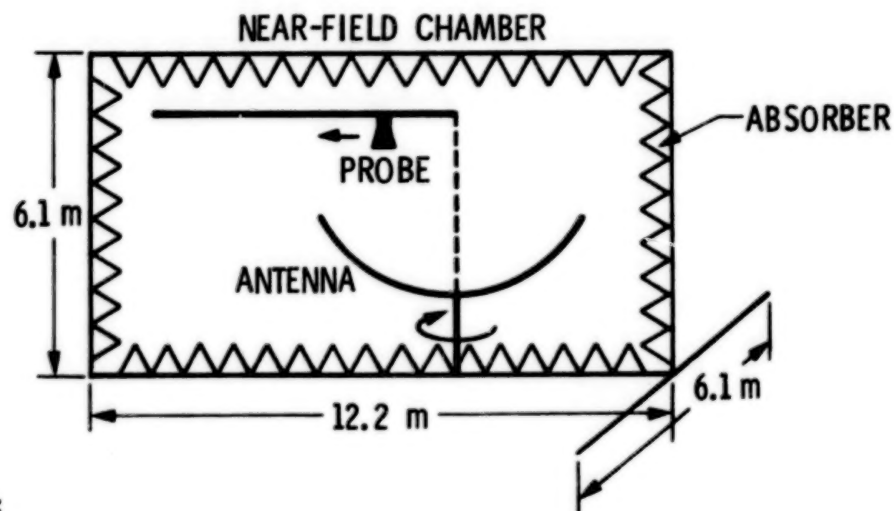


(b)

Figure 12 (Concluded)

FAR FIELDS USING PLANE-POLAR NEAR-FIELD TECHNIQUE

It is well known that at least $2D^2/\lambda$ to $5D^2/\lambda$ of "real estate" is required to measure the far-field patterns of a reflector with diameter D in the far-field range. Unfortunately, in many situations such real estate may not be easily accessible. Also, applications of ever-increasingly fragile antennas necessitate that a controlled measurement environment be used. Near-field measurement techniques are available as alternatives, which include plane-rectangular, cylindrical and spherical techniques. Recently, a new near-field measurement technique, referred to as the plane-polar measurement technique, has been developed and tested at JPL (ref. 5). This technique is particularly suitable for high gain antennas, which also are gravitationally sensitive. The near field of the antenna is measured by a probe moving in a linear direction while the antenna rotates about its axis. Once the amplitude and phase of the near-field measurements are recorded, they are transformed via a Jacobi-Bessel expansion to determine the far-field patterns. Figures 13(a) and 13(b) show both the schematic and actual measurement setup. In the JPL facility antennas up to five meters in diameter have been measured. Figure 13(c) shows the comparison between the far-field patterns obtained using the plane-polar near-field technique and those obtained in the far-field range. These are patterns of the parabolic reflector with 1.5 m (58") diameter measured at X-band (8.415 GHz), as shown in Figure 13(b). Results of the near-field technique for both co-polar (right circular) and cross-polar (left circular) fields show excellent agreement with the actual far-field data. Further tests are needed to assess the applicability of this technique to multiple-beam offset reflector antennas.



FEATURES:

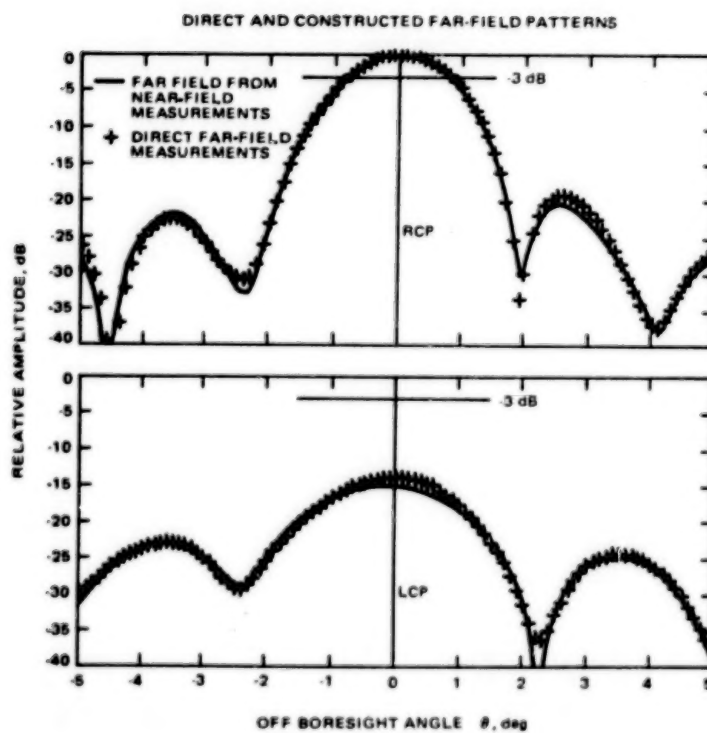
- BOTH THE PROBE AND THE ANTENNA ARE GRAVITATIONALLY BETTER BALANCED
- PROBE MOVES ONLY IN ONE DIRECTION
- ANTENNA ONLY ROTATES (NO DISPLACEMENTS)
- ALLOWS LARGER ANTENNAS FOR THE SAME "REAL ESTATE"
- ANTENNA ALWAYS POINTS IN THE FIXED DIRECTION
- VERY SUITABLE FOR HIGH GAIN ANTENNAS

(a)

Figure 13



(b)



(c)

Figure 13 (Concluded)

REFERENCES

1. Rahmat-Samii, Y., and Galindo-Israel, V., "Shaped Reflector Antenna Analysis Using the Jacobi-Bessel Series," IEEE Transactions on Antennas and Propagation, Vol. 28, pp. 425-435, July 1980.
2. Rahmat-Samii, Y., and Galindo-Israel, V., "Scan Performance of Dual Offset Reflector Antennas for Satellite Communications," Radio Science, Vol. 16, pp. 1093-1099, Nov.-Dec. 1981.
3. Lee, S. W., Cramer, P., Jr., Woo, K., and Rahmat-Samii, Y., "Diffraction by an Arbitrary Subreflector: GTD Solution," IEEE Transactions on Antennas and Propagation, Vol. 27, pp. 305-316, May 1979.
4. Rahmat-Samii, Y., and Salmasi, A., "Vectorial and Scalar Approaches for Determination of Interbeam Isolation of Multiple Beam Antennas -- A Comparative Study," IEEE/AP-S International Symposium, pp. 135-139, June 1981.
5. Rahmat-Samii, Y., Galindo-Israel, V., and Mittra, R., "A Plane Polar Approach for Far-Field Construction from Near-Field Measurements," IEEE Transactions on Antennas and Propagation, Vol. 28, No. 2, pp. 216-230, March 1980.

THE EFFECTS OF MULTIPLE REFLECTING
SURFACES UPON RADIOMETRIC MEASUREMENTS

W. F. Crosswell
Harris Corporation
Melbourne, Florida

Large Space Antenna Systems Technology - 1982
NASA Langley Research Center
November 30 - December 3, 1982

INTRODUCTION

Reflector antennas with mesh surfaces have been used in ground and space applications primarily for communication systems. The purpose of this short paper is to indicate how the requirements for mesh surface reflectors are different for microwave radiometric applications, and to propose a method of measuring the anticipated small dissipation losses of gold-plated mesh using a radiometer system.

REVIEW OF FUNDAMENTALS

The basis geometry used in a spacecraft radiometer system is given in figure 1. The basic scalar relationships between the antenna temperature and brightness temperature are given in figure 2.

The brightness temperature is the sum of the emission from the surface with physical temperature T_S and the reflected sky temperature as received into the antenna terminals. The temperature observed by the antenna, T_A , in its scalar form is the convolution of the power pattern of the antenna with the brightness temperature of the total observed scene $T_B(\theta, \phi)$. The parameter $T_B(\theta, \phi)$ in this form can then be related to the plane wave reflection coefficient R_S and the surface and sky temperatures T_S and T_{SKY} .

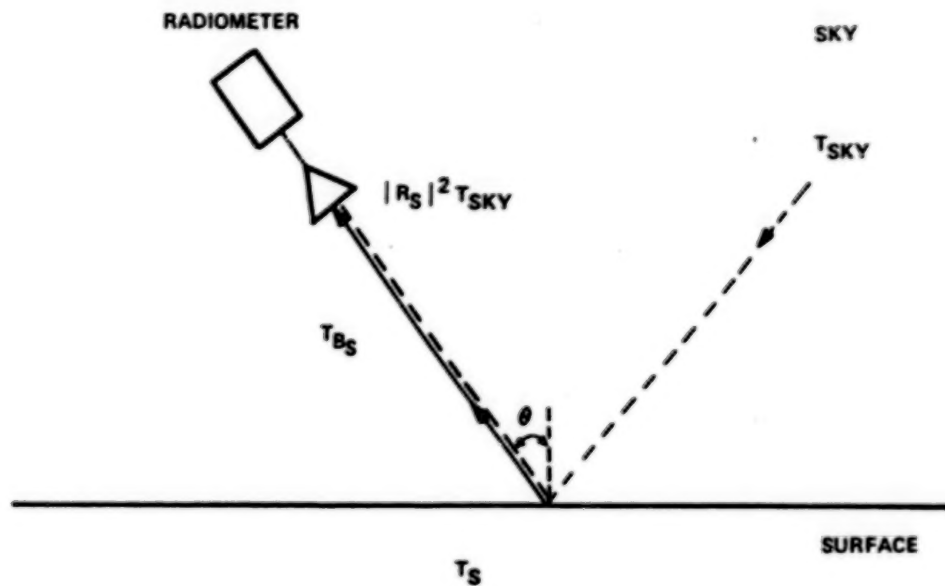


Figure 1.- Typical radiometer scene in microwave remote sensing. $T_{BS} = (1 - |R_S|^2) T_S$.

$$T_A = \frac{\int_0^{2\pi} \int_0^\pi f(\theta, \phi) T_B(\theta, \phi) \sin \theta d\theta d\phi}{\int_0^{2\pi} \int_0^\pi f(\theta, \phi) \sin \theta d\theta d\phi}$$

$$T_B(\theta, \phi) = T_{BS} + |R_S|^2 T_{SKY}$$

SINCE $\epsilon_S = 1 - |R_S|^2$, $T_{BS} = \epsilon_S T_S$

$$T_B(\theta, \phi) = (1 - |R_S|^2) T_S + |R_S|^2 T_{SKY}$$

Figure 2.- Antenna temperature and brightness temperature.

VECTOR PROPERTY OF ANTENNA TEMPERATURE

The antenna temperature is polarization dependent, as is the antenna pattern, and hence the simple scalar expression for T_A in figure 2 must be expressed in vector form, as given in figure 3, where T_{BV} and T_{BH} are the polarized brightness temperatures of the scene, and ψ is the angle between the primary polarization vector of the antenna and the scene coordinate system. Notice that in addition to the expected terms, there is a third term involving the difference in the scene brightness temperature ($T_{BV} - T_{BH}$) and $\sin 2\psi \cos 2\psi$. In this instance, δ is the phase difference between the direct and cross-polarized pattern of the observing antenna. Hence, the amount of cross polarization in the antenna affects the observed antenna temperature.

$$T_A = \frac{\int_0^{2\pi} \int_0^\pi \left\{ (f_\theta \sin^2 \psi + f_\phi \cos^2 \psi) T_{BH} + (f_\theta \cos^2 \psi + f_\phi \sin^2 \psi) T_{BV} + (T_{BV} - T_{BH}) f_\theta f_\phi \sin 2\psi \cos \delta \right\} \sin \theta d\theta d\phi}{\int_0^{2\pi} \int_0^\pi (f_\theta + f_\phi) \sin \theta d\theta d\phi}$$

Figure 3.- Vector property of antenna temperature.

ANTENNA LOSSES AND REFLECTIONS

An additional parameter which must be accounted for in radiometric measurements involves the effects of ohmic losses and reflections in the antenna back to the effective receiver terminals. The simplest form of these effects is given in figure 4, where the antenna losses and mismatch are treated as discrete network parameters.

$$T_a = (1 - l - \rho) T_A + l T_o + \rho T_R$$

ρ = REFLECTION COEFFICIENT

l = FRACTIONAL POWER LOSS IN ANTENNA

T_o = ANTENNA TEMPERATURE

T_R = MICROWAVE TEMPERATURE LOOKING INTO RECEIVER

Figure 4.- Antenna mismatch and losses.

THE OCEAN APPLICATION AND IDENTIFICATION OF PARAMETERS

One of the possible applications of microwave radiometric systems is to measure sea surface temperature. Typical accuracies desired for such systems are on the order of 1 K, so that systems biases for the antenna on the order of 0.1 to 0.2 K are desired to assure the accuracy of the overall measurement. The sea brightness temperatures for 20°C sea water at nadir are on the order of 100 to 110 K, independent of polarization. These temperatures can increase to a nominal 180 K at other commonly employed observation angles for vertical polarization. Hence, at microwave frequencies, sea brightness temperatures can range from 100 to 180 K (ref. 1). The effect of dissipation losses can be quantified, as shown in figure 5. Notice that to achieve small bias temperatures of 0.1 to 0.2 K, a dissipation loss less than 0.005 dB must be achieved when that loss is at a physical temperature of 300 K. Notice that from figure 4 the dissipation loss factor enters into the bias correction as product terms, so that a knowledge of both physical temperature and the loss factor is important.

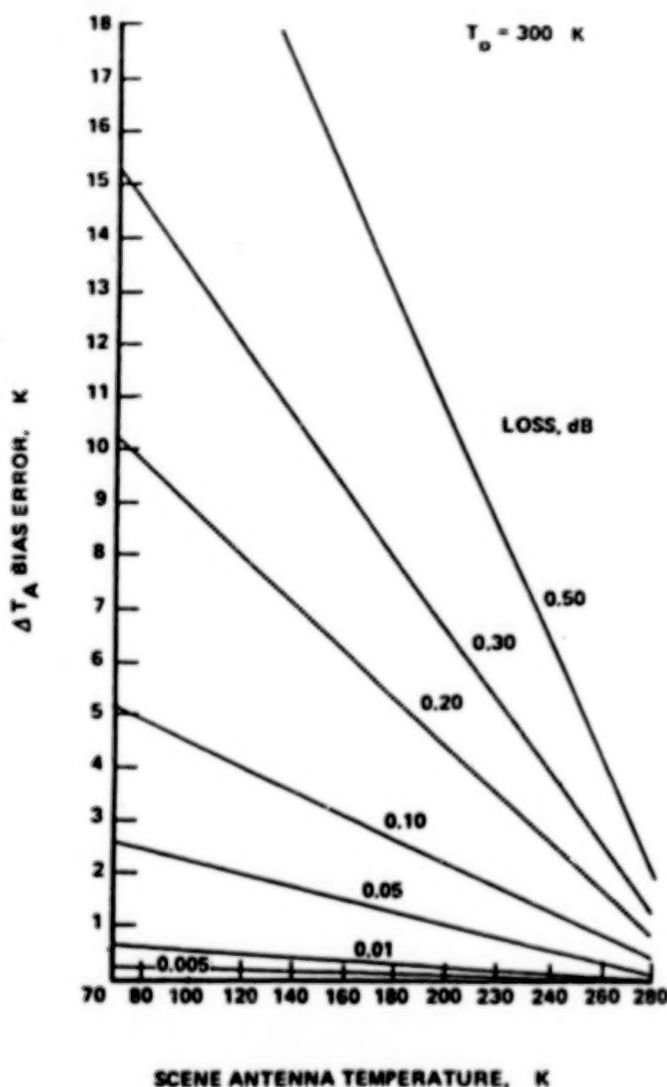


Figure 5.- Effects of losses upon scene antenna temperature. $\Delta T_A = (T_0 - T_A)\ell$.

EFFECT OF POLARIZATION MIXING

The other major bias effect is the polarization mixing, due to a nonperfectly polarized antenna. A measure of the effect of this mixing is illustrated in figure 6, where the cross polarization bias temperature is plotted against differential bias temperature. The parameters $P_{\theta 1,op}$ and $P_{\theta 1,dp}$ represent the total power contained in the main beam angular sector for the opposite and direct polarization. Notice that a cross polarization level of -26 to -27 dB will produce a bias error of less than 0.2 K.

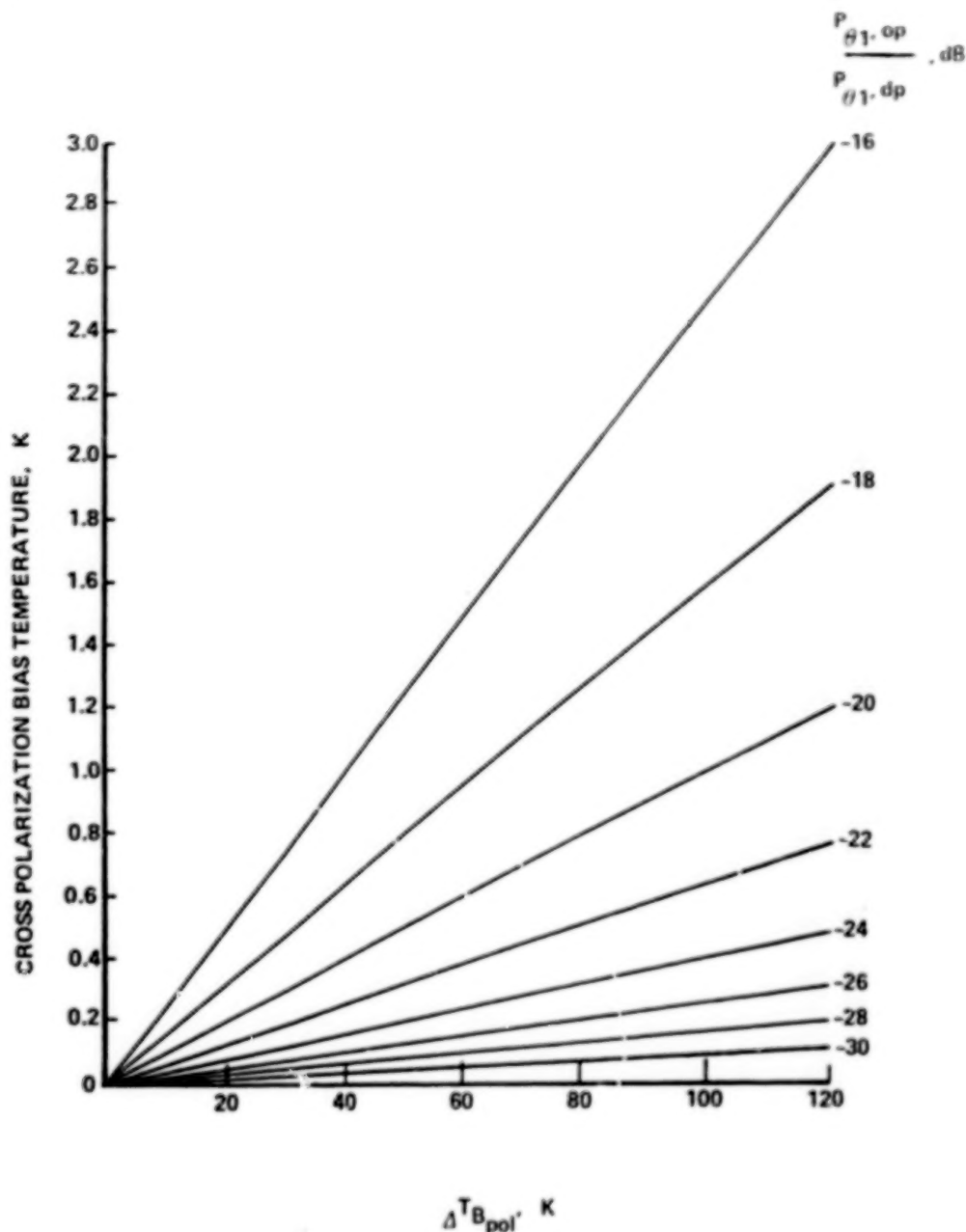


Figure 6.- Effect of antenna cross polarization power on radiometer bias as function of scene polarization difference temperature. $\Delta T_{B_{pol}} = T_{B_{pol}} - T_{B_{op}}$.

TYPICAL MESH REFLECTOR PERFORMANCE

From the previous discussion, the two important mesh reflector properties as applied to radiometer measurements are mesh depolarization and mesh dissipative loss. The data presented here will give the reader a practical insight into the problem.

For microwave radiometer measurements of sea temperature, typical reflection loss data are given in figure 7 for 18 openings (1-in. mesh). The measured data were obtained using a free-space measurement system with an inherent accuracy no better than ± 0.05 dB. The experimental points shown in figure 7 represent the maximum values observed; for the orthogonal polarization, values of 0.05 dB or less were obtained. Assuming the use of an 11-GHz operating frequency, a reflection loss of 0.07 dB is obtained. One now can refer back to figure 5 and observe that if this 0.07-dB loss is all dissipation, a bias of 2 to 3 K may be obtained. The reflection loss observed in this measurement is the sum of dissipation loss and leakage through the mesh. Hence, the measurement method does not allow separation of the two parameters.

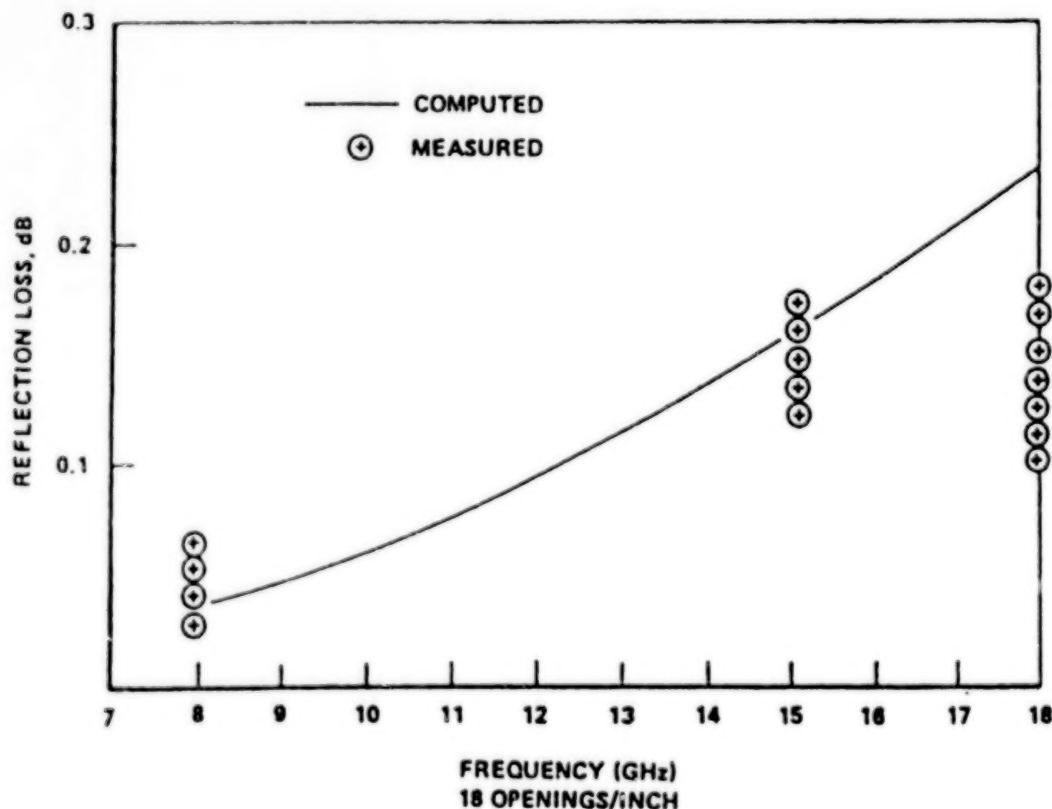


Figure 7.- Calculated and measured reflection loss properties of 18-openings-per-inch mesh.

MESH LOSS PROPERTIES

Using the theoretical model shown in figure 7, a prediction of reflection loss properties at other typical radiometric frequencies for varying mesh size, in openings per inch, is given in figure 8. The behavior shown in figure 8 demonstrates that the reflection properties of mesh tend to scale as a function of opening size per wavelength. Notice that much of the predicted data is below the experimental accuracy of ± 0.05 dB.

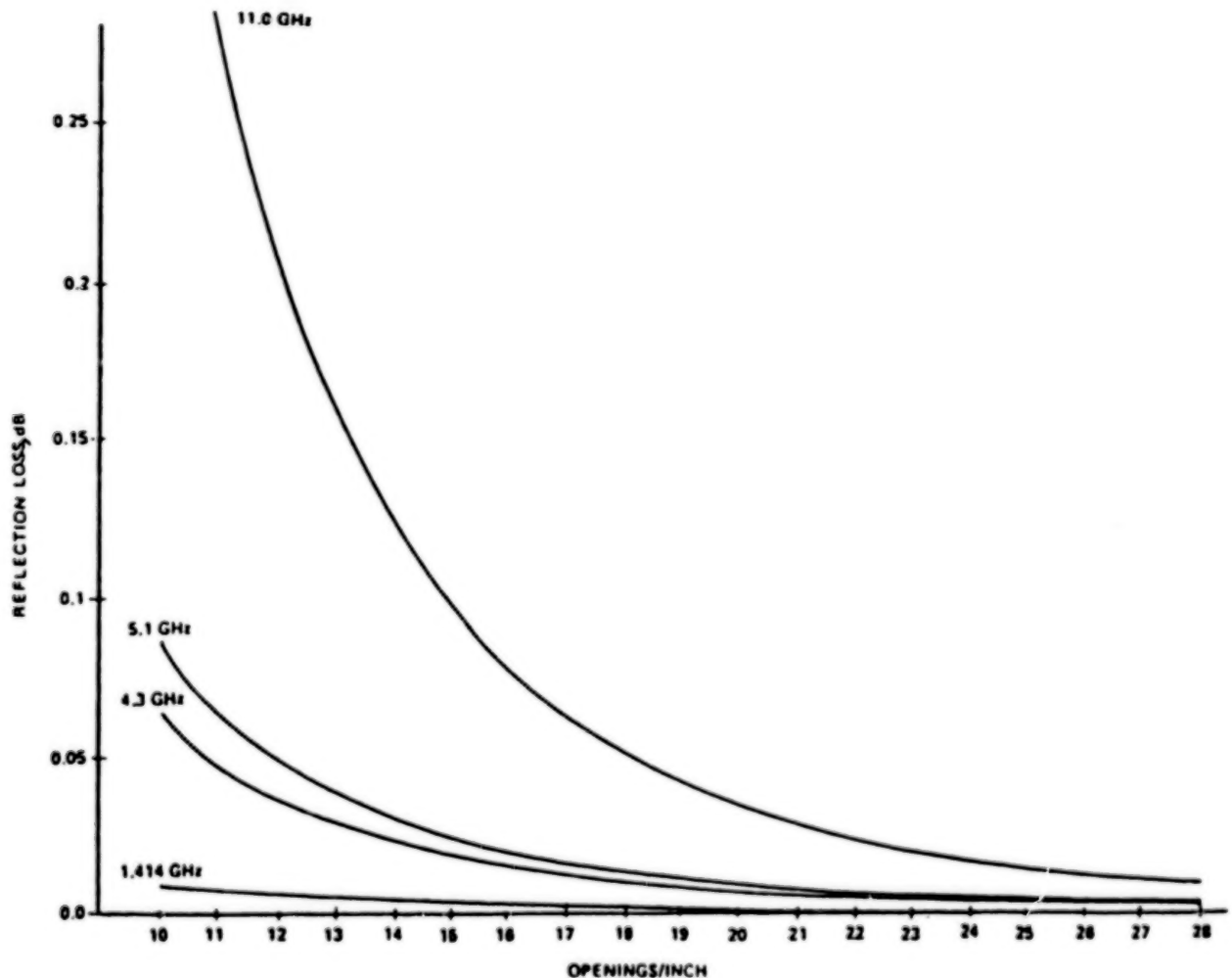


Figure 8.- Mesh loss properties at radiometer frequencies.

FOAM-BACKED MESH REFLECTOR

As indicated previously, the mesh, depending upon the construction technique, may have an anisotropic scattering property. Indeed, for the mesh shown in figure 7, the polarization dependence may be as large as 0.1 dB. The deployable antennas utilizing mesh are generally constructed in gore patterns, which tend to minimize this polarization property in the secondary far-field radiation pattern. In order to quantify this problem, an offset-fed reflector was constructed using 12 gores centered at the offset angle of 32° , as shown in figure 9. The linearly polarized feed horn was a square Cohn multimode horn with a measured cross polarization pattern level of less than -36 dB. The measured and predicted direct and cross polarization patterns from this mesh dish are given in figure 10. Predicted patterns for this geometry using a solid reflector agree closely with the patterns in figure 10, particularly for cross polarization. Hence, cross polarization generated by mesh does not appear significant for the sea surface temperature application.

FOAM AND MESH REFLECTOR GEOMETRY

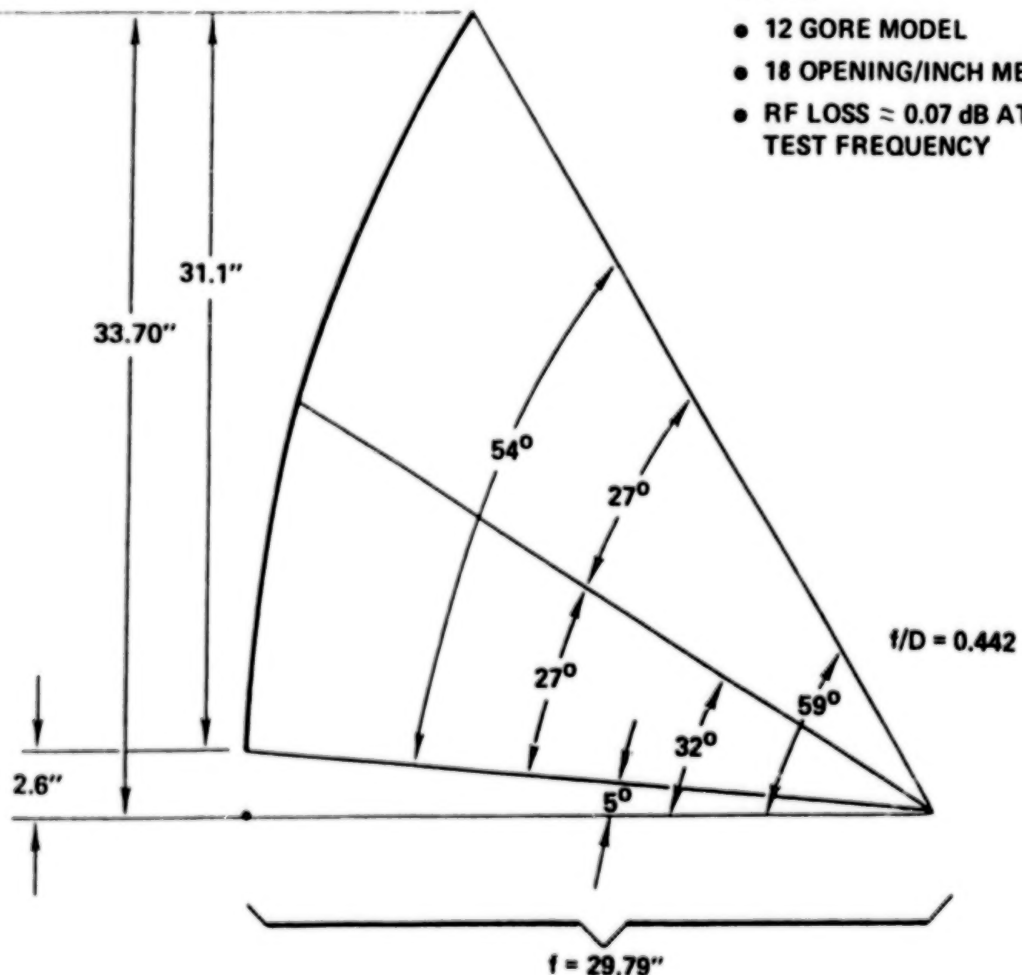


Figure 9.- Foam-backed mesh reflector.

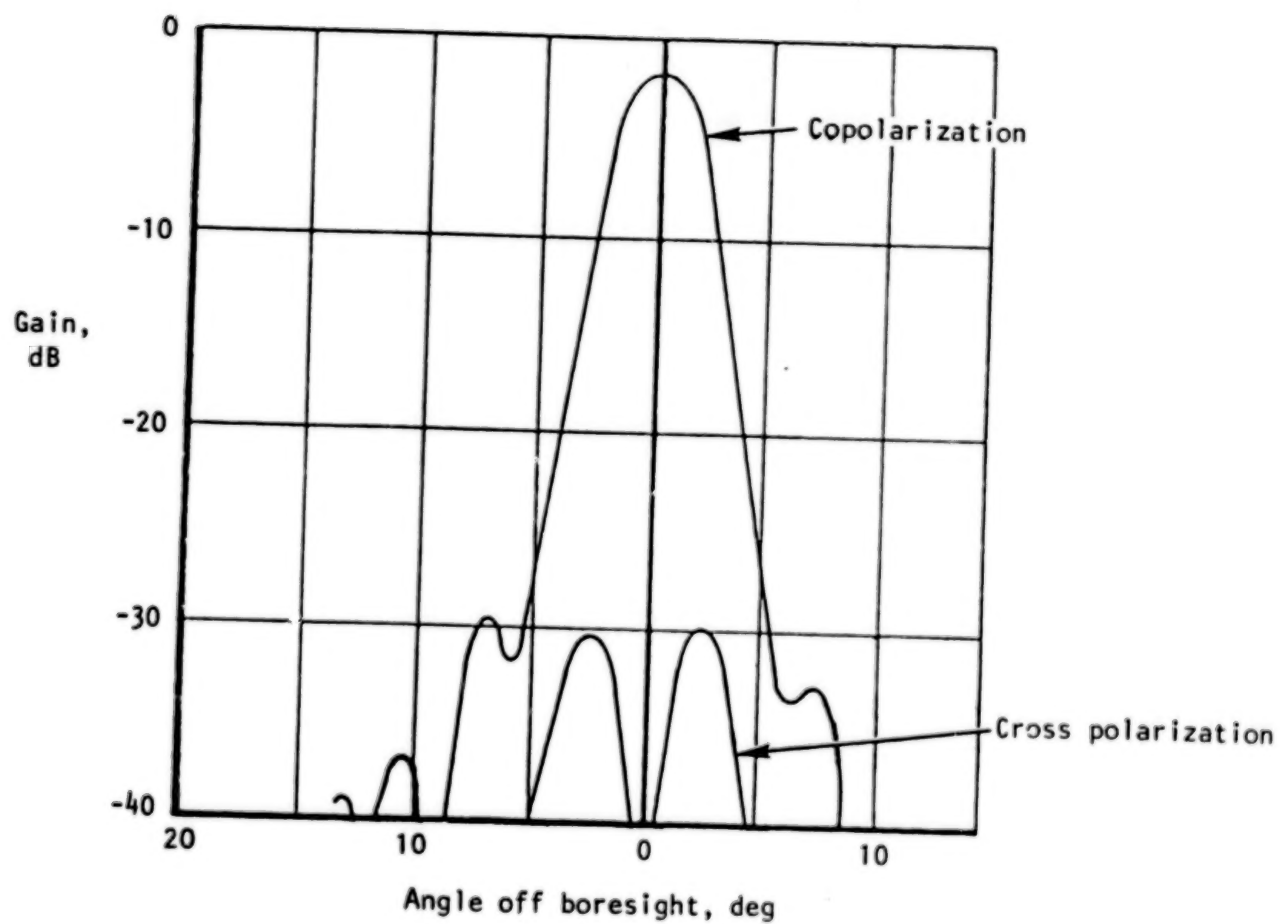
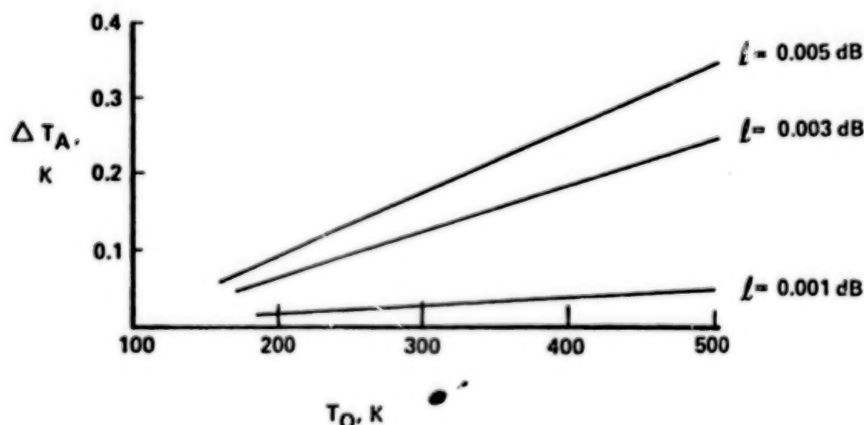


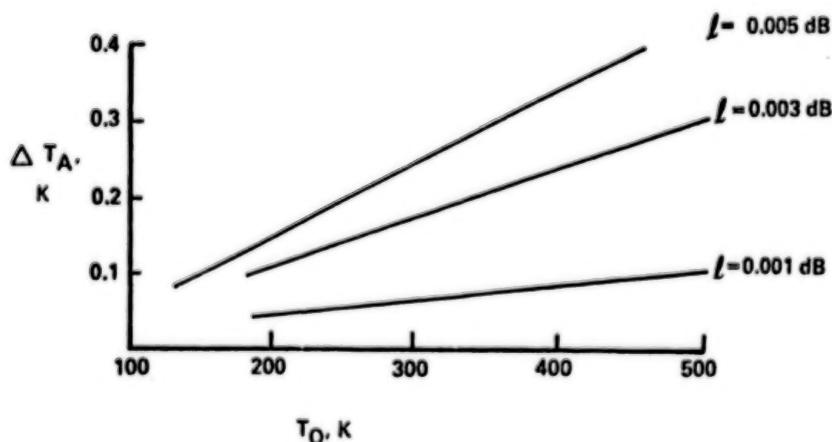
Figure 10.- Foam and mesh reflector patterns.

A METHOD OF MEASURING DISSIPATION LOSS

Due to the rapid heat transfer, gold-plated mesh may experience a temperature change of 300 to 400 K on orbit when passing through certain orbital conditions. The effect of such changes on antenna bias temperature is presented in figure 11. In figure 11(a), the antenna is observing an ocean scene, and in figure 11(b) it is viewing the cold sky. From these data, losses as small as 0.001 to 0.003 dB must be measured to obtain biases less than 0.1 to 0.2 K. To do this, it is proposed that a radiometric method be employed. Two views of the experimental system to perform this measurement are given in figures 12 and 13. The splash plate in this experiment is made of a gold-plated solid conductor for calibration, combined with mesh for loss measurement. The anticipated ΔT_A for low-loss mesh when looking at the cold sky is given in figure 11(b). It is proposed that the mesh be heated and allowed to cool slowly in order to determine the slope of ΔT_A as a function of temperature. The special reflecting plates and platform tilt are necessary to reflect the cold-sky temperature to the region behind the mesh, and hence to minimize the measurement error.



(a) Ocean scene. Scene temperature = 120 K.



(b) Scene temperature = 50 K. (50 K is typical radiometer temperature when observing cold sky of 3 K.)

Figure 11.- Change in antenna temperature due to ohmic losses.

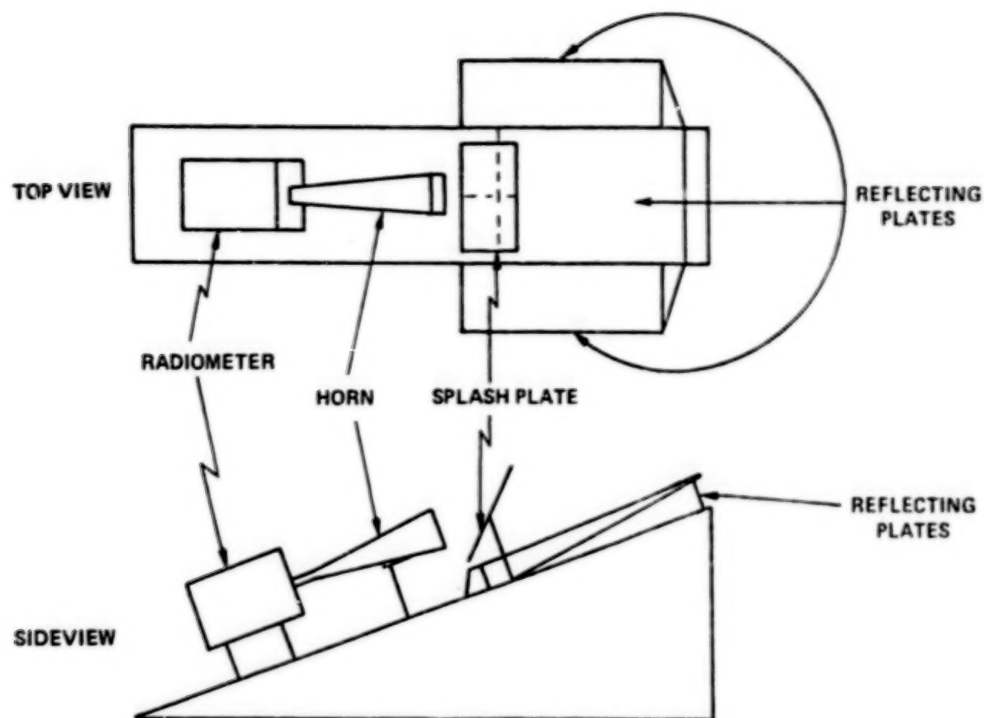


Figure 12.- Radiometer measurement arrangement.

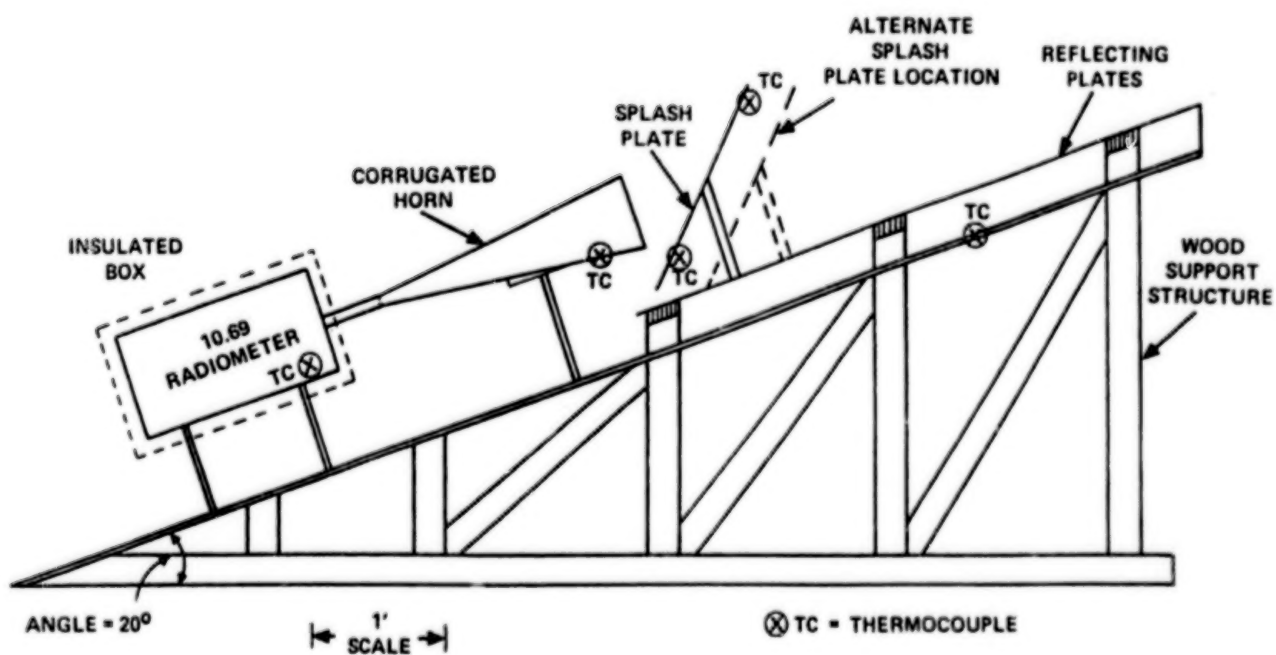


Figure 13.- Arrangement for radiometer measurements of ohmic losses of mesh.

CONCLUSIONS

The use of mesh antennas for space-borne radiometers for precision measurements of surface temperatures requires a measurement of very small dissipation losses over a wide range of temperatures. Indeed, some materials for solid reflectors which use thin metallized coatings may require a similar determination. A method of measuring dissipation loss using a radiometer is proposed.

REFERENCE

1. Staelin, D. H.; and Rosenkranz, P. W.: High Resolution Passive Microwave Satellites. MIT Research Lab for Electronics, Massachusetts Institute of Technology, April, 1977.

DEVELOPMENT OF IMPROVED ANALYTICAL MODELS
FOR MESH REFLECTOR SURFACES

Jerry C. Brand and J. Frank Kauffman
North Carolina State University
Raleigh, North Carolina

Large Space Antenna Systems Technology - 1982
NASA Langley Research Center
November 30 - December 3, 1982

MESH SURFACES

The mesh used to construct large space reflector antennas is typically made from gold-plated molybdenum wire approximately one mil in diameter. The wires are knitted into a fabric suitable for framing and forming a reflector surface. This surface is nonideal, and, as such, displays less than optimum performance. In particular, the wires run and cross in a weave that is periodic in nature, giving rise to a reflecting surface that behaves differently depending on the number of openings per wavelength and the polarization of the incident energy. The undesirable effects resulting from such a surface include transmission loss, resistive loss, and cross-polarization loss.

THE MESH PROBLEM

The Harris mesh shown in figure 1 is typical of the mesh designed for large space reflector antennas (ref. 1). To solve for the reflected field, a combination of the currents on the wire, the aperture field, and the appropriate boundary conditions must be used. One popular model for estimating the reflection from a mesh surface is based on averaged boundary conditions (refs. 2 and 3) and offers good results when the number of mesh openings per wavelength is large (ref. 4). For certain applications, the number of mesh openings per wavelength may become small, and the model (referenced above) breaks down. To overcome this problem, a more accurate model of the mesh must be formulated.

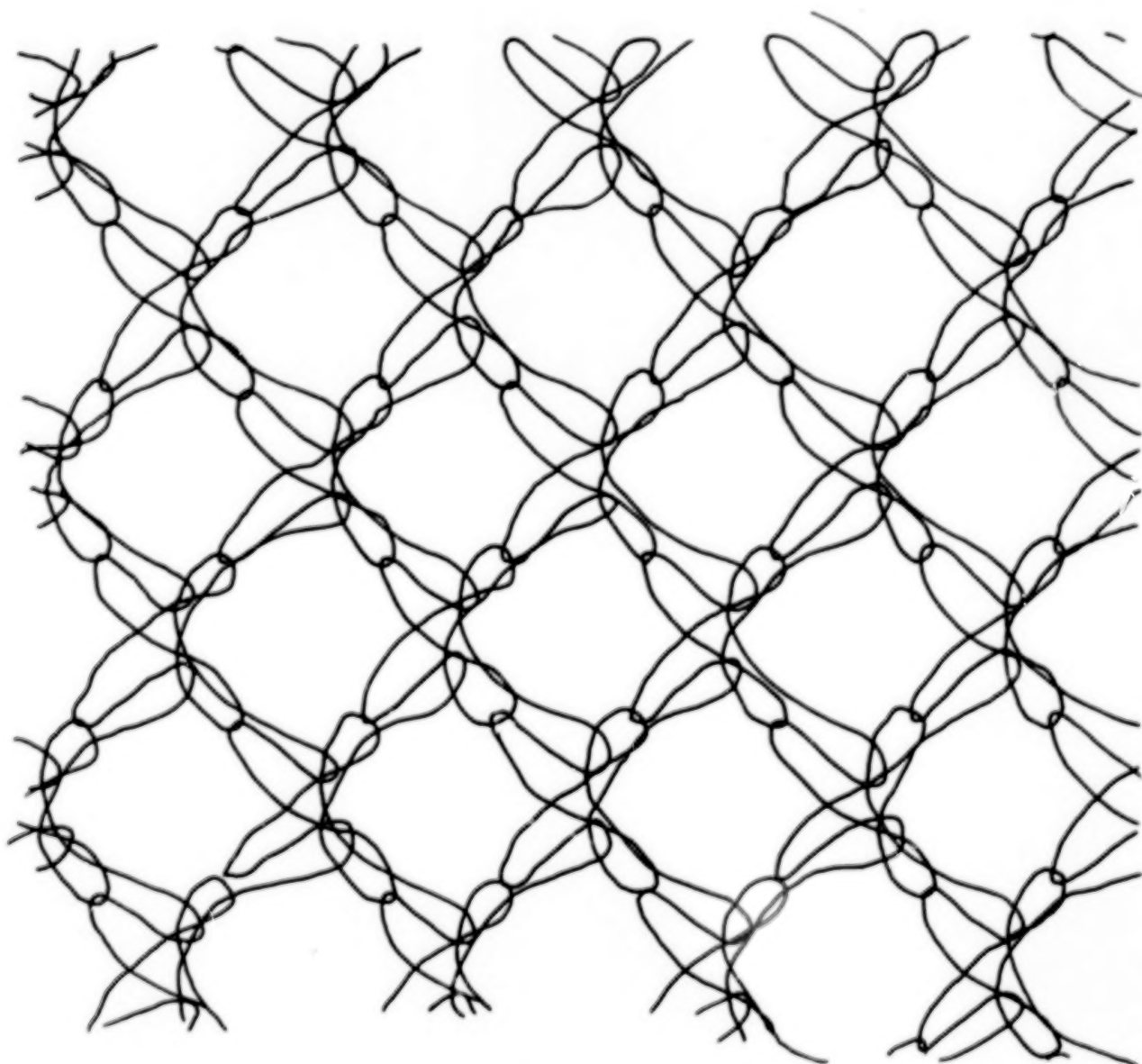


Figure 1

METHODS OF SOLUTION

There are several methods for constructing solutions to the mesh scattering problem. The classical solution involves coupled integral equations, which will not usually yield a solution due to the nature of the integrals. A possible candidate for numerical solution is the method of moments (MoM). This method involves reducing the integral equations in the classical method down to a matrix problem with the proper choice of basis and testing functions. However, the MoM solution generally involves the inversion of a matrix, and this process can become unwieldy. The most likely method to solve the problem appears to originate from the spectral domain approach (ref. 5). This method employs discrete Fourier transforms and Floquet's theorem and avoids the time-consuming matrix inversion involved in the MoM (ref. 6). Table 1 lists several possible methods of solution and also contains short comments on each.

<u>METHODS</u>	<u>COMMENTS</u>
METHOD OF MOMENTS (MoM)	- REPRESENTS INTEGRAL EQUATIONS AS MATRIX; USUALLY REQUIRES MATRIX INVERSION
SINGULARITY EXPANSION METHOD (SEM)	- POSSIBLE IMPEDANCE EXPRESSION AVAILABLE; USUALLY USED IN TRANSIENT ANALYSIS
CLASSICAL METHODS	- INTEGRAL FORMULATION; DIFFICULT TO INVERT INTEGRAL
SPECTRAL DOMAIN	- UTILIZES FOURIER TRANSFORM TECHNIQUE; ELIMINATES CONVOLUTION; MATRIX INVERSION USUALLY NOT REQUIRED

TABLE 1

PERIODIC NATURE OF MESH SURFACES

The mesh surface has a periodic nature which may be described by "cells". One cell consists of a pattern of wires which can be translated to replicate this pattern over the surface. Figure 2 illustrates the nature of these cells and their location over the surface of a typical mesh.

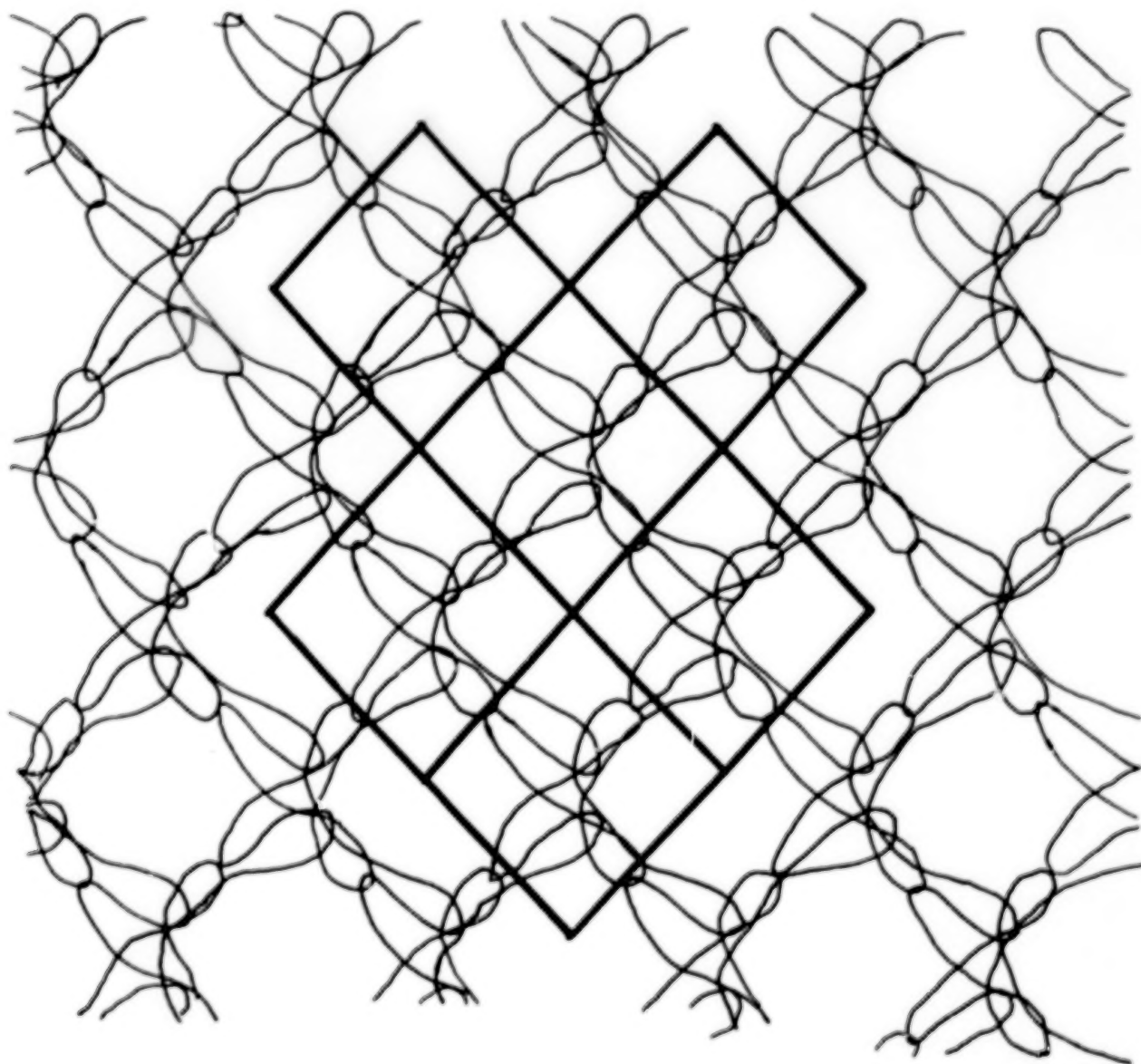


Figure 2

SPECTRAL THEORY AND MESH SURFACES

The spectral theory solution utilizes the discrete Fourier transform (usually in the form of a fast Fourier transform (FFT)) and Floquet's theorem to solve a periodic structure problem (ref. 6). The flow diagram in figure 3 indicates the general nature of solving a problem using the spectral theory referenced above. Even though the formulation is rigorous, certain problems may arise when this approach is applied.

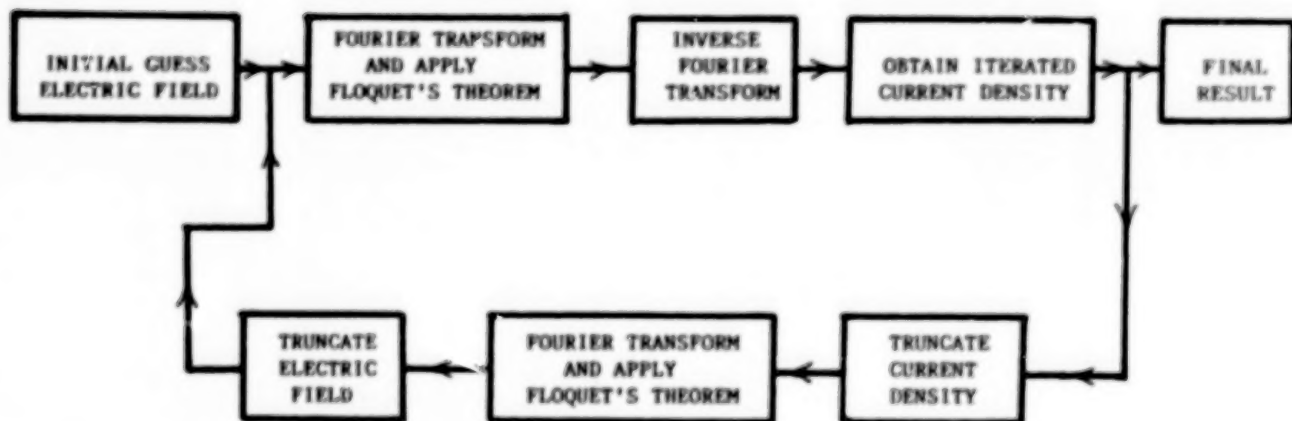


Figure 3

TEST CASE STUDY

A test case using an infinite parallel grid of wires is chosen since the solution is well known (ref. 7). The grid shown in figure 4 indicates the dimensions of the case, the incident wave angle, and the polarization of the incident electric field. The magnitude of the reflection coefficient is shown in figure 5 as a function of incidence angle. The results shown, however, were obtained only after a number of problems inherent in the method were overcome.

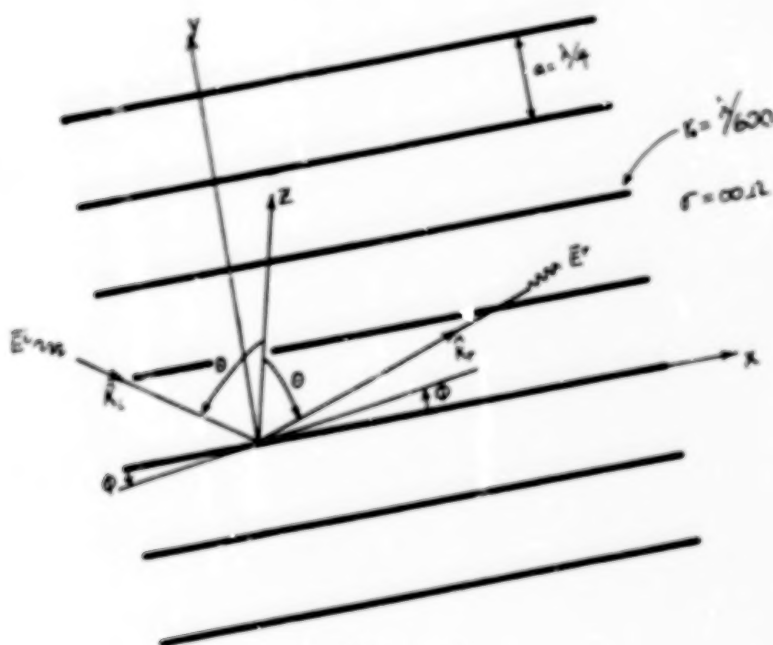


Figure 4

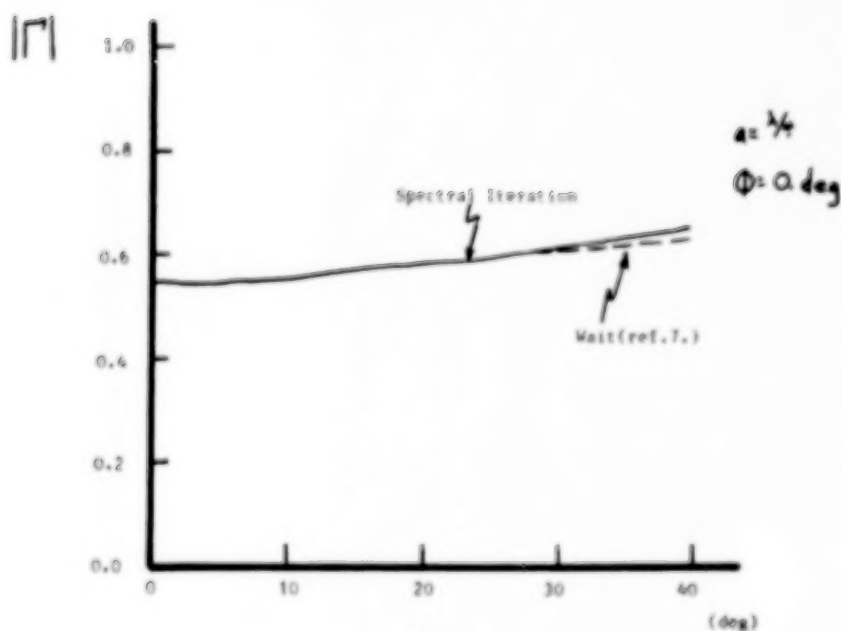


Figure 5

PROBLEMS WITH THE SPECTRAL APPROACH

The spectral approach works well with periodic structures as long as the cell separation is greater than approximately one wavelength. For smaller separations, the field between cells becomes hard to estimate, and convergence is slow (ref. 6). However, an improvement is seen by providing a better estimate of the field between cells. This fact leads to the conclusion that a very good aperture field between cells is required for convergence of the solution for the mesh surface. Additionally, the wires will cross and perhaps lead to an impedance between wires that must be accounted for. Table 2 indicates the types of problems existing with the spectral approach and some possible ideas for solving these problems.

<u>PROBLEM</u>	<u>POSSIBLE SOLUTION</u>
POOR CONVERGENCE DUE TO SMALL FLOQUET CELL SEPARATION	CONSTRUCT BETTER INITIAL ELECTRIC FIELD APPROXIMATION; DETERMINE STATIONARITY OF FORMULATION
"RINGING" IN ITERATIVE PROCEDURE	APPLY SMOOTHING TECHNIQUE TO ITERATIVE CORRECTION VALUE
MESH CROSSINGS	USE FORCED BOUNDARY CONDITIONS TO REPRESENT IMPEDANCE OF WIRE CONNECTION
MESH WIRE NOT THIN	DETERMINE EQUIVALENT RIBBON SIZE FOR WIRE

TABLE 2

CONCLUSION

There are several methods available for computing the reflection coefficients from mesh surfaces. Some methods mentioned have severe limitations, and the spectral approach appears to be the most attractive alternative. In spite of some inherent problems, the solutions obtained with this method will offer not only the reflection coefficients but also the currents carried on the mesh. This would allow separation of the power lost to resistive terms from that due to transmission loss. Overall, good results and rapid convergence should be obtained from this method when proper care is applied.

REFERENCES

1. Blume, Hans-Juergen C.: Measurement of Losses of Mesh Membrane Material for Reflector Applications with an S-Band Radiometer. Large Space Systems Technology - 1981, NASA CP-2215, Part 2, 1982, pp. 611-620.
2. Astrakham, M. I.: Reflecting and Screening Properties of Plane Wire Grids. Telecommunications and Radio Engineering, Vol. 23, Pt. 2, No. 1, January 1968, pp. 76-83.
3. Kontorovich, M. I.: Averaged Boundary Conditions at the Surface of a Grating With a Square Mesh. Radio Engineering and Electronics Physics, Vol. 8, No. 9, September 1963, pp. 1446-1454.
4. Croswell, W. F.: The Suitability of Mesh Membrane Material for Radiometer Reflector Applications. Large Space Systems Technology - 1981, NASA CP-2215, Part 2, 1982, pp. 621-629.
5. Mittra, R.; Ko, W. L.; and Rahmat-Samii, Y.: Transform Approach to Electromagnetic Scattering. Proc. of the IEEE, Vol. 67, No. 11, November 1979, pp. 1486-1503.
6. Tsao, C. H.; and Mittra, R.: A Spectral-Iteration Approach for Analyzing Scattering From Frequency Selective Surfaces. IEEE Trans. Ant. & Prop., Vol. AP-30, No. 2, March 1982, pp. 303-308.
7. Wait, J. R.: Theories of Scattering from Wire Grid and Mesh Structures. Electromagnetic Scattering. Academic Press, Inc., 1978.

A Survey of Near-Field Testing Methods for Large
Aperture Antennas and Future Trends

Allen C. Newell
National Bureau of Standards
Boulder, Colorado

Large Space Systems Technology - 1982
NASA Langley Research Center
November 30 - December 3, 1982

In recent years, near-field antenna measurements have progressed from theoretical concepts to a wide variety of operational measurement systems. This paper will summarize the current status of this work and its possible application to large space antennas.

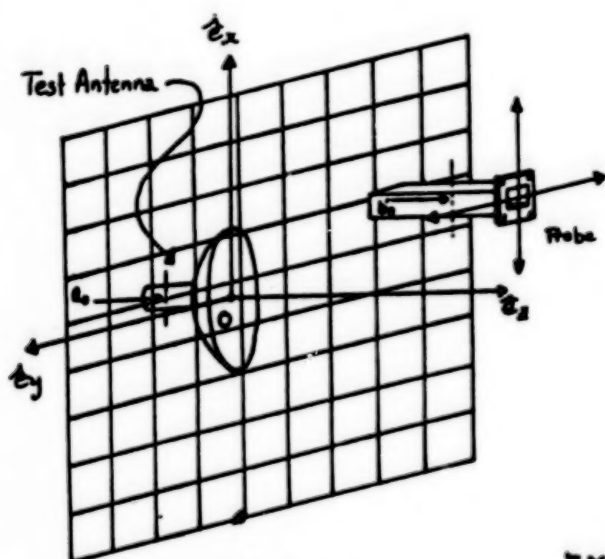
NEAR-FIELD ANTENNA MEASUREMENTS

1. MEASURE THE FIELD VERY CLOSE TO ANTENNA OVER A WELL DEFINED SURFACE (PLANE, CYLINDER, SPHERE)
2. MATHEMATICALLY CALCULATE FAR-FIELD PERFORMANCES

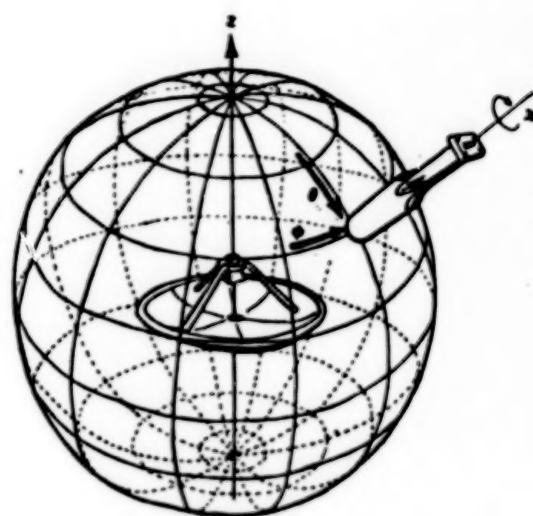
ADVANTAGES

1. NO WEATHER PROBLEMS
2. BETTER ACCESS TO ANTENNA
3. SECURITY AND "CLEAN ROOM"
4. NO INTERFERENCE
5. LESS EXPENSIVE FACILITY
6. MORE ACCURATE AND COMPLETE INFORMATION

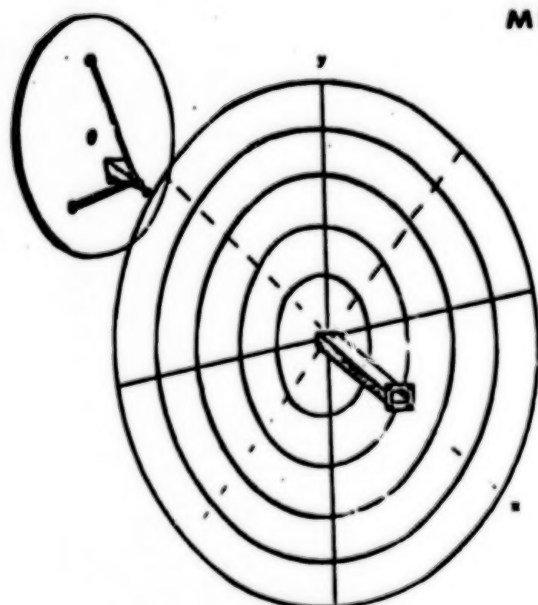
Four types of measurement surfaces or lattice shapes are currently being used. Each has special advantages and applications where it is best suited.



PLANAR

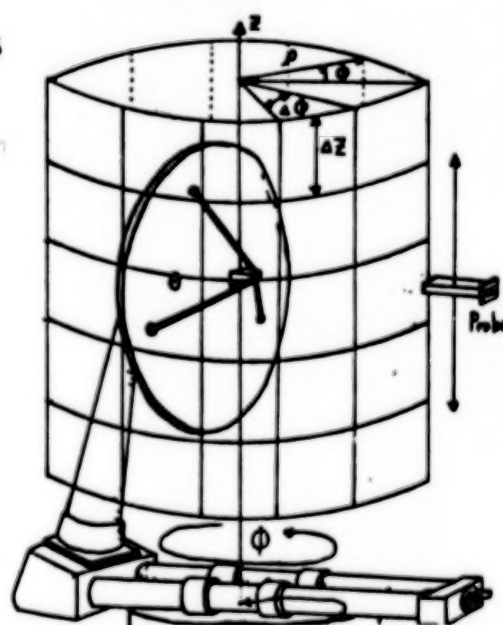


SPHERICAL



PLANE POLAR

**TYPES OF
NEAR FIELD
MEASUREMENTS**



CYLINDRICAL

The planar transmission equation illustrates the general features of each theory. The measured quantity is the probe output voltage as a function of position on the measurement surface. The probe receiving function is known and the test antenna's transmitting function is the object of the measurement.

TRANSMISSION FORMULA CHARACTERISTICS

- GIVES PROBE OUTPUT VOLTAGE AS FUNCTION OF PROBE POSITION & ORIENTATION ON MEASUREMENT SURFACE
- WRITTEN IN TERMS OF MODES (BASIS FUNCTIONS, WAVES) WHICH WILL PROVIDE ORTHOGONALITIES FOR THE MEASUREMENT SURFACE
- VALID FOR NEAR- OR FAR-FIELD DISTANCES
- EXACT EXCEPT FOR MULTIPLE REFLECTIONS
- ALL FUNCTIONS ARE WITH RESPECT TO SINGLE REFERENCE COORDINATE SYSTEM
- CONTAINS FACTORS WHICH CORRESPOND TO OR ARISE FROM:
 - PROBE RECEIVING CHARACTERISTIC
 - ANTENNA UNDER TEST TRANSMITTING CHARACTERISTICS
 - TWO ORTHOGONAL POLARIZATIONS
 - PROBE MOTION ON THE SURFACE

The transmission equation is valid for arbitrary distance and any combination of probe and test antenna. The only simplifying approximation is that multiple reflections are neglected.

NEAR-FIELD THEORY

- DERIVE TRANSMISSION EQUATION APPROPRIATE TO MEASUREMENT SURFACE
- RELATE PROBE RECEIVING FUNCTION, AS DESCRIBED IN ITS OWN COORDINATES, TO ONE DESCRIBED IN REFERENCE COORDINATE SYSTEM (TRANSLATION OF CENTERS)
- DECOUPLE TRANSMISSION EQUATION TO SOLVE FOR TEST ANTENNAS TRANSMITTING FUNCTION
- COMPUTE FAR-FIELD QUANTITIES IN TERMS OF TRANSMITTING FUNCTION

One of the reasons for the success of near-field techniques is the rigor and completeness of the theory. No simplifying assumptions are necessary about the probe or the test antenna.

$$b(x, y, d) = a_0 \iint \left[\sum_{m=1,2} \underbrace{(S_{02}(m, K) e^{i\gamma d})}_{\substack{\text{PROBE RECEIVING FUNCTION} \\ \text{WITH RESPECT TO REFERENCE} \\ \text{COORDINATE SYSTEM}}} \underbrace{T_{10}(m, K)}_{\substack{\text{TEST ANTENNA TRANSMITTING FUNCTION} \\ \text{WITH RESPECT TO REFERENCE COORDINATE} \\ \text{SYSTEM}}} \right] \underbrace{e^{ik_x x} e^{ik_y y}}_{\substack{\text{FACTORS ARISING FROM PROBE} \\ \text{MOTION ON THE PLANE}}} dk_x dk_y$$

PROBE VOLTAGE

PROBE POSITION

POLARIZATION INDEX

The general characters of the transmission formulas for these three surfaces are very similar.

TRANSMISSION FORMULAS

PLANAR
$$b(x,y,d) = a_0 \int_{-\infty}^{\infty} \int_{-\infty}^{\infty} \left[\sum_{m=1}^2 (S'_{02}(m,K) e^{iYd}) T_{10}(m,K) \right] (e^{ik_x x} e^{ik_y y}) dk_x dk_y$$

CYLINDRICAL
$$b(\phi, Z, d) = a_0 \sum_{n=-\infty}^{\infty} \int_{-\infty}^{\infty} \left[\sum_{s=1}^2 R'_n{}^s d(\gamma) T_n{}^s(\gamma) \right] (e^{in\phi} e^{iYZ}) d\gamma$$

SPHERICAL
$$W^A(\chi, \theta, \phi) = \sum_m \sum_n \sum_{\mu} \left[\sum_{s=1}^2 p^{s\mu n A} Q^{smn} \right] (e^{im\phi} d_{m\mu}^{(n)}(\theta) e^{i\mu\chi})$$

The integration of the measured data can be done accurately and efficiently for plane rectangular using the FFT. However, for plane polar, other techniques which may involve approximations are required.

Comparison of Analysis, Plane Rectangular vs. Plane Polar

$$D(\underline{K}) = \frac{e^{-i\gamma d}}{4\pi^2 F' a_0} \iint_{-\infty}^{\infty} b'_0(x, y) e^{-i(k_x x + k_y y)} dx dy$$

Plane Rectangular; 2-D Fourier Transform—FFT

$$D(\underline{K}) = \frac{e^{-i\gamma d}}{4\pi^2 F' a_0} \sum_{n=-\infty}^{\infty} e^{in\theta} e^{-in\eta_1} \int_0^{\infty} \left\{ \int_0^{2\pi} b'_0(\rho, \phi) e^{in\phi} d\phi \right\} J_n(K\rho) \rho d\rho$$

Plane Polar;
1-D Fourier Transform + Hankel Transform

Once the test antennas' spectral coefficients are determined, the far-field pattern is easily obtained.

FAR ELECTRIC FIELD IN TERMS OF TRANSMITTING COEFFECIENTS

PLANAR
$$E(r, \underline{K}) = \frac{ik a_0 e^{ikr}}{r} \left[\underline{t}_{10}(\underline{K}) \cos\theta \right]$$

 (NOTE: $\underline{t}_{10}(\underline{K})$ = COMPLETE VECTOR, $\underline{t}_{10}(\underline{K})$ = TRANSVERSE PART)

CYLINDRICAL
$$E(r, \theta, \phi) = \frac{-2k a_0 \sin\theta e^{ikr}}{r} \sum_{n=1}^{\infty} (-1)^n \left[T_n^1(\gamma) \underline{e}_{\phi}^{-1} T_n^2(\gamma) \underline{e}_{\theta} \right] e^{in\phi}$$

SPHERICAL
$$E(r, \theta, \phi) = \frac{a_0 e^{ikr}}{kr} \sum_{s, m, n} (-1)^{n+1-s} Q^{smn} \underline{G}_n^{sm}(\theta, \phi)$$

Similarly, the power gain is also easily obtained, as are polarization parameters such as axial ratio, tilt angle, and sense of polarization.

ANTENNA GAIN IN TERMS OF TRANSMITTING COEFFICIENTS

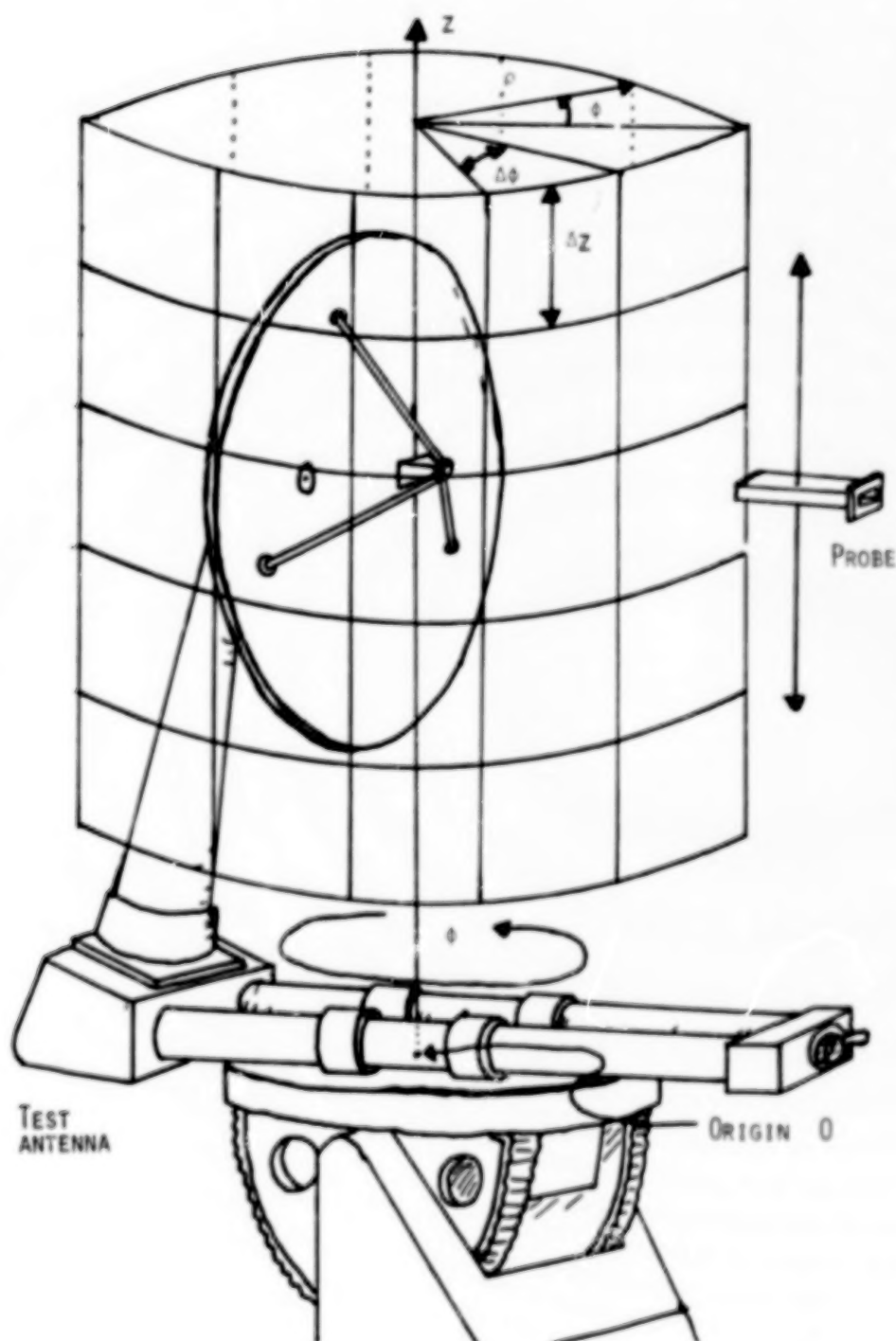
$$\text{PLANAR} \quad G(\underline{k}) = \frac{4\pi k^2 y_0}{(1-|S_{00}|^2)\eta_0} \left[|T_{10}(1,\underline{k})|^2 + |T_{10}(2,\underline{k}) \gamma/k|^2 \right]$$

$$\text{CYLINDRICAL} \quad G(\theta, \phi) = \frac{16\pi k^2 \sin^2 \theta}{z_0 \eta_0 (1-|S_{00}|^2)} \left[\left| \sum_{n=1}^{\infty} (-1)^n T_n^1(\gamma) e^{in\phi} \right|^2 + \left| \sum_{n=1}^{\infty} T_n^2(\gamma) e^{in\phi} \right|^2 \right]$$

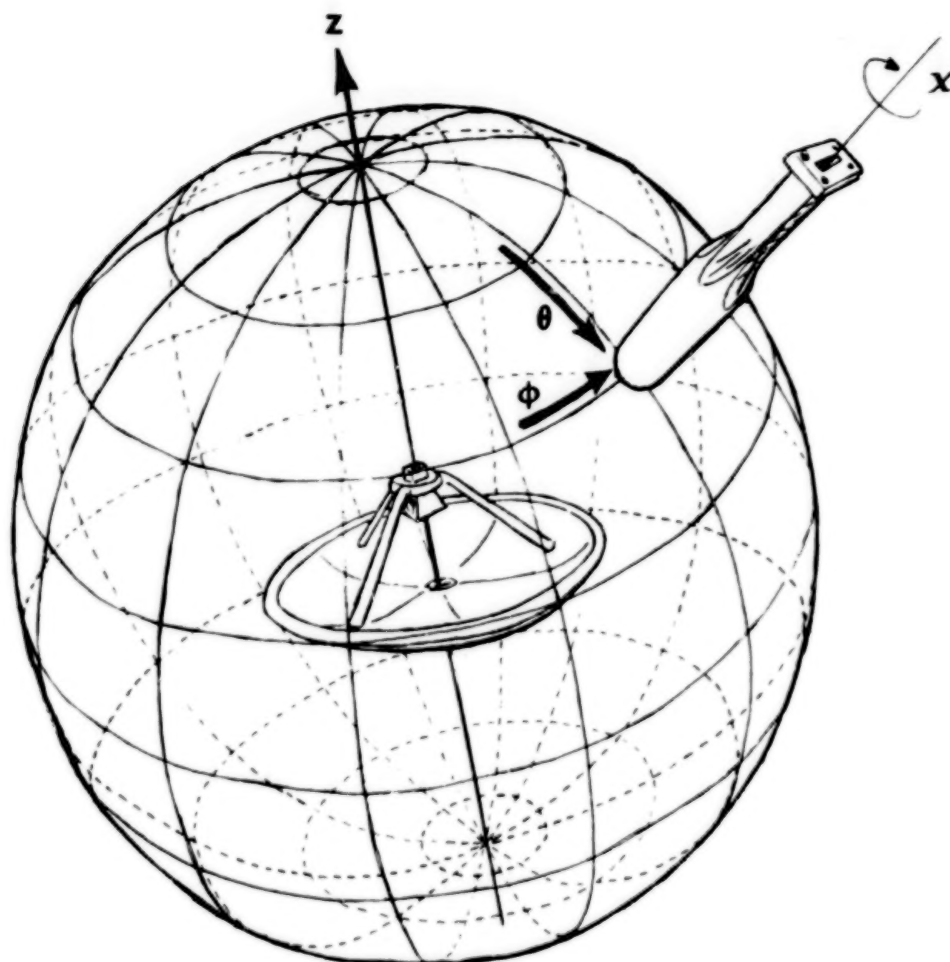
$$\text{SPHERICAL} \quad G(\theta, \phi) = \frac{4\pi \eta_0}{k^2 \hat{n} (1-|S_{00}|^2)} \left| \sum_{smn} (1)^{s-n} Q^{smn} \underline{G}_n^{sm}(\theta, \phi) \right|^2$$

Shown here is a schematic of an experimental set-up for cylindrical near-field scanning, showing the coordinate system for the measurement surface.

CYLINDRICAL SCANNING



Shown below is a schematic of near-field measurements.



$$w^A(\chi, \theta, \phi) = \sum_{m, n, \mu, s} (p_{s\mu n A}^{smn}) \underbrace{e^{im\phi_d(n)} e^{i\mu\chi}}_{\text{FACTORS DUE TO PROBE MOTION ON SURFACE OF SPHERE}} e^{i\mu\chi}$$

PROBE RECEIVING COEFFICIENTS WITH RESPECT TO $oxyz$

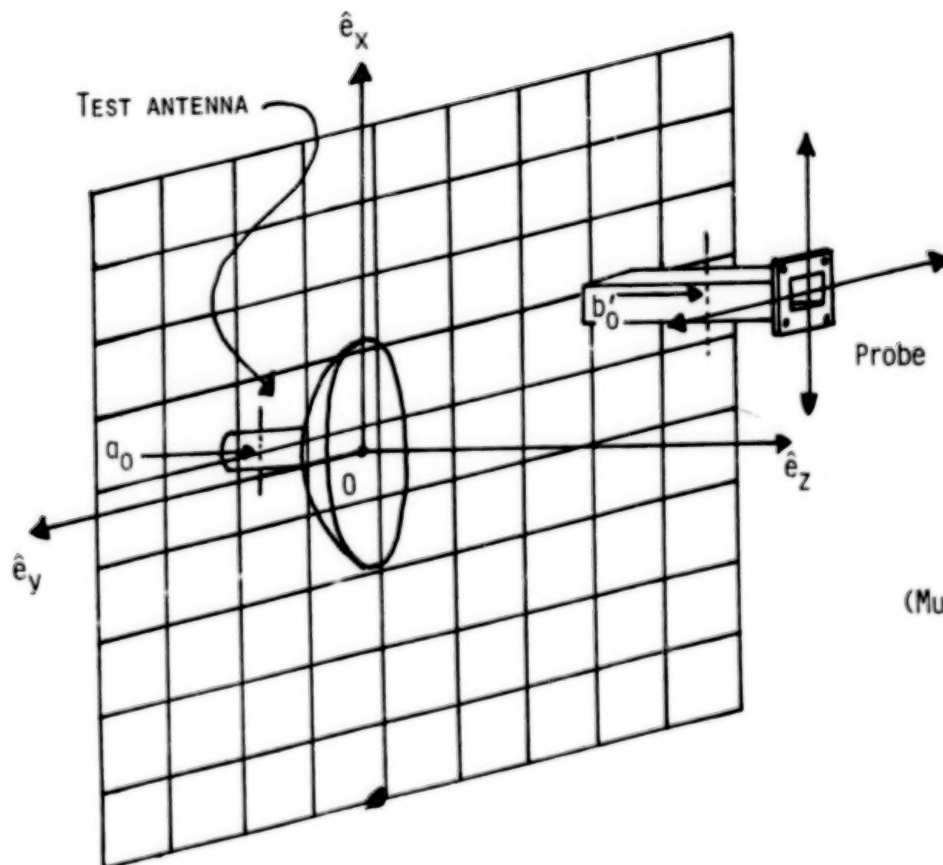
ANT TRANSMITTING COEFFICIENTS WITH RESPECT TO $oxyz$

A = RADIUS OF SPHERE

s = POLARIZATION INDEX

Shown below is a planar scanning schematic. This technique is best suited to narrow-beam antennas.

PLANAR SCANNING



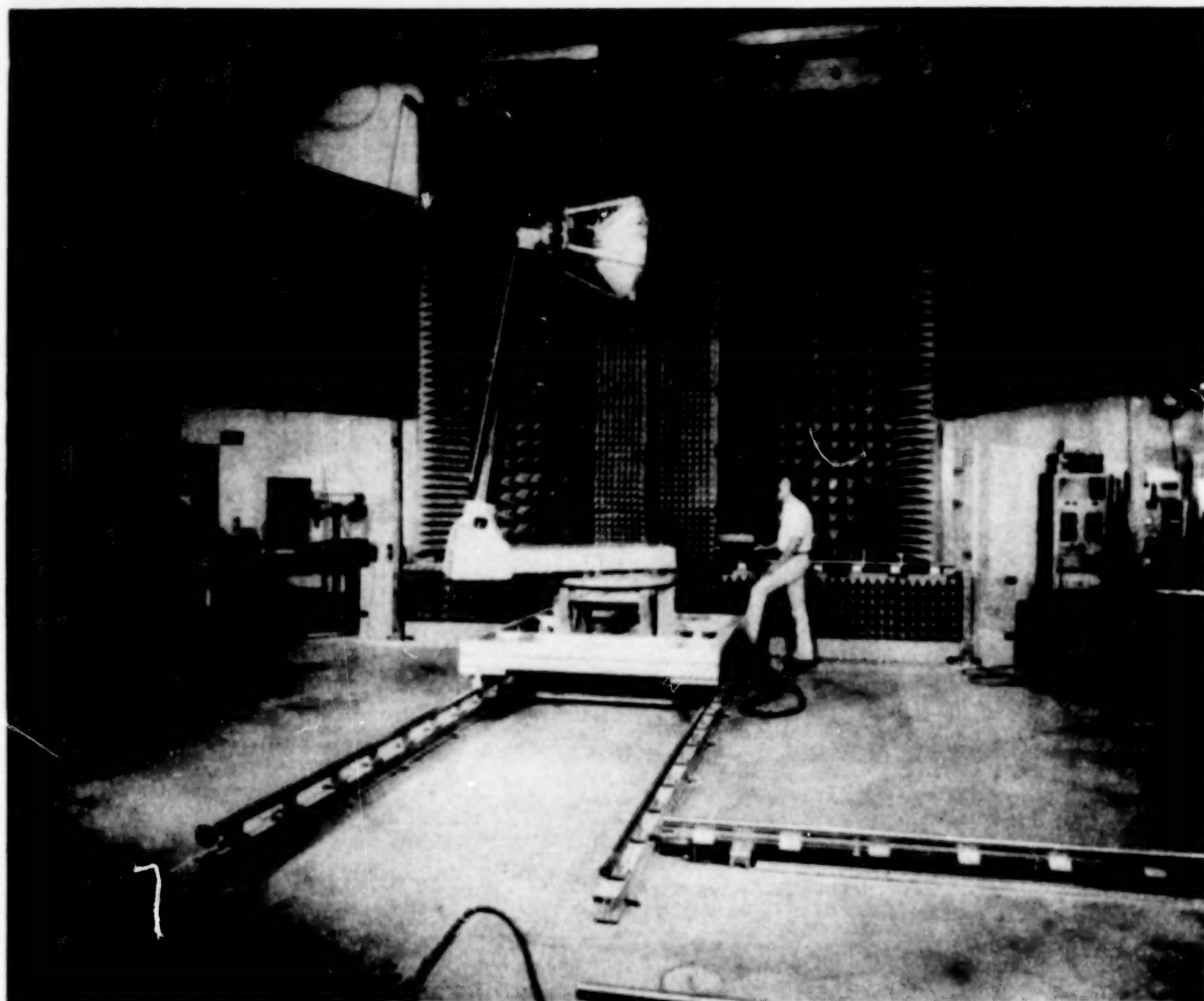
ASSUMPTIONS

- 1) MAXWELL' EQUATIONS
- 2) LINEAR ANTENNAS
- 3) OPERATING CW ($e^{-i\omega t}$) IN FREE SPACE
- 4) SINGLE MODE PROPAGATING IN WAVEGUIDE OF TEST AND PROBE ANTENNAS

ANTENNAS MAY BE LOSSY AND NONRECIPROCAL

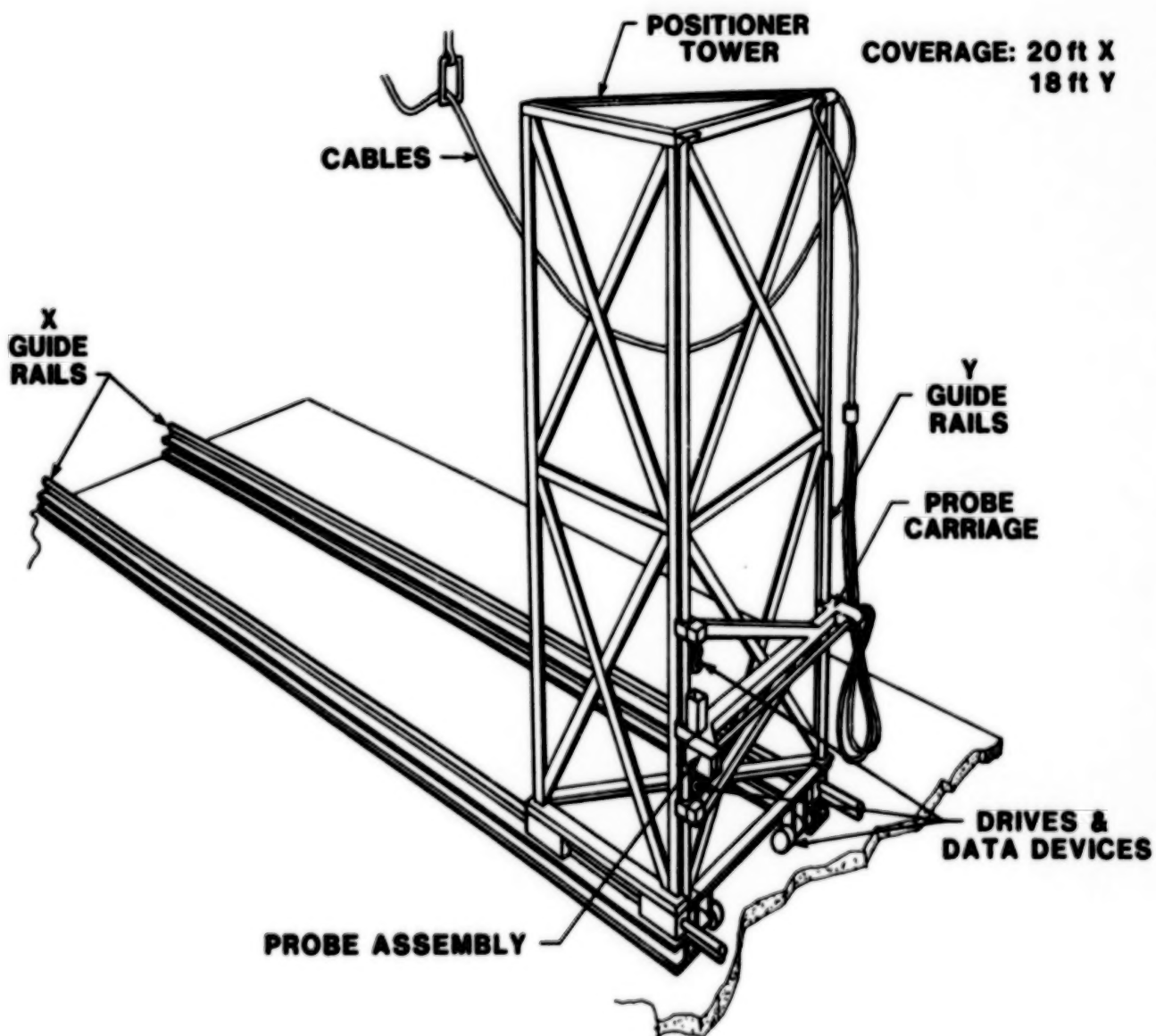
(MULTIPLE REFLECTIONS NEGLIGIBLE)

Shown below is a photograph of the near-field measurement facility at the National Bureau of Standards. Measurements can be performed for all four types of surface/lattice combinations.



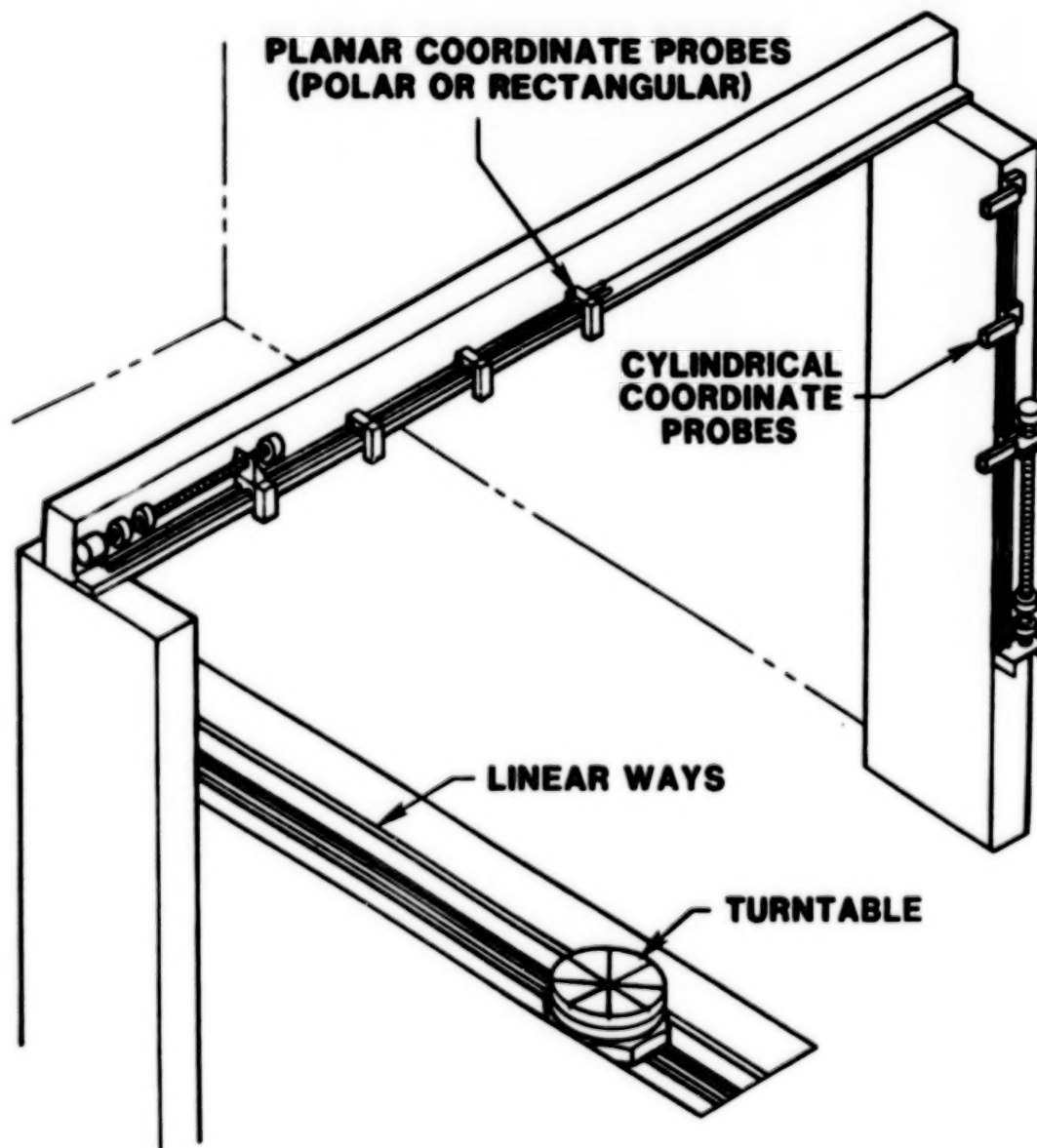
This is a schematic of a planar scanner design using a track and a large rigid probe tower.

SCHEMATIC OF TRACK/TOWER PLANAR SCANNER



Shown below is a schematic of a planar scanner design combining one-dimensional translation of multiple probes with translation and rotation of the test antenna. Very large space-deployable antennas can be measured with this facility.

SCHEMATIC OF TRANSLATION/ROTATION SCANNER



A wide range of antenna types and frequency ranges have been measured at NBS.

SOME ANTENNAS MEASURED AND DATA BASE AVAILABLE

ANTENNA TYPE	FREQUENCY (GHz)	MAJOR DIMENSION	
		IN WAVELENGTH	GAIN (dB)
HORN LENS	48.0	90	47.0
CONICAL HORN (JPL)	8.0	6	22.08
CASSEGRAIN REFLECTOR	60.0	91	46.5
LENS ARRAY (CONSTRAINED LENS)	9.2	23	34.0
PHASED ARRAY (VOLPHASE)	8.4	17	21.5
PHASED ARRAY	7.5	15	30.5
DIPOLE ARRAY	1.4	5	20.3
FAN BEAM RADAR (LINEAR & CIRCULAR POLARIZATION)	9.5	58	30.0
KU-BAND REFLECTOR	14.5	60	42.0
KU-BAND ARRAY (PENCIL & FAN BEAM)	17.00	50	40.0
SHAPED BEAM, C.P. (ARRAY FED REFLECTOR)	4.0	20	27.5
MICROSTRIP ARRAY	1.5	27	30.0
PARABOLIC REFLECTION	1.5-18	15-183	26-47
COMPACT RANGE REFLECTOR	18 & 55	285 & 870	~ 60.0

The validity of the plane rectangular technique has been demonstrated by a combination of approaches. Similar studies are under way for the other techniques.

VALIDITY AND ACCURACY OF PLANAR NEAR-FIELD MEASUREMENTS ESTABLISHED
BY:

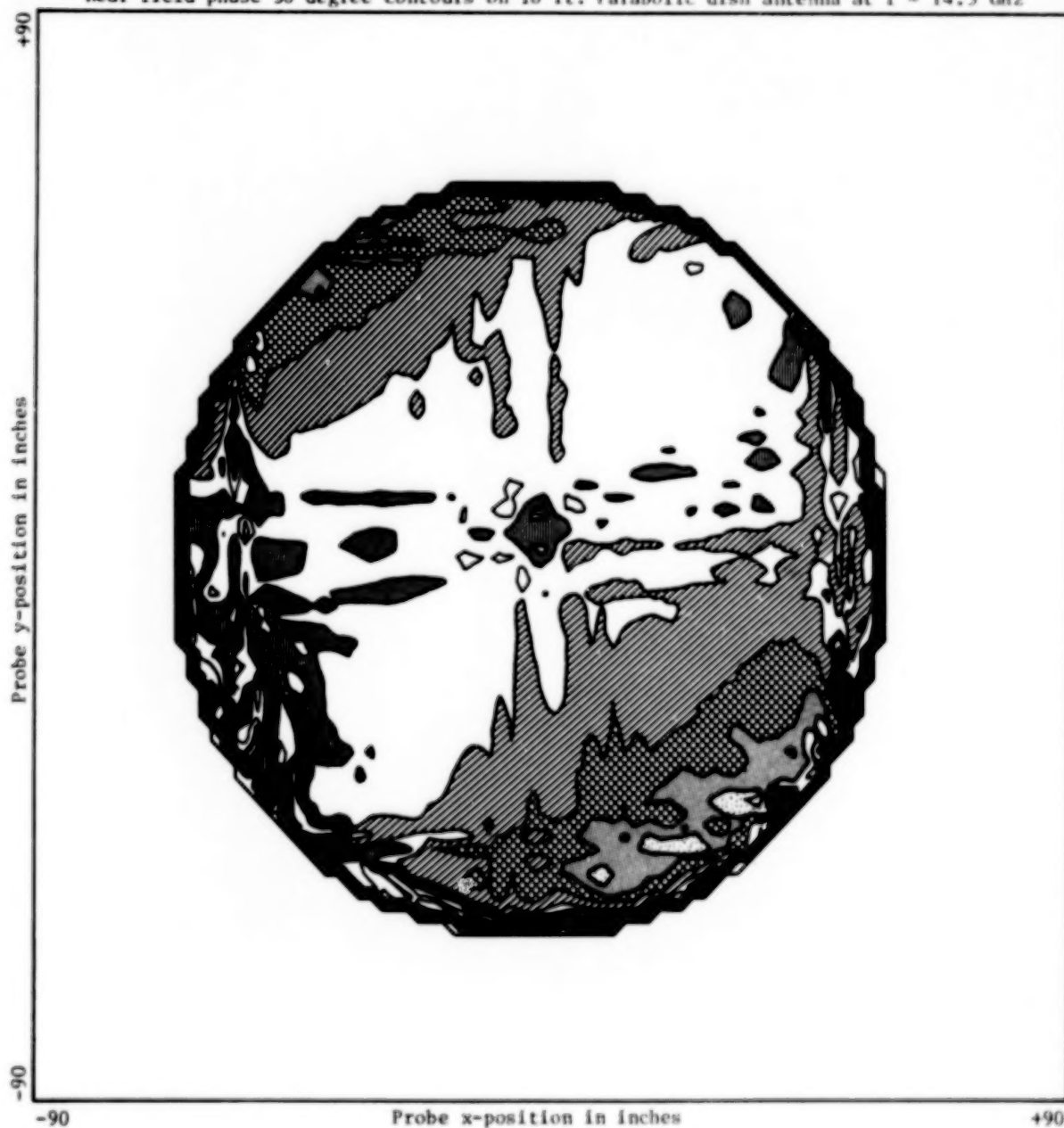
1. COMPARISON WITH OTHER MEASUREMENT TECHNIQUES
2. COMPUTER SIMULATION OF MEASUREMENT ERRORS
3. MATHEMATICAL ANALYSIS OF WORST-CASE SYSTEMATIC AND RANDOM ERROR

ERRORS STUDIED

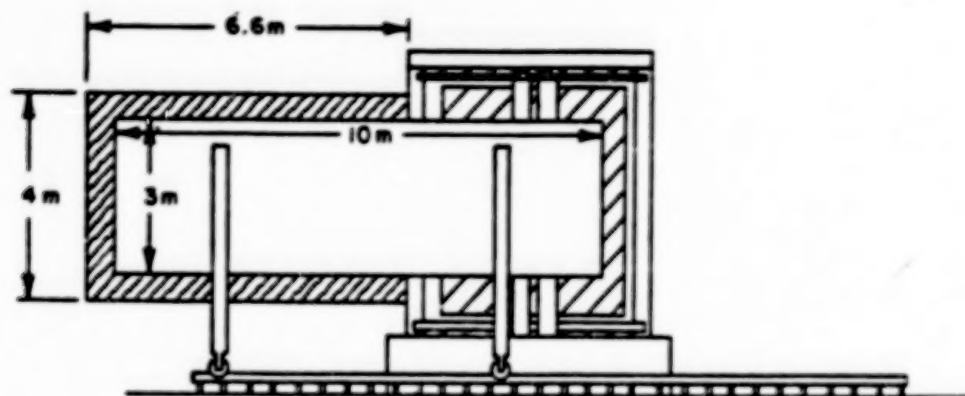
- * TRUNCATION OF MEASUREMENT AREA
- * x , y , AND z PROBE POSITION
- * RECEIVER NON-LINEARITY
- * MULTIPLE REFLECTIONS
- * PROBE PATTERN AND GAIN
- * AMPLITUDE AND PHASE NORMALIZATION



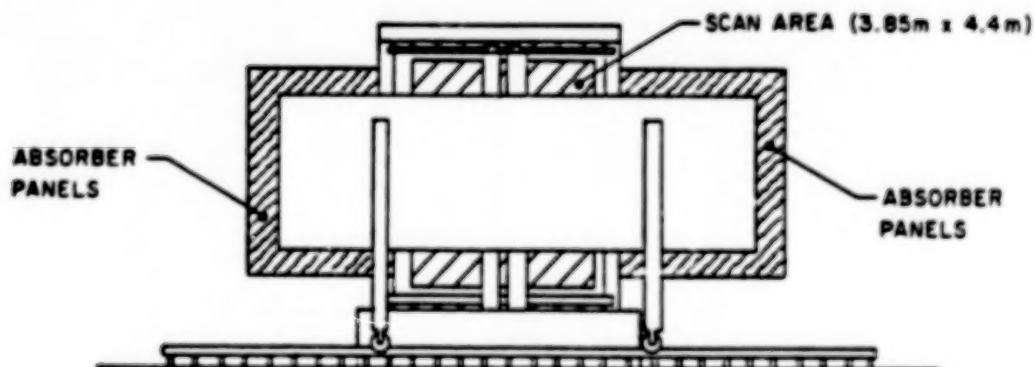
Near field phase 30 degree contours on 10 ft. Parabolic dish antenna at $f = 14.5 \text{ GHz}$



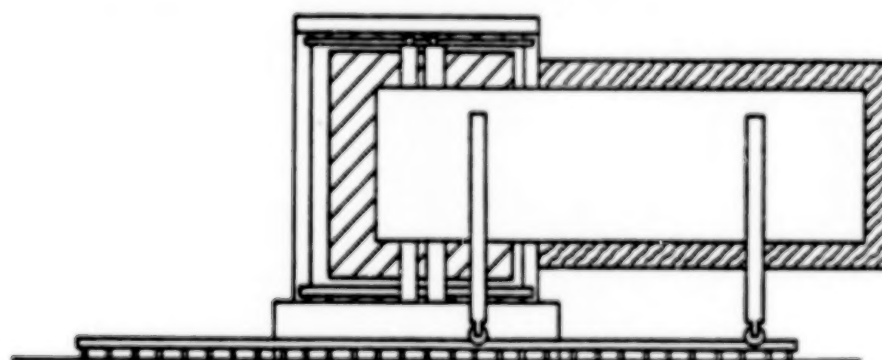
Shown below is another example of how near-field phase is used to determine reflector alignment.



SIR ANTENNA ON NEAR-FIELD SCANNER, POSITION 1



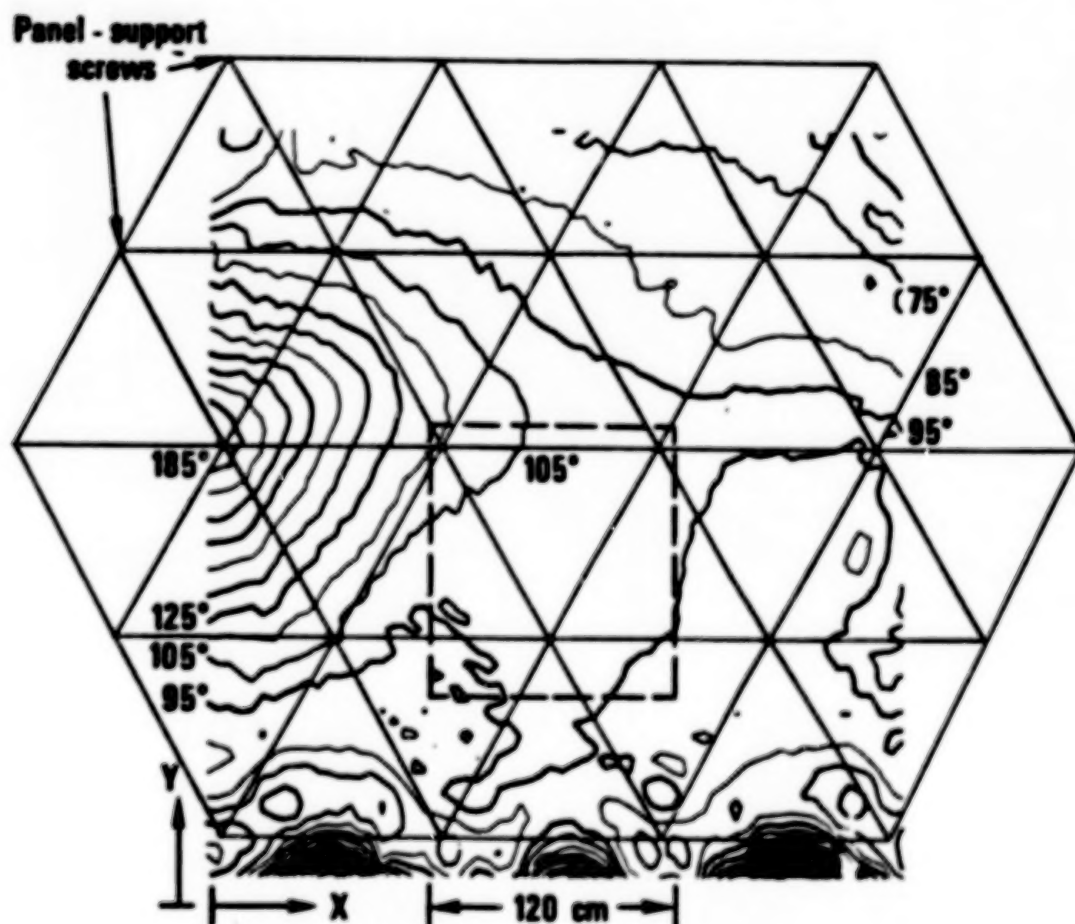
SIR ANTENNA ON NEAR-FIELD SCANNER, POSITION 2



SIR ANTENNA ON NEAR-FIELD SCANNER, POSITION 3

Schematic of SIR antenna in three positions for PNF measurement.

When antennas are larger than the mechanical scanner, it may be possible to obtain the data in segments by translation and/or rotation of the antenna relative to the scanner.



NEAR-FIELD MEASUREMENT FACILITY PLANS AT LEWIS RESEARCH CENTER

R. G. Sharp
NASA Lewis Research Center
Cleveland, Ohio

Large Space Antenna Systems Technology - 1982
NASA Langley Research Center
November 30 - December 3, 1982

INTRODUCTION

The following introductory points provide some background.

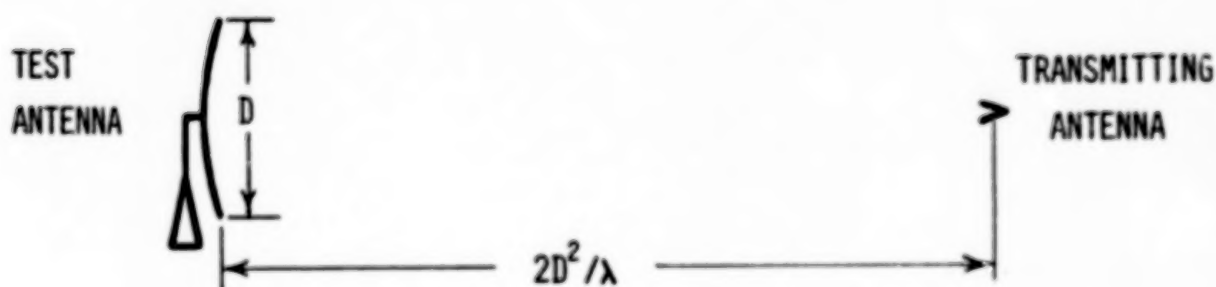
- o NASA LEWIS RESEARCH CENTER IS THE LEAD CENTER FOR THE NASA SPACE COMMUNICATION PROGRAM.
- o ANTENNA TECHNOLOGY HAS BEEN IDENTIFIED AS A CRITICAL TECHNOLOGY FOR FUTURE SPACE COMMUNICATION SYSTEMS.
- o ADVANCED ANTENNA CONCEPTS BASED ON EMERGING TECHNOLOGIES ARE BEING INVESTIGATED IN A BASE RESEARCH AND TECHNOLOGY PROGRAM INVOLVING COORDINATED IN-HOUSE AND CONTRACTUAL EFFORTS.
- o NEAR-FIELD PLANAR SCANNER TESTING WILL PROVIDE AN IN-HOUSE CAPABILITY FOR EXPERIMENTAL INVESTIGATIONS OF ADVANCED ANTENNA CONCEPTS.

FAR-FIELD MEASUREMENT TECHNIQUE

Up until about 20 years ago, all antenna patterns were measured using the far-field technique. The test antenna was required to be mounted at least $2D^2/\lambda$ (out of the Fresnel zone) away from the transmitting antenna in order for far-field conditions to occur. Here, D is the reflector aperture diameter and λ is the wavelength.

BASIC CONCEPT

MEASURE RESPONSE OF TEST ANTENNA IN THE FAR FIELD OF A TRANSMITTING ANTENNA



CONSTRAINTS

1. TEST ANTENNA TO TRANSMITTING PROBE SEPARATION MUST BE $> 2D^2/\lambda$
2. ACCURATE FIELD MEASUREMENTS AS A FUNCTION OF TEST ANTENNA ORIENTATION

FAR-FIELD TECHNIQUE DIFFICULTIES DUE TO THE REQUIRED LARGE TRANSMITTING ANTENNA TO TEST ANTENNA SEPARATION

When the antenna to be measured is of large reflector aperture size D and also high frequency (or of small wavelength λ), the required separation distance from the transmitting antenna to the test antenna can become very great. For example, the required separation distance for a 30 GHz 3-m reflector is 1.8 km in order to meet the minimum separation criteria of $2D^2/\lambda$. As the required separation distance becomes large, the factors shown can present serious difficulties for far-field testing.

- GROUND REFLECTIONS
- INTERFERENCE EFFECTS
- ATMOSPHERIC & WEATHER EFFECTS
- ANTENNA ENVIRONMENTAL CONSTRAINTS
 - TEMPERATURE & HUMIDITY
 - BORESIGHT ORIENTATION
- HIGH POWER, STABLE SOURCE REQUIRED
- LOGISTICS

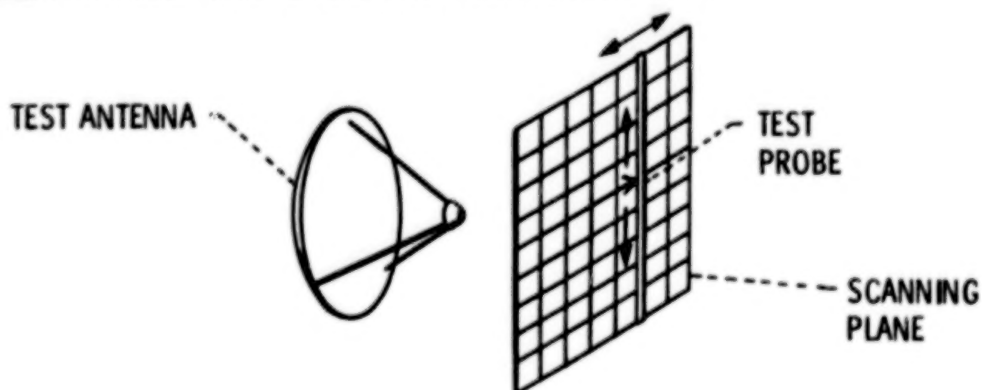
NEAR-FIELD MEASUREMENT TECHNIQUE

In the far-field technique, direct measurements are made of the test antenna response in far-field conditions. However, in the near-field technique, far-field antenna parameters are calculated from phase and amplitude measurements made over a well-defined surface in the near field. Near-field measurements are characterized by the surfaces over which they are made--planar, cylindrical, or spherical.

The figure illustrates a planar near-field scanner with which the phase and amplitude values of an $N \times N$ grid are measured and recorded with a small test probe. Complete 3-dimensional far-field amplitude and polarization information is calculated from the near-field data by a procedure which basically involves performing a discrete fast Fourier transform (DFFT) of the near-field data. The data acquisition constraints are that the scanned surface must intercept essentially all of the antenna's radiation, the surface must be flat to within a small fraction of a wavelength ($\lambda/100$), and the grid point spacing must be on the order of $\lambda/2$. Because all measurements are made in the near field, the measurement system can be located in a controlled indoor environment.

BASIC CONCEPT

1. MEASURE NEAR-FIELD AMPLITUDE AND PHASE OVER WELL-DEFINED SURFACE
2. CALCULATE FAR-FIELD PARAMETERS FROM NEAR-FIELD DATA



PLANAR SCANNER

CONSTRAINTS

1. SCANNED SURFACE INTERCEPTS ESSENTIALLY ALL ANTENNA ENERGY
2. ACCURATE AMPLITUDE AND PHASE MEASUREMENTS AT EACH POINT ON GRID
3. GRID SPACING D : $0.5 \lambda \lesssim D \lesssim \lambda$
4. SCANNED SURFACE SMOOTH TO $\approx \lambda/100$
5. TWO SCANS REQUIRED, ONE FOR EACH OF TWO PROBE POLARIZATIONS
6. PROBE CHARACTERISTICS KNOWN

SATELLITE COMMUNICATION ANTENNA CHARACTERISTICS AND TRENDS

Antennas for communication satellites have increased in frequency, reflector aperture diameter and complexity as these satellites have evolved. The result has been that the electrical size of the antennas D/λ has increased at an even greater rate.

	EARLY BIRD TELSTAR (PAST)		CTS	ACTS (FUTURE)	
	1960	TO	1980	1980	TO 2000
o FREQUENCY	1-2GHz		12-14 GHz	20-30 GHz	60 GHz+
o APERTURE SIZE	1 m		4-m RIGID 9-m DEPLOYABLE	4-m PRECISION	100 m+
o ELECTRICAL SIZE,	3		100-300	300-400	3000+
o COMPLEXITY	SINGLE-ELEMENT RADIATOR		MULTI-ELEMENT FEED/REFLECTOR	MULTIPLE BEAMS, SCANNING BEAM	COMPLEX ACTIVE ARRAY FEEDS

ADVANTAGES OF USING THE NEAR-FIELD METHOD FOR SPACE COMMUNICATION ANTENNAS

The comparison of various antenna measurement techniques is well documented (ref. 1). Each has advantages and disadvantages and the selection of the "best" approach for a given application depends on many factors including antenna size, frequency, type, complexity, desired accuracy, and level of detail required. The near-field method is especially attractive for testing high-frequency, high-gain space communication antennas for the reasons shown.

- o METHOD IS SUITABLE FOR LARGE-APERTURE, HIGH-FREQUENCY ANTENNAS FOR WHICH $2D^2/\lambda$ IS VERY LARGE
- o ANTENNAS ARE TESTED IN A CONTROLLED ENVIRONMENT
- o ANTENNAS MAY BE TESTED IN VERTICAL BORESIGHT CONFIGURATION; MAY BE TESTED WITHOUT BEING MOVED IN ANY WAY
- o ANTENNAS MAY BE TESTED IN TRANSMIT OR RECEIVE MODE
- o COMPLETE FAR-FIELD INFORMATION IS DERIVED FROM SINGLE SET OF NEAR-FIELD MEASUREMENTS
- o METHOD PROVIDES DIAGNOSTIC AND SET-UP INFORMATION

NEAR-FIELD MEASUREMENT FACILITY PLANS AT LeRC

A 22' x 22' horizontal boresight (vertical scan) planar scanner is presently becoming operational at LeRC. The first RF field measurements were made in April of 1982. This facility will provide an essential in-house antenna testing capability in support of the LeRC antenna base research and technology investigations. Future plans call for an Antenna Technology Laboratory (ATL) that will house both the present 22' x 22' scanner and a larger 60' x 60' vertical boresight planar scanner that will be capable of measuring high-frequency, physically and electrically large antennas. Such antennas might be large (up to 15 m diameter) extremely precise reflectors or scale models of very large antennas and antenna systems (the scaled frequency is inversely proportional to the scaled reflector aperture diameter).

- o 22' X 22' HORIZONTAL BORESIGHT PLANAR SCANNER (PRESENTLY EXISTS)

- o 60' X 60' VERTICAL BORESIGHT PLANAR SCANNER (IN PLANNING STAGE)

DESIGN PHILOSOPHY

The plane described by the motion of the probe tip of the planar scanner must be kept very flat over the test period in order to minimize phase error. An extremely rigid mechanical design constructed from a stable material (steel) was chosen in order to minimize the Z-axis (boresight) electrical phase corrections that would otherwise be required. Simple differential screw adjustments are used for alignment of the rails on which the moving components of the scanner are mounted.

DESIGN PHILOSOPHY

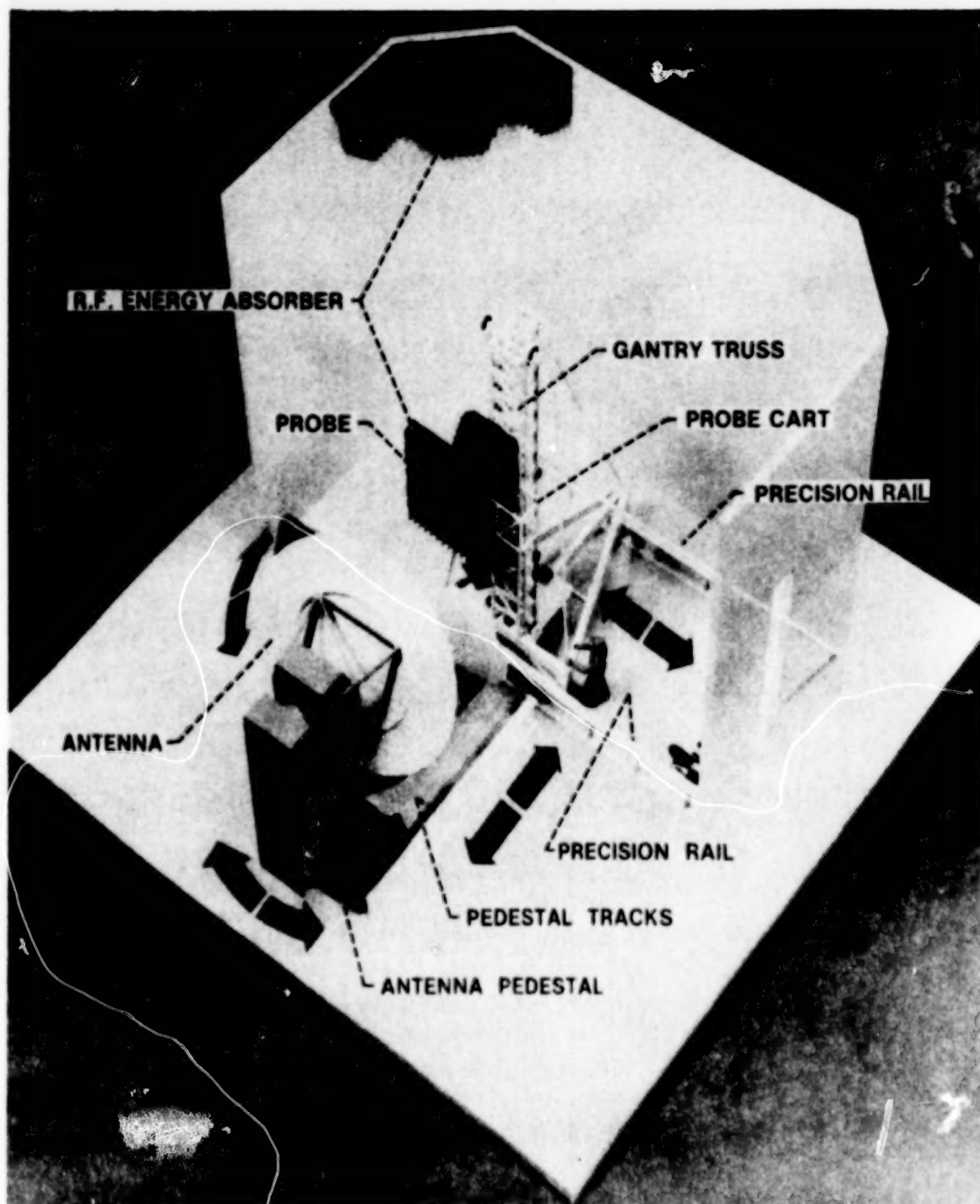
- o PROVIDE AN EXTREMELY RIGID MECHANICAL DESIGN WITH HIGH STRUCTURAL STABILITY
- o PROVIDE CAPABILITY FOR EASY AND ACCURATE MECHANICAL ADJUSTMENT
- o INITIALLY, USE STATE-OF-ART SUBSYSTEM HARDWARE AND COMPUTER PROGRAMS; UPGRADE SYSTEM CAPABILITIES, AS REQUIRED, IN STAGES

DESCRIPTION

- o SCANNING PLANE -VERTICAL, 6.7M x 6.7M OVERALL
- o SCANNING PLANE FLATNESS- \pm 0.005 cm
- o FREQUENCY OF OPERATION -0.8 - 60 GHz
- o PROBE POSITIONING -PROBE POSITION ON GANTRY TRUSS RAILS (VERTICAL AXIS) AND BASE PLATFORM POSITION ON HORIZONTAL RAILS (HORIZONTAL AXIS) DETERMINED BY LASER INTERFEROMETER
- o MECHANICAL ALIGNMENT -LASER STRAIGHTNESS MEASURING DEVICES, PRECISE OPTICAL LEVEL, AND JIG TRANSITS
- o HORIZONTAL DRIVE -CHAIN DRIVEN BY COMPUTER-CONTROLLED D. C. MOTORS WITH PRECISION TACHOMETERS THROUGH A SYNCHRONOUS BELT REDUCTION DRIVE
 - SPEED RANGE: 17.7 TO .012 CM/SEC
- o VERTICAL DRIVE -ESSENTIALLY IDENTICAL TO HORIZONTAL DRIVE
 - SPEED RANGE: 35.4 TO .012 CM/SEC
- o COMPUTER -PRETESTS AND DATA ACQUISITION: PERKIN ELMER 832 (LOCATED IN N-F FACILITY CONTROL ROOM)
 - DATA PROCESSING: UNIVAC 1100 (LOCATED IN LABORATORY CENTRAL COMPUTING FACILITY)
- o RF ABSORBER -18" LOADED URETHANE FOAM (EMERSON CUMING ECCOSORB)

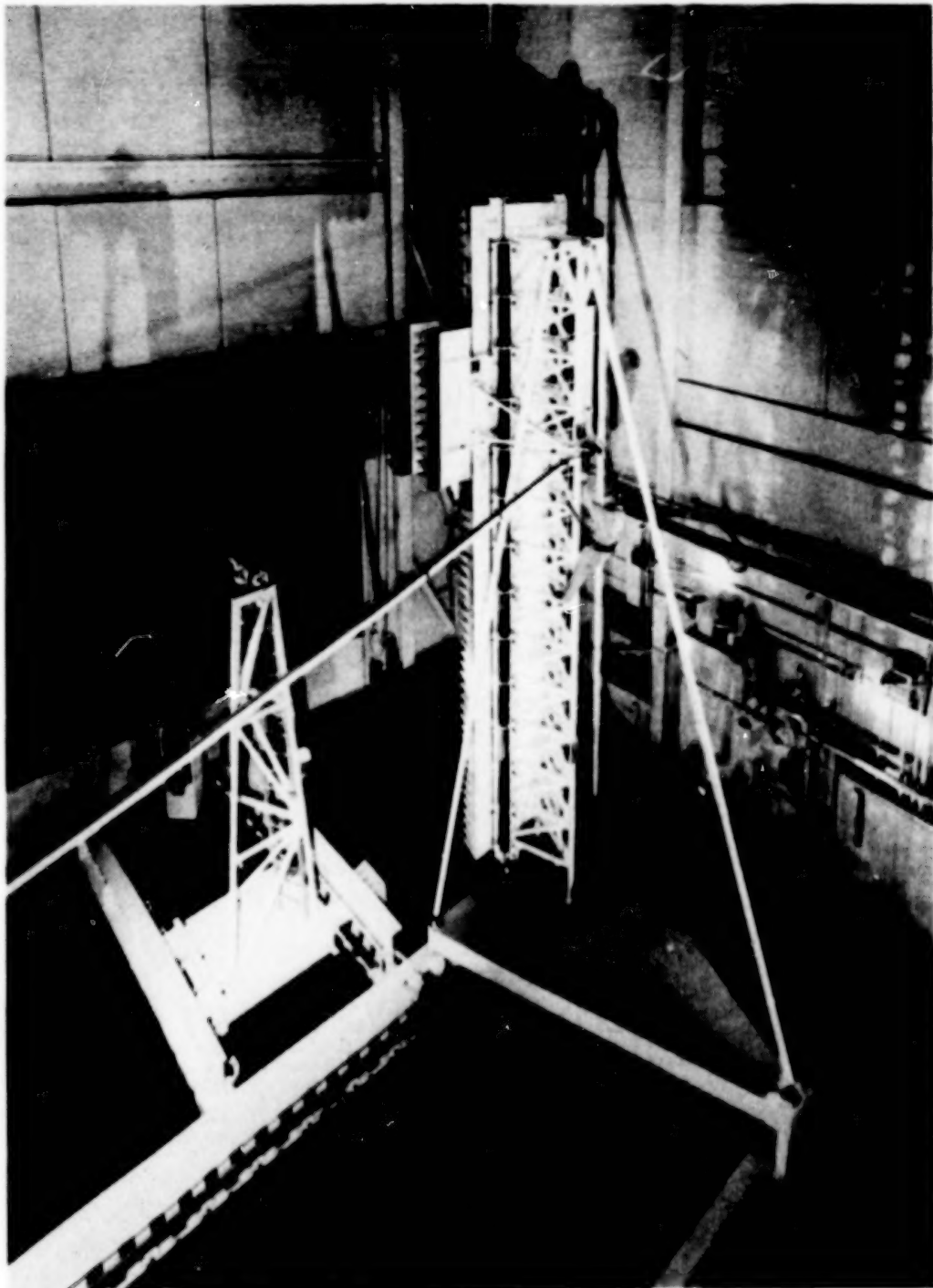
NEAR-FIELD ANTENNA TEST FACILITY

A scale (1/2" per foot) model of the 22' x 22' horizontal boresight near-field scanner is pictured. The major parts are titled and their movements indicated.



VIEW OF 22' x 22' HORIZONTAL BORESIGHT NEAR-FIELD SCANNER
LOOKING INTO THE TEST ANTENNA (BACK OF SCANNER)

This photograph was taken before the RF absorber wall was constructed and shows the back of the scanner. The front (toward the antenna pedestal) rail of the horizontal cart can be seen, including the rail adjustment brackets. The counterweight return tube for the vertical cart can also be seen mounted to the side of the tower.



OVERHEAD VIEW OF 22' x 22' HORIZONTAL BORESIGHT
NEAR-FIELD ANTENNA SCANNER

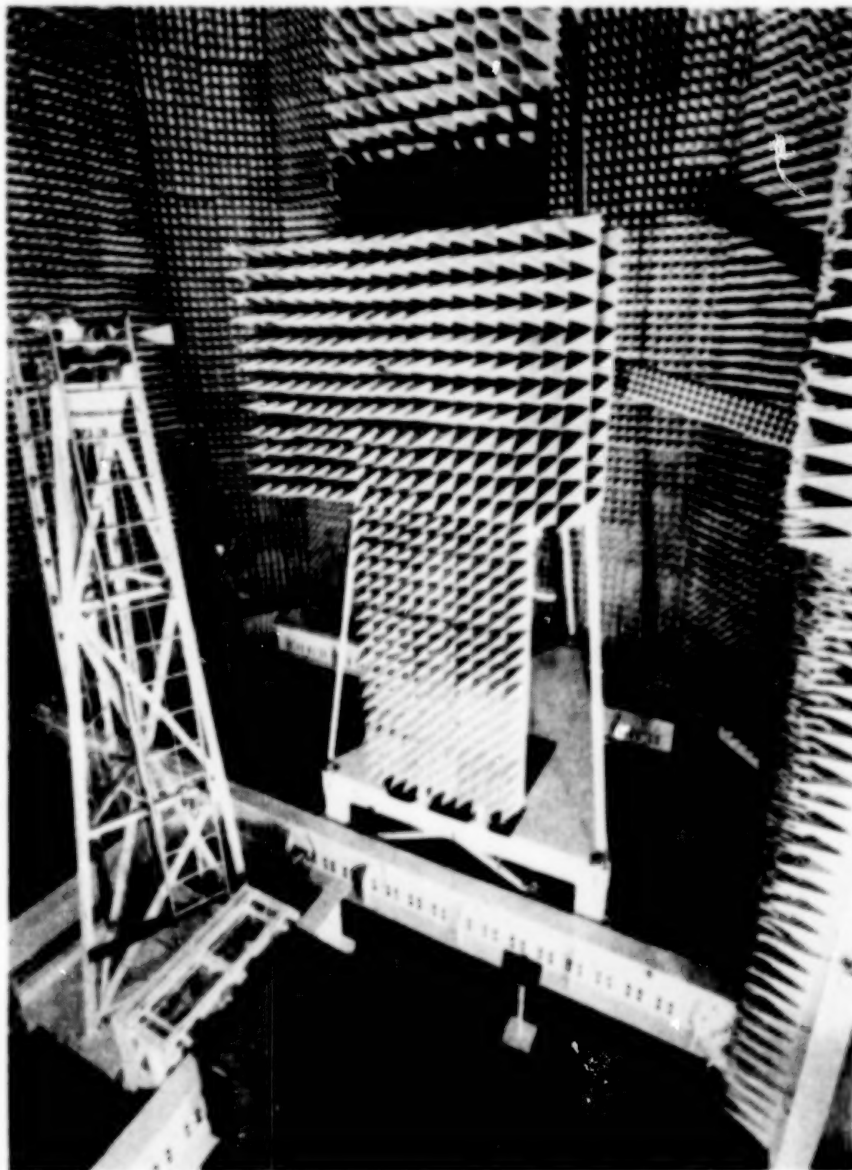
This photograph was taken in November of 1982 after construction of the RF absorber wall was completed. The only RF absorber work remaining is the installation of absorber in front of the large horizontal wide-flange beams that are mounted to the floor.



FRONTAL VIEW OF 22' x 22' HORIZONTAL BORESIGHT
NEAR-FIELD ANTENNA SCANNER

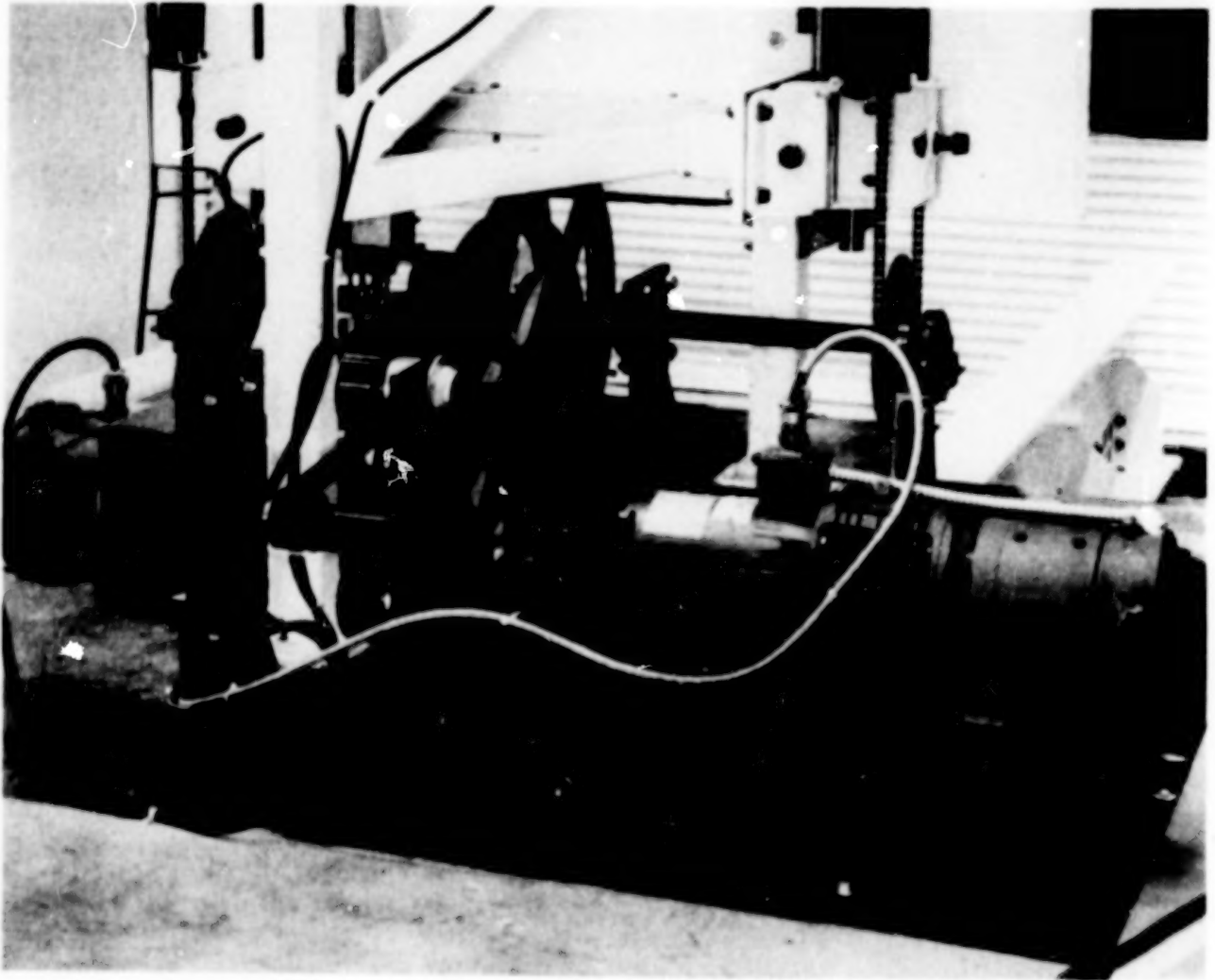
Systems that can be seen in this view are:

- a) the optical blocks and mounting brackets for the laser interferometer position and rail straightness measuring system along the front wide flange beam
- b) the RF system signal source box in the lower left corner and the antenna mounting pedestal which it supplies
- c) the horizontal drive motor and reduction drive belts on the right side of the picture



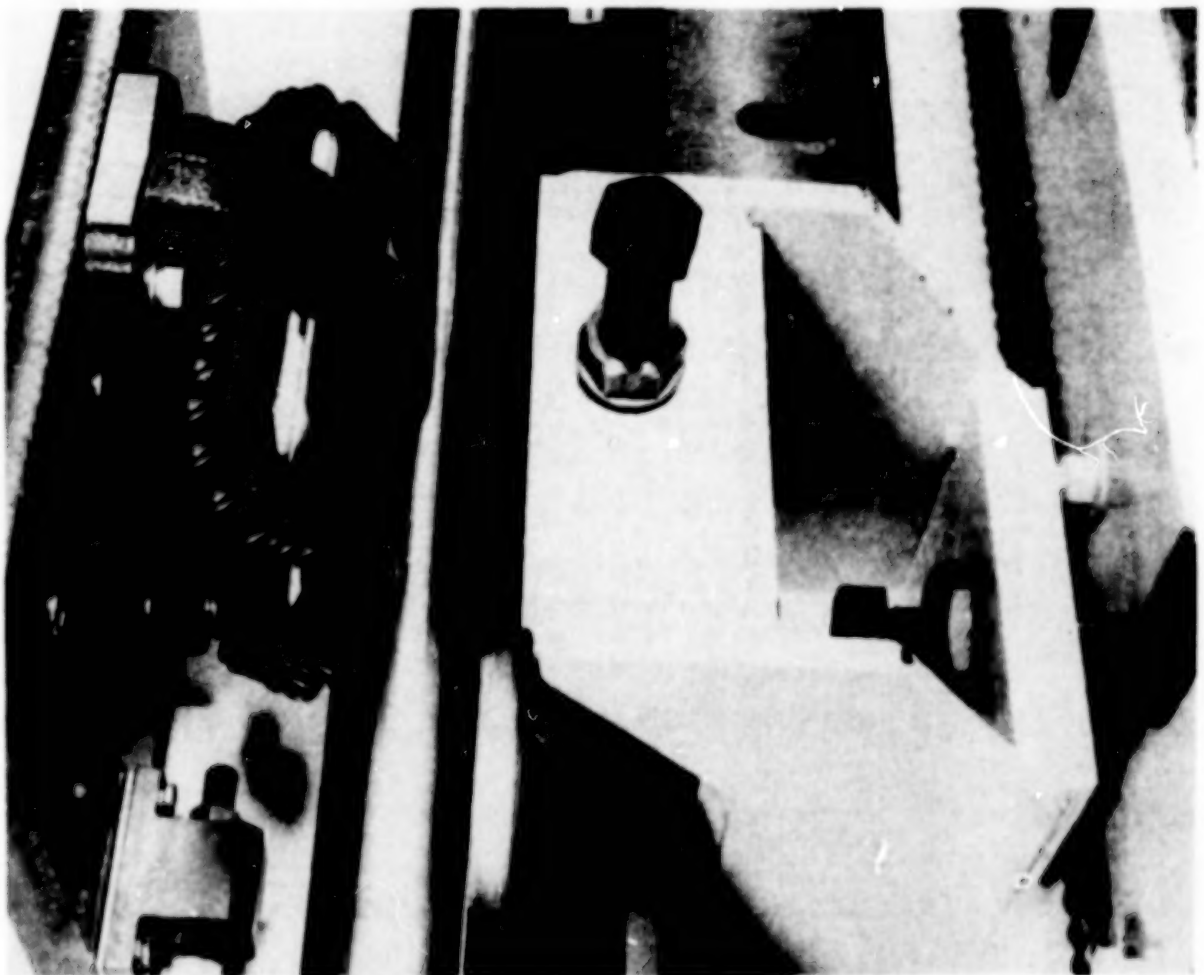
PROBE (VERTICAL) CART DRIVE SYSTEM

The DC drive motor and tachometer, electric brake, synchronous belt reduction setup and vertical drive output shaft (driving the chain sprockets) are shown for the Probe (Vertical) Cart. The probe cart is fully counterweighted and can be positioned within ± 0.001 in.



HORIZONTAL RAIL ADJUSTMENT SYSTEM

The 2" diameter horizontal guide rail and rail adjustment bracket are shown for the front rail of the horizontal cart. V-type linear roller bearings are used to support the corners of the horizontal cart along the front guide rail. The differential screw arrangement for horizontal and vertical rail adjustment is also shown. (The screw is threaded into a nut which is then threaded into the bracket.) If the screw for the horizontal rail adjustment is held stationary and the nut is turned, a one-quarter turn of the nut will adjust the rail horizontally by 0.001 in. All other vertical and horizontal guide rails have similar adjustment mechanisms. These simple accurate rail adjustment features in conjunction with the laser interferometer straightness system will permit frequent verification (and adjustment as required) of system positional alignment.



NEAR-FIELD ANTENNA TEST FACILITY FRONT RAIL VERTICAL STRAIGHTNESS PLOT

During the early stages of assembly a laser interferometer straightness plot was taken of the vertical motion of the horizontal cart as it moved along the front or longer horizontal rail. A straight line was then fitted through the plot using the least squares fit method and the rms deviation from the least squares fit computed as 379 μ in. or 0.0004 in. This vertical motion will be amplified horizontally at the antenna probe in the direction of the antenna boresight. However, these small measured deviations are consistent with the design scan plane accuracy goal of ± 0.002 in. Since this plot was taken, additional rail support brackets have been installed in order to reduce the oscillating motion shown on the plot. (Note also: the west end of the rail appears 4500 μ in. higher than the east end due largely to the limitations of accurately leveling the laser head with our present test setup).

NEAR-FIELD ANTENNA TEST FACILITY FRONT RAIL VERTICAL STRAIGHTNESS PLOT

DATE: March 25, 1982

RAIL: 8

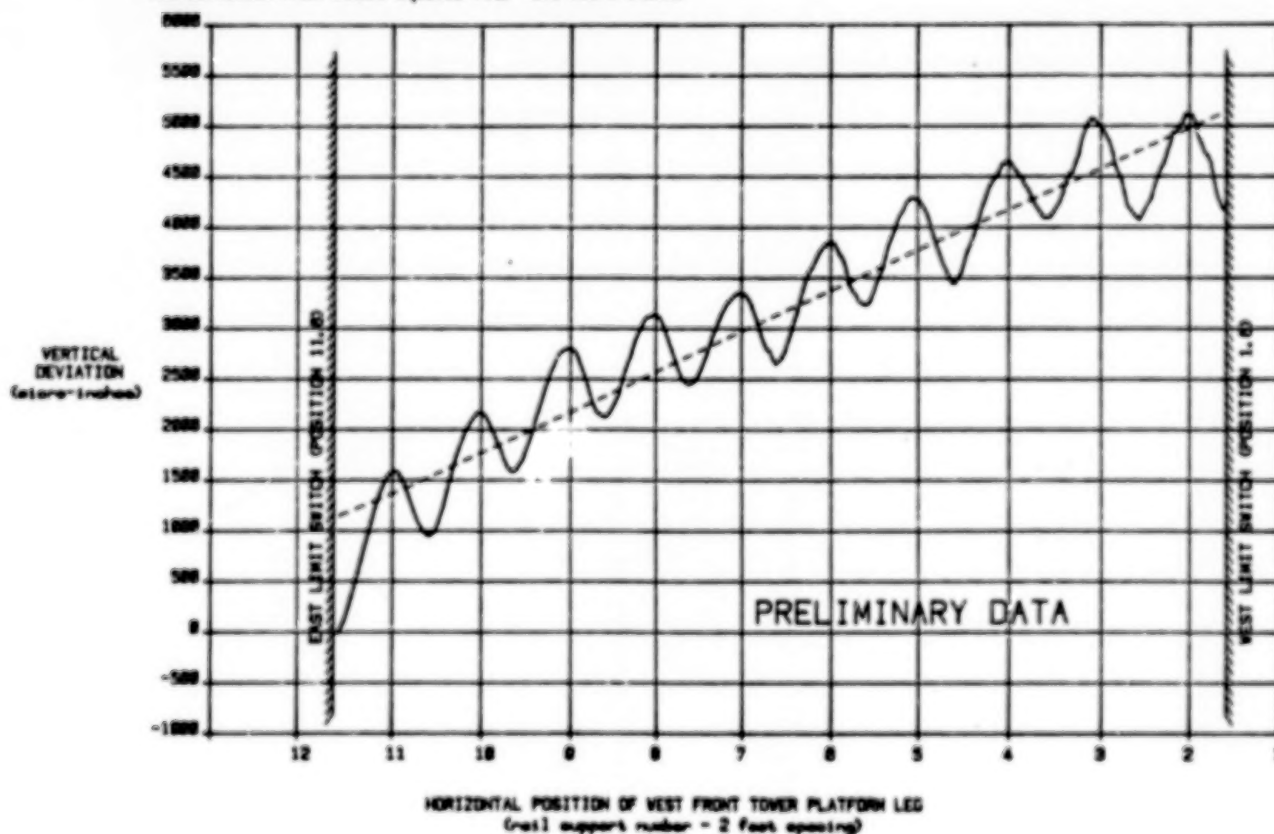
SCAN DIRECTION: East to West

COMMENT: Machine on platform

Max deviation from least squares fit: 1150 micrometers (at position 11.0)

Mean deviation from least squares fit: 315 micrometers

RMS deviation from least squares fit: 379 micrometers



LARGE NEAR-FIELD ANTENNA SCANNER DESIGN PHILOSOPHY

It is essential that large delicate space based antennas or scale models of extremely large (300-m) antennas be tested with the antenna boresight vertical in order to minimize antenna sag and misalignment due to gravity. In order to simulate "0" g in testing a large flexible antenna in the vertical boresight position, it will be necessary to support the reflector centrally and at many points along radial lines emanating from the center of the antenna (along the reflector aperture ribs if the reflector has ribs). In order to keep this support simple and inexpensive it is essential that the antenna not be moved.

It is also essential that the moving mass of the scanner be kept as low as is reasonably possible so that the scanner deflection criteria can be met with a minimum amount of structural steel.

Since scanner alignment on such a large structure would be a very labor intensive operation, it should be made as easy and simple as possible.

An automated antenna probe positioning system (along the antenna boresight axis) should be employed only if absolutely necessary owing to the additional cost, complexity and reliability problems of such a system. Instead, long term scanner dimensional stability should be emphasized. Any phase errors caused by boresight axis probe position errors could then be corrected by measuring the position error and correcting the phase data before the far-field pattern is calculated.

- o ANTENNA SHALL BE TESTED WITH BORESIGHT VERTICAL
-PROVISION MUST BE MADE TO SUPPORT ANTENNA OVER A WIDE AREA
(MANY SUPPORTS) TO SIMULATE 0 g
- o ANTENNA SHALL NOT BE MOVED
- o ANTENNA ERECTION AND SUPPORT SHALL BE KEPT SIMPLE
- o MOVING MASS OF SCANNER SHALL BE MINIMIZED
- o PROVIDE FOR SIMPLE EASILY ADJUSTED SCANNER DIMENSIONAL ALIGNMENT

SCANNER CHARACTERISTICS

The capabilities of the existing 22' x 22' horizontal antenna boresight scanner and the planned 60' x 60' vertical antenna boresight scanner are compared in this chart.

It is not necessary to move the antenna for either scanner. However, with the antenna boresight horizontal, "0" g is difficult to simulate due to the complex antenna support system needed to eliminate antenna sag on large antennas.

Very complex tests (of physically large antennas at high frequency and even including testing of assembled spacecraft) can be accomplished using the large 60' x 60' vertical boresight antenna scanner.

60 X 60' NEAR-FIELD SCANNER 22' X 22' NEAR-FIELD SCANNER

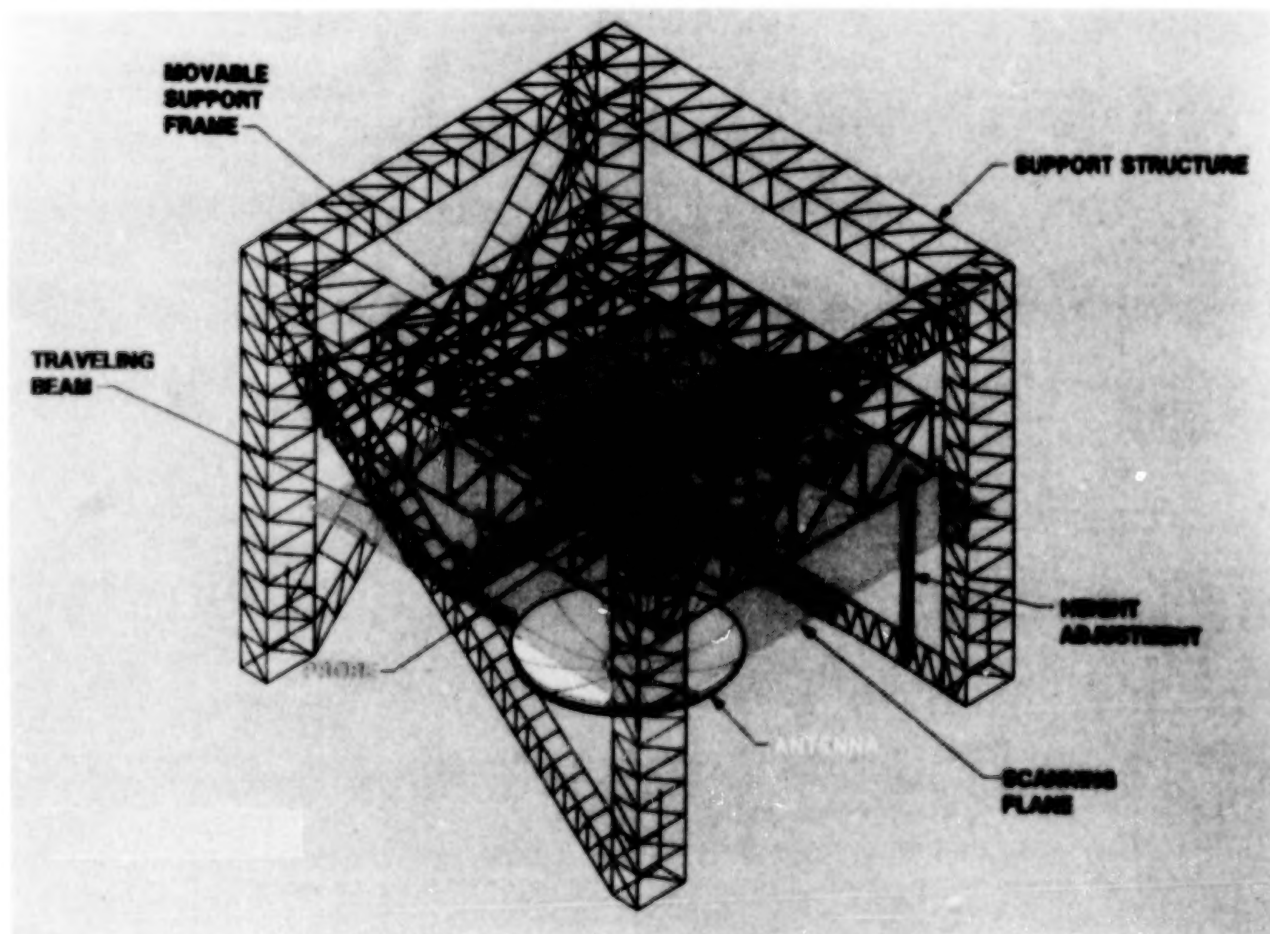
ANTENNA ORIENTATION SCANNING PLANE MOUNTING/SUPPORT CONSIDERATIONS	BORESIGHT VERTICAL HORIZONTAL ANTENNA NOT MOVED DURING TEST ANTENNA CAN EASILY BE SUPPORTED OVER WIDE AREA TO SIMULATE "0" g	BORESIGHT HORIZONTAL VERTICAL ANTENNA NOT MOVED DURING TEST "0" g DIFFICULT TO SIMULATE DUE TO ANTENNA SAG
MAXIMUM ANTENNA APERTURE	D = 15 m (50')	D = 5.5 m (18.3')
MAXIMUM FREQUENCY CAPABILITY	TO 60 GHz	TO 60 GHz +
SCALED TESTING INTEGRATED ANTENNA SYSTEMS TESTING	TO $D/\lambda = 3,000$ CAN DO IN SITU TESTING OF ANTENNAS OF SPACECRAFT OR SPACECRAFT SIMULATORS	TO $D/\lambda = 1100+$ LIMITED CAPABILITY

60' x 60' VERTICAL BORESIGHT NEAR-FIELD PLANAR SCANNER

The stationary scanner support structure will consist of a truss structure composed of four vertical columns coupled together by horizontal trusses at the top and fully cross-braced with trusses to prevent scanner sideways. A vertically adjustable moveable support frame (consisting of a fully triangulated space frame) will be attached to guide rails at the corners of the columns. The scanning plane is described by the motion of the antenna probe tip. The antenna probe will be carried by a probe cart that travels horizontally along a traveling beam truss structure that can also be moved horizontally perpendicular to the motion of the probe cart. Laser interferometer systems will be used to determine guide rail straightness, horizontal axis probe position and vertical position of the moveable support frame.

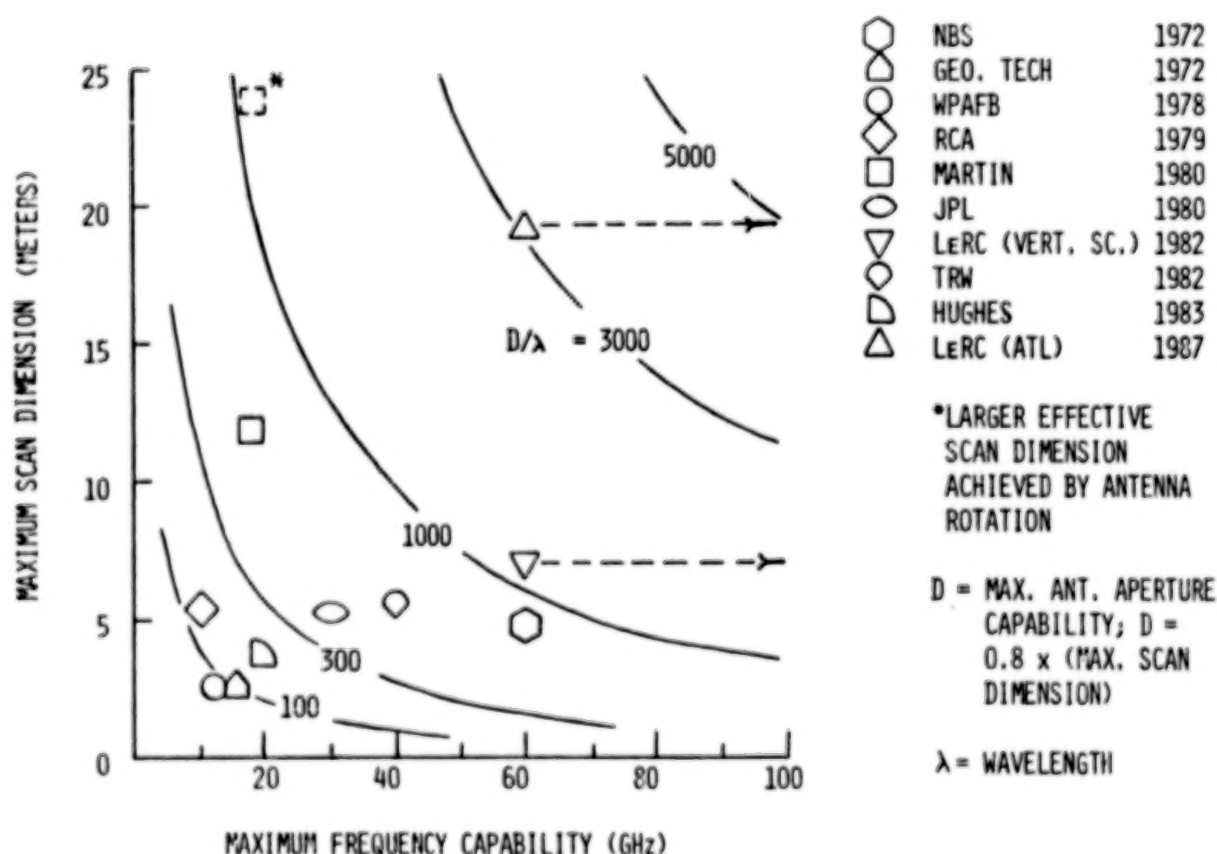
The scanner will be aligned by lowering the moveable support frame and vertically adjusting the horizontal rails on the moveable support platform and the horizontal rails on the traveling beam in order to vertically adjust the probe tip to an accurate plane.

Large (up to 50' aperture) deep (up to 46' deep) antennas will be tested with the moveable support frame raised so that the probe tip clears the highest point of the antenna by a small number of wavelengths. Smaller antennas will be measured by lowering the scan plane to clear the highest point of the antenna by a few wavelengths and then testing over a scan plane smaller than the 60' x 60' maximum capability.



COMPARISON OF U. S. NEAR-FIELD PLANE SCANNER CAPABILITIES

When the maximum scan dimension of currently available near-field planar scanners is plotted against the maximum frequency capability of these scanners, the maximum electrical size of the test antenna D/λ can be parametrically plotted as well. The resulting figure compares the capabilities of the large U. S. near-field facilities in existence (or under construction) with those in existence or planned at LeRC. Each facility is represented by a symbol at the point representing its maximum size and frequency capabilities. Only scanners having a maximum scan dimension of ≥ 2.5 m are shown. The LeRC vertical scanner was designed with appropriate structural stability and alignment precision to support measurements at 60 GHz without corrections. Based on achieved position accuracies, operation could be extended to 100 GHz with first-order corrections for systematic errors. Based on this, the potential for extended frequency range for the LeRC horizontal antenna boresight scanner and the vertical boresight 60' x 60' scanner are shown by dashed lines to a frequency capability of 100 GHz.



DATE: DECEMBER 1982

ANTENNA TECHNOLOGY LABORATORY (ATL) DESCRIPTION

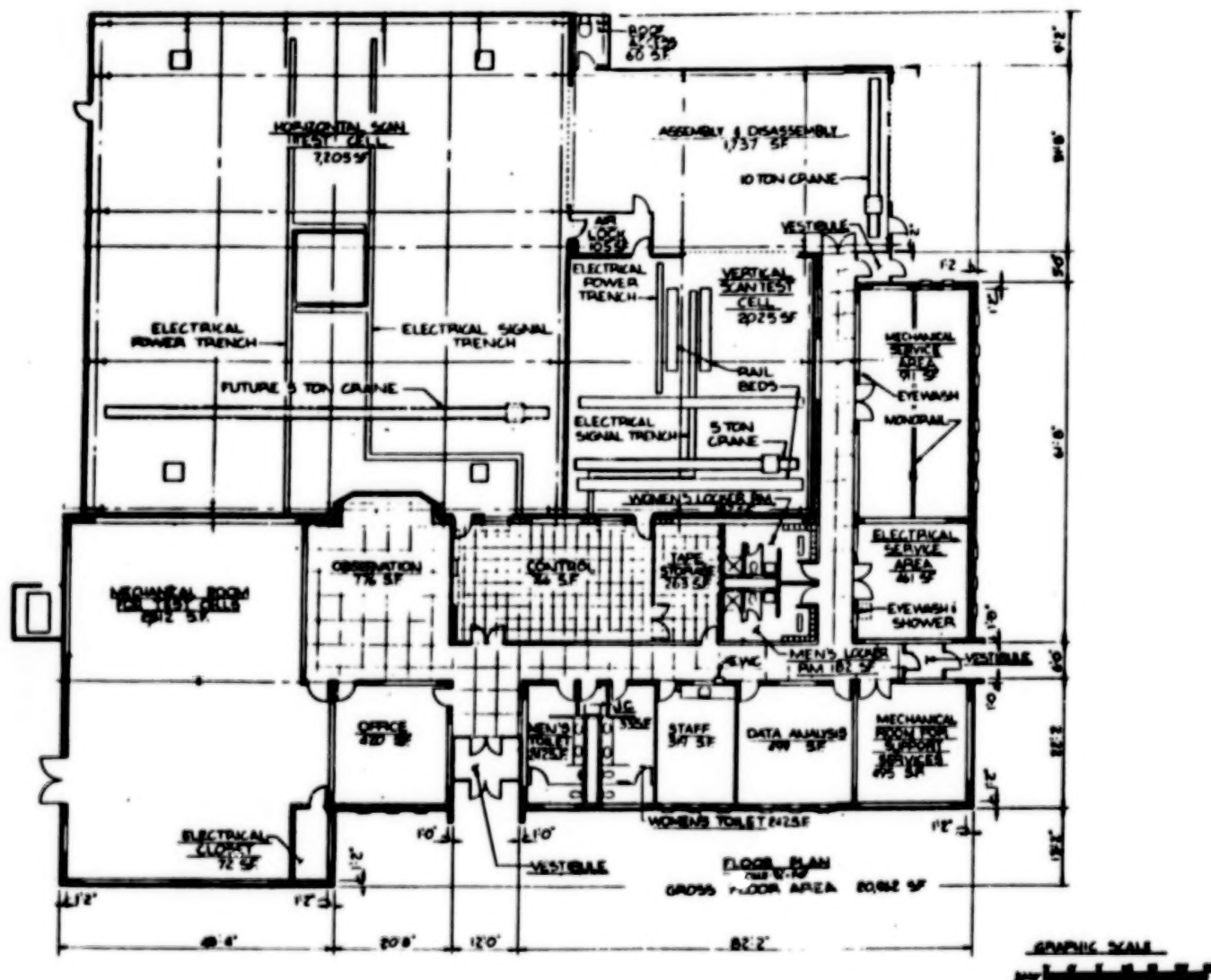
It is planned to permanently house both the existing 22' x 22' scan plane horizontal antenna boresight scanner and the 60' x 60' scan plane vertical antenna boresight scanner in an Antenna Technology Laboratory (ATL). The interior dimensional requirements of the test cells and the environmental specifications for these test cells are given in the figure.

- o LARGE TEST CELL SIZE (FOR 60' X 60' VERTICAL BORESIGHT NEAR-FIELD SCANNER)
INTERIOR DIMENSIONS - 79' X 79' 10" X 71' HIGH (6,300 FT²)
- o SMALL TEST CELL SIZE (FOR 22' X 22' HORIZONTAL BORESIGHT NEAR-FIELD SCANNER)
INTERIOR DIMENSIONS - 42' X 42' X 33' HIGH (1,764 FT²)
- c ENVIRONMENTAL SPECIFICATIONS
 - TEST CELL AND ASSEMBLY AREA AIR FILTRATION
99.97% EFFICIENT ON 0.3 MICRON OR LARGER PARTICLES (PRESSURIZED WITH 25%
OUTSIDE AIR TO MAINTAIN
CLEANLINESS)
 - TEST CELL TEMPERATURE REGULATION
65° LOWEST WINTER TEMPERATURE AND 78° HIGHEST SUMMER TEMPERATURE
1°F TEMPERATURE VARIATION FOR EACH 10 FEET OF HEIGHT VARIATION
 - TEST CELL HUMIDITY REGULATION
40 TO 60% HUMIDITY RANGE

DATE: DECEMBER 1982

ANTENNA TECHNOLOGY LABORATORY FLOOR PLAN

The figure shows the floor plan for the Antenna Technology Laboratory. Large antennas requiring the use of the 60' x 60' scanner would be brought into the assembly and disassembly area where they would be removed from their shipping containers. These antennas would then be mounted to an appropriate cart for transfer to the large test cell. There, the antennas would be mounted and supported from as many points as necessary on a concrete floor in order to compensate for deflections caused by the force of gravity.



CONCLUSIONS

The direction of future antenna technology will be toward antennas which are large, both physically and electrically, will operate at frequencies up to 60 GHz, and are non-reciprocal and complex, implementing multiple-beam and scanning beam concepts and monolithic semiconductor devices and techniques.

The acquisition of accurate antenna performance measurements is a critical part of the advanced antenna research program and represents a substantial antenna measurement technology challenge, considering the special characteristics of future spacecraft communications antennas.

Comparison of various antenna testing techniques and their relative advantages and disadvantages shows that the near-field approach is necessary to meet immediate and long-term testing requirements.

The LeRC facilities, the 22' x 22' horizontal antenna boresight planar scanner and the 60' x 60' vertical antenna boresight planar scanner (with a 60 GHz frequency and $D/\lambda = 3000$ electrical size capabilities), will meet future program testing requirements.

- o SPACE BASED COMMUNICATIONS ANTENNAS ARE RAPIDLY BECOMING PHYSICALLY LARGER, MORE COMPLEX AND ARE OPERATING AT EVER HIGHER FREQUENCIES
- o ACCURATE MEASUREMENT OF THE PERFORMANCE OF THESE ANTENNAS IS ESSENTIAL
- o THE NEAR-FIELD ANTENNA MEASUREMENT TECHNIQUE IS THE MOST FEASIBLE TECHNIQUE FOR OBTAINING THIS MEASUREMENT DATA
- o NEAR-FIELD ANTENNA MEASURING FACILITIES CAPABLE OF ACCURATELY MEASURING LARGE, HIGH FREQUENCY ANTENNAS WILL BE REQUIRED TO MEET FUTURE PROGRAM TESTING REQUIREMENTS
- o THE LeRC 22' X 22' AND 60' X 60' PLANAR NEAR-FIELD SCANNERS WILL MEET THESE FUTURE REQUIREMENTS

REFERENCE

1. Wachter, Paul F.: A Qualitative Survey of Near Field Analyses and Measurements. NBSIR 79-1602, National Bureau of Standards, 1979.

THE NEED FOR SPACE FLIGHT EXPERIMENTS
AND TESTING IN THE DEVELOPMENT OF
LARGE SPACE ANTENNA SYSTEMS TECHNOLOGY

Earle K. Huckins III
NASA Langley Research Center
Hampton, Virginia

Large Space Antenna Systems Technology - 1982
NASA Langley Research Center
November 30 - December 3, 1982

INTRODUCTION

- o TECHNOLOGY DEVELOPMENT FOR LARGE SPACE ANTENNA SYSTEMS CONTINUES TO BE A HIGH-PRIORITY OBJECTIVE BASED ON THE BELIEF THAT
 - LARGE ANTENNAS ARE "NEEDED"
 - FURTHER DEVELOPMENT IS NECESSARY TO REDUCE THE COST AND TECHNICAL RISK TO ACCEPTABLE LEVELS
- o MANY ELEMENTS OF THE TECHNOLOGY PROGRAM ARE REACHING A HIGH LEVEL OF MATURITY IN GROUND-BASED DEVELOPMENT
- o HOWEVER, THE ULTIMATE MEASURE OF SUCCESS IN THESE PROGRAMS IS THE DEGREE TO WHICH THE TECHNOLOGY IS UTILIZED IN FLIGHT SYSTEMS

IN NASA....

**WE WILL SELL NO
FLIGHT EXPERIMENT
BEFORE ITS TIME**

WHAT DO WE MEAN BY A "FLIGHT EXPERIMENT"?

IN SPACE SYSTEMS

- o A FLIGHT EXPERIMENT IS

- A TECHNOLOGY DEVELOPMENT ACTIVITY TO
OBTAIN FLIGHT DATA
FLIGHT VALIDATE A TECHNIQUE, COMPONENT, OR SYSTEM

- o THE FLIGHT EXPERIMENT INCLUDES

- TEST HARDWARE
TEST OBJECTIVES AND PROCEDURES

- o FLIGHT EXPERIMENTS ARE USUALLY CHARACTERIZED BY

- RELATIVELY HIGH COST
LIMITED OPPORTUNITIES
HIGH VISIBILITY
FOCUSED PROJECT - TYPE ACTIVITIES

WHAT CONDITIONS ARE USUALLY NECESSARY FOR A "FLIGHT EXPERIMENT" TO BE UNDERTAKEN ?

- o A NEED FOR THE TECHNOLOGY TO BE DEVELOPED

- o THE TECHNOLOGICAL CAPABILITY IS REQUIRED FOR A BROAD RANGE OF FUTURE HIGH-PRIORITY MISSIONS
 - o THE TECHNOLOGICAL CAPABILITY IS NEEDED IN DIRECT SUPPORT OF A SPECIFIC PLANNED MISSION

- o A SPECIFIC "NEED" FOR FLIGHT EXPERIMENTATION TO COMPLETE THE TECHNOLOGY DEVELOPMENT

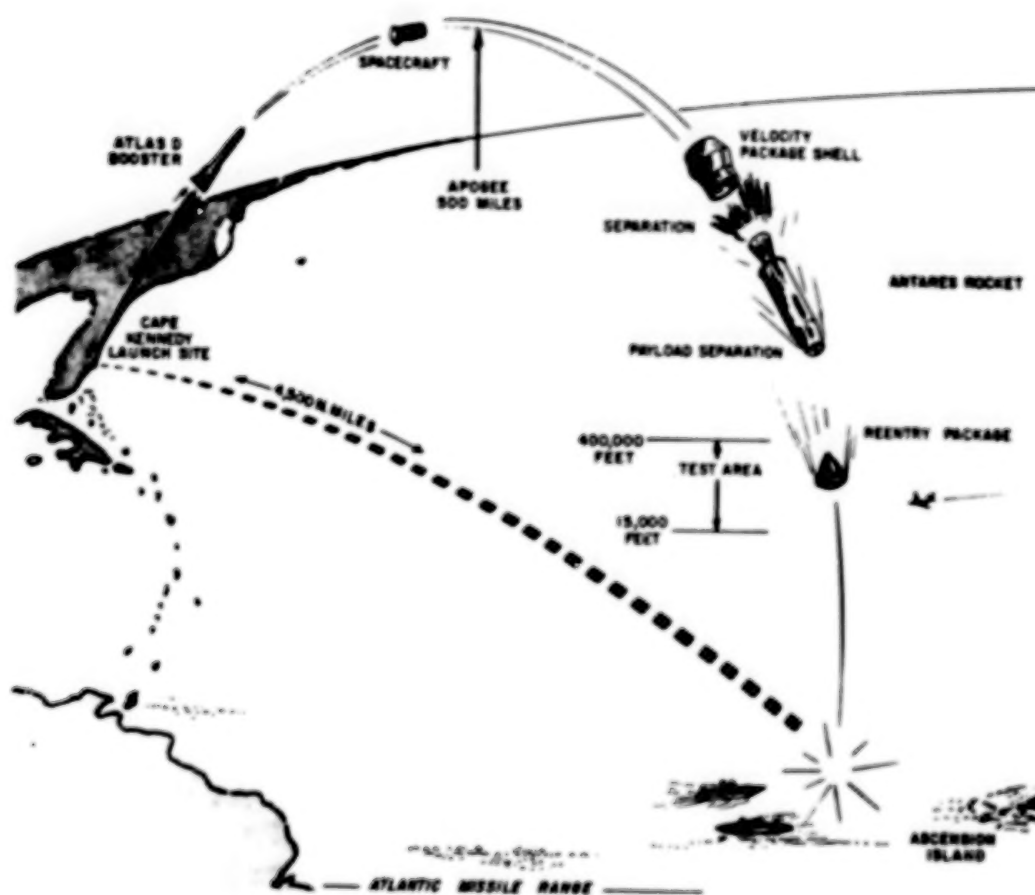
- o THE TECHNOLOGY IS A CLEAR DEPARTURE FROM DESIGN PRACTICE AND/OR FLIGHT EXPERIENCE
 - o THE TECHNOLOGY INVOLVES FLIGHT-SENSITIVE PARAMETERS

**MANY EXAMPLES FROM
THE PAST ILLUSTRATE
THIS HYPOTHESIS**

**FLIGHT EXPERIMENTS IN THE MANNED
SPACECRAFT PROGRAM**

TECHNOLOGY : HEAT SHIELDS FOR BALLISTIC REENTRY

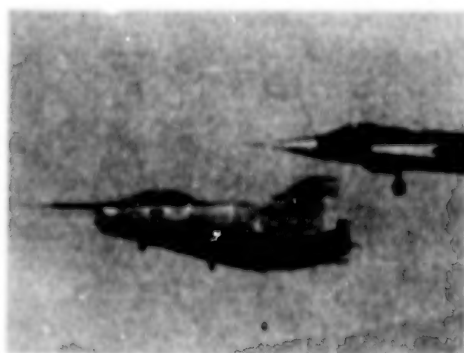
MISSION NEED	FLIGHT EXPERIMENT NEEDS	FLIGHT EXPERIMENTS (Typical)
<hr/>	<hr/>	<hr/>
<ul style="list-style-type: none">o CAPABILITY TO SUCCESSFULLY REENTER THE ATMOSPHERE FROM ESCAPE VELOCITY (25,000 MILES PER HOUR)	<ul style="list-style-type: none">o NO CAPABILITY EXISTED FOR GROUND-BASED SIMULATIONo ANALYTICAL PREDICTIONS VARIED BY AN ORDER OF MAGNITUDE	<ul style="list-style-type: none">o PROJECT FIRE

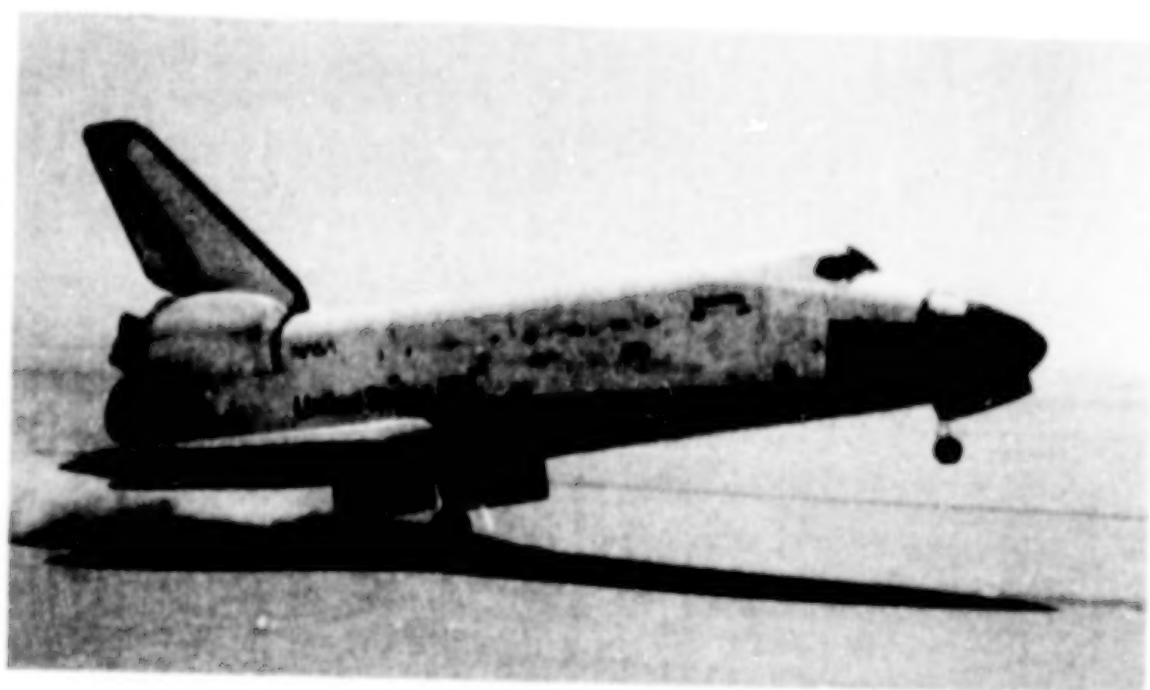


FLIGHT EXPERIMENTS IN SPACE SHUTTLE DEVELOPMENT

TECHNOLOGY : LIFTING REENTRY BODIES

<u>MISSION NEED</u>	<u>FLIGHT EXPERIMENT NEED</u>	<u>FLIGHT EXPERIMENTS (Typical)</u>
o CAPABILITY TO	o NO SIMULATION CAPABILITY	M-2
o REENTER	o NO FLIGHT EXPERIENCE	HL-10
o MANEUVER		
o LAND LIKE CONVENTIONAL AIRCRAFT		





FLIGHT EXPERIMENTS IN PLANETARY SPACECRAFT

TECHNOLOGY : AERODYNAMIC DECELERATION IN LOW-DENSITY ATMOSPHERES

MISSION NEED

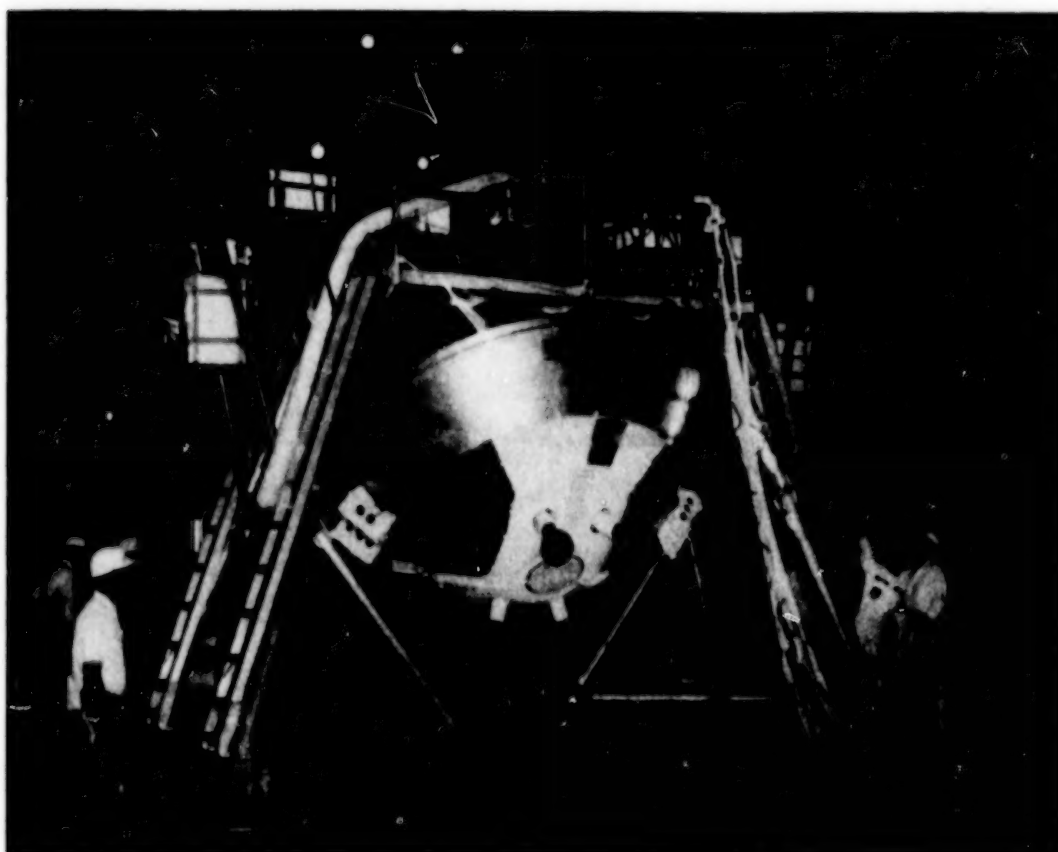
- o DECELERATE THE
VIKING LANDER FOR
TERMINAL DESCENT

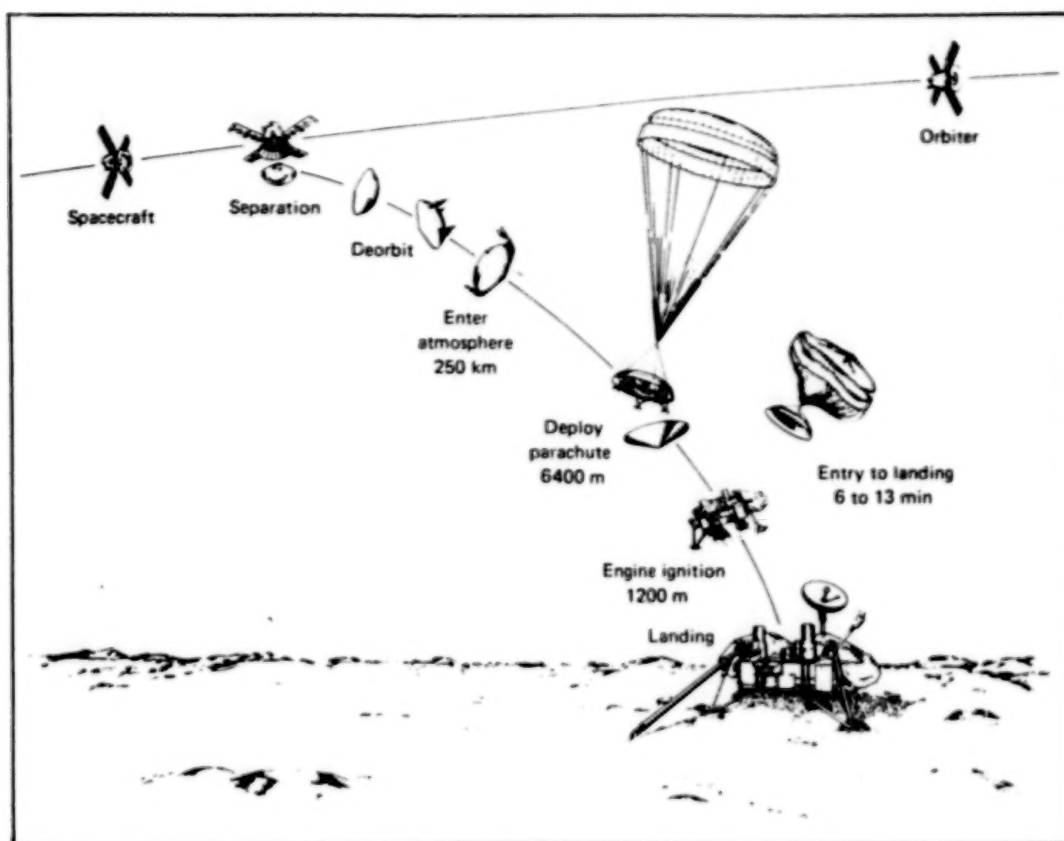
FLIGHT EXPERIMENT NEEDS

- o NO EXISTING EXPERIENCE
WITH PARACHUTE DEPLOYMENT
IN LOW DYNAMIC PRESSURES
- o NO SIMULATION CAPABILITY

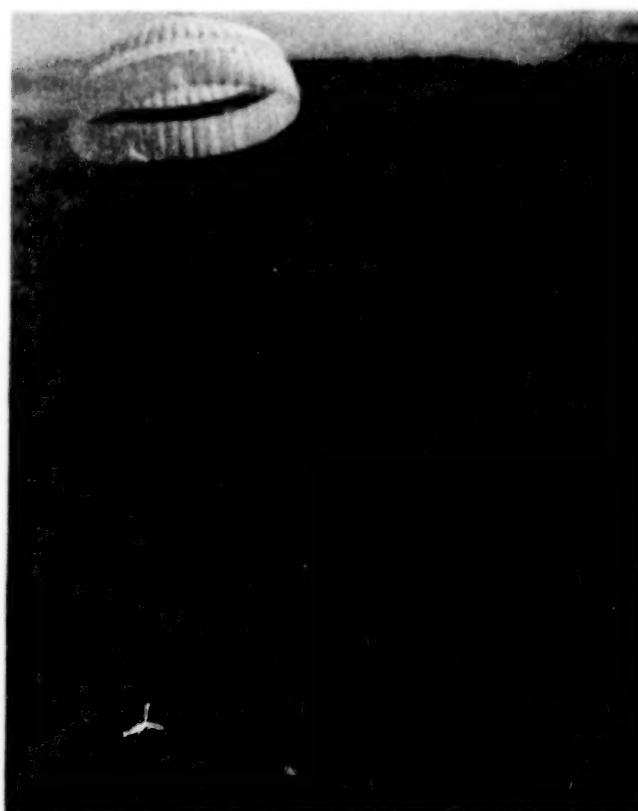
FLIGHT EXPERIMENTS (Typical)

- o PEPP
(PLANETARY ENTRY
PARACHUTE PROGRAM)
- o BLDT
(THE BALLOON-LAUNCHED
DECELERATOR TEST)





[From ref. 1]



OBSERVATIONS ON THE PAST

SPACE FLIGHT EXPERIMENTS WERE UNDERTAKEN WHEN

- o A NEED FOR THE TECHNOLOGY WAS
CLEARLY ESTABLISHED
- o DEVELOPMENT OF THE TECHNOLOGY
REQUIRED FLIGHT EXPERIMENTS

SO WHAT DOES THIS SAY ABOUT

LARGE SPACE ANTENNA SYSTEMS

and , in particular, about

FLIGHT EXPERIMENTS

IN

LARGE SPACE ANTENNA SYSTEMS?

FIRST....WHAT IS A

LARGE SPACE ANTENNA SYSTEM ?

... IT IS A LARGE-AREA SPACECRAFT SYSTEM FOR TRANSMITTING AND/OR RECEIVING
ELECTROMAGNETIC ENERGY



LARGE ENOUGH THAT

IT CANNOT BE TRANSPORTED TO SPACE IN AN OPERATIONAL
CONFIGURATION AND MUST BE

- DEPLOYED
- SPACE ASSEMBLED

STRUCTURAL DENSITY MUST BE LOW

- DIFFICULT (IF NOT IMPOSSIBLE) TO GROUND TEST
- WILL REQUIRE MULTIPOINT CONTROL AND BE
SUBJECT TO STRONG INTERACTIONS BETWEEN THE
STRUCTURAL AND CONTROL SYSTEMS

LARGE SPACE ANTENNA SYSTEMS **ARE "NEEDED"**

BECAUSE

- o MANAGEMENT OF ELECTROMAGNETIC ENERGY IN SPACE

- COLLECTING
- FOCUSING
- RECEIVING (SENSING)
- REFLECTING
- TRANSMITTING

IS ONE OF THE MOST IMPORTANT FUNCTIONS OF SPACECRAFT SYSTEMS

- o IN THE MANAGEMENT OF ELECTROMAGNETIC ENERGY, THERE ARE FEW GOOD SUBSTITUTES FOR PHYSICAL APERTURE

SPECIFIC NEEDS FOR FLIGHT EXPERIMENTS **IN LARGE SPACE ANTENNA SYSTEMS**

(WHAT ARE THE SIGNIFICANT
DEPARTURES FROM CURRENT DESIGN PRACTICE
INVOLVING FLIGHT-SENSITIVE PARAMETERS?)

- o SPACE-BASED FUNCTIONAL TESTING
 - o FULL-SCALE DEPLOYMENT
 - o STRUCTURAL ALIGNMENT AND SURFACE ACCURACY
- o MULTIPOINT CONTROL OF HIGHLY FLEXIBLE SPACE SYSTEMS

DEPLOYMENT OF "LARGE" SPACE ANTENNA SYSTEMS

CURRENT DESIGN PRACTICE

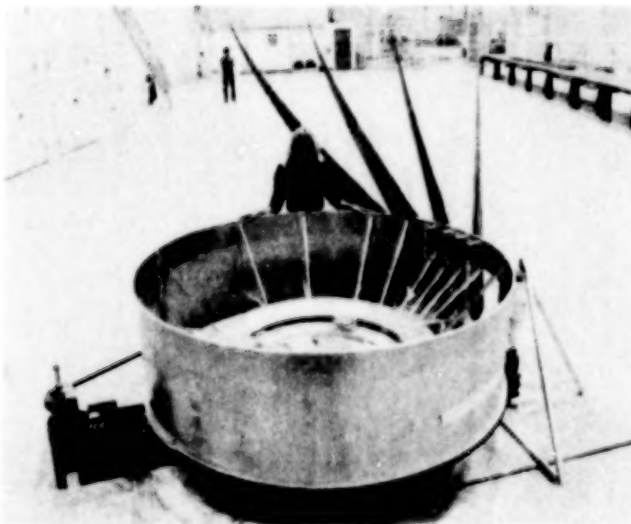
- o ATS-F
- o WRAP-RIB
- o METAL RIBS
- o 9-M

ADVANCED DEVELOPMENT

- o 4-GORE TEST ARTICLE
- o WRAP-RIB
- o COMPOSITE RIBS
- o 55-M

NEED ULTIMATE

- o HIGH CONFIDENCE
THAT LARGE
ANTENNA CAN
BE SUCCESSFULLY
DEPLOYED IN SPACE



STRUCTURAL ALIGNMENT AND SURFACE ACCURACY IN "LARGE" SPACE ANTENNA SYSTEMS

CURRENT DESIGN PRACTICE

TDRSS

- o RADIAL RIB
- o 6-M
- o 15 GHz

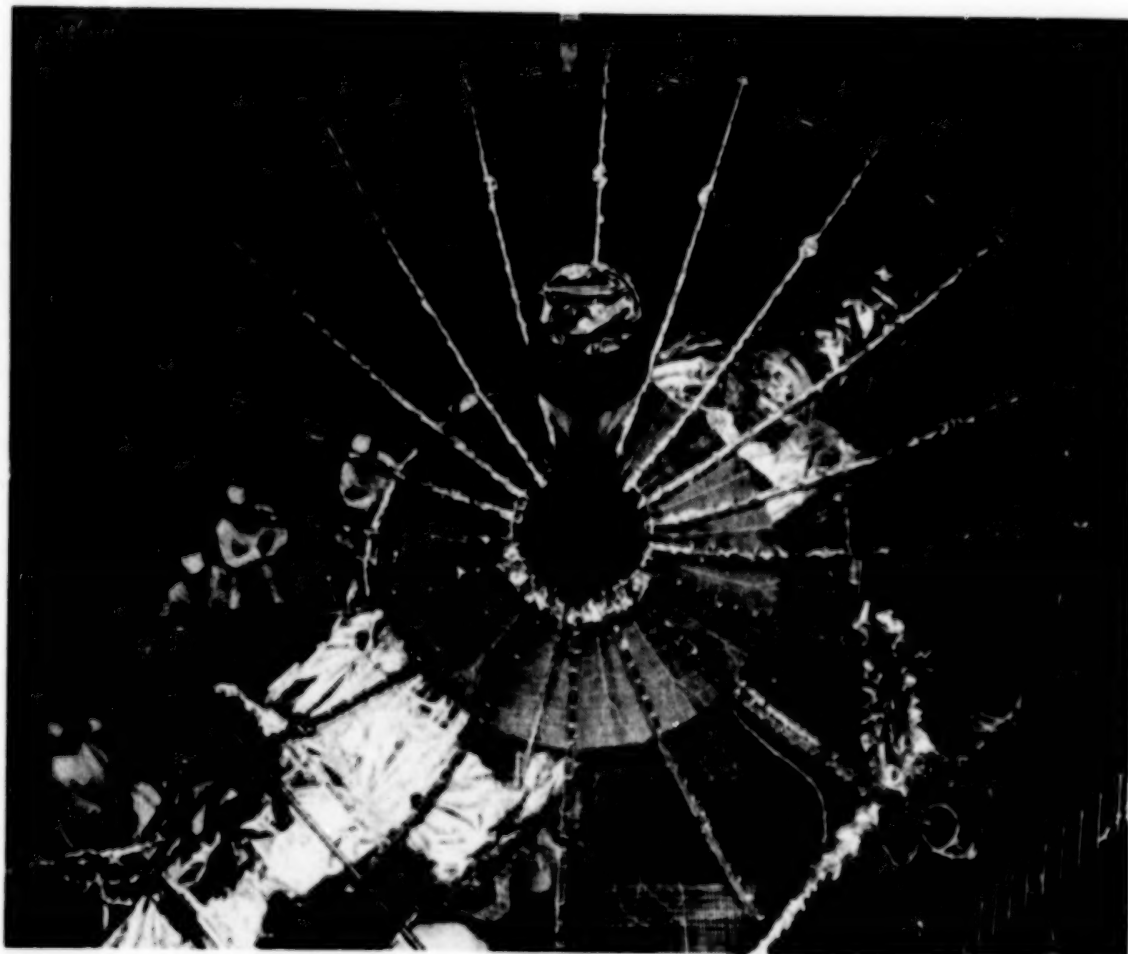
ADVANCED DEVELOPMENT

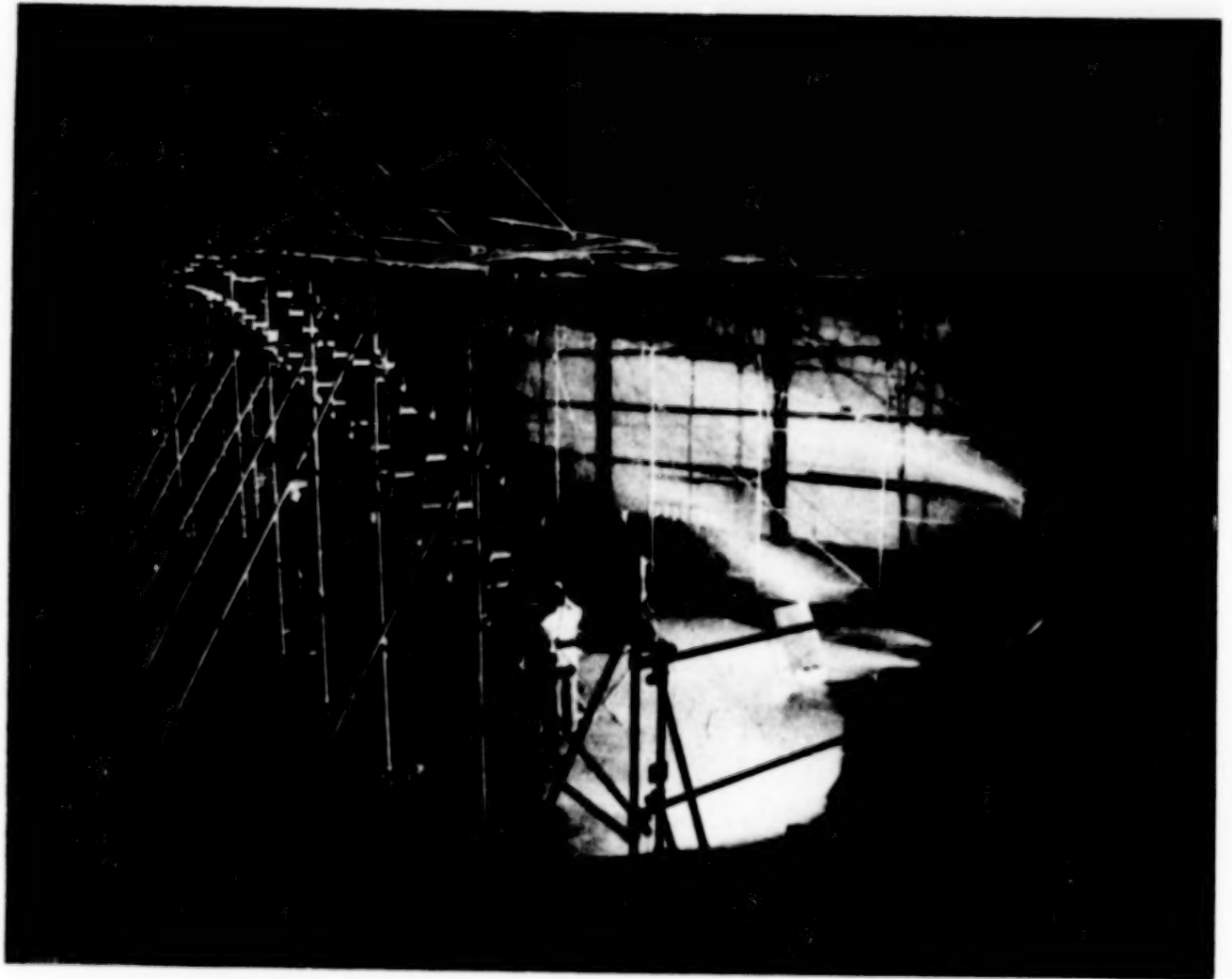
4-GORE SURFACE BREADBOARD

- o HOOP-COLUMN CONCEPT
- o 50-M

ULTIMATE NEED

- o HIGH CONFIDENCE
THAT REQUIRED
SURFACE ACCURACY
CAN BE ACHIEVED
IN SPACE





CONTROL OF HIGHLY FLEXIBLE SPACECRAFT

CURRENT DESIGN PRACTICE

- o CONTROL OF "RIGID"
SPACECRAFT WITH
LOCALIZED FLEXIBILITIES

ADVANCED DEVELOPMENT

(Typical)

LOCKHEED

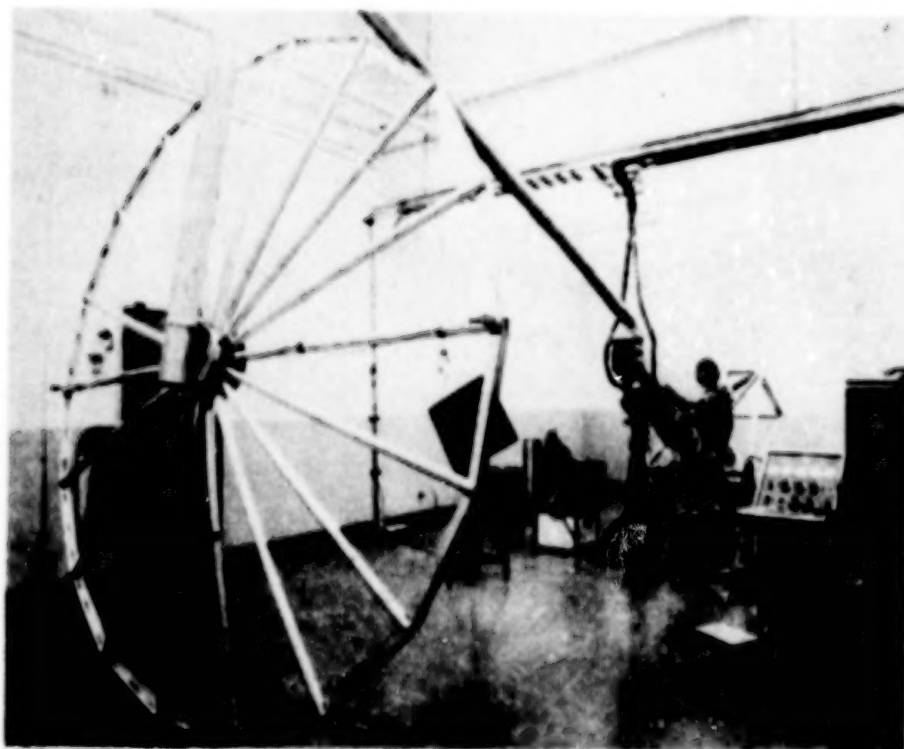
PROOF OF CONCEPT
(P.O.C.)

ULTIMATE NEED

A VALIDATED CAPABILITY
TO PRECISELY POINT AND
CONTROL THE FIGURE OF
STRUCTURAL SYSTEMS
WHICH

--STRONGLY INTERACT
WITH THE CONTROL
SYSTEM

--CANNOT BE
STRUCTURALLY TESTED
ON THE GROUND



SO...., ARE FLIGHT EXPERIMENTS "NEEDED"
FOR THE DEVELOPMENT OF
LARGE SPACE ANTENNA SYSTEMS ?

YES.... BECAUSE

- o LARGE SPACE ANTENNAS ARE "NEEDED"
- o LARGE SPACE ANTENNA SYSTEMS
SIGNIFICANTLY DEPART FROM
CURRENT DESIGN PRACTICE
IN AREAS THAT ARE SENSITIVE TO FLIGHT PARAMETERS
 - o FULL - SCALE DEPLOYMENT FUNCTIONAL TESTING
 - o VALIDATION OF SURFACE ACCURACY
 - o CONTROL OF STRUCTURAL SYSTEMS WHICH
 - STRONGLY INTERACT WITH THE CONTROL SYSTEM
 - CANNOT BE STRUCTURALLY TESTED ON THE GROUND

**"ONE THING WE LEARN
FROM HISTORY....**

IS THAT WE NEVER
LEARN FROM HISTORY"

EPILOG

- o WE STILL HAVE NOT FOUND THE HARD USER FOR LARGE SPACE ANTENNA SYSTEMS
- o HOWEVER
 - o "LARGE" SPACE ANTENNAS REPRESENT A PLATEAU IN SPACECRAFT TECHNOLOGY RATHER THAN EVOLUTIONARY DEVELOPMENT
 - o AND IN SUCH CASES
IDENTIFICATION OF THE FULL MISSION POTENTIAL USUALLY
FOLLOWS TECHNOLOGY DEMONSTRATION
- o WE SHOULD THEREFORE
 - o PRESS ON WITH THE GROUND - BASED TECHNOLOGY DEVELOPMENT
 - o DOUBLE OUR EFFORTS TO "SELL" A WELL - CONCEIVED SYSTEMS TECHNOLOGY FLIGHT EXPERIMENT TO ALL POTENTIAL USERS UNTIL
 - o THE USERS BECOME CONSTITUENTS
 - o THE "NEEDS" MOTIVATE A COMMITMENT

REFERENCE

1. Viking I: Early Results. NASA SP-408, 1976.

A ROBOT IN SPACE AS A LARGE SPACE STRUCTURES CONTROL EXPERIMENT

Richard Gran
Grumman Aerospace Corp.
Bethpage, New York

Large Space Antenna Systems Technology - 1982
NASA Langley Research Center
November 30 - December 3, 1982

BEST AVAILABLE COPY.

CONTROL DESIGN ISSUES

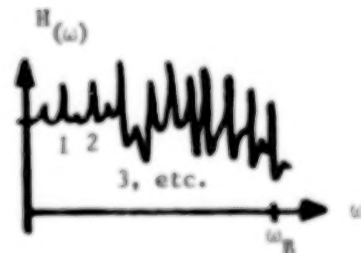
The control systems design issues for large space structure were described in a previous paper in this compilation (ref. 1). The figure below shows the issues in summary form. Each of them can be addressed by a robotics experiment. Thus the following figure gives the seven reasons that an experiment which defines a teleoperator or a robot or uses the RMS can be effective in answering the major LSS control systems design issues.

LSS CONTROL

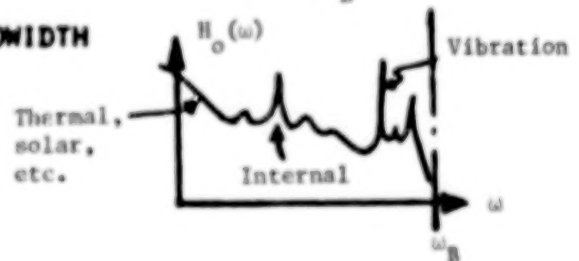
ROBOTICS IN SPACE



DYNAMICS OF COMBINED FLEXIBLE AND RIGID BODY



DISTURBANCES AND THEIR EFFECT ON CONTROL BANDWIDTH



NON-COLLOCATED SENSORS AND ACTUATORS

CONTROL SYSTEM DESIGN ISSUES

1. BOTH LSS AND ROBOTS IN SPACE HAVE MANY CLOSELY SPACED STRUCTURAL MODES BECAUSE OF THE USE OF LIGHTWEIGHT MATERIALS.
2. THE CONTROL REQUIREMENTS ARE DICTATED BY THE DISTURBANCES EXPECTED AND THE SPEED OF RESPONSE REQUIRED TO ADEQUATELY MEET THE MISSION REQUIREMENTS.
3. FOR ROBOTS, SPEED IS OFTEN SACRIFICED TO MAKE THE STRUCTURAL INTERACTIONS UNIMPORTANT (DITTO FOR LSS CONTROL). THE REQUIREMENTS ARE OFTEN COMPROMISED BY THIS APPROACH (ACCURACY IS LOST OR SPEED OF MOTION AND WASTED TIME FOR A ROBOT RESULTS).
4. IF THE CONTROL BANDWIDTH IS MADE LARGE, THEN A STRUCTURAL AND CONTROL INTERACTION RESULTS.
5. GEOMETRY CHANGES MAKE THE CONTROL STRUCTURAL INTERACTION DIFFICULT TO DEAL WITH (MODES CHANGE WITH GEOMETRY, BOTH THEIR FREQ. AND SHAPE).
6. TO COPE WITH GEOMETRY CHANGES THERE MUST BE SOME FORM OF ADAPTATION.
7. SINCE MOTION OF THE END EFFECTOR IS CRITICAL, AND SINCE THE CONTROL IS NOT ACHIEVED BY MOVING ONLY THE END EFFECTOR (ONLY THE ROBOT'S JOINTS), NON-COLLOCATION OF SENSORS AND ACTUATORS IS THE NORM, NOT THE EXCEPTION.,

TRIPLE-DUTY ROBOT/LSS CONTROL EXPERIMENT

The robot experiment does triple duty. It gives a robotics control demonstration, it brings the large space structures control technology to an effective state of readiness, and it could provide a useful robot when the experiment is finished.

1. DEMONSTRATE ROBOT CONTROL FOR FAST MANIPULATOR

- O GEOMETRY CHANGES**
- O NON-COLOLOCATION**
- O WIDE BANDWIDTH**

2. DEMONSTRATE LSS CONTROL

- O ACCOMMODATE WIDEBAND DISTURBANCES**
- O PLUS ALL ISSUES ABOVE**

3. DESIGN AND DEMONSTRATE A DEXTROUS MANIPULATOR

OPTIONS

There are three major options in such an experiment. First, use the RMS. Because of design limitations, safety of flight considerations, and difficulty with modifications of the computer for the RMS controller, this may not be the most desirable alternative.

Second, use a flexible arm that is going to be put on the Shuttle for other reasons (such as the handling and positioning aid (HPA)). Third, design a new dextrous manipulator or teleoperator.

1. USE THE RMS

- * TO MAKE NON-COLLOCATED SENSORS AND ACTUATORS,
USE FEEDBACK FROM THE END EFFECTOR
- * GEOMETRY CHANGES ARE THERE
- * INCREASE BANDWIDTH OF CONTROL BY MOVING RMS FASTER

2. USE HPA

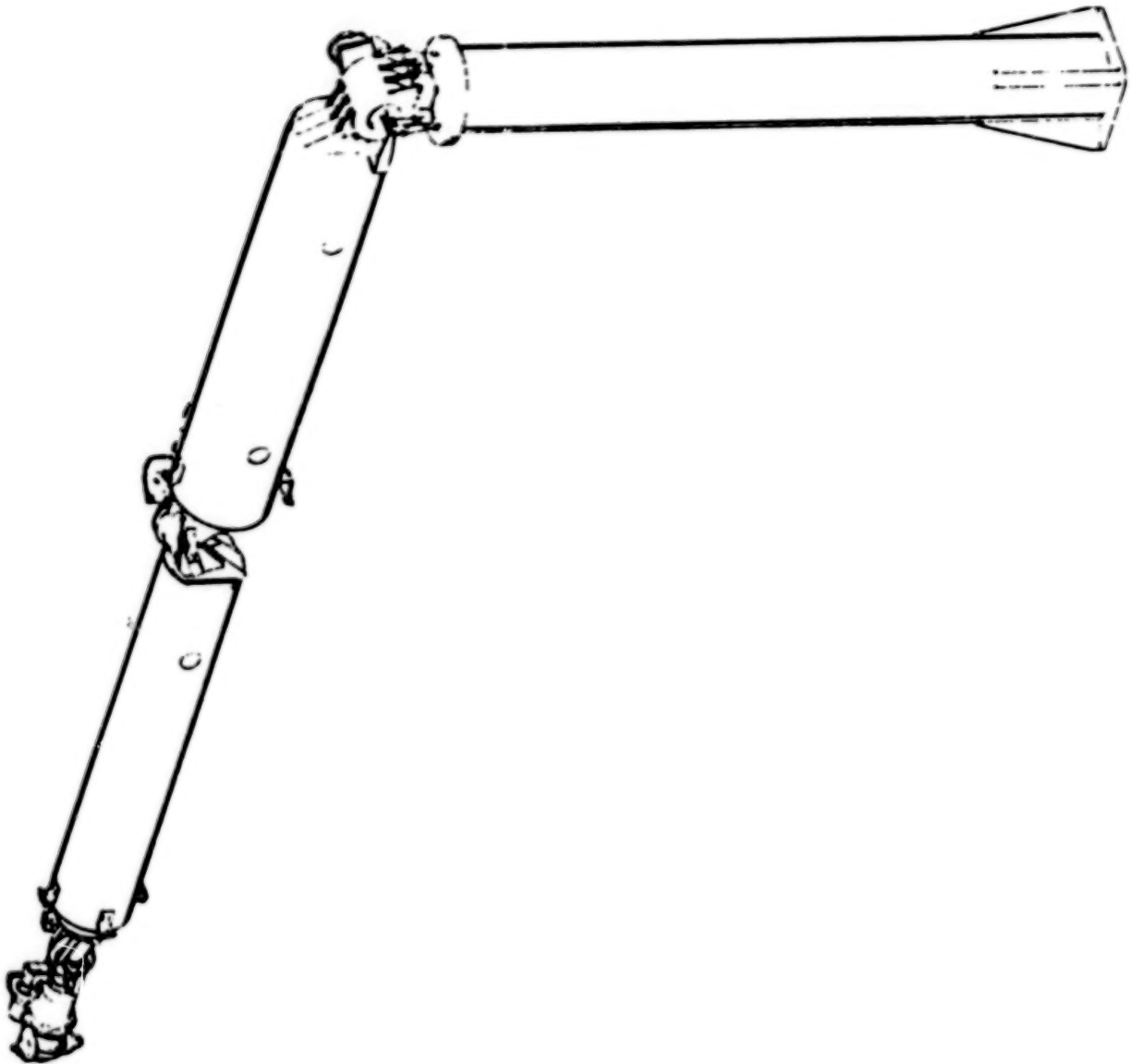
- * MORE RIGID THAN RMS
- * MAY NOT BE USED

3. SEPARATE TELEOPERATOR EXPERIMENT

- * IN CONJUNCTION WITH STEP
- * MAKES SENSE FROM EVOLUTION OF ROBOTICS AND
TELEOPERATORS IN SPACE

HANDLING AND POSITIONING ARM

The HPA that Grumman has designed for JSC is shown in the figure. This device is attractive because (1) it offers the opportunity for use in an experiment, (2) the control system is not a safety-of-flight device, and (3) it could be combined with the STEP pallet.



REFERENCE

1. Gran, Richard: Reduced Order Control Design for Large Space Structures - A Communication Satellite Example. Large Space Antenna Systems Technology, Part 2, NASA CP-2269, 1983, pp. 625-648.

SPACE FLIGHT EXPERIENCE WITH THE
SHUTTLE ORBITER CONTROL SYSTEM

Kenneth J. Cox
NASA Johnson Space Flight Center
Houston, Texas

Kevin C. Daly and Philip D. Hattis
C.S. Draper Laboratory
Cambridge, Massachusetts

Large Space Antenna Systems Technology - 1982
NASA Langley Research Center
November 30 - December 3, 1982

I. INTRODUCTION

Experience gained through the Shuttle Orbital Flight Test (OFT) program has matured the engineering understanding of the Shuttle on-orbit control system. This paper will briefly review the genealogy of the control systems (called digital autopilots, or DAPs, and used by the Shuttle for on-orbit operations), examine the flight experience gained during the flight test program within the context of pre-flight analysis and test results, and address issues for the operational phase of the Shuttle, including constraints upon both operations and analysis still required to increase confidence in the Shuttle's ability to handle capabilities not experienced during the flight test program.

Two orbital autopilots have resulted from computer memory and time constraints on a flight control system, with many different, flight phase unique requirements. The transition DAP, used for insertion and deorbit, has more active sensors and redundancy but a less complex data processing scheme excluding state estimation with fewer choices of operational mode. The on-orbit DAP has capabilities to support operations and long term orbit operations, but generally has only a subset of the sensors available for data acquisition, requiring state estimation.

Extensive pre-flight simulation and design analysis permitted good prediction of performance whenever the environment was properly modelled. OMS residuals, RCS propellant usage, and flexure sensitivity during flight tests were close to expectation.

Most unexpected DAP response in flight can be traced to unmodelled disturbances. Recognition of these factors and their incorporation into simulation have permitted good reconstruction of flight data.

Vernier jets have been found to be limited in life with high duty cycle rates in flight. High maneuver rates, large disturbance torques, and procedural errors inducing simultaneous commands from two control laws have all been responsible for increasing vernier activity. Procedures must be carefully constructed to maximize vernier life. Deadbands must be kept as large as possible, maneuvers may require primary jets more often, and some restrictive software lockouts will be required.

Finally, much work remains to be done to assure effective orbiter control during payload operations. Payload/orbiter dynamic interaction could induce excess RCS activity without adequate control margins being provided by effective pre-mission screening. RMS dynamics can couple into the orbiter dynamics, and mission specific DAP I-loads must reflect these effects.

TOPICS OF DISCUSSION

- **The orbital flight digital autopilots (DAPs)**
- **Flight experience versus pre-flight test results**
 - **Most in-flight performance as predicted in simulation**
 - **Transition DAP showed expected orbiter flexure sensitivity**
 - **Some unmodelled disturbances affected DAP performance**
- **Some suggested constraints on future missions based on flight experience**
- **Analysis required to support undemonstrated capabilities**

II. THE ORBITAL FLIGHT AUTOPILOTS

There are two orbital Digital Autopilots (DAPs) which operate at all times from main engine cutoff in ascent to entry interface at descent. Originally only a single autopilot was developed, but computational and memory constraints from a multitude of flight phase specific requirements necessitated a division into two separate autopilots.

The Transition DAP operates during orbital insertion and deorbit and includes orbiter stabilization between Space Shuttle Main Engine (SSME) cutoff and External Tank (ET) separation, the re-orientation, orbit circularization, Orbital Maneuvering System (OMS) burns, the Jeorbit burn, and dumping of excess forward Reaction Control System (RCS) propellant for entry center-of-gravity control.

The On-Orbit DAP includes all payload deployment related capabilities as well as orbit maintenance and maneuver functions.

The differences in functional requirements of the two DAPs led to different sensor and actuator configurations as well as different data processing mechanizations. The Transition DAP with coarse attitude control requirements excludes use of the six 25-lb vernier jets. Rate Gyro Assemblies (RGAs) are available for angular rate data due to ascent and entry requirements for these sensors. Inertial Measurement Units (IMUs) are operational at this time but CPU time constraints permit incorporating the IMU data only once every 960 ms which is inconsistent with the DAP cycle time of 80 ms. Therefore, the IMU is used only to correct the RGA bias with rates and attitudes derived directly from the RGA data (through digital bending filters which have been added for STS-5 and subsequent flights). For the sake of design simplicity, no state estimation is done, which makes the control system sensitive to the Multiplexer/Demultiplexer (MDM) quantization of 0.04 deg/sec in pitch and yaw and 0.08 deg/sec in roll. The RGA data is corrupted by random noise with a 1 sigma value of approximately one quantum.

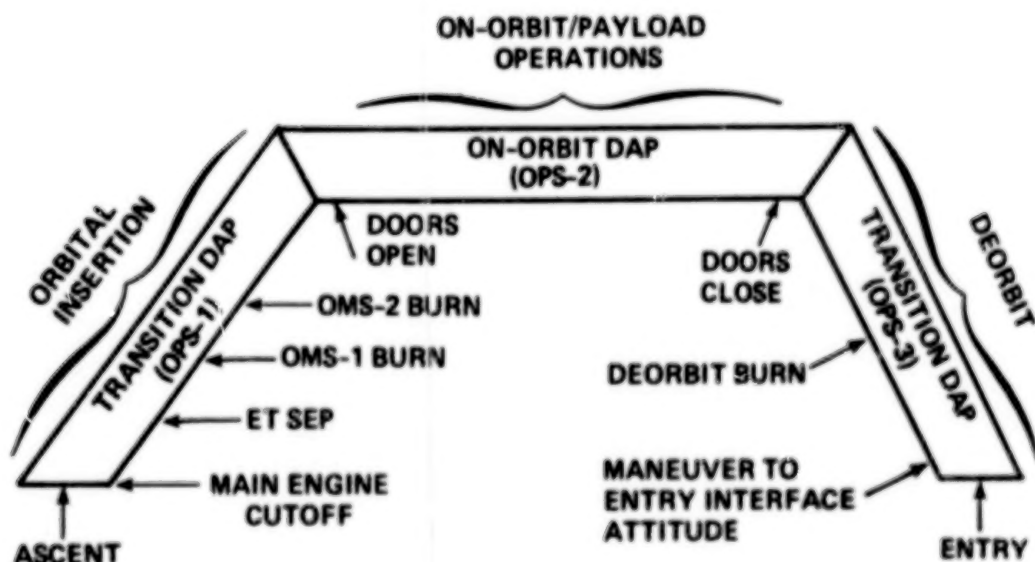
The On-Orbit DAP includes all RCS and OMS system capability. RGAs are not available, requiring state estimation using IMU data to obtain angular rate and disturbance acceleration information. The IMU is processed every 160 ms with an 80 ms DAP cycle time, thus requiring extrapolation as well as estimation.

Redundancy requirements vary between the two DAPs. The Transition DAP does all the flight critical operations in orbit, necessitating use of all three IMUs and four RGAs as well as four primary General Purpose Computers (GPCs). The On-Orbit DAP, used for most of the typical mission, functions in a power-critical environment. Usually one IMU and two GPCs are used, although a full complement of three IMUs may be made temporarily available for critical operations.

THE ORBITAL FLIGHT AUTOPILOTS

- Orbital flight control spans all three flight phases from main engine cutoff to entry interface, each with unique requirements
 - Orbital insertion
 - Mated orbiter/ET coast
 - ET separation
 - OMS-1/OMS-2 orbit circularization burns
 - On-orbit operation
 - Payload operations (tight attitude control may be required)
 - RMS operations
 - Proximity operations
 - RCS/OMS orbit changes
 - Inertial or LVLH maneuvers and track
 - Propellant use balancing
 - Deorbit
 - Deorbit burn
 - RCS propellant dump

TRANSITION/ON-ORBIT DAP TYPICAL FLIGHT PROFILE

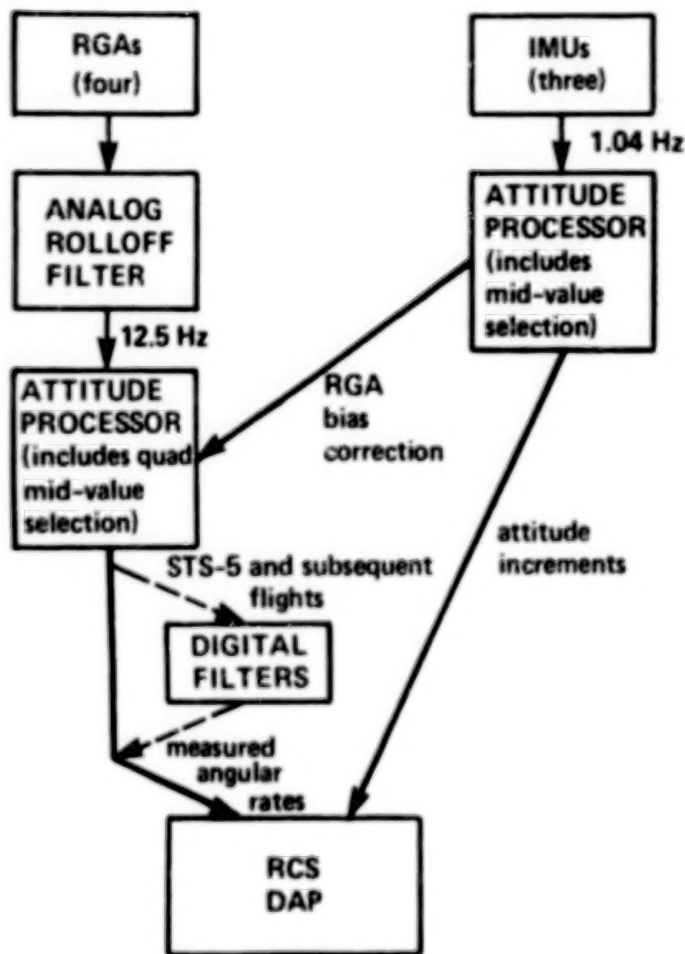


THE ORBITAL FLIGHT AUTOPILOTS (CONT.)

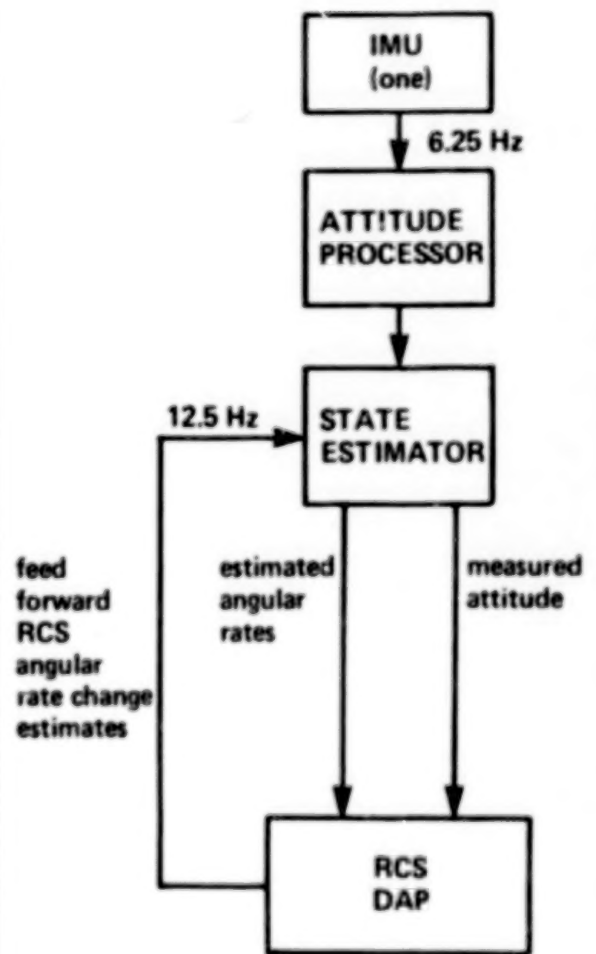
- **Computer core and CPU time overloads from multitude of non-overlapping functions forced split of the three phases into separate software loads with two DAPs**
 - Transition for insertion and deorbit
 - On-orbit
- **Transition DAP has maximum avionic redundancy and design simplicity to support flight critical operations**
 - All sensors and computers powered to span critical flight burns
 - RCS capability only that required for doors closed operations (primaries only)
- **On-orbit DAP has full payload support capability**
 - RCS capability includes options for payload activity
 - Choice of primary and vernier operations
 - RCS control can be optimized for RMS operations in several positions
 - Attitude control precision possible to 0.01 deg relative to sensor platform
- **Data processing differs between DAPs**
 - Transition DAP uses rate gyro assemblies (RGAs) without state estimation
 - RGAs available due to ascent and entry requirements
 - State estimation eliminated to save core (reduced accuracy of state knowledge acceptable for transition)
 - On-orbit DAP uses inertial measurement unit (IMU) as only attitude/angular rate sensor with state estimation
 - RGAs powered down to conserve energy
 - Reduced CPU time load compared to insertion permitted 6.25 Hz IMU read rate

SENSORY DATA PATHS TO DAP

TRANSITION DAP



ON-ORBIT DAP



III. FLIGHT EXPERIENCE VERSUS PRE-FLIGHT TEST RESULTS

The dynamical features of the two orbital autopilots were extensively tested and well understood by the design community before the first Shuttle flight. Consequently most flight experience has validated expected performance. However, some unexpected in-flight disturbances produce interesting responses characteristic of the unique dynamics of each DAP.

Precise OMS and RCS control has been demonstrated for both DAPs within the limits of the RCS and OMS actuator granularity. Also, the on-orbit DAP, with state estimation, shows the expected resistance to orbiter-alone flexure modes at 0.47 Hz or higher frequencies.

The transition DAP, without the digital filters on the first four missions, was sensitive to flexure at frequencies beyond 4 Hz. Main engine slewing during orbiter/ET mated coast excited one such mode inducing rate oscillations sufficient to induce 1.04 Hz periodic RCS firings (1.04 Hz was the SSME step rate). The results are illustrated in the figures that follow.

The transition DAP is also vulnerable to variable initial conditions, such as on STS-3 where an early auxiliary power unit (APU) shutdown occurred, causing an unsymmetric SSME thrust tailoff with high initial rates on the mated orbiter/ET configuration. A special high rotation acceleration feature of the transition mated coast logic proved valuable in assuring that the rates were properly damped before ET separation 12 seconds after transition DAP initiation.

The on-orbit DAP showed response signatures to several unanticipated disturbances. Included were payload bay door motion and remote manipulator system (RMS) activity induced orbiter rate disturbances.

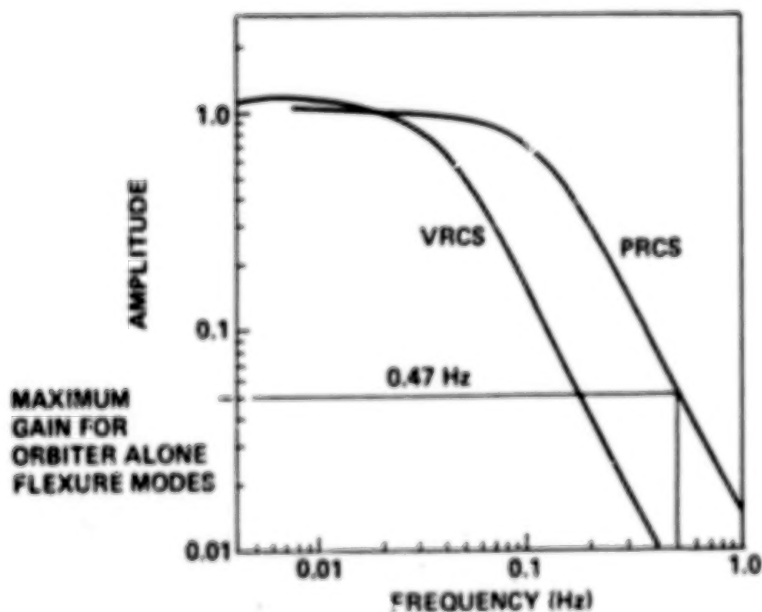
Plume impingement of expanding gas jets on orbiter structure affected both DAPs. Residual dump of SSME propellants at OMS-1 burn initiation caused hydrogen impingement on the port wing with the resultant roll rate disturbance and OMS pitch actuator transient that is illustrated. The on-orbit use of vernier jets caused jet plume impingement on the body flap with a resultant reduction of net thrust. Due to a feed forward extrapolation feature of the state estimator based on preflight jet acceleration estimates, significant estimator transients occurred, as illustrated, causing increased vernier propellant usage and duty cycles.

Trapped water in the tiles on STS-4 was found to induce a diurnal disturbance torque response. Effective gravity gradient attitude hold capability was precluded until water bakeout. The disturbance is illustrated, as is the gravity gradient hold profile after bakeout.

FLIGHT EXPERIENCE VERSUS PRE-FLIGHT TEST RESULTS

- Most in-flight performance as predicted in simulation
 - Nominal OMS burns produce residual velocities of 0.2 ft/s/axis or less
 - Tight attitude control feasible with the RCS
 - Primary jet behavior good to below 1.0 deg deadband and 0.2 deg/s rate limit
 - Vernier jet behavior good to well below 0.1 deg deadband and 0.02 deg/s rate limit
 - On-orbit DAP insensitive to orbiter flexure during RCS activity
 - Lowest orbiter frequency (with doors opened) is 0.47 Hz
 - Estimator attenuation at 0.47 Hz is at least a factor of 20 (doors closed frequencies are higher, so attenuation is greater)

ON-ORBIT DAP
STATE ESTIMATOR FREQUENCY RESPONSE

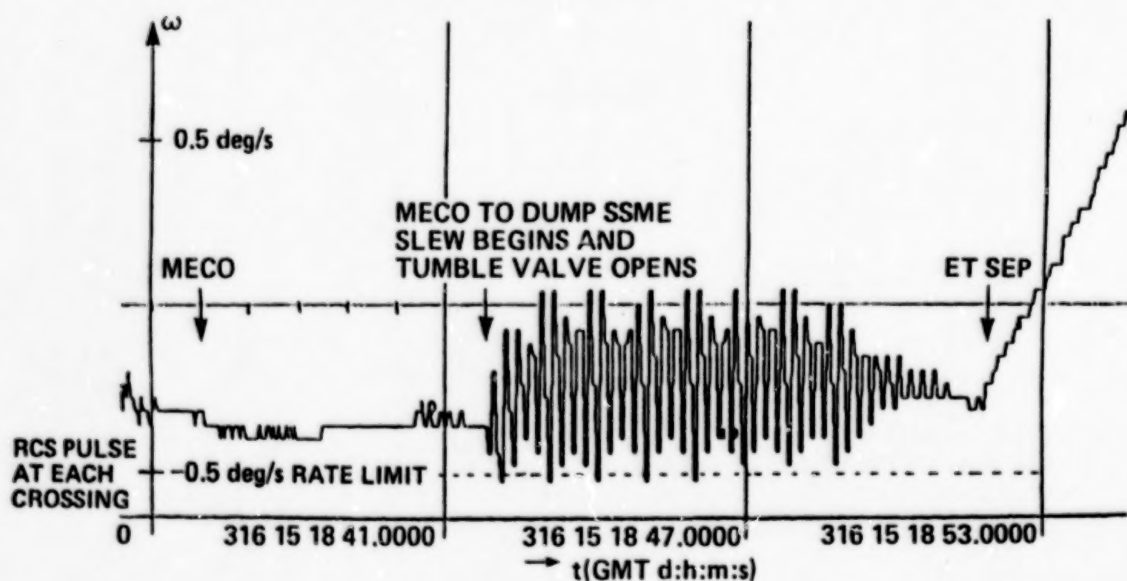


FLIGHT EXPERIENCE VERSUS PRE-FLIGHT TEST RESULTS (CONT.)

- Expected transition DAP sensitivity to direct use of flexure-sensitive rate gyro data caused in flight RCS response to main engine slewing
 - Flight response somewhat worse than expectation due to closer than predicted correlation between mated coast pitch mode frequency and DAP cycle time (frequency approximately 4 minor cycles)
 - Filters already added as of STS-5 should eliminate RCS response to orbiter bending modes
- Some unmodelled disturbances affected DAP performance
 - Early ascent auxiliary power unit shutdown on STS-3 caused high initial mated coast rates
 - Stuck main engine throttle position caused unsymmetric thrust tailoff
 - Mated rates at start of transition DAP were (-0.08, -0.5, +0.5 deg/s)
 - Substantial RCS activity was required to damp rates before tank separation

FLEXURE INDUCED TRANSITION DAP RCS ACTIVITY

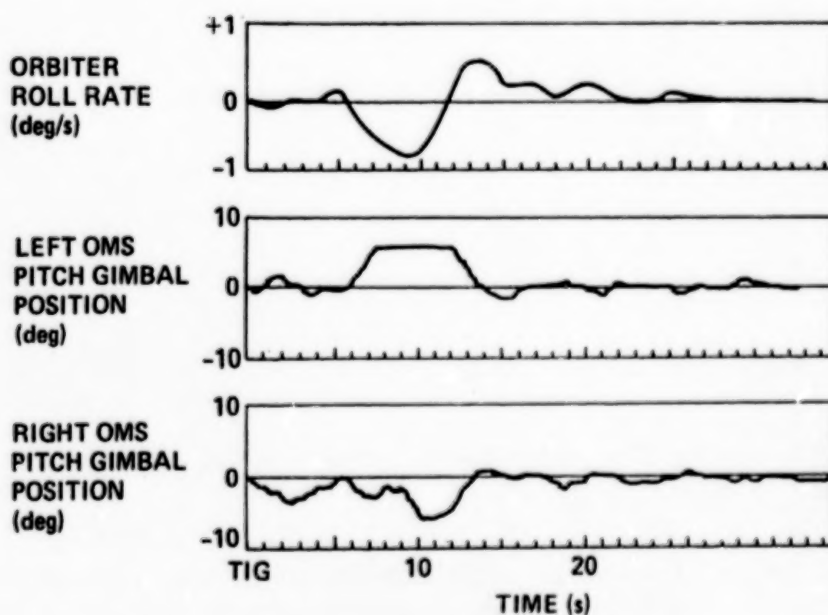
STS-2 MATED COAST PITCH RATES FROM 12.5 Hz SAMPLED DATA DOWNLISTED BY THE BACKUP COMPUTER



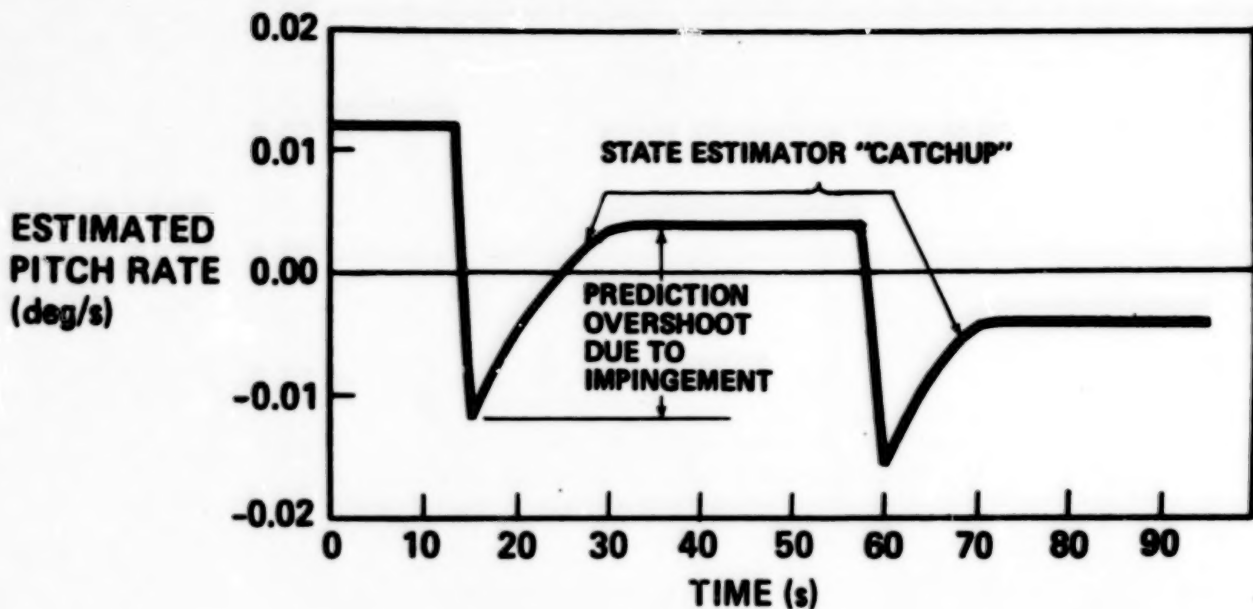
FLIGHT EXPERIENCE VERSUS PRE-FLIGHT TEST RESULTS (CONT.)

- Some unmodelled disturbances (Cont.)
 - Vehicle rates are affected by payload door motions
 - Opening or closing of one door at a time provides disturbance accelerations up to 0.006 deg/s^2
 - Inadequate preflight plume impingement modelling influenced system behavior
 - LH₂ dump during OMS-1 burn produced peak orbiter roll rates of -0.8 deg/s due to plume impingement on port wing
 - Aft down firing vernier jet impingement off body flap causes 45% thrust loss
 - Pitch control acceleration very unsymmetric (+pitch control/-pitch control = 2.2)
 - Unmodelled effect degraded state estimator performance on STS-1
 - Vernier duty cycles were higher than predicted until DAP I-loads were revised to include impingement effects
 - Active attitude control during RMS motion increases RCS activity
 - STS-3 unloaded arm tile survey caused 1% vernier duty cycle with 0.3 deg deadband

OMS-1 LH₂ DUMP DISTURBANCE PROFILE FROM STS-1



STS-1 VERNIER PITCH RATE OVERSHOOT



AFT DOWNFIRING VERNIER JET FORCE MAGNITUDE (lbf)

MODELED (STS-1)

MEASURED

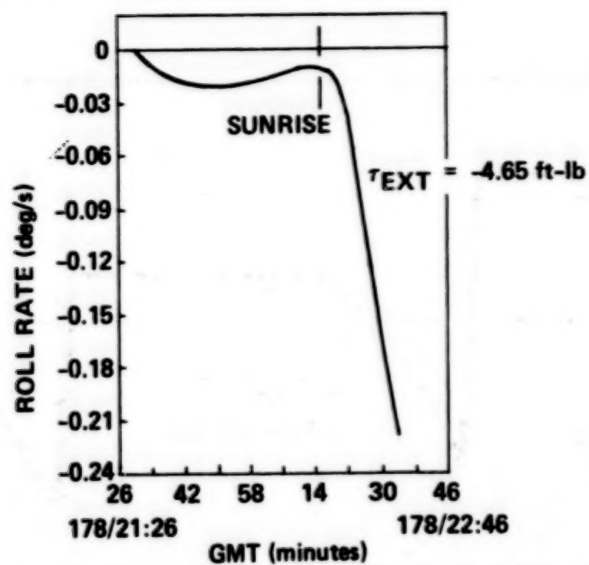
24.0

13.2

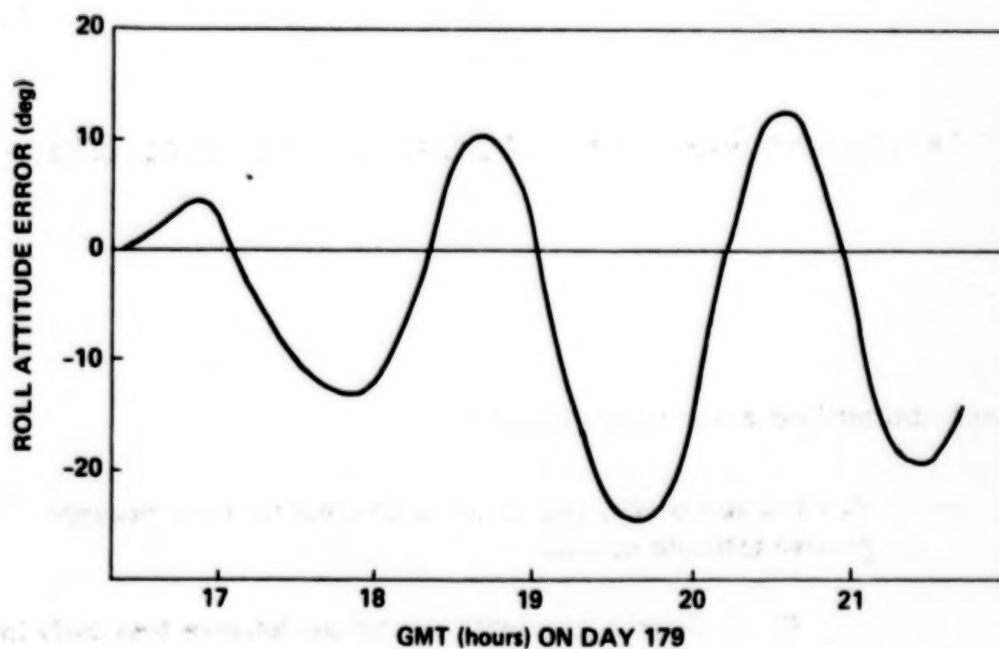
FLIGHT EXPERIENCE VERSUS PRE-FLIGHT TEST RESULTS (CONT.)

- **Some unmodelled disturbances (Cont.)**
 - **Volatization of trapped water in thermal tiles can prevent passive attitude control**
 - **Gravity gradient/aero torque balance test early in STS-4 mission aborted with 100+ deg roll attitude error due to unpredicted venting**

**STS-4 SECOND GRAVITY GRADIENT TEST
(ON MET DAY 1 WITH VOLATIZING WATER)**



**STS-4 MET DAY 2 GRAVITY GRADIENT TEST
(AFTER VENTING STOPPED)**



IV. SOME SUGGESTED CONSTRAINTS ON FUTURE MISSIONS BASED ON FLIGHT EXPERIENCE

Operational experience with the on-orbit autopilot and supporting hardware has demonstrated some responses in particular applications that produce some undesirable propellant expenditures and potential reduction in vernier jet life.

The verniers have been found to have less of a lifetime duty cycle capability than expected, with the ultimate limits determined in part by cyclic thermal shock effects in the ceramic jet lines. The rotation control capability of the vernier jets is highly coupled between body axes, making many duty cycles inevitable to achieve commanded rate changes. Experience has shown that high vernier maneuver rates (above 0.2 deg/s) compound the situation of excessive jet on time. With tight rate limits and deadbanding with high maneuver rates, the limit vernier control authority can induce a target attitude overshoot with required rate reversal resulting in extra jet activity (as illustrated). Also, RMS motion induces orbiter rate changes sufficient to increase vernier activity. Use of APUs on-orbit to test aero surfaces can cause venting torques, which tax vernier control, causing high cycle rates and high peak jet temperatures.

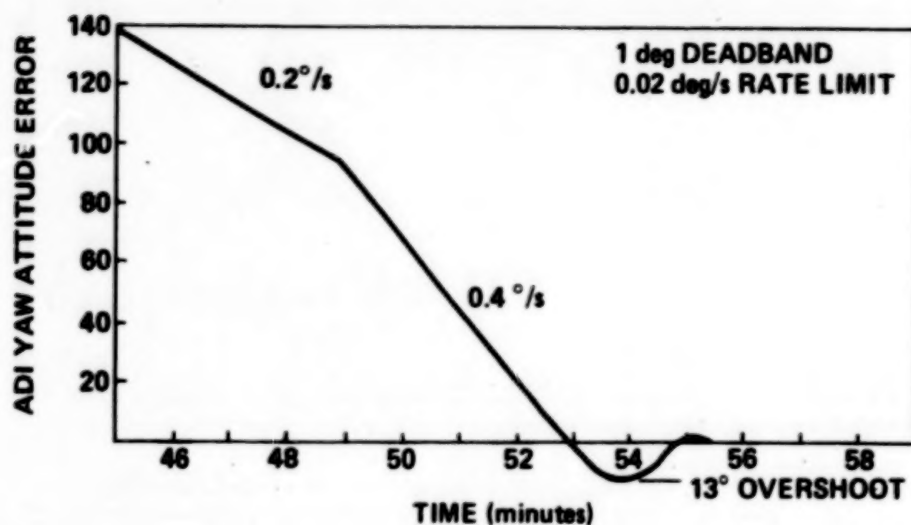
Crew procedural errors can also increase vernier activity. An open loop angular rate compensation capability exists which can be inadvertently selected with phase plane control active (this will change starting STS-12). As is illustrated and has happened several times in flight, the simultaneous commands derived by two incompatible control laws result in very high vernier cycle rates.

The lesson flight experience suggests is to restrict vernier usage to low maneuver rates, use primaries with large disturbances, and carefully select rate and attitude deadbands to conform with the true requirements. Failure to observe the guidelines could increase operational cost due to frequent jet changeout, and reduce orbit stay time from excess propellant expenditures. Also, software lockout of any simultaneous use of incompatible control laws seems advisable.

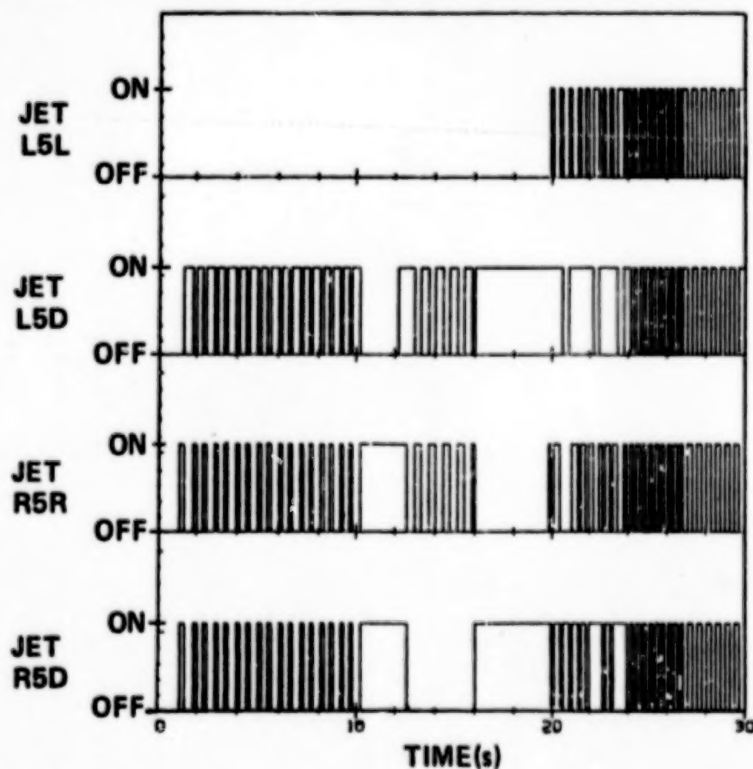
**SOME SUGGESTED CONSTRAINTS ON FUTURE MISSIONS BASED
ON FLIGHT EXPERIENCE**

- Verniers must be protected against excessive duty cycling (thermal shock forced replacement after STS-4)
 - Use primaries for maneuvers at rates higher than 0.2 deg/s
 - Low vernier control authority causes maneuver overshoot when stopping high rates with extra jet activity to damp out errors
 - Use primaries when doors are closed
 - Evaporators observed to cause large disturbance torques which stress vernier control capability
 - Restrict vernier use when RMS motion commanded
 - Momentum exchange of payload and orbiter during RMS acceleration can cause much unnecessary jet activity to control orbiter rates (as seen from STS-3 unloaded arm tile survey — effect will be much worse with payloads)
 - Avoid use of open loop rotation rate compensation during closed loop attitude control
 - COAS alignment maneuver on STS-3 caused high duty cycling due to incompatibility of compensation and phase plane control laws
 - Closed loop control compensation inhibit has been approved effective STS-12

EXAMPLE
STS-3 HIGH RATE VRCS MANEUVER
(RATE INCREASED BY CREW WHEN MANEUVER WAS IN PROGRESS)



VRCS MANEUVER WITH ROTATION COMPENSATION
(AFT JET ACTIVITY FROM SIMULATION REPRODUCING STS-3
COAS MANEUVER WITH 0.003 deg/s COMPENSATION THRESHOLD)



SOME SUGGESTED CONSTRAINTS (CONT.)

- **Carefully choose attitude deadbands and maneuver rates to save propellant and duty cycling during maneuvers**
 - **Excessively small deadbands during maneuvers cause target overshoot with extra RCS recovery activity (similar to effect of high VRCS maneuver rate)**
 - **Care must be taken when collapsing deadbands**
 - **PRCS tight deadband test on STS-4 never achieved stable limit cycle in allocated time (~2 min.) due to excessive residual rates when deadbands were reduced**
 - **Tight deadbands with high maneuver rates specified can cause repeated cycling to maneuver mode to correct large transient errors**

IV. ANALYSIS REQUIRED TO SUPPORT UNDEMONSTRATED CAPABILITY

Payload deployment experience thus far is restricted to PAM-D use on STS-5 and manipulation of RMS payloads less than 1000 lbm on STS-3 and 4. Many dynamical interactions between different classes of payloads, the orbiter, and/or the RMS are possible, some with undesirable forced RCS oscillations resulting if the DAP closes the control loop.

Studies of dynamic interaction must be conducted which quantify the influences of different types of dynamical coupling such as from flexure and rotating bodies. In each case a method must be devised to evaluate stability and control margins available that are needed to contend with unanticipated disturbances either external or introduced by the crew.

In the case of the RMS, envelopes of acceptable operation must be derived as a function of payload characteristics. Alternate I-loads slots are available for vernier use during RMS operation, but they can effectively be used only after computational methodologies to generate the I-loads are developed which incorporate arm flexure effects. Simultaneous orbiter attitude control during commanded RMS motion can complicate the analysis, particularly for large payloads.

Clearly the orbital envelope of operation has not been stretched to anywhere near the intended limits. Further analysis, verification, and possibly DAP design updates are required to permit many desired payload support operations.

ANALYSIS REQUIRED TO SUPPORT UNDEMONSTRATED CAPABILITIES

- **Payload/orbiter dynamic interaction studies**
 - **Influence of payload manipulations on FCS closed loop operation must be quantified**
 - **Inertial effects**
 - **Flexure effects**
 - **Spinning payload coupling effects**
 - **Required control margins must be specified for payload**
 - **DAP parameter variation effects to be included**
 - **Payload physical characteristics must be taken into account**
- **RMS/FCS closed loop behavior**
 - **Stationary arm control envelopes must be evaluated as a function of payload mass properties**
 - **Method for optimal selection of DAP I-loads for payloads deployed on the arm to be developed**
 - **Effects of attitude control during commanded arm motion must be studied**

SPACE TECHNOLOGY EXPERIMENT PLATFORM (STEP).
A SHUTTLE-BORNE SUPPORT FACILITY
FOR STRUCTURES, STRUCTURAL DYNAMICS, AND
CONTROL TECHNOLOGY FLIGHT EXPERIMENTS

Jack E. Harris and Larry D. Pinson
NASA Langley Research Center
Hampton, Virginia

Large Space Antenna Systems Technology - 1982
NASA Langley Research Center
November 30 - December 3, 1982

INTRODUCTION

The NASA Office of Aeronautics and Space Technology (OAST) is actively planning future utilization of the Space Transportation System (STS) for technology experiments in space. STEP is the acronym for the Space Technology Experiment Platform, a Shuttle-borne experiment support facility for use by structures, structural dynamics, and controls technology flight experiments. STEP represents a key element in OAST's commitment to STS utilization.

The STEP concept is undergoing definition for OAST by Langley Research Center.

This paper discusses the STEP concept and definition process, summarizes the results obtained to date on the configuration and function capability, and presents preliminary schedule information.

STEP CONCEPT

As mentioned in previous papers, flight experiments are required in order to accelerate the use of new and high-risk technology that holds promise for new capability, improved performance, and reduced costs. This is particularly true in new technologies for large, lightweight and flexible structures. Maturing ground technology programs in these areas are reaching the point at which further progress and valuable data need to be obtained in the relevant environment of space.

As illustrated in figure 1, STEP's objective is to provide a link between the structures, structural dynamics, and controls research community (NASA, other governmental agencies, universities, and industry) and the relevant space environment conditions (zero gravity, absence of atmospheric damping, and wide thermal excursions) which are accessible through the use of NASA's Space Transportation System (STS). If one thinks of the STS and the Space conditions it can access as being analogous to a wind tunnel, STEP becomes the sting balance upon which test articles are mounted within the tunnel.

To provide such a link, STEP should be configured specifically to support these disciplines and should be responsive to the specialized weight, volume, measurement instrumentation, and operational requirements that they impose.

To facilitate easy access to the STS and to provide a cost-effective link, STEP should utilize standardized hardware and management interfaces with the STS to the maximum extent possible, consistent with the experiment requirements.

To serve the research-oriented user community effectively, STEP should be operated as a research facility and should be responsive to evolving research opportunities. These opportunities will involve a series of flight experiments conducted over a span of several years, thus requiring STEP to have a capability for reuse several times per year.

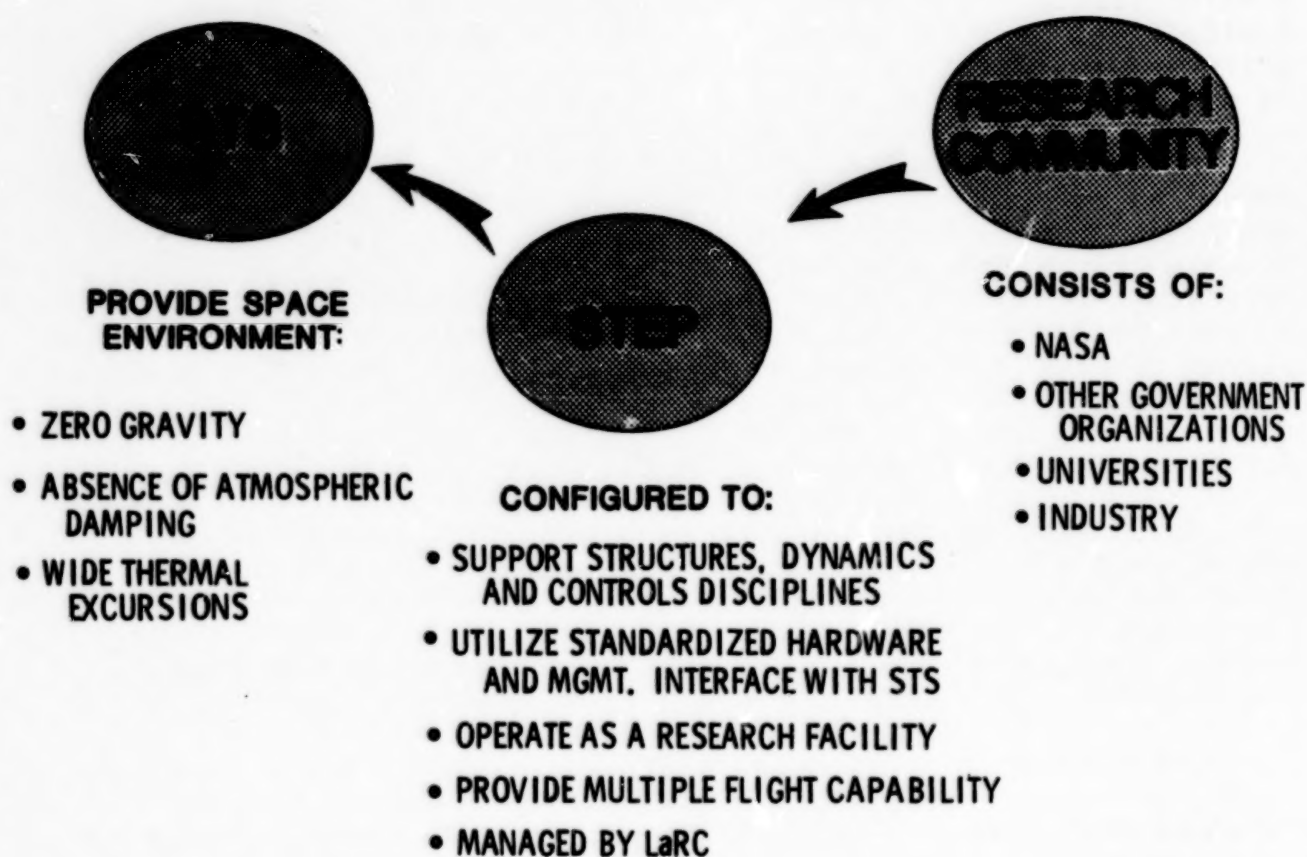


Figure 1.- STEP concept.

SYSTEM DEFINITION STUDY

The Langley Research Center's STEP Project Office is conducting an in-house definition study of the STEP concept. The process of definition is illustrated in figure 2. Several potential large space structures, structural dynamics, and controls technology flight experiments were used to synthesize mission requirements. These requirements, coupled with STS capabilities and constraints and STEP ground rules, were used as drivers for system and subsystem requirements and have culminated in a preliminary statement of STEP capabilities.

Figure 3 illustrates several typical flight experiments that were used to synthesize weight, volume, data handling, command, and power requirements. These particular experiments were used because they represented different levels of complexity. MAST represents component level technology experiments, while the structures/control interaction experiment has an all-up system flavor tending to define the upper boundary on required capability. Experiment classes that are simpler than MAST are also being considered to ensure that the STEP interface mechanization does not force an otherwise inherently simple experiment to become complex.

An initial definition task involved the selection of an appropriate payload carrier to serve as the basic structural interface with the Shuttle orbiter and to provide for mounting the flight experiment and STEP electronics. Figure 4 lists the options considered, identifies the option selected, and summarizes the selection rationale.

The Modular Payload Support Structure (MPSS) being developed by MBB in Germany consists of basic carbon fiber struts and titanium node elements from which a variety of configurations can be assembled. British Aerospace is developing derivatives of the basic Spacelab pallet to provide half-pallet and quarter-pallet sections to increase modularity. The Multipurpose Experiment Support Structure (MPESS) developed by Teledyne Brown Engineering is an aluminum truss structure bridging the cargo bay which is attached to the orbiter through trunnions and a keel fitting. The Experiment Support System (ESS) is being developed for the Air Force by Lockheed Missiles and Space Corporation.

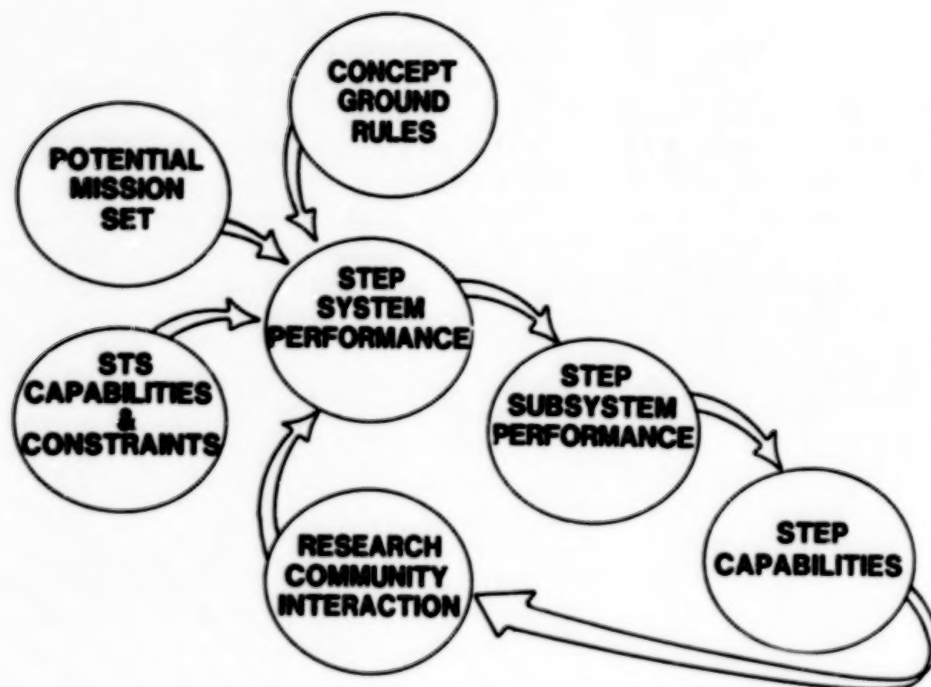


Figure 2.- STEP feasibility and system definition process.

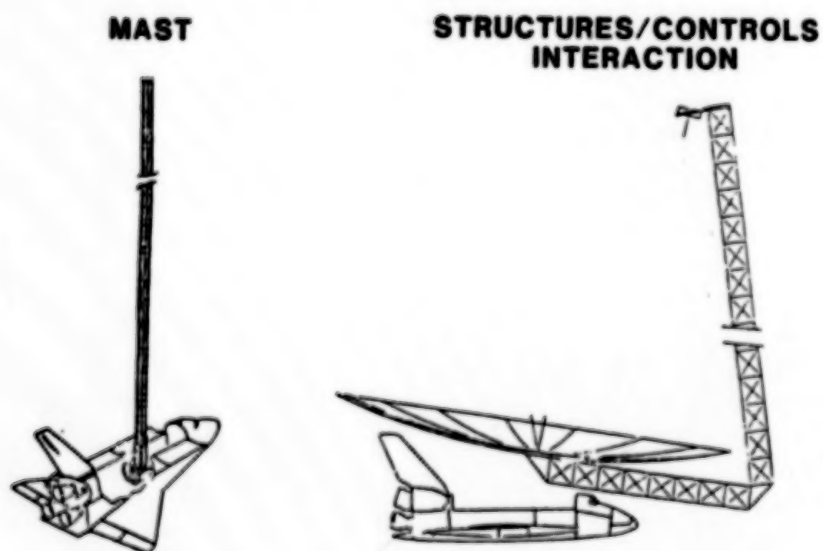


Figure 3.- Typical flight experiments.

PAYLOAD CARRIER OPTIONS
CONSIDERED

° SPACELAB PALLET	
° MODULAR PAYLOAD SUPPORT STRUCTURE (MPSS)	MBB
° SPACELAB PALLET DERIVATIVES	BAE
° MULTIPURPOSE EXPERIMENT SUPPORT STRUCTURE (MPSS)	TELEDYNE BROWN
° EXPERIMENT SUPPORT SYSTEM	LMSC

OPTION SELECTED

SPACELAB PALLET

RATIONALE

- PALLET STRUCTURE DEVELOPED AND SPACE QUALIFIED WITH FLIGHT EXPERIENCE IN THE SORTIE MODE
- MATCHES WEIGHT AND VOLUME NEEDS
- PHYSICAL AND MANAGEMENT INTERFACES DEVELOPED
- CONSISTENT WITH NASA/ESA AGREEMENTS

Figure 4.- Payload carrier selection.

STEP CONFIGURATION

The configuration being considered for STEP is shown in figure 5. This configuration is comprised of three major elements: (1) a standard Spacelab pallet, (2) a modular experiment interface structure, and (3) pallet-mounted electronics.

The Spacelab pallet is a rigid U-shaped structure about 2.9 meters long attached to the orbiter through trunnions and keel fittings. The pallet provides a standardized structural interface with the orbiter. The plan is to obtain the Spacelab pallet from NASA's Spacelab pallet system inventory on a dedicated basis.

The experiment interface structure element consists of three modular shelf-type sections that tie into pallet hard points. The two outboard sections are each roughly one-quarter of the pallet length, while the center section is approximately one-half the length. The sizes are chosen to correspond with the pallet hard point locations and to provide modular flexibility.

In addition to the shelf sections, a unit for one degree of freedom rotation is provided to accommodate experiments that require stowage horizontal with respect to the orbiter cargo bay during launch, descent, and landing but need to be rotated to a vertical or near-vertical position for operation. A quarter-section shelf is used for this mode to maximize available volume.

Experiments that can be vertically accommodated within the Shuttle cargo bay door envelope will be mounted directly on the shelf sections, with the number of sections used in this mode dependent upon the experiment mounting footprint.

The STEP electronics are mounted either on pallet-provided cold plates or directly to the pallet. In figure 5, electronics are shown packaged in a single box directly beneath a shelf section, but they may also be mounted on the sloping surfaces of the pallet in a distributed manner.

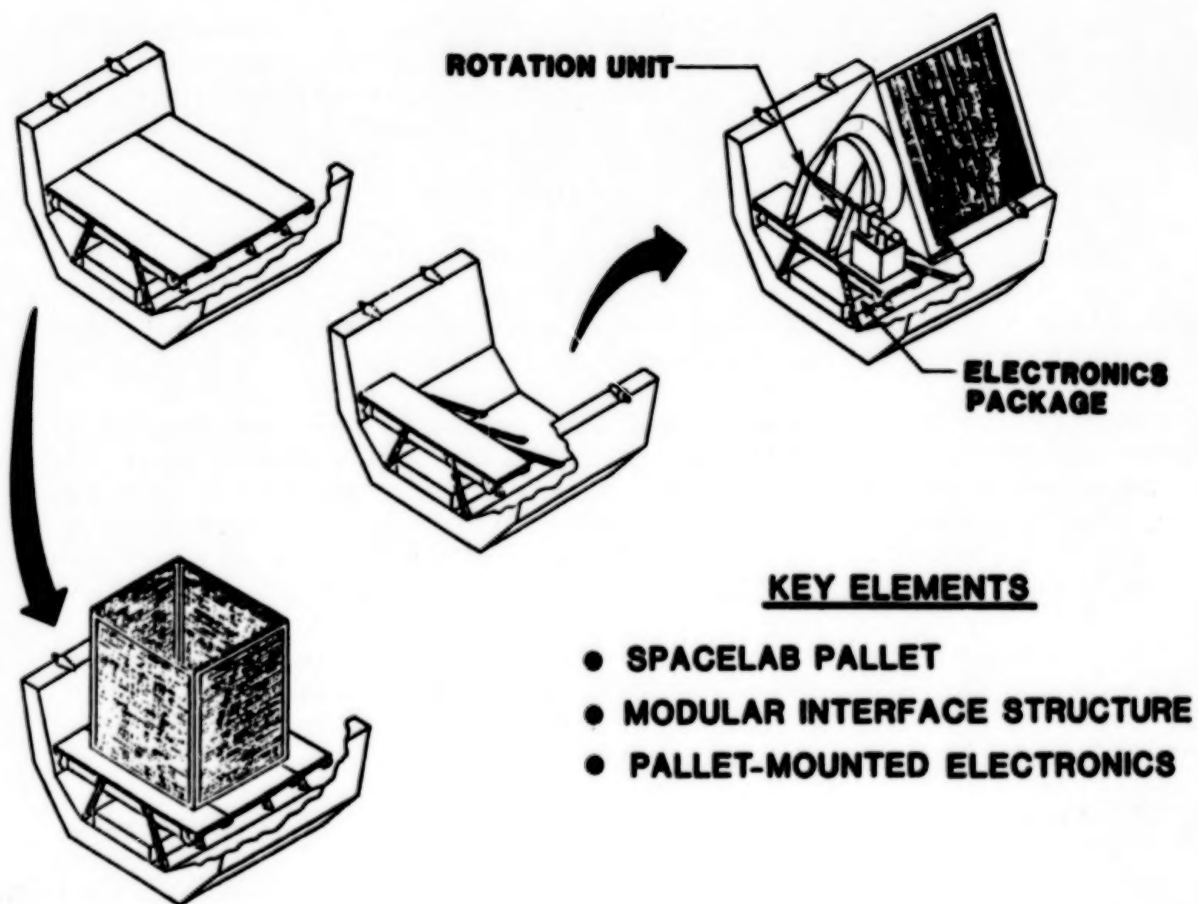


Figure 5.- STEP configuration.

STEP FUNCTIONAL CAPABILITY

Figure 6 outlines the functional capability envisioned for the STEP subsystems. The feasibility and system definition activities have not been completed; thus, these stated capabilities represent a preliminary baseline.

STEP capability can be summarized in the following manner. STEP is a software-controlled system that provides autonomous command, control, data handling and storage, thus freeing the experimenter from many restrictions normally incurred by having to integrate experiment software and data storage needs within available Shuttle orbiter resources and time lines.

<u>SUBSYSTEM</u>	<u>CAPABILITY</u>
SPACELAB PALLET	<ul style="list-style-type: none">* MECHANICAL SUPPORT AND ALIGNMENT OF ALL STEP ELECTRONICS AND INTERFACE STRUCTURE AND MECHANISMS* THERMAL COOLING FOR STEP ELECTRONICS AND THERMAL COOLING INTERFACE FOR EXPERIMENT ELECTRONICS* STANDARDIZED MECHANICAL INTERFACE WITH SHUTTLE ORBITER
INTERFACE STRUCTURE AND MECHANISMS	<ul style="list-style-type: none">* PROVIDES MOUNTING, LATCH AND RELEASE, CONTROLLED ERECTION, AND JETTISON* ACCOMMODATES EXPERIMENT WEIGHTS UP TO 2000 KGS* ACCOMMODATES PACKAGED EXPERIMENT VOLUME UP TO 3.4M DIAMETER AND VARIABLE LENGTH UP TO 6 M
DATA HANDLING AND STORAGE	<ul style="list-style-type: none">* PROVIDES COLLECTION, FORMATTING, SIGNAL CONDITIONING, MULTIPLEXING, STORAGE, AND TRANSFER OF STEP AND EXPERIMENT-GENERATED DATA* ACCOMMODATE EXPERIMENT DATA COMPOSED PRIMARILY OF LOAD, STRAIN, DISPLACEMENT, ACCELERATION AND TEMPERATURE TYPE MEASUREMENTS FROM IN SITU OR REMOTE SENSORS* PROVIDE 10^9 BIT STORAGE* PROVIDE DOWNLINK OF DATA VIA ORBITER KU BAND LINK
COMMAND AND SEQUENCING	<ul style="list-style-type: none">* PROVIDE FOR CONTROL OF STEP AND EXPERIMENT SUBSYSTEMS AND UNITS VIA PRE-STORED COMMAND SEQUENCES DISTRIBUTED AS DISCRETES OR CODED WORDS* PERFORM LIMIT CHECKS AND RESPOND TO INTERRUPTS ACCORDING TO STORED ALGORITHMS TO ALTER SEQUENCES* PROVIDE MANNED INTERACTION VIA KEYBOARD/ DISPLAY UNIT IN AFT FLIGHT DECK* PROVIDE FOR SOFTWARE UPDATE VIA UP-LINK THROUGH ORBITER
POWER DISTRIBUTION AND CONTROL	<ul style="list-style-type: none">* PROVIDE CENTRAL SUPPLY OF POWER TO OPERATE STEP AND EXPERIMENT SUBSYSTEM AND UNITS* PROVIDE REQUIRED SWITCHING AND CONTROL FUNCTIONS FOR POWER MANAGEMENT AND DISTRIBUTION* PROVIDE 28V DC AND 400 Hz 3 PHASE AC* PROVIDE REGULATED AND UNREGULATED POWER

Figure 6.- STEP functional capability.

SCHEDULE

A preliminary STEP development schedule is presented in figure 7. The activity is currently in Phase A with completion scheduled for January 1983. During the system definition phase, the STEP capabilities will be tested against a wider cross section of potential flight experiments and modified appropriately. The development phase involves an in-house design and fabrication activity of the modular experiment interface structure subsystem and a competitively placed contractural effort for the electronics design and fabrication. This will culminate in a first launch availability in 1987.

A preliminary operations flow schedule is presented in figure 8. This flow is based on two flights per year with a typical integration cycle of 18 months. Experiment hardware will be required approximately 6 months prior to launch for STEP compatibility testing and STS physical integration.

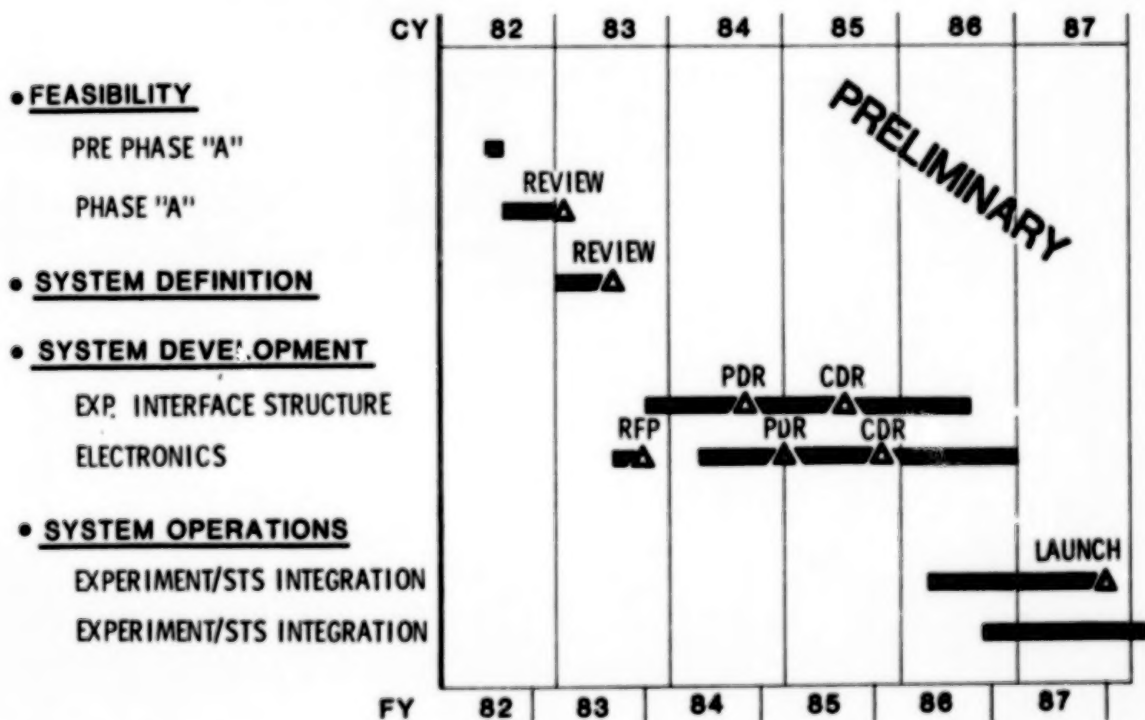


Figure 7.- STEP development schedule.

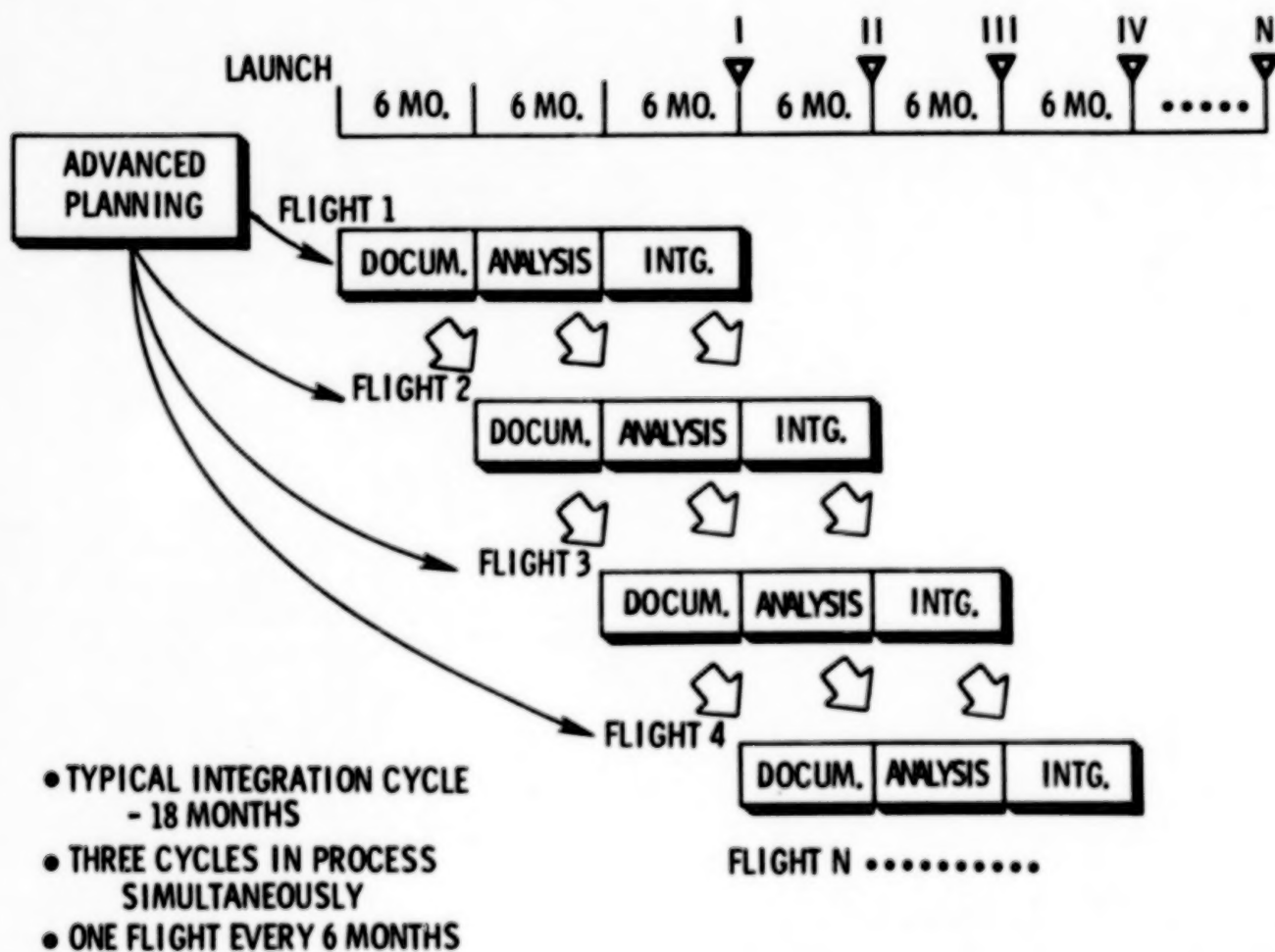


Figure 8.- STEP operations schedule.

SAFE ON-ORBIT EXPERIMENT FOR MEASUREMENT
OF LARGE STRUCTURES DYNAMICS

R. W. Schock
Marshall Space Flight Center
Huntsville, Alabama

Large Space Antenna Systems Technology - 1982
NASA Langley Research Center
November 30 - December 3, 1982

SOLAR ARRAY LSS CHARACTERISTICS

The Solar Array Flight Experiment (SAFE) on-orbit experiment for measurement of large structures dynamics consists of a dynamic sensing system designed to record and analyze the dynamic characteristics of the SAFE.

The early availability of the SAFE and its basic large space structure characteristics make it a logical candidate for verification of the sensing system and the evaluation technique.

The characteristics of the solar array which place it well within the generic class of large space structures are:

1. Large size
2. Low natural frequencies
3. Mechanical complexity of its extendable/retractable mast
4. The inability to dynamically test in the Earth's atmosphere and in one g

The fourth characteristic is due to its size, air damping dominance of the blanket, and structural instability in one g.

The specific characteristics of the solar array are shown in figures 1 and 2 and illustrate the applicability to large space structures.

- ARRAY WT -- 225 Kg
 - BLANKET -- 132 Kg
 - MAST -- 40 Kg
 - CONTAINER -- 40 Kg
 - COVER ASSY -- 14 Kg
- FREQUENCY -- .033 -- .4 Hz
- ARRAY LENGTH -- 3101 CM
- ARRAY WIDTH -- 400 CM
- MAX. ALLOWABLE BM ~ 120.9 N-m

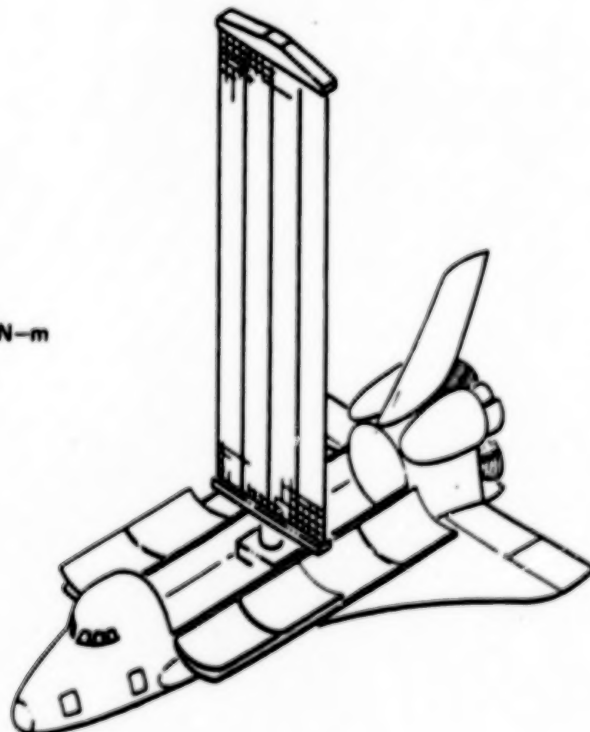


Figure 1

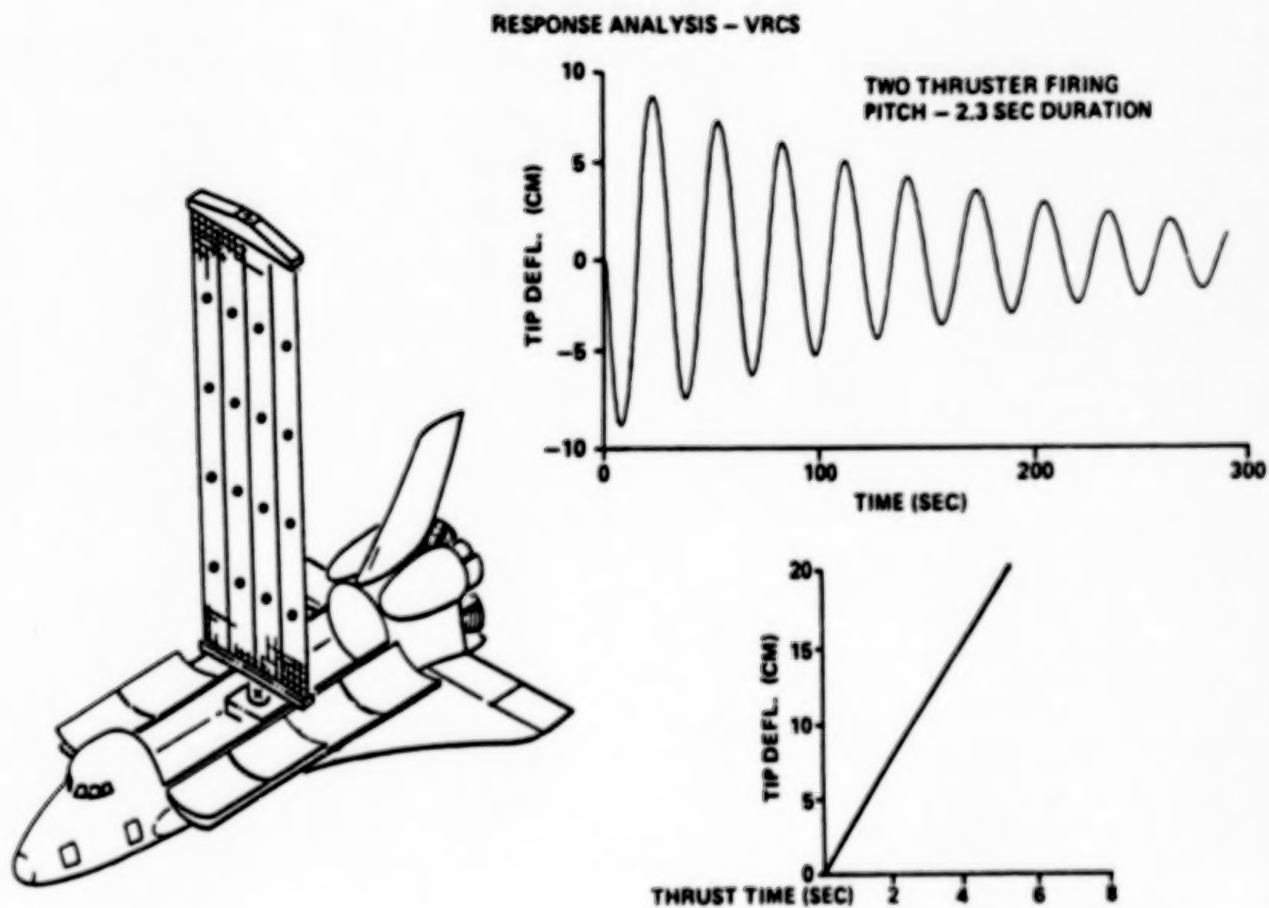


Figure 2

SAFE DYNAMICS AUGMENTATION EXPERIMENT

The basic objectives of the solar array dynamics experiment are:

1. Demonstrate the technology readiness of an on-orbit remote sensing dynamic data processing and recording system for use in large space structure response measurements.
2. Process remotely sensed data to obtain solar array dynamic characteristics for correlation with analysis and ground test and application to response control techniques.

To accomplish these objectives, a remote sensing system is being developed. The sensing system, an adaptation of a multifield star tracker, is being developed by MSFC. The technique is illustrated in figure 3. The emitter, positioned at the base of the solar array, illuminates the array of retroreflectors. The retroreflectors return the emitted energy to the receiver. The receiver focuses the reflector images on a solid-state sensor. A scanner samples the sensor and feeds reflector image positions to a microprocessor. The microprocessor computes the dynamic array displacement from the initial or rest position and provides a digital output through a data conditioner to a digital tape recorder. The recorder data is stored and returned for ground processing.

Ground processing will define the dynamic characteristics of the array such as frequencies, mode shapes, and damping. These characteristics will be used to verify math models, provide test-defined inputs for control software, and provide zero g correlation to one g ground test data.

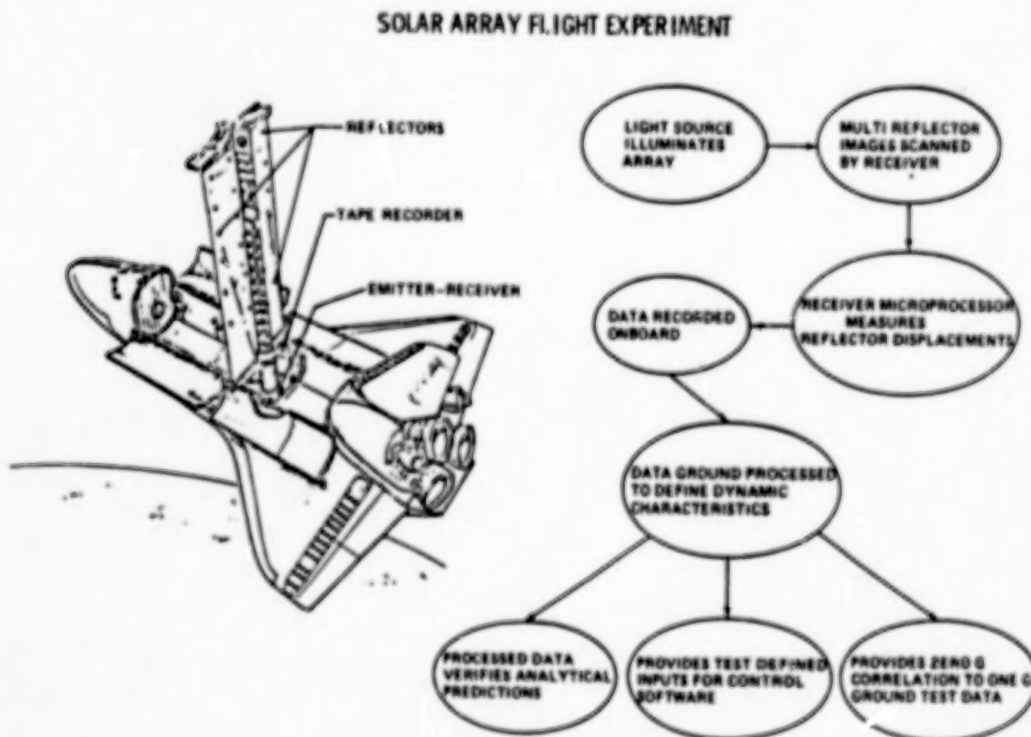


Figure 3

FLIGHT CONFIGURATION AND SYSTEM CHARACTERISTICS

The on-orbit configuration and the basic sensing system characteristics are shown in figures 4 and 5. Twenty-three standoff retroreflecting tape targets have been placed on the solar array blanket and mast. These targets reflect in a -z orbiter direction. The emitter-receiver is positioned within 100 inches of the base of the array to read the x and y motion of the reflectors with minimum error. Data will be taken of the array at both 100% and 70% deployment. Excitation is provided by the orbiter VRCS system, which is designed to maximize response without approaching structural limits. The sensing system is a charge injection device solid-state sensor with a measurement resolution of better than 1/100 of 1%. The sensory frequency bandwidth is 0 to 0.4 Hz.

SAFE DYNAMICS AUGMENTATION EXPERIMENT

SUMMARY

- CONFIGS - FULLY EXTENDED AND 70%-EXTENDED MAST WITH ARRAY
- EXCITATION - VRCS
- INST. - ~ 23 PASSIVE TARGETS (X, Y MOTION RECORDED)

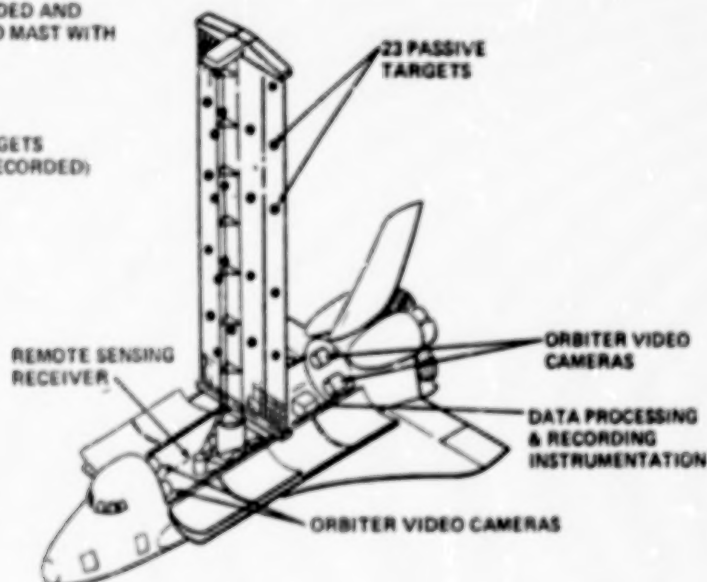


Figure 4

SENSING SYSTEM CHARACTERISTICS

- TWO DIMENSIONAL
- CHARGE INJECTION DEVICE SOLID-STATE DETECTOR
- 0.01 OF 1% RESOLUTION
- 0-0.4 HZ FREQUENCY
- LASER DIODE ILLUMINATION AT 800 NM
- REFLECTORS OF RETROREFLECTIVE HIGH-GAIN SHEETING

Figure 5

OAST-1 PAYLOAD AND DYNAMICS AUGMENTATION EXPERIMENT FLOW DIAGRAM

The OAST-1 experiment with DAE attached is shown in figure 6 along with a flow diagram of the sensor system in figure 7. Although both the solar array dynamic augmentation experiment and the systems are mounted to the mission-peculiar equipment support structures (MPESS), the only interaction between them is optical. The retroreflector field tracker illuminates the solar array reflectors with five 800-nm laser diodes. The retroreflected energy is imaged on a charge injection device solid-state tracker. The tracker is scanned by sensor electronics; the angular deviation from the reference position is measured and converted by a microprocessor to engineering units. This data is digitized and fed through a pulse code modulator (PCM) which conditions the signals for recording on the digital tape recorder. The power control and distribution assembly (PCDA) obtains power from the mission-peculiar equipment (MPE) power control box (PCB) and distributes it to the DAE hardware. The PCDA also receives and distributes commands from the orbiter aft flight deck via the flexible multiplexer demultiplexer (FMDM) and returns housekeeping and indicator data. The scientific dynamic data recorded on the tape recorder is returned for ground data processing.

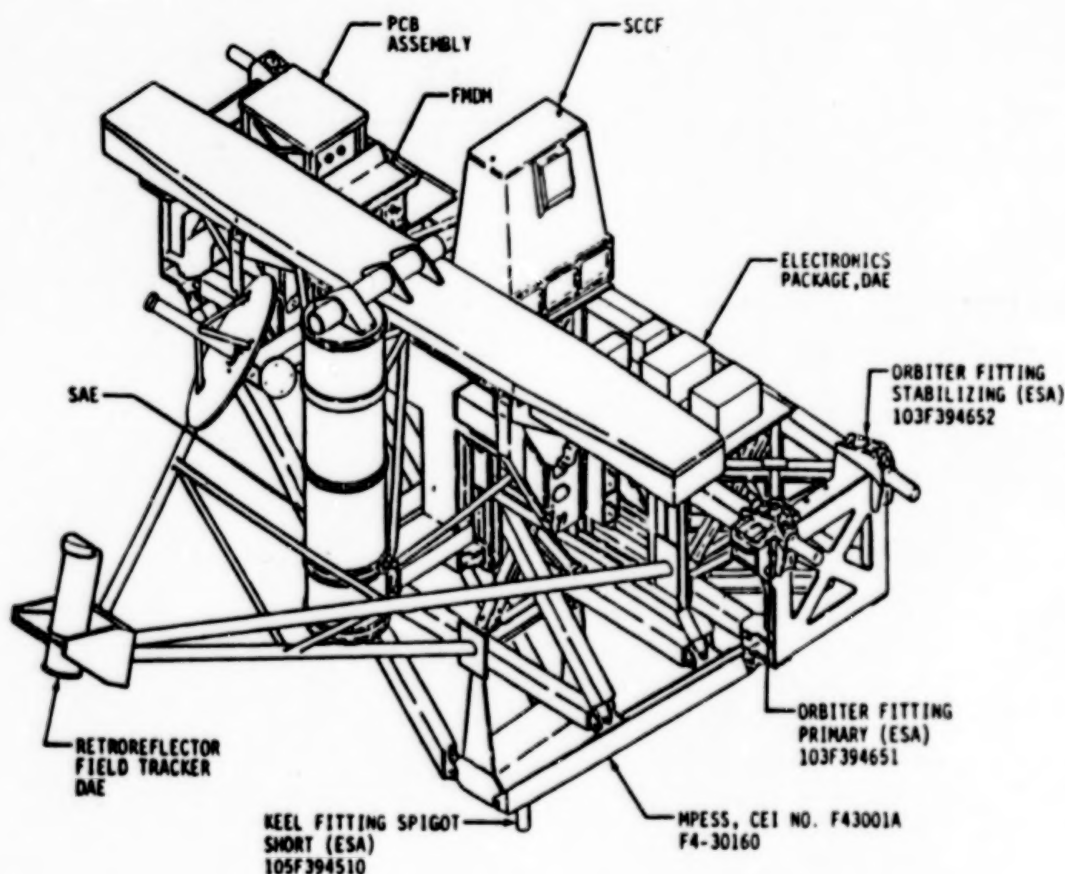


Figure 6

DYNAMICS AUGMENTATION EXPERIMENT

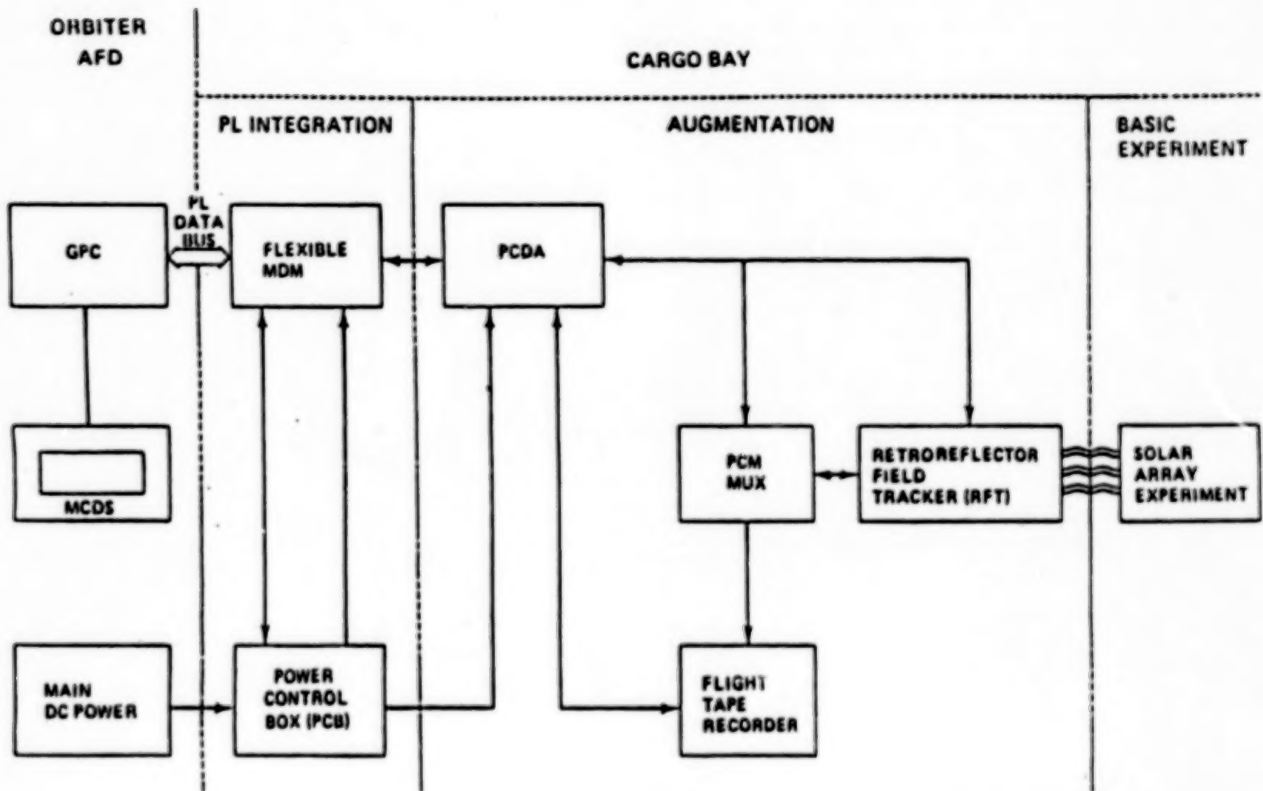


Figure 7

SAFE DYNAMICS AUGMENTATION
GROUND TEST

To provide early verification of the remote sensing data processing concept, a laboratory test is planned for the second and third quarter of FY '83. The ground test approach is illustrated in figure 8. In the tests, light emitting diodes and accelerometers will be mounted to a 16-m, space fabrication-type beam. The beam will be loaded to approximate the natural frequencies of the solar array, and then will be excited by low frequency shakers. Both the LED information and the accelerometers will be processed to assess compatibility of results.

PERSPECTIVE VIEW OF SENSOR MOUNTED FOR MONITORING POINTS ALONG A
16-METER TEST BEAM

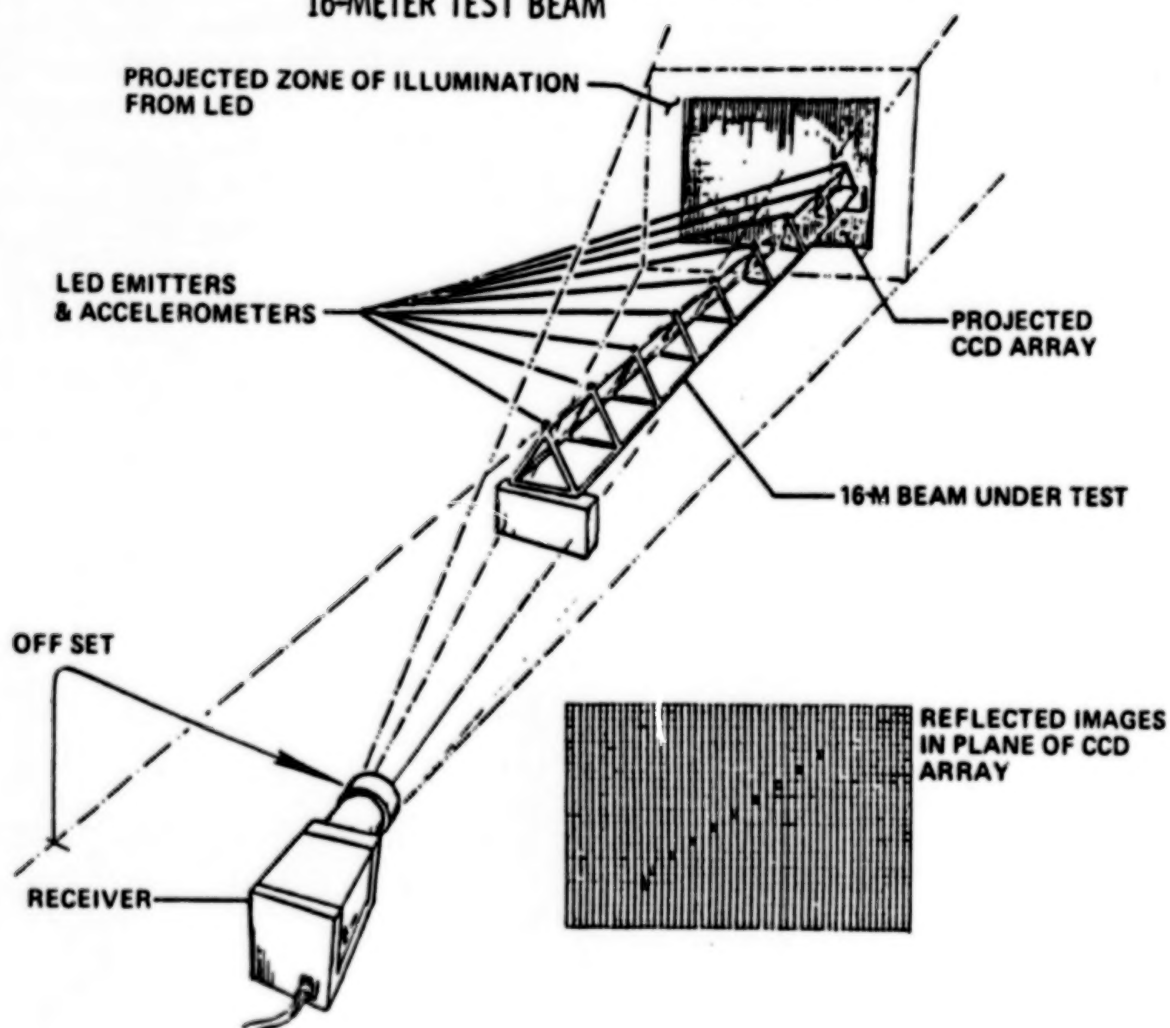


Figure 8

SAFE DYNAMICS AUGMENTATION EXPERIMENT SCHEDULE

The remote sensor hardware is currently scheduled for delivery in mid-May 1983. This appears compatible with delivery of the PCM, tape recorder, and PCDA in March. This allows 6 months of in-house system acceptance testing prior to delivery at KSC in early December. Flight is currently planned for mid-May 1984.

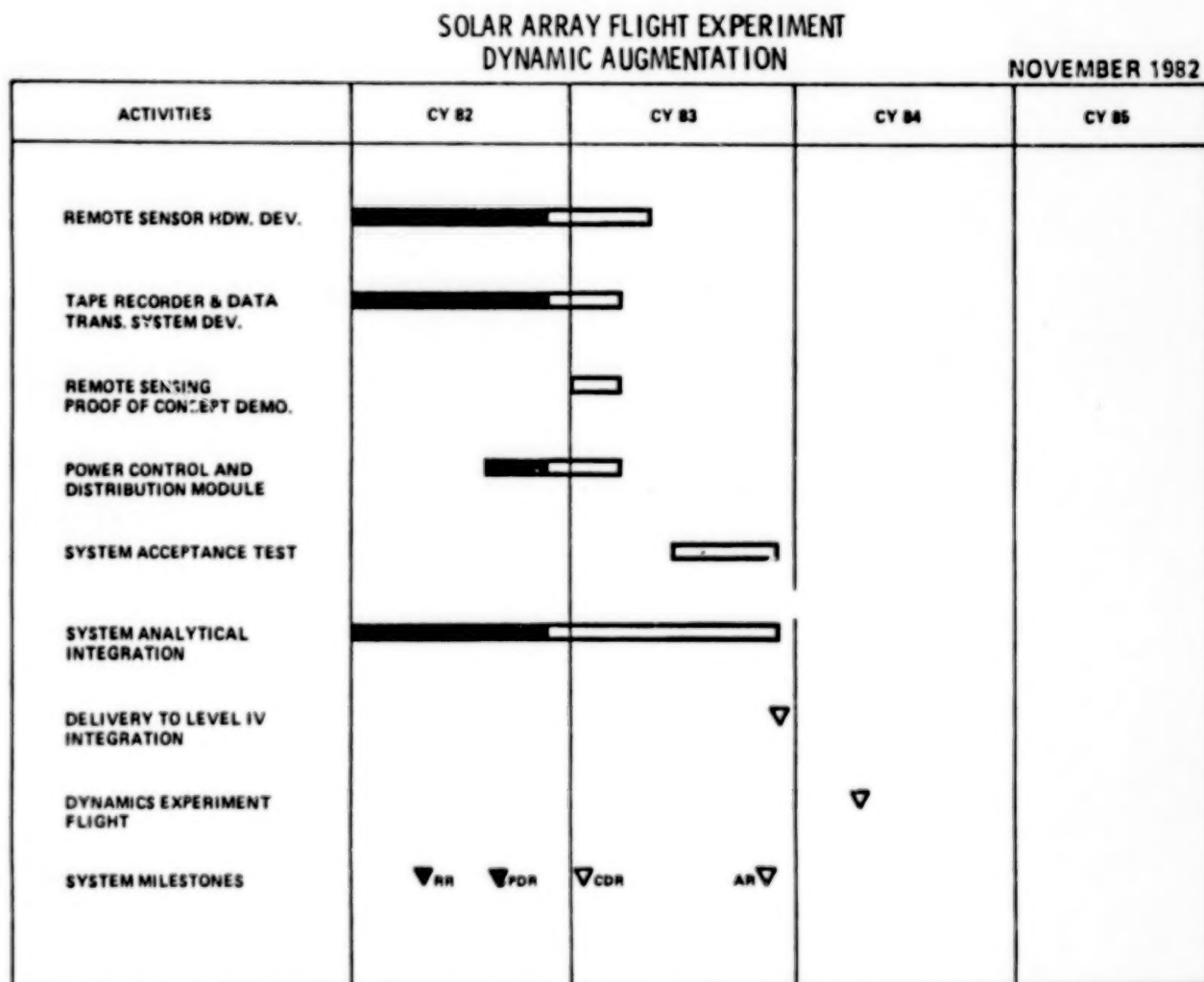


Figure 9

SAFE II - LARGE SYSTEMS SPACE PLASMA EVALUATION EXPERIMENT

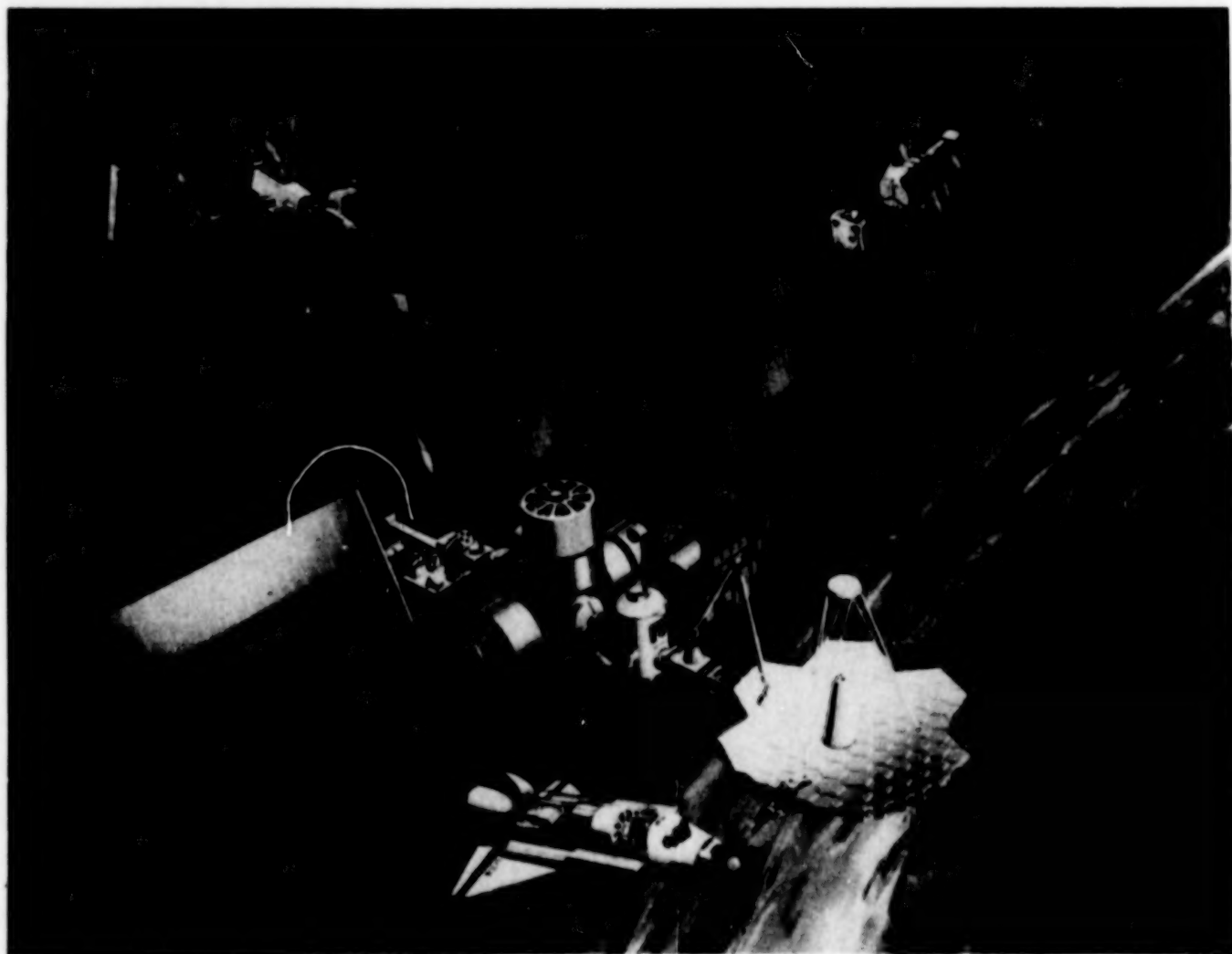
**M. R. Carruth, Jr. and L. E. Young
Marshall Space Flight Center
Marshall Space Flight Center, Alabama**

**C. K. Purvis and N. J. Stevens
NASA Lewis Research Center
Cleveland, Ohio**

**Large Space Antenna Systems Technology - 1982
NASA Langley Research Center
November 30 - December 3, 1982**

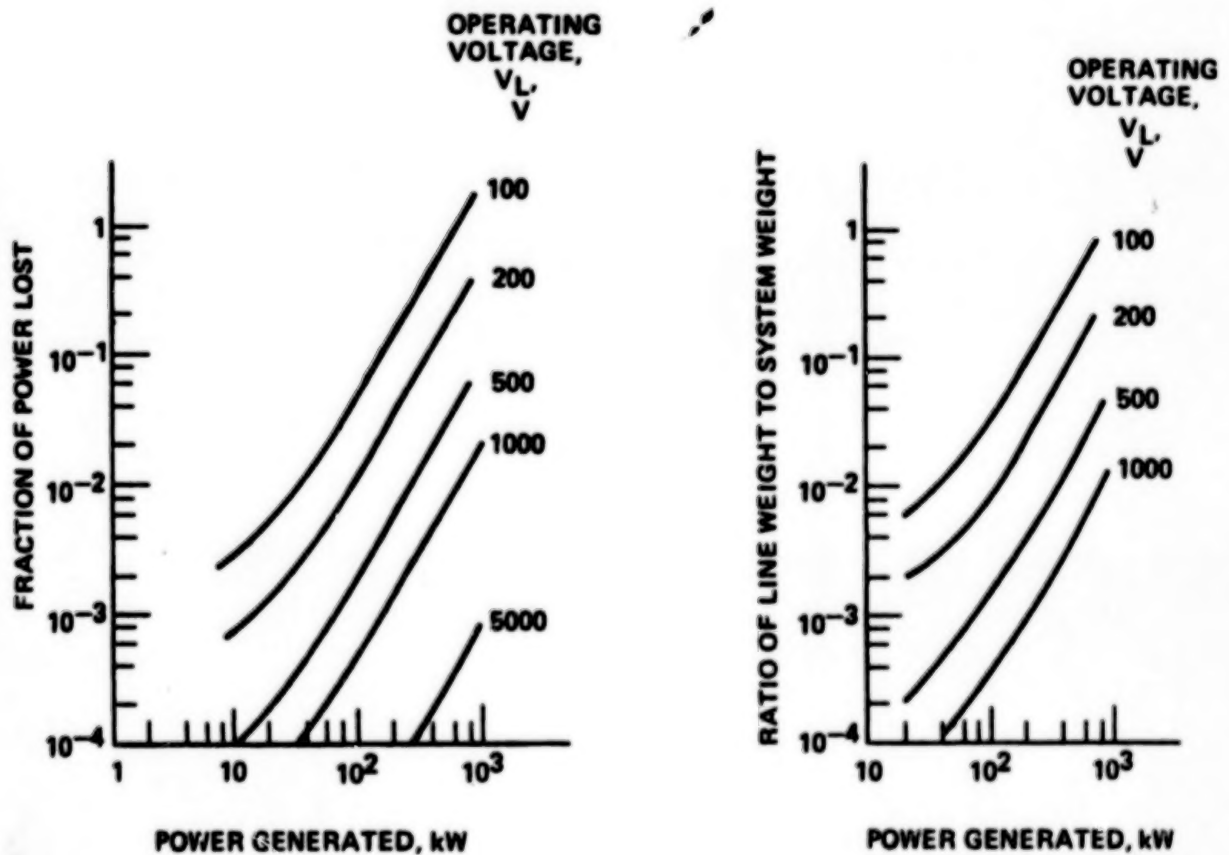
FUTURE MISSIONS UTILIZING LARGE HIGH POWER SOLAR ARRAYS

For a number of years plans for future NASA and USAF missions have concentrated on larger structures and spacecraft utilizing solar arrays which provide tens to hundreds of kilowatts of power. Among these are space based radar, various space platforms, the Solar Electric Propulsion System (SEPS), and most recently Space Station, one concept of which is shown in the figure below. Because these power systems are very much larger than any flown before, there are new areas which must be investigated to insure proper system operation. These include structural, dynamic, and electrical considerations. This paper addresses a Shuttle flight experiment, the purpose of which is to obtain space data on the interaction of a high voltage solar array with the ambient space plasma. This flight experiment will be a reflight of NASA's Solar Array Flight Experiment, SAFE, except that three active solar array panels, electron release devices and plasma diagnostics will be added. This experiment, SAFE II, will evaluate power loss due to parasitic current collected by the solar array, arcing on the solar array and perturbations to the plasma which may increase power loss and disturb plasma and charged particle science acquisition.



HIGH VOLTAGE SOLAR ARRAY

The figure below is the result of one trade study which illustrates the need to operate the high power solar arrays at voltages of at least a few hundred volts in order to reduce internal resistive losses within the array and to reduce the wiring harness mass required to transport the power (ref. 1). It is this need to operate at higher voltages which spawned evaluation of high voltage solar array operation in space. The left figure gives the fraction of power lost in aluminum distribution lines with one square centimeter cross-sectional area. The right figure gives the ratio of transmission line mass to design goal system mass for 5% power loss and a design goal of 10 kg/kW.

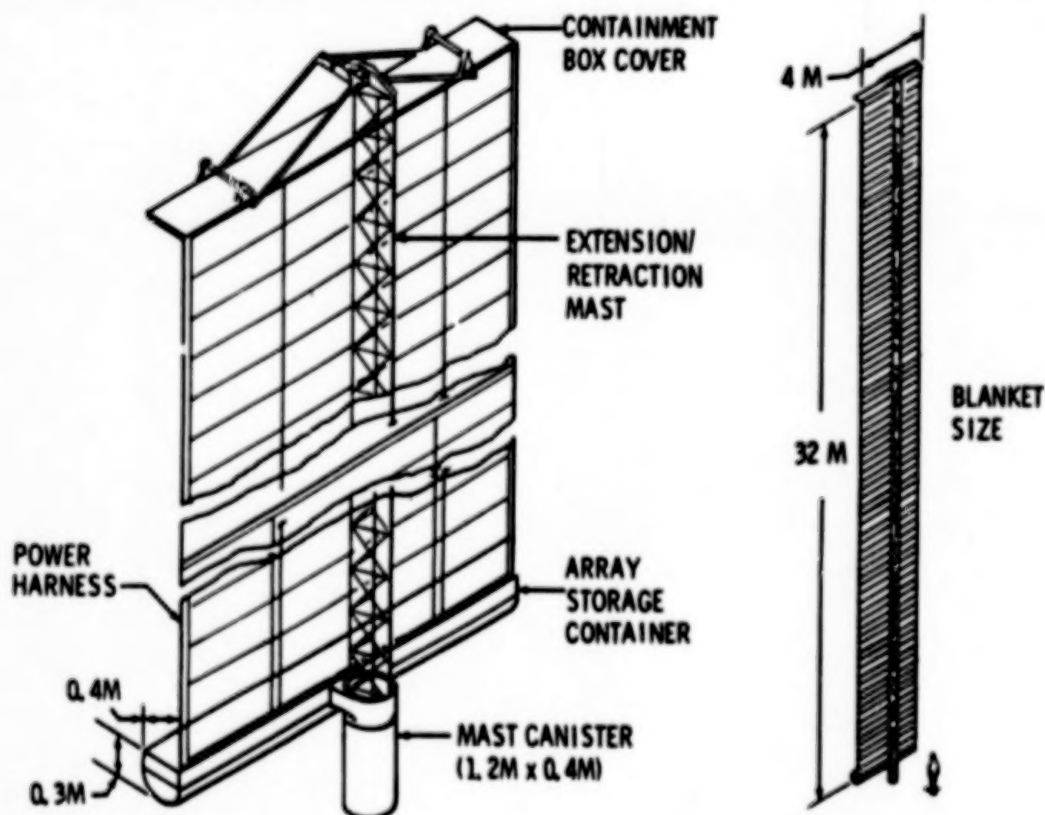


FLEXIBLE FLAT-FOLD SOLAR ARRAY TECHNOLOGY

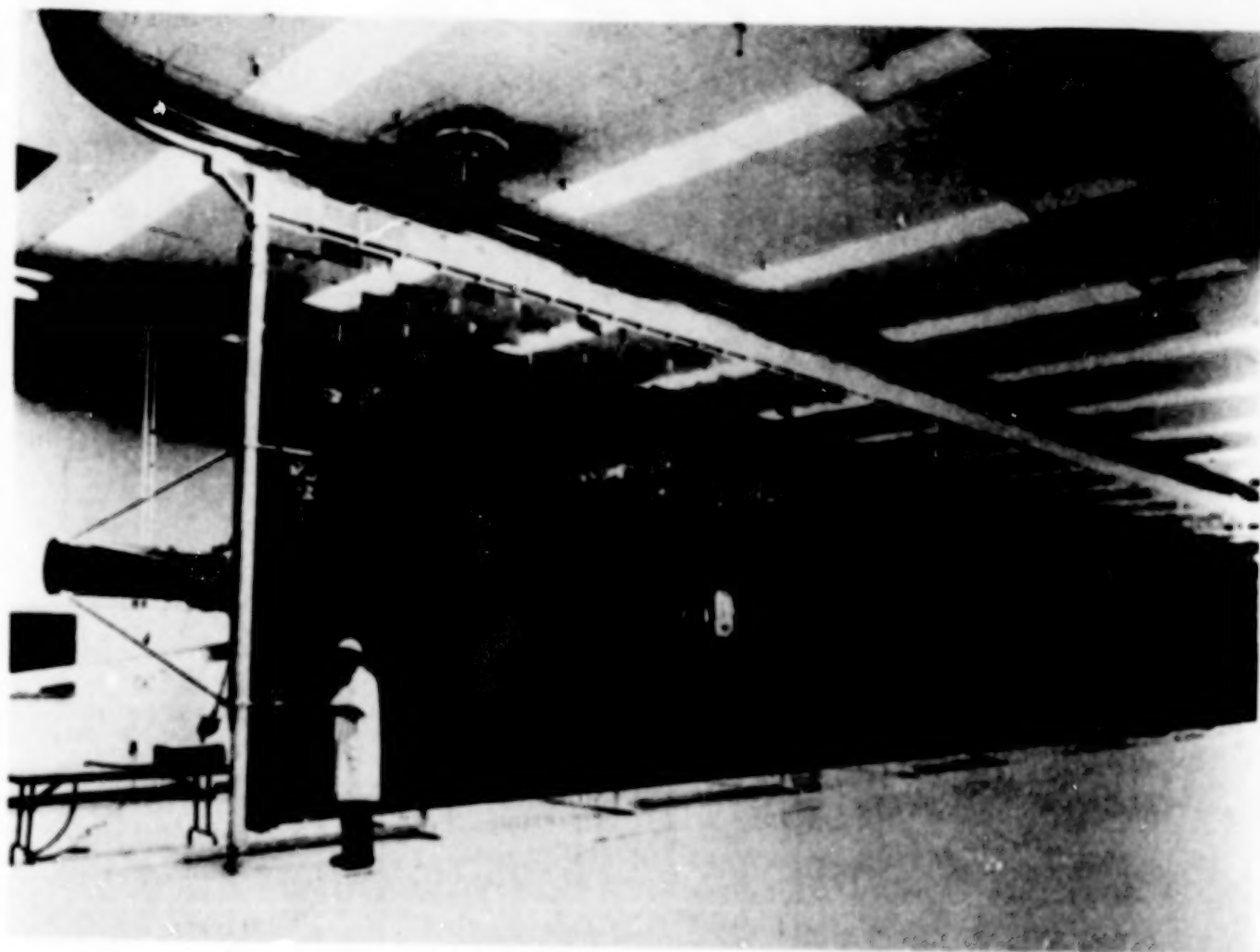
On-going studies of space systems which require large amounts of electrical power, tens to hundreds of kW, generally show flexible flat-fold solar array technology like that originally developed to meet solar electric propulsion mission requirements. The most demanding of these requirements are shown below. The design that meets these requirements utilizes a continuous longeron extension mast to provide the motion for extending and retracting Kapton panels which serve as substrates for the solar cells. Deployed solar array panels are held in tension by negator coils located at the base. The design is shown in the figure below, and an array wing that was built to demonstrate the technology is depicted on the next page.

Technology Development Requirements

- 0 low weight (>66 W/kg)
- 0 retractable
- 0 natural frequency ≥ 0.04 Hz
- 0 low packing volume
- 0 five year lifetime



ARRAY WING



SOLAR ARRAY FLIGHT EXPERIMENT

In 1976, NASA decided to fly the solar array technology development wing shown on the previous page as an experiment on the Space Shuttle. This requirement arose because extension/retraction characteristics and dynamic characteristics of large, lightweight structures like these can only be fully proven in the low gravity, low pressure environment of space. Overall objectives of SAFE are listed below. The wing will be extended and retracted several times during space testing. Accelerometers, photogrammetry, and a star tracker type system will be used to measure the wing dynamic characteristics. The Orbiter Vernier Reaction Control System (VRCS) will be used to dynamically excite the wing. The flight test is scheduled to take place in May 1984.

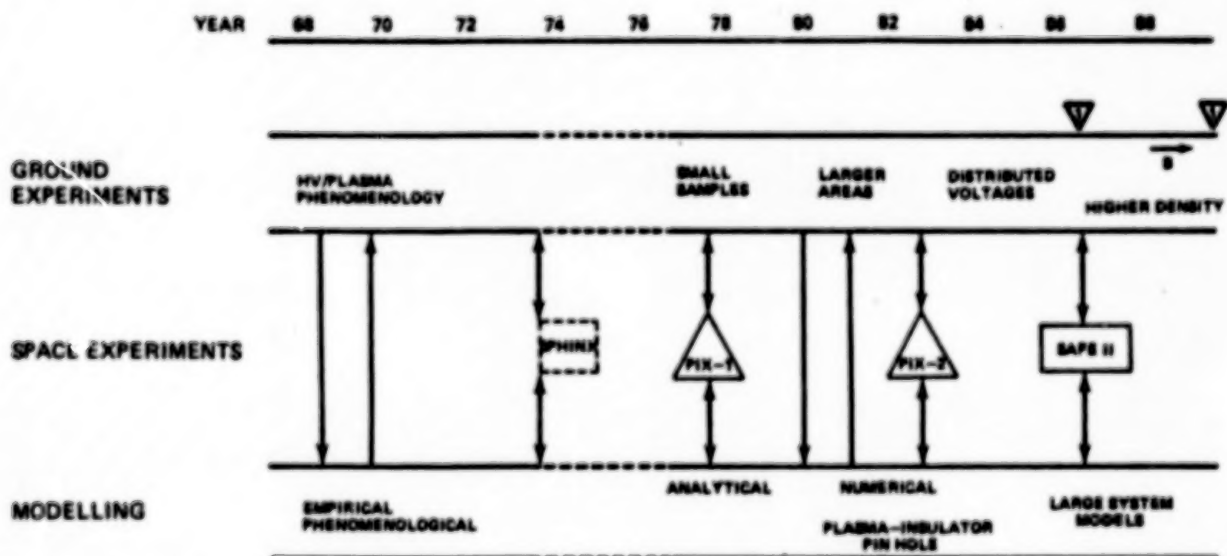
SAFE Objectives

- 0 Demonstrate extension/retraction characteristics of flexible, flat-fold solar array technology
- 0 Measure wing dynamic characteristics and prove analytical models
- 0 Measure electrical and thermal performance
- 0 Identify areas where future work can provide benefits
- 0 Provide space qualification of this technology at low cost and reduce risks for future missions where this technology is applicable



ENVIRONMENTAL INTERACTIONS

Investigation of interactions between high voltage systems and thermal plasmas was begun in the late 1960's. Experimental work using small segments of solar arrays and insulated electrodes with pinholes indicated that the presence of the insulators caused plasma current collection phenomena which departed dramatically from the predictions of Langmuir probe theory. Experiments indicated greatly enhanced electron collection at voltages in excess of about +150 volts, and arcing on solar array segments biased several hundred volts negative with respect to plasma ground. Concern for the implications of these results for high voltage systems in orbit prompted the development of the SPHINX (Space Plasma High Voltage Interactions Experiment) satellite. SPHINX was launched in early 1974 but failed to attain orbit due to a launch vehicle malfunction. Later, two Plasma Interaction Experiments (PIX-1 and PIX-2) were designed and built. PIX-1 flew in March 1978 as a piggy-back on the second stage of the Delta launch vehicle. Approximately two hours of data were returned by real time telemetry. The PIX-1 results verified that the collection enhancement and arcing phenomena observed in ground testing also occur in orbit (ref. 2). PIX-2, scheduled for launch in January 1983 as a piggy-back on the second stage of the IRAS Delta launch, will investigate distributed voltage effects and interactions among four segments of solar arrays independently biasable to ± 1 kV. A third flight experiment, SAFE II, is proposed. This will be carried on an equatorial Shuttle flight in 1986. It will allow experimental investigation of a number of important aspects of power system/environment interactions which cannot be examined except by a flight experiment.

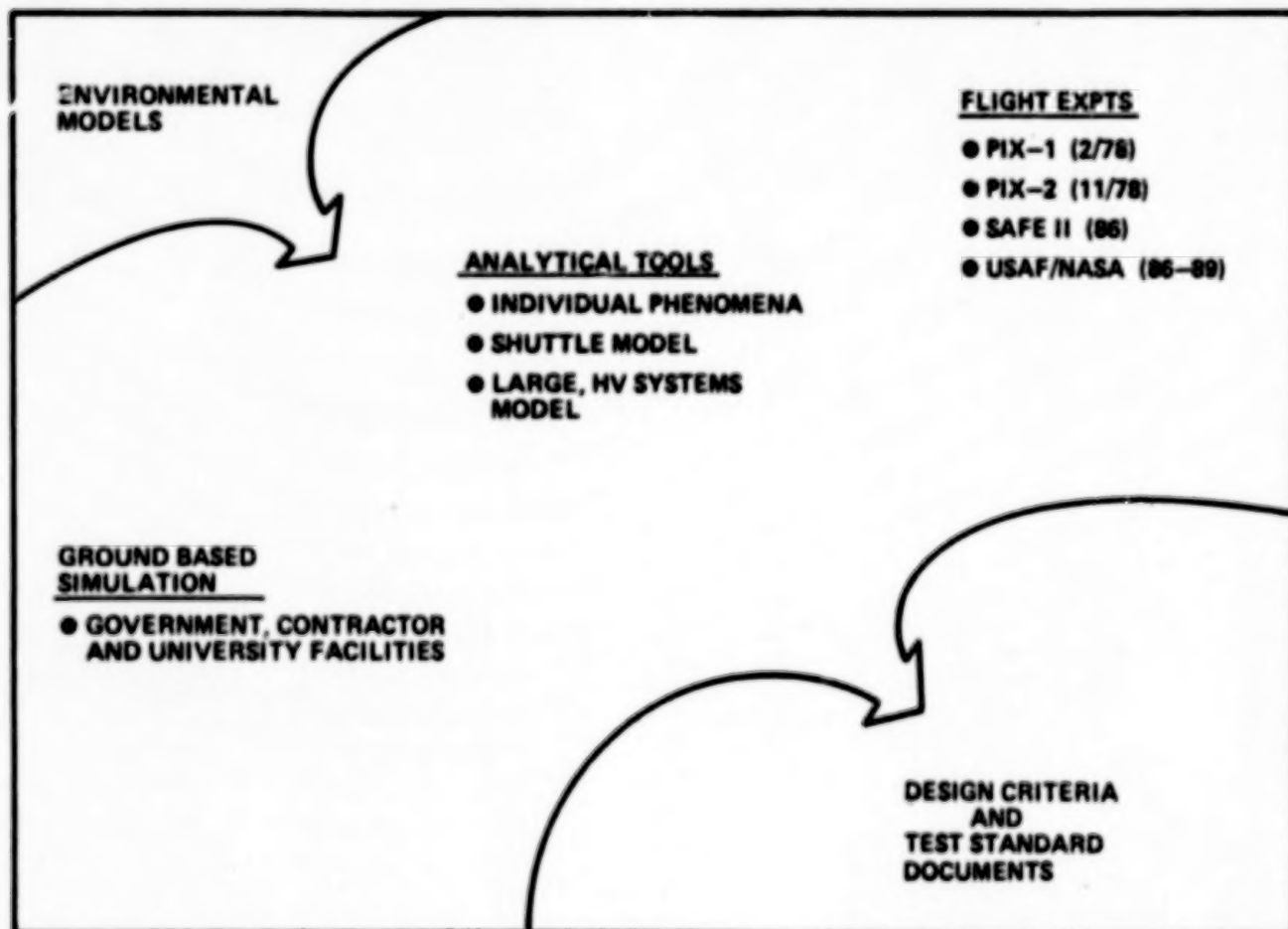


▽ DESIGN GUIDELINES DOCUMENTS

ENVIRONMENTAL INTERACTIONS EVALUATION

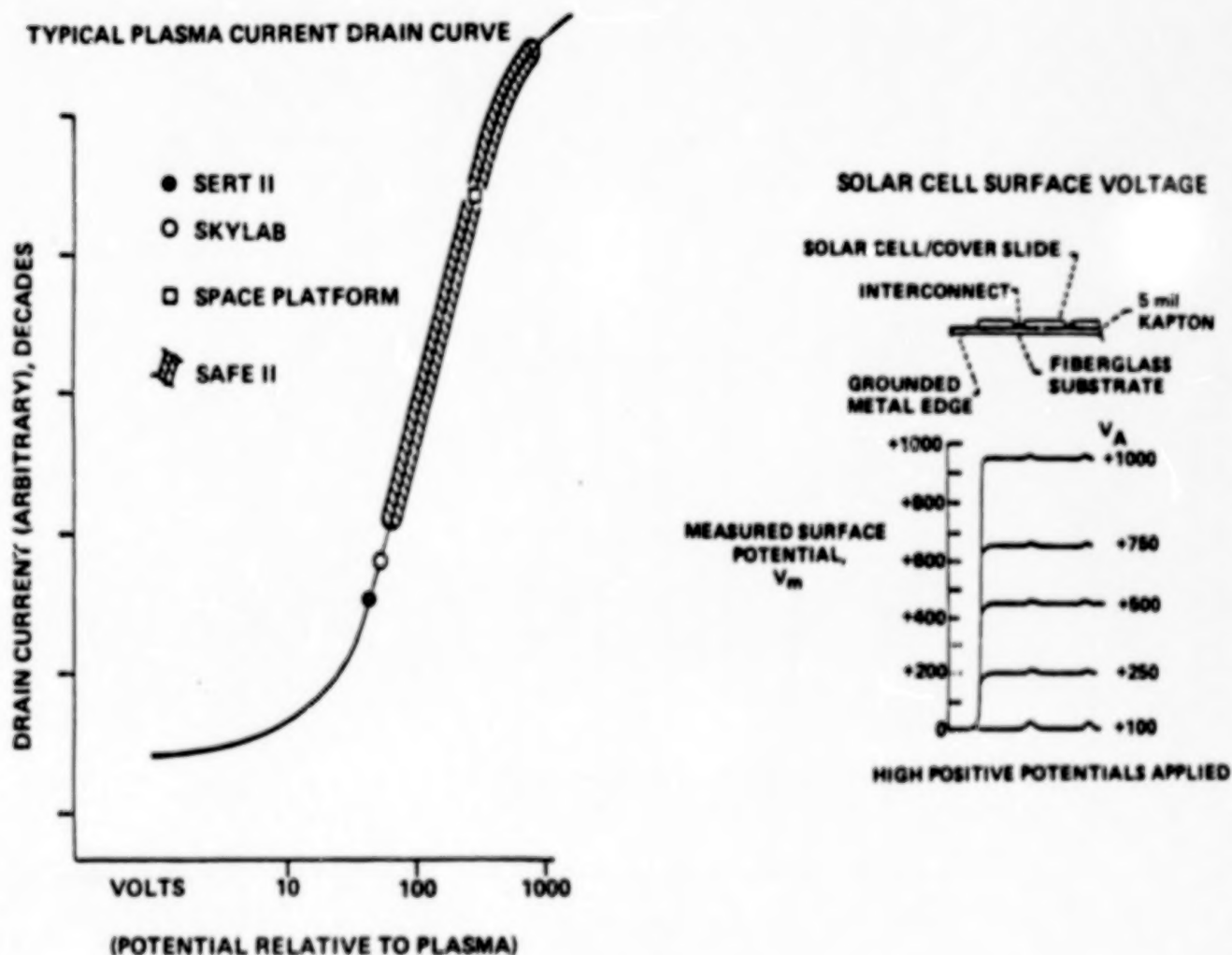
Subsequent to the loss of SPHINX, the attention of the environmental interactions community was for several years focused on the investigation of spacecraft charging, an interaction which had been found to be hazardous for geosynchronous spacecraft and was intensively studied by NASA and the Air Force. In the late 1970's, interest in high voltage interactions again intensified, and their study was resumed under the auspices of the joint NASA/USAF Environmental Interactions Investigation (ref. 3). The ground technology program utilizes the experimental facilities at NASA and USAF centers and builds upon the modeling capabilities developed during the spacecraft charging investigation, as well as utilizing the earlier high voltage study results (refs. 4-10). The goal is to develop design guidelines and analytical tools to guide the design of large high voltage systems in Earth orbit. The approach is to perform experiments and develop models in an interactive program in which experimental results are used to both guide and validate the models.

The ground technology program requires complementary flight experiment data, both to ensure that phenomena observed in ground testing occur in flight and to examine experimental conditions not obtainable in ground facilities.



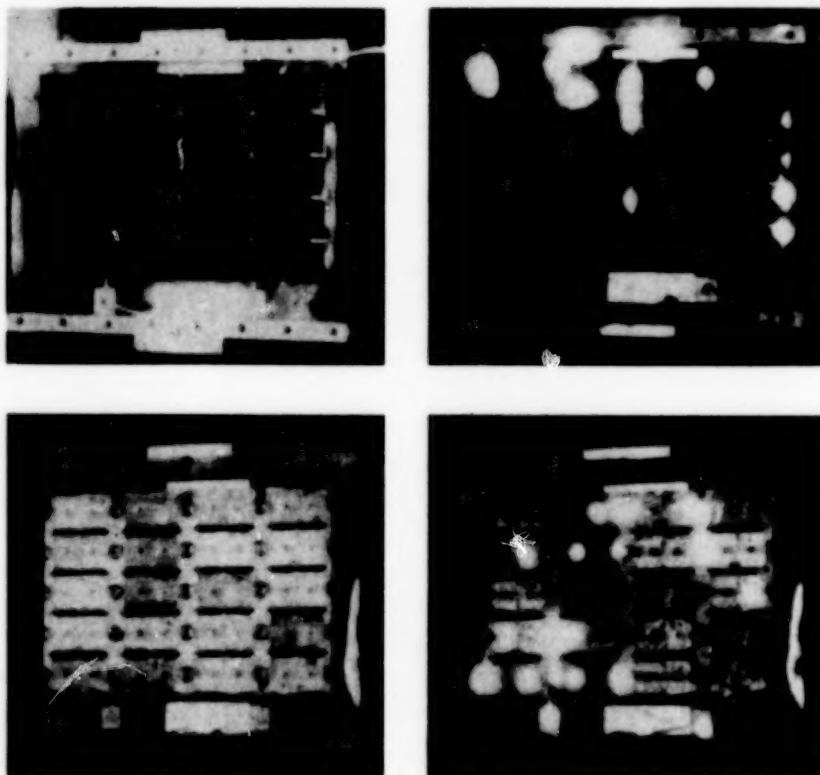
SOLAR ARRAY VOLTAGE POSITIVE RELATIVE TO PLASMA

The figure below represents experimental data of a solar array section biased positive with respect to the plasma it is immersed in (ref. 4). The left half of the figure illustrates that at voltages greater than near 100 volts the electron current collected by the solar array increases dramatically. The right half of the figure illustrates why. Even though the solar array surface is dielectric, the surfaces become highly positive and therefore collect current as though the whole surface were a conductor. The explanation appears to be that as the plasma sheath grows around exposed interconnects or pinholes the accelerated electrons strike the dielectric and low energy secondary electrons are released which are collected by the exposed metal. This leaves the dielectric cover glass positive, allowing the plasma sheath to grow over the solar cells. Therefore, the solar array collects electron current as though it were a conductor. As the voltage on the array segment increases and the collection area increases, the current collected rises, as indicated in the figure below. This current flow through the plasma is current which is not available to the spacecraft and therefore represents a power loss. Depending on the solar array voltage the power loss can be substantial and can seriously impact array performance.



SOLAR ARRAY VOLTAGE NEGATIVE RELATIVE TO PLASMA

The previous figure discussed the observed effects of a solar array segment biased positive of the surrounding plasma. Different effects are observed for a solar array segment biased to a negative voltage relative to the plasma. Unlike the positive voltage case, the solar cell cover glass voltage does not change as the solar cell voltage becomes more negative. A steep voltage gradient exists between the interconnect and other exposed metal parts of the solar cells and the solar cell surface. For impressed voltages of several hundred volts, arcing on the array is observed. Pictures of such arcing events are shown below (ref. 10). The arcing occurs at lower negative voltages for larger plasma densities. Arcing has been observed at voltages of -250 volts on a solar array segment in a plasma with a density of 10^4 electrons/cm³ (ref. 11). Ambient plasma densities of up to 10^6 electrons/cm³ may be encountered in space. Such solar array arcing will introduce large current and voltage transients which may tend to collapse the array voltage.

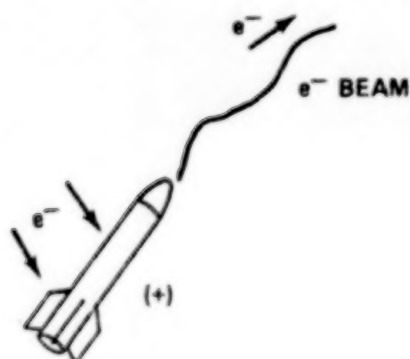


ARCING ON SOLAR CELL ARRAY SAMPLES
2 x 4 cm WRAPAROUND CELLS ON KAPTON
-1 kV BIASED ARRAY CIRCUIT
 10^5 cm⁻³ N PLASMA (25 eV IONS, 3 eV e⁻)

PLASMA PERTURBATION

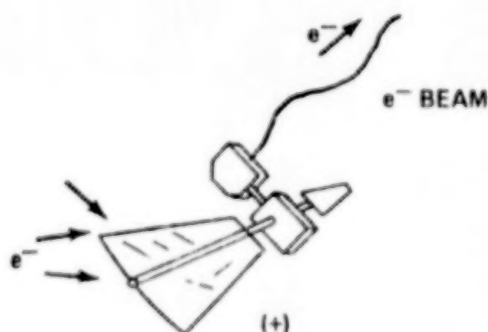
Many sounding rocket experiments have been flown which investigated the magnetosphere by releasing electron beams along the earth's magnetic field lines (ref. 12). It was anticipated that the rocket body would charge hundreds to thousands of volts positive due to the release of a high energy electron beam. This was not observed to be the case. The rocket potentials increased to only 30 to 100 volts positive. Plasma diagnostic devices indicate that the plasma density and temperature increased when the electron beam was released. A local discharge is created around the rocket either by electron bombardment ionization or a beam-plasma discharge (ref. 10). The plasma is also perturbed at large distances from the rocket. An analogous situation can be expected with a spacecraft powered by a high voltage solar array. An electron gun or plasma source operation will raise the spacecraft potential to near space potential and will therefore drive the high voltage solar array very positive of the space plasma potential. The local discharge and plasma perturbations observed during rocket experiments can increase power loss due to parasitic currents and interfere with science data acquisition.

ROCKET EXPERIMENTS



- ROCKET BODY DRIVEN POSITIVE
- RETURN CURRENT COLLECTION UNSTABLE
- PLASMA PERTURBED OVER LARGE VOLUME
 - DENSITY INCREASE
 - T_e INCREASE (DOUBLE POPULATION)
 - WAVES
- LOCAL DISCHARGE AROUND VEHICLE

SPACE STATION

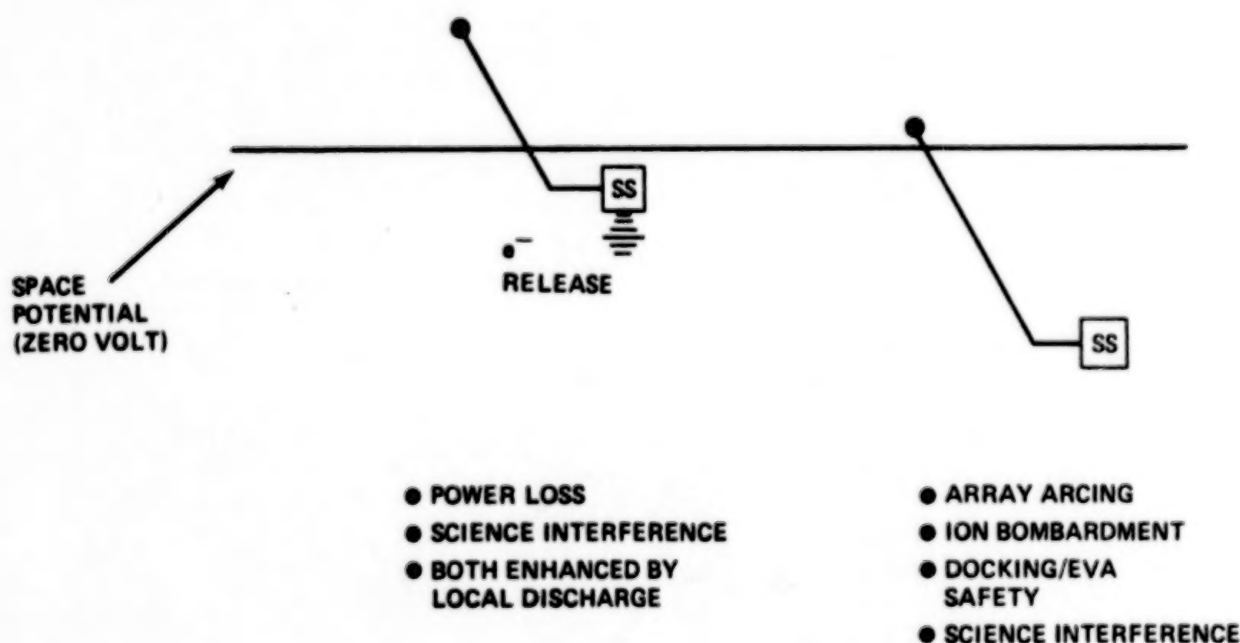


- HIGH VOLTAGE SOLAR ARRAY DRIVEN POSITIVE
- SITUATION ANALOGOUS TO ROCKET EXPERIMENT

SOLAR ARRAY SPACECRAFT SPACE PLASMA POTENTIALS

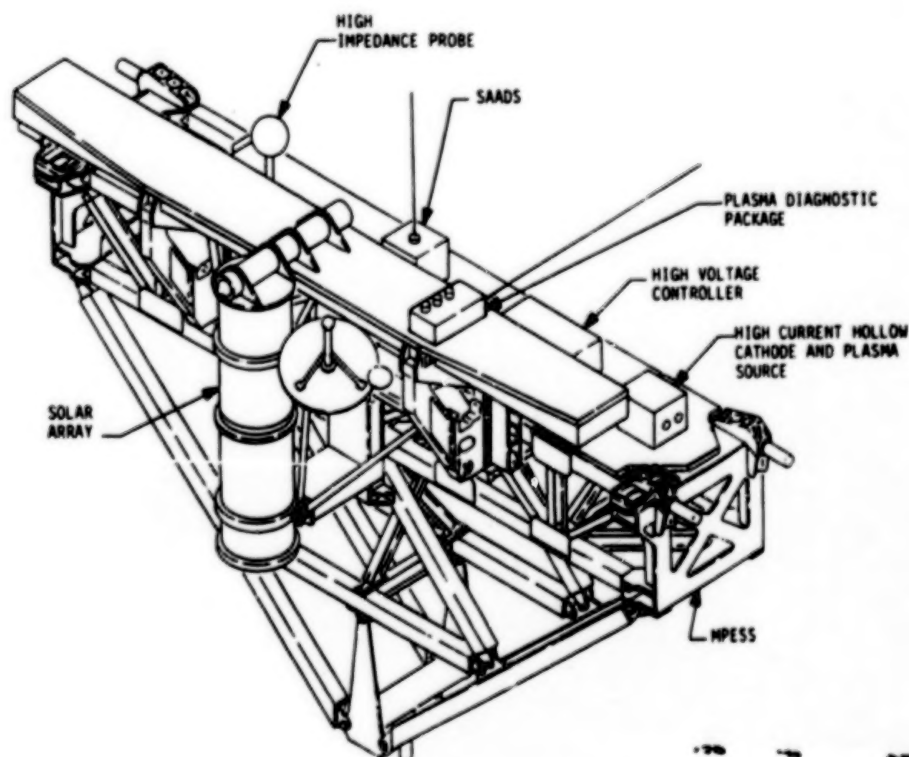
A spacecraft in orbit and immersed in the space plasma will come to a potential relative to the plasma such that no net current is collected. The solar array provides an additional complication since ambient charged particles can be collected. Because of their higher temperature and mobility, electrons are much more easily collected than ions. Therefore, to collect equal electron and ion current a much larger area at a negative potential relative to the plasma is required. For a negative solar array to spacecraft ground, the situation on the right side of the figure below will result. The spacecraft and negative side of the array will be driven negative of space potential. For an array of several hundred volts, solar array arcing may result. Since the spacecraft structure will be several hundred volts negative it will experience a continuous ion bombardment for the spacecraft lifetime which may alter surface thermo-optical properties. Another spacecraft or untethered astronaut will be near space potential. The resulting potential difference between such a free flyer and the highly negative spacecraft can pose safety concerns. The highly negative spacecraft potential will also interfere with some particle and plasma data acquisition.

If an electron gun or plasma source is operated on the spacecraft, electrons collected by the positive portion of the solar array will be released. Large negative potentials will not result, and if electrons are freely released, the situation on the left in the figure below will result. Power loss due to large electron current collection will result. This effect may be enhanced due to creation of a local discharge as previously discussed. Such a discharge will also interfere with science data acquisition of the ambient environment.



SAFE II CONFIGURATION

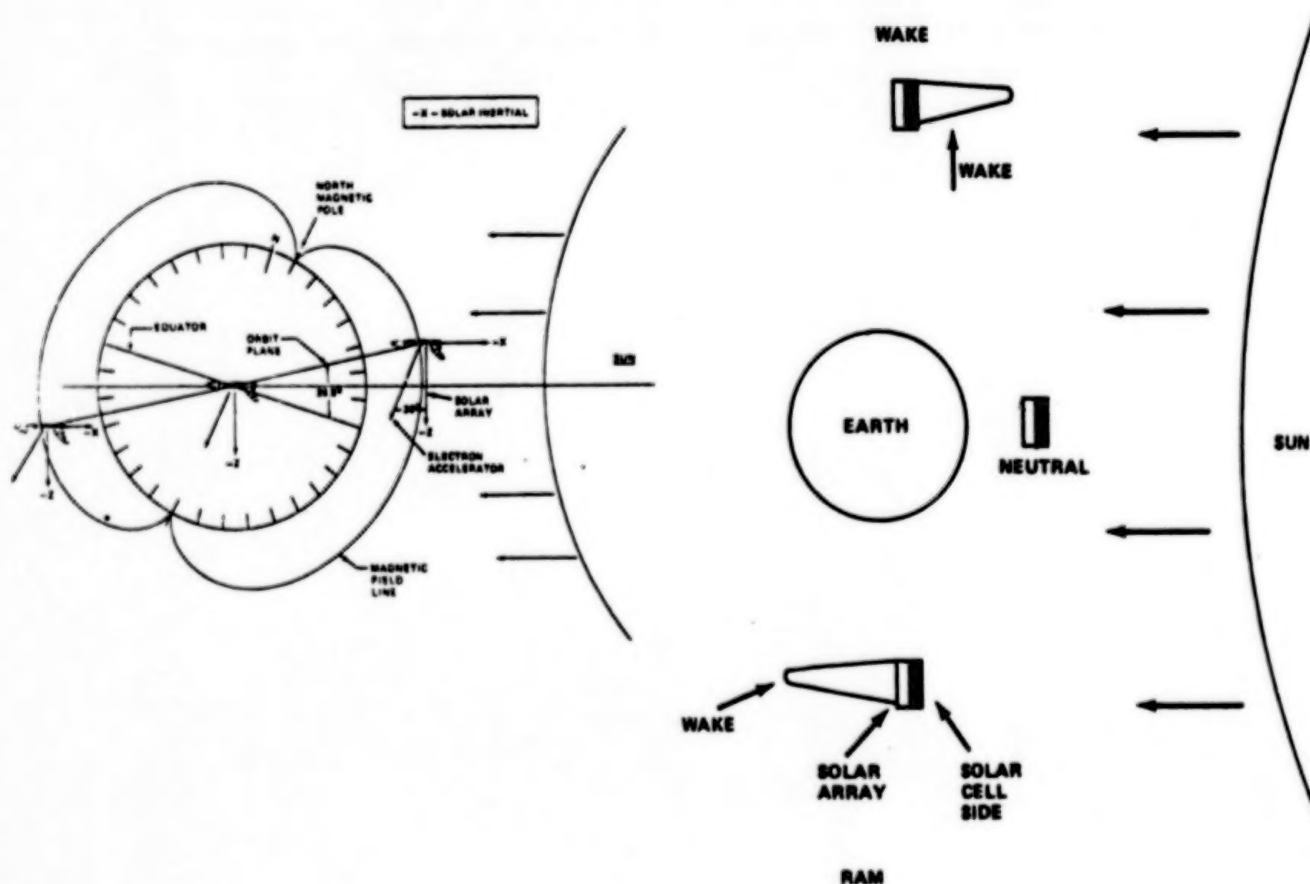
The SAFE II plasma interactions experiment will be a reflight of SAFE with the addition of the required equipment, shown in the figure below. Not shown are the three active panels of solar cells. Each panel will be composed of two modules. All the modules will be placed in various parallel and series configurations to allow testing at solar array voltages from approximately 85 to 500 volts. Tests will include switching the floating solar array from lower to higher voltages. The majority of the array, 80-90%, will float negative and arcing phenomena and floating potential measurements will be made. The high current hollow cathode and plasma source will be operated for positive solar array tests. These sources, possibly with the addition of an electron gun generating an energetic electron beam, will freely emit the solar-array-collected electrons back to space and will control solar array to space potential. The majority of the solar array will be positive of the space potential allowing array power loss evaluation as well as investigation of local discharge phenomena expected in the solar array vicinity. The array potential will be controlled by SAADS, Spacecraft Automatic Active Discharge System, of which the charge release devices are an integral part. Because of their interest in the results of this experiment, the Air Force Geophysics Laboratory intends to furnish this equipment to the SAFE II experiment. Some plasma diagnostics associated with SAADS will be located on the Mission Peculiar Experiment Support Structure, MPESS. Plasma diagnostics including a neutral density instrument, a Langmuir probe and a Differential Ion Flux Probe (ref. 13) will be mounted on the end of the solar array. These instruments will allow determination of the ambient conditions in which the plasma interaction experiment is conducted as well as evaluation of perturbations to the plasma due to the high voltage solar array operation.



ORBITAL CONFIGURATION

The figure below illustrates the anticipated orbital configuration of the SAFE II experiment. The left side of the figure indicates that the solar array and Shuttle tail will be pointed toward the Sun. This configuration is particularly advantageous for experiments involving electron release by electron gun. The beam can be projected along the magnetic field line and not strike the solar array. The generated plasmas will also tend to diffuse along magnetic field lines and away from the solar array.

The orbital velocities of spacecraft in low Earth orbit (LEO) are much greater than the thermal ion velocity but much less than the thermal electron velocity. The result is that as a spacecraft moves through the plasma it sweeps out the ions, leaving a much decreased plasma density in its wake, which is occupied by an excess of electrons. As observed in the figure below, there will be positions in the orbit where the wake is on the solar cell side and the backside of the solar array, and where no wake exists (when the spacecraft velocity vector and Sun line are perpendicular). Data acquisition at these various positions will allow determination of power loss, arcing and plasma perturbation over the range of anticipated orbital plasma conditions.



SUMMARY

For a number of years NASA and the USAF have planned space missions utilizing solar arrays which generate orders of magnitude more power and operate at a much higher voltage than has been flown previously. During this same time ground technology programs have addressed the interactions between such a high voltage solar array and the ambient space plasma. These programs have given us a basic understanding of what interactions to anticipate and under what conditions. Ground test information has been augmented by flight tests which verified that the effects observed on the ground are observed in space. However, it has long been recognized that ground tests are limited by facility size, facility effects on plasma and electric field conditions and the capability to accurately simulate space plasma conditions. It is very important to test actual solar array performance with a large, self-generated voltage so that effects of large array area, surface voltage gradients and varying currents in the solar array can be evaluated. It is not possible to do this adequately in a ground test chamber.

The SAFE II experiment will allow collection of data on high voltage solar array operation under actual operating conditions. Experiments with both extreme negative and positive potentials, relative to space, will be conducted. These will be performed with the solar cells in plasma ram, wake, and neutral conditions. Plasma diagnostics will allow determination of ambient and perturbed plasma conditions for all experiments conducted as part of SAFE II. The SAFE II experiment will allow direct data acquisition on high voltage solar array operation in space, which is required to verify ground based interaction concepts and analytical models.

REFERENCES

1. Stevens, N. J.: Interactions Between Spacecraft and the Charged-Particle Environment. Spacecraft Charging Technology - 1978, NASA CP-2071, 1978.
2. Grier, N. T.; and Stevens, N. J.: Plasma Interaction Experiment (PIX) Flight Results. Spacecraft Charging Technology - 1978, NASA CP-2071, 1978.
3. Pike, C. P.; and Stevens, N. J.: Agreement for NASA/OAST - USAF/AFSC Space Interdependency on Spacecraft - Environmental Interaction. Spacecraft Charging Technology - 1980, NASA CP-2182, 1980.
4. Kennerud, K. L.: High Voltage Solar Array Experiments. NASA CR-121280, 1974.
5. McCoy, J. E.; and Konradi, A.: Sheath Effects Observed on a 10-Meter High Voltage Panel in Simulated Low Earth Orbit Plasmas. Spacecraft Charging Technology - 1978, NASA CP-2071, 1978.
6. McCoy, J. E.; and Martucci, D. T.: Experimental Plasma Leakage Currents to Insulated and Uninsulated 10-m² High Voltage Panels. Spacecraft Charging Technology - 1980, NASA CP-2182, 1980.
7. Katz, I.; Cassidy, J. J.; Mandell, M. J.; Parks, D. E.; Schnuelle, G. W.; Stannard, P. R.; and Steen, P. G.: Additional Application of the NASCAP Code. Vol. I: NASCAP Extension. NASA CR-165349, 1981.
8. Nonhaast, J. H.; Chaky, R. C.; Armstrong, T. P.; Enoch, J.; and Wiseman, G. G.: Numerical Simulation of Plasma-Insulator Interactions in Space. Part I: The Self-Consistent Calculation. Spacecraft Charging Technology - 1980, NASA CP-2182, 1980.
9. Chaky, R. C.; Nonnast, J. H.; Armstrong, T. P.; Enoch, J.; and Wiseman, G. G.: Numerical Simulation of Plasma-Insulator Interactions in Space. Part II: Dielectric Effects. Spacecraft Charging Technology - 1980, NASA CP-2182, 1980.
10. Stevens, N. J.; Roche, J. C.; and Grier, N. T.: Large Space System: Charged Particle Environment Interaction Technology. NASA TM-79156, 1979. (Also AIAA Paper No. 79-0913.)
11. Grier, N. T.: Experimental Results on Plasma Interactions With Large Surfaces at High Voltage. NASA TM-81423, 1980.
12. Winckler, J. R.: The Application of Artificial Electron Beams to Magnetospheric Research. Rev. Geophys. and Space Phys., vol. 18, no. 3, Aug. 1980.
13. Stone, N. H.: Technique for Measuring the Differential Ion Flux Vector. Rev. Sci. Instrum., vol. 48, no. 11, 1977.

MAST SPACE RESEARCH FLIGHT EXPERIMENT

John L. Allen and Brantley Hanks
NASA Langley Research Center
Hampton, Virginia

Large Space Antenna Systems Technology - 1982
NASA Langley Research Center
November 30 - December 3, 1982

INTRODUCTION

Over the last few years, NASA has been developing the Space Shuttle in order to place in orbit a new class of spacecraft which we have called large space systems (LSS). During the same time many of the organizations of the agency have been exploring the character of these systems, from large orbital antennas to manned space stations, and have initiated the development and ground-based testing of technologies required to accomplish those next-generation missions.

Now that the operational Shuttle exists, there is the opportunity and the need to test and validate in space the theories, structural concepts, and system components required by those missions.

It is not our intention to discuss the need for space testing, but rather to outline a flight research program focused on discipline-based issues in structures, dynamics, and controls. Hopefully this will be affordable, and will be defined by a series of flights building progressively from modeling and modal characterization of large space structures to the more complex issues of flexible-body interactive control. The approach described is one that incrementally builds modal and functional complexity into a baseline configuration, allowing the design of a sequence of phenomena model test articles that address a chosen set of LSS discipline issues. In this way the discipline research objectives, and therefore the phenomena model configuration, can be tailored to the major concerns of LSS spacecraft, but may be independent of the specific configurations ultimately chosen for these new missions.

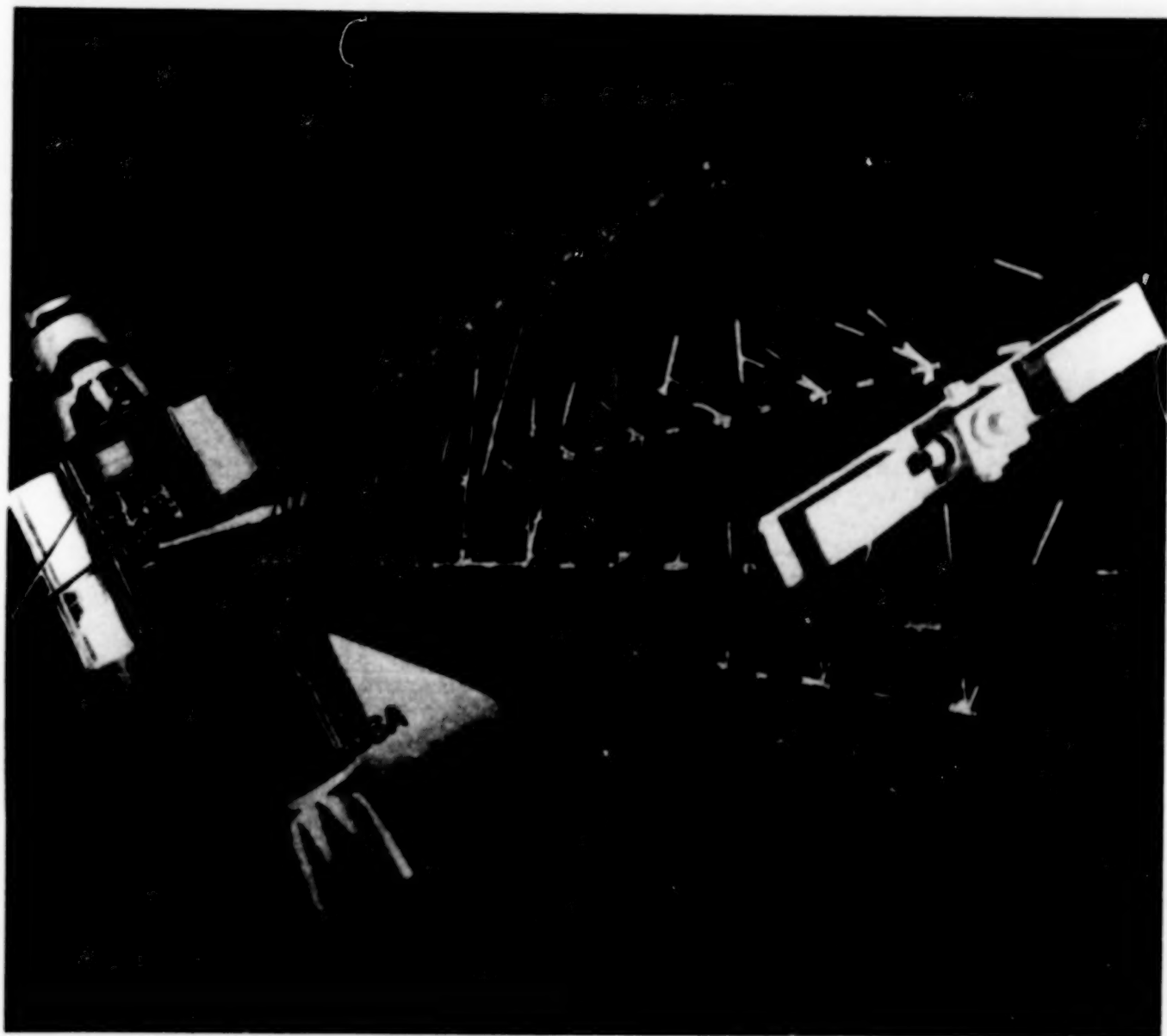
LARGE SPACE SYSTEMS

THE SPACE STATION



LARGE SPACE ANTENNA SYSTEMS





BEST AVAILABLE COPY

MAST FLIGHT RESEARCH PROGRAM OVERVIEW

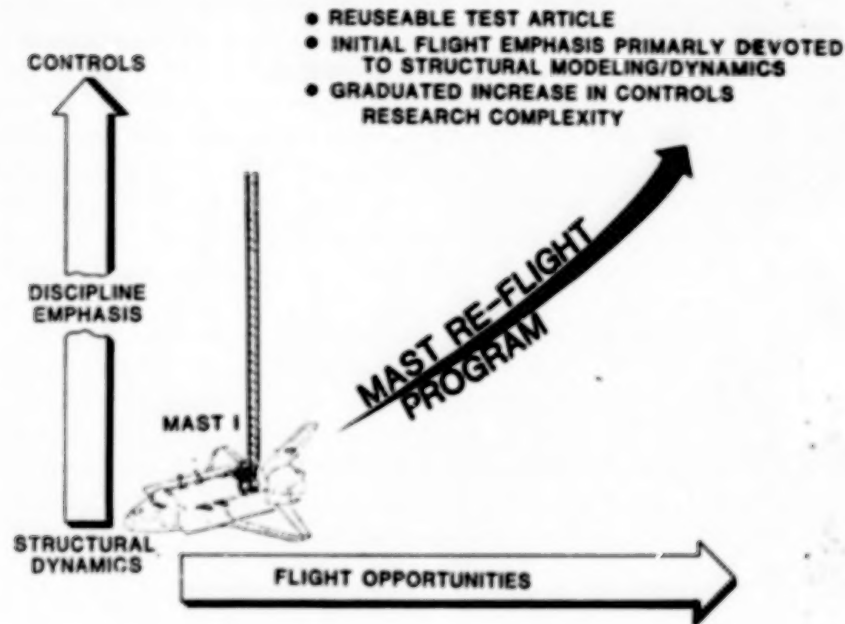
The MAST flight experiments comprise a research program focusing on major LSS issues for which it is deemed necessary to test, measure, and validate techniques and concepts in the space environment. In this sense, the program is a logical extension of the standard development and test flow that we have all used. In the standard flow, most development activity would terminate at the successful conclusion of ground-based testing. There are elements of large space systems which cannot be characterized or validated on Earth to the extent that mission success or system performance is assured. These particular research activities must be moved to the Laboratory of space and those findings integrated into the analytical and ground-based data before it can be said that "technology readiness" has been achieved.

The MAST Shuttle-attached test articles will be transported to space by the STEP experiment carrier and will be compatible with STEP interfaces in all configurations.

As the experiments require no particular orbit and the operational timelines needed for mission performance are not extensive, it is foreseen that the STEP/MAST combination could provide an attractive repetitive element within the Shuttle mixed-cargo manifesting process. Using the STEP experiment carrier and a retractable reusable test article will allow repetitive flight research to the extent that the STEP is able to be manifested on a regular basis.

Since this research program will be examining generic phenomena, maximum emphasis will be placed upon information quality and the fidelity with which the phenomena model emulates the LSS issue. As such, the MAST research does not constitute a hardware demonstration program, nor is it focused on any particular mission or space structure. However, the developed test articles will be spacecraft-quality space-qualified structures. The characteristics of the MAST test article will be driven by the nature of next-generation LSS structural systems such as large antenna spacecraft and space stations. In addition, the end item structure will be characteristically suitable to serve as a space test bed for evaluation and validation of newly developed LSS sensor and actuator devices.

MAST MULTI-FLIGHT RESEARCH PROGRAM



MAST EXPERIMENT OVERVIEW

MAST IS:

- MULTI-FLIGHT EXPERIMENTAL RESEARCH PROGRAM CONDUCTED IN THE LABORATORY OF SPACE VIA STEP EXPERIMENT CARRIER
- MULTI-DISCIPLINE EFFORT IN STRUCTURES/STRUCTURAL DYNAMICS AND CONTROLS
- SHUTTLE-ATTACHED EXPERIMENT FOR INVESTIGATING GENERIC PHENOMENA AND ISSUES OF LARGE FLEXIBLE SPACE STRUCTURES
- WEIGHTED TOWARD MAXIMUM INFORMATION (INSTRUMENTATION) AS OPPOSED TO MAXIMUM UTILITY (HARDWARE DEVELOPMENT)

MAST IS NOT:

- A HARDWARE DEMONSTRATION PROGRAM
- FOCUSED ON ANY PARTICULAR MISSION OR SPACE STRUCTURE

TECHNICAL THRUSTS OF LARGE SPACE STRUCTURES DISCIPLINES

The basic technical thrusts of the MAST space research program are expressed in three disciplines of large space structures. Within the structures area, the development of a precision, efficiently packaged, space-qualified truss structure is the primary focus. The structural dynamics discipline will drive toward the definition of dynamic response prediction techniques, particularly joint damping phenomena in a flexible-joint-dominated truss and the correlation of ground and flight dynamic test data. In the controls area, space validation of multivariable control techniques for flexible body spacecraft is the primary motivation.

STRUCTURES

- PRECISION LIGHTWEIGHT DEPLOYABLE STRUCTURES

STRUCTURAL DYNAMICS

- STRUCTURAL DYNAMIC RESPONSE PREDICTION TECHNIQUES

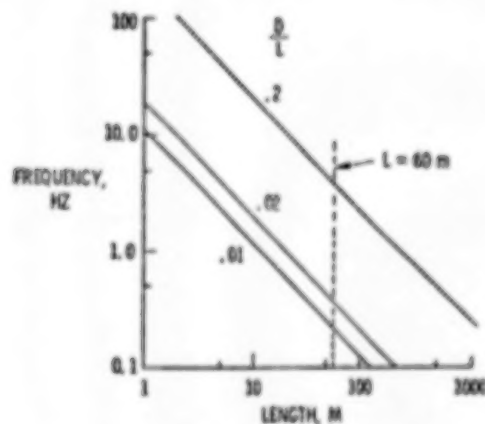
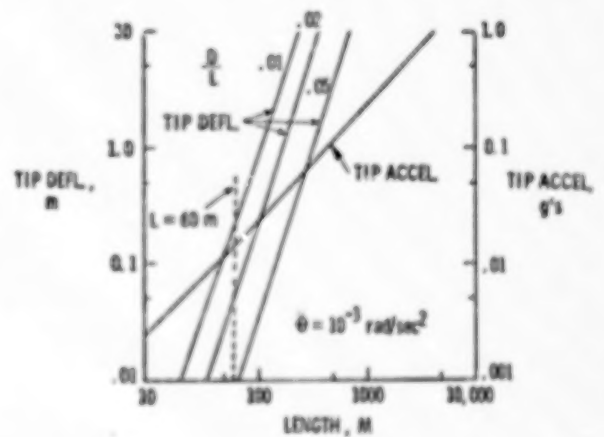
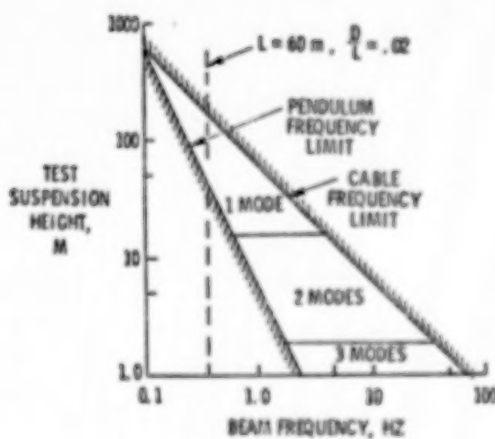
CONTROLS

- MULTI-VARIABLE CONTROL TECHNIQUES

MAST DESIGN CONSIDERATIONS

The deployable beam, which will serve as the MAST test article, must satisfy the needs of each of the three technical disciplines. It must have the qualities of a usable piece of spacecraft structure and have flexible properties which are of interest to the dynamicist and controls designer. It must also be ground testable through some of its deployed states, and must maintain structural margins cantilevered from the Orbiter bay while the Shuttle is operating in the vernier reaction control system mode.

Meeting of all these conditions has provided a major challenge to the MAST principal investigator. The characteristics that have to be balanced against one another are typified in part by the curves shown below. These allow consideration of characteristics such as beam diameter and length (D/L), bending mode frequency, tip deflection and acceleration, and ground test feasibility for the examined combinations. Through the use of such trades, we have selected a characteristic set for the baseline test article which meets the test of all three participating disciplines and will meet the operating structural and dynamic constraints of the STS. These characteristics are displayed in the following figure.



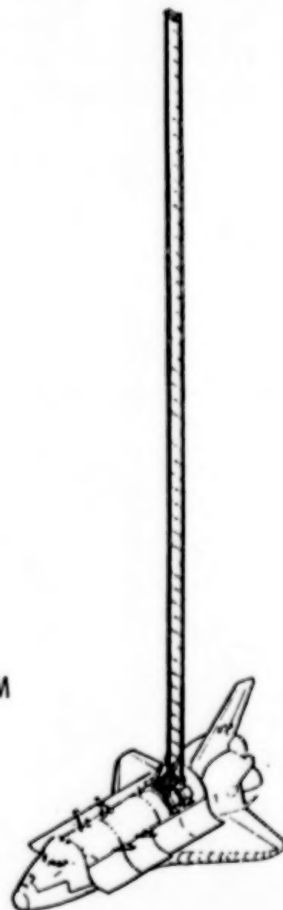
PRELIMINARY REQUIREMENTS OF BASELINE CONFIGURATION MAST

The requirements shown are for the MAST program in its simplest configuration, the baseline configuration. Expanded configurations will be described later which provide added degrees of structural, dynamic, and avionic complexity.

The length of the composite deployable beam, 60 m, may seem short in the figure, but in earthbound terms it is approximately the height of a twenty-story building. The truss depth, 1.2 to 1.4 m, is three or more times the depth of the continuous longeron mast to be flown in the SAFE experiment, and the truss of entirely different construction.

The root acceleration shown is a design specification based upon inputs generated by the vernier RCS of the Shuttle. The 0.15-Hz lowest natural frequency is selected in order to escape experiment interaction with the Shuttle digital autopilot. Tip position and truss displacement measurements will be provided by an optical system. An active actuator/damper set will be installed at the beam tip in order to provide modal excitation for the systems identification activity, and to provide test article damping to shorten test timelines during space-based model surveys. With the tip actuator set, the baseline truss can be excited at either extremity, by base inputs from the Shuttle using the vernier RCS, or by actuator inputs at the truss tip.

- GENERAL SIZE/CONFIGURATION
 - 60-METER LENGTH/COMPOSITE MATERIAL
 - 1.2 - 1.4 METER DIAMETER
 - LOWEST NATURAL FREQUENCY ≥ 0.15 Hz
 - UNLOADED/UNLOADABLE JOINTS
 - SEQUENTIALLY DEPLOYABLE TRUSS BEAM
 - ROOT MOMENT ACCELERATION 10^{-3} RAD/SEC² DOUBLE PULSE
 - COMPATIBLE WITH STEP EXPERIMENT CARRIER
- INSTRUMENTATION/DATA ACQUISITION
 - MODE SHAPES OF FIRST 5 MODES EACH AXIS
 - TIP POSITION ACCURACY TO 1 CM, MAXIMUM RESPONSE 0.5M
 - LINEAR SHAPE TO 1 CM
 - TEMPERATURE MEASUREMENTS AT TBD LOCATIONS
 - LOADS AT STEP INTERFACE
 - TIP MOUNTED ACTIVE ACTUATOR/DAMPER SET



MAST FLIGHT EXPERIMENT OBJECTIVES

The specific objectives listed here define the development flight activity required to support the LSS technical discipline thrusts in structures, structural dynamics, and controls.

The structures objectives are obvious--the development, fabrication, modeling, and testing of a lightweight, efficiently packaged, LSS-deployable truss test article. The development of a spacecraft-quality composite "zero"-CTE deployable structure of this size will be a major activity and should provide valuable insight into those problems inherent in fabrication, assembly, and test of first-generation large-scale composite structures.

The structural dynamics objectives relate to the ability to model and predict the dynamic character of a flexible-joint-dominated truss system, and particularly to assess damping phenomena and deployment dynamics. The ability to modally characterize the structural system by system identification techniques will also be evaluated.

The development and evaluation of multivariable techniques for the control of flexible structure in the presence of system uncertainty are the concerns of the controls experiment objectives. The objectives of the structures and dynamics disciplines can be completed using the baseline cantilevered beam, as defined in previous sections. The controls discipline objectives can be probed in part by the same baseline configuration; however, additional complexity must be included before the full set of controls objectives may be addressed.

MAST FLIGHT EXPERIMENT OBJECTIVES

STRUCTURES

- DEVELOPMENT AND GROUND TEST OF AN EFFICIENT PRECISION DESIGN 60-METER DEPLOYABLE TRUSS
- EVALUATE STRUCTURAL MODELING AND ANALYTICAL TECHNIQUES THROUGH MEASUREMENT OF FIGURE FIDELITY AND MAST TIP LOCATION
- EVALUATE THERMAL DISTORTION EFFECTS IN LARGE SPACE STRUCTURES
- VALIDATE SPACE TRUSS DEPLOYMENT WITHIN OPERATIONAL SPACECRAFT ENVIRONMENT

DYNAMICS

- DETERMINE THE DEGREE TO WHICH THEORY AND GROUND TESTING CAN PREDICT FLIGHT PERFORMANCE OF LOW-FREQUENCY STRUCTURES
- EVALUATE MATH MODELING OF LARGE LIGHTWEIGHT COMPLEX SYSTEMS ON WHICH GROUND TEST RESULTS ARE QUESTIONABLE
- EVALUATE SYSTEM IDENTIFICATION TECHNOLOGY ON COMPLEX LIGHTWEIGHT STRUCTURES IN REAL SPACE ENVIRONMENT
- EVALUATE DEPLOYMENT DYNAMICS IN ZERO-G
- EVALUATE JOINT DAMPING PHENOMENA IN ZERO-G

CONTROLS

- EVALUATE TECHNIQUES FOR RESPONSE CONTROL ON LOW-FREQUENCY, LIGHTWEIGHT STRUCTURES
- EVALUATE SYSTEM PERFORMANCE FOR FINE FIGURE/POINTING CONTROL OF FLEXIBLE STRUCTURES
- EVALUATE "ROBUST" DESIGNS IN PRESENCE OF UNCERTAINTY OF DYNAMIC CHARACTERISTICS
- EVALUATE ON-LINE SYSTEM IDENTIFICATION ALGORITHMS
- EVALUATE SENSOR/MEASUREMENT TECHNIQUES AND ACTUATOR APPLICATIONS IN LOW FREQUENCY SYSTEMS

MAST BASELINE EXPANSION

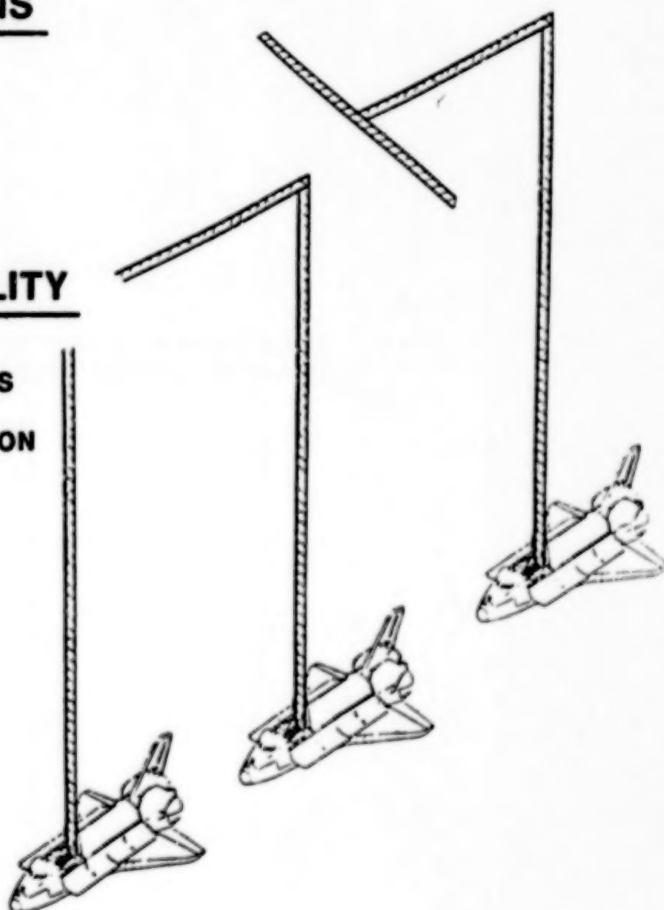
Examples of configurational alterations are displayed in the figure below. With the addition of distributed actuators and sensors and a flight controls computer, evaluation of multivariable control techniques can be initiated using the baseline cantilevered mast. With the addition of structural appendages with selected characteristics, the closely spaced modal frequencies and complex coupled motions required for the LSS research program can be produced. These phenomena model configurations will be designed to achieve the full range of characteristics necessary for a broad flight experiment program in LSS controls and dynamics.

CONFIGURATIONAL ALTERATIONS

- STRUCTURAL APPENDAGES
- DISTRIBUTED ACTUATORS/SENSORS
- FLIGHT CONTROL COMPUTER

EXTENDED RESEARCH CAPABILITY

- CLOSELY SPACED MODAL FREQUENCIES
- MODES WITH COMPLEX COUPLED MOTION
- MULTI-VARIABLE CONTROL
- ON-LINE SYSTEMS IDENTIFICATION



CONTROLS DISCIPLINE RESEARCH ISSUES

The controls objectives listed previously represent the broad goals of LSS controls research. The issues which may be addressed in part by the expanded baseline phenomena models are presented below.

- **SYSTEM MODEL IDENTIFICATION**
- **DISTRIBUTED CONTROL**
- **FIGURE CONTROL**
- **POINTING CONTROL/POSITION CONTROL**
- **SLEWING/SETTLING**
- **MODAL DAMPING**
- **DISTURBANCE ACCOMMODATION**
- **FAILURE IDENTIFICATION/RECONFIGURATION**
- **STABILITY/ROBUSTNESS**
- **ACTUATORS/SENSORS/INSTRUMENTATION EVALUATION**

SUMMARY

The flight test approach which has been described here provides an affordable and achievable bridge between today's technology level and the development and validation of a new plateau which must be reached in order to build and operate the large antenna spacecraft and the space station and space platform configurations which we envision.

- The experiments are incremental and build in complexity.
- The research is a generalized discipline-based activity, yet traceability to LSS issues and to next-generation mission configurations should be apparent.
- When next-generation configurations are known, the MAST Program will be amenable to configurational modification in order to address specific mission research, as opposed to generic research, and the system will be in place to meet that need when it arises.

We do not intend to state that the MAST program meets all needs for future LSS-related problems, nor that it is the only acceptable approach. However, an end-to-end flight research program has to be devised which will address the broad range of concerns. It should be flexible in its ability to grow as new mission configurations are defined and as component technology matures.

- **PROVIDES A PLANNED AND AFFORDABLE BRIDGE BETWEEN TODAY'S GENERAL RESEARCH/TECHNOLOGY EFFORTS AND TOMORROW'S LARGE SPACE FLIGHT INITIATIVES**

- **PROGRESSIVE MAST PHENOMENA MODEL FLIGHT EXPERIMENT PROGRAM**
 - LOW COST INCREMENTAL EXPERIMENTS
 - GENERALIZED DISCIPLINE-BASED RESEARCH
 - READILY EXPANDABLE TO MEET CONFIGURATION-RELATED SPACE EXPERIMENTS

**A LARGE ANTENNA SYSTEM
FLIGHT EXPERIMENT**

**Keto Soosaar
The Charles S. Draper Laboratory, Incorporated
Cambridge, Massachusetts**

**Large Space Antenna Systems Technology - 1982
NASA Langley Research Center
November 30 - December 3, 1982**

A LARGE ANTENNA SYSTEMS FLIGHT EXPERIMENT

PROBLEM : BY WHAT PROCESS DO WE ACQUIRE CONFIDENCE IN OUR
ABILITY TO DESIGN, BUILD, FLY, AND OPERATE A
LARGE ORBITING ANTENNA STRUCTURE?

A BASIC ASSUMPTION

- A SERIOUS NEED ALREADY EXISTS FOR LARGE ANTENNAS

OR

- USERS WILL EMERGE ONCE DEVELOPMENT RISKS HAVE BEEN BOUNDED
AND SOME EFFORT HAS BEGUN

CURRENT UNCERTAINTIES WITH LARGE ANTENNAS

- RESULT MAINLY FROM INCREASED SIZE (5 TO 10x)
 - INCREASED FLEXIBILITY, NATURAL PERIODS, DISTURBANCE SUSCEPTIBILITY
 - TOLERANCES TIGHTENING WITH SIZE
- MAJOR UNCERTAINTIES
 - REALISTIC PERFORMANCE TEST IN 1 "G" NOT POSSIBLE
 - HIGH PACKAGING RATIO - COMPLEX AND RISKY DEPLOYMENT
 - POSSIBILITY OF VIBRATION CONTROL (ALIGNMENT AND SURFACE)
 - UNCERTAINTY THAT ANALYSIS CAN SUBSTITUTE FOR TESTS

PROCESS FOR ASSESSING SOME UNCERTAINTIES

- PRELIMINARY SYSTEMS DESIGN EXERCISE VERY USEFUL
 - DEFINE BASELINE SYSTEM GOALS AND PERFORMANCE OBJECTIVES
 - DEVELOP CONFIGURATION FOR SATELLITE AND ANTENNA
 - DEVELOP GOALS FOR MAJOR SUBSYSTEMS
 - PERFORM PRELIMINARY DESIGN OF SUBSYSTEMS
 - DEVELOP FIRST-ORDER MODELS FOR SUBSYSTEMS
- ANALYSIS, MODELLING, AND SIMULATION WILL INDICATE
 - POSSIBLE PERFORMANCE
 - WITH RESPECT TO SYSTEM OBJECTIVES
 - WITH RESPECT TO STATE OF ART
 - AREAS OF DEFICIENCY IN ANALYSIS TOOLS
 - MULTIDISCIPLINARY INTERACTION
 - REGIMES WHERE BEHAVIOR VIOLATES ASSUMPTIONS
 - AREAS WHERE ANALYSIS AND MODELLING TOOLS DO NOT EXIST
- ANALYSIS WILL OBVIOUSLY NOT UNCOVER UNMODELLED UNEXPECTED BEHAVIOR
 - THUS TEST PROGRAMS ARE CRUCIAL

TEST PROGRAMS WILL REDUCE RISKS THROUGH

- IDENTIFICATION AND QUANTIFICATION OF SUSPECTED PHENOMENA
- VERIFICATION OF THEORY, ANALYSIS, MODELLING APPROACHES
- DEMONSTRATION OF COMPLEX SUBSYSTEM
- PROTOTYPE FEASIBILITY DEMONSTRATION

SCOPE OF TEST PROGRAMS

- IDEALIZED--FLIGHT ARTICLE IN REAL SPACE ENVIRONMENT
- REALITY--COST, RISK, COMPLEXITY OF FULL-UP SPACE TEST
 - QUALIFIES ONLY SPECIFIC ARTICLE
 - PROVIDES LITTLE GENERIC GUIDANCE
 - SHOULD ONLY FOLLOW MUCH OTHER WORK
- DESIRABLE
 - PARALLEL DEVELOPMENT OF CONFIDENCE
 - ANALYSIS, SIMULATION TOOLS FOR COMPONENTS AND SYSTEM
 - LABORATORY EXPERIMENTS TO IMPROVE/CORROBORATE ANALYSIS
 - SPACE TESTS
 - TO OBSERVE IMPORTANT PHENOMENA OTHERWISE MASKED
 - TO DEMONSTRATE FULL INTEGRATED PERFORMANCE (SYSTEMS PRECURSOR)

VALIDATION OF STRUCTURAL BEHAVIOR - I

- EVEN WITH CONVENTIONAL SATELLITE STRUCTURE GROUND TEST
 - SIGNIFICANT DEPARTURE BETWEEN ANALYSIS AND SHAKER TESTS
 - GENERALLY UNABLE TO
 - ACCOUNT FOR DIFFERENCES
 - MODIFY MODEL APPROPRIATELY
 - NOT CERTAIN WE UNDERSTAND PHYSICS OF STRUCTURAL ASSEMBLIES
 - TO BOUND RISKS ON ANTENNA PROGRAMS
 - CAREFULLY PLANNED LABORATORY TESTS
 - RESEARCH ON STRUCTURAL BEHAVIOR
 - IMPROVEMENT OF ANALYSIS AND MODELLING TOOLS
 - DEVELOPMENT OF HIGH-ORDER SYSTEMS IDENTIFICATION APPROACHES
 - A FINAL VERIFICATION IN SPACE ON SUITABLE ASSEMBLAGES DESIRABLE BUT NOT CRUCIAL

VALIDATION OF STRUCTURAL BEHAVIOR - II

- WITH LARGE FLEXIBLE ANTENNA GROUND TEST
 - GRAVITY EFFECTS CAN BE ENORMOUS ON FLIMSY STRUCTURES
 - STIFFNESS PROPERTY CHANGES RESULT IN
 - LARGER/SMALLER STATIC DEFLECTIONS
 - HIGHER/LOWER NATURAL FREQUENCIES
 - BUCKLING/STABILITY MARGINS ALTERED
 - NONLINEAR (LARGE-DEFLECTION) BEHAVIOR
 - STRENGTH AND PLASTICITY MARGIN CHANGES
 - EFFECTS ON MODAL SURVEYS
 - FREQUENCY, MODE SHAPE SHIFT DUE TO GRAVITY
 - ATMOSPHERIC DAMPING
 - JOINTS BOTTOMED OUT BY GRAVITY
 - BUNGEE CORD PHENOMENA (IF USED)
- SYSTEM ACCEPTANCE WILL ULTIMATELY DEPEND ON COMBINATION OF
 - ANALYTICAL PREDICTION
 - GROUND TESTS
 - SPACE TESTS

VALIDATION OF DYNAMICS, DEPLOYMENT AND UNPACKAGING

- COMPLEX INTERACTION BETWEEN RIGID BODY, FLEX BODY, POSSIBLE CONTROL
- FEW SPACE SYSTEMS HAVE BEEN FREE OF DEPLOYMENT PROBLEMS
- WITH LARGE ANTENNAS, SCALE OF PROBLEM BECOMES ENORMOUS

—DYNAMICS PHENOMENOLOGY UNCERTAIN

- POSSIBLE NONLINEARITIES IN DYNAMICS AND STRUCTURE
- STABILITY RISKS IN DYNAMICS AND STRUCTURE
- MUCH BASIC WORK NEEDED
 - THEORETICAL MODELS FOR 1g AND 0g
 - LAB TESTS TO VERIFY 1g MODELS
 - SPACE TESTS TO VERIFY 0g (FREE FLYER?)

—MANY INTERACTING AND INTERDEPENDENT DEPLOYMENT DEVICES

- RELIABILITY OF PROCESS CRUCIAL
- SYNCHRONOUS VERSUS SEQUENTIAL APPROACHES
- MUCH RESEARCH AND EXPERIMENT NECESSARY

VALIDATION OF FLEXIBLE CONTROL

- GROUND-BASED EXPERIMENTS CAN BE MADE ON ANALOGS OF FLIGHT ARTICLE TO PROVE SOME PERFORMANCE AND ROBUSTNESS PARAMETERS
- GROUND-BASED EXPERIMENTS ON REAL ANTENNA STRUCTURES
 - STRONGER, LONGER ACTUATORS
 - STRUCTURAL NONLINEARITIES MAY BE SIGNIFICANT
 - IDENTIFICATION AND ROBUSTNESS EXPERIMENTS MAY BE VERY INCONCLUSIVE AND NON-REPRESENTATIVE
- SPACE EXPERIMENTS WILL BE CRUCIAL
 - PRIMARILY BECAUSE OF STRUCTURAL/DYNAMIC UNCERTAINTIES
 - CONTROL SYSTEM CONFIGURED TO BE ROBUST FOR 1g TO 0g WILL EXCESSIVELY PENALIZE PERFORMANCE
- FULL-UP SYSTEM SPACE TEST CRUCIAL IF CONTROL IS ONLY MEANS TO ACHIEVE PERFORMANCE

VALIDATION OF SYSTEM PERFORMANCE

- EXPERIMENTALLY UNLIKELY IN 1g
- INITIALLY - MUST BE BASED ON SPACE TESTS
- ULTIMATELY -
 - BASED ON VALIDATED ANALYSIS AND SIMULATION TOOLS
 - AS NEW PHENOMENA ARE FOUND
 - SUPPLEMENTED BY GROUND TESTS
 - RARE SPACE TEST

SUMMARY : TO VALIDATE DESIGN AND ACCEPTANCE PROCESS WE NEED TO DO THE FOLLOWING

THEORY DEVELOPMENT : (START NOW)

- BEHAVIOR OF STRUCTURAL ASSEMBLIES UNDER VIBRATION
- BEHAVIOR OF FLIMSY STRUCTURES UNDER 1g
- COMPLEX DYNAMICS - ESPECIALLY DEPLOYMENT
- IMPROVED SYSTEMS IDENTIFICATION - OPEN & CLOSED LOOP

LAB TESTS : (START NOW)

- CAREFULLY MONITORED SHAKER TESTS
- FLIMSY STRUCTURES - MODEL VERIFICATION
- DEPLOYMENT MODEL VERIFICATION
- CONTROLS AND IDENTIFICATION DEMONSTRATIONS

SIMULATION DEVELOPMENT : (START NOW)

- CAPABLE OF MULTIDISCIPLINARY INTEGRATION/INTERACTION
- VERIFICATION THROUGH SUBSYSTEM TEST

SIMPLE FLIGHT EXPERIMENTS : (PLAN FOR EARLY FLIGHTS)

- STRUCTURAL RESPONSE, SYSTEM IDENTIFICATION, ZERO-G VALIDATION
- DEPLOYMENT DEMONSTRATION, MODEL VERIFICATION
- CONTROL AUTHORITY DEMONSTRATION VERSUS UNCERTAINTY
- LIMITED SIMULATION VERIFICATION

FULL-UP ANTENNA EXPERIMENTS : (EXPECT TO NEED)

- SYSTEMS-LEVEL VERIFICATION OF PERFORMANCE AND SIMULATION

**SADE – A SPACE EXPERIMENT TO DEMONSTRATE
STRUCTURAL ASSEMBLY**

**James K. Harrison and David C. Cramblit
National Aeronautics and Space Administration
Marshall Space Flight Center
Huntsville, Alabama**

**Large Space Antenna Systems Technology – 1982
NASA Langley Research Center
November 30 – December 3, 1982**

INTRODUCTION

During the last several years, the large space structures work at the Marshall Space Flight Center has followed the routine program scheme of planning exercises, analysis, and contractor studies followed by the ground tests of hardware components and systems. As the next step in this scheme a Structural Assembly and Demonstration Experiment (SADE) is proposed as a flight test to corroborate these previous steps and to demonstrate the space construction of a simple truss structure approximately 100 feet in length. It uses both deployable and erectable construction methods and will be built in the Shuttle bay where it remains throughout the flight. The SADE is scheduled to fly in 1985. Figure 1 shows SADE with some possible future applications of structural members like the SADE truss.

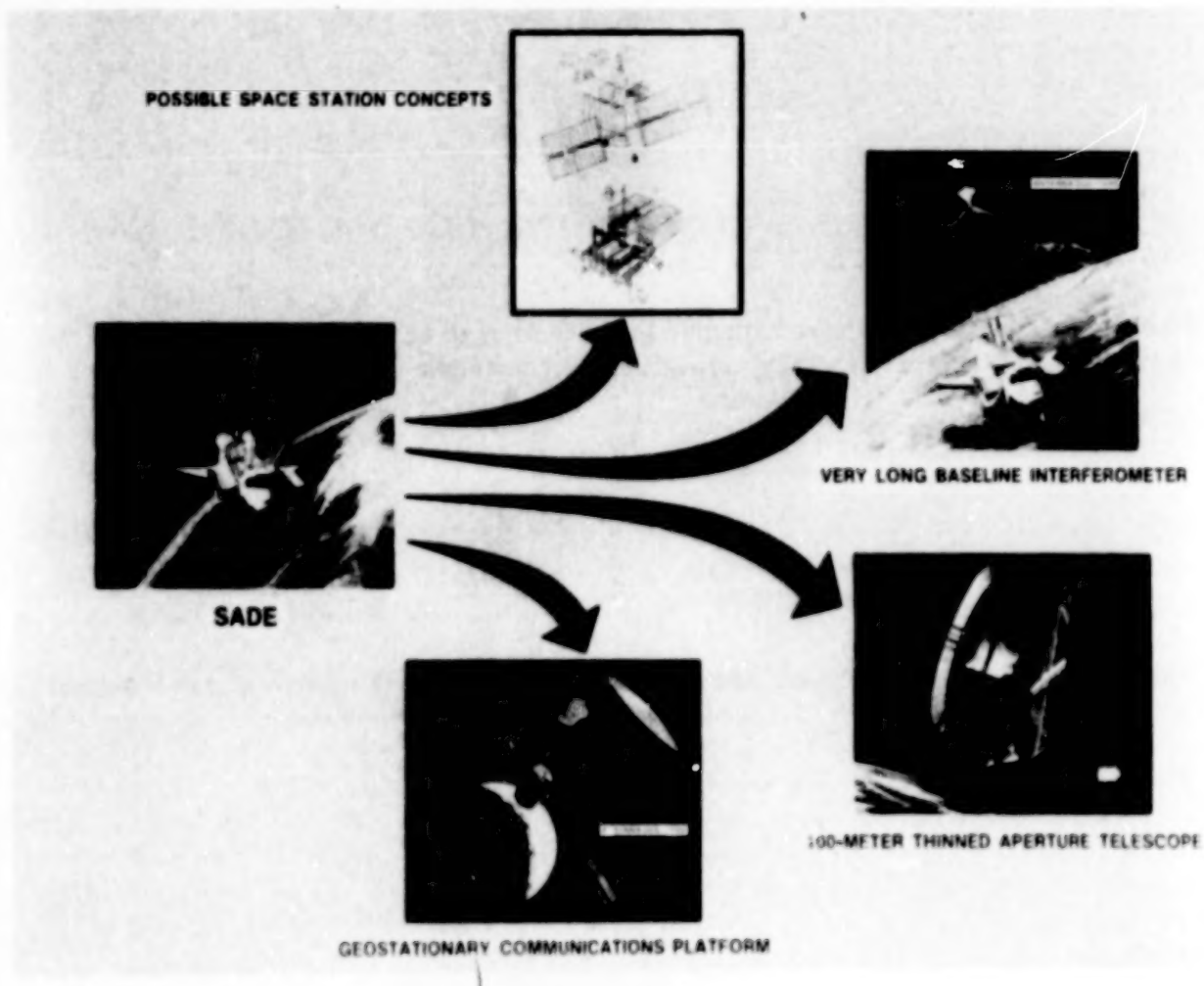


Figure 1. SADE showing some future possible applications.

PURPOSE

The purpose of SADE is first to demonstrate that the Shuttle is a suitable base for space construction; this includes a test of the Shuttle's control system to determine its performance when a long attached truss or beam is extended from the bay. Examples of Shuttle-related systems that will receive special attention are the RMS, the lighting system, and the crew assembly capabilities. A second purpose is to determine the extent to which the assembly results from the Neutral Buoyancy Simulator can be used to forecast the results of space assembly. And, finally, the SADE truss design will be validated by measuring the performance of the deployment, the special connectors, and the assembly methods.

MISSION

A single flight is planned in 1985. The precise construction sequence has not yet been developed; that will be done by MIT during the next 12 months and by the engineers at MSFC with help from the SADE tests to be run next year in the Neutral Buoyancy Simulator (NBS).

A possible construction sequence is shown in figure 2 and is as follows: Alternately erect one bay and deploy two until 9 bays are constructed. Then, automatically deploy the remaining bays until a length of approximately 100 feet is reached. The final length will be set by the truss frequency needed for a meaningful Shuttle control system-beam interaction experiment. A heavy mass — on the order of 5000 pounds — to influence the frequency will be placed on top of the truss using the RMS. Of course, this will have to be done early in the construction sequence so as to be within the reach of the RMS. EVA and the RMS will be used extensively throughout the construction of the truss.

The disassemble sequence of the truss is a reverse sequence to the assembly, except the automatic deployment is replaced by a manual retraction operation.

Three crewmen will be required for these construction operations. Two will participate in the EVA while the third one operates the RMS and the TV and photographic cameras, and reads the crew checklist.

The assembly and disassembly will each require about 3 hours with perhaps a span of several days in between during which time no firing of the Shuttle primary RCS can occur.

The suitability of the Shuttle to serve as a base for this type of activity will be determined primarily from the performance of the construction crew as recorded by the TV and photographic cameras. The capability of the Shuttle control system to damp undesirable oscillations in the truss structure will be tested during the time span between assembly and disassembly. JSC and Draper Labs are working with MSFC to define this control experiment. The final length and tip mass will depend on the truss frequency requirements set by this definition.

The camera data will also be used to measure and compare the on-orbit construction activity with similar preflight activity done in the NBS. This is especially useful with regard to the bays that are erected since they are built member by member requiring considerably more EVA assistance than the bays that are deployed.

Strain gages and accelerometers will be located on some of the structural members to measure the loads and forces encountered during the experiment.

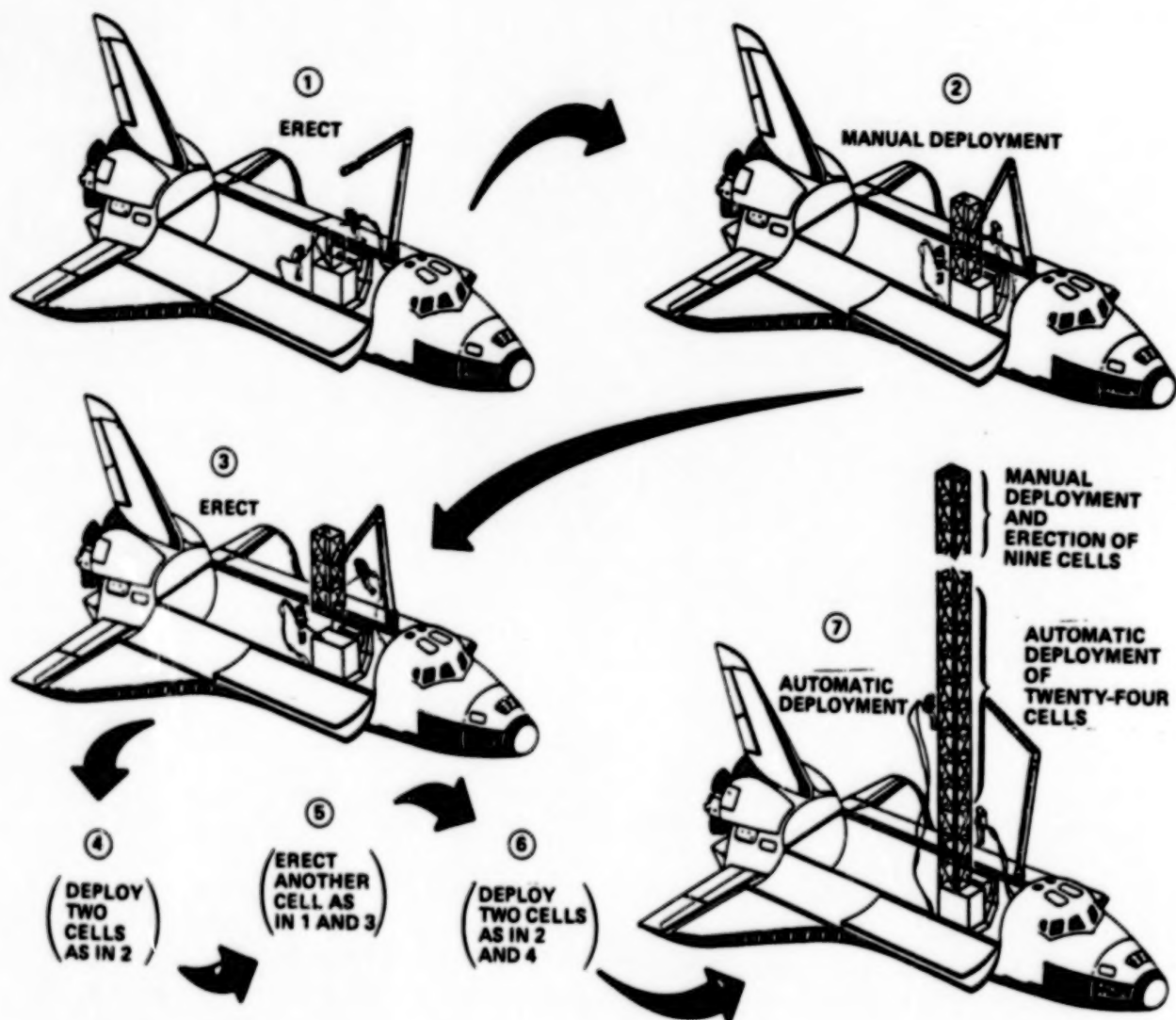


Figure 2. One possible SADE assembly sequence.

SYSTEMS

The principal SADE pieces (figure 3) are the truss structure, the launch assembly platform (LAP), the Spacelab pallet, the grapple fixtures, the connectors, and perhaps a data recording system if the Shuttle data system is not used.

The truss structure will be derived from the SASP ground truss now undergoing tests at MSFC and shown in a later figure. The exact length has not been determined but will be about 100 feet. The truss is aluminum (the bare structural weight is about 400 pounds) and is made up of cells or bays equal in size and cube-shaped; each is 5 feet on a side. A few cells are erected member by member, but the majority are deployed either manually or by using an automatic deployment system that has an electric motor driven cable that runs through the telescoping diagonal members of each bay. Retraction is done manually.

An interface structure between the truss and the Spacelab pallet is required to store the folded truss and perhaps other components as well, and to serve as a platform during the construction period. This structure is the LAP.

Grapple fixtures, somewhat modified for SADE, will be needed to permit the use of the RMS in handling the truss.

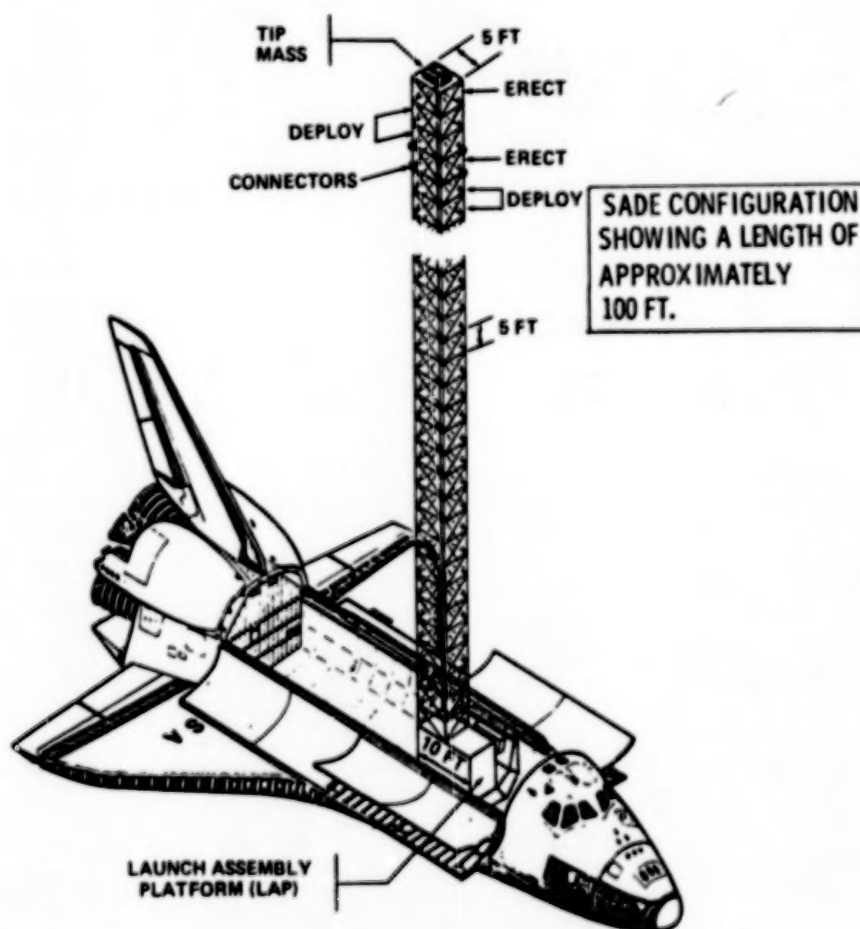


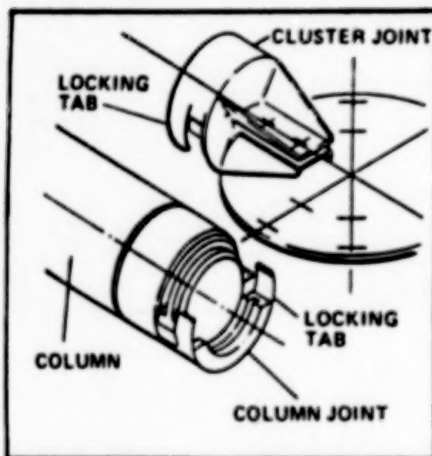
Figure 3. Principal SADE pieces.

CONNECTORS

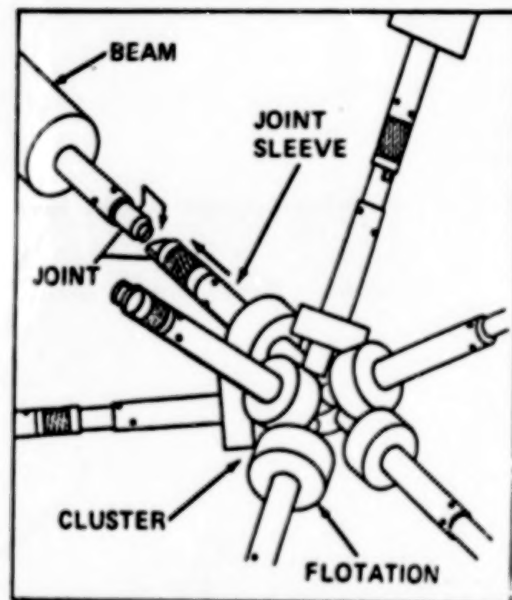
Four different connectors (figure 4) will be evaluated for use in the assembly of the SADE truss so that the most effective and satisfactory design for joining these types of structural members can be determined. The connectors join the erectable cells to the deployable cells (figure 3).

Whether or not SADE will use the Shuttle data recording system or provide its own will be determined when a more accurate estimate is made of the number of measurements and the sampling frequency.

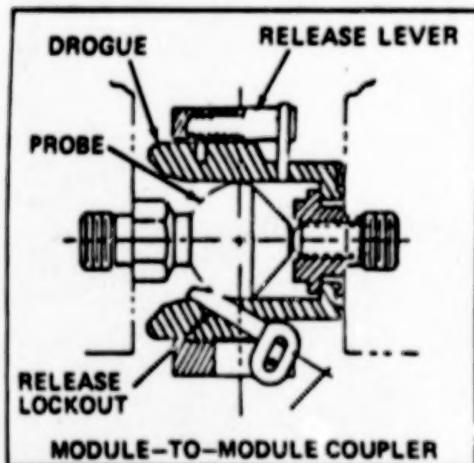
SADE CONNECTORS



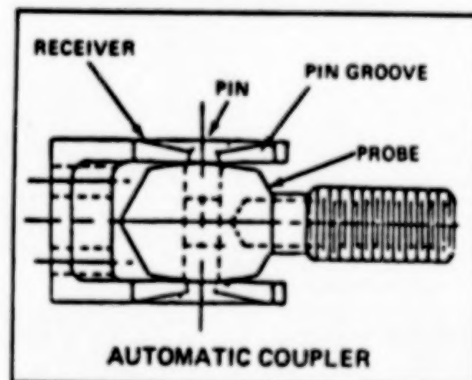
LARC SNAP-JOINT UNION



MIT CLUSTER SLIP-JOINT



VOUGHT MODULE-TO-MODULE COUPLER



VOUGHT QUICK-CONNECT COUPLER

Figure 4. Connectors to be evaluated for SADE assembly.

NEUTRAL BUOYANCY TESTS AND TRAINING

A key SADE objective is to correlate the Neutral Buoyancy Simulator (NBS) assembly activity and the space assembly activity. In future NBS activities this will permit a sort of calibration with respect to the tank's ability to simulate space construction.

To meet this objective, the assembly activity planned in the Shuttle bay will first be done in the NBS. The tank hardware will be as similar as possible to that used in space except, of course, the full deployed length cannot be handled by the NBS.

Training of the crew to handle the on-orbit assembly tasks will occur in the NBS using procedures and hardware similar to that used during the flight.

Some recent activities in the NBS that relate to SADE are depicted in figure 5.

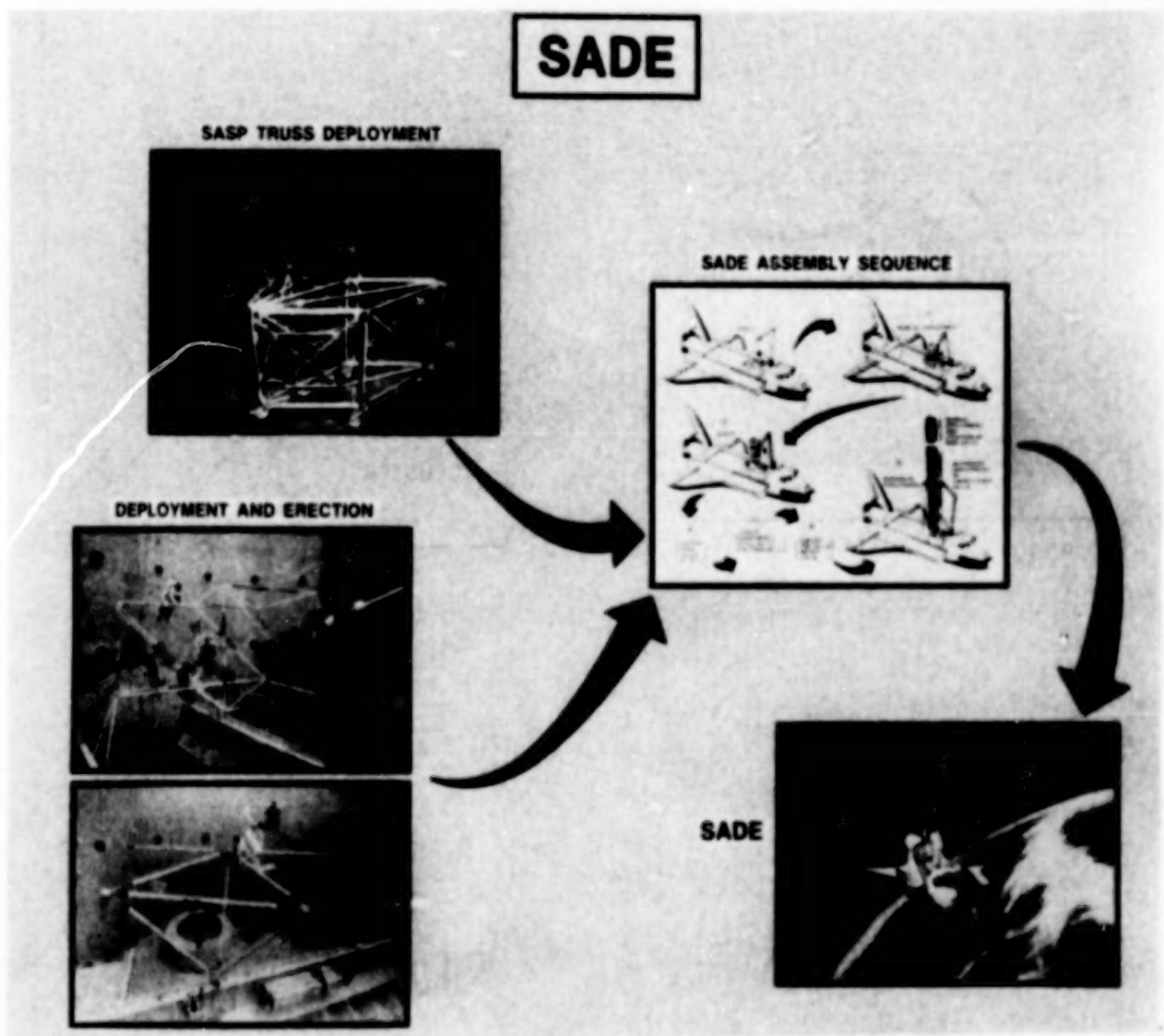


Figure 5. Recent activities that lead to SADE.

FINAL REMARKS

The principal in-house activity at the moment is the design of the hardware to be tested late next summer (1983) in the NBS. The schedule calls for this design activity to be completed this spring (1983) followed by completion of the fabrication work in time for the tests next summer. These tests will guide the flight hardware design which begins in January 1984 and is to be followed by the flight hardware fabrication which ends in the fall of 1984. This will allow time for the qualification and acceptance tests so that SADE can meet its mid-1985 launch date.

Out-of-house activity mainly involves help from MIT's Space Systems Laboratory in developing a detailed space assembly procedure plus some hardware for the NBS tests and the procurement of an underwater camera system for the NBS work. JSC, MSFC, and Draper Labs are working together to define a Shuttle control system-truss interaction experiment.

SADE (figure 6) is the first flight experiment devoted solely to large space structures. It represents a very simple yet significant step along the way leading to space construction of complete and complex systems. It will give the first indication of the Shuttle's capability to serve as a base for building these kinds of systems at a later date. It will also give the first indication of the value of both deployable and erectable construction methods, and finally, it will give the first indication of the value of the Neutral Buoyancy Simulator to simulate space assembly.

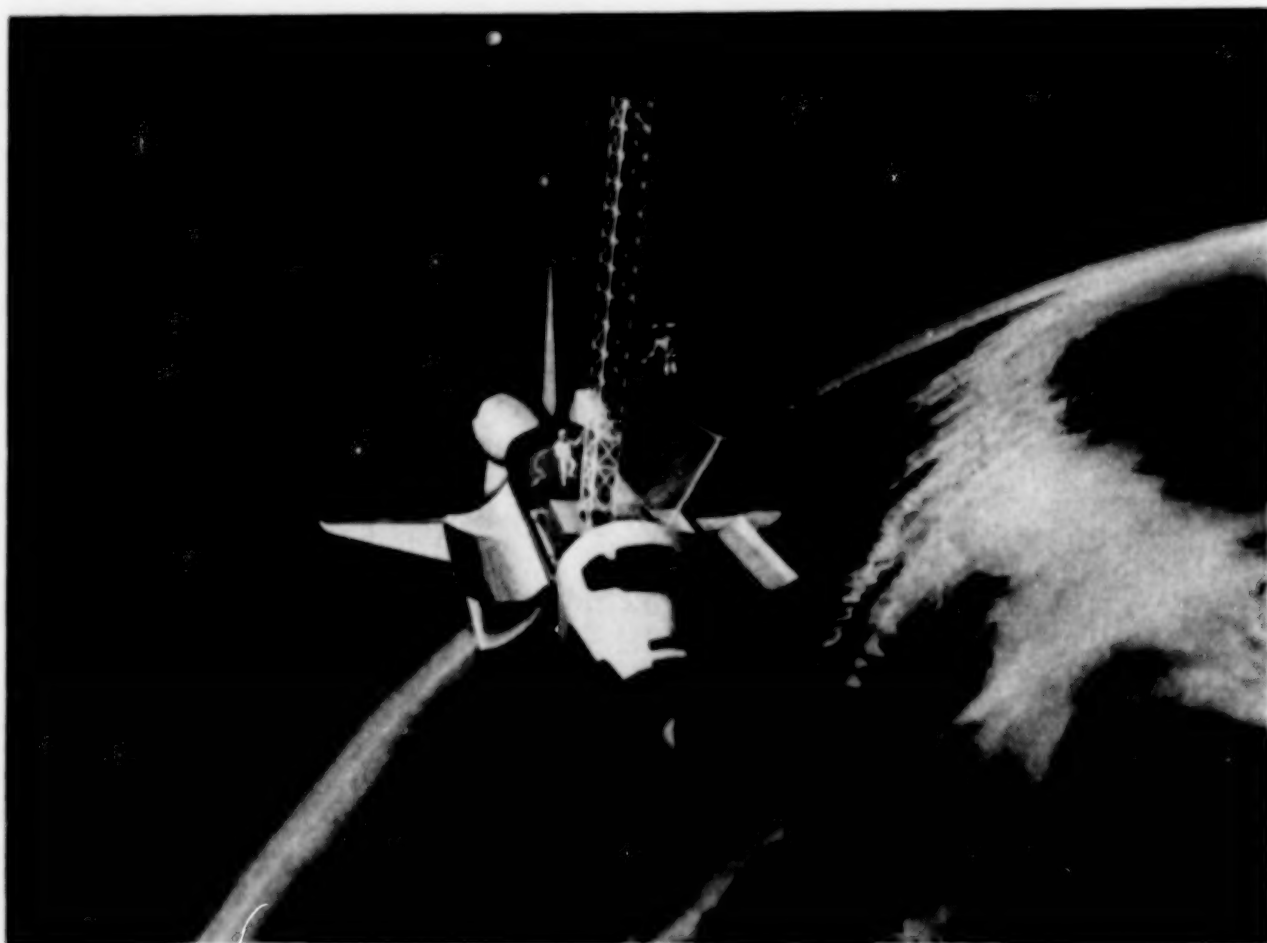


Figure 6. SADE structural assembly and demonstration experiment.

1. Report No. NASA CP-2269, Part 2		2. Government Accession No.		3. Recipient's Catalog No.	
4. Title and Subtitle LARGE SPACE ANTENNA SYSTEMS TECHNOLOGY - 1982				5. Report Date May 1983	
				6. Performing Organization Code 506-62-23-01	
7. Author(s) E. Burton Lightner, compiler				8. Performing Organization Report No. L-15614	
9. Performing Organization Name and Address NASA Langley Research Center Hampton, VA 23665				10. Work Unit No.	
				11. Contract or Grant No.	
12. Sponsoring Agency Name and Address National Aeronautics and Space Administration Washington, DC 20564				13. Type of Report and Period Covered Conference Publication	
				14. Sponsoring Agency Code	
15. Supplementary Notes					
16. Abstract This publication is a compilation of the unclassified papers presented at the NASA Conference on Large Space Antenna Systems Technology, which was held at the Langley Research Center, Hampton, Virginia, November 30 - December 3, 1982. The conference, which was sponsored jointly by the NASA Office of Aeronautics and Space Technology (OAST) and the NASA Langley Research Center, was organized into five sessions: Systems, Structures Technology, Control Technology, Electromagnetics, and Space Flight Test and Evaluation. All speakers and topics were selected by the session cochairmen and included representation from industry, universities, and government. The program was organized to provide a comprehensive review of space missions requiring large antenna systems and of the status of key technologies required to enable these missions.					
17. Key Words (Suggested by Author(s)) Large space systems Large antenna systems Structures, materials, and analyses Flight technology experiments			18. Distribution Statement Unclassified - Unlimited Subject Category 15		
19. Security Classif. (of this report) Unclassified	20. Security Classif. (of this page) Unclassified	21. No. of Pages 468	22. Price A20		